Vol. 61 May, 1957 No. 5

THE JOURNAL OF PHYSICAL CHEMISTRY

(Registered in U. S. Patent Office)

CONTENTS

THE JOURNAL OF PHYSICAL CHEMISTRY

(Registered in U. S. Patent Office)

Published monthly by the American Chemical Society at 20th and Northampton Sts., Easton, Pa.

Entered as second-class matter at the Post Office at Easton, Pennsylvania.

The *Journal of Physical Chemistry* is devoted to the publication of selected symposia in the broad field of physical chemistry and to other contributed papers.

Manuscripts originating in the British Isles, Europe and Africa should be sent to F. C. Tompkins, The Faraday Society, 6 Gray's Inn Square, London W. C. 1, England.

Manuscripts originating elsewhere should be sent to W. Albert Noyes, Jr., Department of Chemistry, University of Rochester, Rochester 20, N. Y.

Correspondence regarding accepted copy, proofs and reprints should be directed to Assistant Editor, Allen D. Bliss, Department of Chemistry, Simmons College, 300 The Fenway, Boston 15, Mass.

Business Office: Alden H. Emery, Executive Secretary, American Chemical Society, 1155 Sixteenth St., N. W., Washington 6, D. C.

Advertising Office: Reinhold Publishing Corporation, 430 Park Avenue, New York 22, N. Y.

Articles must be submitted in duplicate, typed and double spaced. They should have at the beginning a brief Abstract, in no case exceeding 300 words. Original drawings should accompany the manuscript. Lettering at the sides of graphs (black on white or blue) may be pencilled in and will be typeset. Figures and tables should be held to a minimum consistent with adequate presentation of information. Photographs will not be printed on glossy paper except by special arrangement. All footnotes and references to the literature should be numbered consecutively and placed in the manuscript at the proper places. Initials of authors referred to in citations should be given. Nomenclature should conform to that used in *Chemical Abstracts*, mathematical characters marked for italic, Greek letters carefully made or annotated, and subscripts and superscripts clearly shown. Articles should be written as briefly as possible consistent with clarity and should avoid historical background unnecessary for specialists.

Notes describe fragmentary or less complete studies but do not otherwise differ fundamentally from articles. They are subjected to the same editorial appraisal as are Articles. In their preparation particular attention should be paid to brevity and conciseness.

Communications to the Editor are designed to afford prompt preliminary publication of observations or discoveries whose value to science is so great that immediate publication is imperative. The appearance of related work from other laboratories is in itself not considered sufficient justification for the publication of a Communication, which must in addition meet special requirements of timeliness and significance. Their total length may in no case exceed 500 words or their equivalent. They differ from Articles and Notes in that their subject matter may be republished.

Symposium papers should be sent in all cases to Secretaries of Divisions sponsoring the symposium, who will be responsible for their transmittal to the Editor. The Secretary of the Division by agreement with the Editor will specify a time after which symposium papers cannot be accepted. The Editor reserves the right to refuse to publish symposium articles, for valid scientific reasons. Each symposium paper may not exceed four printed pages (about sixteen double spaced typewritten pages) in length except by prior arrangement with the Editor.

Remittances and orders for subscriptions and for single copies, notices of changes of address and new professional connections, and claims for missing numbers should be sent to the American Chemical Society, 1155 Sixteenth St., N. W., Washington 6, D. C. Changes of address for the *Journal of Physical Chemistry* must be received on or before the 30th of the preceding month.

Claims for missing numbers will not be allowed (1) if received more than sixty days from date of issue (because of delivery hazards, no claims can be honored from subscribers in Central Europe, Asia, or Pacific Islands other than Hawaii), (2) if loss was due to failure of notice of change of address to be received before the date specified in the preceding paragraph, or (3) if the reason for the claim is "missing from files."

Subscription Rates (1957): members of American Chemical Society, $8.00 for 1 year; to non-members, $16.00 for 1 year. Postage free to countries in the Pan American Union; Canada, $0.40; all other countries, $1.20. $12.50 per volume, foreign postage $1.20, Canadian postage $0.40; special rates for A.C.S. members supplied on request. Single copies, current volume, $1.35; foreign postage, $0.15; Canadian postage $0.05. Back issue rates (starting with Vol. 56): $15.00 per volume, foreign postage $1.20, Canadian, $0.40; $1.50 per issue, foreign postage $0.15, Canadian postage $0.05.

The American Chemical Society also publishes *Journal of the American Chemical Society, Chemical Abstracts, Industrial and Engineering Chemistry, Chemical and Engineering News, Analytical Chemistry, Journal of Agricultural and Food Chemistry* and *Journal of Organic Chemistry*. Rates on request.

THE JOURNAL OF
PHYSICAL CHEMISTRY

VOLUME 61 MAY 27, 1957 NUMBER 5

DISSOCIATION PRESSURE AND COHESIVE ENERGY OF INDIUM PHOSPHIDE

BY KURT WEISER

RCA Laboratories, Radio Corporation of America, Princeton, N. J.

Received July 27, 1956

The dissociation pressure of solid InP has been measured between 700 and 1045°. From the temperature dependence of the vapor pressure and the known heat of vaporization of indium and heat of dissociation of P_4 molecules, the cohesive energy of InP was calculated to be 154,000 cal./mole.

I. Introduction

In view of the current interest in the semi-conducting properties of InP,[1] a measurement of its dissociation pressure as a function of temperature is of considerable technological importance. Furthermore, such measurements together with existing data on the heat of vaporization of indium and the heat of dissociation of phosphorus enable one to calculate the cohesive energy of the compound, *i.e.*, the energy necessary to dissociate the solid into the gaseous atoms of its components.

II. Experimental Methods and Results

Crystals of InP heated in a sealed, evacuated vial, will partly decompose until the pressure of the vapor in the vial equals the dissociation pressure of the compound. Since, at the temperatures investigated, the phosphorus pressure is always many orders of magnitude larger than the vapor pressure of indium,[2] the dissociation pressure of InP is essentially equal to its phosphorus pressure.

The phosphorus pressure over solid indium phosphide was measured by the method of the "dew-point," *i.e.*, by determining the temperature at which the vapor pressure of pure phosphorus is equal to the dissociation pressure of the compound. This method has long been used for the study of aqueous solutions[3] but apparently has not been applied to measurements of the dissociation pressures of phosphides. In the comprehensive study of many other phosphides undertaken by Biltz and his collaborators[4] the dissociation pressure was determined by measuring the *total* pressure over the solid investigated. Compared to the method described below, this procedure suffers from the possible error of the compound having an appreciable vapor pressure so that the total pressure does not necessarily equal the dissociation pressure.

In carrying out the experiments, crystals of high purity InP (the impurity content, as determined from electrical measurements, was less than one part in 10^5), were sealed into an evacuated quartz tube, as shown schematically in Fig. 1. The bulb containing the crystals was made of heavy wall tubing (appr. 2.5 mm. wall thickness) in order to minimize both the danger of explosions and temperature fluctuations inside the bulb. To determine a pressure, the crystals were kept in the "front furnace" at a controlled "decomposition temperature" T_D, while the temperature in the "rear furnace" was decreased in intervals. At each interval, temperature equilibration was permitted (5 to 10 minutes), and then a short blast of air was directed at the tip through the tapered tube J. If the blast lowered the temperature sufficiently, a condensate of phosphorus in the form of a few droplets would be induced. If the temperature of the "rear furnace" was higher than the condensation temperature T_C of the phosphorus, the condensate disappeared rapidly after the blast of air was turned off. As T_C was approached, the droplets would disappear more slowly, and eventually they would persist when T_C was reached; below T_C the condensate would spread rapidly. The condensation temperature can be established in this manner with an accuracy of better than 10°, and the dissociation pressure of InP at T_D can then be determined from the vapor pressure data of phosphorus at T_C.[5] The air-blast method prevented supersaturation of the phosphorus vapor, as well as permitting an accurate determination of the dew-point by giving warning of its approach.

The determination of the dissociation pressures at the two lowest temperatures investigated was carried out by a slightly modified procedure, since the dew-points of phosphorus fell below room temperature. The tip of the vial was kept in a beaker full of water, first slightly below room temperature, and then at ice temperature. The tempera-

(1) (a) H. Welker, *J. Electronics*, [1] **1**, 181 (1955); (b) O. G. Folberth and H. Weiss, *Z. Naturforschung*, **10a**, 615 (1955); (c) O. G. Folberth, *ibid.*, **10a**, 502 (1955); (d) F. Oswald, *ibid.*, **9a**, 181 (1954); (e) H. Welker, *ibid.*, **8a**, 248 (1953); (f) **7a**, 744 (1952); (g) *Physica*, **XX**, No. 11, 893 (1954).

(2) L. L. Quill, "Chemistry and Metallurgy of Miscellaneous Materials Chemistry," Ch. III, McGraw-Hill Book Co., New York, N. Y., 1950.

(3) See for example, J. N. Friend, "Textbook of Physical Chemistry," Vol. II, J. B. Lippincott, 1935, p. 125.

(4) W. Biltz, *Z. physik. Chem.*, **189A**, 10 (1941).

(5) (a) F. S. Dainton, *Trans. Faraday Soc.*, **46**, 912 (1950); (b) "Handbook of Physics & Chemistry," 1955–1956.

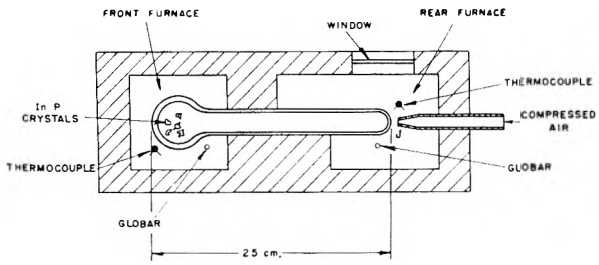

Fig. 1.—Schematic diagram of apparatus for determining dissociation pressures of InP.

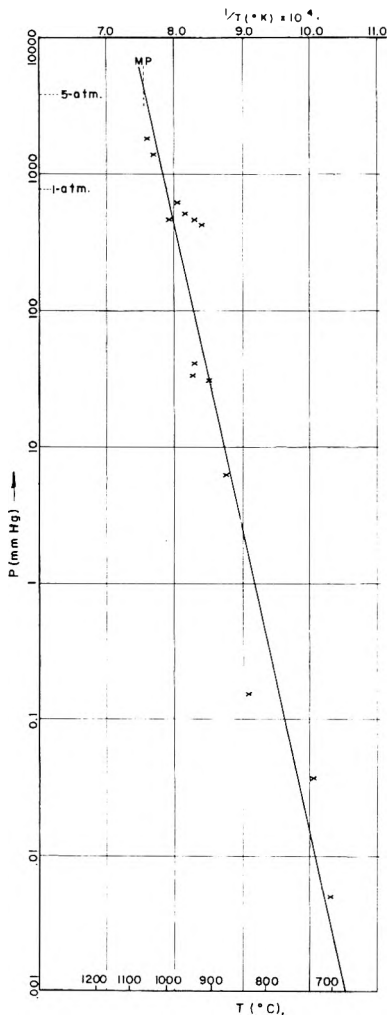

Fig. 2.—Dissociation pressure of InP from 700° to 1045°.

ture of the crystals, T_D, was raised gradually until a condensate of phosphorus appeared at the tip. The decomposition temperature corresponding to a given "dew-point" was thus determined.

The results of four separate runs are shown in Fig. 2, where the logarithm of the dissociation pressure is plotted against the reciprocal of the absolute temperature. For each run, a new quartz vial and different crystals were used. The data represented true equilibrium values since the same results were obtained when the data were taken with increasing or with decreasing temperature.

The two main difficulties encountered during the experiments were due to the presence of an indium phosphide layer on the walls of the vial, and to the occasional conversion of white to red phosphorus. The indium phosphide layer was due to slow sublimation of the compound, and obscured the appearance of the phosphorus condensate. The trouble was overcome by focusing a strong lamp on the tip, and by occasionally heating the tip to drive off the sublimate.[6] The occasional conversion of the white phosphorus condensate to the red modification resulted in an uncertainty as to the proper vapor pressure to be assigned to the condensate. If, however, the condensate induced by the air blast was kept at a minimum, the difficulty was avoided since the phosphorus would evaporate before it had a chance to convert to the red form. For the data shown in Fig. 2, only those measurements were used in which the appearance and disappearance of the condensate were readily visible, and in which no conversion to red phosphorus took place.

III. Discussion

It is a well known result of thermodynamics[7] that the temperature dependence of the equilibrium constant for a chemical reaction at constant volume can be expressed by the equation

$$\ln K_v = E^0/RT + \Delta c^0_v/R) \ln T + \text{const.} \qquad (1)$$

provided that Δc^0_v is constant over the temperature range investigated. In this equation, K_v represents the equilibrium constant at constant volume, E^0 is the heat of the reaction over the temperature range investigated, Δc^0_v is the difference in heat capacity at constant volume between products and reactants, R is the gas constant, and T is the absolute temperature. Since for a typical chemical reaction, E^0 is of the order of 10 to 100 kcal., while Δc_v is of the order of calories per degrees, a plot of ln K against $1/T$ may appear linear over a considerable temperature range.

The chemical equilibria studied here can be represented by the equations

$$InP_s \rightleftharpoons In_l + {}^1/_4P_4(g) \qquad (2a)$$

$$In_l + y.InP_s \rightleftharpoons (In.y.InP)_l \quad \text{where } 0 < y < 1 \qquad (2b)$$

The subscripts s, l and g stand for solid, liquid and gas, respectively. The notation $(In.y.InP)_l$ indicates a saturated solution of InP in indium. Equation 2b indicates the fact that the free indium which is formed by the decomposition of some of the indium phosphide, according to equation 2a, dissolves some additional indium phosphide until the saturated solution $(In.y.InP)_l$ results. The solid solubility of indium in solid indium phosphide has been shown to be negligible by electrical measurements. The assumption of P_4 molecules is based on the measurements of Stock and coworkers[8] who showed that fewer than 10% of the P_4 molecules are dissociated at the highest temperatures investigated here. Since the vapor pressure of indium is negligible at these temperatures[2] the equilibrium constant for the reaction is given by the phosphorus pressure to the one fourth power, or $K = P_4{}^{1/4}$.[7] The assumption of vapor ideality seems reasonable in view of the high temperature and moderate pressures involved.

The data of Fig. 2 can be fitted by the equation

$$\log p = 4 \log K = -23{,}000/T + 21.0 \qquad (3)$$

(6) The gradual sublimation of InP affects the measurements only near the melting point. As long as solid InP is in equilibrium with the indium produced by the decomposition the amount of solid InP is immaterial. After complete melting, however, the system becomes bivariant so that the pressure is no longer a unique function of the temperature but depends on the melt composition as well. This composition will depend on the amount of InP which had sublimed during the course of the experiment.

(7) See, for example: S. Glasstone, "Textbook of Physical Chemistry," Sec. ed., Ch. XI, D. Van Nostrand Co., New York, N. Y., 1946.

(8) A. Stock, *et al.*, *Ber.*, **45**, 3527 (1912).

The heat for the over-all reaction (equations 2a and 2b), as calculated from the slope of Fig. 2 is therefore equal to 26,000 ± 3600 cal./mole. It is clear that this heat consists of two terms, the heat necessary to dissociate one mole of InP (eq. 2a), and the heat involved in dissolving some of the remaining InP in the indium resulting from the dissociation (eq. 2b). Since the solubility of InP in indium increases with temperature,[9] the heat of solution also increases, so that a linear relationship between log p and $1/T$ should not really be expected. It will be shown, however, that the heat of the reaction 2b is small over most of the temperature range of Fig. 2, and in fact falls within the experimental error of the value calculated for the heat of the over-all reaction.

The heat required for reaction 2b can be estimated from a knowledge of the phase diagram for the system In–InP.[10] By plotting the logarithm of the liquidus composition on the InP side of the eutectic against the inverse of the freezing temperature, one can calculate the molar heat of solution of InP; if the melt behaves ideally this heat should equal the heat of fusion of InP. Only the points from about 800° down to the eutectic temperature can be used, however, since above that temperature the liquidus curve begins to flatten markedly, indicating increasing dissociation of the compound in the molten state; the interpretation of the data is then no longer simple. To calculate the heat for reaction 2b, it is only necessary to multiply the molar heat of solution of InP by the number of moles of InP soluble in one g-atom of indium at a given temperature. It was found that up to 900° the heat of reaction 2b was less than the experimental error of the over-all heat of the reaction, as determined from Fig. 2. Above 900° the log p *vs.* $1/T$ curve should increase somewhat in slope but this effect apparently is obscured by experimental error. From the portion of Fig. 2 below 900° we can therefore calculate a value of 26,000 ± 3600 cal./mole for the dissociation energy of indium phosphide into liquid indium and phosphorus.

To find the cohesive energy it is necessary to add to this figure the heat of vaporization of liquid indium and one quarter of the heat of dissociation of P_4 molecules into phosphorus atoms. From published data, we find 56,000 cal./g. atom for the former[2] and one quarter of 288,000 cal./mole for the latter.[11] The cohesive energy of InP is thus 154,000 cal./mole in the temperature range investigated.

It is of interest to compare this result to the cohesive energy of InP as calculated on the model of purely ionic bonding between the components, assuming singly charged indium and phosphorus ions.[12] Using the Madelung constant for the zinc blende structure and the known inter-atomic distance for InP, [16] one obtains a value of 84,000 cal./mole. In making this calculation the ionization energy of indium was taken as 132,000 cal./g. atom,[5b] while the electron affinity of phosphorus had to be estimated by Mulliken's rule[13]; a value of nine was taken for the compressibility parameter n. Any reasonable value for n and for the electron affinity of phosphorus yield a cohesive energy for InP, as calculated on a purely ionic model, which is far smaller than that determined experimentally. One, therefore, reaches the not too surprising conclusion that the bonding in the compound is largely covalent.

Comparing the cohesive energy of indium phosphide to that of two gram atoms of germanium, namely, 178,000 cal.,[14] one finds that the former is somewhat smaller. This result seems to conflict with Welker's prediction[1f] that III-V compounds would have a greater bond strength than the bracketed Group IV element due to the partly ionic nature of the bond. It seems plausible, however, that this prediction would apply more readily to "horizontal" III-V compounds (*i.e.*, both elements in the same Period) than to "diagonal" ones, in which the atoms differ markedly both in nuclear charge and in size.

(9) The phase diagram of the system In–InP has been determined by M. W. Shafer of the College of Mineral Industries, Penna. State Univ. (to be published). The system is simple, showing complete miscibility in the liquid state, immiscibility in the solid state, and a simple eutectic. The flatness of the liquidus curve near the melting point of InP indicates dissociation of the compound in the molten state.

(10) See, for example, ref. 7, chapter X.

(11) (a) F. S. Dainton, *Trans. Faraday Soc.*, **43**, 244 (1947); (b) G. Wetroff, *Compt. rend.*, **208**, 903 (1939).

(12) See F. Seitz, "The Modern Theory of Solids," Ch. I, McGraw-Hill Book Co., New York, N. Y., 1940.

(13) L. Pauling, "Nature of the Chemical Bond," Cornell Univ. Press, Ithaca, N. Y., 1948, Ch. II.

(14) R. E. Honig, *J. Chem. Phys.*, **22**, 1610 (1954).

THE COMPRESSIBILITIES OF THE SILICATES: THE Li_2O–SiO_2 SYSTEM

BY HARRY BLOOM AND JOHN O'M. BOCKRIS

The John Harrison Laboratories of Chemistry, The University of Pennsylvania, Philadelphia, Pa.

Received August 3, 1956

Two models for the liquid silicates indicate different courses for the compressibility isotherms as a function of composition. An apparatus is described which permits measurement of the compressibilities of liquids up to $T = 1350°$. Compressibilities have been measured for the Li_2O–SiO_2 system over the composition range 24–55% Li_2O. Results are in disagreement with the classical model and give some support to the discrete anion model.

Introduction

In the classical view of the structure of liquid silicates[1] it is assumed that the orthosilicate composition (66.7 mole % M_2O)[2] consists of $4M^+$ and SiO_4^{4-} ions. Addition of silica to this composition results in the formation of silicon–oxygen chains in

(1) *Cf.* H. Stanworth, "The Properties of Glass," Oxford, 1950, p. 89.

(2) Throughout this paper, compositions are given in mole %.

which each Si atom has attached to it two charged O atoms. The M^+ is assumed to be located in wells of minimum potential energy near an O^- atom. This theory requires lengthening of the chains as the proportion of SiO_2 increases, the length tending to increase indefinitely as the composition of the mixture approaches 50% SiO_2. Further addition of SiO_2 causes the structure to become two dimensional, the extent of the ionic sheets increasing until the SiO_2 content is 66.7%, when further addition causes the sheets to give way to a three-dimensional structure. This three-dimensional structure becomes more extensive with further addition of SiO_2, tending eventually to the three-dimensional structure of pure silica.

A model for the liquid silicate lattice has recently been suggested[3-5] which differs from the classical one in that instead of the infinite chains and two-dimensional sheets of this theory, it postulates the existence of discrete cyclic silicate anions, essentially polymers of the ion $Si_3O_9^{6-}$, which exist at compositions between 50% M_2O and about 10% M_2O in the alkali oxide–silica systems. At compositions near to 10%, three-dimensional bonding is supposed to be taken up throughout the structure which in these low M_2O contents then becomes identical to that of the classical theory. These two theories of the liquid silicate structures therefore differ essentially in the composition at which the three-dimensionally bonded lattice is supposed to be taken up.

As the extent of continuously bonded areas of Si–O becomes larger in the liquid lattice, the compressibility of the liquid silicate should become less. Thus, if the classical theory were correct, inflections should occur on the compressibility–composition isotherm at the 50% M_2O composition (where a rapid increase of Si–O–Si chain length occurs), and again at 33% M_2O, where the structure commences to exhibit three dimensional bonding. Because from a composition of 33% M_2O to pure SiO_2, the three-dimensional bonding is gradually taken up, there should be no particular inflection in the compressibility isotherm at composition of less than 33% M_2O. Conversely, according to the discrete ion theory, the ion type and shape is supposed to remain unaltered between the compositions 50 and 10% M_2O, the size of the cyclic anion uniformly increasing until this latter composition. The compressibility would be expected to decrease smoothly over the range 50-10% and undergo a rapid decrease at compositions of less than 10% M_2O, where, according to the discrete anion theory, there commences a rapid spread of three-dimensional (silica-like) bonding. The compressibility isotherms thus proffer a clear diagnostic in distinction between classical and discrete ion theories.

Experimental

Ultrasonic velocity measurements were made by the method of Richards, Brauner and Bockris.[6] Use is made of phase interference of two wave trains, one passing through the liquid, and the other, a reference signal.

For measurements on liquid silicates, several modifications to the technique of Richards, *et al.*, were made. Heating was carried out in a carbon tube resistance furnace similar to the one described by Mackenzie.[7] Control of furnace temperature could be obtained by manual adjustment of the "Powerstat" to ±5° over 30 minutes. As the time required to take 5 duplicate measurements of wave length is of this order, such temperature control is satisfactory. Temperature was measured by means of calibrated 20% Rh–Pt *vs.* 40% Rh–Pt thermocouples in Alundum sheaths.

The crucibles for containing the melt were manufactured by a process described by Tomlinson, *et al.*,[8] from molybdenum sheet of thickness 0.006". Specially ductile Mo sheet was used for the bottoms. The crucibles were 1.5" in diameter and 6" tall.

The rods used for propagating the ultrasonic vibrations were high density Alundum. They were circular in cross-section, 0.6" diameter by 18" long, with flat ends. The accuracy of measurement depends largely on the flat nature of the ends of these rods. As the alumina was rapidly attacked by the liquid the end in the melt became seriously corroded after two or three hours and did not allow accurate measurement after that time. The ends were therefore ground flat after each run.

During a run, the alumina rods were supported in two clamps, which were attached by means of a long screw to the upper end and lower parts of the frame, respectively. The rods could be advanced or retracted in the furnace by means of knurled nuts working in the clamps. To the cool end of each rod, a barium titanate, piezoelectric transducer was cemented. The transducers were 0.5" in diameter. The crucible containing the weighed mixture of lithium carbonate and powdered quartz was supported on the top face of the lower Alundum rod. The furnace was assembled, helium passed in and the temperature brought up to just about the liquidus temperature within 5 hours. Heating was continued at this temperature overnight so as to decompose all the carbonate and measurements of sound velocity were begun.

Ultrasonic vibrations generated by the bottom transducer passed *via* the bottom of the crucible into the melt and after being propagated through it, were picked up by the upper alumina rod, conducted along the rod to the transducer at the top and converted by this transducer into electrical impulses. The wave train from the upper transducer was mixed with the attenuated direct signal in the electronic apparatus as described by Richards, *et al.*, and complete interference resulted when the two wave trains were out of phase. When this took place, a null was observed at a certain position on the cathode ray tube detector. The upper rod was advanced or retracted until a second complete null appeared in the same position on the cathode ray screen. The distance traversed by the upper rod between the two nulls was then the wave length of the ultrasonic vibration in the melt. During this process the attenuation was checked to ensure that the direct signal was reduced in amplitude to the same amount as that of the transmitted signal. The frequency (ν) was measured by a frequency meter and was checked during each reading for constancy. From the frequency and wave length (λ) the velocity of the ultrasonic vibrations in the melt was calculated from the equation $v = \nu\lambda$. The displacement of the upper rod was made to cover three or four complete wave lengths so that a more accurate measure of wave length could be made. The displacement of the upper rod was measured by means of a cathetometer.

At least six readings were taken at each temperature. The first measurement was taken at 20° above the liquidus temperature. The temperature was increased by amounts of about 20° and measurements taken at each new temperature up to 1300°. This upper limit was the temperature at which absorption of the ultrasonic vibrations by the alumina rods became too great to enable further measurements to be made.

(3) J. O'M. Bockris and D. C. Lowe, *Proc. Roy. Soc.* (*London*), **226A**, 423 (1954).

(4) J. O'M. Bockris, J. W. Tomlinson and J. L. White, *Trans. Faraday Soc.*, **52**, 299 (1956).

(5) J. O'M. Bockris, J. D. Mackenzie and J. A. Kitchener, *ibid.*, **51**, 1734 (1955).

(6) N. E. Richards, E. Brauner and J. O'M. Bockris, *British J. Applied Phys.*, **6**, 387 (1955).

(7) J. D. Mackenzie, Thesis, London, 1954.

(8) J. W. Tomlinson, D. C. Lowe, G. W. Mellors and J. O'M. Bockris, *J. Sci. Instr.*, **31**, 107 (1954).

TABLE I

RESULTS IN THE Li_2O–SiO_2 SYSTEM

Composition mole % Li_2O	Velocity, m./sec. 1150°	1200°	1300°	Density 1150°	1200°	1300°	Compressibility (cm.² dyne⁻¹) 1150°	1200°	1300°
25	..	..	2850	...	...	2.17	0.3	..	5.7
30	3000	2890	2725	2.179	2.166	2.16	5.1	5.5	6.3
32.8	3000	2900	2700	2.171	2.159	2.15	5.1	5.5	6.4
37	3000	2850	2475	2.159	2.148	2.13	5.1	5.7	7.7
43	..	2490	2120	...	2.128	2.11	..	7.6	10.6
55	..	1930	1500	...	2.066	2.04	..	13.0	21.8

The reproducibility of velocity measurements at each temperature was ±100 meters/sec., *i.e.*, 3–6%.

Mixtures were made up by weighing calculated quantities of lithium carbonate and powdered quartz into a bottle which was shaken for 30 minutes. The quartz was washed with boiling, concentrated HCl, followed by distilled water, and dried. The lithium carbonate (A. R. Quality) had been heated in an oven at 200° for 4 hours and cooled in a desiccator. Duplication of measurements was carried out on several compositions. Reproducibility was obtained to within 3–6%.

Results

Velocity (v), density (ρ) and adiabatic compressibility (β) are given at 1150, 1200 and 1300° in Table I.

Figure 1 shows velocity isotherms as a function of composition at the same three temperatures and Fig. 2 shows isotherms of the adiabatic compressibility (calculated from the general equation $v = \sqrt{1/\rho\beta}$) as a function of composition.

Discussion

Figure 2 shows clearly that there are no breaks in the compressibility isotherms corresponding to the changes in nature of the silicate groups present in the liquid according to the classical theory.[1]

The isothermal compressibility does, however, decrease uniformly, as required by the discrete anion model, over the composition range 55% M_2O–25% M_2O. That this change of isothermal compressibility (β_s) with composition is consistent with the form expected according to the discrete ion model for liquid silicates may be demonstrated in two specific ways.

Firstly, the discrete ion theory indicates that at any given composition of the silicate between 66% M_2O and 10% M_2O, the predominant silicate anions should have a characteristic length. Further, between c_{M_2O} = 50% and c_{M_2O} = 10%, the cross-section of the silicate anion should be constant, whilst the length, l, should increase with decrease of c_{M_2O}. If β_s (exptl.) is plotted against the theoretical value of l calculated[5] on the basis of the discrete anion theory, it is found that

$$\beta_s \propto \alpha \frac{1}{l^{1/2}} \qquad (1)$$

over the composition range 50%–24% M_2O. Hence, as, over this range according to the discrete anion theory, the cross-sectional area of the silicate anions is supposed to be constant, the empirical result (1) is equivalent to the relation

$$\beta_s \propto \alpha \frac{1}{V_A^{1/2}} \qquad (2)$$

where V_A is the molar volume of the silicate anion. However, according to the theory of liquids in terms of holes[9]

(9) R. Furth, *Proc. Camb. Phil. Soc.*, **37**, 252 (1941).

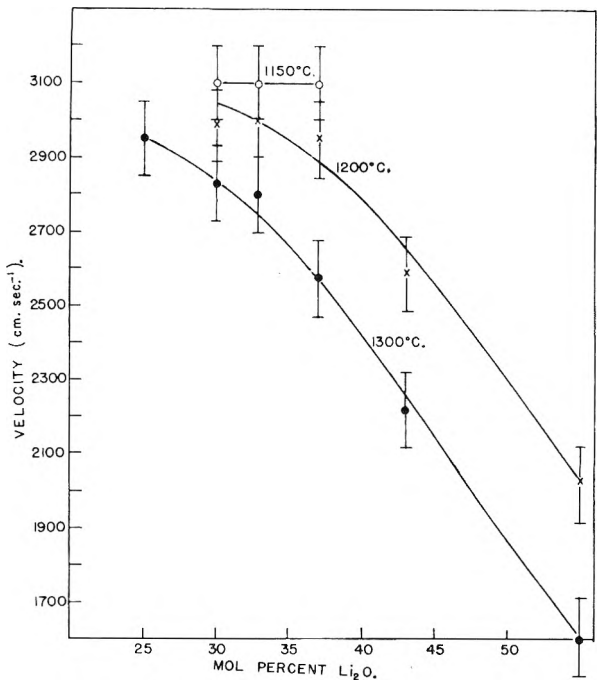

Fig. 1.—Velocity of sound in meters per second as a function of the molar percentage of lithium oxide.

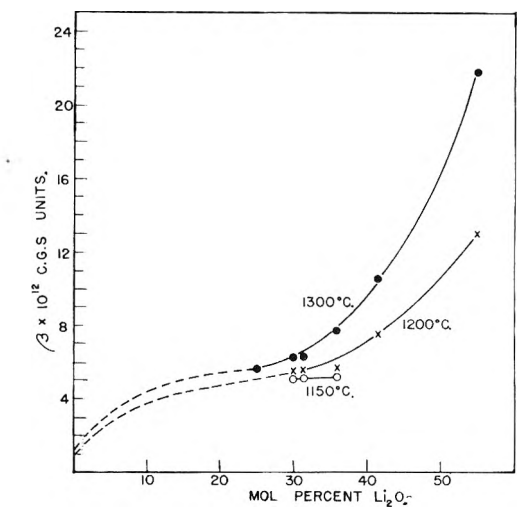

Fig. 2.—Compressibility in cm.² dyne⁻¹ as a function of the molar composition of the molar percentage of lithium oxide.

$$\beta_s \propto \alpha (\Delta V_M / V_M) \qquad (3)$$

where ΔV_M is the change of volume on melting and V_M is the molar volume of the liquid. The change of ΔV_M on composition would not be expected to be great in a series of similar liquids such as the lithium silicates between the composition range 50–

24% Li_2O. Let it be assumed here to be negligible. V_M for a pure electrolyte C^+A^- can be regarded as having effectively the value $(V_C V_A)^{1/2}$, where V_C is the molar volume of the cation, which in the system at present under consideration is V_{Li}, and is constant for the series of liquids examined (whilst V_A varies, if the discrete anion theory is correct). Hence, for a system such as the lithium silicates over the range of compositions stated, $V_M \propto V_A^{1/2}$. It follows that for the systems considered equation 3, based on the general theory of holes in liquids, takes the special form

$$\beta_s \propto \alpha \frac{\Delta V_M}{V_A^{1/2}} \propto \alpha \frac{1}{V_A^{1/2}} \qquad (4)$$

if ΔV_M is assumed independent of composition and the discrete anion theory is applicable. The theoretical equation 4 therefore has the same form as the empirical equation 2, thus lending support to the assumptions made in the deduction of 4.

Secondly, the dotted line in Fig. 2 (obtained by extrapolating the experimental relation shown by the solid line to the value for the compressibility of vitreous SiO_2 at the same temperature[10]) suggests that an inflection in the compressibility–composition relation occurs between $c_{M_2O} = 25$ and $c_{M_2O} = 0$%. If the inflection implied in Fig. 2 is assumed to occur approximately half way between 0 and 25% Li_2O, the composition at which it takes place is about 12% Li_2O. However, it is just at a composition near to this, namely, 10% Li_2O, that, according to the discrete ion theory,[3] there is a radical change in the structure of the liquid, the discrete ion structure becoming, for compositions containing $c_{Li_2O} < 10$%, a partially broken down three-dimensional lattice. The latter structure would be expected to have a considerably lesser compressibility (*i.e.*, fewer holes per cc.) than that of a series of discrete ions of nearly the same Si/O ratio (where holes and free space exist), so that the compressibility would indeed be expected to undergo a sudden decrease in just that region of composition where the experimental results of Fig. 2 suggest that such a decrease occurs.

Acknowledgments.—The authors are grateful to the Atomic Energy Commission for a grant in support of this work under Contract Number AT (30-1)-1769.

(10) W. G. Cady," Piezoelectricity," Academic Press, New York, N. Y., 1946, p. 140.

THERMODYNAMIC PROPERTIES OF METHYL ALCOHOL–CHLOROMETHANE SOLUTIONS

BY E. A. MOELWYN-HUGHES AND R. W. MISSEN

Department of Physical Chemistry, University of Cambridge, Cambridge, England

Received August 10, 1956

Excess free energies and heats of mixing have been measured at 35° for binary solutions of methyl alcohol and methylene dichloride, chloroform and carbon tetrachloride, respectively. The excess entropies of mixing obtained from them show that the systems are very irregular. The abnormal behavior is most marked for solutions dilute in alcohol. For these solutions, the partial molar properties of the alcohol become very large as dilution is increased. This behavior requires exponential equations for an adequate description of the compositional dependence of the thermodynamic functions, but power-series equations are applicable at most compositions. Refractive indices of the solutions have also been measured at 20°.

Several theories have been advanced recently of binary solutions of which one component is an alcohol.[1] The experimental data with which any of them can be compared, however, are often inadequate in that the entropy changes which occur on mixing are not obtained from free energy and thermal changes measured at the same temperature. As part of a program[2] of investigating properties of solutions, we have measured free energies and heats of mixing of solutions of methyl alcohol with methylene dichloride, chloroform and carbon tetrachloride, respectively, at 35°. The free energy changes for methyl alcohol and carbon tetrachloride solutions at this temperature have been well defined by Scatchard and his co-workers,[3,4] and those for methyl alcohol and chloroform solutions by Kireev and Sitnikov,[5] but the thermal changes have not been similarly treated. It is known, however, that these solutions have large, non-zero excess entropies of mixing, and are thus far from regular in Hildebrand's sense.[6] As far as we know, there is no other available information about the behavior of mixtures of methyl alcohol and methylene dichloride.

Experimental

Purification and Physical Properties of the Liquids.—The purification and physical properties of the methylene dichloride, chloroform and carbon tetrachloride used have been described.[2] A. R. methyl alcohol was purified by fractionation, the product being removed over a temperature range of 0.02 to 0.04°. It had a refractive index ($n^{20}D$) of 1.3287 and a density (d^{25}_4) of 0.7867. Vapor pressures measured at 5° intervals in the equilibrium still from 25 to 65° are reproduced by equation (1) with a standard deviation of 0.4 mm.

$$\log_{10} p^0 = 17.3506 - 2.9314 \log_{10} T - 2383.7/T \qquad (1)$$

in which p^0 is the vapor pressure, mm. and T the absolute temperature, and the constants were determined by the method of least squares. The boiling point calculated from this equation is 64.59°.

Apparatus.—Excess free energies of mixing were calculated from equilibrium data measured in a modified Gillespie,

(1) See, for example, J. A. Barker, *J. Chem. Phys.*, **20**, 1526 (1952); C. B. Kretschmer and R. Wiebe, *ibid.*, **22**, 1697 (1954).

(2) E. A. Moelwyn-Hughes and R. W. Missen, *Trans. Faraday Soc.*, in press.

(3) G. Scatchard, S. E. Wood and J. M. Mochel, *J. Am. Chem. Soc.*, **68**, 1960 (1946).

(4) G. Scatchard and L. B. Ticknor, *ibid.*, **74**, 3724 (1952).

(5) V. A. Kireev and I. P. Sitnikov, *J. Phys. Chem.* (*U.S.S.R.*), **15**, 492 (1941).

(6) J. H. Hildebrand, *J. Am. Chem. Soc.*, **51**, 66 (1929); *Faraday Soc. Disc.*, **15**, 3 (1953).

condensate-recirculation still, which is described elsewhere.[2] Difficulties similar to those described by Scatchard and Ticknor[4] were encountered in the operation of the still. Boiling and pumping became less smooth as the composition of the contents approached that of pure alcohol. This could be offset by using a high current (up to 5 amp.) in the internal heater. A steady state, that is, a temperature fluctuation not exceeding 0.02°, could not be attained for dilute solutions of methyl alcohol in carbon tetrachloride and of methylene dichloride in methyl alcohol. Fluctuations as large as 0.1 to 0.15° were experienced. For such solutions the composition of the vapor differs greatly from that of the liquid, and it may be necessary to use a vapor-recirculation, instead of a condensate-recirculation, still in order to eliminate the fluctuation. Otherwise, a steady state was attained in less than an hour, and boiling was usually interrupted after 1.25 hours.

The calorimeter for the measurement of heat of mixing is also described elsewhere.[2] This, too, did not operate as successfully as with methyl iodide solutions. The first thermistor had to be replaced by another of similar type, which was enclosed in an all-glass envelope. The mounting was not as successful in the second case, with the result that mechanically the thermistor was not completely stable on rotation. This was offset by the fact that the heat effects were generally larger, and so the sensitivity could be reduced. In addition, there was some reaction between the methyl alcohol and the copper of the calorimeter. This is not thought to have seriously affected the results, however, as some measurements of the heat of mixing of methyl alcohol and chloroform at 25° agreed with those of Hirobe[7] within 2%. Discs of electrolytic copper foil were used instead of tin as the diaphragm between the pure liquids.

Results

In the following, subscript 1 denotes methyl alcohol or component 1 in general, 2 methylene dichloride or component 2, 3 chloroform and 4 carbon tetrachloride. Except where otherwise stated, the constants of the empirical equations have been determined by the method of least squares.

Refractive Index—The measured refractive indices which were used to construct the calibration curves for the analysis of the samples from the still can best be reproduced analytically in terms of volume fractions by the following equations with a standard deviation less than 0.0002

$$(n^{20}\mathrm{D})_{12} = 1.4244 - 0.0957\theta_1 - 0.0040\theta_1\theta_2 \quad (2a)$$

$$(n^{20}\mathrm{D})_{13} = 1.4462 - 0.1175\theta_1 + 0.0020\theta_1\theta_3 \quad (2b)$$

$$(n^{20}\mathrm{D})_{14} = 1.4604 - 0.1317\theta_1 \quad (2c)$$

Here θ represents volume fraction and is calculated without regard to volume changes on mixing. Our data for methyl alcohol and carbon tetrachloride solutions do not agree with those obtained by Hipkin and Myers[8] at 20°. The average absolute deviation is 0.0009, and the algebraic deviation changes sign at a composition near that of the azeotrope. The linearity with respect to volume fraction expressed by equation 2c, however, agrees with the finding of Pesce and Evdokimoff[9] at 25°.

Free Energy of Mixing.—The measured excess free energies of mixing, ΔG^E, of the three systems at 35° are plotted as circles in Fig. 1, 2 and 3. Let x and y denote the compositions of the liquid and vapor phases in equilibrium, both expressed in mole fraction, and P the total pressure in mm. Then ΔG^E may be calculated from the equilibrium data by means of the equations

(7) H. Hirobe, *J. Fac. Sci., Tokyo*, [I] **1**, 155 (1925).
(8) H. Hipkin and H. S. Myers, *Ind. Eng. Chem.*, **46**, 2524 (1954).
(9) B. Pesce and V. Evdokimoff, *Gazz. chim. ital.*, **70**, 723 (1940).

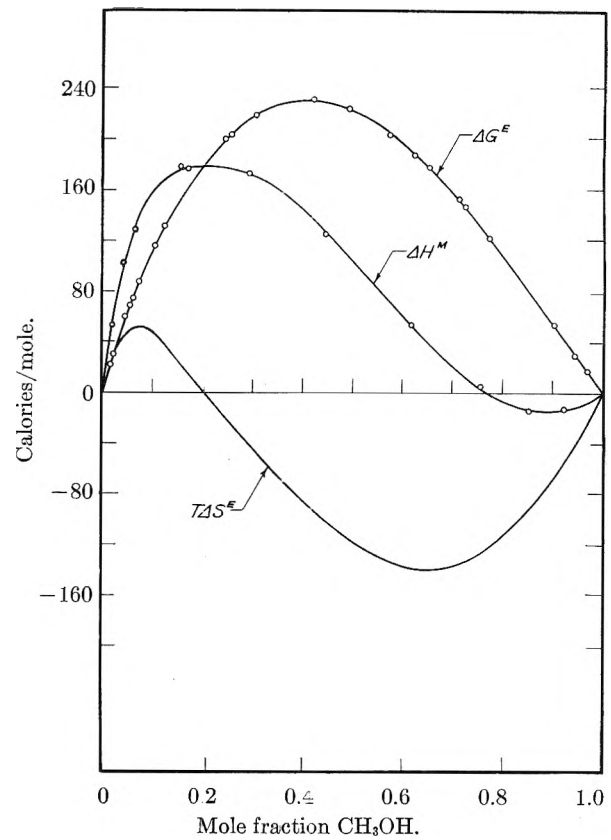

Fig. 1.—Excess thermodynamic functions: CH_3OH–CH_2Cl_2 at 35°.

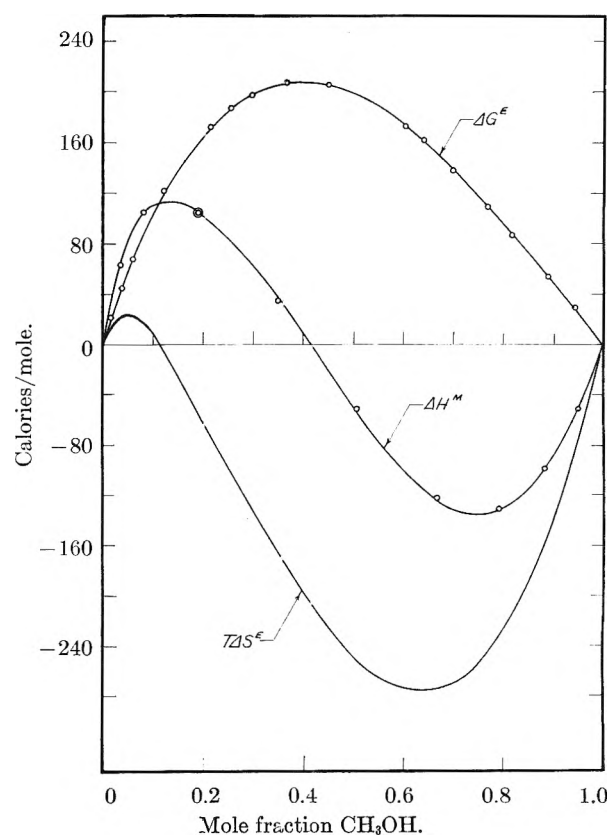

Fig. 2.—Excess thermodynamic functions: CH_3OH–$CHCl_3$ at 35°.

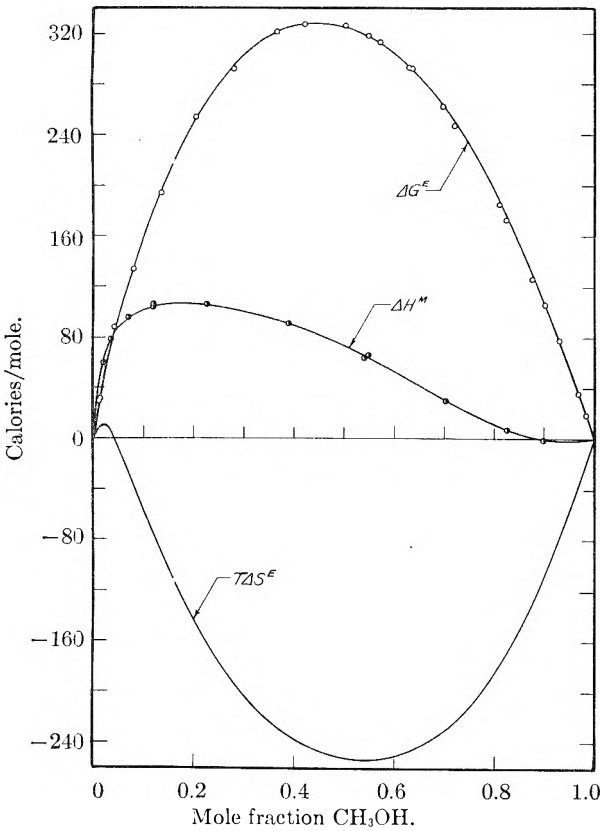

Fig. 3.—Excess thermodynamic functions: CH_3OH–CCl_4 at 35°.

$$\Delta G_{12}^{E} = x_1\mu_1^{E} + x_2\mu_2^{E} \quad (3)$$

and

$$\mu_1^{E} = RT \ln (y_1P/x_1p_1^{0}) \quad (4)$$

where μ_1^{E} is the excess chemical potential of component 1, and a similar relation applies for component 2. We have here assumed that the vapor phase behaves as an ideal solution, so that the partial pressure of component 1 is $p_1 = y_1P$.

In all three cases the excess free energies do not vary symmetrically with respect to composition expressed as mole fraction. In order to represent the compositional dependence of the experimental data adequately, we have found it necessary to use two types of equations for different regions of composition. An exponential equation has thus been used for solutions dilute in methyl alcohol, and a power-series equation for other solutions, except in the case of mixtures of methyl alcohol and carbon tetrachloride, for which two exponential equations have been used. The forms of these equations are

$$\Delta G^{E} = x_1x_2[g_0 + g_1(x_1 - x_2) + g_2(x_1 - x_2)^2] \quad (A)$$

$$\Delta G^{E} = x_1x_2 \exp[g_0 + g_1(x_1 - x_2) + g_2(x_1 - x_2)^2] \quad (B)$$

and

$$\Delta G^{E} = x_1x_2[g_0 + \exp(g_1 + g_2(x_1 - x_2))] \quad (C)$$

where g_0, g_1 and g_2 are empirical constants. In some cases, two-constant forms of these equations are adequate. The form of equation A has been used extensively by Scatchard.[10] The type of equation used, the values of the constants and the valid composition range are given in Table I, in which σ is the standard deviation in comparing observed and calculated values. The continuous free energy curves of Fig. 1, 2 and 3 were calculated from these equations. This smoothing procedure has one disadvantage apart from the inconvenience of determining and using two sets of constants. The two sets should be made mutually consistent so that the resulting calculated data rigorously satisfy the Gibbs–Duhem equation. This has not been done, however, because, as is described later, the calculated data reproduce the experimental data as closely as the latter obey the above relation.

TABLE I

CONSTANTS OF THE EXCESS FREE ENERGY OF MIXING EQUATIONS AT 35°

System	Eq. type	g_0	g_1	g_2	σ, cal./mole	x_1 range
CH_3OH–CH_2Cl_2	B[a]	7.082	0.588	0.795	1	<0.2
	A	892	−352	.....	1	> .2
CH_3OH–$CHCl_3$	B[a]	6.983	0.546	0.772	1	< .2
	A	794	−354	56	1	> .2
CH_3OH–CCl_4	B[a]	11.452	10.735	7.200	2	< .1
	C	1200[b]	4.635	−2.086	2	> .1

[a] Constants obtained by method of averages. [b] Obtained by inspection from $(\Delta G^{E}/x_1x_4) - x_1$ plot.

The calculated data for methyl alcohol and chloroform solutions agree with those of Kireev and Sitnikov[5] within an average of 5 cal./mole. Scatchard, Wood and Mochel[3] have measured ΔG^{E} for methyl alcohol and carbon tetrachloride solutions at 35 and 55°. Their data have been recalculated by Scatchard and Ticknor[4] and smoothed in the form of a 5-constant equation of type A, which reproduces their data well when $x_1 > 0.1$ but not when $x_1 < 0.1$. In the former region their calculated data agree with the present data within an average of 3 cal./mole. Both sets of calculated data yield total free energies of mixing which barely escape the "two-phase catastrophe" between $x_1 = 0.1$ and 0.2.

These three systems are azeotropic. The compositions of the minimum-boiling azeotropes were determined graphically from y–x plots, and are $x_1 = 0.143$ for methyl alcohol and methylene dichloride, $x_1 = 0.295$ for methyl alcohol and chloroform and $x_1 = 0.503$ for methyl alcohol and carbon tetrachloride.

The equilibrium data were tested for internal consistency by plotting $\mu_1^{E} - \mu_2^{E}$ against x_1.[11] The ratios of the areas below and above the composition axis were 1.01, 1.02 and 1.04 for the methyl alcohol–methylene dichloride, methyl alcohol–chloroform and methyl alcohol–carbon tetrachloride systems, respectively.

Heat of Mixing.—The measured heats of mixing for the three systems at 35° are given in Table II and are plotted as circles in Fig. 1, 2 and 3. As in the case of ΔG^{E}, more than one equation is required to smooth the data adequately for each system. The type of equation used, the values of the constants and the valid composition range are given in Table III, in which the constants h_0, h_1 and h_2 replace g_0, g_1 and g_2 of equations A, B and C. For

(10) G. Scatchard, *Chem. Revs.*, **44**, 7 (1949).

(11) O. Redlich and A. T. Kister, *Ind. Eng. Chem.*, **40**, 345 (1948).

dilute solutions of methyl alcohol in carbon tetrachloride, no equation of the above types with less than 5 constants has been found to fit the experimental data without introducing inflection points. These data have therefore been smoothed graphically. The continuous heat of mixing curves in Fig. 1, 2 and 3 were calculated from the constants of Table III.

TABLE II

HEATS OF MIXING AT 35° IN CAL./MOLE

CH_3OH–CH_2Cl_2 x_1	ΔH_{12}^M	CH_3OH–$CHCl_3$ x_1	ΔH_{13}^M	CH_3OH–CCl_4 x_1	ΔH_{14}^M
0.019	53	0.035	63	0.019	60
.042	103	.081	105	.035	79
.065	129	.191	105	.070	96
.155	179	.192	105	.119	104
.171	177	.350	35	.120	106
.292	173	.507	− 51	.226	106
.447	125	.669	−122	.389	91
.618	53	.792	−131	.542	65
.758	4	.883	− 99	.550	64
.854	−14	.949	− 51	.703	29
.929	−13			.827	6
				.900	0

TABLE III

CONSTANTS OF THE HEAT OF MIXING EQUATIONS AT 35°

System	Eq. type	h_0	h_1	h_2	σ, cal./mole	x_1, range
CH_3OH–CH_2Cl_2	B[a]	6.524	0.310	1.886	2	<0.3
	A	420	−894	191	2	> .3
CH_3OH–$CHCl_3$	B[a]	4.414	−3.390	.....	1	< .25
	A	−198	−1166	226	2	> .25
CH_3OH–CCl_4	...	Data graphically smoothed			..	< .35
	A	296	−380	.....	1	> .35

[a] Constants obtained by the method of averages.

Hirobe[7] has measured the heat of mixing of methyl alcohol and chloroform solutions at 25°, but there is a systematic deviation between his results and ours, which is believed to be caused by the temperature dependence of ΔH_{13}^M. Scatchard, Ticknor, Goates and McCartney[12] have measured ΔH_{14}^M at 20° and Scatchard and Ticknor[4] have adjusted these to 35° with the help of data on the temperature dependence of ΔG_{14}^E. As well as can be judged from their graph, our values agree with theirs within 2 to 3 cal./mole for $x_1 > 0.5$, but their endothermic maximum of 86 cal./mole is considerably lower than ours of 106 cal./mole.

Entropy of Mixing.—The excess entropies of mixing were calculated from the free energies and heats of mixing from

$$T\Delta S^E = \Delta H^M - \Delta G^E \qquad (4)$$

The calculated data are plotted as the entropy of mixing curves in Fig. 1, 2 and 3, which show that these solutions are far from regular. For each system there is a small region of positive ΔS^E and a much greater region of negative ΔS^E. The former is greatest for the methyl alcohol–methylene dichloride system and least for the methyl alcohol–carbon tetrachloride system.

(12) G. Scatchard, L. B. Ticknor, J. R. Goates and E. R. McCartney, *J. Am. Chem. Soc.*, **74**, 3721 (1952).

Discussion

The highly irregular behavior of solutions of methyl alcohol and the chloromethanes contrasts greatly with that of solutions of methyl iodide and the chloromethanes, which we have shown to be nearly regular.[2] Molecules of methyl iodide and methyl alcohol have net dipole moments of about the same magnitude, 1.6×10^{-18} e.s.u., but, as has been pointed out,[13,14] this is not a reliable criterion for similarity of behavior in solution. The presence of the hydroxyl group in the alcohol molecule gives rise to the conventionally accepted view that liquid methyl alcohol is a mixture of monomeric, dimeric and polymeric molecules held together in chain-fashion by transient hydrogen bridges.[15] There is no comparable "structure" in methyl iodide.

The features of the excess entropy of mixing curves of Fig. 1, 2 and 3 have been discussed qualitatively on several previous occasions.[1,3,16,17] The positive excess entropies of mixing for solutions dilute in alcohol have thus been attributed, in part, to increased rotational entropy as the hydrogen-bridged network of alcohol molecules is endothermally broken up. The large negative excess entropies of mixing over the greater part of the composition range are due to clustering of like molecules, or perhaps even of unlike molecules in definite proportions in the case of methyl alcohol and chloroform.[16]

In agreement with the positive values of ΔS^E for solutions dilute in alcohol is the fact that the partial molar properties of the alcohol are unusually large in these solutions. The excess chemical potential (μ^E) of the alcohol in dilute solution of chloromethane as calculated by equation B is about twice that of the chloromethane in dilute solution of alcohol. Differentiation of the heat of mixing equations would show a similar abnormality for the partial molar heat content. It is this feature, which results in correspondingly large values of the total molar properties in this region, which makes it impossible for power-series expansions to describe adequately the compositional dependence of the excess free energies and heats of mixing.

Acknowledgment.—R. W. Missen thanks the Athlone Fellowships Managing Committee for financial assistance during the period of this work.

(13) J. D. Bernal, *Trans. Faraday Soc.*, **33**, 210 (1937).

(14) J. H. Hildebrand and R. L. Scott, "Solubility of Non-electrolytes," 3rd ed., Reinhold Publ. Corp., New York, N. Y., 1950, p. 2.

(15) W. H. Zachariasen, *J. Chem. Phys.*, **3**, 158 (1935).

(16) G. Scatchard and C. L. Raymond, *J. Am. Chem. Soc.*, **60**, 1278 (1938).

(17) S. E. Wood, *J. Chem. Phys.* **15**, 358 (1947).

LOW TEMPERATURE HEAT CAPACITIES AND RELATED PROPERTIES OF POTASSIUM AND Na_2K[1,2]

BY C. A. KRIER, R. S. CRAIG AND W. E. WALLACE

Contribution No. 999 from the Department of Chemistry, University of Pittsburgh, Pittsburgh, Pa.

Received August 24, 1956

Constant pressure heat capacities between 12 and 320°K. are presented for potassium and an alloy of composition Na_2K. The Na_2K–K eutectic point was established to be $-12.65 \pm 0.01°$, and the incongruent melting point or meritectic point for Na_2K was established to be $6.90 \pm 0.00°$. From the heat capacity data the entropies at 273.16 and 298.16°K., relative to absolute zero, are found to be, 14.77 ± 0.03 and 15.38 ± 0.03 e.u./g. atom for potassium, and 12.48 ± 0.02 and 16.07 ± 0.03 e.u./g. atom for Na_2K, respectively. A residual entropy for Na_2K at absolute zero was estimated, assuming an ideal entropy of mixing, to be -0.05 e.u./g. atom; this result suggests that the entropy of formation of Na_2K exceeds the ideal mixing entropy. No low temperature "transition anomalies" of the type reported for sodium, rubidium and cesium were detected. Anomalous rising of the heat capacity of Na_2K about 100 degrees below the incongruent melting point, as found for the pure metals, indicates that the cause of the excess heat capacity is not the open structure of the body-centered cubic lattice. The alloy deviates negatively from the Kopp–Neumann rule below 50°K. and in a positive manner thereafter.

Introduction

The present study is part of a continuing series of investigations being carried out in this Laboratory dealing with the thermodynamics of metallic elements and selected intermediate phases.[3] Na_2K was selected for inclusion in the group of studies because it seems to be an excellent example of a size stabilized compound.[4] In addition the thermal and electrical properties of sodium and potassium exhibit a number of peculiarities, and there was hope that a study of the thermal properties of the alloy might further our understanding of the behavior of these elements.

There are at least three unusual properties of the alkali metals. First, the constant volume heat capacities of sodium and potassium begin to exceed the Dulong–Petit limit at 240 and 150°K., respectively. Second, Dauphinee, MacDonald and Preston-Thomas[5] have shown that sodium in the Dry Ice range exhibits a specific heat anomaly which depends upon the thermal history of the sample. Third, MacDonald[6] has pointed out that potassium, rubidium and cesium have resistance-temperature characteristics between 150 and 200°K. which are time dependent. These phenomena clearly indicate complexities with the alkali metals which are not in accord with the usual concepts of these substances as simple and well understood metals. MacDonald's resistance measurements suggested the possibility of a heat capacity anomaly in potassium around 175°K. This possibility, the paucity of reliable heat capacity data for potassium, and the need for such data in connection with the study of Na_2K were the factors responsible for the decision to redetermine the heat capacity of potassium over the range covered in the present work.

(1) From a thesis submitted by C. A. Krier in partial fulfillment of the requirements for the Ph.D. degree at the University of Pittsburgh, January, 1955.

(2) This work was assisted by the U. S. Atomic Energy Commission.

(3) L. W. Coffer, R. S. Craig, C. A. Krier and W. E. Wallace, *J. Am. Chem. Soc.*, **76**, 241 (1954).

(4) B. Chalmers, "Progress in Metal Physics," Vol. I. Interscience Publishers, New York, N. Y., 1949, Chapter 1 by G. V. Raynor, "Progress in Theory of Alloys," p. 34.

(5) T. M. Dauphinee, D. K. C. MacDonald and H. Preston-Thomas, *Proc. Roy. Soc.* (*London*), **221A**, 267 (1954).

(6) D. K. C. MacDonald, *Phil. Mag.*, **43**, 479 (1952).

Experimental Aspects

Apparatus Used.—The equipment and technique were, in the main, the same as have been in use in this Laboratory for several years.[7] The only change necessary was to adapt the sample container to accommodate reactive metals. Ordinarily the sample container is sealed in the open. This practice cannot be followed in the present instance due to atmospheric attack of the samples. Accordingly an inner container was provided which held the potassium or Na_2K and which was sealed off under an atmosphere of helium in a special "dry-box" arrangement.[8] The inner container was a cylindrical copper vessel with a monel top and bottom. It was provided with a tapered hole lying along the axis of the cylinder and extending entirely through it. The tapered pin of the regular sample container fitted into the tapered hole. The tapered pin was lubricated with a small amount of Apiezon grease to assist in making a good thermal bond between the inner container and the sample container. Further constructional details of the inner container are given elsewhere.[9] After the sample had been introduced into the inner container (the sample being liquid in each case as it was introduced), and that container sealed, all under an atmosphere of purified helium, the inner container was placed in the regular sample container and sealed in the usual way.

It was of course necessary to recalibrate the sample container with the inner container in place. The recalibration consisted of 109 determinations of the heat capacity of the empty calorimeter extending from 10 to 325°K.

Preparation of Materials.—The starting materials for the samples were a pound of nominally pure potassium and a pound of sodium–potassium alloy (approximately 44% by weight potassium). These were donated by the Mine Safety Appliances Company of Callery, Pa.[10]

The potassium was triple distilled under high vacuum in an all-Pyrex still and only the first 40% of the material distilling over was retained for use. The purified potassium was a sample having a volume of 250 cm.^{3}. Portions of this were used for the determinations on pure potassium and for preparing the sample of Na_2K. To ascertain the extent of the impurities present, small samples of the pure metal and the alloy were converted to the chloride and analyzed in this state spectroscopically. Metallic impurities, other than tin, aluminum, boron and silicon were found to be present only in spectroscopic traces. It seems fairly certain that these four elements, which were present in only slightly greater amounts, were introduced in the process of converting the metals into salts. Further details of the analysis are given elsewhere.[9]

The bulk supply of alloy had a composition of approximately 44% potassium by weight whereas the percentage of

(7) R. S. Craig, C. A. Krier, L. W. Coffer, E. A. Bates and W. E. Wallace, *J. Am. Chem. Soc.*, **76**, 238 (1954).

(8) E. E. Ketchen, F. A. Trumbore, W. E. Wallace and R. S. Craig *Rev. Sci. Instruments*, **20**, 524 (1949).

(9) C. A. Krier, Ph. D. Dissertation, University of Pittsburgh, 1955.

(10) The authors acknowledge with thanks the cooperation of Dr. C. B. Jackson in obtaining the samples.

potassium in Na_2K is 45.96. To facilitate the preparation of Na_2K, a portion of the bulk supply was enriched with potassium to a percentage of about 47. The compositions of these two stock alloys were then determined to be 47.44 ± 0.02 and 42.95 ± 0.04 weight % potassium by converting weighed samples into the chloride. Appropriate volumes of the two stock solutions were mixed under helium to give an alloy of composition Na_2K.

The prepared sample was analyzed in two ways, by conversion to the chloride and with a flame photometer. The results obtained by these two independent schemes of analysis were 46.07 ± 0.02 and 46.08 ± 0.16 weight % potassium, respectively. The Na_2K sample therefore contained a slight excess of potassium, 0.0030 ±0.0006 gram atom out of a total of 2.0027 gram atoms of sodium and potassium.

The presence of excess potassium in the sample also could be demonstrated calorimetrically. The calorimetric equipment was used to determine cooling curves in the usual way and an arrest at −12.65 ± 0.01° was observed. This temperature corresponds to the Na_2K–K eutectic point.[11] It was a simple matter to determine the energy associated with this arrest, which was found to be 2.44 cal. From this it was possible to estimate the amount of excess potassium present in the sample as 0.0018 gram atom. However, this computation involves the heat of mixing of the supercooled liquid metals, a quantity which is very imperfectly known, so that the estimate of the potassium excess obtained in this way may be in error by as much as 50%. If this is borne in mind, it is seen that the thermal and analytical methods are in substantial agreement as regards the excess of potassium in the sample.

Synthesis of Na_2K.—The preparation of the intermediate phase Na_2K, which is the stable form of the system below 7°, presented some difficulties. Above 20° Na_2K is liquid; on cooling, sodium begins to precipitate out at 20°. Na_2K forms by a meritectic reaction beginning at 7°. If this reaction is not allowed to run to completion, the system below 7° consists of Na_2K plus a mixture of sodium and potassium. The magnitude of the heat effect at the eutectic temperature can be used to estimate the degree of completion of the reaction. In the early attempts there was a comparatively large heat effect at the eutectic point indicating the reaction to be far from completion. The preliminary work indicated that to effect a complete transformation it was necessary to cool through the two-phase region (20 to 7°) as rapidly as possible. Under these conditions the precipitated sodium is well dispersed and the meritectic reaction occurs at a maximum rate. If the cooling through the two-phase region is slow, the sodium particles apparently increase in size to the point that completion of the reaction cannot be achieved in a length of time which is experimentally feasible. In the technique which proved to be successful the sample was cooled using liquid nitrogen. With this procedure, its temperature dropped to the meritectic point in less than 9 min. and to 198°K. in a total of 70 min. It was then raised to 272°K. and kept there for six hours with the adiabatic shield control, and was kept an additional 37 hours at temperatures between 265 and 275°K. Since heat is evolved as Na_2K forms, it was possible to ascertain whether the reaction was still under way by noting the temperature rise of the sample container under adiabatic conditions. At the end of 43 hours the warm-up rate had fallen to essentially zero and the reaction seemed to have run its course. After another 24 hours a measurement was made to see how much heat was absorbed on warming through the eutectic point; from the observed heat effect the conclusion was reached that the reaction was better than 99.8% complete. The sample was held an additional 12 hours at 275°K. and was then permitted to drift down in temperature toward the Dry Ice point.

These various operations were, of course, carried out with the sample in the calorimeter.

Experimental Results

Heat Capacities of Potassium.—Measurements were made using 52.8823 g., or 1.3525 g. atoms, of potassium. Six series of determinations were carried out as shown

Series	Temp. range, °K.	Thermal history
I	292–321	As sealed into calorimeter
II	277–325	As sealed into calorimeter
III	200–289	Cooled from 294 to 200°K. in 45 min.
IV	203–289	Cooled from 289 to 203°K. in 26 hr.
V	101–199	Cooled from room temp. to 134°K. in 65 hr., then from 134 to 10°K. in one hr. Mechanical failure occurred in Collins Machine so that experiments below 100°K. could not be performed cooled from room temp. to 144°K. in 47 hr., from 144 to 10°K. in one hr.
VI	10–230	

Results of the individual measurements and smoothed heat capacities are given in Tables I and III. Precision of the measurements is of the order of 0.1%. The average deviation of the individual determinations from a smooth curve drawn through all the points is 0.075% and only 11 of the 110 measurements deviate by more than 0.15%.

TABLE I

HEAT CAPACITY VALUES OF POTASSIUM FROM INDIVIDUAL DETERMINATIONS

Temp., °K.	C_p, cal./deg. g. atom	Temp. °K.	C_p, cal./deg. g. atom	Temp. °K.	C_p, cal./deg. g. atom
Series I		Series IV		Series VI	
295.09	7.048	205.79	6.470	11.12	0.840
300.32	7.096	210.48	6.497	12.62	1.102
305.68	7.163	215.42	6.519	14.64	1.446
311.50	7.205	220.52	6.536	16.99	1.851
317.61	7.313	225.65	6.567	19.51	2.260
		230.91	6.595	22.16	2.685
Series II		236.34	6.625	25.03	3.092
		241.80	6.653	28.10	3.473
279.94	6.898	247.30	6.684	31.36	3.818
284.92	6.931	252.85	6.714	34.76	4.130
290.08	6.976	258.36	6.745	38.29	4.384
295.34	7.036	263.85	6.775	41.98	4.616
300.63	7.069	269.31	6.816	45.82	4.799
306.08	7.154	274.87	6.856	49.80	4.979
311.69	7.218	280.54	6.911	54.14	5.135
317.33	7.295	286.21	6.948	59.06	5.278
322.80	7.404			64.32	5.416
		Series V		69.67	5.519
Series III				75.32	5.604
		103.73	5.917	81.26	5.702
202.17	6.456	109.03	5.965	87.32	5.783
206.63	6.477	114.43	6.000	93.62	5.836
211.31	6.501	119.82	6.036	100.05	5.889
216.26	6.522	125.10	6.069	106.35	5.939
221.34	6.544	130.43	6.099	112.46	5.987
226.44	6.562	135.80	6.132	118.43	6.023
231.69	6.606	141.23	6.164	124.27	6.064
237.10	6.626	146.71	6.196	129.99	6.099
242.54	6.662	152.12	6.225	135.81	6.133
248.00	6.681	157.46	6.267	141.74	6.167
253.48	6.717	162.88	6.290	147.57	6.205
258.92	6.747	168.36	6.307	153.52	6.230
264.37	6.775	173.85	6.326	159.61	6.258
269.82	6.820	179.36	6.353	165.63	6.290
275.37	6.854	184.82	6.376	171.77	6.316
281.02	6.894	190.42	6.399	178.02	6.382
286.62	6.953	196.14	6.424	184.20	6.370
				190.37	6.397
				196.38	6.423
				202.20	6.453
				207.39	6.477
				212.07	6.499
				217.01	6.519
				222.09	6.550
				227.15	6.568

(11) G. L. C. M. Van R. H. Van Eleiswijk, *Z. anorg. Chem.*, **74**, Band S 152 (1912).

Previously measurements of the heat capacity of potassium have been made by Simon and Zeidler,[12] Carpenter and Steward,[13] and Douglas, *et al.*[14] Simon and Zeidler covered the range 15 to 275°K. but the other two studies were for higher temperatures and only a few measurements overlapped the temperature range covered in the present study. Above 60°K. the deviation of Simon and Zeidler's results from those in this study never exceeds 1%. Between 60 and 160°K. the two sets of data are in agreement to within about 0.2% but above 160°K. their data are consistently higher by about 0.8%. Below 60°K. their data fall well below the present determinations, being 10% lower at 15°K. The results of Carpenter and Douglas are in most cases higher than the present data, but the scatter is large, averaging about 2%. After the present study was completed, it was learned that Dauphinee, Martin and Preston-Thomas had determined the heat capacities of potassium between 30 and 320°K. Their results, which have since been published,[15] are in good agreement with the results obtained in this study. Above 50°K. their data show an average deviation of 0.2% from the present results. The deviations are larger below 50°K. but even here the differences average only 0.4%.

Heat Capacities of Na_2K in the Single Phase Temperature Regions.—Measurements were made using 56.832 g. or 2.0027 g. atoms of alloy.[16] A total of 115 determinations in the range 12 to 321°K. were made. The original 85 measurements were made in six series of determinations. Series I (68–205°K.): after being prepared the sample was cooled from 275 to 222°K. in 13 hours, from 222 to 68°K. in two hours. Series II (10–78°K.): it was necessary to transfer the calorimeter from the liquid nitrogen cryostat used in Series I to the Collins helium cryostat without warming above the meritectic point for Na_2K. The sample was cooled to 86°K. and the vacuum broken with helium. The assembly then was detached from the nitrogen cryostat vacuum line, connected temporarily with a portable vacuum system, and placed in the helium cryostat which then was set in operation. When it had cooled to about 200°K., the vacuum in the calorimeter was broken with helium, the temporary system detached, and the permanent system connected. During these operations the sample temperature was monitored, and it at no time rose above 200°K. The sample was cooled to 148°K. in 16 hours and from there to 4°K. in 40 min. Series III (195 to 263°K.): the assembly was transferred from the helium cryostat to a Dry Ice–acetone cryostat after Series II using the auxiliary vacuum system as described above. Series IV (237–324°K.): the sample was held at 196°K. for two weeks while results of the earlier series were calculated. Series V (301–324°K.): the sample was held at room temperature for five days. Series VI (281–303°K.): after Series V the temperature was dropped from 324 to about 275°K. in 20 min. and a slow heating of the sample was begun to establish the Na_2K meritectic temperature. Heating was interrupted four times and the equilibrium temperature was measured. The equipment was left for 9 hours during which time the temperature fell from 281 to 262°K. With resumption of work it was heated to 281°K. and the Series VI measurements begun.

The results of the determinations are assembled in Table II and smoothed results are given in Table III. In each case a correction has been

(12) F. Simon and W. Zeidler, *Z. physik. Chem.*, **123**, 383 (1926).

(13) L. G. Carpenter and C. J. Steward, *Phil. Mag.*, **27**, 202 (1939).

(14) T. B. Douglas, A. F. Ball, D. C. Ginnings and W. D. Davis, *J. Am. Chem. Soc.*, **74**, 2472 (1952).

(15) T. M. Dauphinee, D. L. Martin and H. Preston-Thomas, *Proc. Roy. Soc.* (*London*), **A233**, 214 (1955).

(16) The sample mass was not obtained by direct weighing. Initially the calorimeter was loaded with 57.4049 g. or 2.0229 g. atoms of sample. After the entire temperature range had been covered, the equipment was taken apart to introduce another sample whereupon it was found that the calorimeter had been filled too full. The sample had expanded at the highest temperatures, broken open the seal, and a small amount had dropped onto the adiabatic shield. Repetition of the entire work hardly seemed a justifiable expenditure of time considering that the error in mass was small, about 1%, and could be estimated. It was not clear when the pendulant drop detached itself from the calorimeter but the possibilities were limited to two times: (1) before any data were taken, since the sample was, for purposes of homogenization, warmed up to 320°K. prior to any measurements and (2) at the time solid Na_2K was converted into liquid alloy and solid sodium, that is, at 280°K. Continuity of heat capacity data excluded any other times. Accordingly, the container was resealed with a weighed portion of Na_2K and thirty additional heat capacity determinations were made, distributed equally above and below 280°K. By comparing these with the original 85 determinations it was possible to determine the mass of the sample involved in the original work. In this way it was found that the loss in mass occurred before any measurements were made. The mass was determined by this procedure to be 56.832 g. with a probable error of the mean of ±0.021 g.

TABLE II

HEAT CAPACITY VALUES OF Na_2K FROM INDIVIDUAL DETERMINATIONS

Temp., °K.	C_p, cal./deg. g. atom	Temp., °K.	C_p, cal./deg. g. atom	Temp., °K.	C_p, cal./deg. g. atom
Series I		Series II		Series IV	
71.22	4.995	12.19	0.320	240.21	6.701
80.48	5.226	15.15	0.600	245.52	6.767
86.62	5.349	16.35	0.732	250.80	6.793
93.16	5.462	17.84	0.916	256.13	6.929
99.43	5.547	20.56	1.265	265.49	7.052
105.51	5.617	23.66	1.675	268.68	7.142
111.43	5.687	26.34	2.018	271.89	7.237
117.20	5.742	29.34	2.380	275.89	7.469
122.86	5.796	32.86	2.774	284.91	15.135
128.41	5.850	32.53	2.732	288.17	14.833
133.87	5.890	36.60	3.137	291.55	13.430
139.27	5.934	40.98	3.490	295.33	11.422
144.58	5.967	45.57	3.834	299.71	10.085
149.81	5.999	50.37	4.147	304.50	8.997
154.95	6.032	54.97	4.394	309.73	8.402
160.24	6.062	59.43	4.589	315.51	8.040
165.66	6.094	64.31	4.745	321.42	7.996
171.00	6.126	69.54	4.945		
176.31	6.156	74.94	5.092	Series V	
181.59	6.192				
186.82	6.216	Series III		303.57	8.148
192.12	6.258			308.01	8.113
197.51	6.295	197.88	6.309	312.12	8.082
202.84	6.326	202.63	6.350	316.32	8.042
		207.56	6.382	321.00	8.007
		212.59	6.424		
		217.70	6.488	Series VI	
		222.90	6.543		
		228.11	6.587	282.27	15.973
		233.34	6.636	284.12	16.156
		238.60	6.698	286.14	16.263
		243.89	6.763	288.17	15.996
		249.21	6.825	290.42	14.875
		254.49	6.884	293.19	12.624
				296.65	10.408
				300.87	9.142

made for the heat capacity of the 0.0030 g. atom of excess potassium present.

TABLE III

SMOOTHED ATOMIC HEAT CAPACITY OF K AND Na_2K

Temp., °K.	C_p, cal./deg. g. atom K	Na_2K	Temp., °K.	C_p, cal./deg. g. atom K	Na_2K
12	0.993	0.304	155	6.239	6.030
14	1.337	.483	160	6.263	6.061
15	1.508	.583	165	6.287	6.090
16	1.678	.691	170	6.309	6.120
18	2.014	.931	175	6.331	6.150
20	2.345	1.193	180	6.353	6.181
22	2.661	1.458	185	6.375	6.211
24	2.952	1.719	190	6.396	6.243
25	3.088	1.847	195	6.418	6.278
26	3.218	1.974	200	6.441	6.316
28	3.462	2.219	205	6.466	6.358
30	3.681	2.454	210	6.489	6.402
35	4.150	2.984	215	6.514	6.448
40	4.494	3.416	220	6.538	6.498
45	4.765	3.791	225	6.564	6.548
50	4.987	4.123	230	6.590	6.601
55	5.163	4.394	235	6.617	6.654
60	5.307	4.611	240	6.644	6.711
65	5.427	4.798	245	6.670	6.769
70	5.526	4.959	250	6.697	6.828
75	5.612	5.094	255	6.725	6.891
80	5.685	5.215	260	6.754	6.961
85	5.749	5.319	265	6.784	7.043
90	5.802	5.409	270	6.818	7.178
95	5.847	5.486	273.16	6.840	7.302
100	5.890	5.553	275	6.854	7.407
105	5.929	5.615	280	6.893	...
110	5.968	5.671	280.06	...	7.909 Solid
115	6.004	5.721	285	6.933	...
120	6.038	5.771	290	6.976	...
125	6.070	5.816	295	7.022	...
130	6.099	5.860	298.16	7.052	...
135	6.128	5.900	300	7.071	...
140	6.157	5.937	305	7.126	8.140 Liquid
145	6.186	5.971	310	7.188	8.093
150	6.213	6.001	315	7.262	8.050
			320	7.348	8.012

The precision of the results is of the order of 0.1%. The average deviation of the individual determinations from a smooth curve is 0.06% and 59 out of the 69 measurements made led to results which deviated from the smoothed curve by less than 0.1%.

Heat Capacities of Na_2K in Two Phase Temperature Regions.—Up to this point, except for Table II, data for the temperature region between 280 and 295°K., in which range the stable state of the system is solid sodium plus liquid alloy, have been excluded from consideration. This range was covered in the measurements in Series IV and VI. The results, shown in Fig. 1, of the two series of determinations reveal (1) an excess in the heat capacity and (2) discrepancies between the two sets of measurements. Part of the excess heat capacity probably is due to a destruction of local order in the liquid alloy, which is just above its solidification point. The majority, however, seems to originate with the heat of solution of sodium in the alloy, a process which undoubtedly is endothermal and comparable with the heat of fusion of sodium. The existence of the excess heat capacity above 295°K. and the discrepancies between the series IV and Series V determinations between 303 and 315°K. show clearly that the measurements above 280°K. do not refer to the system in an equilibrium state. Sodium apparently did not dissolve sufficiently rapidly to maintain saturation in the region below the liquidus and solution was continuing above 295°K. Series VI was carried out more slowly than Series IV and the heat capacity excess was more nearly concentrated in the temperature range expected from the equilibrium diagram.[11]

It was of interest to ascertain whether the integrated excess heat capacity in Fig. 1 agreed with that which was expected from the heat of solution of the amount of sodium involved. This was possible only for the results of Series IV since the sample had not been completely transformed prior to Series VI and the amount of sodium present was not known. With the aid of Van Bleiswijk's phase diagram it is possible to ascertain the relative amounts of sodium and liquid alloy, and the composition of the latter, for temperatures just above the meritectic point. One can then write down a series of simple thermochemical steps to represent the change of state of the system between that point and 320°K. Using the thermal data of Ginnings,[17] *et al.*, for the necessary heat capacity and heat of fusion information for sodium the enthalpy change (ΔH_c) for raising the temperature from 280.06 to 320°K. is calculated[18] to be 443 cal./g. atom. The measured value (ΔH_m) is also 443 cal./g. atom. The maximum uncertainty in $\Delta H_m - \Delta H_c$ is estimated to be ± 4 cal./g. atom. Thus a good accounting for the excess heat capacity is made on the basis of the dissolving of sodium.

Determination of Fixed Point Temperatures and the Heat Effect at the Na_2K Meritectic Point.—The Na_2K–K eutectic point was established during the preparation of Na_2K by heating the sample with low power input and by allowing the sample to cool. The heating was interrupted three times and the equilibrium temperature determined. The average value was 260.524 ± 0.003°K. In the cooling experiment the temperature was constant for 16 min. at 260.500°K. The eutectic temperature is taken to be 260.51 ± 0.01°K. or −12.65 ± 0.01°. This may be compared with −12.6, −12.5 and −12.3° obtained by Van Bleiswijk,[11] Rinck[19] and Miller, Ewing, Hartman and Atkinson,[20] respectively.

The incongruent melting point, or meritectic point, for Na_2K was established in an experiment in which the sample was heated and the equilibrium temperature measured for various fractions of the solid melted. The heating was interrupted four times and the equilibrium temperature established. When the fractions melted were 0.003, 0.015, 0.11 and 0.65 the observed temperatures were 280.0581, 280.0584, 280.0585, 280.0582°K., respectively. The meritectic point is therefore taken to be 280.058 ± 0.001°K. or 6.90 ± 0.00°. This temperature was determined by Van Bleiswijk[11] to be 6.90° and by Rinck[19] to be 6.6°.

(17) D. C. Ginnings, T. B. Douglas and A. F. Ball, *J. Research Natl. Bur. Standards*, **45**, 23 (1950).

(18) The calculation is made under two assumptions: (1) that the atomic heat capacity of liquid Na–K alloy is independent of composition between 42 and 33.44% potassium and (2) that the mixing of (supercooled) sodium and liquid alloy at 320°K. is athermal. The heat of mixing is small and independent determinations vary even as to its sign.

(19) E. Rinck, *Compt. rend.*, **197**, 49 (1933).

(20) R. R. Miller, C. T. Ewing, R. S. Hartman and H. B. Atkinson, Jr., Naval Research Laboratory Report No. C-3105 (1947).

The phase change occurring at 280.06°K. can be represented as

$$1/3\ Na_2K(s) \rightarrow 0.794\text{Alloy}(1, 42\ \text{atomic}\ \%\ K) + 0.206\ Na(s)$$

To obtain ΔH for the process one heats the sample from T_1 to T_2, where these are temperatures just below and above 280.06°K., respectively. Correction for the heat absorbed between T_1 and 280.06 was made using the measured heat capacities of Na_2K. A similar correction for the heat absorbed between 280.06 and T_2 involved the heat capacity data for the two phase region, which as indicated earlier are not entirely satisfactory. The correction is small, however, and the error introduced into ΔH for the process is slight. Using the Series IV data ΔH = 700 cal./g. atom whereas with the Series VI data, ΔH = 697 cal./g. atom. One can also estimate, using the extrapolated data in the Series V determinations, together with the data obtained in Series IV, the enthalpy change associated with the process

$$1/3\ Na_2K(s) \rightarrow 1/3\ Na_2K(\text{supercooled liq.})$$

$$\Delta H = 829\ \text{cal./g. atom}$$

Derived Results

Entropy of Potassium.—The heat capacity data were used to establish the entropy changes for various temperature intervals. The value of the heat capacity at 12°K. indicated a Debye θ of 88°K. Extrapolation below 12°K. was made using a Debye function with this value as the characteristic temperature. The entropies at 273.16, 298.16 and 320°K. are 14.77 ± 0.03, 15.38 ± 0.03 and 15.89 ± 0.03 e.u./g. atom, respectively, of which 0.33 ± 0.02 is due to the extrapolation below 12°K. The result at 298.16°K. may be compared with the value recommended by Kelley[21] of 15.2 ± 0.2 e.u./g. atom.

Entropy of Na_2K.—Results of the calculations are given in Table IV. Extrapolation below 12°K. was made using the Debye T^3 law. The entropy increments associated with the phase transformation at 280.06°K. and the increase of temperature in two phase region were both slightly uncertain due to the lack of (1) reproducibility of the heat capacities in the two phase region and (2) knowledge of the exact course of the heat capacity curve immediately above the transformation temperature. The lack of reproducibility stems from the inability to maintain the system in an equilibrium state. Sodium is dissolved at too high a temperature. This results in a displacement of part of the heat capacity excess upward on the temperature scale. The usual integration employing the measured (non-equilibrium) heat capacities will therefore lead to a ΔS which is too small. However, it is possible to estimate the error in ΔS by displacing the heat capacity excess downward on the temperature scale in accordance with expectations from the phase diagram. The alteration in ΔS for warming through the two phase region is 0.005 e.u./g. atom and errors due to failures to maintain equilibrium in the two phase region are therefore negligible. An uncertainty of ± 0.04 e.u./g. atom is assigned to the entropy of the phase transformation, 0.03 of which is due to the uncertainty in the course of the heat capacity curve from 280 to 283°K. This is perhaps an overly generous estimate of the error which could arise in this way. The entropy increment between 280.06 and 320°K. is the average of values obtained using the two series of heat capacity measurements covering the two phase range, which differ by only 0.02 e.u./g. atom.

(21) K. K. Kelley, Bureau of Mines Bulletin 477 (1950).

TABLE IV

ENTROPY CHANGES OF Na_2K FOR VARIOUS TEMPERATURE INTERVALS

Temp. interval, °K.	ΔS, e. u./g. atom
0–12 (extrap.)	0.102 ± 0.005
12–273.16	12.381 ± .009
12–280.06 (solid)	12.570 ± .010
Phase transformation at 280.06	2.50 ± .04
0–273.16	12.48 ± .02
0–280.06 (solid)	12.67 ± .02
0–280.06 (2 phase)	15.17 ± .06
0–298.16 (liquid)	16.07 ± .03
0–320 (liquid)	16.66 ± .03

The uncertainties listed in Table IV are estimated from the scatter in the heat capacities together with allowance for those factors such as non-equilibrium results, etc., mentioned above. As 298.16°K. is just above the liquidus, it was not possible to obtain the result for liquid Na_2K at this temperature by direct integration from 0 to 298.16°K. The heat capacity of the system near the upper limit of temperature is, as mentioned earlier, incorrect due to inability to preserve equilibrium during the measurements. Accordingly, the entropy increment was evaluated by using the value for the system at 320°K. and integrating between this temperature and 298.16°K., using the results of the C_p data obtained in the Series V measurements extrapolated downward slightly. The result for Na_2K as undercooled liquid at 280.06°K. can be obtained in a similar way using extrapolated Series V heat capacity data. From this one can estimate the entropy change at 280.06°K. associated with the congruent melting of Na_2K. This entropy change is calculated to be 2.88 e.u./g. atom.

The entropy contribution due to the stoichiometric excess of 0.0030 g. atom of potassium has been neglected throughout this section since it in no case amounts to more than 0.005 e.u.

Estimate of the Residual Entropy of Na_2K.—To make this estimate the entropy data in Table IV were extended to 420°K. using data of Douglas, *et al.*[14] This temperature was chosen since at this point both metals are liquid, and in addition Douglas, *et al.*, have shown that the heat capacity per gram atom is independent of alloy composition. The system thus has at this temperature one feature of an ideal solution. It is found that $S_{420°K.} - S_{0°K.}$ = 18.74 e.u./g. atom. The entropy of $^2/_3$ g. atom of sodium and $^1/_3$ g. atom of potassium at this temperature is 17.42 e.u. If one assumes that the system behaves like a regular solution,[22] that is, that the entropy of mixing is nearly ideal, one obtains ΔS_{mixing} = 1.27 e.u./g. atom. Thus,

(22) J. H. Hildebrand and R. L. Scott, "The Solubility of Nonelectrolytes," Reinhold Publ. Corp., New York, N. Y., 1950, pp. 119–154.

$S_{420°K.}$ for the system is 18.69 e.u./g. atom which leads to a residual entropy of −0.05 e.u./g. atom. A similar calculation at 320°K., involving the mixing of the undercooled liquid metals, gives 16.66 e.u./g. atom for $S_{320°K.} - S_{0°K.}$ for the alloy and 16.61 for $S_{320°K.}$ for the mixture, again yielding $S_{0°K.} = -0.05$ e.u./g. atom. This estimated negative value of the residual entropy suggests that the entropy of formation of Na_2K exceeds the ideal value calculated as the entropy of mixing.

In much work dealing with the thermodynamics of alloys one assumes that the heat capacity of the alloy is additively related to the heat capacities of the components This assumption is without theoretical foundation and the small amount of suitable experimental work has failed to supply it with an experimental basis. Comparison of the measured heat capacities of Na_2K with those computed assuming additivity is made in Table V. Data for the pure metals were obtained as follows: potassium up to 320°K.—the present work; sodium up to 55°K.—Pickard and Simon,[23] Parkinson and Quarrington[24] and Simon and Zeidler,[13] 55 to 320°K.—Dauphinee, *et al.*[5]

TABLE V

DEVIATION OF C_p FOR Na_2K FROM VALUES CALCULATED ASSUMING ADDITIVITY

Temp., °K.	Deviation $(C_p)_{Na_2K} - 2/3(C_p)_{Na} - 1/3(C_p)_K$ cal./deg. g. atom	Dev., %
12	−0.20	−66
14	− .23	−48
15	− .23	−39
16	− .23	−33
18	− .21	−23
20	− .19	−16
25	− .15	− 8.1
30	− .11	− 4.5
40	− .07	− 2.0
50	− .09	− 2.2
60	+ .015	+ 0.3
70	.017	0.3
80	.019	0.4
90	.010	0.2
100	.007	0.1
110	.006	0.1
120	.015	0.3
130	.024	0.4
140	.026	0.4
150	.022	0.4
160	.023	0.4
170	.026	0.4
180	.023	0.4
190	.024	0.4
200	.042	0.7
210	.079	1.2
220	.126	1.9
230	.184	2.8
240	.249	3.7
250	.311	4.6
260	.387	5.6
270	.545	7.6
280.06	(1.214)	15.3
305	0.380[a]	4.7
310	0.343	4.2
315	0.310	3.9
320	0.292	3.6

[a] Comparison made for supercooled pure metals.

The deviations from additivity are in some cases quite large and in most cases outside the experimental error. One can see that the Kopp–Neumann Rule is satisfactory with this system only when fairly crude results will suffice.

Discussion of Results

Mention was made earlier of the discovery by Dauphinee, *et al.*, of a thermal anomaly in sodium in the Dry Ice range. Later work[15] has revealed the existence of a similar anomaly in rubidium but not in potassium. The present measurements had been made before these findings had been presented and special care was taken in the potassium work to vary the thermal history of the sample so as to reveal any unusual behavior. In agreement with the findings of Dauphinee, Martin and Preston-Thomas there was no indication of a "sodium-type" anomaly in the case of potassium. The only peculiarity revealed by the potassium results is the well known fact that the Dulong–Petit limit is reached at about 150°K. Nothing similar to the time-dependent resistance effects observed by MacDonald[6] appear in the thermal behavior.

Debye θ values at various temperatures are shown in Table VI. These calculations are made only up to 130°K. At and above 150°K. the value of θ is meaningless since C_v exceeds $3R$. The tendency toward an abnormally large heat capacity is already apparent between 100 and 130°K. as evidenced by the rapid fall in the θ values in this temperature interval.

TABLE VI

DEBYE θ VALUES FOR POTASSIUM AT SEVERAL TEMPERATURES

T, °K.	12	20	50	80	100	130
θ, °K.	88	96	98	93	85	59

In a sense the transformation in Na_2K is an order-disorder transformation, the disordered alloy being a two-phase system. At the outset of this work it was of interest to know if Na_2K would exhibit an excess heat capacity below the transformation point as is the case with the usual disordering of ordered alloys. The metallic radii of sodium and potassium differ by roughly 20% and it was difficult to visualize a process in which these were interchanged in the lattice. The data are plotted in Fig. 2 along with results for the two pure metals. It is clear that there is a very pronounced rise in heat capacity before the melting point. However, since there is similar behavior in the pure materials, the rapid increase in heat capacity above 200°K. cannot be ascribed unambiguously to a disordering of the alloy.

The excess heat capacity of Na_2K near its transformation point is of some interest in relationship to attempts to determine the origin of the excess heat capacities of the several pure alkali metals near their melting points. One possibility is that, due to their open structures, there is considerable

(23) C. L. Pickard and F. Simon, *Proc. Phys. Soc.*, **61**, 1(1948).
(24) D. E. Parkinson and J. E. Quarrington, *ibid.*, **68B**, 762 (1955).

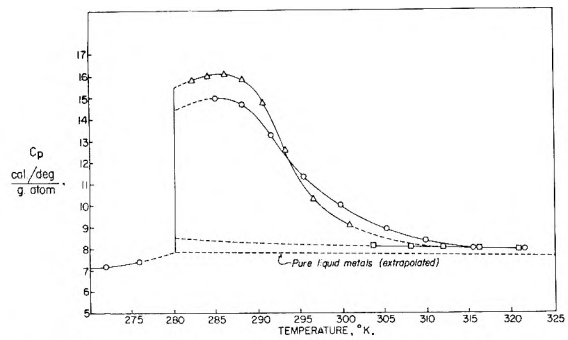

Fig. 1.—Heat capacities of Na_2K in the two-phase region: O, Series IV; □, Series V; △, Series VI.

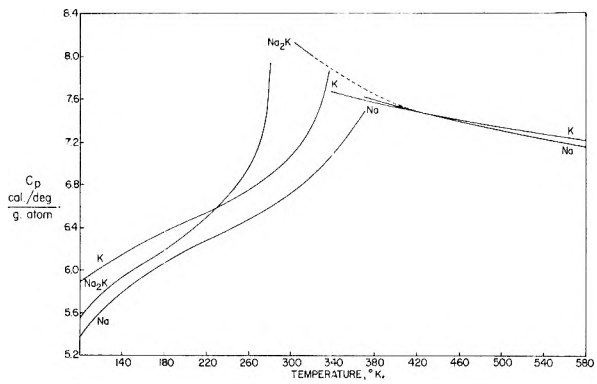

Fig. 2.—Temperature dependence of the heat capacities of sodium, potassium and Na_2K.

anharmonicity in the atomic vibrations at higher temperatures and it is this which permits C_v to exceed $3R$.[25] If so, it seems likely that Na_2K would behave in a strikingly different way. Its structure is one of very close packing and one would expect the vibrational characteristics of the oscillators in Na_2K to differ substantially from those in the pure components. The fact that the variation of the heat capacities of sodium, potassium and Na_2K with temperature is similar for all three of the metallic species suggests that anharmonicities in the vibrations are not responsible for the anomalous specific heat, thus agreeing with recent theoretical treatments of the effect of anharmonicity on specific heats.[26,27]

Carpenter[28] has discussed the possibility that lattice defects of either the Schottky or Frenkel type are responsible for the extra heat capacity. Introduction of either of these defects into the lattice is an endothermal process and since the number of defects increases with temperature, there would be a contribution to the specific heat from this source over and above that of the lattice vibrations. From the observed excess specific heat one computes the mole percentage of defects to be 0.5 if they are of the Schottky type or about 0.3 if they are Frenkel defects. These figures apply to temperatures near the melting point. If the rise of C_p for Na_2K above 180°K. is due to the same factors which are responsible for the excess heat capacity in the elements, one would conclude from the data in Fig. 2 that the energy of defect formation in the alloy is less than the corresponding energies for sodium and potassium. This follows from the fact that the excess heat capacity appears at a lower temperature with the alloy. The notion that the energy of vacancy formation is least for the intermediate phase is not entirely satisfactory in view of the exothermal formation of the alloy from the elements. One might reasonably expect an increased lattice energy to be accompanied by an increase in the energy required to introduce a defect into the lattice.

A third possibility for explaining the excess heat capacity is in terms of what have been called heterophase fluctuations.[29] At temperatures near the equilibrium temperature between two phases each phase experiences rather wide fluctuations from its equilibrium properties. Consider a solid, for example, near its melting point. Due to fluctuation, rather large regions within the solid acquire liquid-like characteristics so that a crude description of the solid might consist in representing it as being partly liquid. The "liquid fraction" would increase with increasing temperature up to the melting point. This is a type of pre-melting which results in the appearance of part of the latent heat below the melting point in the form of extra heat capacity of the solid. In a like manner a portion of the heat of fusion would be deferred and contribute positively to the heat capacity of the liquid just above the melting point.

The data for the alkali metals suggest the possibility that heterophase fluctuations may be responsible for extra heat capacity in the solid below and in the liquid above the melting point. If so, perhaps the same mechanism is operating in Na_2K with it fluctuating either toward solid disordered Na_2K or liquid alloy of this composition. In this connection it is of interest to report on a series of measurements which were made but which do not appear in Table II. In one of the early attempts to prepare Na_2K only partial conversion of the alloy into hexagonal Na_2K was achieved. Heat capacity measurements were made on this heterogeneous sample at temperatures immediately below the Na_2K–K eutectic point. A sharp rise in heat capacity, above that expected for the mixture, was found as the eutectic point was approached. It is not clear why this should have happened, but some type of pre-melting or heterophase fluctuation effect seems to offer the best opportunity for interpreting this result.

The data for liquid Na_2K between 310 and 320°K. show the alloy to have a heat capacity about 3% in excess of that computed assuming additivity of the heat capacities of the pure supercooled liquid metals. This again would suggest that there remains in the system some solid-like alloy which is being destroyed endothermally. It therefore seems that much of the unusual thermal behavior in sodium, potassium and Na_2K can be qualitatively explained in terms of heterophase fluctuations although this kind of explanation leaves

(25) F. A. Lindemann, *Phil. Mag.*, **45**, 1119 (1923).

(26) J. S. Dugdale and D. K. C. MacDonald, *Phys. Rev.*, **96**, 57 (1954).

(27) D. K. C. MacDonald and S. K. Roy, *ibid.*, **97**, 673 (1955).

(28) L. G. Carpenter, *J. Chem. Phys.*, **21**, 2244 (1953).

(29) J. F. Frenkel, "Kinetic Theory of Liquids," Clarendon Press, Oxford, 1946, p. 387.

much to be desired since a detailed description of this kind of fluctuation is yet to be provided.

The estimated residual entropy for Na_2K must be regarded with caution until an experimental value for the entropy of formation of liquid alloy is provided. It will be of considerable interest to establish this value without making use of ideal solution theory, for if there are lattice defects in this alloy in substantial amounts, they may become frozen-in and contribute to the residual entropy in a way similar to that which has been observed for $MgCd_3$ in this Laboratory.[30] Calculations of this type may shed further light upon the possibility of the existence of defects to the extent of 0.5% or more in these materials.

Acknowledgment.—The authors wish to express their appreciation to Dr. M. G. Zabetakis for his generous assistance in the making of the measurements reported in this paper.

(30) L. W. Coffer, R. S. Craig, C. A. Krier and W. E. Wallace, *J. Am. Chem. Soc.*, **76**, 241 (1954).

RETENTION OF LIQUID BY CALCIUM STEARATE–CETANE GELS STABILIZED BY ADDITIVES[1]

By Robert D. Vold and Richard J. Coswell[2]

Department of Chemistry, University of Southern California, Los Angeles, Calif.

Received September 4, 1956

Data are presented on the amount and rate of loss of liquid by calcium stearate gels in cetane as a function of gel composition and thermal history, together with the results of X-ray diffraction studies of the gels and visual observations of phase transitions and physical characteristics. Only additives which reduce the viscosity of the high temperature melt are effective stabilizers of the gels present at room temperature. It is shown that the observed behavior cannot be interpreted in terms of the phases present in the gel, or compound formation between additive and soap, but must be related to such variables as particle size and shape, degree and kind of particle interaction, effect of rate of cooling and degree of dispersion at the elevated temperatures of the phase from which the gel was formed. The results suggest that the pore volume of the gels is divisible into two categories, fine pores within the homogeneous soap network and larger pores corresponding to irregularities in the structure, with a characteristic difference between gels formed from solutions more or less concentrated than 18% soap.

This study was undertaken to investigate the dependence of the stability of gels of calcium stearate in cetane on such factors as the concentration of metal soap, the thermal history of the sample and the presence of variable small amounts of additives. The results obtained show that neither the phase state of the soap at room temperature nor the ability or lack of ability of the additive to form an addition compound with the soap are of primary importance. Instead the stability appears to depend principally on the degree of subdivision of the soap in the solid state, and on the fineness and degree of coherence of the gel skeleton formed by aggregation of the ultimate particles of soap. This conclusion is strongly supported by the observation that all additives which reduce the viscosity of the solutions at high temperature are also effective stabilizers of the gels formed on cooling.

The data obtained also help to establish the probable location of some phase boundaries in systems of calcium stearate in cetane[3-7] containing a variety of organic additives, and in a number of liquids which have been proposed as oil substitutes in greases in recent years.

Techniques and Materials[8]

Materials.—Sources of all materials used are given in Table I. Most of the experiments were carried out with calcium stearate 5R3AH although a few were made with calcium stearate 4 with no measurable difference in the results. Unless otherwise stated the various liquids were used without purification other than drying over appropriate desiccants. This latter was done in all cases for liquids used for measurement of liquid loss but not always for samples used only for visual observations. The soap was dried to constant weight at 105° before use. During the heating of soap and cetane in contact with the air remaining in the sealed tube noticeable darkening occurred with nitroethane and nitrobenzene as additives, but not with any of the other samples.

Preparation of Samples.—Soap, solvent and additive (5.0-g. samples for liquid loss experiments, one to two gram samples for visual observation) were sealed into glass tubes, heated to fluidity, mixed thoroughly, equilibrated at the desired temperature and quenched in a Dry Ice–acetone bath. Cooling in running tap water did not provide sufficiently rapid crystallization throughout the sample to give gels of reproducible liquid loss characteristics.

Visual Observations.—These were made in an electrically heated air oven with glass windows, a device for rocking the tubes, and crossed Polaroid sheets to facilitate detection of phase changes. Transition temperatures reported in the present investigation are slightly higher than the equilibrium values since they were made while the temperature was rising 1 to 2° per minute rather than after equilibration at each temperature. In the one case where equilibrium values are available for comparison[5,7] (anhydrous calcium stearate in cetane) the difference is not more than a few degrees.

X-Ray Diffraction Patterns.—These were obtained on a

(1) This work was supported by the Office of Naval Research under Contract N6-on-238-TO-2 and by the National Lubricating Grease Institute, and presented in part at the San Francisco Meeting of the American Chemical Society in 1949 and in part at a Symposium on Colloids in Bombay, India, in 1956 while the senior author was Guest Professor of Physical Chemistry at the Indian Institute of Science, Bangalore.

(2) General Electric Co., Pittsfield, Mass.

(3) R. D. Vold, "Phase Studies of Greases," First Annual Report, Contract N6-onr-238-TO-2, 2-19-48.

(4) R. D. Vold, Second Technical Report, Contract N6-onr-238-TO-2, Project No. NRO57057, 2-28-49.

(5) R. D. Vold, Third Technical Report, Contract N6-onr-238-TO-2, Project No. NRO57057, 3-15-50.

(6) R. D. Vold, Final Technical Report, Contract N6-onr-238-TO-2, Project No. NRO57057, 9-1-50.

(7) M. J. Vold and R. D. Vold, *J. Inst. Pet.*, **38**, 155 (1952).

(8) Further experimental details may be found in the M.S. Thesis of R. J. Coswell, University of Southern California Library, 1949.

TABLE I

CHARACTERISTICS OF MATERIALS USED

Calcium stearate 5R3AH	As in ref. 15
Calcium stearate IV	As in ref. 13
Li Str.	Technical Li Str, Metasap Chemical Co., 1 to 2% free fatty acid by titration of dried soap in ethanol
Nujol	Medicinal grade
Decalin	Eastman Kodak Practical grade
Cetane	Du Pont Co., n_D 1.4345
Stearic acid 5R3	As in ref. 15
Methanol	Baker and Adamson, reagent grade
Acetone	Dried over K_2CO_3 and distilled, b.p. 56.5°
α-Tetralone	Student preparation
Nitroethane	Commercial Solvents Company
Pyridine	Eastman Kodak, Karl Fischer, reagent grade
n-Heptanol	Eastman Kodak, reagent grade
Di-n-butylamine	Paragon Testing Laboratories
Calcium acetate monohydrate	Baker and Adamson, reagent grade
Nitrobenzene	Paragon Testing Laboratories, redistilled
Di-(2-ethylhexyl) sebacate	Resinous and Chemical Products Co.
Diethylene glycol	Carbide and Carbon Chemical Co., max. 0.3% water
Methyl stearate	Prepared by Dr. L. L. Lyon: yielded stearic acid A of ref. 15 on hydrolysis
Amyl acetate	Baker and Adamson, reagent grade
Aluminum grease Al-4	*Cf.* Vold, Hattiangdi and Vold, *Ind. Eng. Chem.*, **41**, 2539 (1949)
Lithium grease Li-6	
Lithium grease Li-1	
Calcium grease Ca-3	
Sodium grease Na-2	

number of gels using an X-ray spectrometer as previously described.[9]

Liquid Loss under Pressure.—The apparatus consisted of a medium porosity Alundum filter thimble of 22 mm. inside diameter and 5 mm. inside depth, sample weights in different thimbles varying between 1.4 and 1.9 g. The thimble was placed in a 6 in. × 1 in. metal pipe on a rubber washer over a 1/4 in. drain, the pipe being closed on top with a screw cap with an outlet tube for application of gas pressure. In order to obtain reproducible results the thimbles were cleaned with carbon tetrachloride before and after each use and oven dried. Each soap preparation provided enough material to fill two thimbles, the gel being first worked on a watch-glass with a spatula for three minutes, pressed lightly into the thimble with the spatula, and smoothed off on top. Samples were studied immediately after rewarming to room temperature after quenching, since an isolated experiment had shown that although ultimate liquid loss remained virtually unchanged after two weeks aging at room temperature the rate of loss nearly quadrupled, changing most rapidly during the first day.

Application of gas pressure for 60 to 100 minutes, generally at 10 lb./in.^{2}, forced liquid out through the pores of the thimble, which drained out through the outlet drain in the bottom of the cylinder. Liquid loss as a function of time was determined by removing and weighing the thimble six to eight times during the course of a run. Refractometric examination of the expressed liquid showed it had the same refractive index within experimental error (0.0002) as pure cetane.

At the conclusion of an experiment the grease cake was removed and the small residue of liquid remaining in the pores of the thimble determined by weight. This amounted to about 0.08 g., a correction of about 5 absolute %, which was added to the values for amount of liquid lost by the gel. Values reported are generally the average of four determinations made on two different sample preparations. Reproducibility of results for ultimate liquid loss, both on duplicate runs on portions of the same sample and on independently prepared samples of the same composition, were usually within 3% absolute corresponding with many systems to about 10% relative deviation.

Data obtained by this technique were generally fitted very well by the empirical linear relationship of Farrington and Humphreys.[10]

$$t/s = a + bt$$

where $1/a = (ds/dt)_{t=0}$ and $1/b = S_{t=\infty}$; where s is the % loss in weight of the sample in time t (minutes) and a and b are constants determined from the intercept and the slope of the line. Neither the observed loss of weight (w) at a given time (t), nor this quantity plus the weight of liquid retained in the pores of the thimble at the end of the experiment (p), gives a proper value for s since the one procedure assumes no liquid escapes from the thimble until its pores are filled completely while the other assumes that liquid flows out through the larger pores before the bulk of the finer pores have filled. Actually both the functions t/w and $t/w + p$ are linear functions of time except at short times (less than five minutes in the case of cetane systems). In the first case the reciprocal of the slope of the line plus the experimental value of p gives the ultimate liquid loss by the sample while in the second the reciprocal of the slope gives this value directly. Within the experimental error identical values of $S_{t=\infty}$ were obtained by the two procedures. However, values for the initial rate of loss, which are obtained from the intercepts of the extrapolated straight lines, differed by as much as 40% in some cases, indicative of the fact that at very short times the curve does not follow the same linear course as over most of the time range.

In subsequent tables the reported values of $1/a$ and $(1/b + p)$ obtained from plots of t/w *vs.* t, are used to represent, respectively, the initial rate of loss and the ultimate liquid loss. The values for ultimate liquid loss can be taken to be correct on an absolute basis whereas the parameter $1/a$ is not related entirely unambiguously to the initial rate of loss, although the reported values are comparable from one system to another.

In measurements made on commercial greases, where loss of liquid occurs very slowly because of the high viscosity of the oil, the standard procedure was modified by letting the sample stand in the thimble two days before application of pressure, thus allowing the oil to fill the pores of the thimble. This alteration of technique caused no change in the ultimate liquid loss from that of samples subjected to pressure immediately after filling, but it greatly decreased the time required after application of pressure for attainment of a linear relation between t/w and t, which amounted to as long as 500 minutes in samples studied immediately. However, values of $1/a$ calculated from such curves may not be directly comparable with those obtained by the standard technique, since in these cases the experimentally measured rate of loss at very short times is slower than this extrapolated value, *i.e.*, the actual curve is not linear during the early stages of loss of oil.

The commercial greases were also examined by a modification of the "filter paper test."[11] Brass rings 13.2 mm. in diameter and 20 mm. in height were completely filled with grease, placed on 11 cm. circles of Whatman No. 1 filter paper, and the position of the advancing oil front in the paper observed periodically. Plots of area of spread oil *vs.* logarithm of time were linear, results following the equation $A = Kt^{0.66}$ as contrasted with the equation for rate of capillary rise, $A = Kt^{0.5}$.[12] Likewise a plot of $1/a$, the initial rate of loss, for different greases against the time at

(9) R. D. Vold and M. J. Vold, THIS JOURNAL, **52**, 1424 (1948).

(10) B. B. Farrington and J. Humphries, *Ind. Eng. Chem.*, **31**, 230 (1939).

(11) E. N. Klemgard, "Lubricating Greases: Their Manufacture and Use," Reinhold Publ. Co., New York, N. Y., 1937.

(12) E. W. Washburn, *Phys. Rev.*, **17**, 273 (1921).

which A, the area of oil spread in the filter paper, equaled 1000 mm.^{2}, showed a simple proportionality suggesting that the filter paper test may also give an indication of the storage stability of a grease.

Experimental Results

Visual Observations.—As is clear from the results assembled in Table II there is a perfect correlation between the viscosity of the solutions and the stability of the gels formed on cooling. All solvents or additives giving rise to fluid isotropic solutions also formed firm, grease-like gels, while those solutions which, though isotropic, were less translucent and very viscous, formed a more paste-like gel readily undergoing syneresis.

TABLE II

APPEARANCE OF SOLUTIONS AND GELS OF 18% CALCIUM STEARATE WITH VARIOUS ADDITIVES

Solvent	Additive	Concn. (moles/mole soap)	Solution viscosity	Gel type[a]
Cetane	None	...	High	B
Cetane	Water	1.0	Low	A
Cetane	Stearic acid	0.24	Low	A
Cetane	Methanol	1.6	Low	A
Cetane	Acetone	3.0	Low	A
Cetane	α-Tetralone	3.0	Low	A
Cetane	Nitroethane	0.94	Low	A
Cetane	n-Heptanol	.58	Low	A
Cetane	Di-(n-butyl)-amine	.54	Low	A
Cetane	Diethylene glycol	1.1	Low	A
Cetane	Pyridine	5.1	Low	A
Cetane	Methyl stearate	0.22	High	B
Cetane	Nitrobenzene	3.2	High	B
Cetane	Di-(2-ethylhexyl) sebacate	0.3	High	B
Cetane	Amyl acetate	0.6	High	B
Cetane	Calcium acetate	1.0	...	A[b]
Di-(2-ethyl-hexyl) sebacate	None	..	High	B
Di-(2-ethyl-hexyl) sebacate	Water	1.0	Low	A
n-Heptanol	None	...	Low	A
Di-n-butyl-amine	None	...	Low	A
Diethylene glycol[c]	None	...	Insoluble	..

[a] Type B gels, formed on cooling in a Dry Ice–acetone bath from 120° or higher, are translucent, "pasty," and spontaneously syneretic. Type A gels, formed by the same procedure, are relatively stable, non-syneretic, and grease-like in texture. [b] Instead of dissolving to isotropic liquid forms a stiff brilliantly anisotropic liquid crystalline phase at 170°; and a firm non-syneretic grease on cooling. [c] Insoluble even at 240° and does not form a gel.

The effect of additive concentration was investigated for water, methanol, stearic acid and pyridine. With water concurrent reduction in viscosity of the hot solution and decreased syneresis of the gel at room temperature is already marked at 0.19 mole ratio of water to soap and is maintained with increasing amounts of water even up to a mole ratio of 14.9, where part of the water remains as visible droplets dispersed in the soap solution in cetane. With both methanol and stearic acid the stabilizing effect of the additive first increases with increasing concentration and then decreases sharply. The unstable systems containing large amounts of these additives are mushy pastes rather than transparent gels. The samples containing stearic acid exhibited marked age-hardening.

Calcium stearate–cetane systems to which small amounts of third components were added become nearly transparent homogeneous solutions at temperatures a few degrees higher than in the absence of additive (115° at 18%) consistent with the hypothesis that the position of the isotropic solution boundary is qualitatively similar in these cases to that of the simple binary system. In di-(2-ethylhexyl) sebacate, solution occurred at temperatures about 13° higher than with cetane and with heptanol and di-(n-butyl)-amine 15 and 5° lower, respectively.

Liquid Loss under Pressure.—Figures 1 and 2 summarize the effect of soap concentration on rate and amount of liquid loss at 10 p.s.i. for samples of calcium stearate monohydrate in cetane quenched from 155°. Marked changes in the behavior of the gels occur at about 18% soap for both properties.

Figures 3 and 4 show the effect on the rate and amount of liquid loss, respectively, after quenching from 155°, of increasing concentrations of water, methanol and stearic acid added to 18% systems of calcium stearate in cetane. It is noteworthy that there exists an optimum ratio of additive to soap for minimizing both initial rate of loss of liquid and ultimate amount lost, but that these compositions are different for the two properties. In agreement with the visual observations of the effect of additive concentration on stability, the rate of loss of liquid remains low over a wide range of added concentration of stearic acid and methanol indicative of the instability of these gels.

Table III shows the effect of changing the applied pressure or the quenching temperature on the stability of 18% gels of calcium stearate in cetane containing one mole water per mole of soap. Both initial rate of loss and ultimate loss of liquid of gels prepared by quenching from 155° is lower than from other temperatures investigated.

TABLE III

LIQUID LOSS FROM 18% GELS OF CALCIUM STEARATE MONOHYDRATE IN CETANE AS A FUNCTION OF QUENCHING TEMPERATURE AND APPLIED PRESSURE

Quenching temp., °C.	Applied pressure, p.s.i.	Ultimate liq. loss, % of sample	Initial loss rate, %/min.
120	10	39.8 ± 1.0	2.8 ± 0.2
155	10	30.0 ± 2.6	0.56 ± .12
175	10	39.4 ± 0.6	2.1 ± .2
190	10	40.3 ± 0.3	4.1 ± .5
155	25	37.2 ± 1.4	2.9 ± 1.0
155	40	37.3 ± 0.6	3.9 ± 0.3
280	0	63.3[a]	

[a] This is the % spontaneously exuded on standing one week by an 18% anhydrous system rather than a molar ratio of water to soap of unity as in the other experiments.

Table IV shows that commercial greases behave in approximately the same fashion when studied by this technique as do the calcium stearate gels although generally the total amount of oil expressed is greater while the initial rate of loss is significantly slower. This is in accord with the greater storage

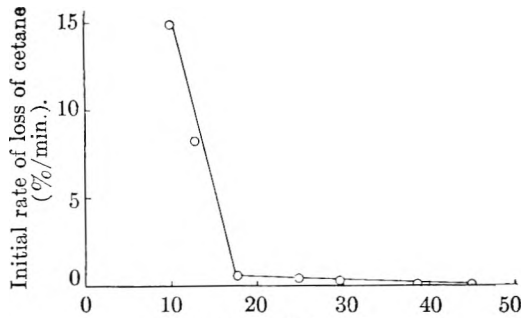

Fig. 1.—Initial rate of outflow of cetane at 10 p.s.i. from greases containing calcium stearate in cetane, stabilized by the incorporation of one mole of water per mole of soap.

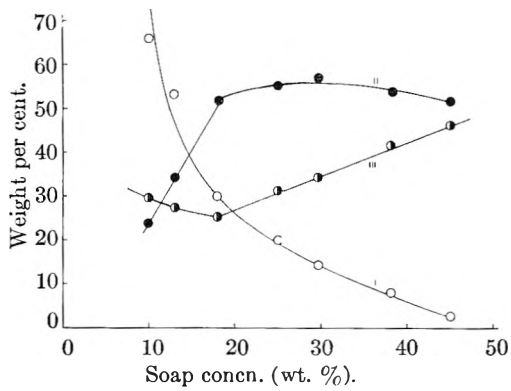

Fig. 2.—Ultimate loss of cetane at 10 p.s.i. from greases containing calcium stearate in cetane, stabilized by the incorporation of one mole of water per mole of soap: I, liquid lost (based on original weight of sample), ○; II, liquid retained (based on original weight of sample), ●; III, soap content of pressed cake (wt. %), ◑.

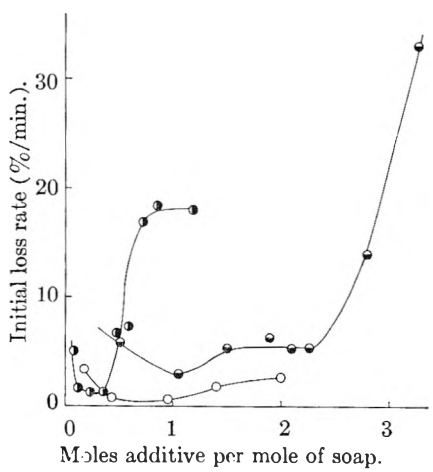

Fig. 3.—Initial rate of loss of cetane at 10 p.s.i. from gels of 18% calcium stearate in cetane, stabilized by various additives: ○, water; ◑, stearic acid; ◒, methanol.

stability of the commercial preparations and with the known empirical relation between storage stability and initial rate of loss ($1/a$) in these accelerated experiments.[10] The variation in rate of expression of liquid is also as would be expected from the higher viscosity of lubricating oils as contrasted with cetane. This effect of viscosity of the "oil" is also evident in comparison of the rate of initial loss of liquid from gels of calcium stearate monohydrate in various liquids, also given in Table IV.

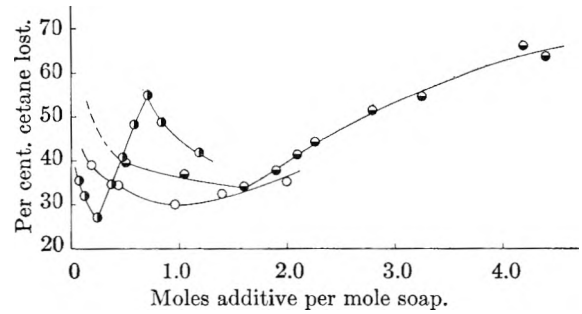

Fig. 4.—Ultimate loss of cetane from gels of 18% calcium stearate in cetane at 10 p.s.i. stabilized by various additives: ○, water; ◑, stearic acid; ◒, methanol.

TABLE IV

LIQUID LOSS AT 10 P.S.I. FROM COMMERCIAL GREASES AND FROM CALCIUM STEARATE MONOHYDRATE GELS IN VARIOUS LIQUIDS AT 10 P.S.I., QUENCHED FROM 155°

Sample	Soap, wt. %	Ultimate loss, wt. % (1/b)	Initial loss rate, %/min. (1/a)	Obsd. loss after %	Min.
Grease Al-4	12	52.3	0.17	41.4	870
Grease Li-6	*ca.* 6	79.9	.15	44.9	373
Grease Li-1	10	45.9	.16	22.4	136
Grease Ca-3	18	51.5	.11	42.6	859
Grease Na-2	16	42.6	.08	34.3	1023
$Ca(Str)_2 \cdot H_2O$–acetone	18	30.0	.56	...	...
$Ca(Str)_2 \cdot H_2O$–decalin	18	49.1	4.3	...	...
$Ca(Str)_2 \cdot H_2O$–white mineral oil (Nujol)	18	40.1	0.40	...	...
$Ca(Str)_2 \cdot H_2O$–diethylhexyl sebacate	18	37.3	1.8	...	...

A few investigations also were made on lithium stearate–cetane gels, these results being presented in Table V. As expected, the slow-cooled gel, in which relatively large crystals can grow, is much less stable and loses a much greater fraction of its liquid than does the quenched sample. Incorporation of water into the lithium stearate–cetane gels decreases their stability, whereas within limits it enhances the stability of the calcium stearate–cetane system. The X-ray diffraction patterns show that the lithium stearate is in the same phase state in all samples regardless of differences in their preparation.

X-Ray Data.—The phases present at room temperature in the calcium stearate gels are identified by their X-ray diffraction patterns in Table VI. Four principal types of pattern have been reported[13–15] for anhydrous calcium stearate. The VI-N pattern is believed to correspond to a layer-like structure of extended calcium stearate molecules, mutually parallel but disordered with respect to lateral separation, roughly approximating hexagonal packing of cylinders.[14,16] It is the least crystalline of the patterns and is obtained on quenching anhydrous calcium stearate. The VI-H

(13) R. D. Vold, J. D. Grandine, 2nd, and M. J. Vold. *J. Colloid Sci.*, **3**, 339 (1948).

(14) R. D. Vold and T. D. Smith, *J. Am. Chem. Soc.*, **73**, 2006 (1951).

(15) M. J. Vold, G. S. Hattiangdi and R. D. Vold, *J. Colloid Sci.*, **4**, 93 (1949).

(16) A. J. Stosick, *J. Chem. Phys.*, **8**, 1035 (1950).

TABLE V

LIQUID LOSS AND X-RAY DIFFRACTION PATTERNS OF LITHIUM STEARATE–CETANE SYSTEMS

% Li Str.	Solvent	% additive (basis of system)	Thermal treatment	Ultimate liq. loss, % of sample	Initial loss rate, %/min.	Long spacing, Å.	Other values d/n
100	...	...	Dried at 105°	...	...	40.0	4.23, 4.01, 3.97, 3.73, 3.58, 2.37, 2.28
100	...	...	Cooled slowly from 200°	...	...	40.2	4.24, 4.04, 3.97, 3.74, 3.58, 2.37, 2.28
100	...	...	Quenched from 155°	...	...	40.6	4.23, 4.07, 3.77, 3.63
18.0	Cetane	None	Cooled slowly from 200°	39.5	3.1	40.6	4.26, 4.07, 3.97, 3.77, 3.63, 4.66, halo
18.0	Cetane	None	After heating to 210° cooled to 155° and then quenched	16.9	0.22	40.6	4.23, 4.07, 3.77, 3.63, 4.66, halo
18.0	Cetane	0.6%	After heating to 210° cooled slowly to 155° and then quenched	45.0	6.3	40.3[a]	4.23, 4.01, 3.73, 3.57, 4.66, halo

[a] In this case the diffraction pattern was obtained on the press cake of 32.6% Li Str content after the liquid loss experiment rather than on the initial gel.

TABLE VI

CHARACTERIZING FEATURES OF THE X-RAY DIFFRACTION PATTERNS OF CALCIUM STEARATE GELS

Composition (% by wt. of system)	Moles additive per mole soap	Temp. from which quenched, °C.	Long spacing, Å.	Principal short spacings,[a] Å.	Other short spacings	Pattern type
100% calcium stearate monohydrate[a]	...	155	49.7	4.15	4.42, 3.86, 3.42	VI-N, VI-H
86.4% calcium stearate,[a] cetane	...	160	49.9	4.19	.....	VI-N
17.4% calcium stearate,[a] cetane	...	160	49.8	4.26	.....	VI-N
14.3% $Ca(Str)_2$, 0.43% H_2O, cetane	1.0	130	50.0	4.39 (0.55) 4.19 (1.0)	3.87	VI-H
17.5% $Ca(Str)_2$, 2.1% Str, cetane	0.24	155	51.0	4.17 (0.40)	3.77, 2.49, 2.35, 2.22, 2.11	VI-N
18.0% $Ca(Str)_2$, 5.9% H Str, cetane	0.72	155	51.0	4.18 (.45)	3.77, 2.50, 2.23, 2.10	VI-N
17.4% $Ca(Str)_2$, 1.1% methanol, cetane	1.0	130	50.1	4.52 (.15) 4.17 (.80)	3.92, 3.77	VI-S and VI-N
18.0% $Ca(Str)_2$, 1.0% methanol, cetane	1.0	155	50.2	4.55 (.16) 4.41 (.38) 4.17 (.53)	3.92, 3.47, 2.97, 2.50	VI-S and VI-H
15.0% $Ca(Str)_2$, 2.8% methanol, cetane	3.54	130	50.2	4.42 (.19) 4.16 (.57)	3.71	VI-H and VI-A
17.9% $Ca(Str)_2$, 0.6% H_2O, di-(2-ethylhexyl) sebacate	1.0	155	49.8	4.42 (.65) 4.17 (.55) 3.89 (.20) 3.41 (.25)	2.21	VI-H
17.5% $Ca(Str)_2$, *n*-heptanol	...	155	50.9	4.38 (.29) 4.15 (.42) 3.42 (.13)	3.94	VI-H

[a] Values from ref. 14. [b] Also present as a short spacing is the broad halo due to the solvent. These values are 4.66 for cetane, (P.T.O.).

and VI-S patterns are believed to correspond to different types of stacking disorder of layers within which the lateral arrangement of the extended calcium stearate molecules is similar, and the VI-A pattern to a second type of lateral arrangement within the layers. VI-A patterns are obtained on slow-cooling (1 to 2°/min.) from the melt of the purest preparations of anhydrous calcium stearate. VI-H and VI-S patterns occur on slow cooling of solutions of calcium stearate in various solvents or from melts containing water. The VI-H pattern of anhydrous calcium stearate is indistinguishable from that of pure calcium stearate monohydrate. It is apparent, even though all patterns obtained conform to one or another of these types, that the values of the spacings between interatomic planes are affected by the presence of various solvents or additives during crystallization.

Figure 5 presents the results of an X-ray study of the binary system calcium stearate–stearic acid undertaken to ascertain whether the acid forms an addition compound with the soap analogous to monohydrate formation with water. Although no lines were found in the pattern of mixtures of calcium stearate and stearic acid which are not present in one or another of the modifications of the soap or the acid, the over-all behavior strongly suggests that in certain ranges of compositions a crystalline addi-

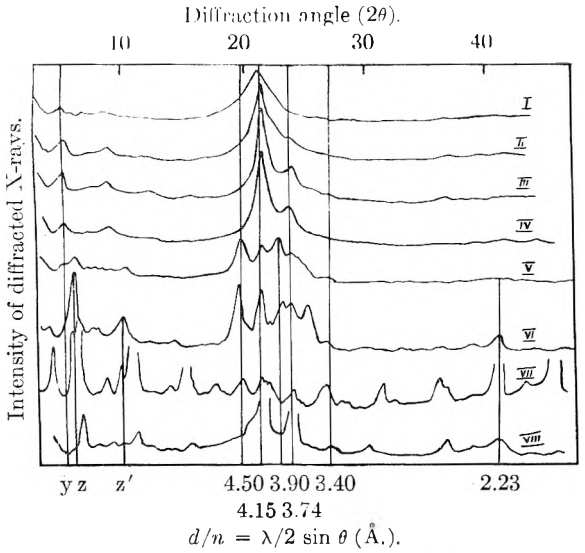

Fig. 5.—X-Ray diffraction patterns of systems of calcium stearate with stearic acid: I, $Ca(Str)_2$ with $^1/_8$ mole HStr, quenched from 155°; VI-N type pattern; II, $Ca(Str)_2$ with 0.25 mole HStr, quenched from 155°, mixed VI-A and VI-N pattern; III, $Ca(Str)_2$ with 0.50 mole HStr, quenched from 155°, VI-A type pattern; IV, $Ca(Str)_2$ with 1 mole HStr, quenched from 155°, VI-A type pattern; V, $Ca(Str)_2$ with 1 mole HStr, slow-cooled from 155°; VI, $Ca(Str)_2$ with 2 moles HStr, slow-cooled from 155°; VII, stearic acid, crystallized from ethanol; VIII, stearic acid, solidified melt. Curve VIII pertains to substantially pure C form of stearic acid while curve VII indicates a mixture of B and C forms. Of the lines marked, Y is the third order of a long spacing of 50.5 Å. and pertains to calcium stearate; Z and Z′ are third and fifth orders of a long spacing of 43.3 Å. (form B of stearic acid). Lines near 4.15, 3.74 and 3.40 Å. could belong to either acid or soap. Lines near 4.5 and 3.9 Å. are present in the VI-S pattern of calcium stearate.

tion compound is formed on cooling.[17] Thus, even though the patterns of both calcium stearate and stearic acid remained unchanged after a certain heat treatment similar treatment of a mixture resulted in a different value of the long-spacing. Moreover, after heat treatment of mixtures containing excess stearic acid and washing with chloroform the stearic acid peak at 40 Å. had disappeared, proving that the new peak at 44 Å., which remained, must be due to an addition compound rather than to a polymorphic form of stearic acid with a peak at this spacing.

Discussion

Peptization and Gel Stabilization by Additives.—Presumably the high viscosity of solutions of calcium stearate in cetane is due to the presence of large aggregates held together in much the same way as in the crystal, with the further possibility of cross-linking between the aggregates themselves. In the crystal, whether of hydrate or of anhydrous soap, it appears[18] that the calcium ions form a sort of one-dimensional lattice perpendicular to the direction of the hydrocarbon chains, in which each calcium is effectively shared among four carboxyl groups as illustrated in Fig. 1b of that paper. Accordingly a tendency toward linear extension of the aggregates would be expected in hydrocarbon solutions with resultant high viscosity. However, formation of additional sheaths, as in the crystal, would be difficult in view of the absence of any tendency to form two-dimensional ionic planes, because of the inaccessibility of the calcium ion to additional oxygens, and the virtually identical interaction between cetane molecules and stearate chains.

Effective viscosity reducers are then those substances which are capable of blocking this extended growth of chains. This can be accomplished either by coördinating some other atom than calcium with oxygens of the carboxylate groups of calcium stearate molecules, or by coördinating some other atom than oxygen from an adjoining carboxylate with calcium atom. This conclusion explains the fact that although none of the non-effective additives (forming type B gels) are capable of hydrogen bonding there are also some molecules incapable of hydrogen bonding which are effective peptizers and stabilizers (forming type A gels) even though most of this group can form hydrogen bonds. There seems to be no simple relation between the effectiveness or lack of effectiveness of the non-hydrogen bonding additives and such characteristics as molecular size or availability of free electron pairs.

Recent work on the viscosity of hydrocarbon solutions of aluminum soaps[19,20] and of sodium phenyl stearate[21–23] confirms that also in these systems reduction of viscosity can be due to hydrogen bonding or to competition between the additive and the carboxylate ion for positions in the coördination sphere of the metal ion. Infrared studies of gels of aluminum hydroxy dilaurate in benzene showed conclusively that in this system the peptizers acted by breaking chains formed by aluminum–oxygen–aluminum coördination with concomitant formation of hydrogen bonds with the peptizer. With the sodium soap stearic acid was the most powerful peptizer and some molecules capable of hydrogen bonding, such as amylamine, were ineffective. The initial conclusion was that only molecules with an acid hydrogen were effective for breaking the soap chains, water and alcohol being effective only because of the formation of stearic acid by hydrolysis.[21] However, infrared spectroscopy[22] showed that although under some conditions hydrolysis was rapid, under other conditions it was negligible, and X-ray studies[14] showed no measurable formation of stearic acid in the case of calcium stearate in cetane heated with excess water. Later[23] it was recognized that the viscosity decrease on addition of phenylstearic acid, ethanol or phenol to solutions of alkaline or alkaline earth phenyl stearates in benzene might be due either to hydrogen bonding or to formation of coördination complexes between the additive and calcium ion.

(17) E. Stanley, Research Report, "An X-Ray Study of the Structure of Calcium Stearate Monohydrate," University of Southern California Science Library, 1954; personal communication, August 30, 1955.

(18) E. Stanley, *Nature*, **175**, 165 (1955); Research Report, "An X-Ray Study of the Structure of Calcium Stearate Monohydrate," University of Southern California Science Library, August, 1954.

(19) F. A. Scott, J. Goldenson, S. E. Wiberley and W. H. Bauer, THIS JOURNAL, **58**, 61 (1954).

(20) W. O. Ludke, S. E. Wiberley, J. Goldenson and W. H. Bauer, *ibid.*, **59**, 222 (1955).

(21) J. G. Honig and C. R. Singleterry, *ibid.*, **58**, 201 (1954).

(22) R. E. Kagarise, *ibid.*, **59**, 271 (1955).

(23) J. G. Honig and C. R. Singleterry, *ibid.*, **60**, 1114 (1956).

Gelation of alkaline and alkaline earth metal soaps in oils is now generally attributed to development of a three-dimensional fibrous network in the system although the nature of the bond at contact points between separate ultimate fibers is still uncertain, proposals ranging from simple mechanical entanglement at one extreme to common crystallization at contact points at the other.[24-26] The stability of the gels (decreased rate of loss of liquid, increased yield value, etc.) would be expected to be greater the more proliferated the form in which the soap exists at room temperature. It seems quite possible that smaller size of the micelles in the isotropic solution is conducive to formation of smaller fibers and more highly organized and interconnected networks in the solid formed on cooling. The same factors which enable additives to reduce the size of the micelles in solution will also be operative in preventing the growth of large coherent crystallites on solidification. The lower viscosity of the solution brought about by effective additives may also facilitate formation of complicated "dendritic" structures during the short interval between incipient crystallization and the prevention of further rapid changes because of the falling temperature.

The plausibility of this concept is supported by electron micrographs[26] which show larger crystals in slow-cooled systems with correlating lower yield values, and also by the present data where slow-cooled systems of both calcium and lithium stearates in cetane were found to lose liquid much faster and in greater amount than those which were prepared by quenching. It resembles somewhat the mechanism of gelation postulated by Boedtker and Doty[27] for gelatin in water, where the gel skeleton is regarded as being formed in part by agglutination of more or less intact micelles of the solution phase. There are difficulties with this hypothesis, however, since Table III shows that gels formed by quenching from 155° are more stable than those quenched from higher or lower temperatures, whereas a regular change in stability with quenching temperature might be expected if micellar size in solution were the primary variable. Possibly the explanation is the occurrence of markedly different properties in different regions of the same isotropic phase field, as found in sodium soap solutions in water,[28] or a variable extent of reincorporation of water into the condensed phase from the vapor space on cooling the system.

That melt viscosity may be important is suggested by the results shown in Fig. 5, where quenching a very viscous melt of pure calcium stearate results in the formation of the disordered VI-N form while the more fluid systems resulting from addition of stearic acid yield the more highly ordered VI-A form. The VI-A modification is still formed when stearic acid is present even in cases where slow-cooling of the pure calcium stearate results in the VI-H form, the change in type presumably being due to the effect of stearic acid in removing traces of adsorbed calcium ion which inhibits crystallization of the VI-A modification.[15]

Capillary Characteristics of the Gel.—If the size distribution of capillary spaces within which liquid is immobilized in a gel is treated as an equivalent system of uniform cylindrical capillaries the radius, r, of the pore which can just retain liquid against any applied pressure, P, can be calculated by the equation $r = 2\gamma \cos\theta/P$, where θ is the contact angle and γ the surface tension of the liquid. The ultimate loss of liquid at a given pressure can be regarded as being determined by the total pore volume of spaces so small that outflow from them is prevented by the surface tension of the entrained liquid. On this basis the liquid content of the gel after pressing is a measure of the pore volume of capillary spaces smaller than the limiting radius determined by the applied pressure. That it is not due to the residue having a composition corresponding to a phase boundary is shown by the fact that a new system made at this composition initially loses further liquid on exposure to the same pressure. Differences in ultimate liquid loss of comparable gels are then a result of either differences in the pore size and pore volume of the initial gels or of weaker interparticle binding in one case than the other, resulting in a greater degree of collapse of the structure under pressure. That some collapse of empty pores occurs is evident since a 30% calcium stearate gel prepared by pressing a 10% system had virtually the same density as a freshly prepared 30% gel. Moreover, the ultimate liquid loss of 18% calcium stearate–water–cetane gels increased gradually as pressure was increased from 10 to 30 lb./in.^{2}, but at pressures between 40 and 50 lb./in.^{2}, the liquid loss was less than at lower pressures, suggesting that the applied pressure had exceeded some intrinsic collapse pressure of the soap network in the oil system, with formation of a system of finer pores in the pressed cake.

The fraction of the total pore volume made up of large pores (>7978 Å. for cetane gels at 10 lb./in.^{2} pressure, assuming $\cos\theta = 1$ and $\gamma = 27.5$) may be calculated from the difference in liquid content of the original and the pressed gel. That many spaces of this order of magnitude may actually be present in the gel framework has been shown by electron micrographs of thin sections of lithium soap–cetane gels.[29] The fraction of cetane in large pores is plotted as a function of initial liquid content in Fig. 6. The proportion of large pores decreases with increasing soap concentration, as would be expected, but the most striking result is that the points fall on two intersecting curves rather than varying continuously with composition. This suggests that the total pore volume is composed of voids of two different types.

It may be postulated that there is in the gel, in addition to the primary soap particles a three-di-

(24) A. Bondi, J. P. Caruso, H. M. Fraser, J. D. Smith, S. T. Abrams, A. M. Cravath, R. J. Moore, W. H. Peterson, A. E. Smith, F. H. Stross, E. R. White and J. N. Wilson, *Proc. Third World Pet. Congress*, Section VII, 373 (1951).

(25) M. J. Vold, *NLGI Spokesman*, **19**, 20 (1955).

(26) R. D. Vold, H. F. Coffer and R. F. Baker, *Institute Spokesman*, **15**, 9 (1952).

(27) H. Boedtker and P. Doty, THIS JOURNAL, **58**, 968 (1954).

(28) D. G. Dervichian, M. Joly and R. S. Titchen, *Kolloid Z.*, **136**, 6 (1954).

(29) V. Artel, Research Report, "Electron Microscope Studies of Lithium Soap-Cetane Gel Systems," University of Southern California Science Library, September, 1955.

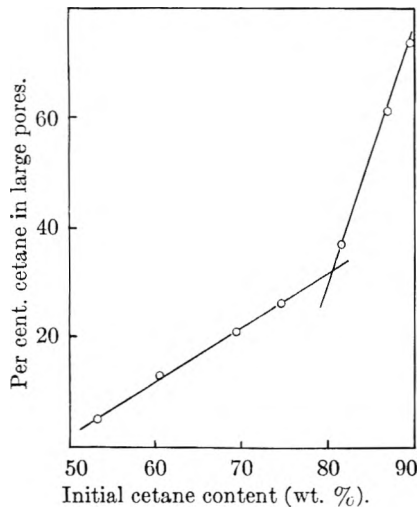

Fig. 6.—Fraction of capillary volume present as large pores. Calculated for calcium stearate monohydrate–cetane gels under a pressure of 10 p.s.i. assuming $\theta = 0$ and $\gamma = 27.5$.

mensional network formed by aggregation of the ultimate particles, and a series of voids where portions of the network which formed in spatially different regions of the solution come into irregular contact. The soap crystallites or fibrils are essentially nonporous, the homogeneous regions of the network or skeleton provide a mesh of pores of both large and small size, while the zones where the different regions join together would be characterized by larger voids. As the solution from which the gel is formed is diluted the average size of the pores in the homogeneous regions of the gel skeleton will increase since less soap is available for cross-linking and formation of a fine network, thus giving rise to a regular increase in the fraction of large pores. When the solution becomes sufficiently dilute, however, the extent to which homogeneous gel structure can develop may be limited by the low concentration, with a resultant increase in the volume occupied by the irregular contacts between such regions. This may account for the rapid increase in the proportion of large pores with further increase in cetane content beyond 81%, although the possibility cannot be excluded that this effect might be due to a change in the nature of the micellar solution at this concentration resulting in formation of a gel skeleton of different porosity.

Alternative Explanations of Gel Stability.—Since the properties of soap gels in oil at room-temperature may depend both on the phases present at room-temperature and on those at higher temperatures where the gel was formed[9,13,14,30,31] it might be thought possible that additives owe their effectiveness to alteration of the phase behavior, although even in the earlier work in many cases the controlling variable appeared to be the size and shape of the soap fibers present[30–32] rather than the phase behavior itself. This supposition was strengthened by the fact that after quenching calcium stearate–cetane systems from 130° X-ray data[9,14] showed that distinctive changes in diffraction pattern occurred sharply at several compositions, with changes in microscopic and visual appearance at roughly the same places, even though all systems there and in the present work were isotropic solutions at elevated temperatures and, according to the equilibrium phase diagram,[7] should have contained only mixtures of the same solvent-free calcium stearate and nearly pure cetane at temperatures below 100°.

Nevertheless, the stability and consistency of the gels are not sensitive to these possible differences in the soap phase. Figures 1 and 2 show that both the ultimate loss of liquid and the initial rate of loss appear to vary continuously with soap content with no discontinuities at the compositions where the diffraction patterns change, although there is an abrupt change of slope at 18% calcium stearate monohydrate. Moreover, gels giving the same X-ray diffraction pattern often differ greatly in stability while gels of the same stability can show different diffraction patterns. Among the former group are 18% gels of lithium stearate in cetane prepared by slow-cooling and by quenching (Table V), and anhydrous and water-containing lithium stearate gels prepared by quenching. Gels of calcium stearate–stearic acid–cetane containing 0.24 and 0.72 mole of stearic per mole of soap have virtually identical diffraction patterns (Table VI) even though ultimate liquid loss is minimum at the first composition and maximum at the second (Fig. 4). Conversely, an 18% calcium stearate–cetane gel with 2.1 moles water per mole of soap has nearly the same rate of loss of liquid (Fig. 3) and ultimate loss (Fig. 4) as a similar system with 1.0 mole methanol/mole soap even though in the alcohol system the soap is present as a mixture of VI-S and VI-H crystalline forms (Table VI) while in the water-containing system it is in the VI-N form.[14]

It may therefore be concluded that it is not the phase which is present but the nature of the solid skeleton of the gel which is of primary significance. In this connection a combination of factors will be important, including not only the size and shape of the particles from which the gel skeleton is formed but also the number of cross links between particles and the strength of the binding at these points of closest approach, together with such characteristics of the network as its average porosity and proportion of "open" to "closed" pores. On this view changes in the soap phase would not *per se* result in changes in gel behavior since they would not necessarily alter the geometrical structure of the network. Thus the attraction between two fibers directly in contact on their hydrocarbon surfaces,[26] or separated by a bimolecular film of adsorbed cetane or additive, would not be expected to vary appreciably because of small differences in packing[14] of the soap molecules in the crystal lattice.

Another hypothesis which might be proposed to account for the action of additives is to postulate that they form addition compounds with the soap, thus resulting in changes in crystal habit which can be very important in determining the physical

(30) D. Evans, J. F. Hutton and J. B. Matthews, *J. Applied Chem.*, **2**, 252 (1952).

(31) M. J. Vold, THIS JOURNAL, **60**, 439 (1956).

(32) R. J. Moore and A. M. Cravath, *Ind. Eng. Chem.*, **43**, 2892 (1951).

TABLE VII

IDENTIFICATION OF HYDRATION STATE OF CALCIUM STEARATE FROM X-RAY DIFFRACTION PATTERNS

Soap from stearic acid sample	Ref.	Feasibility of detection of hydration state from diffraction pattern
I	13	Readily
5R3	14	Possible, but some variations from standard pattern
5R3	15	Only after a considerable aging period
II, III, 5	13, 15	Not possible with these less pure fatty acids

Form present at room temp. after thermal treatment

Sample	Ref.	Phase	Prior treatment
5R3AH	14	VI-N	Quenched from cetane–water systems
5R3	33	Hydrate	Quenched from cetane–water systems

Ease of rehydration of various forms under different conditions

Sample	Ref.	Phase	Thermal treatment	Ease of rehydration
I	13	VI-A	.....	No hydrate after 36 hr. in water at 60°
I	13	VI-A	.....	Hydrate present after 1 hr. in water at 100°
I	13	VI-N	Quenched from 155°	Reverted readily to hydrate at room temp.
5R3AH	14	VI-N	Quenched	Rehydrated partially after 1 mo. at room temp.
5R3AH	14	VI-A	.....	No hydrate formation on exposure to laboratory air at room temp.
5R3AH	14	VI-A	.....	Hydrated completely at room temp. on sealing in a tube with water

properties of greases.[33] Although water can form a monohydrate with calcium stearate,[13] after equilibration of systems at 155°, which is above the decomposition temperature, hydrate can be present only if it reforms during quenching or on standing at room temperature. There is some difficulty in identification by X-ray diffraction techniques since the pattern obtained is strongly dependent on the presence or absence of traces of adsorbed salts,[15] the available evidence as to change of pattern with hydration state and ease of hydration of the dry soap being summarized in Table VII. Under the conditions of the present experiments even in the water-containing systems the soap must have been present at room temperature predominantly in the anhydrous VI-N form in all cases with possible traces of VI-A and monohydrate. In the case of stearic acid the X-ray evidence (Fig. 5) indicates the formation of a molecular compound with calcium stearate under some conditions.[17]

However, if the effect of the additive were due solely to formation of an addition compound with the soap it would be expected that the ultimate liquid loss and initial rate of loss would be minimum at a composition ratio of additive to soap corresponding to complete formation of the complex, and that this would occur at low integral molal ratios. Study of Figs. 3 and 4 shows that the molal ratio of additive to soap is usually non-integral at the minima, is different at the compositions of minimum rate of loss of liquid and of minimum ultimate loss, and again different at the composition of maximum yield value of the gel.[26,34] In view of the variability of these ratios and their failure to accord with the compositions of any plausible addition compound it seems unlikely that compound formation can be adduced as the mechanism of stabilization by these additives.

(33) D. H. Birdsall and B. B. Farrington, THIS JOURNAL, **52**, 1415 (1948).

(34) H. F. Coffer, Ph.D. Dissertation, University of Southern California Library, 1951.

HOMOGENEOUS DECOMPOSITION OF HYDROGEN PEROXIDE VAPOR

BY CHARLES N. SATTERFIELD AND THEODORE W. STEIN

Department of Chemical Engineering, Massachusetts Institute of Technology, Cambridge, Mass.

Received September 10, 1956

Studies of the thermal decomposition of hydrogen peroxide vapor under flow conditions in a relatively inert glass reactor show a transition from heterogeneous to homogeneous reaction in the temperature range of 400 to 450°, at a partial pressure of 0.02 atmosphere. The homogeneous reaction was of 3/2 order and had an activation energy of 55,000 cal. The decomposition mechanism appears to involve very long straight chains.

Numerous studies have been made of the thermal decomposition of hydrogen peroxide vapor (these have been summarized[1] recently) but only in the study by McLane[2] were experimental conditions such that at least a portion of the reaction seemed to be occurring homogeneously. The present study shows quite clearly the conditions under which a transition from heterogeneous to homogeneous de-

(1) W. C. Schumb, C. N. Satterfield and R. L. Wentworth, "Hydrogen Peroxide," A. C. S. Monograph No. 128, Reinhold Publ. Corp., New York, N. Y., 1955, pp. 447–458.

(2) C. K. McLane, *J. Chem. Phys.*, **17**, 379 (1939).

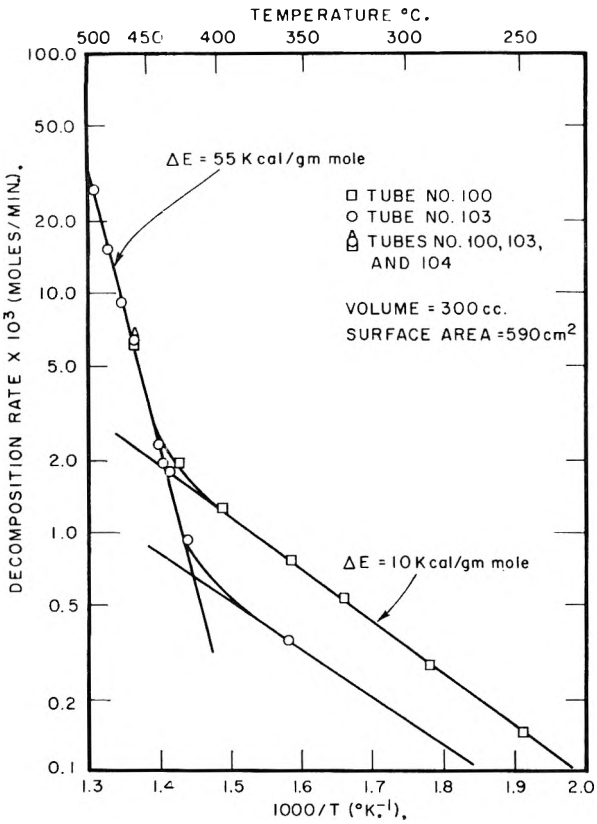

Fig. 1.—Effect of temperature on the decomposition rate of hydrogen peroxide vapor ($P_{H_2O_2}$ = 0.02 atm.).

composition may be observed and provides some information on the kinetics of the homogeneous reaction.

A mixture of hydrogen peroxide and water vapor at one atmosphere total pressure was produced at a constant rate and composition by boiling an aqueous solution of hydrogen peroxide of appropriate composition. The vapor was passed continuously through a Pyrex tube held in a constant temperature bath. The amount of decomposition occurring in the tube was determined by continuous removal of vapor samples before and after the tube, with quick quenching, followed by analysis of the condensate with standardized permanganate in the usual fashion. The apparatus is described in more detail elsewhere.[3]

In a series of studies at temperatures up to 250°, and hydrogen peroxide concentrations up to 0.20 atmosphere the rate per unit of surface area was found to be independent of the surface–volume ratio, for the most inert surfaces studied[3] showing, in agreement with previous investigators, that the homogeneous reaction cannot be detected at these temperatures. The temperature range from 215 to 490° was then investigated in three Pyrex tubes, each of which previously had been treated with 4 *N* phosphoric acid to provide a highly inert surface. Each tube had a surface area of 590 cm.² and a volume of 300 cm.³ The results are shown on Fig. 1.

Two facts show quite clearly that a transition from heterogeneous to homogeneous decomposition occurred in the temperature range of 400 to 450°; (1) the sharp increase in the temperature coefficient of the decomposition rate and (2) the fact that different tubes showed different decomposition rates in the lower (heterogeneous) temperature region but the same results in the higher temperature region. The data in the heterogeneous range were obtained at average hydrogen peroxide partial pressures of 0.025 to 0.038 atmosphere, those in the homogeneous range from 0.006 to 0.029 atmosphere. To put the results on a comparable basis, the rates of decomposition were recalculated for a hydrogen peroxide partial pressure of 0.02 atmosphere, assuming that in the homogeneous range the rate is proportional to the 3/2 power of the hydrogen peroxide concentration, and in the heterogeneous range that the concentration effect is the same as that found at lower temperatures[3]—slightly greater than first order.

The homogeneous reaction is so rapid under these conditions that a large fraction of the hydrogen peroxide entering the Pyrex tube decomposed therein, so that it must be treated as an "integral reactor." To determine the correct manner in which to average inlet and exit hydrogen peroxide concentrations, data obtained at a common temperature of 460° and several concentrations were plotted as on Fig. 2. The slope corresponds to a 3/2 order reaction

$$-\frac{dn_{H_2O_2}}{V\,d\theta} = kP_{H_2O_2}^{3/2} \qquad (1)$$

where the average value of $P_{H_2O_2}$ is given by

$$P_{H_2O_2} = \left[\frac{P_{in}P_{out}^{1/2} + P_{out}P_{in}^{1/2}}{2}\right]^{2/3} \qquad (2)$$

Homogeneous rate data obtained at slightly different average partial pressures were recalculated to a common basis of a hydrogen peroxide partial pressure of 0.02, yielding the curve in Fig. 1 for the homogeneous reaction. The slope of this curve corresponds to an activation energy of about 55 kcal./g. mole.

The temperatures reported are an average of the bath temperature and that of the vapor entering the reactor. This is a satisfactory measure of reaction temperature when reaction takes place exclusively on the tube wall. However in the homogeneous range the exothermicity of the reaction may cause the vapor to be appreciably hotter than the tube wall. To estimate this factor, the temperature variation of the vapor as a function of tube length was calculated for the various H_2O_2 concentrations studied, assuming the heat transfer coefficient to be 3.5 BTU/(hr.)(°F.)(ft.²), the latter being based on the Reynolds number with allowance for entering turbulence. It was concluded that for only one set of runs (those at an average hydrogen peroxide partial pressure of about 0.03 atm.) was this factor an appreciable source of error and that here the vapor temperature was about 10° higher than the wall temperature. For plotting on Fig. 2 this one set of observed values were therefore corrected using the Arrhenius equation with an activation energy of 55 kcal.

Further evidence for a 3/2 order reaction comes from the data of Miss Huang[4] which were obtained

(3) C. N. Satterfield and T. W. Stein, *Ind. Eng. Chem.*, in press.

(4) Y. M. Huang, S.M. thesis in Chemical Engineering, M.I.T., August, 1955.

in the same type of apparatus, differing principally in that the reaction temperature was determined from five thermocouple wells placed equidistantly along the reaction tube. A group of nine runs at temperatures between 466 and 489° and at average hydrogen peroxide partial pressures of from 0.001 to 0.035 atmosphere were available for evaluation. Her rate data were adjusted to the common temperature of 475° using the Arrhenius equation and an activation energy of 55,000 kcal. Although the data scatter slightly, the results, shown on Fig. 3, clearly correspond to a 3/2 order expression rather than to a first or a second order. The data of Miss Huang when recalculated to 475° and 0.02 partial pressure of hydrogen peroxide and allowing for the difference in reactor volumes correspond to a rate of homogeneous reaction about 30% less than that shown in Fig. 1.

McLane[2] obtained data in boric acid-coated Pyrex at average concentrations of 0.002 atmosphere pressure of hydrogen peroxide and below and at temperatures of 470–540°. His rate reportedly followed a first-order expression and in the lowest surface–volume ratio vessel studied (S/V = 3 cm.$^{-1}$) he reported an activation energy of 50,000 cal.

There are several important differences between his experimental conditions and those in the present study. The hydrogen peroxide concentrations here were one to two orders of magnitude greater; the surface–volume ratio of the present vessel was about 2 cm.$^{-1}$, compared to 3 cm.$^{-1}$ of McLane, and the flow pattern here approximated slug flow whereas that of McLane appeared to be close to that of a completely mixed reactor. The present rate data are about twice those reported by McLane if the rate is taken to be proportional to the 3/2 power, or about ten times those of McLane if the reaction were assumed to follow a first-order expression. This most probably reflects an increase in chain length of the reaction as the surface–volume ratio is lowered and the H_2O_2 concentration is raised.

The most probable initiating step in the reaction is

$$H_2O_2 + M \longrightarrow 2OH \qquad (3)$$

The energy required for this reaction is about 52.6 kcal./g. mole whereas about 90 kcal./g. mole would be needed for the only alternate initiating step, formation of H and OOH.

Chain propagation is most probably by

$$OH + H_2O_2 \longrightarrow OOH + H_2O \qquad (4)$$

and

$$OOH + H_2O_2 \longrightarrow H_2O + O_2 + OH \qquad (5)$$

both of which are exothermic whereas all chain branching steps are endothermic. Chain breaking can occur by adsorption of radicals on the walls or by 3-body combination reactions of OH or OOH, thus

$$2OH + M \longrightarrow H_2O_2 \qquad (6a)$$
$$OH + HO_2 + M \longrightarrow O_2 + H_2O_2 \qquad (6b)$$
$$2HO_2 + M \longrightarrow H_2O_2 + O_2 \qquad (6c)$$

If the rates of reactions 3, 4, 5 and 6a are formulated in terms of the appropriate rate constants and

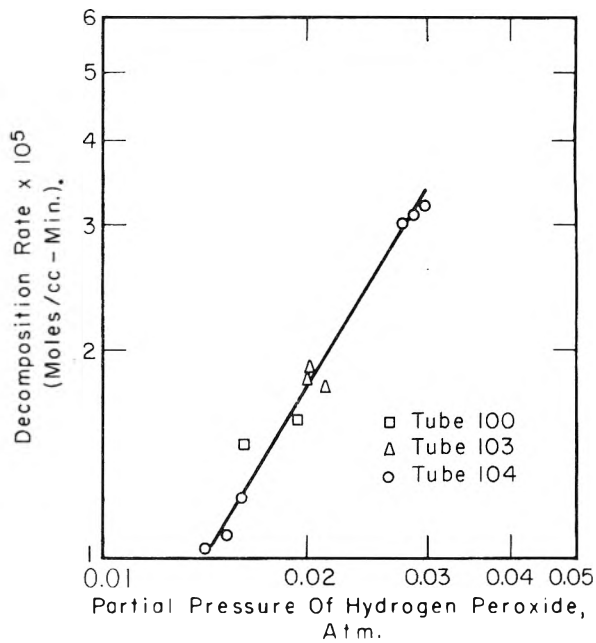

Fig. 2.—Effect of concentration on the homogeneous decomposition rate of hydrogen peroxide, T = 460°

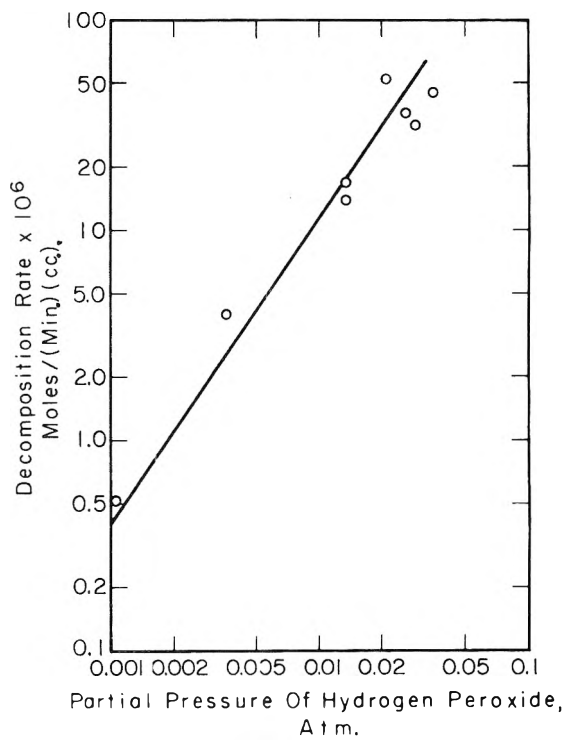

Fig. 3.—Effect of concentration on the homogeneous decomposition rate of hydrogen peroxide (from Huang), T = 475°.

reactant concentrations, and the rate of production and destruction of each of the free radicals is equated, one can derive the expression

$$-\frac{dn_{H_2O_2}}{V\,d\theta} = 2k_4\sqrt{\frac{2k_3}{k_{6a}}}\left(\frac{1}{RT^{3/2}}\right)P_{H_2O_2}^{3/2} \qquad (7)$$

A 3/2 order expression is also obtained if one of the other free radical combination reactions is chosen instead of 6a. However, if 3-body free radical combination reactions are regarded as negligible and chain stopping is assumed instead to occur by

adsorption on walls, the mathematical formulation leads to a second-order expression. The fact that the decomposition rate in fact followed a 3/2-order expression suggests that the 3-body free radical recombinations were the chain stopping mechanism here and not wall reactions.

It is interesting to compare the observed decomposition rate with the number of collisions of hydrogen peroxide molecules in which the energy is greater than 55,000 cal./g. mole. The measured decomposition rate at 460° and hydrogen peroxide partial pressure of 0.02 atmosphere corresponds to about 1.9×10^{17} molecules decomposing per cc. per second. Assuming that the fraction of collisions having activation energies greater than 55,000 cal./g. mole equals $e^{-E/RT}$, the number of such activated collisions involving a hydrogen peroxide molecule is about 1.8×10^{10} collisions per cc. per second. There are, of course, considerable sources of error in calculating the number of "effective collisions," such as the uncertainty as to the value of the activation energy and as to the collision cross-sections, and also the possibility that the activation energy may be shared between more than two "square terms," and therefore that the fraction of effective collisions may be somewhat greater than $e^{-E/RT}$. Nevertheless, the enormous difference between the two numbers clearly indicates that long chains are involved here.

Acknowledgment.—The authors wish to acknowledge the financial support of the Office of Naval Research, under Contract Nonr-1841 (11).

CALCULATION OF EXPERIMENTAL ISOTOPE EFFECTS FOR PSEUDO FIRST-ORDER IRREVERSIBLE REACTIONS

BY JAMES YING-PEH TONG AND PETER E. YANKWICH

Contribution from the Noyes Chemical Laboratory, University of Illinois, Urbana, Illinois

Received September 24, 1956

Four exact equations are derived for the calculation of experimental isotope effects of systems of pseudo first-order irreversible reactions. The input data are either measured isotope ratios alone, or a combination of isotope ratios with the measured reaction coördinate. The advantages and disadvantages of these equations over those of the zero-time approximation method are discussed.

Introduction

In this paper, we are concerned with a system of pseudo first-order irreversible reactions

$$A' + pP + qQ \longrightarrow B' + uU + vV \quad (1)$$
$$A'' + pP + qQ \longrightarrow B'' + uU + vV \quad (2)$$

where one atom of the element Z is transferred from a molecule of A to one of B during one stoichiometric unit of reaction. The symbols A′ and B′ stand for the compounds A and B containing the lighter isotope Z′, and the symbols A″ and B″ stand for the compounds A and B containing the heavier isotope Z″. The rate equations are assumed to be

$$-d(A')/dt = k'(A')F \quad (3)$$
$$-d(A'')/dt = k''(A'')F \quad (4)$$

where F is a function of the concentrations of reactants, catalysts and products, other than A and B. Conventionally, the *isotope effect* is defined as the deviation from unity of the ratio of isotopic rate constants r; *i.e.*

$$(r - 1) = (k'/k'') - 1 \quad (5)$$

An approximate method[1] which has been employed in several studies[2,3] involves the determination of the isotope ratios R_{bt} and $R_{b\infty}$ (or R_{a0}), the corrected isotope ratios (B″)/(B′) of product accumulated to times t and infinity; collection of the sample with which the former measurement is to be made is stopped at a value of the reaction coördinate, f, so small that the time t may be considered equal to zero. The isotope effect, then is computed from the relation

$$(r - 1) = (R_{b\infty}/R_{bt})_{t\to 0} - 1 \quad (6)$$

Several other workers[4-6] have published the results of studies based on other approximation methods which employ isotope ratios determined on product material accumulated up to large values of the reaction coördinate f; in all of these, the approximation has been the application of an equation valid only when one isotope is present at the trace level.

In a system of two simultaneous irreversible reactions involving isotopically different reactants and products, one can measure three isotope ratios and the reaction coördinate; the isotope effect can be computed from any grouping of three of these quantities. In this paper we shall examine four *exact* equations applicable to systems of any original isotopic constitution and each of which employs a different grouping of the input data. For each of these equations and equation 6 we shall calculate and compare the errors in r arising from typical imprecisions in the input data.

Derivations

The four measurable quantities are: the isotope ratio of the starting material, R_{a0} (which is the same as that of the accumulated product at complete reaction, $R_{b\infty}$); the isotope ratio of the residual reactant at time t, R_{at}; the isotope ratio of

(1) J. Bigeleisen, *Science*, **110**, 14 (1949).

(2) J. Bigeleisen, *J. Chem. Phys.*, **17**, 425 (1949).

(3) P. E. Yankwich, R. L. Belford and G. Fraenkel, *J. Am. Chem. Soc.*, **75**, 832 (1953).

(4) A. A. Bothner-By and J. Bigeleisen, *J. Chem. Phys.*, **19**, 755 (1951).

(5) J. A. Schmitt, A. L. Myerson and F. Daniels, THIS JOURNAL, **56**, 917 (1952).

(6) A. M. Downes, *Australian J. Sci. Research*, **A5**, 521 (1952).

the product accumulated to time t, R_{bt}; and the reaction coördinate at time t, f. Let us define a quantity g as

$$g = (A'')_t/(A'')_0 = e^{-k''\int F dt} \tag{7}$$

then

$$(A')_t/(A')_0 = e^{-\kappa''\int F dt} = g^r \tag{8}$$

The above four input data can be expressed as

$$R_{a0} = R_{b\infty} = \frac{(A'')_0}{(A')_0} \tag{9}$$

$$R_{at} = \frac{(A'')_t}{(A')_t} = \frac{R_{a0}}{g^{r-1}} \tag{10}$$

$$R_{bt} = \frac{(B'')_t}{(B')_t} = \frac{R_{a0}(1 - g)}{(1 - g^r)} \tag{11}$$

$$f = \frac{(B')_t + (B'')_t}{(A')_0 + (A'')_0} = \frac{(1 - g^r) + R_{a0}(1 - g)}{1 + R_{a0}} \tag{12}$$

Three exact relations for r are obtained by elimination of g between each of the three pairs of equations chosen from the triad (10), (11) and (12); the fourth such relation requires elimination of both g and R_{a0} from among the three.

When R_{a0}, R_{at} and R_{bt} are determined

$$r = \frac{\ln\left[\frac{(R_{bt} - R_{a0})}{(R_{bt} - R_{at})}\right]}{\ln\left[\frac{R_{at}(R_{bt} - R_{a0})}{R_{a0}(R_{bt} - R_{at})}\right]} \tag{I}$$

When R_{a0}, R_{at} and f are determined

$$r = \frac{\ln\left[\frac{(1 - f)(R_{a0} + 1)}{(R_{at} + 1)}\right]}{\ln\left[\frac{R_{at}(1 - f)(R_{a0} + 1)}{R_{a0}(R_{at} + 1)}\right]} \tag{II}[7]$$

When R_{a0}, R_{bt} and f are determined

$$r = \frac{\ln\left[1 - \frac{f(R_{a0} + 1)}{(R_{bt} + 1)}\right]}{\ln\left[1 - \frac{R_{bt}f(R_{a0} + 1)}{R_{a0}(R_{bt} + 1)}\right]} \tag{III}$$

When R_{at}, R_{bt} and f are determined

$$r = \frac{\ln\left[\frac{1}{(1 - f)} - \frac{f(R_{bt} - R_{at})}{(1 - f)(R_{bt} - 1)}\right]}{\ln\left[\frac{1}{(1 - f)} + \frac{f(R_{bt} - R_{at})}{(1 - f)R_{at}(R_{bt} + 1)}\right]} \tag{IV}$$

In those experimental situations where g and g^r can be measured directly, r can be obtained by combination of the logarithms of equations 7 and 8; such a relation has been employed and an analysis of the associated errors given by Jones.[10]

Error Analysis

The deviations in the calculated rate constant ratio, Δr, due to deviations in the measured isotope ratios, ΔR, and the measured reaction coördinate, Δf, can be obtained from an approximation of a Taylor series expansion in these quantities.

If r is a function of the variables w_i, the Taylor series expansion of Δr in terms of corresponding Δw_i's is

$$\Delta r = \sum_i \left[\sum_{n=1}^{\infty} \frac{1}{n!}\frac{\partial^n r}{\partial w_i^n}(\Delta w_i)^n\right] \tag{13}$$

When Δw_i's are small, terms of equation 13 containing $(\Delta w_i)^n$ for n equal to two or greater may be ignored. We have, then, as an approximation

$$\Delta r = \sum_i \frac{\partial r}{\partial w_i}(\Delta w_i) \tag{14}$$

Equation 14 can be modified easily to express all the deviations as fractional deviations (or percentage deviations) to read

$$\frac{\Delta(r - 1)_k}{(r - 1)} = \frac{\Delta r_k}{(r - 1)} = \sum_i C_{ki}\frac{\Delta w_i}{w_i} \tag{15}$$

where

$$C_{ki} = \frac{w_i}{r - 1}\left(\frac{\partial r}{\partial w_i}\right)_k \tag{16}$$

The calculation of the error in $r - 1$ by equation 15 requires the use of the signs of the individual contributing deviations; these signs are usually unknown and may vary with experimental conditions, etc. In order to evaluate the usefulness of equations I through IV, we shall consider the *maximum fractional deviation in r − 1* calculated by each equation for a given set of values of fractional deviations in isotope ratios and reaction coördinates.[11] The maximum fractional deviation in $r - 1$ (henceforth abbreviated to S_k) is defined as

$$S_k = \sum_i \left|c_{ki}\frac{\Delta w_i}{w_i}\right| \tag{17}$$

The expressions for the coefficients c_{ki} and the related g's are summarized in the Appendix.

A similar analysis has been given by Bigeleisen and Allen[13] on an equation[4] when expressed in our notation reads

$$r = \ln(1 - f')/\ln\left(1 - \frac{R_{bt}}{R_{a0}}f'\right) \tag{18}$$

which can be obtained by combining equations 11 and 19, or by combining equations III and 20.

$$f' = 1 - g^r \tag{19}$$

$$f' = f(R_{a0} + 1)/(R_{bt} + 1) \tag{20}$$

The approximation made by the authors was $f' = f$.

Calculations and Discussion

The coefficients c_{ki} were calculated for r values of 1.01, 1.03, 1.10, 1.35, 2.00 and 4.00, and for R_{a0} values of 1, 0.1 and 0.011111.[14] Maximum fractional deviations in $r - 1$, S_k, were calculated for the above values of r and R_{a0} using assumed

(7) Equation II can be obtained by rearrangement of the Rayleigh distillation formula[8] as given by Urey.[9]

(8) John William Strutt (3rd Baron Rayleigh), *Phil. Mag.*, [5] **42**, 493 (1896).

(9) H. C. Urey, *Repts. Progr. Phys.*, **6**, 48 (1939).

(10) W. M. Jones, *J. Chem. Phys.*, **19**, 78 (1951).

(11) A more conventional statistical formulation of the fractional error S'_k, is

$$S'_k = \left[\sum_i (c_{ki}\Delta w_i/w_i)^2\right]^{1/2}$$

If the assumption is made that the measurements of the various input data are independent, then both this S'_k and that given by equation 17 are derived from Taylor's Theorem expansion neglecting terms of higher order than the first.[12] Thus the value of S_k computed from equation 17 is always equal to or larger than S'_k.

(12) See for example: J. Reilly and W. N. Rae, "Physico-Chemical Methods," fifth edition, Vol. I, D. Van Nostrand Co., Inc., New York, N. Y., 1954, p. 180.

(13) J. Bigeleisen and T. L. Allen, *J. Chem. Phys.*, **19**, 760 (1951). A factor $[1 + (N_{x_0} - N_x)f/N_{x_0}(1 - f)]$ is missing from the denominator of the first term on the left of their equation 6.

(14) The values for ρ_{a_0}, see Appendix, actually employed in the computer work were 1, 10 and 90; the last value was chosen to correspond to the approximate situation in natural carbon.

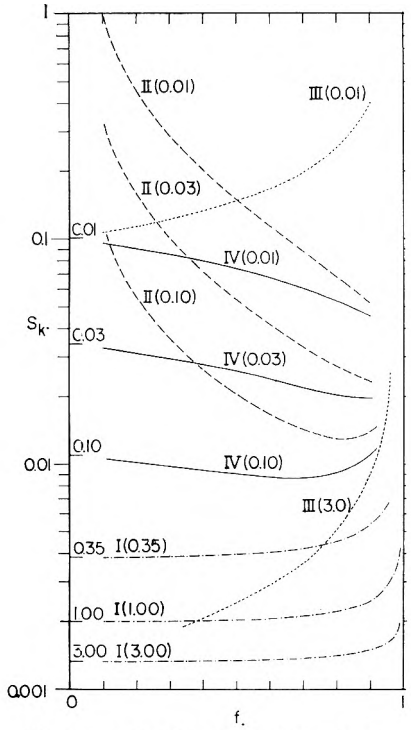

Fig. 1.—Maximum fractional deviation in $r - 1$, S_k, of equations I (- · - · - · -), II (- - - -), III (. . . .), IV (——), and (6) (short lines on the inside left edge of frame) as a function of f and $r - 1$ (arabic numbers) at $R_{a0} = 0.011111$.

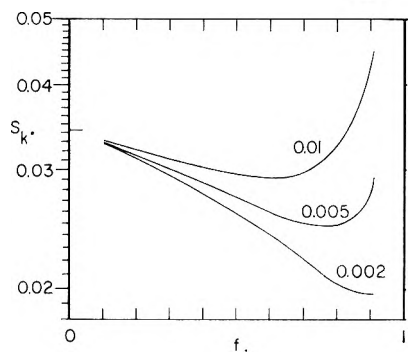

Fig. 2.—Maximum fractional deviation in $r - 1$, S_k, of equation IV as a function of f at $\Delta f/f$ levels of 0.01, 0.005 and 0.002; $R_{a0} = 0.011111$; $r - 1 = 0.03$. Corresponding S_k of equation 6 is 0.0343.

$\Delta R/R$ and $\Delta f/f$ of 0.0005 and 0.002, respectively. These error levels of 0.05% in an isotope ratio and 0.2% in the determination of a reaction coördinate have been found to be representative in the work carried out in this Laboratory. All computations were performed on the University of Illinois digital computer *Illiac*; the program was checked by hand computation to the same degree of precision (~8 decimal significant figures).

The calculated S_k values for $R_{a0} = 0.011111$ for equations 6, I, II, III and IV are summarized as functions of the reaction coördinate f in Fig. 1. In the calculation of S_k values for equation 6 we assume that the ratio R_{bt} is determined at a reaction coördinate sufficiently small that the approximation $t = 0$ does not introduce significant error.

Since the application of equation 6 requires the determination of only two quantities while the use of other equations requires three, and for some systems the two quantities involved in equation 6 are particularly convenient to determine, we base the following discussion on a comparison of the present four equations with equation 6.

At reaction coördinates of 0.5 or less the S_k values from equation I are between 1 and 1.05 times the S_k values from equation 6 for all values of r between 1.01 and 4.00 and all values of R_{a0} between 0.01 and 1. Results obtained by equation I are comparable in accuracy to those derived by equation 6. Equation I is the more useful, however, in the study of reactions involving large isotope effects. For example: if $r = 2$, $R_{a0} = 0.0111$, and $f = 0.5$, $S_k = 0.00204$; similarly, for $R_{a0} = 1$, $S_k = 0.00208$. In order to achieve a S_k value no larger than 0.00220 with equation 6 for $r = 2$, product collection must be stopped at reaction coördinates of 0.0004 and 0.0003 for R_{a0} values of 0.0111 and 1, respectively.

For small isotope effect ($r = 1.03$) equation II yields smaller S_k values at large reaction coördinates ($f \sim 0.7$) than the zero time approximation method, equation (6). Equation IV is even more advantageous than equations II and 6 at small isotope effect. For equation IV, the S_k values at some reaction coördinates are still smaller than those given by equation 6 even when the reaction coördinates are measured with 1% accuracy as illustrated in Fig. 2.

Equation III which involves a measurement of f in addition to other input data similar to those of equation 6 offers no advantage over equation 6.

The changes in S_k due to changes in R_{a0} are only significant at large isotope effect. The S_k values of equations I and III increase and those of equations II and IV decrease as R_{a0} is increased. The application of equation I is, therefore, more favorable the smaller the R_{a0}.

We have also calculated S_k' as defined in footnote 11 but found that the trends described in the above discussion are not seriously altered except in the case of equation I. The S_k' values from equation I at reaction coördinates of 0.5 or less are always slightly less than those obtained with equation 6 under the conditions considered.

Acknowledgment.—It is a pleasure to acknowledge the interest and assistance of Professors J. P. Nash and D. E. Muller of the Digital Computer Laboratory. This paper is based on research supported by the U. S. Atomic Energy Commission.

Appendix

Coefficients c_{ki} and Equations for g.—In the expressions summarized below all isotope ratios R appear as their reciprocals: $\rho_{a0} = 1/R_{a0}$, etc. The coefficients c_{ki} are defined by equation 16 above, while g is defined in equation 7; the signs given for the c_{ki} below are those which will yield the proper deviation in r if values of $\Delta\rho/\rho$ are inserted in equation 15 rather than values of $\Delta R/R$. The subscript $k = 0$ refers to the zero-time approximation method, equation 6; the subscripts $k = 1$, 2, 3 and 4, refer to equations I, II, III and IV, respectively. The second subscripts, $i = 1$, 2, 3 and 4, refer to the quantities $\Delta\rho_{a0}/\rho_{a0}$, $\Delta\rho_{at}/\rho_{at}$, $\Delta\rho_{bt}/\rho_{bt}$ and $\Delta f/f$, respectively.

Equation 6.—

$$C_{01} = -\frac{r}{r-1} \tag{21}$$

$$C_{03} = +\frac{r}{r-1} \tag{22}$$

Equation I.—

$$g = \frac{\rho_{bt} - \rho_{a0}}{\rho_{bt} - \rho_{at}} \tag{23}$$

$$C_{11} = \frac{1}{(r-1)\ln g}\left[\frac{(r-1)(1-g)}{g(1-g^{r-1})} - 1\right] \tag{24}$$

$$C_{12} = \frac{1}{(r-1)\ln g}\left[1 - \frac{(r-1)(1-g)g^{r-1}}{(1-g^{r-1})}\right] \tag{25}$$

$$C_{13} = \frac{-1}{(r-1)\ln g}\left[\frac{(r-1)(1-g)(1-g^{r})}{g(1-g^{r-1})}\right] \tag{26}$$

Equation II.—

$$g = \frac{(1-f)(\rho_{a0}+1)}{(\rho_{at}+1)} \tag{27}$$

$$C_{21} = \frac{-1}{(r-1)\ln g}\left(\frac{r\rho_{a0}+1}{\rho_{a0}+1}\right) \tag{28}$$

$$C_{22} = \frac{1}{(r-1)\ln g}\left(\frac{r\rho_{at}+1}{\rho_{at}+1}\right) \tag{29}$$

$$C_{24} = \frac{1}{(r-1)\ln g}\left[\frac{(r-1)f}{(1-f)}\right] \tag{30}$$

Equation III.—

$$g = 1 - \frac{(\rho_{a0}+1)f}{(\rho_{bt}+1)} \tag{31}$$

$$C_{31} = \frac{1}{(r-1)\ln g}\left[\frac{(1-g^{r}) + r(1-g)g^{r-1}\rho_{a0}}{g^{r}(\rho_{a0}+1)}\right] \tag{32}$$

$$C_{33} = \frac{-1}{(r-1)\ln g}\left[\frac{(1-g^{r}) + r(1-g)g^{r-1}\rho_{bt}}{g^{r}(\rho_{bt}+1)}\right] \tag{33}$$

$$C_{34} = \frac{-1}{(r-1)\ln g}\left[\frac{(1-g^{r}) - r(1-g)g^{r-1}}{g^{r}}\right] \tag{34}$$

Equation IV.—

$$g = \frac{(\rho_{bt}+1)(1-f)}{(\rho_{bt}+1) - (\rho_{bt}-\rho_{at})f} \tag{35}$$

$$C_{42} = \frac{1}{(r-1)\ln g}\left[\frac{(1-g^{r}) + r(1-g)\rho_{at}}{\rho_{at}+1}\right] \tag{36}$$

$$C_{43} = \frac{-1}{(r-1)\ln g}\left[\frac{(1-g^{r}) + r(1-g)\rho_{bt}}{\rho_{bt}+1}\right] \tag{37}$$

$$C_{44} = \frac{1}{(r-1)\ln g}\left[\frac{-(1-g^{r}) + r(1-g)}{1-f}\right] \tag{38}$$

GRADIENT ELUTION THEORY

By Edward C. Freiling

Nuclear and Physical Chemistry Branch, Chemical Technology Division, U. S. Naval Radiological Defense Laboratory, San Francisco 24, California

Received October 8, 1956

Freiling's theory of gradient elution has been extended to include the variation of the number of plates with increasing eluent strength. As before, three principal equations are derived. The first equation predicts the peak locations and is identical to that obtained previously. The second equation predicts peak shapes on the simplifying assumption of Gaussian shaped solute distribution on the column. Since the second equation is manageable only with difficulty, a third equation is derived which, while more approximate, is more easily handled. Tests of the theory were performed by eluting Na^{22} and Cs^{137} on Dowex-50 using HCl eluent. Calibration runs showed a reproducibility of 3% in peak location but only 30% in the number of plates. Gradient elution runs were next performed under a variety of conditions. Application of theory and calibration data to these results indicated that the peak locations could be predicted well within the experimental error. The shapes of the gradiently eluted peaks were calculated by both equations. Reasonably good agreement was obtained between the data and the exact equation over 98% of the elution history curve. Both exact and approximate formulas were found to give better fits of the leading edge than of the trailing edge. Goodness of fit appears to be lost more by two rapid elutions.

Introduction

Since the discovery of the technique,[1-3] gradient elution analysis (*i.e.*, elution chromatography with continuously varying eluent strength) has been applied successfully to numerous chromatographic separations. These include the separation of oligosaccharides,[4] organic acids[2,3,5-7] amino acids and peptides,[3,8,9] high polymer silicones,[10] sugar and sugar phosphates,[11] ketosteroids,[12] DNA,[13,14] nucleotides,[15] oxyhemoglobin,[16] purine bases,[17] rare earths,[18,19] alkali metals[20] and various other cations.[21] Initial theoretical work was primarily concerned with either the calculation of the influent concentration under various conditions of mixing[7,22-24] or qualitative discussion.[1,12]

(1) R. S. Alm, R. J. P. Williams and A. Tiselius, *Acta Chim. Scand.*, **6**, 826 (1952).

(2) K. O. Donaldson, V. J. Tulane and L. M. Marshall, *Anal. Chem.*, **24**, 185 (1952).

(3) H. Busch, R. B. Hurlburt and V. R. Potter *J. Biol. Chem.*, **196**, 717 (1952).

(4) R. S. Alm, *Acta Chim. Scand.*, **6**, 1186 (1952).

(5) L. M. Marshall, K. O. Donaldson and F. Friedberg, *Anal. Chem.*, **24**, 773 (1952).

(6) R. W. Scott, *ibid.*, **27**, 367 (1955).

(7) C. Mader, *ibid.*, **26**, 566 (1954).

(8) R. J. P. Williams, *Analyst*, **77**, 905 (1952).

(9) P. N. Campbell, S. Jacobs, T. S. Work and T. R. E. Kresman, *Chemistry and Industry*, 117 (1955).

(10) D. W. Bannister, C. S. G. Phillips and R. J. P. Williams, *Anal. Chem.*, **26**, 1451 (1954).

(11) C. W. Parr, *Biochem. J.*, **56**, xxvii (1954).

(12) T. K. Lakshmanan and S. Lieberman, *Arch. Biochem. Biophys.*, **53**, 258 (1954).

(13) A. Bendich, I. R. Fresco, H. S. Rosenkranz and S. M. Beiser, *J. Am. Chem. Soc.*, **77**, 3671 (1955).

(14) R. K. Main and L. J. Cole, paper presented at 129th Meeting of the American Chemical Society, April, 1956, Dallas, Texas.

(15) R. B. Hurlburt, H. Schmitz, A. F. Brumm and V. R. Potter, *J. Biol. Chem.*, **23**, 209 (1954).

(16) M. Morrison and J. L. Cook, *Science*, **122**, 920 (1955).

(17) K. Jackson, to be submitted to *Am. J. Physiol.*

(18) W. E. Nervik, This Journal, **59**, 690 (1955).

(19) L. R. Bunney, E. C. Freiling, L. D. McIsaac and E. M. Scadden, *Nucleonics*, **15**, No. 2, 81 (1957).

(20) B. Drake, *Arkiv. Kemi*, **8**, 189 (1955).

(21) M. Lederer, *Nature*, **172**, 727 (1953).

More recently, the theoretical details of chromatographic elution with a graded eluent have received closer attention. Freiling[25] has extended the batch equilibrium plate theory of Mayer and Tompkins[26] and Martin and Synge[27] to the case of varying eluent and arrived at equations for predicting peak locations and peak shapes. Simultaneously, Drake[28] formulated peak location equations for the cases of both linear and non-linear absorption of the gradient and solute substances. For the case of a non-absorbed gradient substance, Drake's peak location equation becomes identical to that of Freiling.

Freiling's peak shape equations were derived on the basis of a constant number of theoretical plates during the course of a gradient elution. Since this is in general not the case, they are of limited value.

In this communication the previous peak shape equations are first extended to the case of a varying number of plates. Experiments are described which were designed to test the equations derived by eluting a relatively loosely held solute (Na) and a relatively tightly held solute (Cs) under conditions of constant and variable eluent strength. Predictions based on constant strength elutions and theoretical considerations are compared with the results of gradient elutions and the results discussed.

Theoretical

The models to be considered in attacking this problem are those used already to describe constant strength elutions, namely, (1) equilibrated discontinuous bed with discontinuous flow, according to Mayer and Tompkins[26]; (2) equilibrated discontinuous bed with quasi-continuous flow, originated by Martin and Synge[27]; (3) equilibrated discontinuous bed with continuous flow developed by Glueckauf[29] and Said[30]; (4) unequilibrated discontinuous bed with continuous flow devised by Glueckauf,[31]; (5) unequilibrated continuous bed with continuous flow used by Vermeulen and Hiester.[32]

Because of the necessity of making P and C variables, and for the sake of simplicity, it was considered desirable to utilize the methods and results of models 1 and 2. The following notation is used:

L = column length
C = equilibrium ratio of fraction of solute in resin phase to fraction of solute in liq. phase in any given plate of the column
P = no. of theoretical plates $P = P(C)$
ΔF = vol. increment of eluent in free column vols.
F = total vol. of eluent leaving column in free column vols.
F_e = value of F for which $t^2 = 2$
F_f = value of F at the peak solute concn. in the effluent
l = distance down the column
t = Gaussian distribution parameter
C_f = value of C at the peak solute concn. in the effluent

Consider a column of length L containing a unit amount of solute adsorbed on an infinitesimally thin layer at the top. Let a volume increment of eluent $(\Delta F)_1$ be put through the column and followed by a neutral solution which does not effect the solute distribution. Let P_1 and C_1 be the values of P and C for eluent of this strength. Proceeding on the Mayer–Tompkins assumptions of batch equilibrium and linear isotherms one finds as in the previous treatment (ref. 25) that the peak solute concentration has moved down the column a distance

$$l_1 = \frac{L(\Delta F)_1}{C_1}$$

and has a distribution given approximately by

$$t_1^2 = \frac{P_1 C_1^2 (l - l_1)^2}{(\Delta F)_1 L^2 (1 + C_1)}$$

Consider, now, a second column through which is put a volume increment $(\Delta F)_{1,2}$ of an eluent of strength C_2 and for which the number of plates is P_2. If $(\Delta F)_{1,2}$ is so chosen that the resulting solute distribution is the same as in the previous case

$$t_1^2 = t_{1,2}^2$$

from which it follows that

$$(\Delta F)_1 \frac{(1 + C_1)}{P_1 C_1^2} = (\Delta F)_{1,2} \frac{(1 + C_2)}{P_2 C_2^2}$$

This situation is illustrated by Fig. 1.

If a volume increment $(\Delta F)_2$ of the second eluent is now put through each column, the distribution will be the same in each case and be given by

$$t_2^2 = \frac{P_2 C_2^2 (l - l_2)^2}{[(\Delta F)_{1,2} + (\Delta F)_2]\, L^2 (1 + C_2)} = \frac{(l - l_2)^2}{\left[(\Delta F)_1 \frac{(1 + C_1)}{P_1 C_1^2} + (\Delta F)_2 \frac{(1 + C_2)}{P_2 C_2^2}\right] L^2}$$

while the distance of the peak in the first column is now

$$l_2 = L\left[\frac{(\Delta F)_1}{C_1} + \frac{(\Delta F)_2}{C_2}\right]$$

The movement of the peak down the column is illustrated by Fig. 2. Generalizing

$$l_n = L\Sigma \frac{(\Delta F)_n}{C_n}$$

$$t_n^2 = \frac{(l - l_n)^2}{L^2 \Sigma \frac{(1 + C_n)}{P_n C_n^2} \Delta F_n}$$

As the volume increments become infinitesimal the equations become

$$1 = L \int_0^F dF/C$$

$$t^2 = \frac{(l - l_n)^2}{L^2 \int_0^F \frac{(1 + C)}{PC^2} dF}$$

As in the previous derivation (ref. 25) it is found that when $F = F_f$ and $1 = L$ the peak location is given by

(22) T. K. Lakshmanan and S. Lieberman, *Arch. Biochem. Biophys.*, **45**, 235 (1953).

(23) A. Cherkin, F. E. Martinez and M. S. Dunn, *J. Am. Chem. Soc.*, **75**, 1244 (1953).

(24) M. Bock and N. Ling, *Anal. Chem.*, **26**, 1543 (1954).

(25) E. C. Freiling, *J. Am. Chem. Soc.*, **77**, 2067 (1955).

(26) S. W. Mayer and E. R. Tompkins, *ibid.*, **69**, 2866 (1947).

(27) A. V. P. Martin and R. L. M. Synge, *Biochem. J.*, **35**, 1358 (1941).

(28) B. Drake, *Arkiv. Kemi*, **8**, 1 (1955).

(29) E. Glueckauf, *Trans. Faraday Soc.*, **51**, 34 (1955).

(30) A. S. Said, *J. A. I. Ch. E.*, **2**, 477 (1956). Said extends his theory to gradient elution assuming a constant number of plates, arriving at a peak location equation identical to Freiling's and Drake's and an equation for peak shapes

(31) E. Glueckauf, *Soc. Chem. Industry*, 27 (1954).

(32) T. Vermeulen and N. K. Hiester, *Ind. Eng. Chem.*, **44**, 636 (1952).

$$1 = \int_0^{F_f} dF/C \qquad (1)$$

The elution history curve is easily obtained by calculating the amount of solute which has passed from the end of the resin bed on to an imaginary extension as shown in Fig. 3. Here l is replaced by L and l_n by

$$\int_0^F dF/C$$

Then

$$t^2 = \left[\int_{F_f}^{F} \frac{dF}{C}\right]^2 \left[\int_0^F \frac{1 + C}{PC^2} dF\right]^{-1} \qquad (2)$$

A less exact but more easily manageable equation can be obtained by approximating the elution curve with a normal error curve, using the slope of eq. 2 at F_f

$$\left(\frac{dF}{dt}\right)^2_{F=F_f} = C_f^2 \int_0^{F_f} \frac{1 + C}{PC^2} dF \qquad (3)$$

Although this type of approximation has been successfully used by a number of investigators,[26,27,29-32] its application to gradient elution history curves must be made with caution, as the results will show.

When an arithmetic-probability plot of the data is made, eq. 3 predicts the slope of the tangent to the curve at the peak. Equation 2 predicts that the actual points obtained with an increasing concentration should lie above this tangent on both side of the peak, the degree of departure being greater for steeper gradients. For the decreasing concentration gradient, the reverse would be expected.

Equation 3 reduces to Matheson's equation when P and C are constant, t^2 is taken as 2 and F as F_e. Equation 2 does not reduce to Mayer and Tompkins' equation

$$t^2 = \frac{P(F - C)^2}{C(1 + C)}$$

but to

$$t^2 = \frac{P(F - C)^2}{F(1 + C)}$$

because the assumption here is that the solute distribution on the column is Gaussian after the eluent is removed, while Mayer and Tompkins assumed a Gaussian shape while the eluent was still present in the column.

Experimental

Column.—The ion-exchange column used in these experiments was constructed from 6 mm. i.d. glass tubing fitted with a stopcock on the bottom and a 50-ml. reservoir at the top. The glass tubing was calibrated with water at 0.5-cc. intervals to determine the cross-sectional area, which was 0.24 cm.^{2}. The resin bed was made from analytical grade Dowex-50 in the H^+ form (purchased from Bio-Rad Laboratories, Berkeley, Calif.) and graded to settle at the rate of 7 min./in. The bed depth was 14 cm. and the free column volume 1.34 ml. The drop size was measured at various flow rates so that drops could be converted to free column volumes.

Reagents.—The absorbates used were carrier free solutions of Na^{22} and Cs^{137}, purchased from Oak Ridge.

Eluents were made from C.P. grade HCl diluted with distilled water.

Conduct of Runs.—Prior to a run the column was washed free of acid with distilled water until the pH of the wash was reduced to 5. Supernatant water was then withdrawn and microliter quantities of tracers added to the top of the column in such a manner that contact with the glass tubing

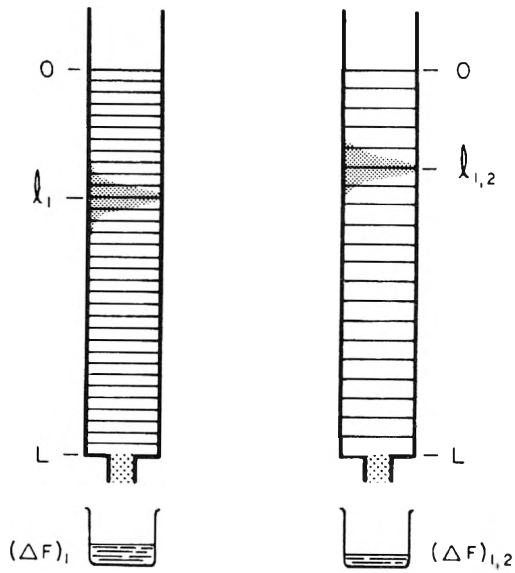

Fig. 1.—Comparison of actual and equivalent columns.

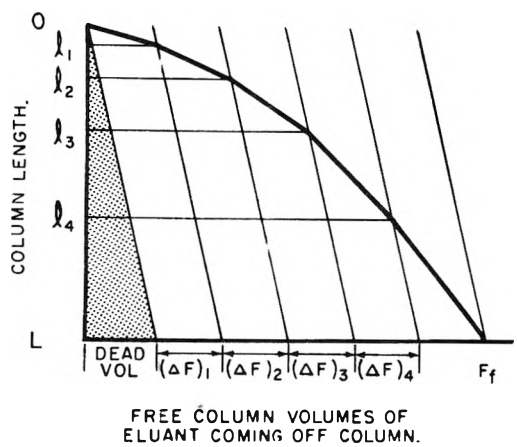

Fig. 2.—Progress of solute in a stepwise elution.

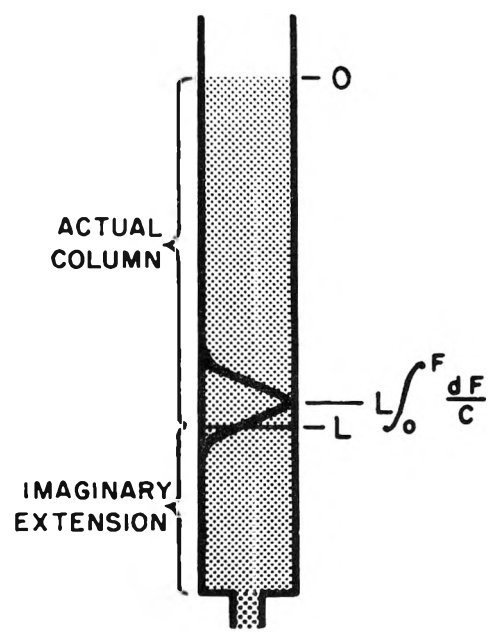

Fig. 3.—Use of imaginary column extension to calculate peak shape.

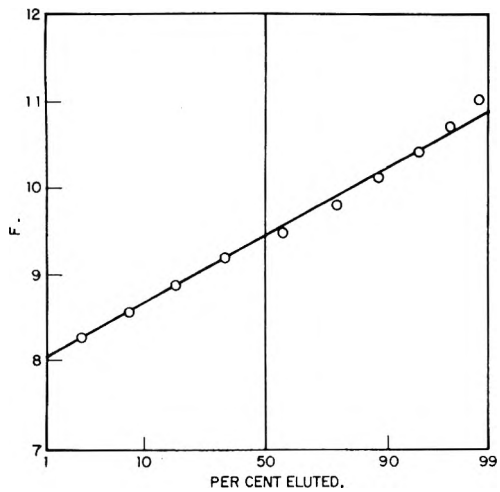

Fig. 4.—Arithmetic-probability plot of Cs peak in run 10.

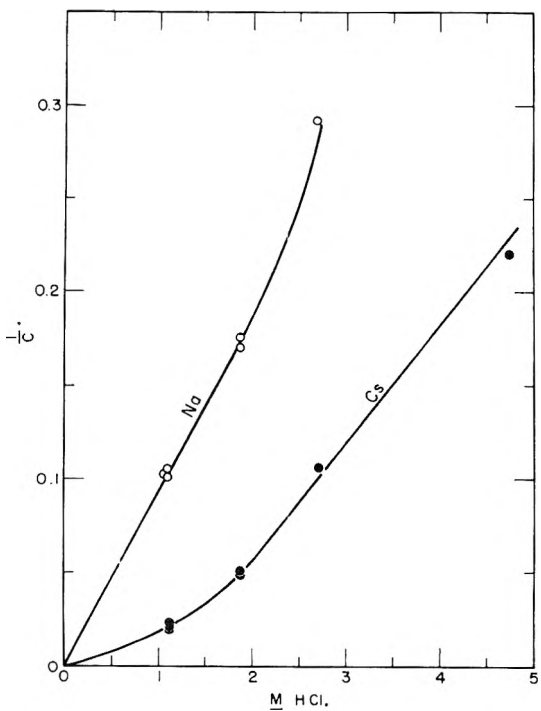

Fig. 5.—Value of $1/C$ for Na and Cs as a function of HCl concentration.

was kept at a minimum. The tracers were allowed to sink into the resin bed and these were followed by two or three water washes to bring any residual tracers down into the column. There followed two or three washes of the exposed glass stem with eluent, which was pipetted out of the top of the column, to free the walls of adhering activity. The reservoir was next filled with eluent and the column allowed to drip under its own head at a rate of about 80 sec./drop or 0.14 cm./min. The reservoir was fitted with a capillary tube air inlet to prevent change in eluent concentration by evaporation during the course of a run. Three drop fractions were then collected in test-tubes using a drop counting fraction collector. In the calibration runs, initial test-tubes each contained a scrap of *p*H paper so that the presence of acid in the effluent was sharply signalled by the color change. The fraction size was then altered to some more expedient number of drops. The quantity of tracer in each fraction was measured by counting the tubes in a well-type γ-ray scintillation counter. The eluent concentrations in the gradient elution runs were determined by titration.

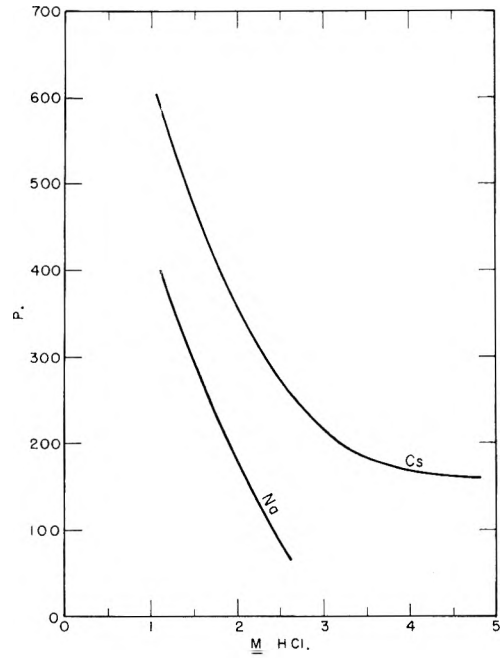

Fig. 6.—Number of plates for Na and Cs as a function of HCl concentration.

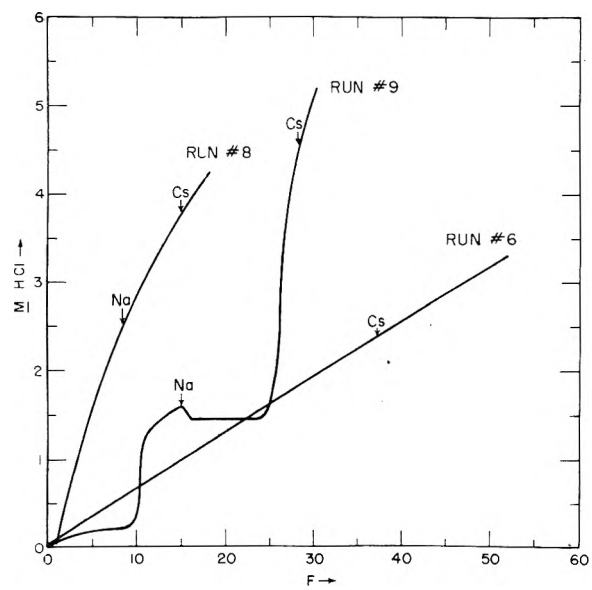

Fig. 7.—Normality of HCl *vs.* volume in free column volume units for the gradient elution runs. Positions of eluted peaks are indicated with arrows.

Results and Discussion

The first three runs were performed at a flow rate of 15 sec./drop. Arithmetic-probability plots of these runs indicated that tailing ensued when only 80–85% of the activity had been removed from the column. In order to reduce the tailing, the remaining runs were carried out at flow rates in the neighborhood of 100 sec./drop. Tailing was thereby reduced to the order of 5–10%. From the initial runs, however, it was established that the degree of reproducibility was approximately 3% for C and 30% for P. The values of C and P were determined from arithmetic-probability plots as described in ref. 25 and illustrated by a typical example in Fig. 4.

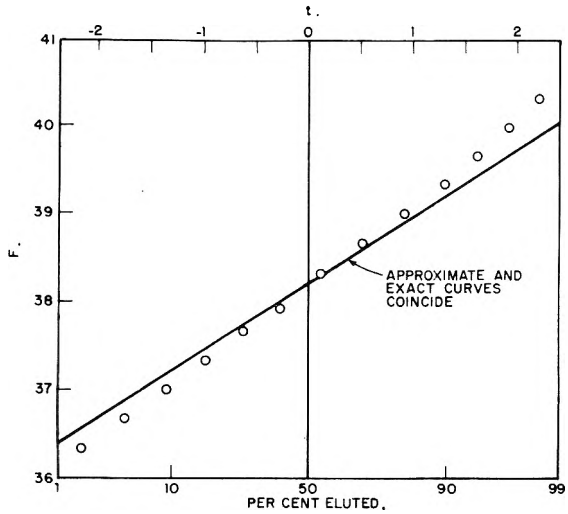

Fig. 8.—Arithmetic-probability plot of Cs peak obtained in run 6. Solid line calculated by eq. 2 or eq. 3.

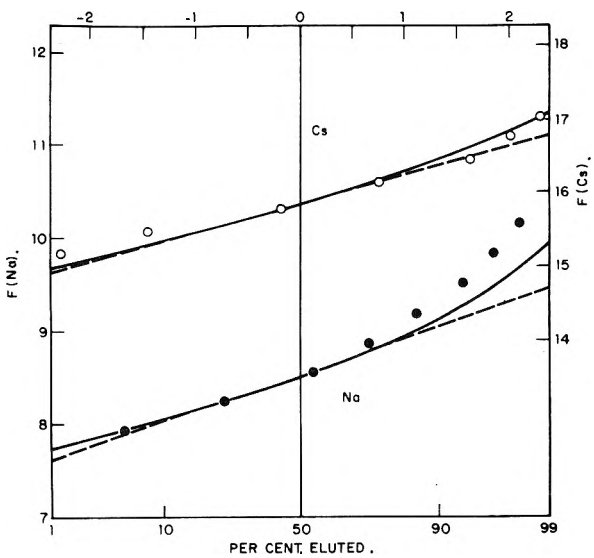

Fig. 9.—Arithmetic-probability plot of Na and Cs peaks obtained in run 8; solid lines calculated by eq. 2; dashed lines by eq. 3.

The results of the calibration runs are summarized in Table I and illustrated in Figs. 5 and 6. Since the value of C did not vary with flow rate, the C values obtained for the first three runs are included in Fig. 5.

Three gradient elution runs were performed. The shapes of the gradients, as shown in Fig. 7, cover a wide variety of conditions. Run 6 was performed with a relatively slow increase in HCl concentration, run 8 with a relatively sharp increase, and run 9 is essentially a stepwise elution with the Na eluting on a flat portion and the Cs

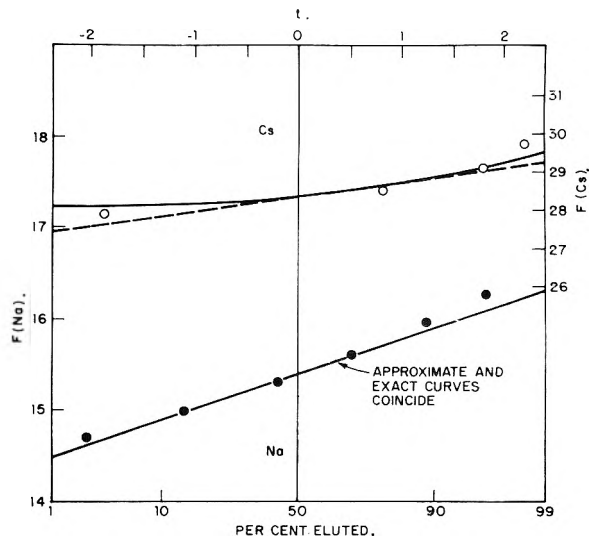

Fig. 10.—Arithmetic-probability plot of Na and Cs peaks obtained in run 9; solid lines calculated by eq. 2; dashed lines by eq. 3.

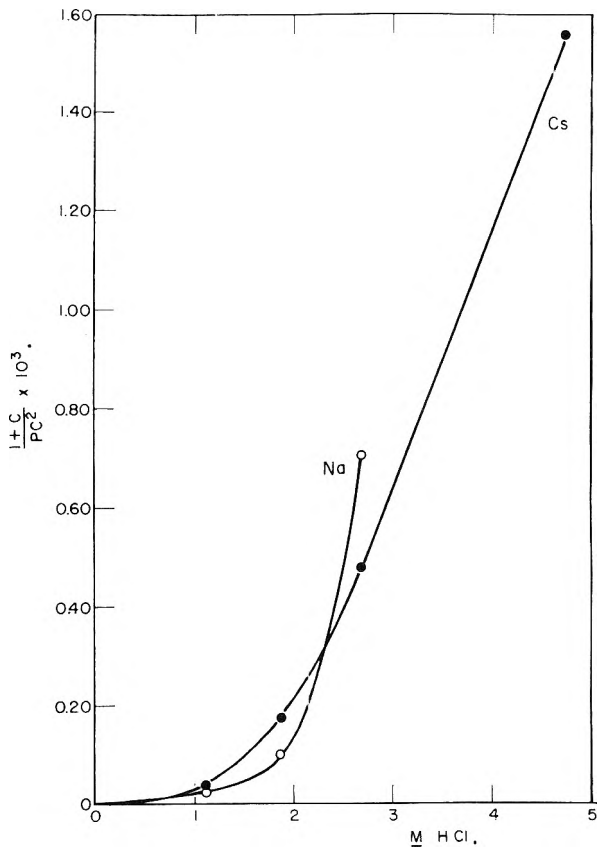

Fig. 11.—The value of $(1 + C)/PC^2$ as a function of HCl concentration for Na and Cs.

TABLE I

CALIBRATION RUN RESULTS

Run	HCl concn. (M)	Flow rate (sec./drop)	Na Peak C	Na Peak P	Cs Peak C	Cs Peak P
5	1.10	80	9.90	400	45.1	600 ± 200
4	1.87	80	5.68	210	20.0	450
10	2.68	100	3.43	53 ± 13	9.39	250
7	4.74	80	...	..	4.56	170

TABLE II

COMPARISON OF CALCULATED AND OBSERVED PEAK LOCATIONS FOR THE GRADIENT ELUTION RUNS

Run	Flow rate (sec./drop)	Na peak location: Predicted F_f	Na peak location: Obsd. F_f	Na peak location: Error, %	Cs peak location: Predicted F_f	Cs peak location: Obsd. F_f	Cs peak location: Error, %
6	100	...	...	...	38.2	37.4	+2.1
8	120	8.47	8.50	−0.4	15.0	14.9	+0.7
9	100	15.9	15.4	+3.2	27.7	28.4	−2.5

eluting on a very steep portion. Arithmetic-probability plots of the peaks obtained with these runs are shown in Figs. 8, 9 and 10.

In order to test the reliability of eq. 1, graphs of $1/C$ *vs.* F were prepared for the gradient elutions. The values of F at unit area were determined by graphical integration and compared with the values obtained from the arithmetic-probability plots. Observed values obtained in this manner are actually center of mass locations. The results are given in Table II and show agreement well within the experimental error in all cases.

Calculations based upon eq. 2 and 3 were obtained by plotting $(1 + C)/PC^2$ *vs.* F for each run and integrating graphically to F_f. The variation of $(1 + C)/PC^2$ with HCl concentration is shown in Fig. 11. From the shape of this curve it can be seen that differences between experimental and assumed conditions at the initial stages of a run are minimized by the relatively low value of the function for low HCl concentrations. For most cases the application of eq. 2 could be simplified by using the equation

$$t^2 = \frac{\left\{(F - F_f)\left[\frac{1}{C_f} + K(F - F_f)\right]\right\}^2}{\int_0^{F_f} \frac{1 + C}{PC^2}\,dF + (F - F_f)\left[\frac{1 + C_f}{P_f C_f^2} + K^1(F - F_f)\right]}$$

where K and K^1 are the half slopes of the $1/C$ *vs.* F and $(1 + C)/PC^2$ *vs.* F curves respectively at F_f.

In Figs. 8, 9 and 10, theoretical curves based on eq. 2 are shown as solid lines, while those based on eq. 3 are shown as dashed lines. In general reasonably good fits are obtained, the goodness of fit increasing with F_f. The leading edges of the curve generally show better fit than the trailing edges, as would be expected from the tailing found in the calibration runs.

The greatest source of error in this work is obviously the poor plate reproducibility. This irreproducibility appears to stem from three sources: the difficulty of controlling the flow rate, the variations inherent in the technique, and the interpretations of arithmetic probability curves which are complicated by tailing and minor fluctuations. The magnitude of the last limitation, when present, is indicated by the plus-or-minus figures in Table I. Evidently more testing with improved experimental conditions is in order. Resin of lower cross linkage, elevated temperatures, and better flow rate control should do much to reduce the errors.

The degree of experimental approach to the assumed equilibrium conditions is best illustrated by reference to Glueckauf's "Ion Exchange and its Application."[31] According to Fig. 9 of this report, the gradient elution runs were begun under conditions in the effective equilibrium zone, but decreasing C gradually shifted them to the particle diffusion zone.

From a practical point of view, the present theory would be best utilized in predicting peak locations from distribution curves obtained by equilibrations. The availability of Glueckauf's theory[31] for predicting H.E.T.P. should materially reduce the number of necessary column calibrations. Development of empirical formulas for the indicated functions would eliminate the need for graphical integration.

Acknowledgment.—The author is indebted to Dr. E. R. Tompkins for valuable advice and encouragement.

ELECTROLYTE THEORY AND THE DONNAN MEMBRANE EQUILIBRIUM

BY TERRELL L. HILL

Naval Medical Research Institute, Bethesda, Md.

Received October 11, 1956

In Sec. II, an earlier Donnan method calculation of the osmotic pressure second virial coefficient, in the Donnan membrane equilibrium, is extended to ions of finite size. It is found, as before, that this coefficient disagrees with the corresponding result from the McMillan–Mayer method. The discrepancy is attributed to missing higher terms in the Debye–Hückel interionic potential of average force. In Sec. III, formal and exact equations are given which show that one can view refinements in the Debye–Hückel theory in terms of the introduction of "local activity coefficients." In Sec. IV, an intuitive and semi-empirical argument is used to illustrate the application of local activity coefficients and to obtain a refinement of the Debye–Hückel interionic potential of average force. Although not satisfactory in some other respects, this potential gives the same osmotic pressure second virial coefficient in the Donnan equilibrium problem as does the Donnan method. It is pointed out that local activity coefficients might also prove useful in problems involving double layers, adsorption, surface tension, etc.

I. Introduction

The osmotic pressure second virial coefficient in the Donnan membrane equilibrium can be calculated[1] (1) by equating the electrochemical potentials of diffusible ions on the two sides of the membrane (Donnan method), using Debye–Hückel activity coefficients, or (2) from the McMillan–Mayer solution theory, using the Debye–Hückel potential of average force between a pair of non-diffusible ions. In Sec. II we extend our earlier[1] Donnan method calculation of the second virial coefficient to ions of finite size and find, as before, that this coefficient disagrees with the corresponding result obtained from the McMillan–Mayer method. The discrepancy is attributed to missing higher terms in the interionic potential of average force. In Sec. III we give formal and exact equations showing that one can view refinements in the

(1) T. L. Hill, *Disc. Faraday Soc.*, **21**, 31 (1956); *J. Chem. Phys.*, **22**, 1251 (1954).

Debye–Hückel theory in terms of the introduction of "local activity coefficients." Incidentally, this approach provides a very simple way of deriving the basic integral equations of Kirkwood's theory of fluid mixtures.[2,3] Finally, in Sec. IV, we use a strictly intuitive argument, based on the concept of "local activity coefficients," to obtain, as an illustration, a refinement of the Debye–Hückel interionic potential of average force. Although not completely satisfactory in other respects, this new potential gives the same osmotic pressure second virial coefficient in the Donnan equilibrium problem as does the Donnan method.

II. Osmotic Pressure Second Virial Coefficient in the Donnan Equilibrium.—We consider a Donnan equilibrium in which the j-th species of diffusible ion (valence z_j) has a concentration c^0_j on the "outside" of the membrane and c_j on the "inside"; there is also a non-diffusible species of valence z and concentration ρ on the inside. The outside electrolyte is assumed dilute enough to follow the Debye–Hückel theory. All ions are considered hard spheres of diameter a and are immersed in a continuous medium of dielectric constant D (see Fig. 1). The membrane potential is $\psi = \psi_{in} - \psi_{out}$.

On equating inside and outside electrochemical potentials for the j-th species, we have

$$c_j \gamma_{j(in)} e^{z_j \epsilon \psi / kT} = c^0_j \gamma_{j(out)} \tag{1}$$

where

$$\ln \gamma_{j(out)} = -\frac{z_j^2 \epsilon^2 \kappa}{2DkT(1 + \kappa a)} + \frac{4\pi a^3 c^0}{3} \tag{2}$$

$$\ln \gamma_{j(in)} = -\frac{z_j^2 \epsilon^2 \kappa_{in}}{2DkT(1 + \kappa_{in} a)} + \frac{4\pi a^3}{3}\left(\sum_s c_s + \rho\right) \tag{3}$$

and we have introduced the definitions

$$\kappa^2 = \frac{4\pi\epsilon^2 \Sigma_2}{DkT} \tag{4}$$

$$\kappa^2_{in} = \frac{4\pi\epsilon^2}{DkT}\left(\sum_s c_s z_s^2 + \rho z^2\right) \tag{5}$$

$$c^0 = \sum_s c^0_s \qquad \Sigma_n = \sum_s c^0_s z_s^n$$

The terms in a^3 in eq. 2 and 3 are "hard sphere" corrections for a dilute solution.[4]

In order to ensure that the inside solution is also sufficiently dilute to follow the Debye–Hückel theory, we use expansions in powers of ρ and retain linear terms only. Also, to be consistent with the well-known linearization introduced in the derivation of the Debye–Hückel equations, we use only linear terms in α, where

$$\alpha = \epsilon^2 \kappa / DkT$$

We write

$$c_j = c^0_j + a_j \rho + \ldots \tag{6}$$

$$\epsilon\psi/kT = A\rho - \ldots \tag{7}$$

where A and the a_j are to be determined. Substitution of these series in eq. 1 and expansion of the exponentials leads to

(2) J. G. Kirkwood, *J. Chem. Phys.*, **3**, 300 (1935).

(3) T. L. Hill, "Statistical Mechanics," McGraw-Hill Book Co., Inc., New York, N. Y., 1956, Chap. 6.

(4) R. H. Fowler and E. A. Guggenheim, "Statistical Thermodynamics," Cambridge, 1939, eq. 704, 5. These terms also follow from λ_i in eq. 26 and 40.

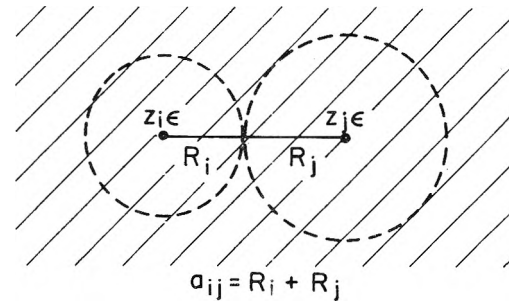

Fig. 1.—Ions of types i and j in contact in continuous dielectric medium. For most purposes we take all ions of same size, $a = 2R$.

$$c_j = c^0_j + a_j\rho + \ldots = c^0_j\left[1 - z_j A\rho + \frac{z_j^2\beta(z^2 + \Sigma)\rho}{4\Sigma_2} - \frac{4\pi a^3 S\rho}{3} + \ldots\right] \tag{8}$$

where

$$\beta = \frac{\alpha}{(1 + \kappa a)^2} \qquad \Sigma = \sum_s a_s z_s^2 \qquad S = 1 + \sum_s a_s$$

Thus, from eq. 8

$$a_j = -z_j A c^0_j + \frac{z_j^2\beta(z^2 + \Sigma)c^0_j}{4\Sigma_2} - \frac{4\pi a^3 S c^0_j}{3} \tag{9}$$

Now we sum eq. 9 over j (a) as it stands, (b) after multiplication by z_j, and (c) after multiplication by z_j^2. These summations lead, respectively, to the linear equations in S, Σ and A

$$S - \frac{\beta}{4}\Sigma = 1 + \frac{\beta z^2}{4} \tag{10}$$

$$\frac{\beta\Sigma_3}{4\Sigma_2}\Sigma - \Sigma_2 A = -z - \frac{\beta z^2 \Sigma_3}{4\Sigma_2} \tag{11}$$

$$\frac{4\pi a^3}{3}\Sigma_2 S + \left(1 - \frac{\beta\Sigma_4}{4\Sigma_2}\right)\Sigma + \Sigma_3 A = \frac{\beta z^2 \Sigma_4}{4\Sigma_2} \tag{12}$$

We neglect terms of order $4\pi a^3 c^0/3$ compared to unity (dilute solution). The solution of eqs. 10–12 is

$$S = 1 + \frac{\beta}{4}\left(z^2 - z\frac{\Sigma_3}{\Sigma_2}\right) \tag{13}$$

$$\Sigma = -z\Sigma_3/\Sigma_2 \tag{14}$$

$$A = \frac{z}{\Sigma_2} + \frac{\beta\Sigma_3}{4\Sigma_2^2}\left(z^2 - z\frac{\Sigma_3}{\Sigma_2}\right) \tag{15}$$

Eq. 7 and 15 give the membrane potential, and the second virial coefficient is,[1] from eq. 9

$$B_2 = -\frac{1}{2}\frac{a_j}{c^0_j}(z_j = z) = \frac{2\pi a^3}{3} + \frac{z^2}{2\Sigma_2} - \frac{\alpha}{8\Sigma_2(1 + \kappa a)^2}\left(z^2 - z\frac{\Sigma_3}{\Sigma_2}\right)^2 \tag{16}$$

Turning now to the McMillan–Mayer method, we have seen[1] already that the Debye–Hückel potential of average force

$$\frac{W(r)}{kT} = +\infty \qquad r < a$$

$$= \frac{z^2\epsilon^2 e^{-\kappa(r-a)}}{DrkT(1 + \kappa a)} \qquad r \geq a \tag{17}$$

when substituted in

$$B_2 = -2\pi\int_0^\infty [e^{-W(r)/kT} - 1]\, r^2\, dr \tag{18}$$

gives

$$B_2 = \frac{2\pi a^3}{3} + \frac{z^2}{2\Sigma_2} - \frac{\alpha z^4}{8\Sigma_2(1 + \kappa a)^2} \tag{19}$$

This differs from eq. 16 through the omission of the terms in $z^2\alpha$ and $z^3\alpha$.

Because it is possible to obtain B_2 in the Donnan method without going beyond linear terms in ρ and α, we can have confidence in eq. 16. On the other hand, as Mayer has pointed out in another connection,[5] higher terms in eq. 17 will contribute to the virial coefficients, including possibly B_2. This will be illustrated in Sec. IV where we find that α^2 terms in $e^{-W/kT}$ lead to α terms in B_2 by the McMillan–Mayer method while α^2 terms in γ_j (from α^2 terms in $e^{-W/kT}$) lead to α^2 terms in B_2 by the Donnan method. This is at once an advantage of the Donnan method and a way of checking the self-consistency of the α and α^2 terms in $e^{-W/kT}$.

III. Electrolyte Theory—General.—We are specifically interested here in spherically symmetrical electrolyte ions, so we restrict the general argument to monatomic molecules. However, the extension to the polyatomic case is straightforward.[2,3]

We write the Helmholtz free energy as $A = A' + A^e$ where A' would be the free energy in the absence of intermolecular forces. Then

$$\mu_i = \partial A/\partial N_i = \mu_i' + \mu_i^e \tag{20}$$

where

$$\mu_i' = \mu_i^\circ + kT \ln c_i^0 \tag{21}$$

$$\mu_i^e = kT \ln \gamma_i \tag{22}$$

Eq. 21 gives the "ideal" chemical potential and γ_i is an activity coefficient which corrects for the effects of intermolecular forces. Also

$$\mu_i^e = \partial A^e/\partial N_i = A^e(N_i) - A^e(N_i - 1) = W_i^e \tag{23}$$

where W_i^e is the isothermal, reversible work that has to be done against intermolecular forces in order to add one more molecule of species i to the system.

Let $u_{is}(r)$ be the interaction energy between a molecule of species i and one of species s. Let ξ_i be a coupling or "charging" parameter such that $\xi_i u_{is}(r)$ is the interaction energy when the i molecule is coupled to the extent ξ_i.

In electrolyte theory

$$u_{is}(r) = +\infty \qquad r < a_{is}\,, \tag{24}$$
$$= \frac{z_i z_s \epsilon^2}{Dr} \qquad r \geq a_{is}$$

where u_{is} is actually a free energy. For present purposes, however, the solvent is treated as a continuum of dielectric constant D and not one of the molecular components of the system. The model of an ion of type i implicit here is a point charge immersed in the dielectric continuum with a hard shell of radius a_i centered about the point charge (see Fig. 1).

The average number of molecules of species s in the element of volume $d\mathbf{r}_s$ in the neighborhood of a partially coupled molecule of species i is

$$c^0{}_s e^{-W_{is}(r_{is},\xi_i)/kT} d\mathbf{r}_s \tag{25}$$

where W_{is} is the potential of average force.[2,3] The contribution to W_i^e, arising from interactions with these molecules, when ξ_i is increased by $d\xi_i$, is (25) multiplied by $u_{is}(r_{is})d\xi_i$. Therefore, if we integrate over $\mathbf{r}_s$ and ξ_i, and sum over s, we have

$$W_i^e = kT \ln \gamma_i = \sum_s c^0{}_s \int_0^1 \int_V u_{is} e^{-W_{is}(\xi_i)/kT} d\mathbf{r}_s d\xi_i \tag{26}$$

Now consider an element of volume $d\mathbf{r}$ near a fixed molecule of species j (chosen as origin of the coördinate system for $\mathbf{r}$ and $\mathbf{r}_s$), and the equilibrium between i molecules in $d\mathbf{r}$ and i molecules at a very large distance from the fixed j molecule. We can write

$$\mu_i(\infty) = \mu^0{}_i + kT \ln c^0{}_i + kT \ln \gamma_i$$
$$= \mu_i(r) = \mu^0{}_i + kT \ln c_i{}^j(r) + kT \ln \gamma_i{}^{*j}(r) + u_{ij}(r) \tag{27}$$

where $c_i{}^j$ is the average concentration of i molecules in $d\mathbf{r}$, $\gamma_i{}^{*j}$ is a "local activity coefficient," and u_{ij} is included because we are considering a concentration equilibrium in the field of the fixed j molecule (analogous to, say, a gravitational field). The term in $\gamma_i{}^{*j}$ in eq. 27 represents the work that has to be done against intermolecular forces (excluding the fixed j molecule) in order to add an i molecule to the system at $\mathbf{r}$.

The average number of s molecules in $d\mathbf{r}_s$, when a j molecule is fixed at the origin and a partially coupled i molecule is at $\mathbf{r}$, is

$$c^0{}_s e^{-W^s{}_{ij}(\mathbf{r},\mathbf{r}_s,\xi_i)/kT} d\mathbf{r}_s$$

where $W^s{}_{ij}$ is an unsymmetrical[2,6] potential of average force. Then the total work of coupling or "charging" i at $\mathbf{r}$ is

$$kT \ln \gamma_i{}^{*j}(r) = \sum_s c^0{}_s \int_0^1 \int_V u_{is}\, e^{-W^s{}_{ij}(\xi_i)/kT} d\mathbf{r}_s d\xi_i \tag{28}$$

From eq. 27

$$c_i{}^j(r) = \frac{c^0{}_i \gamma_i e^{-u_{ij}(r)/kT}}{\gamma_i{}^{*j}(r)} \tag{29}$$

We also have the relation

$$c_i{}^i(r) = c^0{}_i e^{-W_{ij}(r)/kT} \tag{30}$$

On combining eq. 29 and 30, we obtain

$$\frac{W_{ij}(r)}{kT} = \frac{u_{ij}(r)}{kT} + \sum_s c^0{}_s \int_0^1 \int_V \frac{u_{is}}{kT}$$
$$[e^{-W^s{}_{ij}(\xi_i)/kT} - e^{-W_{is}(\xi_i)/kT}] d\mathbf{r}_s d\xi_i \tag{31}$$

This is the basic integral equation for the pair potential of average force (or the negative of the logarithm of the distribution function) in Kirkwood's theory.[2,3] By choosing a group of fixed molecules (instead of just one j molecule), analogous equations[3] in higher distribution functions can also be deduced. The introduction of a local activity coefficient provides a relatively simple derivation of eq. 31, and an alternative approach to electrolyte theory, which we now point out.

Electrolyte Solutions.—The same equilibrium as in eq. 27 may be considered, but here it is more convenient to write

$$\mu_i(\infty) = \mu_i{}^0 + kT \ln c_i{}^0 + kT \ln \gamma_i$$
$$= \mu_i(r) = \mu_i{}^0 + kT \ln c_i{}^j(r) + kT \ln \gamma_i{}^j(r)$$
$$+ z_i \epsilon \psi_j(r) \tag{32}$$

where $\psi_j(r)$ is the mean electrostatic potential at $\mathbf{r}$, a distance r from the fixed j ion, with $\psi_j(\infty) = 0$. This defines a new "local activity coefficient" $\gamma_i{}^j$

(5) J. E. Mayer, *J. Chem. Phys.*, **18**, 1426 (1950).

(6) See pp. 186–188 of ref. 3: $e^{-W^s{}_{ij}/kT} = g^{(3)}(\mathbf{r}_i, \mathbf{r}_j, \mathbf{r}_s)$.

analogous to the "bulk" activity coefficients conventionally used with electrostatic potentials in electrochemical systems. Of course γ_i^j and γ_i^{*j} must be related by

$$\gamma_i^j(r)e^{z_i\epsilon\psi_j(r)/kT} = \gamma_i^{*j}(r)e^{u_{ij}(r)/kT} \quad (33)$$

From eq. 32, and corresponding to eq. 29

$$c_i^j(r) = \frac{c_i^0\gamma_i e^{-z_i\epsilon\psi_j(r)/kT}}{\gamma_i^j(r)} \quad (34)$$

The Poisson–Boltzmann equation for $\psi_j(r)$ is, from eq. 30

$$\nabla^2\psi_j(r) = -\frac{4\pi\epsilon}{D}\sum_s z_s c_s^j(r) = -\frac{4\pi\epsilon}{D}\sum_s z_s c_s^0 e^{-W_{sj}(r)/kT} \quad (35)$$

Alternatively, from eq. 34

$$\nabla^2\psi_j(r) = -\frac{4\pi\epsilon}{D}\sum_s \frac{z_s c_s^0\gamma_s e^{-z_s\epsilon\psi_j(r)/kT}}{\gamma_s^j(r)} \quad (36)$$

whereas the approximate equation

$$\nabla^2\psi_j(r) = -\frac{4\pi\epsilon}{D}\sum_s z_s c_s^0 e^{-z_s\epsilon\psi_j(r)/kT} \quad (37)$$

is often used. Equations 35 and 36 are both exact, though eq. 35 is simpler. However, in theories which attempt to improve eq. 37, yet which are still approximate, eq. 36 may prove quite useful since it suggests an alternative way (*via* the local activity coefficient) of considering the correction to eq. 37 which has to be introduced. Section IV provides an illustration.

We now derive an exact expression for $\gamma_i^j(r)$. Corresponding to eq. 24, the electrostatic potential a distance r from and due to an ion of species s is $z_s\epsilon/Dr$. The contribution to the potential at $\mathbf{r}$, due to s ions in $d\mathbf{r}_s$, is then

$$\frac{z_s\epsilon}{Dr_{is}} c_s^0 e^{-W_{sj}(r_s)/kT}d\mathbf{r}_s$$

where $r_{is} = |\mathbf{r}_s - \mathbf{r}|$. Hence the total potential at $\mathbf{r}$, arising from the fixed j ion and its ion atmosphere, is

$$\psi_j(r) = \frac{z_j\epsilon}{Dr} + \sum_s c_s^0\int_V \frac{z_s\epsilon}{Dr_{is}} e^{-W_{sj}/kT}d\mathbf{r}_s \quad (38)$$

This is, of course, the solution of eq. 35.

We now use eq. 24 for u_{is} in eq. 26 and 28. It is then convenient to divide the integral over V into two parts: the region $r_{is} < a_{is}$ and the region $(V')r_{is} \geq a_{is}$. From the first region we obtain a small term[4] which we denote by λ_i in eq. 26 and by λ_{ij} in eq. 28. For consistency, we break up V in eq. 38 in the same way, even though there is no discontinuity in the integrand here. From the region $r_{is} < a_{is}$ we obtain, in eq. 38, a small term which we denote by λ_{ij}'. If we now substitute eq. 28 and 38 in eq. 33, we find, for $r \geq a_{ij}$,

$$kT\ln\gamma_i^j(r) = \lambda_{ij} - \lambda'_{ij} + \sum_s c_s^0 \int_0^1\int_{V'} \frac{z_i z_s\epsilon^2}{Dr_{is}}[e^{-W_{sij}(\xi_i)/kT} - e^{-W_{sj}/kT}]d\mathbf{r}_s d\xi_i \quad (39)$$

In eq. 39, the concentration $c_s^0[\ ]$ of s ions at $\mathbf{r}_s$ is that in the ion atmosphere of an i (with ξ_i) and a j ion less that in the ion atmosphere of a j ion alone. This is equal to the concentration of s ions at $\mathbf{r}_s$ in the ion atmosphere of an i ion (with ξ_i), *as perturbed by the presence of the j ion.* In the Debye–Hückel linear approximation, there is superposition in the potentials of average force and hence the perturbation does not exist. In general, however, the perturbation is responsible for departures of the quotient $\gamma_s/\gamma_s^j(r)$ from unity in eq. 36. Explicitly, from eq. 26 and 39

$$kT\ln\frac{\gamma_i^j(r)}{\gamma_i} = \lambda_{ij} - \lambda'_{ij} - \lambda_i + \sum_s c_s^0\int_0^1\int_{V'}\frac{z_i z_s\epsilon^2}{Dr_{is}}[e^{-W_{sij}(\xi_i)/kT} - e^{-W_{sj}/kT} - e^{-W_{is}(\xi_i)/kT}]d\mathbf{r}_s d\xi_i \quad (40)$$

It is easy to see that $\gamma_i^j(r)/\gamma_i \to 1$ in the Debye–Hückel approximation or when $r \to \infty$.

Finally, for completeness, we should rewrite eq. 26 in more conventional form. Let $\psi_i^{atm}(0, \xi_i)$ be the potential at $\mathbf{r}$ due to the ion atmosphere of an i ion (with ξ_i) fixed at $\mathbf{r}$. Then

$$\psi_i^{atm}(0, \xi_i) = \sum_s c_s^0\int_{V'}\frac{z_s\epsilon}{Dr_{is}} e^{-W_{is}(\xi_i)/kT}d\mathbf{r}_s \quad (41)$$

Comparing this with eq. 26

$$kT\ln\gamma_i = \lambda_i + \int_0^1 z_i\epsilon\psi_i^{atm}(0, \xi_i)d\xi_i \quad (42)$$

IV. Electrolyte Theory—Approximate.—In this section we give a rough argument which serves two purposes. First, it shows that it is possible, by modifying the Debye–Hückel potential of average force (eq. 17), to obtain a Donnan membrane, osmotic pressure second virial coefficient from the McMillan–Mayer method which agrees with eq. 16, deduced by the Donnan method. Second, the argument illustrates the use of local activity coefficients to improve the Poisson–Boltzmann equation as ordinarily written (eq. 37). Although local activity coefficients are introduced in this section in a very approximate way, it is hoped that the present treatment will at least serve to stimulate other, more refined, applications of this point of view.

As a first approximation, we assume that $\gamma_i^j(r)$ has the Debye–Hückel form but that the parameter κ depends on the *local* ionic strength a distance r from a j ion rather than on the bulk ionic strength. That is, ignoring the small term in a^3

$$\ln\gamma_i^j(r) = \frac{-z_i^2\epsilon^2\kappa_j(r)}{2DkT[1 + \kappa_j(r)a]} \quad (43)$$

where

$$\kappa_j^2(r) = \frac{4\pi\epsilon^2}{DkT}\sum_s c_s^j(r)z_s^2 \quad (44)$$

We use the Debye–Hückel linear approximation for $c_s^j(r)$ to obtain the desired first-order correction

$$c_s^j(r) = c_s^0\left[1 - \frac{z_s\epsilon\psi_j(r)}{kT}\right] = c_s^0\left[1 - \frac{z_s z_j\epsilon^2 e^{-\kappa(r-a)}}{DkTr(1 + \kappa a)}\right] \quad (45)$$

and therefore

$$\frac{\kappa_j^2(r)}{\kappa^2} = 1 - \frac{\alpha z_j\Sigma_2 e^b}{\Sigma_2(1 + b)}\frac{e^{-x}}{x} + O(\alpha^2) \quad (46)$$

where

$$x = \kappa r \quad b = \kappa a$$

It should of course be noted that $\Sigma_3 = 0$ for a symmetrical electrolyte. For the ratio $\gamma_i/\gamma_i^j(r)$ we then find, to the term in α^2

$$\frac{\gamma_i}{\gamma_i^j(r)} = \frac{\exp\,[-z_i^2\alpha/2(1+\kappa a)]}{\exp\,\{-z_i^2\alpha(\kappa_j/\kappa)/2[1+\kappa a(\kappa_j/\kappa)]\}} = 1 - \frac{A'z_i^2\Sigma_2}{\Sigma_3}\frac{e^{-x}}{x} + \ldots \quad (47)$$

where

$$A' = \frac{\alpha^2 z_j\Sigma_3^2 e^b}{4\Sigma_2^2(1+b)^3}$$

We use eq. 47 for γ_s/γ_s^j in eq. 36, and retain up to the quadratic term in ψ_j in the expansion of the exponential, giving a non-linear differential equation. But since we are not keeping terms beyond those in α^2, the only contribution to ψ_j^2 that concerns us is from the Debye–Hückel term. Hence, with the substitution of the Debye–Hückel ψ_j in the ψ_j^2 term, the non-linear equation becomes linear

$$\frac{d^2y}{dx^2} - y = A'\frac{e^{-x}}{x} + B\frac{e^{-2x}}{x} \quad (48)$$

where

$$y = x\varphi,\ \varphi = \epsilon\psi_j/kT$$
$$B = -\frac{\alpha^2 z_j^2\Sigma_3 e^{2b}}{2\Sigma_2(1+b)^2}$$

The solution of eq. 48, satisfying the usual boundary conditions of the Debye–Hückel theory, is

$$\varphi = \left[\frac{\alpha z_j e^b}{1+b} + \frac{A'b^2}{2(1+b)} - \frac{BF(b)}{2} + \frac{B(1-b)e^{2b}F(3b)}{2(1+b)}\right]\times\frac{e^{-x}}{x} - \frac{A'}{2}e^{-x} + \frac{B}{2}\frac{e^{-x}F(x)}{x} - \frac{B}{2}\frac{e^xF(3x)}{x} \quad (49)$$

where

$$F(x) = \int_x^\infty \frac{e^{-t}}{t}\,dt$$

Then from

$$e^{-W_{ij}/kT} = \frac{\gamma_i}{\gamma_i^j}e^{-z_i\epsilon\psi_j/kT} \quad (50)$$

and eqs. 47 and 49, we obtain, to terms in α^2

$$e^{-W_{ij}/kT} = 1 - \left[\frac{\alpha z_i z_j e^b}{1+b} + \frac{A'z_i^2\Sigma_2}{\Sigma_3} + \frac{A'z_ib^2}{2(1+b)} - \frac{Bz_iF(b)}{2} + \frac{Bz_i(1-b)e^{2b}F(3b)}{2(1+b)}\right]\frac{e^{-x}}{x} + \frac{A'z_i}{2}e^{-x} - \frac{Bz_i}{2}\frac{e^{-x}F(x)}{x} + \frac{Bz_i}{2}\frac{e^xF(3x)}{x} + \frac{\alpha^2z_i^2z_j^2e^{2b}}{2(1+b)^2}\frac{e^{-2x}}{x^2} \quad (51)$$

Eq. 51 satisfies the neutrality condition

$$\int_b^\infty \sum_s c_s^0 z_s e^{-W_{sj}/kT}4\pi r^2\,dr = -z_j \quad (52)$$

But we note two deficiencies in this equation. (1) While there is one term in $z_i^2z_j$, there are four in $z_iz_j^2$; thus W_{ij} is not symmetrical in z_i and z_j as it should be. (2) Substitution of eq. 51 (putting $z_i = z_j = z$) in eq. 18 gives almost but not quite the correct second virial coefficient B_2 (eq. 16): the term in αz^3 in eq. 16 is multiplied by an extra factor

$$(1+b)e^bF(b) - (1-b)e^{3b}F(3b)$$

though otherwise B_2 is correct. These results confirm, as expected, the fact that eq. 43, though a plausible semi-quantitative correction, is not exact.

As an essentially empirical further step, let us symmetrize eq. 51 with respect to z_i and z_j by the arbitrary substitution of

$$-\frac{A'z_iz_j\Sigma_2}{\Sigma_3}\frac{e^{-x}}{x} \quad (53)$$

for the four terms in $z_iz_j^2$ referred to above. This gives

$$e^{-W_{ij}/kT} = 1 - \left[\frac{\alpha z_i z_j e^b}{1+b} + \frac{\alpha^2(z_i+z_j)z_iz_j\Sigma_3 e^b}{4\Sigma_2(1+b)^3} + \frac{\alpha^2z_iz_j\Sigma_3^2b^2e^b}{8\Sigma_2^2(1+b)^4}\right]\frac{e^{-x}}{x} + \frac{\alpha^2z_iz_j\Sigma_3^2e^b}{8\Sigma_2^2(1+b)^3}e^{-x} + \frac{\alpha^2z_i^2z_j^2e^{2b}}{2(1+b)^2}\frac{e^{-2x}}{x^2} \quad (54)$$

Rather surprisingly, we then find that eq. 54 satisfies the neutrality condition, eq. 52, and also gives the correct second virial coefficient (eq. 16).

To find the potential ψ_j associated with W_{ij} in eq. 54, we integrate eq. 35 using the Debye–Hückel boundary conditions. The result is

$$\varphi(x) = \left[\frac{\alpha z_j e^b}{1+b} + \frac{\alpha^2z_j\Sigma_3^2b^2e^b}{8\Sigma_2^2(1+b)^4} + \frac{\alpha^2z_j^2\Sigma_3e^b}{4\Sigma_2(1+b)^3}\right]\frac{e^{-x}}{x} - \frac{\alpha^2z_j\Sigma_3^2e^b}{8\Sigma_2^2(1+b)^3}e^{-x} - \frac{\alpha^2z_j^2\Sigma_3e^{2b}}{4\Sigma_2(1+b)^2}\frac{e^{-2x}}{x} + \frac{\alpha^2z_j^2\Sigma_3e^{2b}F(2x)}{2\Sigma_2(1+b)^2} \quad (55)$$

The corresponding γ_i/γ_i^j is, from eq. 50, 54 and 55

$$\frac{\gamma_i}{\gamma_i^j} = 1 - \frac{\alpha^2z_i^2z_j\Sigma_3e^b}{4\Sigma_2(1+b)^2}\frac{e^{-x}}{x} - \frac{\alpha^2z_iz_j^2\Sigma_3e^{2b}}{4\Sigma_2(1+b)^2}\frac{e^{-2x}}{x} + \frac{\alpha^2z_iz_j^2\Sigma_3e^{2b}F(2x)}{2\Sigma_2(1+b)^2} \quad (56)$$

The activity coefficient γ_i can be calculated either from eq. 26 and 54, or from Eq. 42 and 55 (using the fact that $\psi_i^{atm}(0) = \psi_i^{atm}(a)$). The result is (omitting the term in a^3)

$$\ln\gamma_i = -\frac{\alpha z_i^2}{2(1+b)} - \frac{\alpha^2z_i^2\Sigma_3^2}{16\Sigma_2^2(1+b)^4} - \frac{\alpha^2z_i^3\Sigma_3}{12\Sigma_2(1+b)^3} + \frac{\alpha^2z_i^3\Sigma_3e^{2b}F(2b)}{6\Sigma_2(1+b)^2} \quad (57)$$

In view of the approximate nature of the present argument, there seems little point in calculating other thermodynamic functions or in comparing results with, say, the work of Mayer.[5]

It is easy to see that, if eq. 57 is used in the Donnan method, eq. 1, α^2 terms in $\ln\gamma_i$ lead to α^2 terms in B_2, as already mentioned in Sec. II.

Differentiation shows that, in common with most approximate treatments of electrolyte solutions, eq. 55 fails to satisfy the well-known condition

$$\frac{\partial\psi_i^{atm}(0)}{\partial z_j} = \frac{\partial\psi_j^{atm}(0)}{\partial z_i} \quad (58)$$

The same is true of eq. 49, incidentally.

While eq. 54–57 are undoubtedly improvements over the Debye–Hückel theory (for unsymmetrical electrolytes), they clearly have only an intuitive (eq. 43) and semi-empirical (eq. 53) foundation. However, it is believed that this treatment achieves the modest goals set forth in the first paragraph of the present section.

It should be emphasized that both the general discussion of local activity coefficients in Sec. III and approximate applications as in Sec. IV might profitably be extended to any problem that involves concentration gradients on a molecular scale, at equilibrium. For example, (1) plane (see the Appendix), spherical and cylindrical double layers, (2) adsorption of a gas or solute at a surface, (3)

the interface between two fluid phases, etc. In (1) and (2), the molecules or ions on or in the surface take the place of the "group of fixed molecules" referred to following eq. 31; and in (1) we would have a Poisson–Boltzmann equation as in eq. 36.

Finally, the comparison of Donnan equilibrium osmotic virial coefficients, obtained by the two methods considered here, might well be used as a consistency check on any theory of electrolytes.

Appendix

We discuss a plane double layer here in a manner analogous to Section IV. There is a fixed surface charge density σ on the plane $\eta = 0$. Electrolyte ions of diameter a (Fig. 1) and a continuum of dielectric constant D occupy the region $\eta \geq 0$, except that ionic centers cannot approach the surface $\eta = 0$ closer than $\eta = d$. The potential $\psi(\eta)$ satisfies Laplace's equation for $\eta < d$ and (see eq. 36)

$$\frac{d^2\psi(\eta)}{d\eta^2} = -\frac{4\pi\epsilon}{D}\sum_s \frac{z_s c_s^0 \gamma_s e^{-z_s\epsilon\psi(\eta)/kT}}{\gamma_s^\sigma(\eta)} \qquad (59)$$

for $\eta \geq d$, where γ_s^σ is the local activity coefficient of species s. Using the local ionic strength at η from the linearized Poisson–Boltzmann equation (eq. 37), we find, as in eq. 47, to quadratic terms in α and θ

$$\frac{\gamma_s}{\gamma_s^\sigma(y)} = 1 - \frac{Cz_s^2\Sigma_2}{\Sigma_3}e^{-\nu} + \ldots \qquad (60)$$

where

$$y = \kappa\eta,\ \delta = \kappa d$$
$$C = \frac{\alpha\theta\Sigma_3^2 e^\delta}{4\Sigma_2^2(1+b)^2}$$
$$\theta = 4\pi\sigma\epsilon/DkT\kappa$$

Instead of eq. 48, we have

$$\frac{d^2\rho}{dy^2} - \varphi = Ce^{-\nu} + D'e^{-2\nu} \qquad (61)$$

where

$$\varphi = \epsilon\psi/kT$$
$$D' = -\frac{\theta^2\Sigma_3 e^{2\delta}}{2\Sigma_2}$$

With appropriate boundary conditions at $\eta = 0$ and $\eta = d$, we find, for $\eta \geq d$

$$\varphi = \left[\theta e^\delta + \frac{C(\delta-1)}{2} - \frac{2D'e^{-\delta}}{3}\right]e^{-\nu} - \frac{C}{2}ye^{-\nu} + \frac{D'}{3}e^{-2\nu} \qquad (62)$$

and

$$e^{-W_s/kT} = \frac{\gamma_s e^{-z_s\varphi}}{\gamma_s^\sigma}$$
$$= 1 - \left[z_s\theta e^\delta + \frac{Cz_s(\delta-1)}{1} - \frac{2D'z_s e^{-\delta}}{3} + \frac{\alpha\theta z_s^2\Sigma_4 e^\delta}{4\Sigma_2(1+b)^2}\right]e^{-\nu} + \frac{Cz_s}{2}ye^{-\nu} + \frac{D'z_s}{3}e^{-2\nu} + \frac{1}{2}\times\theta^2 z_s^2 e^{2\delta}e^{-2\nu} \qquad (63)$$

Equation 63 satisfies the condition of electrical neutrality but not the symmetry condition that W_s should remain unchanged if both σ and z_s change sign.

The formal expression for γ_i^σ is easily seen to be (compare eq. 39)

$$kT\ln\gamma_s^\sigma(\eta) = \lambda_{i\sigma} - \lambda'_{i\sigma} + \sum_s c_s^0\int_0^1\int_{V'}\frac{z_i z_s\epsilon^2}{D\eta_{is}}[e^{-W^{s_i\sigma}(\xi_i)/kT} - e^{-W_s/kT}]d\eta_s d\xi_i \qquad (64)$$

where the notation is obvious or has been used before.

STUDIES OF DIFFUSION FLAMES. III. THE DIFFUSION FLAMES OF THE BUTANOLS

BY S. RUVEN SMITH, ALVIN S. GORDON AND MAYNARD H. HUNT

Michelson Laboratory, U. S. Naval Ordnance Test Station, China Lake, Calif.

Received October 15, 1956

Using a quartz probe technique in conjunction with precision mass spectrometer analyses and gas chromatographic analyses, samples of the precombustion products have been removed from the diffusion flames of the four isomeric butanols and analyzed. Analyses of these products indicate that the mechanism of burning involves an oxygen induced pyrolysis of the alcohol followed by oxidation of the ultimate pyrolysis products, H_2, CO and carbon particles. The mechanisms of these pyrolyses are discussed.

Introduction

In the earlier papers of this series[1,2] it has been demonstrated that the main process occurring inside the flame cone is oxygen induced pyrolysis of the parent compound. The present paper shows that the same process occurs inside the diffusion flame mantle of the more complex alcohols. The ultimate pyrolysis products, H_2, CO and carbon particles burn at the edge of the flame.

The original free radical formed by hydrogen abstraction from the parent compound decomposes to give a smaller free radical, and an olefinic compound because the energy regained in the formation of the double bond results in an over-all considerably lower activation energy than competitive paths involving just the breaking of a carbon–carbon bond.

Experimental

The apparatus and procedures are similar to those described previously[2]: an alcohol burner with a Pyrex glass wool wick set up on a micromanipulator in a Plexiglas hood. A quartz probe with a ground diaphragm opening was sealed into position above the burner and the samples probed from the flame were expanded into previously evacuated flasks. Samples have been probed along the central axis near the wick and toward the tip of the flame.

The samples probed from the flames were analyzed with a Consolidated Analytical Mass Spectrometer. Analyses

(1) S. R. Smith and A. S. Gordon, THIS JOURNAL, **60**, 759 (1956).
(2) S. R. Smith and A. S. Gordon, *ibid.*, **60**, 1059 (1956).

were carried out in triplicate. After proper equilibration and conditioning of the sample system, the second and third analyses gave reproducible results for the water and alcohol components.

The identification of the components in the mass spectra was aided by three techniques. The samples were thermally fractionated from a series of temperatures from liquid nitrogen to room temperature, and the spectra of each fraction were examined. High mass resolution was used to identify formaldehyde in the presence of ethane at mass 30, using the mass difference between $C^{12}H_2{}^1O^{16}$ and $C_2{}^{12}H_6$.[1] The positive identification of products in the C_3 and C_4 region has been accomplished by gas chromatography used in conjunction with the mass spectrometer.[3] Samples of the effluent gas from the chromatography column coincident with peaks in the region of interest were collected and analyzed with the mass spectrometer. In this manner it has been possible to identify quantitatively allene in the presence of propyne and to separate the butene isomers.

Temperatures of the flame zones were measured with a 0.001" Pt–Pt-Rh hairpin thermocouple enclosed in a 0.004" o.d. quartz tube to prevent catalytic reactions on the platinum. Temperatures were recorded simultaneously with photographic records.

The temperatures measured on the central axis of all the butanol flames are shown in Fig. 1. Figure 2 is a typical temperature profile across the flame. Although catalysis errors have been removed, the errors due to conductivity along the thermocouple exist. Because of thermal conductivity by the wire in the thermocouple, the measured maximum temperature at the edge of the flame is too low; however, in the central pyrolysis region, the temperature gradients are small and the conductivity corrections are small.

Discussion

The product distribution at any volume element is influenced by diffusion of the various species as well as by the reaction taking place in the given volume. Also, secondary reactions play a prominent role. Thus we cannot interpret our data quantitatively. However, the data show qualitatively which homogeneous processes are most important.

1-Butanol.—The analyses of the samples probed from the various regions on the central axis of the 1-butanol flame are reported in Table I. Sample 1 was probed about 1 mm. above the wick of the burner, sample 2 was probed halfway between the wick and the tip of the flame, and sample 3 was probed two thirds of the way to the top of the flame.

It will be observed that in sample 2 although the concentration of 1-butanol has dropped to 0.01%, pyrolysis of ethylene causes the concentration of acetylene to continue to increase. In sample 3, however, where the ethylene has almost disappeared, the concentration of acetylene falls.

In the following the primary free radical abstraction is illustrated by using O_2 as the abstraction agent.

$$CH_3CH_2CH_2CH_2OH + O_2 \longrightarrow CH_2CH_2CH_2CH_2OH + HO_2 \quad (1)$$

$$CH_3CH_2CH_2CH_2OH + O_2 \longrightarrow CH_3CHCH_2CH_2OH + HO_2 \quad (2)$$

$$CH_3CH_2CH_2CH_2OH + O_2 \longrightarrow CH_3CH_2CHCH_2OH + HO_2 \quad (3)$$

$$CH_3CH_2CH_2CH_2OH + O_2 \longrightarrow CH_3CH_2CH_2CHOH + HO_2 \quad (4)$$

$$CH_3CH_2CH_2CH_2OH + O_2 \longrightarrow CH_3CH_2CH_2CH_2O + HO_2 \quad (5)$$

(3) C. M. Drew, J. R. McNesby, S. R. Smith and A. S. Gordon, *Anal. Chem.*, **28**, 979 (1956).

The primary free radicals formed decompose to form a doubly bonded compound and a smaller free radical.

$$CH_2CH_2CH_2CH_2OH \longrightarrow C_2H_4 + CH_2CH_2OH \quad (6)$$

CH_2CH_2OH radical abtracts H and forms ethanol. In certain regions the temperature is high enough so that the radical can also lose OH and simultaneously

Table I

Samples Probed from *n*-Butyl Alcohol Diffusion Flame

	No. 1	No. 2	No. 3
n-Butyl alcohol	16.61	0.01	0.01
Toluene	0.01	0.01	...
Benzene	0.03	0.13	...
Cyclopentadiene	0.02	0.01	...
Butene-1	0.38	...	...
1,3-Butadiene	0.09	0.02	...
Vinylacetylene	0.07	0.10	...
Diacetylene	0.01	0.07	0.02
Ethyl alcohol	0.05	...	...
Acetaldehyde	0.35	...	...
Carbon dioxide	7.22	8.91	10.63
Propylene	0.38	0.05	0.01
Propane	0.01	...	...
Propyne	0.09	0.12	0.01
Allene	0.09		
Ethylene	3.01	1.47	0.01
Acetylene	1.37	2.48	0.49
Oxygen	0.08	0.01	0.02
Argon	0.44	0.63	0.71
Water	11.88	13.84	12.76
Methane	1.26	1.25	0.07
Ethane	0.17	0.02	...
Formaldehyde	0.10	0.01	0.01
Carbon monoxide	6.53	8.87	7.69
Nitrogen	47.18	59.26	65.84
Hydrogen	2.58	2.73	1.72
	100.00	100.00	100.00
T, °C.	550	950	975

give a C_2H_4 molecule. This process has a much higher energy of activation than the hydrogen abstraction process; however, it probably has a much more favorable steric factor.

$$CH_3CHCH_2CH_2OH \longrightarrow CH_3CH{=}CH_2 + CH_2OH \quad (7)$$

with the CH_2OH radical pyrolyzing into formaldehyde and an H atom.

$$CH_3CH_2CHCH_2OH \longrightarrow CH_3CH_2CH{=}CH_2 + OH \quad (8)$$

$$CH_3CH_2CH_2CHOH \longrightarrow \begin{cases} CH_3CH_2 + CH_2{=}CHOH & (9) \\ CH_3 + C_2H_4 + CH_2O & (10) \end{cases}$$

The $CH_3{=}CHOH$ rearranges itself to acetaldehyde and the ethylene radical stabilizes itself as ethane and ethylene, ethylene predominating in the higher temperature regions of the flame.

$$CH_3CH_2CH_2CH_2O \longrightarrow CH_3CH_2CH_2 + CH_2O \quad (11)$$

and the *n*-propyl radicals pyrolyze to CH_3 and C_2H_4.

Methyl radicals form CH_4 by H abstraction and C_2H_5 by combination; the ethane is pyrolyzed subsequently to ethylene and this in turn to acetylene. Only butene-1 is found in the products as would be

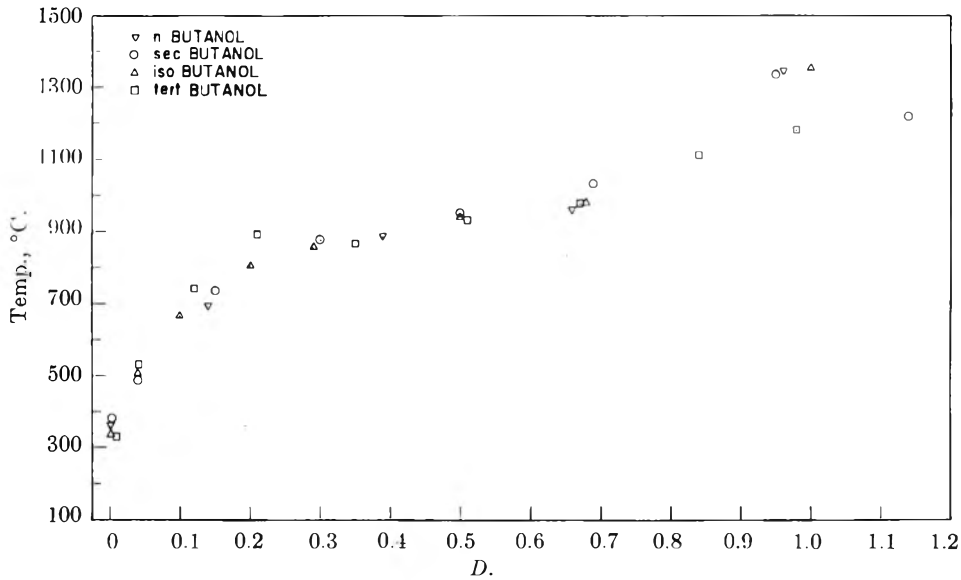

Fig. 1.—Central axis temperature of butanol diffusion flames (D = ratio of distance above wick to height of flame).

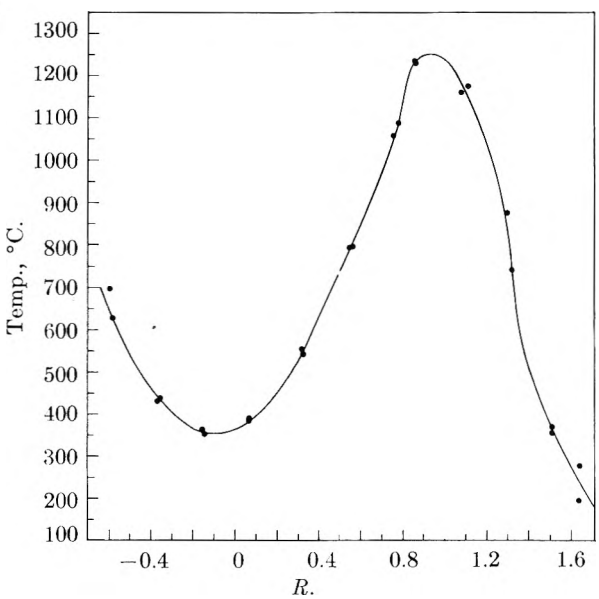

Fig. 2.—Temperature profile of *n*-butanol flame at wick (R = ratio of distance of thermocouple to central axis over the radius of the flame).

expected from the pyrolysis mechanism (reaction 3 followed by reaction 8).

In the remainder of the paper, the primary H atom abstraction step will not be discussed, since it is entirely analogous to the 1-butanol flames.

***sec*-Butyl Alcohol.**—The analysis of the sample probed from the *sec*-butyl alcohol flame is reported in Table II. Sample 1 was probed on the central axis about 0.5 mm. above the wick and sample 2 was probed about a quarter of the way to the tip of the flame. The radicals formed by H abstraction from the parent molecule are pyrolyzed by the mechanisms shown

$$CH_3CH_2\underset{\displaystyle OH}{\underset{|}{C}}HCH_3 \longrightarrow C_2H_4 + \underset{\displaystyle OH}{\underset{|}{C}}HCH_3 \qquad (12)$$

and the CH_3–CHOH radical forms ethanol by H abstraction and acetaldehyde by loss of an H atom.

TABLE II

SAMPLES PROBED FROM *sec*-BUTYL ALCOHOL DIFFUSION FLAME

	No. 1	No. 2
Styrene	0.01	0.01
Ethynylbenzene	0.01	0.04
Toluene	0.02	0.03
Benzene	0.07	0.20
Cyclohexadiene	0.02	0.01
sec-Butyl alc.	18.42	0.05
Methyl ethyl ketone	0.09	...
2-Methyl-2-butene	0.03	...
1,3-Pentadiene	0.03	...
Cyclopentadiene	0.03	0.04
Acetone	0.44	0.06
Propionaldehyde	0.01	...
Butene-1	0.45	0.07
Butene-2	0.19	
1,3-Butadiene	0.21	0.17
Vinylacetylene	0.11	0.15
Diacetylene	0.02	0.04
Propane	0.01	...
Acetaldehyde	0.67	0.16
Carbon dioxide	7.29	8.52
Propylene	0.39	0.23
Propyne	0.15	0.18
Allene	0.05	
Argon	0.51	0.71
Oxygen	0.03	0.13
Ethanol	0.12	...
Ethane	0.37	0.24
Ethylene	3.08	2.01
Acetylene	0.95	1.84
Water	8.08	11.65
Methane	1.98	2.44
Carbon monoxide	5.62	5.79
Nitrogen	48.00	62.05
Hydrogen	2.54	3.15
	100.00	100.00
T, °C.	375	800

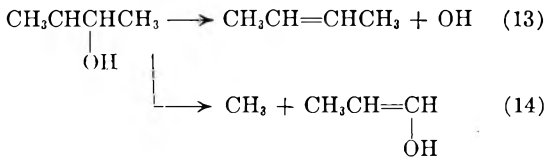

$CH_3CH{=}CHOH$ rearranges to propionaldehyde. Since the propionaldehyde is present in very small percentage, we may conclude that reaction 14 is inefficient.

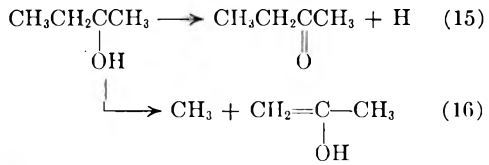

The $CH_2{=}C(OH){-}CH_3$ rearranges to acetone.

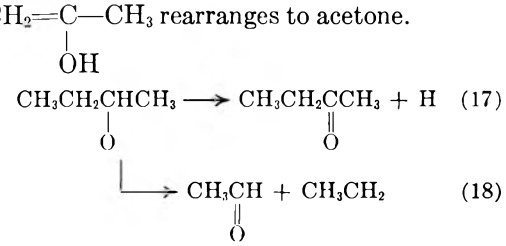

Methyl ethyl ketone is present in small concentration so that over-all reactions 14 and 16 are comparatively slow.

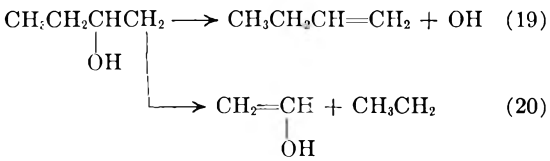

The $CH_2{=}CH(OH)$ rearranges to CH_3CHO.

It is noted that both butene-1 and butene-2 are present in the products, consistent with the mechanism proposed.

Isobutyl Alcohol.—The analysis of the samples probed from the isobutyl alcohol diffusion flame are reported in Table III. Sample 1 was probed on the central axis about 1 mm. above the wick, and sample 2 was probed about a quarter of the way to the tip of the flame.

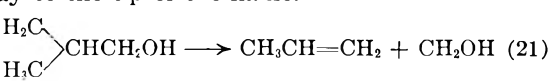

and CH_2OH pyrolyzes to CH_2O and H.

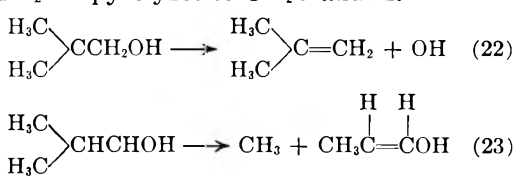

The $CH_3CH{=}CHOH$ rearranges to propionaldehyde.

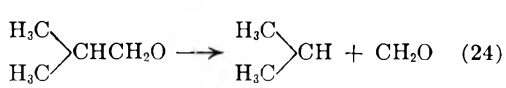

The isopropyl radical rearranges to the *n*-propyl radical which pyrolyzes to CH_3 and ethylene or loses an H to give propylene. The isopropyl radical

Table III

Samples Probed from Isobutyl Alcohol Diffusion Flame

	No. 1	No. 2
Toluene	0.01	0.02
Benzene	0.05	0.17
1,3-Cyclohexadiene	0.01	...
Isobutyl alcohol	22.87	0.09
2-Methyl-1-butene	0.04	...
2-Methyl-1,3-butadiene	0.03	...
Cyclopentadiene	0.02	0.01
Propionaldehyde	0.40	...
Isobutylene	0.47	...
1,3-Butadiene	0.10	0.03
Vinylacetylene	0.08	0.08
Diacetylene	0.02	0.05
Carbon dioxide	6.51	8.20
Propane	0.01	...
Propylene	1.00	0.06
Propyne	0.06	0.18
Allene	0.18	
Oxygen	0.06	0.05
Argon	0.44	0.65
Ethane	0.28	0.03
Formaldehyde	0.27	0.06
Ethylene	1.23	1.01
Acetylene	1.19	2.11
Water	10.96	14.31
Methane	1.64	1.61
Carbon monoxide	6.31	8.48
Nitrogen	44.21	59.75
Hydrogen	1.56	3.05
	100.00	100.00
T, °C.	400	800

at lower temperatures abstracts H to give propane. Propane is more stable thermally than formaldehyde, and so should appear in at least equal concentration. Since propane is present as only a few per cent. of the formaldehyde, the isopropyl radical does not primarily disappear by H abstraction.

***t*-Butyl Alcohol.**—The analyses of the samples probed from the *t*-butyl alcohol flame are reported in Table IV. Sample 1 was removed from the central axis about 2 mm. above the wick, and sample 2 was removed from the central axis about a quarter of the distance to the tip of the flame.

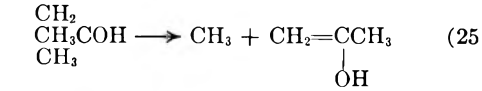

and the $CH_2{=}C(OH){-}CH_3$ rearranges to acetone.

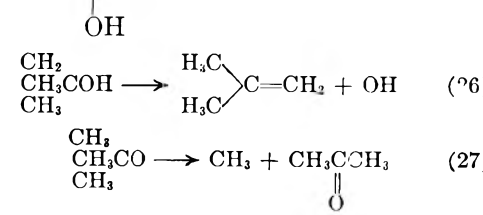

It is of some interest to compare some of the products in the butanol flames. It may be noted that ethylene is present in large concentrations in the 1-butanol and secondary butanol flames, and in considerably lower concentrations in the isobu-

TABLE IV

SAMPLES PROBED FROM *t*-BUTYL ALCOHOL FLAME

	No. 1	No. 2
t-Butyl alc.	12.18	0.04
Toluene	0.03	0.07
Benzene	0.14	0.39
1,3-Cyclohexadiene	0.03	0.03
Acetone	0.41	0.16
Isobutylene	1.78	1.04
1,3-Butadiene	0.17	0.22
2-Methyl-2-butene	0.10	0.04
Vinylacetylene	0.12	0.19
Diacetylene	0.05	0.05
Carbon dioxide	8.49	9.32
Propylene	0.23	0.30
Methylacetylene	0.07	0.74
Allene	0.43	
Ethane	0.28	0.26
Formaldehyde	0.02	0.04
Ethylene	0.82	1.07
Acetylene	1.03	1.53
Water	11.55	14.1
Methane	2.19	3.5
Carbon monoxide	4.13	5.28
Nitrogen	52.90	58.24
Hydrogen	2.09	2.60
Oxygen	0.08	0.03
Argon	0.68	0.74
	100.00	100.00
T, °C.	450	750

tyl alcohol and *t*-butyl alcohol flames. The ethane concentration is no greater in the first two flames, so that pyrolysis of ethane is not the important route for ethylene formation. Rather, hydrogen abstraction reactions such as reaction 1 followed by reaction 6 give rise to ethylene. In addition, ethyl radicals are formed by reactions such as reaction 9. Since ethane is not appreciably increased in this flame over butanol flames in which no ethyl radicals are formed, it may be concluded that the ethyl radicals form ethylene. Ethylene also may be formed by reaction 2, followed by

$$CH_3CHCH_2CH_2OH \longrightarrow CH_2CH_2 + CH_2CH_2OH \quad (28)$$

At this time there is experimental evidence indicating that reaction with hydrogen migration can occur.[4]

Methane and ethane probably are formed from methyl radicals by abstraction and recombination, respectively. In the acetone flame[5] methyl radicals must play a dominant role. Here we find the methane/ethane ratio roughly the same as in the butanol flames.

Propylene is in especially high concentration in the isobutyl alcohol flame since a direct path for its formation is available in reaction 21. Its formation in the other butanols is probably by pyrolysis of some of the stable primary products. Thus isobutene and butene-1 have been shown to generate propylene.

Butene-1, but no butene-2, is formed in the 1-butanol flame, as would be predicted from the mechanism. It is interesting to note that butene-1 does not isomerize. As would be predicted, both butene-1 and butene-2 are formed in the *sec*-butyl alcohol flame. Contrary to our observations we would predict that butene-2 should be present in greater concentration than butene-1, since both the relative rates of hydrogen abstraction from the *sec*-butanol as well as the relative stabilities of the butene-1 and butene-2 would favor butene-2. No butene-1 or butene-2 is found in the 2-butanol or *tert*-butanol flames, and no mechanism is available for their formation. Instead, consistent with the mechanism, isobutene is found in these flames, but not in the 1-butanol and *sec*-butyl alcohol flames.

Propyne and allene must be formed from the pyrolysis products of the butanols.

It may be noted that allene is especially high in the *t*-butyl alcohol flame. Propylene pyrolysis results in allene,[6] but the isobutylene flame, which is richest in propylene, is not richest in allene. It is probable, therefore, that isobutylene is the major precursor of allene.

$$\begin{matrix} H_3C \\ H_3C \end{matrix}\!\!>\!C{=}CH_2 + R \longrightarrow RH + \begin{matrix} H_2C \\ H_3C \end{matrix}\!\!>\!C{=}CH_2 \quad (29)$$

$$\begin{matrix} H_3C \\ H_2C \end{matrix}\!\!>\!C{=}CH_2 \longrightarrow CH_3 + CH_2{=}C{=}CH_2 \quad (30)$$

Propyne probably results from the pyrolysis of propylene and butene-2.

$$CH_3CH{=}CH_2 + R \longrightarrow RH + CH_3C{=}CH_2 \quad (31)$$

$$\longrightarrow RH + CH_3CH{=}CH \quad (32)$$

$$CH_3C{=}CH_2 \longrightarrow CH_3C{\equiv}CH + H \quad (33)$$

$$CH_3CH{=}CH \longrightarrow CH_3C{\equiv}CH + H \quad (34)$$

$$CH_3CH{=}CHCH_3 + R \longrightarrow RH + CH_3C{=}CHCH_3 \quad (35)$$

$$CH_3C{=}CHCH_3 \longrightarrow CH_3 + CH_3C{\equiv}CH \quad (36)$$

As would be expected, formaldehyde is found in the 1-butanol and isobutyl alcohol flames where R–CH_2OH group is present.

Acetaldehyde is found in the *sec*-butyl alcohol and 1-butanol flames where the structure R–$\underset{\underset{OH}{|}}{CH}CH_3$ or RCH_2CH_2OH is present. The first structure does not involve a hydrogen shift along the carbon skeleton and is probably an easier path, so that a higher concentration of acetaldehyde is found in the *sec*-butyl alcohol flame than in the 1-butanol flame.

Propionaldehyde is rarely found in any alcohol flames; an exception is the isobutyl alcohol flame where reaction 23 is quite favorable.

Acetone is found only in the *sec*-butyl alcohol and *t*-butyl alcohol flame where the structure of the parent butanol has the skeleton of the acetone molecule.

Methyl ethyl ketone is found only in the *sec*-butyl alcohol flame because only this butanol has a methyl and an ethyl group on the carbon containing the OH.

(4) J. R. McNesby and A. S. Gordon, *J. Chem. Phys.*, **25**, 582 (1956).

(5) S. R. Smith and A. S. Gordon, "Diffusion Flames of Ketones," in preparation.

(6) Observation in our laboratories.

Acknowledgment.—The authors wish to acknowledge the assistance of Andreas V. Jensen in the operation of the mass spectrometer, of Helen R. Young in the reduction of the mass spectral data and of Mr. Joseph H. Johnson in the operation of the gas chromatography apparatus.

CONTRIBUTIONS TO THE THERMODYNAMICS OF THE SYSTEMS PbS–Sb_2S_3, Cu_2S–Sb_2S_3, Ag_2S–Sb_2S_3 AND Ag–Sb

BY A. G. VERDUCH AND CARL WAGNER

Department of Metallurgy, Massachusetts Institute of Technology, Cambridge, Massachusetts

Received October 15, 1956

Formulae for the calculation of the free energies of formation of double sulfides from measurements of reduction equilibria and from e.m.f. measurements are derived and applied to the systems PbS–Sb_2S_3, Cu_2S–Sb_2S_3 and Ag_2S–Sb_2S_3. On the basis of reduction equilibrium measurements by Schenck, Hoffmann, Knepper and Vögler, the free energies of formation of the double sulfides $Pb_3Sb_2S_6$, $PbSb_2S_4$, Cu_3SbS_3, $CuSbS_2$, Ag_3SbS_3 and $AgSbS_2$ from the corresponding simple sulfides at 400° are found to be −286, −242, −725, −787, −751 and −538 cal./equivalent, respectively. The values for Ag_3SbS_3 and $AgSbS_2$ deduced from e.m.f. measurements at 275° are −710 and −565 cal./equivalent, respectively. As an auxiliary value, the free energy of formation of the intermetallic compound $Ag_{0.75}Sb_{0.25}$ = $^1/_4Ag_3Sb$ has been determined with the help of e.m.f. measurements between 200 and 375° and has been found to be $[-745 - 1.16(t - 300)]$ cal./g.-atom where t is temperature in °C.

Many sulfides of heavy metals form double sulfides, *e.g.*, Ag_3SbS_3, Cu_3SbS_3, $PbSb_2S_4$, which are especially known as minerals. In view of geological and metallurgical problems, an attempt has been made in order to determine the free energy of formation of double sulfides from the constituent simple sulfides by using investigations on reduction equilibria and galvanic cells.

General Equations for the Evaluation of Reduction Equilibria.—Darken[1] has shown that the molar free energy of a ternary system may readily be obtained from measurements of the partial molar free energy of a single component. A similar treatment is used for the present problem, but certain modifications are profitable.

The sulfide-forming metals are denoted by A and B and their valences in the sulfides under consideration by z_A and z_B, respectively. Thus the formulas of the binary sulfides are $A_2S_{z_A}$ and $B_2S_{z_B}$. Let n_A, n_B and n_S be the number of moles of A, B and S, respectively. Then the number of equivalents are z_An_A, z_Bn_B and $2n_S$. The composition of the ternary system A–B–S is determined by two independent variables, *e.g.*, by the ratio of the number of equivalents of B to the sum of the number of equivalents of A and B

$$\xi = z_Bn_B/(z_An_A + z_Bn_B) \quad (1)$$

and by the ratio of the number of equivalents of sulfur to the sum of the number of equivalents of A and B

$$\eta = 2n_S/(z_An_A + z_Bn_B) \quad (2)$$

The partial free energies of the components per equivalent are denoted by $\bar{F}_{A(eq)}$, $\bar{F}_{B(eq)}$ and $\bar{F}_{S(eq)}$, respectively. Hence the free energy F of a system involving $(1 - \xi)$ equivalent of metal A, ξ equivalent of metal B, and η equivalent of sulfur is

$$F = (1 - \xi)\bar{F}_{A(eq)} + \xi\bar{F}_{B(eq)} + \eta\bar{F}_{S(eq)} \quad (3)$$

In view of the Gibbs-Duhem equation

$$(1 - \xi)\mathrm{d}\bar{F}_{A(eq)} + \xi\mathrm{d}\bar{F}_{B(eq)} + \eta\mathrm{d}\bar{F}_{S(eq)} = 0 \quad (4)$$

it follows from equation 3 that

$$\partial F/\partial\eta = \bar{F}_{S(eq)} \quad (5)$$

Integration of eq. 5 with $\eta = 0$ as the lower limit and $\eta = 1$ as the upper limit at constant ξ yields

$$F(\xi, \eta = 1) = F(\xi, \eta = 0) + \int_0^1 \bar{F}_{S(eq)}(\xi, \eta)\,\mathrm{d}\eta \quad (6)$$

The free energy of formation $\Delta F_{eq}(\xi, \eta = 1)$ of one equivalent of a phase or a mixture of phases of the quasi-binary system $A_2S_{z_A}$–$B_2S_{z_B}$ from $(1 - \xi)$ equivalent of sulfide of metal A, and ξ equivalent of sulfide of metal B is

$$\Delta F_{eq}(\xi, \eta = 1) = F(\xi, \eta = 1) - (1 - \xi)F(\xi = 0, \eta = 1) - \xi F(\xi = 1, \eta = 1) \quad (7)$$

where $F(\xi = 0, \eta = 1)$ and $F(\xi = 1, \eta = 1)$ are the free energies of one equivalent of the sulfides of metals A and B, respectively.

Substitution of eq. 6 in eq. 7 yields

$$\Delta F_{eq}(\xi, \eta = 1) = \Delta F_{eq}(\xi, \eta = 0) + (1 - \xi)\int_0^1 [\bar{F}_{S(eq)}(\xi, \eta) - \bar{F}_{S(eq)}(\xi = 0, \eta)]\,\mathrm{d}\eta + \xi\int_0^1 [\bar{F}_{S(eq)}(\xi, \eta) - \bar{F}_{S(eq)}(\xi = 1, \eta)]\,\mathrm{d}\eta \quad (8)$$

where $\Delta F_{eq}(\xi, \eta = 0)$ is the free energy of formation of the alloy from $(1 - \xi)$ equivalent of metal A and ξ equivalent of metal B

$$\Delta F_{eq}(\xi, \eta = 0) = F(\xi, \eta = 0) - [(1 - \xi)F(\xi = 0, \eta = 0) + \xi F(\xi = 1, \eta = 0)] = (1 - \xi)F_A{}^M/z_A + \xi F_B{}^M/z_B \quad (9)$$

and $F_A{}^M$ and $F_B{}^M$, respectively, are the partial molar free energies of mixing of metals A and B in the alloy. Equation 9 holds for homogeneous or heterogeneous alloys involving solid solutions or intermetallic compounds.

The partial equivalent free energy of sulfur, $\bar{F}_{S(eq)}$, is given by the equilibrium ratio $q = p_{H_2S}/p_{H_2}$ of the gas phase

$$\bar{F}_{S(eq)} = \text{constant} + {}^1/_2\,RT\ln q \quad (10)$$

Measurements for various systems have been made especially by Schenck and his associates.[2–4]

(1) L. S. Darken, *J. Am. Chem. Soc.*, **72**, 2909 (1950).

(2) R. Schenck, I. Hoffmann, W. Knepper and H. Vögler, *Z. anorg. allgem. Chem.*, **240**, 173 (1939).

(3) R. Schenck and P. von der Frost, *ibid.*, **241**, 145 (1939).

(4) R. Schenck and P. von der Frost, *ibid.*, **249**, 76 (1942).

Substitution of eq. 10 in eq. 8 yields

$$\Delta F_{eq}(\xi, \eta = 1) = \Delta F_{eq}(\xi, \eta = 0) + \frac{1}{2} RT[(1 - \xi) \int_0^1 \ln \frac{q(\xi, \eta)}{q(\xi = 0, \eta)} d\eta + \xi \int_0^1 \ln \frac{q(\xi, \eta)}{q(\xi = 1, \eta)} d\eta] \quad (11)$$

Equation 11 also holds for systems involving intermediate phases with a sulfur content $\eta < 1$ which have been claimed to occur, *e.g.*, in the system Ag–Sb–S[2].

If metal A has a much higher affinity for sulfur than metal B, and no sulfide phases involving lower valences of metals A and B exist, removal of sulfur from a system of the initial composition ξ_0, $\eta = 1$ leads to the formation of metal B and phases along the quasi-binary section $\eta = 1$ with values of ξ smaller than ξ_0. Thus H_2S/H_2 ratios for phases of the quasi-binary system $A_2S_{z_A}$–$B_2S_{z_B}$ in equilibrium with metal B are obtained. The reduction reaction

$$(1/2 z_B)B_2S_{z_B} + 1/2 H_2(g) = (1/2 z_B)B + 1/2 H_2S(g) \quad (12)$$

has the equilibrium condition

$$\Delta F^\circ + 1/2 RT \ln q - (\bar{F}_{B,S(eq)} - \bar{F}^\circ_{B,S(eq)}) = 0 \quad (13)$$

where ΔF° is the standard free energy change of reaction 12, $\bar{F}_{B,S(eq)}$ is the partial equivalent free energy of the sulfide of metal B in the mixture being reduced, and $F^\circ_{B,S(eq)}$ is its standard free energy value. From eq. 13 it follows that the relative partial equivalent free energy of the sulfide of metal B is

$$\bar{F}_{B,S(eq)} - F^\circ_{B,S(eq)} = 1/2 RT \ln (q/q_0) \quad (14)$$

where q_0 denotes the H_2S/H_2 equilibrium ratio over pure $B_2S_{z_B}$ and pure metal B.

The partial equivalent free energy of the sulfide of metal A may be calculated from that of the sulfide of metal B with the aid of the Gibbs–Duhem equation. Finally the value of $\Delta F_{eq}(\xi, \eta = 1)$ may be calculated as[5]

$$\Delta F_{eq}(\xi, \eta = 1) = (1 - \xi) \int_0^\xi \frac{\bar{F}_{B,S(eq)} - F^\circ_{B,S(eq)}}{(1 - \xi)^2} d\xi \quad (15)$$

If the quasi-binary system of the sulfides of metals A and B involves only compounds without appreciable homogeneity ranges, the plot $(\bar{F}_{B,S(eq)} - F^\circ_{B,S(eq)})$ *vs.* ξ is a staircase curve. In this case, the integral in eq. 15 can be evaluated as a sum.[6]

Thermodynamics of the Systems PbS–Sb_2S_3 and Cu_2S–Sb_2S_3.—Reduction of the systems PbS–Sb_2S_3 and Cu_2S–Sb_2S_3 gives virtually pure antimony as the only reduction product. The corresponding H_2S/H_2 equilibrium ratios at 400° have been determined by Schenck, Hoffmann, Knepper and Vögler.[2] These data can be substituted in eq. 14 and 15. For the reduction of the system PbS–Sb_2S_3, there have been reported seven steps, each representing supposedly the equilibrium between three solid phases, *viz.*, pure antimony and two sulfide phases. Hence the relative partial equivalent free energies of the quasi-binary system PbS–Sb_2S_3 are staircase functions shown in Fig. 1. The function $\Delta F_{eq}(\xi, \eta = 1)$ is a polygon shown in Fig. 2. The most conspicuous phases have the formulas $Pb_3Sb_2S_6$ (falkmanite) and $PbSb_2S_4$ (zinckenite), whose free energies of formation from PbS and Sb_2S_3 at 400° are −286 and −242 cal./equivalent, respectively.

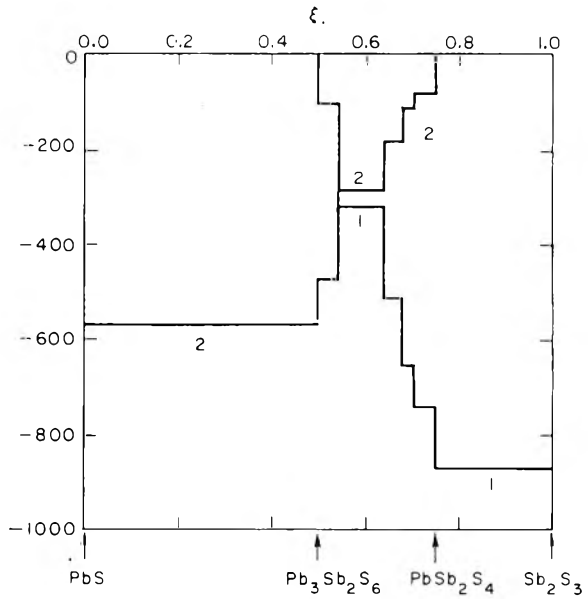

Fig. 1.—Relative partial equivalent free energies for the system Sb_2S_3–PbS at 400°: 1, $\bar{F}_{Pb,S(eq)} - F^\circ_{Pb,S(eq)}$ (cal.) *vs.* ξ; 2, $\bar{F}_{Sb,S(eq)} - F^\circ_{Sb,S(eq)}$ (cal.) *vs.* ξ.

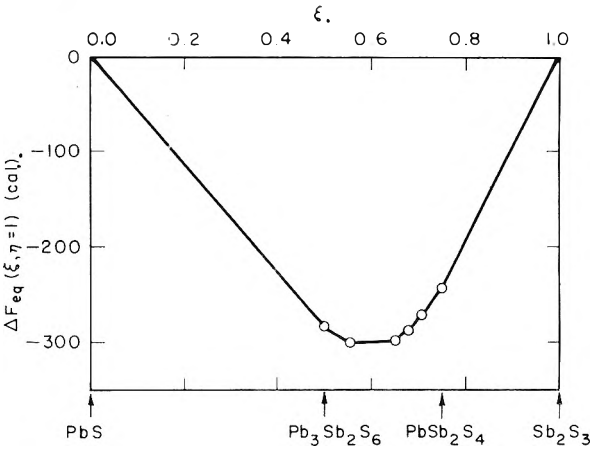

Fig. 2.—Free energy of formation ΔF_{eq} for the quasi-binary system PbS–Sb_2S_3 at 400°.

For the system Cu_2S–Sb_2S_3, there have been reported two regions involving a continuous variation of the H_2S/H_2 ratio with ξ corresponding supposedly to solid solutions in phases having the ideal formulas Cu_3SbS_3 and $CuSbS_2$ whose free energies of formation from Cu_2S and Sb_2S_3 at 400° are found to be −725 and −787 cal./equivalent, respectively.

Although details of the plots $\bar{F}_{Sb,S(eq)} - F^\circ_{Sb,S(eq)}$ *vs.* ξ in Figs. 1 and 3 are uncertain and the reality of small steps may be questioned, these uncertainties introduce only small errors in the calculation of the values of $\Delta F_{eq}(\xi, \eta = 1)$ shown in Figs. 2 and 4 because integration smooths the resulting function.

(5) C. Wagner, "Thermodynamics of Alloys," Addison–Wesley Press, Cambridge, Mass., 1952, p. 14.

(6) Ref. 5, p. 28.

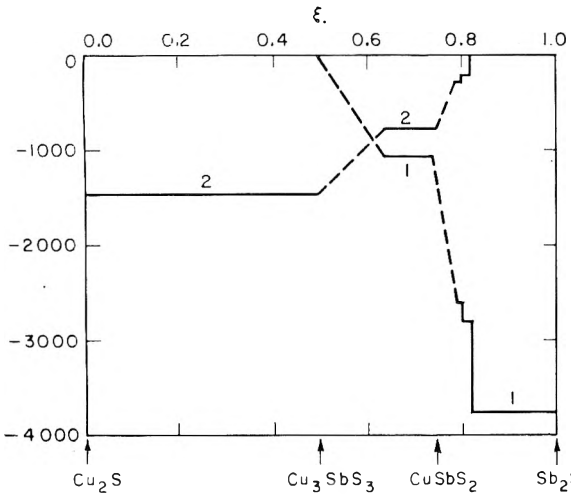

Fig. 3.—Relative partial equivalent free energies for the system Sb_2S_3–Cu_2S at 400°: 1, $\bar{F}_{Cu,S(eq)} - F^0_{Cu,S(eq)}$ (cal.) *vs.* ξ; 2, $\bar{F}_{Sb,S(eq)} - F^0_{Sb,S(eq)}$ (cal.) *vs.* ξ.

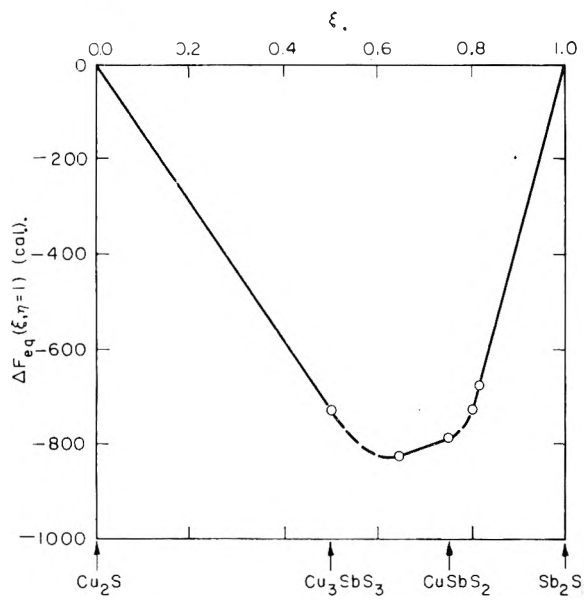

Fig. 4.—Free energy of formation ΔF_{eq} for the quasi-binary system Cu_2S–Sb_2S_3 at 400°.

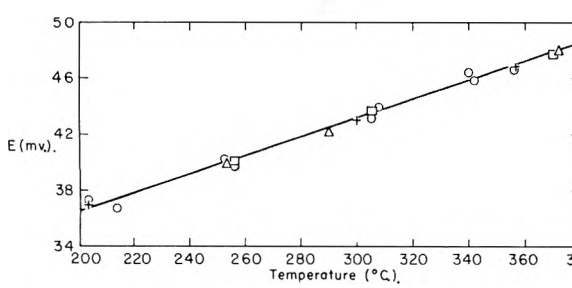

Fig. 5.—Electromotive force E of the cell II: Ag|AgI|Ag–Sb alloy: □, $x_{Sb} = 0.322$; ○, $x_{Sb} = 0.420$; +, $x_{Sb} = 0.469$; Δ, $x_{Sb} = 0.622$.

Electrochemical Measurements on Ag–Sb Alloys.—The reduction of the quasi-binary system Ag_2S–Sb_2S_3 yields various phases of the system Ag–Sb.[2] In order to evaluate available data for the reduction equilibria with the help of eq. 11, it is, therefore, necessary to determine the free energy of formation of Ag–Sb alloys at 400° between $\xi = 0.5$ and $\xi = 1$ where the alloy consists of virtually pure antimony and the intermetallic compound Ag_3Sb.[7–10]

Weibke and Effinger[11] have tried to determine thermodynamic quantities of Ag–Sb alloys between 400 and 500° with the aid of the cell

$$\text{Sb} \mid \text{SbCl}_3\text{–KCl–LiCl melt} \mid \text{Ag–Sb alloy} \qquad \text{(I)}$$

The observed e.m.f. values, however, were ill-defined. Presumably, the displacement reaction $Ag + {}^1/_3\,SbCl_3 = {}^1/_3\,Sb + AgCl$ interferes.

To minimize the effect of displacement reactions, the free energy of formation of the salt used as electrolyte must be sufficiently more negative than that for the salt of the other component of the alloy.[12] This requirement is satisfied when the cell

$$\text{Ag(s)} \mid \text{AgI(s)} \mid \text{Ag–Sb alloy (s)} \qquad \text{(II)}$$

is used since the heats of formation of AgI and SbI_3 at 25° are −14.91 and −7.7 kcal./equivalent, respectively.[13]

Cell II involving small pellets of Ag, AgI and the alloy was assembled in the same way as recently described for cells involving solid oxides as electrolyte.[14] Results are shown in Fig. 5.

From the observed values of the e.m.f. E, the partial molar free energy of mixing of silver has been calculated from the formula

$$F_{Ag}{}^M = -E\mathfrak{F} \qquad (16)$$

where $\mathfrak{F}$ is the Faraday constant.

Values of E and $F_{Ag}{}^M$ were found to be independent of ξ in accord with the fact that the alloy consists of the solid phases Ag_3Sb and Sb if $0.5 < \xi < 1.0$, or $0.25 < x_{Sb} < 1.0$ where x_{Sb} is the mole fraction of antimony. The dependence on temperature t in °C. is represented by the formula

$$F_{Ag}{}^M \text{ (cal.)} = -994 - 1.55(t - 300) \quad \text{if } 0.25 < x_{Sb} < 1.0 \qquad (17)$$

whereas $F_{Sb}{}^M \cong 0$ since virtually pure antimony is present.

Available phase diagram data[7–10] indicate that the compound co-existing with Sb deviates only slightly from the formula Ag_3Sb. Thus the integral free energy of formation of this compound is found to be

$$F^M (Ag_{0.75}Sb_{0.25}) \text{ (cal./g.-atom)} = 0.75F_{Ag}{}^M + 0.25F_{Sb}{}^M = -745 - 1.16(t - 300) \qquad (18)$$

The heat of formation calculated from eq. 18 with the help of the Gibbs–Helmholtz equation is $H^M(Ag_{0.75}Sb_{0.25}) = -80$ cal./g.-atom at 300°. A direct calorimetric determination at 450° by Kleppa[15] gives a value of +26 cal./g.-atom, which has to be regarded as the more accurate value since deviations from the ideal formula Ag_3Sb have been ignored in the evaluation of the e.m.f. measure-

(7) G. J. Petrenko, *Z. anorg. allgem. Chem.*, **50**, 139 (1906).
(8) A. Westgren, G. Hagg and S. Erickson, *Z. physik. Chem.*, **B4**, 453 (1929).
(9) M. Hansen, "Der Aufbau der Zweistofflegierungen," Springer, Berlin, 1936, pp. 55–58.
(10) F. Weibke and I. Effinger, *Z. Elektrochem.*, **46**, 53 (1940).
(11) F. Weibke and I. Effinger, *ibid.*, **46**, 61 (1940).
(12) Ref. 5, p. 91f.
(13) Circular 500 of the National Bureau of Standards, Washington, D. C., 1952.
(14) K. Kiukkola and C. Wagner, *J. Electrochem. Soc.*, in press.
(15) O. J. Kleppa, THIS JOURNAL, **60**, 846 (1956).

ments. In view of this neglect, the difference between the two values is within the limits of error.

Electrochemical Measurements on the System Ag_2S–Sb_2S_3.—The phase diagram of the system Ag_2S–Sb_2S_3 has been investigated by various authors, especially by Jaeger and van Klooster[16] and by Jensen,[17] whose results agree closely. Two double sulfides, Ag_3SbS_3 ($\xi = 0.50$) and $AgSbS_2$ ($\xi = 0.75$), with congruent melting points have been found. Gaudin and McGlashan[18] have confirmed these compounds by microscopical examination of solidified mixtures and have found one additional phase designated as B phase with excess sulfur at Ag/Sb ratios greater than 3 ($\xi < 0.5$), whereas no phase involving a noticeable excess of sulfur in mixtures richer in antimony sulfide has been found. In accord with the observations by Gaudin and McGlashan, Ag_2S–Sb_2S_3 pellets heated at 275° in nearly saturated sulfur vapor did not change their weight if $\xi > 0.5$, whereas a weight increase of about 1.3% was found for a pellet involving $\xi = 0.40$.

Since phases of the system Ag_2S–Sb_2S_3 show electronic conduction, thermodynamic measurements on galvanic cells require use of an auxiliary electrolyte involving ionic conduction. To this end, silver iodide is suitable. In view of available data for the heats of formation at 25°, it can be estimated that neither the displacement reaction $AgI + {}^1/_3\,Sb = Ag + {}^1/_3\,SbI_3$ nor the displacement reaction $AgI + {}^1/_6\,Sb_2S_3 = {}^1/_2\,Ag_2S + {}^1/_3\,SbI_3$ is likely to interfere.

Three different types of cells may be considered.

(1) In the cell

$$Pt, S_x(g)|Ag_2S(s)|AgI(s)|(Ag_2S, Sb_2S_3)(s)|Pt, S_x(g) \qquad (III)$$

the half-cell reactions on the left-hand and the right-hand side, respectively, on passing one faraday are

$${}^1/_2Ag_2S(s) = Ag^+(\text{in AgI}) + e^- + ({}^1/_2x)S_x(g) \qquad (19)$$

$$Ag^+(\text{in AgI}) + e^- + ({}^1/_2x)\,S_x(g) = {}^1/_2Ag_2S\ (\text{in } Ag_2S\text{–}Sb_2S_3) \qquad (20)$$

Upon combining eq. 19 and 20, the over-all cell reaction is found to be

$${}^1/_2Ag_2S(s) = {}^1/_2Ag_2S\ (\text{in } Ag_2S\text{–}Sb_2S_3) \qquad (21)$$

Hence

$${}^1/_2[\bar{F}_{Ag_2S} - F^\circ_{Ag_2S}] = -E\mathfrak{F} \qquad (22)$$

where $\bar{F}_{Ag_2S}$ is the partial molar free energy of Ag_2S in the system Ag_2S–Sb_2S_3 on the right-hand side of cell III.

Since the over-all cell reaction does not involve sulfur vapor, the e.m.f. of cell III is supposed to be independent of the sulfur partial pressure provided that the sulfur partial pressures at the two electrodes are equal.

Investigations on cell III were confined to Ag_2S–Sb_2S_3 mixtures with values of ξ greater than 0.5 at which no B phase is formed. To prepare a mixture, appropriate amounts of Ag_2S and Sb_2S_3 obtained by synthesis from the elements were melted, the solidified melt was ground in an agate mortar, and tablets 6 mm. in diameter were pressed in a die.

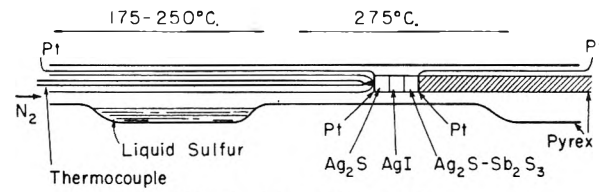

Fig. 6.—Vessel for cell III.

Figure 6 shows schematically the vessel used for measurements on cell III. The vessel was installed in a two-stage furnace which had a total length of 50 cm. A gentle stream of nitrogen entering the vessel at the left-hand side was saturated with sulfur vapor at temperatures ranging between 175 and 250° and was passed along electrodes of cell III at 275°. The temperature of 275° was selected because above 315° a liquid phase of the ternary system Ag_2S–Sb_2S_3–AgI is formed.

The e.m.f. of cell III was found to be well defined and independent of the sulfur partial pressure when the temperature of the sulfur saturator was between 200 and 250°, whereas at lower temperatures the e.m.f. was lower and not well reproducible presumably because equilibrium between the electrodes and sulfur vapor of low partial pressure is attained slowly. Results are listed in Table I.

TABLE I

ELECTROMOTIVE FORCE E OF CELL III AT 275°

ξ	Phases	E (mv.)
0.580	$Ag_3SbS_3 + AgSbS_2$	43 ± 0.4
.603	$Ag_3SbS_3 + AgSbS_2$	43 ± .4
.670	$Ag_3SbS_3 + AgSbS_2$	43 ± .4
.820	$AgSbS_2 + Sb_2S_3$	99 ± 1.0
.885	$AgSbS_2 + Sb_2S_3$	98 ± 1.0
.900	$AgSbS_2 + Sb_2S_3$	97 ± 1.0

(2) In the cell

$$Ag(s)|AgI(s)|(Ag_2S, Sb_2S_3)|Pt, S(l) \qquad (IV)$$

the cell reaction on passing one faraday would be

$$Ag(s) + {}^1/_2S(l) = {}^1/_2Ag_2S\ (\text{in } Ag_2S\text{–}Sb_2S_3) \qquad (23)$$

Hence the e.m.f. of cell IV gives the free energy of formation of Ag_2S in the system Ag_2S–Sb_2S_3 from silver and sulfur. Upon combining results with the e.m.f. for a cell involving Ag_2S alone[14] the difference ${}^1/_2[\bar{F}_{Ag_2S} - F^\circ_{Ag_2S}]$ is obtainable. Since this difference has been determined directly with the help of cell III, no measurements on cell IV have been made, but cells of type IV may be found to be profitable for investigations on other systems.

(3) In addition, the cell

$$Ag|AgI|AgSbS_2 + Sb_2S_3|Sb \qquad (V)$$

has been investigated. Assuming that the antimony electrode is reversible, the cell reaction on passing one faraday would be

$$Ag + {}^2/_3Sb_2S_3 = {}^1/_3Sb + AgSbS_2 \qquad (24)$$

The e.m.f. of cell V was found to be about 300 mv. at 300°. Considerations not presented in detail in this paper show that this value is in conflict with results obtained for cell III. When the anti-

(16) F. Jaeger and H. S. van Klooster, *Z. anorg. allgem. Chem.*, **78**, 245 (1912).

(17) E. Jensen, *Avhandl. Norske Widenskaps. Akad. Oslo, I. Mat.-Naturv. Klasse*, No. 2 (1947).

(18) A. M. Gaudin and D. W. McGlashan, *Econom. Geol.*, **33**, 143 (1938).

mony electrode in cell V was replaced by a platinum electrode, the e.m.f. was found to be about the same as for cell V. This result indicates that the antimony electrode in cell V is not reversible at 300° but shows some kind of passivity which prevents adjustment of the sulfur activity in $AgSbS_2$–Sb_2S_3 mixtures to the two-phase equilibrium value of the system Sb–Sb_2S_3. This interpretation is in accord with the fact that antimony reacts very slowly with sulfur. An antimony pellet having a surface area of 0.5 cm.^{2} showed a weight increase of only 4.6 mg. after heating in sulfur vapor at 400° during 64 hours.

Thermodynamics of the System Ag_2S–Sb_2S_3.—In the first place, ΔF_{eq} for the phases Ag_3SbS_3 and $AgSbS_2$ may be calculated from eq. 11 by using reduction equilibrium data obtained by Schenck and his associates[2] and data for Ag–Sb alloys reported above.

Upon reduction of $Ag_3SbS_3(\xi = 0.5)$ with hydrogen, the H_2S/H_2 ratio was found to be constant over most of the ranges of η. Thus the integrals in eq. 11 may be evaluated as products.

When $AgSbS_2(\xi = 0.75)$ was reduced, two plateaus of the plot q *vs.* η were found. In addition, a further decrease of q at low values of η was observed. This tail in the q *vs.* η plot has been ascribed to the formation of a phase designated as Z with the approximate formula $Sb_2S_3 + 2Ag_2S + 31Ag$, but the existence of this phase has not yet been proved by other methods, *e.g.*, X-ray investigations. In the following evaluation, the tail of the q *vs.* η plot has been disregarded because detailed data are not available and the contribution of the tail is only minor.

Substituting numerical values in eq. 11, we obtain for Ag_3SbS_3

$$\Delta F_{eq}(\xi = 0.50, \eta = 1; 400°) = -575 - 176 = -751 \text{ cal./equivalent} \quad (25)$$

and for $AgSbS_2$

$$\Delta F_{eq}(\xi = 0.75, \eta = 1; 400°) = -288 - 250 = -538 \text{ cal./equivalent} \quad (26)$$

In each of these equations, the first term represents the value of $\Delta F_{eq}(\xi, \eta = 0)$ for the alloy, and the second term is the sum of the integrals involving values of q.

In addition, values of ΔF_{eq} for Ag_3SbS_3 and $AgSbS_2$ have been calculated from eq. 15 with partial equivalent free energies of Ag_2S derived from e.m.f. measurements listed in Table I. Equation 15 yields for Ag_3SbS_3

$$\Delta F_{eq}(\xi = 0.5, \eta = 1; 275°) = -710 \text{ cal./equivalent} \quad (27)$$

and for $AgSbS_2$

$$\Delta F_{eq}(\xi = 0.75, \eta = 1; 275°) = -565 \text{ cal./equivalent} \quad (28)$$

In spite of different temperatures, 400 and 275°, the values of ΔF_{eq} in eq. 25 and 27 for Ag_3SbS_3 and in eq. 26 and 28 for $AgSbS_2$ differ only to a minor extent in accord with the rule that the free energy change of reactions involving solid phases of virtually invariable composition varies only slightly with temperature.

Acknowledgment.—This work was supported by Office of Ordnance Research, U. S. Army, under Contract DA-19-020-ORD-3661. A. G. Verduch acknowledges gratefully the receipt of a Fulbright Fellowship.

THEORY OF SOLVENT EFFECTS ON MOLECULAR ELECTRONIC SPECTRA. FREQUENCY SHIFTS[1]

BY E. G. McRAE

Department of Chemistry, Florida State University, Tallahassee, Florida

Received October 15, 1956

The effects of electric dipole interactions on electronic band frequencies in solution spectra are analyzed theoretically. A general expression for the frequency shift is derived by perturbation theory. The frequency shift is the sum of contributions from dispersive and static dipole interactions. The dispersive contribution represents the *general red shift*, which is present in all solution spectra; it depends in part on the *weighted mean wave length* characteristic of the solvent. In the electrostatic contribution the role of the quadratic Stark effect is emphasized. The introduction of a simple electrostatic model permits the derivation of formulas relating frequency shifts in both emission and absorption spectra to the refractive index and static dielectric constant of the solvent. Illustrative numerical applications are described.

I. Introduction

In several recent discussions of solvent effects on electronic spectra, solvent-induced frequency shifts have been interpreted in terms of electric dipole interactions. The well-known red shift[2] in the spectra of non-polar solutes has been related by Bayliss[3] to the solvation energy of the transition dipole, while the work of Ooshika[4] indicates that the red shift is caused by dispersive interactions. Several authors[4–6] have discussed frequency shifts in the spectra of polar solutes in terms of the relative solvation energies of the permanent dipoles appropriate either to the combining states of the

(1) This work was carried out under a contract between the U. S. Air Force, Office of Scientific Research, ARDC, and the Florida State University.

(2) Shifts to lower frequencies relative to the vapor frequency are called red shifts, and shifts to higher frequency, blue shifts. In algebraic expressions, red shifts will be designated by a negative sign, blue shifts by a positive sign.

(3) N. S. Bayliss, *J. Chem. Phys.*, **18**, 292 (1950).

(4) Y. Ooshika, *J. Phys. Soc. Japan*, **9**, 594 (1954).

(5) L. G. S. Brooker, *Experientia Supplementum II*, (*XIVth International Congress of Pure and Applied Chemistry*), 229 (1955).

(6) N. S. Bayliss and E. G. McRae, THIS JOURNAL, **58**, 1002 (1954).

solute, or to the resonance structures contributing to those states. As has been stressed by Bayliss and McRae,[6] it is necessary in general to consider the frequency shifts arising from interactions involving the solute permanent dipoles as superposed on a *general red shift*,[7] which is present in all solution spectra.

In this paper we present a further discussion of frequency shifts caused by dipole interactions. The most important contribution of this study is the derivation, by perturbation theory, of a general expression for the frequency shift. It is hoped that this formulation will serve to correlate previous interpretations, and provide the basis for a more precise and complete qualitative interpretation. A second contribution of the present work is the derivation, from the general expression, of formulas linking the frequency shift to the solvent refractive index and static dielectric constant. The formulas presented here are more widely applicable than those previously put forward.[3,4]

II. Theoretical

The method of treatment consists of the application of second-order perturbation theory to the calculation of the electronic state energies of a solution containing N identical solvent molecules and one solute molecule. We suppose in the beginning that the molecules have fixed positions and orientations. In view of the comparative rapidity of electronic transitions, the same positions and orientations are appropriate to the ground and excited states of the solute.

In the zeroth order of approximation, we consider the molecules not to interact. The zeroth-order electronic state functions of the solution are then made up of products of state functions for the unperturbed component molecules. Neglecting the non-orthogonality of the latter, we shall employ simple product functions, for which we introduce notations such as

$$\Phi^0_{a(p)b(q)j} = \phi_0^{v(1)} \cdots \phi_a^{v(p)} \cdots \phi_b^{v(q)} \cdots \phi_0^{v(N)} \phi_j^u$$
$$\Phi^0_{a(p)j} = \phi_0^{v(1)} \cdots \phi_a^{v(p)} \cdots \phi_0^{v(q)} \cdots \phi_0^{v(N)} \phi_j^u \text{ and}$$
$$\Phi^0_{a(p)0} = \phi_0^{v(1)} \cdots \phi_a^{v(p)} \cdots \phi_0^{v(q)} \cdots \phi_0^{v(N)} \phi_0^u$$

where for example $\Phi^0_{a(p)b(q)j}$ denotes the zeroth-order function representing the state of the solution in which the solute molecule is in its jth excited electronic state ϕ_j^u, and the pth and qth solvent molecules are in their ath and bth excited states $\phi_a^{v(p)}, \phi_b^{v(q)}$, respectively.[8] Throughout this paper the notations u and $v(p)$ will refer to the solute and the pth solvent molecules, and the subscript zero will indicate the ground electronic state of a single molecule.

The zeroth-order electronic state energies are sums of the electronic state energies of the unperturbed component molecules; *e.g.*, the energy corresponding to $\Phi^0_{a(p)j}$ is given by $W^0_{aj} = (N-1)w_0^v + w_a^v + w_j^u$, where w denotes the electronic state energy of an unperturbed molecule. Energy differences will be expressed in cm.$^{-1}$, and denoted by ν; thus, for example, the energy difference between the ith and jth states of the solute will be expressed by

$$\nu^u_{ji} = (w_j^u - w_i^u)/hc = -\nu^u_{ij}$$

where h and c have the usual meanings.

We represent the energy of interaction of the molecules in solution by the classical energy of dipole interaction, which is given in the point-dipole approximation by

$$\mathcal{H}' = -\sum_{p=1}^{N} \Theta^{uv(p)} \mathfrak{M}^u \mathfrak{M}^{v(p)} - (1/2) \times \sum_{p=1}^{N} \sum_{q=1}^{N} \Theta^{v(p)v(q)} \mathfrak{M}^{v(p)} \mathfrak{M}^{v(q)} \quad (1)$$

where $\mathfrak{M}$ denotes the instantaneous magnitude of the dipole moment of a molecule and Θ is a geometrical factor dependent on the mutual orientation and separation of two dipoles.

The energy of the state Φ_i, corresponding in the zeroth order of approximation to Φ^0_i, is governed principally by the matrix elements $H_{j,i} = W^0\delta_{ji} + \int \Phi^0_j \mathcal{H}' \Phi^0_i d\tau$ (δ_{ji} is the Kronecker delta), $H_{a(p)j,i} = \int \Phi^0_{a(p)j}, \mathcal{H}' \Phi^0_i d\tau$ and $H_{a(p)b(q)i,i} = \int \Phi^0_{a(p)b(q)i} \mathcal{H}' \Phi^0_i d\tau$. Here and in what follows, the state functions are for simplicity taken to be real. In view of (1), the matrix elements may be written

$$H_{j,i} = W^0_i \delta_{ji} - \sum_{p=1}^{N} \Theta^{uv(p)}_{ji,00} M^u_{ji} M^v_{00} - (1/2) \sum_{p=1}^{N} \sum_{q=1}^{N} \Theta^{v(p)v(q)}_{00,00} (M^v_{00})^2 \delta_{ji} \quad (2)$$

$$H_{a(p)j,i} = -\Theta^{uv(p)}_{ji,a0} M^u_{ji} M^v_{a0} - (1/2) \sum_{\substack{q=1, \\ \neq p}}^{N} \Theta^{v(p)v(q)}_{a0,00} M^v_{a0} M^v_{00}$$

and

$$H_{a(p)b(q)i,i} = -(1/2) \sum_{\substack{q=1, \\ \neq p}}^{N} \Theta^{v(p)v(q)}_{a0,b0} M^v_{a0} M^v_{b0} \quad (3)$$

Here M denotes a matrix element of the dipole moment (*e.g.*, $M^u_{ij} = \int \phi^u_j \mathfrak{M}^u \phi^u_i d\tau$), and Θ denotes a geometrical factor of proportionality between the product of the moments of two rigid point dipoles and their energy of interaction (*e.g.*, the energy of interaction of two rigid point dipoles whose moments are, respectively, M^u_{ji} and M^v_{a0}, and which belong, respectively, to the solute and pth solvent molecules, is given by $-\Theta^{uv(p)}_{ji,a0} M^u_{ji} M^v_{a0}$).

Confining our attention to non-degenerate states of the solute, the energy of the state Φ_i is given according to second-order perturbation theory[9] by

(7) Bayliss and McRae[6] used the term *polarization red shift*.

(8) (a) It should be noticed that the subscripts for unexcited solvent molecules are omitted, but the subscript for the unexcited solute molecule is retained. (b) The above notations embrace all of the required zeroth-order functions, for in the approximations of the present treatment, matrix elements involving zeroth-order functions corresponding to the simultaneous excitation of more than two solvent molecules are zero.

(9) H. Eyring, J. Walter and G. E. Kimball, "Quantum Chemistry," John Wiley and Sons, Inc., New York, N. Y., 1944, p. 95.

$$W_i = H_{i,i} + \sum_{j\neq i}\frac{(H_{j,i})^2}{W_i^0 - W_j^0} + \sum_{p=1}^{N}\sum_{a\neq 0}\frac{(H_{a(p)i,i})^2}{W_i^0 - W_{ai}^0} + \sum_{p=1}^{N}\sum_{a\neq 0}\sum_{j\neq i}\frac{(H_{a(p)j,i})^2}{W_i^0 - W_{aj}^0} + (1/2)\sum_{p=1}^{N}\sum_{\substack{q=1,\\ \neq p}}^{N}\sum_{a\neq 0}\sum_{b\neq 0}\frac{(H_{a(p)b(q)i,i})^2}{W_i^0 - W_{abi}^0} \quad (4)$$

A similar expression for W_0 is obtained by replacing i by 0. The frequency shift, $\Delta\nu$, is given by

$$hc\Delta\nu = (\overline{W_i - W_0}) - (W_i^0 - W_0^0) \quad (5)$$

where the bar indicates a time-average value.

General Formula.—In order to obtain a simple expression for the frequency shift, it will be assumed that all the (point) dipoles associated with any one molecule (*i.e.*, transition dipoles as well as permanent dipoles) may be considered to lie at the same point in the molecule. Equation 4 can then be reduced to a form in which the energy is related explicitly to environmental contributions to the electric field at the solute dipoles. The time-average of this expression yields, through (5), a general formula for the frequency shift.

In the explicit reduction of (4), it will be assumed that the molecules can be considered as optically isotropic. However, as will be shown later, the formulas given below require only minor modification, if either the solute or the solvent molecules or both can be considered *rod-like*, in the sense of having all dipole moments parallel.

The term by term reduction of (4) can be accomplished without further gross approximations. Let $\mathbf{E}^u$ denote the field at the solute dipoles, due to the permanent dipoles of the surrounding solvent molecules. In view of (2), the first term in (4) reduces to

$$W_i^0 - \mathbf{M}_{ii}^u\cdot\mathbf{E}^u - (1/2)\sum_{p=i}^{N}\sum_{\substack{q=1\\ \neq p}}^{N}\Theta_{00,00}^{v(p)v(q)}(M_{00}^v)^2 \quad (6)$$

The terms under summation in (6) represent the energy of interaction of solvent permanent dipoles, and make no contribution to the frequency shift.

The second term in (4) can be written

$$-\frac{1}{hc}\sum_{j\neq i}\frac{(\mathbf{M}_{ji}^u\cdot\mathbf{E}^u)^2}{\nu_{ji}^u}$$

For an isotropic molecule, the value of $(\mathbf{M}_{ji}^u\cdot\mathbf{E}^u/M_{ji}^uE^u)^2$ averaged over all states $j \neq i$ is 1/3. Consequently the second term in (4) becomes approximately

$$-\frac{(E^u)^2}{3hc}\sum_{j\neq i}\frac{(M_{ji}^u)^2}{\nu_{ji}^u}$$

Making use of the usual expression for the isotropic polarizability of a molecule,[10] this becomes

$$-(1/2)(E^u)^2\alpha_i^u \quad (7)$$

where α_i^u denotes the static isotropic polarizability of the solute molecule in its ith excited electronic state.

With the aid of (2), the third term in (4) can be written

(10) Reference 9, p. 121.

$$-\frac{1}{hc}\sum_{p=1}^{N}\sum_{a\neq 0}\frac{(\Theta_{ii,a0}^{uv(p)}M_{ii}^uM_{a0}^v)(\Theta_{ii,a0}^{uv(p)}M_{ii}^uM_{a0}^v + \sum_{\substack{q=1,\\ \neq p}}^{N}\Theta_{a0,00}^{v(p)v(q)}M_{a0}^vM_{00}^v)}{\nu_{a0}^v} - \frac{1}{4hc}\sum_{p=1}^{N}\sum_{a\neq 0}\frac{\left(\sum_{\substack{q=1,\\ \neq p}}^{N}\Theta_{a0,00}^{v(p)v(q)}M_{a0}^vM_{00}^v\right)^2}{\nu_{a0}^v}$$

The second sum represents the energy of interaction of permanent and induced solvent dipoles, and makes no contribution to the frequency shift. The first sum can be written

$$-\frac{1}{hc}\sum_{p=1}^{N}\sum_{a\neq 0}\frac{(\mathbf{E}_i^{v(p)u}\cdot\mathbf{M}_{a0}^{v(p)})\left(\mathbf{E}_i^{v(p)u} + \sum_{\substack{q=1,\\ \neq p}}^{N}\mathbf{E}^{v(p)v(q)}\right)\cdot\mathbf{M}_{a0}^{v(p)}}{\nu_{a0}^v}$$

where $\mathbf{E}_i^{v(p)u}$ denotes the field at the dipoles belonging to the pth solvent molecule, due to the permanent dipole of the solute molecule in its ith excited state, and $\mathbf{E}^{v(p)v(q)}$ denotes the field at the same point, due to the permanent dipole of the qth solvent molecule. The second factor in parentheses in the above expression represents the field at the pth solvent molecule, due to the permanent dipoles of the surrounding molecules. We shall neglect the contribution of solvent dipoles to this field, on the ground that the percentage error thereby incurred in the above sum will be large only when the solvent is highly polar, and in that case terms of the type we are discussing at present make a relatively small contribution to the frequency shift. Making use of the properties of isotropic molecules, we obtain

$$-(1/2)\sum_{p=1}^{N}(E_i^{v(p)u})^2\alpha_0^v$$

where α_0^v denotes the static isotropic polarizability of a solvent molecule in its ground state. Let $\mathbf{m}_i^{v(p)}$ denote the moment of the dipole induced in a solvent molecule by the field $\mathbf{E}_i^{v(p)u}$. The above expression then becomes

$$-(1/2)\sum_{p=1}^{N}\mathbf{E}_i^{v(p)u}\cdot\mathbf{m}_i^{v(p)}$$

which can be written alternatively

$$-(1/2)M_{ii}^u e_i^u \quad (8)$$

where $\mathbf{e}_i^u$ denotes the field at the solute dipoles, due to solvent induced dipoles such as that with moment $\mathbf{m}_i^{v(p)}$.

Utilizing (2), the fourth term in (4) can be written

$$\sum_{p=1}^{N}\sum_{a\neq 0}\sum_{j\neq i}\left(1 - \frac{\nu_{ji}^u}{\nu_{a0}^v}\right)(\Theta_{ji,a0}^{uv(p)}M_{ii}^u)^2\frac{1}{hc}\frac{\nu_{a0}^v(M_{a0}^v)^2}{(\nu_{a0}^v)^2 - (\nu_{ii}^u)^2}$$

From the above expression, we obtain

$$\sum_{p=1}^{N}\sum_{a\neq 0}\sum_{j\neq i}\left(1 - \frac{\nu_{ji}^u}{\nu_{a0}^v}\right)\frac{1}{hc}\frac{\nu_{a0}^v(\mathbf{E}_{ji}^{v(p)u}\cdot\mathbf{M}_{a0}^{v(p)})^2}{(\nu_{a0}^v)^2 - (\nu_{ii}^u)^2}$$

which for isotropic molecules may be written approximately

$$\sum_{p=1}^{N}\sum_{a\neq 0}\sum_{j\neq i}\left(1-\frac{\nu_{ji}^{u}}{\nu_{a0}^{v}}\right)(E_{ji}^{v(p)u})^2\frac{1}{3hc}\frac{\nu_{a0}^{v}(M_{a0}^{v})^2}{(\nu_{a0}^{v})^2-(\nu_{ji}^{u})^2}$$

It is convenient to introduce a *weighted mean wave length*, defined by

$$L_{ji}=\sum_{a\neq 0}\frac{(M_{a0}^{v})^2}{(\nu_{a0}^{v})^2-(\nu_{ji}^{u})^2}\Big/\sum_{a\neq 0}\frac{\nu_{a0}^{v}(M_{a0}^{v})^2}{(\nu_{a0}^{v})^2-(\nu_{ji}^{u})^2}$$

We then obtain, for the fourth term in (4)

$$-(1/2)\sum_{p=1}^{N}\sum_{j\neq i}(1-\nu_{ji}^{u}L_{ji})(E_{ji}^{v(p)u})^2\alpha_0^{v}(\nu_{ji}^{u})$$

Here $\alpha_0^{v}(\nu_{ji}^{u})$ denotes the isotropic polarizability of a solvent molecule, appropriate to an oscillating field of frequency ν_{ji}^{u}. Let $m_{ji}^{v(p)}$ denote the amplitude of the dipole moment induced in a solvent molecule by an oscillating field of amplitude $E_{ji}^{v(p)u}$ and frequency ν_{ji}^{u}. We then obtain

$$-(1/2)\sum_{p=1}^{N}\sum_{j\neq i}(1-\nu_{ji}^{u}L_{ji})E_{ji}^{v(p)u}m_{ji}^{v(p)}$$

which can be written alternatively

$$-(1/2)\sum_{j\neq i}(1-\nu_{ji}^{u}L_{ji})M_{ji}^{u}e_{ji}^{u} \qquad (9)$$

Here e_{ji}^{u}, for example, denotes the field at the solute dipoles, due to a solvent induced dipole with moment $\mathbf{m}_{ji}^{v(p)}$.

As is made clear by (3), the fifth term in (4) represents the energy of an interaction between solvent molecules only. Consequently, this term makes no contribution to the frequency shift.

From (6), (7), (8) and (9) we find an expression for the energy W_i, and a similar expression for W_0 results on replacing i by 0. The frequency shift in the transition between the ground state and the ith excited state is given, according to (5), by

$$\begin{aligned}\Delta\nu_{i0}=(1/2hc)\Big[&\sum_{j\neq 0}(1-\nu_{j0}^{u}L_{j0})M_{j0}^{u}\overline{e_{j0}^{u}}-\\&\sum_{j\neq i}(1-\nu_{ji}^{u}L_{ji})M_{ji}^{u}\overline{e_{ji}^{u}}\Big]\\&+(1/2hc)(M_{00}^{u}\overline{e_{0}^{u}}-M_{ii}^{u}\overline{e_{i}^{u}})\\&+(1/hc)\overline{(\mathbf{M}_{00}^{u}-\mathbf{M}_{ii}^{u})\cdot\mathbf{E}^{u}}\\&+(1/2hc)(\alpha_0^{u}-\alpha_i^{u})\overline{(E^{u})^2}\end{aligned} \qquad (10)$$

where the bars indicate time-average values.

If either the solute or solvent molecules or both can be considered rod-like instead of isotropic, (4) can be reduced in a manner similar to that described above. If the solute molecule is rod-like, the final formula differs from (10) only in the fourth term, which becomes

$$(3/2hc)(\alpha_0^{u}-\alpha_i^{u})\overline{(\mathbf{M}_{00}^{u}\cdot\mathbf{E}^{u}/M_{00}^{u})^2}$$

where α_0^{u} and α_i^{u} again denote isotropic polarizabilities. If the solute molecule is not rod-like, the final formula is the same as (10).

Relationship to Macroscopic Properties.—Equation 10 may be written in a form involving the reaction fields of the solute dipoles. These may in turn be related to macroscopic properties of the solvent. We may identify $\overline{e_{ji}^{u}}$, for example, with the reaction field r_{ji} of the dipole whose moment is M_{ji}^{u}. The reaction field r_{ji} arises formally from the polarization of the solvent by an oscillating field whose frequency is ν_{ji}^{u}; therefore it should be related to the square of the solvent refractive index at this frequency. A slightly different interpretation should be placed on the reaction fields r_i and r_0, which are to be identified, respectively, with $\overline{e_i^{u}}$ and $\overline{e_0^{u}}$. These reaction fields arise from the contribution of induced dipoles to the static polarization of the solvent, and should therefore be related to the square of the solvent refractive index, extrapolated to zero frequency. The third term in (10) may be written $(1/hc)(\mathbf{M}_{00}^{u}-\mathbf{M}_{ii}^{u})\cdot\mathbf{R}$, where $\mathbf{R}$ denotes the reaction field corresponding to $\mathbf{E}^{u}$. (Obviously, R should not be identified with $\overline{E^{u}}$). $\mathbf{R}$ arises from the contribution of the solvent permanent dipoles to the static polarization of the solvent, and should therefore be related to that part of the static dielectric constant attributable to orientation polarization.

A difficulty arises in the treatment of the fourth term in (10), since $\overline{(E^{u})^2}$ cannot be related to macroscopic solvent properties through identifications such as those indicated above. However we may be sure that when R is comparatively large, $\overline{(E^{u})^2}$ will be of the same order of magnitude as R^2. Somewhat arbitrarily we adopt $\overline{(E^{u})^2}=3R^2$ (R large). For a rod-like solute molecule, we choose $\overline{(\mathbf{M}_{00}^{u}\cdot\mathbf{E}^{u}/M_{00}^{u})^2}=R^2$ (R large). The advantage of these assumptions is that the last term in (10) and the corresponding expression for a rod-like solute molecule become the same, *viz.*, $(3/2hc)(\alpha_0^{u}-\alpha_i^{u})R^2$.

We shall utilize the well known expression for the reaction field, derived on the basis of a point dipole at the center of a spherical cavity in a homogeneous dielectric.[11] For an absorption transition starting from the ground state, we have for an isotropic solute molecule

$$R=\frac{2(M_{00}^{u}+\alpha_0^{u}R)}{a^3}\frac{D'-1}{2D'+1}$$

where D' denotes the contribution of the permanent dipoles to the static dielectric constant of the solvent, and a denotes the cavity radius. The expression in parentheses represents the dipole moment of the solute molecule in solution. For most molecules, the ground-state isotropic polarizability is about one-half the cube of the most suitable cavity radius,[12] so that we derive approximately

$$R=\frac{2M_{00}^{u}}{a^3}\left[\frac{D-1}{D+2}-\frac{n_0^2-1}{n_0^2+2}\right] \qquad (11)$$

where we have substituted for $(D'-1)/(D'+2)$ by the factor in brackets, involving D, the static dielectric constant of the solvent, and n_0, the solvent refractive index extrapolated to zero frequency.

The value of R appropriate to emission bands depends on the degree of dipole reorientation occurring in the interval between population of the excited state, and emission. We consider two limiting cases: if there is negligible dipole reorientation,

(11) C. J. F. Bottcher, "Theory of Electric Polarization," Elsevier Publishing Co., Amsterdam, 1952, p. 64.

(12) Reference 11, p. 206.

the value of R is the same as that for the corresponding absorption band. On the other hand, if there is complete dipole reorientation, we have for a transition starting from the ith excited state

$$R = \frac{2(M_{ii}^{u} + \alpha_i^{u}R)}{a^3}\,\frac{D' - 1}{2D' + 1}$$

Neglecting terms involving powers of $(D'-1)/(D'+2)$ higher than the second, we obtain after a short calculation similar to the derivation of (11)

$$R = \frac{2M_{ii}^{u}}{a^3}\left[\frac{D-1}{D+2} - \frac{n_0^2-1}{n_0^2+2}\right]\times \left\{1 - \frac{2(\alpha_0^{u} - \alpha_i^{u})}{a^3}\left[\frac{D-1}{D+2} - \frac{n_0^2-1}{n_0^2+2}\right]\right\} \quad (11')$$

For the remaining reaction fields, we have in both absorption and emission bands

$$r_{ji} = \frac{2M_{ji}^{u}}{a^3}\,\frac{n_{ji}^2-1}{2n_{ji}^2+1} \qquad r_{j0} = \frac{2M_{j0}^{u}}{a^3}\,\frac{n_{j0}^2-1}{2n_{j0}^2+1} \quad (12)$$

$$r_i = \frac{2M_{ii}^{u}}{a^3}\,\frac{n_0^2-1}{2n_0^2+1} \qquad r_0 = \frac{2M_{00}^{u}}{a^3}\,\frac{n_0^2-1}{2n_0^2+1} \quad (13)$$

where n_{ji}, for example, denotes the solvent refractive index for light of frequency ν_{ji}^{u}. In (13) it would have been more accurate to write $M_{ii}^{u} + \alpha_i^{u}R$ in place of M_{ii}^{u}, and a similar expression in place of M_{00}^{u}. However this refinement would not greatly improve the accuracy of the final expression for the frequency shift, because whenever R is large, the term involving the reaction fields r_i and r_0 makes a relatively small contribution to the shift.

In view of the above discussion, including (11), (12) and (13), we obtain for the frequency shift in an absorption transition from the ground state to the ith excited state of an isotropic molecule

$$\Delta\nu = 2.13\times10^{-30}\left[\sum_{j\neq0}\left(\frac{1}{\nu_{j0}^{u}} - L_{j0}\right)\frac{f_{j0}^{u}}{a^3}\,\frac{n_{j0}^2-1}{2n_{j0}^2+1} - \sum_{j\neq i}\left(\frac{1}{\nu_{ji}^{u}} - L_{ji}\right)\frac{f_{ji}^{u}}{a^3}\,\frac{n_{ji-1}^2}{2n_{ji+1}^2}\right] + \frac{1}{hc}\,\frac{(M_{00}^{u})^2 - (M_{ii}^{u})^2}{a^3}\times \frac{n_0^2-1}{2n_0^2+1} + \frac{2}{hc}\,\frac{\mathbf{M}_{00}^{u}(\mathbf{M}_{00}^{u} - \mathbf{M}_{ii}^{u})}{a^3}\left[\frac{D-1}{D+2} - \frac{n_0^2-1}{n_0^2+2}\right] + \frac{6}{hc}\,\frac{(M_{00}^{u})^2(\alpha_0^{u} - \alpha_i^{u})}{a^6}\left[\frac{D-1}{D+2} - \frac{n_0^2-1}{n_0^2+2}\right]^2 \quad (14)$$

where in the first term we have introduced the oscillator strength, which, for a transition between the ith and jth states of the solute, for example, is given by[13]

$$f_{ji}^{u} = 4.704\times10^{29}\,\nu_{ji}^{u}\,(M_{ji}^{u})^2 = -f_{ij}^{u}\quad (M_{ji}^{u}\text{ in e.s.u.})$$

Equation 14 is applicable to emission transitions only in the cases in which there is no appreciable dipole reorientation in the excited state. If there is complete dipole reorientation, (11'), (12) and (13) are applicable, and give for the frequency shift in the emission transition from the ith excited state to the ground state of an isotropic solute molecule

$$\Delta\nu = 2.13\times10^{-30}\left[\sum_{j\neq0}\left(\frac{1}{\nu_{j0}^{u}} - L_{j0}\right)\frac{f_{j0}^{u}}{a^3}\,\frac{n_{j0}^2-1}{2n_{j0}^2+1} - \sum_{j\neq i}\left(\frac{1}{\nu_{ji}^{u}} - L_{ji}\right)\frac{f_{ji}^{u}}{a^3}\,\frac{n_{ji}^2-1}{2n_{ji}^2+1}\right] + \frac{1}{hc}\,\frac{(M_{00}^{u})^2 - (M_{ii}^{u})^2}{a^3}\times \frac{n_0^2-1}{2n_0^2+1} + \frac{2}{hc}\,\frac{\mathbf{M}_{ii}^{u}(\mathbf{M}_{00}^{u} - \mathbf{M}_{ii}^{u})}{a^3}\left[\frac{D-1}{D+2} - \frac{n_0^2-1}{n_0^2+2}\right] + \frac{2}{hc}\,\frac{\mathbf{M}_{ii}^{u}(5\mathbf{M}_{ii}^{u} - 2\mathbf{M}_{00}^{u})(\alpha_0^{u} - \alpha_i^{u})}{a^6}\left[\frac{D-1}{D+2} - \frac{n_0^2-1}{n_0^2+2}\right]^2 \quad (14')$$

where we have neglected terms involving powers of $[(D-1)/(D+2) - (n_0^2-1)/(n_0^2+2)]$ higher than the second.

From (14) and (14'), the frequency difference between the O–O bands in the absorption and emission transitions between the ground and the excited states of an isotropic solute molecule is predicted to be

$$\Delta\nu(\text{absorption}) - \Delta\nu(\text{emission}) = \frac{2}{hc}\,\frac{(\mathbf{M}_{00}^{u} - \mathbf{M}_{ii}^{u})^2}{a^3}\times \left[\frac{D-1}{D+2} - \frac{n_0^2-1}{n_0^2+1}\right] + \frac{2}{hc}\,\frac{(\alpha_0^{u} - \alpha_i^{u})[3(M_{00}^{u})^2 - 5(M_{ii}^{u})^2 + 2\mathbf{M}_{00}^{u}\cdot\mathbf{M}_{ii}^{u}]}{a^6}\times \left[\frac{D-1}{D+2} - \frac{n_0^2-1}{n_0^2+2}\right]^2 \quad (15)$$

III. Discussion

The result of the treatment given in Sec. II is embodied in eq. 10, 14 and 14.[14]

Equation 10 is limited to transitions between non-degenerate states of the solute, but is otherwise generally applicable. It is fundamentally correct even though it is approximate, and therefore provides the basis for a sound qualitative interpretation of frequency shifts caused by dipole interactions. Because of the simplifications invoked in its derivation, especially the point-dipole approximation and the approximations inherent in second-order perturbation theory, the environmental fields appearing in (10) should not always be taken literally. For example, if the solute permanent charge distribution consists of positive and negative charges separated by several Å., it does not make sense to speak literally of the field at the solute dipole. Instead, the environmental fields should be considered simply as parameters whose qualitative variation from solvent to solvent can often be inferred, either from the macroscopic properties of the solvent or through consideration of hydrogen bonding. Again, if either the solute or solvent molecule is non-polar, but contains highly polar groups whose moments cancel, it is not realistic to put the time-average of the field $\mathbf{E}^{u}$ equal to zero, even though this is implied formally in the derivation of eq. 10.

Equation 14 represents the frequency shift in absorption bands. Unless the solvent and solute are both polar, frequency shifts in corresponding absorption and emission bands are predicted to be equal. When the solvent and solute are both polar, frequency shifts in emission bands are represented by (14) if there is negligible dipole reorientation in the excited state, or by (14') if there is complete di-

(13) R. S. Mulliken and C. A. Rieke, *Rep. Prog. Phys.*, **8**, 231 (1941).

(14) These equations represent the solvent effect on the frequency of the O–O band. As the O–O band cannot always be identified in solution spectra, the equations must be compared with observed frequency shifts in band maxima, relative to the corresponding band maxima in the vapor spectrum. The latter should be determined by drawing the envelope of the vibrational structure. Unless the frequency shifts are comparable with or larger than the band width, the above procedure for applying the equations cited is valid only insofar as there is no significant solvent effect on band shape. Similar remarks apply to eq. 15.

pole reorientation. For example, frequency shifts induced in fluorescence spectra by rigid-glass solvents are represented by (14), since in such solvents the dielectric relaxation times are some orders of magnitude greater than the lifetime of the excited state ($\sim 10^{-8}$ second). On the other hand the relaxation times of most liquid solvents at room temperature are about 10^{-10} second,[15] so that shifts induced by them in fluorescence spectra are represented by (14′). In the application of (14) to frequency shifts induced by solid polar solvents, the adopted dielectric constant should be the value extrapolated from that of the liquid solvent.

Equations 14 and 14′ are of course subject to the same limitations as (10), and an additional limitation is imposed by the use of the simple model for the solute in solution. In particular, (14) and (14′) do not apply to frequency shifts caused in part by hydrogen bonding.

Because of the assumption of identical solvent molecules in the derivation of (10), this formula and the formulas derived from it apply to frequency shifts induced by pure solvents only. The generalization to mixed solvents can be achieved in cases in which the solvent composition near the solute molecule can be assumed equal to the bulk composition. In that case, the weighted mean wave length of a mixed solvent is a linear combination of weighted mean wave lengths of the solvent components, the coefficients being the appropriate mole fractions.

Dispersive Interactions.—The first term in (10) represents a contribution from dispersive interactions. It will ordinarily be negative, because $\nu^{u}_{j0} > \nu^{u}_{ji}$ for $j>i$ (the states being numbered in order of increasing energy). In practice we observe frequency shifts in only the first few electronic bands of the solute, and these lie at lower frequencies than that of the onset of solvent absorption. The first term represents the *general red shift.*

The expression for the general red shift consists of a sum of terms, each of which corresponds to a virtual transition starting from one of the combining states of the solute. Each term contains the reaction field of a dipole whose moment oscillates with a frequency equal to the appropriate transition frequency and with amplitude equal to the appropriate transition dipole moment. According to the present formulation, the general red shift depends in part on the *weighted mean wave length*, which is a function of the frequency, characteristic of the solvent.

If none of the transitions which make an important contribution to the general red shift lie close in frequency to a solvent absorption band, the weighted mean wave length may be considered approximately as a constant. Whenever this is the case, we shall for definiteness adopt the value at zero frequency, denoting it by L_0.

The weighted mean wave length may be taken as a constant in all applications to strong transitions ($f \sim 1$), because any frequency shifts are governed mainly by the term corresponding to the transition in question. In applications to weak transitions, the frequency-dependence of the weighted mean wave length may be important if the solvent begins to absorb at a frequency close to that of the transition in question.

Limits are set on L_0, the weighted mean wave length at zero frequency, by the inequalities

$$\sum_{a\neq 0}{}' \frac{(M^{\nu}_{a0})^2}{(\nu^{\nu}_{a0})^2} \Big/ \sum_{a\neq 0}{}' \frac{(M^{\nu}_{a0})^2}{\nu^{\nu}_{a0}} > L_0 > \frac{2}{3hc} \sum_{a\neq 0}{}' \frac{(M^{\nu}_{a0})^2}{(\nu^{\nu}_{a0})^2} \Big/ \alpha^{\nu}_0$$

where the primes indicate summation over terms corresponding to known transitions in the absorption spectrum of the solvent in question.

As long as the frequency and intensity of at least one strong transition is known, the limits are sufficiently close that their arithmetic mean is a good estimate of L_0. For example, we have for the solvent benzene, utilizing the known polarizability, the formula relating the oscillator strength to the transition dipole moment and the information in Table I: $1850 > L_0 > 650$ (Å.) yielding $L_0 \approx 1250$ Å. This value is quite insensitive to refinements such as taking into account some Rydberg transitions. It is appropriate to many benzene derivatives as well as to benzene itself.

Unfortunately the ultraviolet absorption spectra of most other common solvents are not sufficiently well known for the above method to be useful. However we discuss a few typical solvents as follows.

TABLE I

FREQUENCY SHIFTS IN THE BENZENE SPECTRUM

Transition[a]	f	ν(cm.$^{-1}$)	n	Contribution to $\Delta\nu$ (cm.$^{-1}$) λ2500 Å. band	λ2000 Å. band
$A_{1g} \rightarrow B^{+}_{2u}$	0.002[b]	40,000	1.49[f]	−3	2
$A_{1g} \rightarrow B^{+}_{1u}$	.12[c]	50,000	1.56[g]	112	−238
$A_{1g} \rightarrow E^{+}_{1u}$	1.2[c]	55,000	1.58[g]	951	951
$B_{2u} \rightarrow E_{2g}$	(0.72)[d]	30,000[e]	1.45[f]	(−1368)[d]	0
$B_{1u} \rightarrow E^{-}_{2}$	(.50)[d]	19,000[e]	1.43[f]	0	(−1785)[d]
		Obsd. shift		−308[b]	−1070[b]

[a] Notations and assignments of Pariser.[20] [b] Reference 21. [c] Reference 16. [d] Values required to fit observed shifts. [e] Differences of energies calculated by Pariser.[20] [f] Landolt-Bornstein, "Physikalisch-chemisch Tabellen," Springer, Berlin, 1935, Part 3 (II), p. 1683. [g] Extrapolated from literature values.

Cyclohexane.—From the absorption spectrum[16] we have $L_0 < 1450$ Å., and guess $L_0 \approx 1000$ Å. This value should be equally applicable to most saturated hydrocarbon solvents.

Dioxane.—From the absorption spectrum[17] we have $L_0 < 1800$ Å. Since the oscillator strength of the first band (0.11) is less than that of the λ 1800 Å. band of benzene, the value of L_0 for dioxane probably lies between those for benzene and cyclohexane.

Water.—From the absorption spectrum[18] we have $L_0 <$ 1350 Å., suggesting a value of L_0 approximately equal to or less than that for cyclohexane.

It should be noted that the values of L_0 tend to increase in the same order as the solvent refractive index.

Comparison with Previous Work.—In the first term in (14), the general red shift is related to the solvent refractive index. This expression may be compared in an interesting way with that previously derived by Bayliss.[3] To facilitate the comparison, we write the result of the present treatment in the form

$$1.07 \times 10^{-14} \left\{ -\frac{2L_{i0}f^{u}_{i0}}{a^3} \frac{n^2_{i0}-1}{2n^2_{i0}+1} + \sum_{\substack{j\neq 0,\\ \neq i}} \left[\left(\frac{1}{\nu^{u}_{j0}} - L_{j0} \right) \frac{f^{u}_{j0}}{a^3} \frac{n^2_{j0}-1}{2n^2_{j0}+1} - \right. \right.$$

(15) D. H. Whiffen, *Quart. Rev. Chem. Soc.*, **4**, 131 (1950).

(16) L. W. Pickett M. Muntz and E. M. McPherson, *J. Am. Chem. Soc.*, **73**, 4862 (1951).

(17) L. W. Pickett, N. J. Hoeflich and Tien-Chuan Liu, *ibid.*, **73**, 4865 (1951).

(18) K. Watanabe and M. Zelikoff, *J. Opt. Soc. Amer.*, **43**, 753 (1953).

$$\left(\frac{1}{\nu^{u}_{ji}} - L_{ji}\right)\frac{f^{u}_{ji}}{a^3}\frac{n^2_{ii}-1}{2n^2_{ii}+1}\Bigg] \quad (16)$$

whereas the Bayliss expression is

$$-1.07\times 10^{-14}\,\frac{1}{\nu^{u}_{i0}}\,\frac{f^{u}_{i0}}{a^3}\,\frac{n^2_{i0}-1}{2n^2_{i0}+1}$$

The first term in (16) differs from the Bayliss expression in that it contains $2L_{i0}$ in place of $1/\nu^{u}_{i0}$. Terms such as those under summation in (16) appear also in the treatment due to Ooshika.[4] However, the result of the present treatment is not identical with that obtained by Ooshika. In particular, the weighted mean wave length appears, in the present work, in place of the wave length of onset of solvent absorption in Ooshika's expression. This modification is considered to be quite important, because the two wave lengths do not in general vary in the same way from solvent to solvent.

Application to Benzene.—The terms under summation in (16) make a dominant contribution to the red shift in weak transitions, since f^{u}_{i0} is then small. This point may be illustrated by a numerical application of (16) to the shifts induced by the solvent cyclohexane in the λ 2500 Å. and λ 2000 Å. absorption bands of benzene. We assume that the shifts are caused by the transitions indicated in the first column of Table I,[19] the notations and assignments being those of Pariser.[20] Since the intensities of the transitions between excited states are unknown, we prefer to apply (16) in an indirect way, by calculating the intensities that these transitions must have in order to account for the observed shifts. Possible contributions from forbidden transitions between excited states will be neglected. For the radius of the benzene molecule, we adopt $a = 3.0$ Å. Since the first absorption band of cyclohexane lies at a considerably higher frequency than any of the benzene transitions indicated in the table, the weighted mean wave length may be considered approximately as a constant. We adopt the value indicated above, *viz.*, $L_0 = 1000$ Å. With the transition intensities, transition frequencies and solvent refractive indices, n, indicated in the table, we require in order to fit the observed shift of 308 cm.$^{-1}$ in the λ 2500 Å. band[21] that the oscillator strength of the $B^{-}_{2u} \rightarrow E^{+}_{2g}$ transition be 0.7. This value is in accord with the fact that the transition is allowed. The fifth column in the table shows the contribution of each transition to the shift. The $A^{-}_{1g} \rightarrow B^{-}_{2u}$ transition itself is seen to contribute only one per cent. of the total. A similar calculation shows that in order to fit the observed shift of 1070 cm.$^{-1}$ in the λ 2000 Å. band,[21] the oscillator strength of the $B^{+}_{1u} \rightarrow E^{-}_{2g}$ transition must be 0.5, again an appropriate value for an allowed transition. The last column of the table shows that the $A^{-}_{1g} \rightarrow B^{+}_{1u}$ transition itself contributes about one-quarter of the total shift.

(19) Transitions to still higher energy states must unfortunately be omitted, for practical reasons. However, the contributions of such transitions probably tend strongly to cancel.

(20) R. Pariser, *J. Chem. Phys.*, **24**, 250 (1956).

(21) N. S. Bayliss and L. Hulme, *Australian J. Chem.*, **6**, 257 (1953).

The above example indicates that the frequency shifts are caused predominantly by strong transitions. The intensities of these transitions are probably not greatly altered upon the introduction of substituents into the benzene ring. Consequently, we are able to explain Ferguson's[22] observation that in the λ2500 Å. bands of weakly polar substituted benzenes, the frequency shifts are all about the same, and in particular are independent of the λ2500 Å. band intensities.

Effect of the Weighted Mean Wave Length.—The influence of the weighted mean wave length is manifest in the relative magnitudes of the general red shift induced by different solvents. The general red shift is observed directly only when both the solvent and solute are non-polar. In such cases, it is known that the frequency shift is approximately proportional to $(n^2 - 1)/(2n^2 + 1)$, where n denotes the solvent refractive index at some particular visible or near-ultraviolet frequency.[3,21,23] (The linearity is also observed in certain other cases, which will be discussed later.) From the relatively few studies in which frequency shifts have been referred to the vapor frequency,[3,21,24,25] it appears that the plots of $\Delta\nu$ *vs.* $(n^2 - 1)/(2n^2 + 1)$ do not in general extrapolate to the origin, as they should according to Bayliss' theory, but tend to cut the frequency axis beyond the origin. This behavior led Bayliss[3] to suggest that the frequency shift is caused in part by interactions other than those accounted for by his theory. Actually, the discrepancy may arise from the slightly incorrect form of the Bayliss expression. According to the present theory, the frequency shift is approximately proportional to $(AL_0 + B)(n^2 - 1)/(2n^2 + 1)$, which is a form of (16) obtained by replacing refractive indices and weighted mean wave lengths at all frequencies by n and L_0, respectively. A and B denote constants characteristic of the solute. Since the weighted mean wave length tends to be shorter for solvents of lower refractive index, the plot of $\Delta\nu$ *vs.* $(AL_0+B)(n^2 - 1)/(2n^2 + 1)$ should pass nearer the origin than that of $\Delta\nu$ *vs.* $(n^2-1)/(2n^2+1)$, while still retaining the linearity of the latter plot. Because of the difficulty of estimating L_0, A and B, the possibility of the former plot cutting the frequency axis far on the red-shift side of the origin cannot definitely be excluded, although this appears unlikely if AL_0 and B are of comparable magnitude. Inspection of (16) suggests that this is actually the case; AL_0 probably predominates slightly in strong transitions, B in weak transitions.

Electrostatic Interactions.—The remaining terms in (16) represent the contribution of electrostatic interactions. The second term represents the contribution of interactions between the solute permanent dipoles and the solvent dipoles thereby induced, and the third term represents the contribution of interactions between the permanent dipoles

(22) J. Ferguson, *J. Chem. Phys.*, **24**, 1263 (1956).

(23) (a) N. D. Coggeshall and A. Pozefsky, *ibid.*, **19**, 980 (1951); (b) G. M. Badger and R. S. Pearce, *Spectrochim. Acta*, **4**, 280 (1951); (c) J. Ham, *J. Am. Chem. Soc.*, **76**, 3875 (1954).

(24) (a) S. Sambursky and G. Wolfsohn, *Trans. Faraday Soc.*, **36**, 427 (1940); (b) G. Kortüm and B. Finckh, *Z. physik. Chem.*, **B52**, 263 (1942). This work has been summarized and discussed by Förster.[25]

(25) Th. Förster, "Fluoreszenz Organischer Verbindungen," Vandenhoeck and Ruprecht, Gottingen, 1951, p. 135.

of the solute and solvent molecules. The fourth term represents the contribution of the interactions between the permanent dipoles of the solvent molecules and the solute dipoles thereby induced. Since it is proportional to the square of the field intensity produced by the solvent permanent dipoles, the fourth term may be said to represent the quadratic Stark effect.

The representation of the electrostatic contribution as a sum of terms is somewhat artificial, being a consequence of second-order perturbation theory. The same expressions could have been derived by the conventional methods of electrostatics, with due cognizance of the non-equilibrium polarization of the solvent immediately after the transition. The treatment by perturbation theory is preferable, because it is consistent with the treatment of the dispersive interactions.

In the last three terms in (14) and in (14′), the contributions of electrostatic interactions are expressed in terms of the static dielectric constant of the solvent and the solvent refractive index extrapolated to zero frequency. It will be recalled that the third terms were derived on the assumption of an isotropic solute molecule, and the fourth terms were derived on an assumption which is likely to be valid only when both the solvent and the solute are highly polar.

The dependence on the solvent of the frequency difference between the O–O bands of corresponding absorption and fluorescence bands should be interpretable in terms of electrostatic interactions only. Since the interpretation is complicated neither by the general red shift nor by solute dipole-induced solvent dipole interactions, concurrent studies of absorption and fluorescence spectra should provide more definite information about the dipole moment of the solute in its lowest excited singlet state than can be inferred from data on absorption spectra alone. Equation 15 represents the frequency difference mentioned above.

Comparison with Previous Work.—Equation 14 may be compared with the formula derived by Ooshika.[4] As far as the electrostatic contributions are concerned the two expressions appear to be quite different, but the difference is probably superficial. However, the present result has the substantial advantage that the electrostatic contribution is expressed in closed form.

The present theory leads naturally to a classification of solutions previously adopted by Bayliss and McRae.[6] In their case I (both solute and solvent non-polar) the first term in (10) alone contributes to the frequency shift. In case II (solute non-polar, solvent polar) the first and fourth terms contribute, while in case III (solute polar, solvent non-polar) the first and second terms contribute. In case IV (both solute and solvent polar), all four terms make a contribution. Case I has already been discussed above. In the following discussion of cases II–IV, we shall avoid unnecessary duplication of that given in the previous paper,[6] with which we are substantially in agreement, confining our attention to certain modifications or extensions suggested by the present work.

Cases II and III of Bayliss and McRae.—In the discussion of case I, it was mentioned that the frequency shifts vary approximately linearly with $(n^2 - 1)/(2n^2 + 1)$. The same behavior is ordinarily observed in cases II and III, although in case II, apparently anomalous shifts are produced by highly polar solvents such as water,[21] methanol[24,25] and ethanol.[21,26] The phenomena in case II do not necessarily conflict with the theory, since we may say that the first term in (10) is ordinarily much larger than the fourth (*i.e.*, the general red shift is dominant) but that if the solvent is highly polar the fourth term (*i.e.*, the quadratic Stark effect) may make an important contribution. In case III, the dependence of the frequency shift on the solvent refractive index is represented by the first two terms in (14) (or 14′). Since n_0 ordinarily differs little from n,[27] the theory readily explains the observed behavior.

Case IV of Bayliss and McRae.—To simplify this discussion, we write the last two terms of (10) in the form involving the reaction field, *viz.*, $(1/hc)\cdot(\mathbf{M}_{00}^{u} - \mathbf{M}_{ii}^{u})\cdot\mathbf{R}$ and $(3/2hc)(\alpha_0^u - \alpha_i^u)R^2$, respectively. Here, the significance of the reaction field is analogous to that of $\mathbf{E}^u$, as discussed at the beginning of this section. The nature of the phenomena in case IV depends critically on the relative magnitude of the above terms. In all cases of practical interest, the first of the two terms contributes a significant proportion of their sum. Whether or not the contribution of the second term is important can only be judged from the experimental results, because the difference between ground and excited state polarizabilities (indeed, even the sign of the difference) is in general difficult to predict.

If the contribution of the quadratic Stark effect is indeed negligible,[29] the qualitative interpretation is the same as that previously proposed.[6] However, we are able to give semi-quantitative expression to the qualitative theory, with the aid of (14) or (14′). We illustrate this by the application of an approximate form of (14) to the λ 5500 Å. absorption band of phenol blue.

Application to Phenol Blue.—Solvent effects in the phenol blue spectrum have been studied by Brooker and Sprague,[30] whose results imply that the frequency shifts increase in the order of solvent dielectric constant. The more extensive study by LeRosen and Reid[31] shows that there is no correlation with the dielectric constant, but that the shifts induced by hydrocarbon and aryl halide solvents vary regularly with the solvent refractive index. LeRosen and Reid found no correlation of the shifts induced by other solvents with any solvent macroscopic property or combination of such properties. They did, however, present a qualitative inter-

(26) R. Schnurmann and W. F. Maddams, *J. Chem. Phys.*, **19**, 1430 (1951).

(27) The solvent water is exceptional in this respect. The value of n_0^2 is about 5, while n^2 for visible light is 1.77.[28]

(28) R. A. Robinson and R. H. Stokes, "Electrolyte Solutions," Butterworth, London, 1955, p. 10.

(29) "Negligible" has a different meaning in the discussion of case IV than in that of the preceding cases, the discussion of case IV being carried on at a lower level of approximation.

(30) L. G. S. Brooker and R. H. Sprague, *J. Am. Chem. Soc.*, **63**, 3214 (1941).

(31) A. L. LeRosen and C. E. Reid, *J. Chem. Phys.*, **20**, 233 (1952).

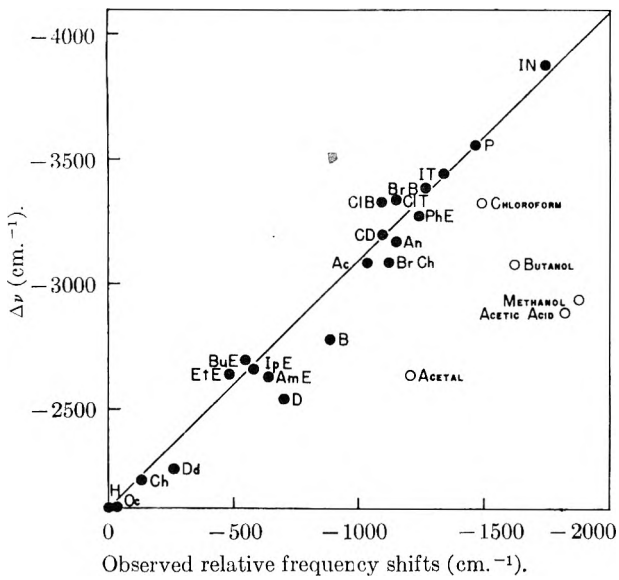

Fig. 1.—Calculated *vs.* observed frequency shifts in the λ5500 Å. band of phenol blue. The frequency shifts are calculated from eq. 17 ($A = -5.5 \times 10^8$ cm.$^{-2}$, $B' = -5500$ cm.$^{-1}$, $C = -1530$ cm.$^{-1}$). Hydrogen bonding solvents (open circles) are indicated by name. The remaining solvents (full circles) are indicated as shown below. In the following list of solvents, the refractive index and static dielectric constant of each solvent are quoted in that order. In a few cases, static dielectric constants are not available; values estimated from those for related compounds were used in the calculation, and the estimated values are given below in parentheses. The solvents are listed in the order in which they induce increasing red shifts.

H	Heptane	1.390	1.9
Oc	Octane	1.391	1.9
Ch	Cyclohexane	1.419	2.0
Dd	Dodecane	1.417	2.0
EtE	Ethyl ether	1.345	4.4
BuE	Butyl ether	1.393	(3.4)
IpE	Isopropyl ether	1.363	(3.9)
AmE	Amyl ether	1.409	2.8
D	Dioxane	1.417	2.2
B	Benzene	1.493	2.3
Ac	Acetone	1.360	21.0
ClB	Chlorobenzene	1.519	5.5
CD	Carbon disulfide	1.618	2.6
BrCh	Bromocyclohexane	1.491	7.9
ClT	*p*-Chlorotoluene	1.516	5.6
An	Anisole	1.509	4.3
PhE	Phenyl ether	1.574	3.7
BrB	Bromobenzene	1.553	5.2
IT	*o*-Iodotoluene	1.603	(5)
P	Pyridine	1.502	12.4
IN	1-Iodonaphthalene	1.695	(4)

pretation of the results in terms of various types of intermolecular interactions, including hydrogen bonding.

Equation 14 may be written in the approximate form

$$\Delta\nu = (AL_0 + B')\frac{n_D^2 - 1}{2n_D^2 + 1} + C\left[\frac{D - 1}{D + 2} - \frac{n_D^2 - 1}{n_D^2 + 2}\right] \quad (17)$$

where refractive indices at all frequencies have been replaced by the value appropriate to the sodium-D line, and the quadratic Stark effect has been neglected. A, B' and C are constants characteristic of the solute. Figure 1 illustrates the fit of the above equation to the experimental results for phenol blue.

In Fig. 1, points are shown for all solvents whose effects have been measured,[30,31] except water. In the case of water, (17) is inapplicable because of the considerable difference between n_0 and n_D.[27]

For saturated hydrocarbon solvents, bromocyclohexane, aliphatic alcohols and water, the value of L_0 was taken to be 1000 Å.; for other solvents, 1250 Å. was adopted. The fit of predicted and observed shifts was insensitive to B'/A; the assumed ratio, which is arbitrary, places equal weight on AL_0 and B for saturated hydrocarbon solvents. The best value of C/A was determined by the method of least squares, omitting the points represented in the figure by open circles. The value of A was adjusted to make the theoretical straight line pass through the points for *n*-heptane and pyridine (the vapor spectrum is not available). The neglect of the quadratic Stark effect is justified by the fit of the points to a straight line, as shown in the figure.

A glance at Fig. 1 shows that the solvents are separated into two distinct series according to their ability to form a hydrogen bond with the solute. Although (14) is not applicable to the total frequency shifts caused in part by hydrogen bonding, it may be capable of predicting that part of the shift exclusive of the contribution of hydrogen bonding. The points representing non-hydrogen bonding solvents are fitted to the full straight line with a root mean square deviation of about 100 cm.$^{-1}$, which is of the same order of magnitude as the experimental error in the determination of band frequencies in solution spectra (~50 cm.$^{-1}$). The points representing non-polar solvents illustrate the behavior mentioned above as typical of class III. The remaining points (non-hydrogen bonding polar solvents) show that frequency shifts in class IV may be correlated with a particular function of both the dielectric constant and refractive index of the solvent, even though there is no general correlation with either quantity separately.

The theory is evidently capable of reproducing the gross features of the phenomena, but not all of the finer details. For example, all of the points representing the aliphatic ethers lie near the full straight line, but the relative shifts induced by different members of this group of solvents do not support the theory. No doubt the discrepancies are due in part to the simplifying assumptions about the refractive index and the weighted mean wave length, the crudity of the model, and the anisotropy of phenol blue. At least one of the discrepancies, in the case of the solvent dioxane, may reflect a more fundamental failure of the approach based on (14). The dioxane molecule has two non-adjacent dipolar groups whose moments cancel, so that the effective reaction field **R** is probably greater than is indicated by the macroscopic properties (*cf.* the discussion of (10) at the beginning of this Section).

LeRosen and Reid[31] tried to explain the results which they obtained with non-hydrogen bonding solvents in terms of solute dipole-induced solvent dipole interactions only. The present work indicates that permanent dipole interactions make an important contribution to the frequency shifts induced by polar solvents.

The constant C, which appears in the approximate form of (14), corresponds to $(2/hca^3)(\mathbf{M}_{00}^{y} - \mathbf{M}_{00}^{y})\cdot\mathbf{M}_{01}^{y}$ in (14), so that from the best value of C found as indicated above (-1530 cm.$^{-1}$) we may calculate the excited state permanent dipole moment of phenol blue. The ground state dipole

moment is 5.80 Debye.[32] The most appropriate cavity radius probably lies between 4 and 5 Å. If we assume that the ground and excited state dipole moments are parallel, we calculate the excited state dipole moment to be between 7.5 Debyes (a = 4 Å.) and 9.1 Debyes (a = 5 Å.). Both are of the expected order of magnitude, but they do not offer strong support for the suggestion[20] that a Zwitterion structure contributes heavily to the excited state.

Application to Merocyanines.—We now discuss the remarkable solvent-induced frequency shifts observed in the lowest-frequency singlet–singlet absorption bands of merocyanine dyes. The results of extensive studies, mainly by Brooker and co-workers,[33,34] are typified by those illustrated in Fig. 2a. The three dyes IV, V and IX (notations of Brooker, Keyes and Heseltine[34]) have a common acidic (electron-attracting) nucleus, and basic (electron-repelling) nuclei whose basicity decreases in the order IV > V > IX.[34] Almost certainly, this is the order of decreasing ground state permanent dipole moment. The outstanding feature of the frequency shifts, as revealed by Fig. 2a, is that the band of the most highly polar dye IV shifts to higher frequencies as the water content of the solvent is increased, while the band of the least polar dye IX shifts initially to lower and then to higher frequencies. Intermediate behavior is exhibited by the dye of intermediate dipole moment.

The phenomena have been interpreted by Brooker[5] in terms of the relative solvent stabilization of polar and non-polar resonance structures, and this approach has been elaborated by Simpson[35] and by Platt.[36] As a particular application of the present theory, we advance an alternative (but not fundamentally different) explanation in terms of the quadratic Stark effect.

The merocyanine dyes have just the right combination of properties to favor the quadratic Stark effect. First, they are highly polar, implying that in moderately or highly polar solvents R (and hence R^2) is particularly large; second, the first singlet transition is strong ($f \sim 1$). The second property makes it reasonable to assume, as is necessary in the following interpretation, that the polarizability of any given dye in its lowest singlet excited state is considerably less than in its ground state. This can be understood upon inspection of the usual formula for the polarizability.[10] The lowest singlet transition, being strong, makes a sizable contribution to the ground state polarizability, and a negative contribution of the same magnitude to the lowest excited singlet state polarizability.

A particularly simple discussion is made possible by writing (10) in a form appropriate to the limiting case of large R, *viz.*

$$\Delta\nu - \Delta\nu_{ref} = (1/hc)(\mathbf{M}^u_{00} - \mathbf{M}^u_{ii})\cdot\mathbf{R} + (3/2hc)(\alpha^u_0 - \alpha^u_i)\,R^2 \qquad (18)$$

where $\Delta\nu_{ref}$ represents the frequency shift induced by a non-polar reference solvent, and the frequency shift as again expressed in terms of $\mathbf{R}$ instead of $\mathbf{E}^u$. We assume that in order to preserve the orthogonality of ground and excited electronic state functions in a series of merocyanines of decreasing ground state dipole moment, the excited state dipole moments either stay nearly constant or tend to increase in the same order as the ground state dipole moments decrease. In Fig. 2b, the frequency shift $\Delta\nu - \Delta\nu_{ref}$ is plotted against R in the three possible cases: $M^u_{00} - M^u_{ii}$ greater than, less than and equal to zero. (In the discussion of visible merocyanine spectra, the ground and excited state permanent dipole moments may be considered parallel.) The comparison of Figs. 2a and 2b shows that (18) is capable of reproducing the gross features of the phenomena, for R may be assumed to increase

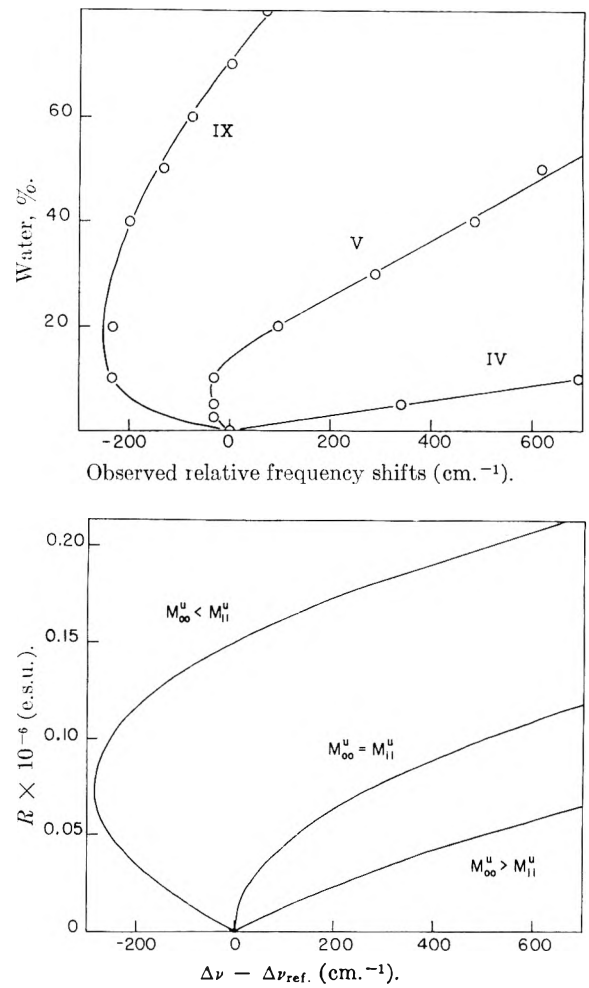

Fig. 2.—(a, top) variation of merocyanine band frequency with percentage of water in aqueous pyridine solvent. The abscissa is the frequency shift relative to the shift induced by pure pyridine. Curves are drawn for three merocyanine dyes, whose ground state dipole moments are considered to decrease in the order: IV > V > IX (see text). The optical data and dye notations are those of Brooker, Keyes and Heseltine.[34] (b, bottom) variation of band frequency with the reaction field, according to eq. 18 ($\alpha^u_0 - \alpha^u_i = 0.67 \times 10^{-23}$ cm.^{3}, $M^u_{00} - M^u_{ii}$ = 1.5, 0, −1.5 Debyes). These curves are meant to illustrate the general behavior predicted by the theory. The numbers are considered to be of the correct order of magnitude (see text), but are otherwise arbitrary. The curves do not refer specifically to the dyes of Fig. 2a.

(32) C. P. Smyth, "Dielectric Behavior and Structure," McGraw-Hill Book Co., Inc., New York, N. Y., 1955, p. 348.

(33) L. G. S. Brooker, G. H. Keyes, R. H. Sprague, R. H. Van Dyke, E. Van Lare, G. Van Zandt, F. L. White, H. W. J. Cressman and S. G. Dent, *J. Am. Chem. Soc.*, **73**, 5332 (1951).

(34) L. G. S. Brooker, G. H. Keyes and D. W. Heseltine, *ibid.*, **73**, 5350 (1951). Brooker and co-workers have studied solvent effects on maximum extinction coefficients as well as band frequencies.

(35) W. T. Simpson, *J. Am. Chem. Soc.*, **73**, 5359 (1951).

(36) J. R. Platt, *J. Chem. Phys.*, **25**, 80 (1956).

monotonically with water content in an aqueous pyridine solvent. The comparison must remain purely qualitative, because there is in this case no reliable way of relating R to the solvent composition. Indeed, the reaction field has only formal significance in the present application. The reason for this has been explained, with explicit reference to $\mathbf{E}^u$, at the beginning of this section. Equation 18 itself is far from realistic, because the first two terms in (10) may well suffer significant changes on passing from solvent to solvent. However it is unlikely that the consideration of the general red shift, for example, would alter the qualitative conclusions drawn here.

In spite of the drastic simplifications which have been introduced, the present discussion is readily shown to involve quantities of the correct order of magnitude. For this purpose the ordinate in Fig. 2b was chosen to run to 2×10^5 e.s.u., which is the order of magnitude of the reaction field indicated by the simple model, for a solvent of high dielectric constant and $M^u_{00} = 10$ debyes. The difference between the ground and excited state permanent dipole moments is almost certainly of the order of a few debyes, and 1.5 debyes was chosen for the sake of illustration. In order to reproduce the gross features of the phenomena within the chosen range of R, the difference between the ground and excited state isotropic polarizabilities must be $0.5–1.0 \times 10^{-23}$ cm.^{3}, *i.e.*, about one-third of the contribution of a strong visible transition to the ground state polarizability.

In his discussion of the phenomena, Brooker[5] has focused attention on the plot of the peak extinction coefficient ϵ_m against the corresponding wave length λ_m, and he has associated the maxima in such curves with the *isoenergetic point*, at which the principal polar and non-polar resonance structures have equal energies. At the isoenergetic point the ground and excited state dipole moments of the solute in solution should be equal. From (18) we find that the condition for a minimum value of $\Delta\nu - \Delta\nu_{ref}$ ($M^u_{ii} > M^u_{00}$) is $M^u_{00} + 3\alpha^u_0 R = M^u_{ii} + 3\alpha^u_i R$. For a rod-like solute molecule, $3\alpha^u_0$ and $3\alpha^u_i$ are polarizabilities appropriate to a field directed parallel to the dipole moments, so that $M^u_{00} + 3\alpha^u_0 R$ and $M^u_{ii} + 3\alpha^u_i R$ represent dipole moments of a rod-like solute molecule in solution. Since the merocyanines may be considered nearly rod-like, the present theory suggests that in the approximation of neglecting the first two terms in (10), the minimum in $\Delta\nu - \Delta\nu_{ref}$ should be associated with the isoenergetic point. The minimum in $\Delta\nu - \Delta\nu_{ref}$ and the maximum in the plot of ϵ_m *vs.* λ_m ordinarily occur at nearly the same solvent composition.[37] The present discussion thus tends to support the views previously expressed by Brooker,[5] and in fact indicates that Brooker's conclusions remain valid even if there are more than two resonance structures making important contributions to the combining states.

(37) This is not the case in the curves for Brooker, Keyes and Heseltine's dyes IX and X.[34] However, since these dyes are relatively weakly polar, the first two terms in (10) may make an important contribution.

Other Interactions.—Finally we point out that not all frequency shifts are caused entirely by dipole interactions, but that other types of interaction may make important or even dominant contributions in certain cases. For example, charge-transfer complex formation is generally accompanied by shifts in band frequencies; this topic has been reviewed recently.[38] Again, a large frequency shift may arise from intermolecular repulsive forces, in the event that the solute molecule suffers a marked change of equilibrium size[39] or shape[40,41] upon excitation.

Since the completion of the present work, some important contributions to the theory of solvent effects have come to the author's attention. From Ooshika's formula,[4] Mataga, Kaifu and Koizumi[42] have deduced an expression for the solvent effect on the frequency separation of the O—O bands in corresponding absorption and fluorescence transitions. This expression differs only slightly from the first term of that derived in the present work (eq. 15). Mataga, Kaifu and Koizumi have applied their formula in the evaluation of excited-state dipole moments.[43] Another method for evaluating excited-state dipole moments has been proposed by Lippert.[44]

The writer has been privileged to read, in manuscript form, a new treatment by Longuet-Higgins and Pople[45] of solvent-induced frequency shifts arising from dispersive interactions. The conclusions drawn by Longuet-Higgins and Pople are similar to those reached in the present work, but are expressed in a simpler form.

Acknowledgments.—The writer gladly acknowledges the award of a Hackett Studentship by the University of Western Australia, and the kind interest of Dr. N. S. Bayliss, Dr. H. C. Longuet-Higgins, Dr. M. Kasha and Mr. M. F. O'Dwyer.

(38) (a) L. J. Andrews, *Chem. Revs.*, **54**, 713 (1954); (b) L. E. Orgel, *Quart. Rev. Chem. Soc.*, **8**, 422 (1954).

(39) (a) N. S. Bayliss and A. L. G. Rees, *J. Chem. Phys.*, **8**, 377 (1940); (b) N. S. Bayliss, A. R. H. Cole and B. G. Green, *Australian J. Sci. Res.*, **A1**, 472 (1948); (c) A. L. G. Rees, *J. Chem. Phys.*, **8**, 429 (1940).

(40) K. W. Hausser, R. Kuhn and E. Kuhn, *Z. physik. Chem.*, **B29**, 417 (1935). This work has been summarized and discussed by Förster.[41]

(41) Reference 25, p. 136.

(42) N. Mataga, Y. Kaifu and M. Koizumi, *Bull. Chem. Soc. Japan* **29**, 115 (1956).

(43) N. Mataga, Y. Kaifu and M. Koizumi, *ibid.*, **29**, 465 (1956).

(44) E. Lippert, *Z. physik. Chem.* (N.F.), **6**, 125 (1956); *Z. Naturforsch.*, **10a**, 541 (1955).

(45) H. C. Longuet-Higgins and J. A. Pople, to be published in the *Journal of Chemical Physics*.

IDEALIZED MODELS FOR ADSORPTION FROM SOLUTION. I. VAN DER WAALS ADSORPTION FROM REGULAR SOLUTIONS

BY ROBERT S. HANSEN AND URSULA H. MAI

Contribution No. 498 from the Ames Laboratory, Ames, Iowa[1]

Received October 15, 1956

The theory of ideal van der Waals adsorption from regular solutions of equal sized molecules is developed, and explicit limiting forms for high and low concentrations of preferentially adsorbed components and for slightly soluble systems are given. Salient properties of the model are the following: (1) one component is preferentially adsorbed over the entire concentration range, (2) adsorption of the preferentially adsorbed component is proportional to $\ln^{-1/3}1/a$, where a is the component activity at low concentrations and to $(1 - x)$, where x is the component mole fraction at high concentrations, (3) in slightly soluble systems the adsorption is proportional to $\log^{-1/3} x'/x$ over the entire concentration range except for minor corrections. Comparisons with available experimental data are given.

Introduction

A number of idealized models suitable for discussion of unimolecular adsorption of gases have been proposed, and have been well summarized by Fowler and Guggenheim.[2] A number of idealized models for multimolecular adsorption of gases have been advanced.[3-6] Kipling and Tester,[7] in particular, have developed a Langmuir-like model for unimolecular adsorption from solution. There have been no quantitative models treated for multimolecular adsorption from solution, although Hansen, Fu and Bartell[8] used the Brunauer–Emmett–Teller equation in treating their data, and Brown[9] has used the Harkins–Jura equation in treating the same data.

In treating adsorption from solution, one must consider both component–adsorbent and component–component interactions. A simple model for consideration of component–component interactions is the so-called "regular" solution model extensively developed by Hildebrand and co-workers.[10] Van der Waals interaction energy between adsorbent and polarizable adsorbate, to the extent that this interaction can be properly represented by the London model, has been shown by Polanyi and London[11] and subsequently, apparently independently, by Hill[5] to be inversely proportional to the third power of the distance between component molecule and adsorbent surface. Information as to the component–adsorbent interactions furnished by the Polanyi–London theory can then be combined in the general theory of adsorption from solution given by Hansen and Fackler[12] to give isotherm forms explicitly.

(1) Work was performed in part in the Ames Laboratory of the U. S. Atomic Energy Commission.

(2) R. H. Fowler and E. A. Guggenheim, "Statistical Thermodynamics," Cambridge University Press, 1949 (Chapter X).

(3) (a) S. Brunauer, P. H. Emmett and E. Teller, *J. Am. Chem. Soc.*, **60**, 309 (1938); (b) W. D. Harkins and G. Jura, *ibid.*, **66**, 1366 (1944).

(4) G. D. Halsey, Jr., *J. Chem. Phys.*, **16**, 931 (1948).

(5) T. L. Hill, *ibid.*, **17**, 590 (1949).

(6) G. F. Huttig, *Monatsh.*, **78**, 177 (1948).

(7) J. J. Kipling and D. A. Tester, *J. Chem. Soc.*, 4123 (1952).

(8) R. S. Hansen, Y. Fu and F. E. Bartell, THIS JOURNAL, **53**, 769 (1949).

(9) C. Brown, *ibid.*, **54**, 1278 (1950).

(10) J. H. Hildebrand and R. L. Scott, "Solubility of Non-Electrolytes," 3d Ed., Reinhold Publ. Corp., New York, N. Y., 1950.

(11) M. Polanyi and F. London, *Naturw.*, **18**, 1099 (1930).

(12) R. S. Hansen and W. V. Fackler, Jr., THIS JOURNAL, **57**, 634 (1953).

Theoretical

In a generalization of the Polanyi[13] theory of adsorption of slightly soluble solutes from solution, Hansen and Fackler[12] showed that if the Polanyi gas adsorption theory[14] applied to the pure gaseous components, then the surface excess of component 1 in binary solution with component 2 was given by

$$\Gamma_1^{(v)} = \int_0^{\infty} \frac{x_{1r}}{\bar{v}_r} - \frac{x_{1B}}{\bar{v}_B}\, dr \qquad (1)$$

where x_{1r} is obtained from

$$\frac{a_{1r}}{a_{2r}^{\alpha}} = \frac{a_{1B}}{a_{2B}^{\alpha}} \exp\left\{\frac{E_1(r) - \alpha E_2(r)}{RT}\right\} \qquad (2)$$

In eq. 1, $\Gamma_1^{(v)}$ is the surface excess in the Guggenheim and Adam "v" contention,[15] x_{1r} and $\bar{v}_r$ are the mole fraction of component 1 and molar volume of solution at a distance r from the surface, and x_{1B} and $\bar{v}_B$ are the corresponding quantities in bulk solution (*i.e.*, at infinite distance from the surface). In eq. 2, a_{1r} and a_{2r} are the activities of components 1 and 2 at a distance r from the surface, referred to standard states of pure liquid components also at a distance r from the surface. a_{1B} and a_{2B} are activities of the bulk components, referred to standard states of pure liquid components in bulk. $\alpha = \bar{v}_{1r}/\bar{v}_{2r}$, where $\bar{v}_{ir}$ is the partial molal volume of component i at r. $E_1(r)$ and $E_2(r)$ are the Polanyi potentials at position r. It is assumed that the function a_{1r}/a_{2r}^{α} depends on x_{1r} in the same way that a_{1B}/a_{2B}^{α} depends on x_{1B}; since this latter dependence and the Polanyi potentials can be established experimentally, x_{ir} can be established from eq. 2, and hence $\Gamma_1^{(v)}$ can be obtained from eq. 1.

We now consider specialization of the theory of Hansen and Fackler to regular solutions and Polanyi potentials arising from dispersion forces.

For regular solutions the activity coefficients, referred to pure liquids (in the same external fields) as standard states are given by[10]

$$\ln \gamma_1 = \beta x_2^2 \qquad (3a)$$

$$\ln \gamma_2 = \beta x_1^2 \qquad (3b)$$

in which γ_1 and γ_2 are the activity coefficients of components 1 and 2, x_1 and x_2 their mole fractions, and β is a constant. For the purpose of this paper we shall also assume that the partial molal volumes of the two components are equal and constant;

(13) M. Polanyi, *Z. Physik*, **2**, 111 (1920).

(14) M. Polanyi, *Verh. physik. Ges.*, **18**, 55 (1916).

(15) E. A. Guggenheim and N. K. Adam, *Proc. Roy. Soc.* (*London*), **A139**, 218 (1933).

strictly speaking this assumption is a part of the regular solution model in the sense that it is necessary to a statistical derivation of eq. 3a and 3b.

According to the theory of Polanyi and London[11]

$$E(r) = Kr^{-3} \tag{4}$$

Since $\bar{v}_1 = \bar{v}_2$, $\alpha = 1$, and therefore

$$\frac{1}{RT}\{E_1(r) - \alpha E_2(r)\} = \frac{1}{RTr^3}(K_1 - K_2) = \left(\frac{r^\circ}{r}\right)^3 \tag{5}$$

r_0 is defined by eq. 5, and is a constant with dimension of length.

By combining eq. 3a, 3b and 5 we obtain

$$\frac{x_{1r}}{1 - x_{1r}} e^{-2\beta x_{1r}} = \frac{x_{1B}}{1 - x_{1B}} e^{-2\beta x_{1B}} e^{(r^\circ/r)^3} \tag{6}$$

Let $z = x_{1r} - x_{1B}$, and let $u = r/r_0$. Then eq. 6 can be rearranged to obtain

$$\ln \frac{1 + z/x}{1 - z/(1 - x)} - 2\beta z = \frac{1}{u^3} \tag{7}$$

In this and subsequent expressions, x will be used to denote x_{1B} when this is the only mole fraction occurring explicitly in the expression. For a given x, a value of u can be calculated for each choice of z in the range $0 < z < 1 - x$ and the function $z(u)$ can be plotted.

With the assumptions made as to partial molal volumes, $\bar{v}_r = \bar{v}_B = \bar{v}$, hence by eq. 2

$$\Gamma_1^{(v)} = \frac{1}{\bar{v}}\int_0^\infty (x_{1r} - x_{1B})dr = \frac{r_0}{\bar{v}}\int_0^\infty (x_{1r} - x_{1B})d\left(\frac{r}{r_0}\right) \tag{8}$$

or

$$\frac{\bar{v}\Gamma_1^{(v)}}{r_0} = \int_0^\infty z\, du \tag{9}$$

Having obtained the function $z(u)$ by means of eq. 7, we can obtain the dimensionless group $v\Gamma_1^{(v)}/r_0$ proportional to the surface excess $\Gamma_1^{(v)}$ by graphical integration. For large u, eq. 7 readily can be expanded to show that

$$z \longrightarrow \frac{x(1 - x)}{1 - 2\beta x(1 - x)}\frac{1}{u^3}$$

as $u \rightarrow \infty$, so that $zu \rightarrow 0$ as $u \rightarrow \infty$, and since $1 - x$ is the upper limit for z, $zu \rightarrow 0$ as $u \rightarrow 0$. Hence

also

$$\frac{\bar{v}\Gamma_1^{(v)}}{r_0} = \int_0^{1-x} u\, dz = \int_0^{1-x}\left[\ln\left(1 + \frac{z}{x}\right) - \ln\left(1 - \frac{z}{1 - x}\right) - 2\beta z\right]^{-1/3} dz \tag{10}$$

The following limiting forms are of interest.

(a) For large x, let $y = 1 - x$ assumed small, and let $1 - z/y = e^{-t}$. Eq. 10 becomes

$$\frac{\bar{v}\Gamma_1^{(v)}}{r_0} = y\int_0^\infty t^{-1/3}e^{-t}\left[1 + y\frac{1 - e^{-t}}{t}\left\{\frac{1 - 2\beta(1 - y)}{1 - y} - \frac{1}{2}\frac{y}{(1 - y)^2}(1 - e^{-t}) + \ldots\right\}\right]^{-1/3} dt \tag{11}$$

Since $(1 - e^{-t})/t$ does not exceed 1 for $0 \leq t < \infty$ the second term in the bracket is at most of order y; using the binomial expansion, integrating term by term, and ordering terms in powers of y we obtain

$$\frac{\bar{v}\Gamma_1^{(v)}}{r_0} = y\,\Gamma\left(\frac{2}{3}\right)[1 + y(2^{1/3} - 1)(2\beta - 1) - y^2\{2^{4/3} - 3^{1/3} + 6\beta(3^{1/3} - 2^{1/3}) - 2\beta^2(1 - 2^{7/3} + 3^{4/3})\} + \ldots] \tag{12}$$

where $\Gamma(2/3)$ is the Γ-function of argument 2/3. Collecting constants and substituting $(1 - x)$ for y we obtain

$$\frac{\bar{v}\Gamma_1^{(v)}}{r_0} = 1.354(1 - x)[1 + 0.260(2\beta - 1)(1 - x) - (1.078 + 1.092\beta - 0.572\beta^2)(1 - x)^2 + \ldots] \tag{13}$$

Hence as $x \rightarrow 1$, the effect of solution component interactions, represented by the parameter β, becomes apparent only in second order terms, and curves of $v\Gamma_1^{(v)}/r_0$ as functions of x approach $x = 1$ with common magnitudes and slopes.

(b) As x becomes small, $z(u)$ approaches a step function of u, *i.e.*, $z \approx 1 - x$ if $u < u'$, and $z \approx 0$ if $u > u'$. Let $z = 0.5 + y - x$, and obtain

$$\frac{\bar{v}\Gamma_1^{(v)}}{r_0} = \left\{\ln\frac{1 - x}{x} - \beta(1 - 2x)\right\}^{-1/3}\int_{-(0.5 - x)}^{0.5}\left\{1 + \frac{\ln(0.5 + y) - \ln(0.5 - y) - 2\beta y}{\ln\frac{1 - x}{x} - \beta(1 - 2x)}\right\}^{-1/3} dy \tag{14}$$

$$= A^{-1/3}\int_{-(0.5 - x)}^{0.5}\left(1 - \frac{1}{3}g + \frac{2}{9}g^2 - \ldots\right)dy \tag{15}$$

where

$$A = \ln\frac{1 - x}{x} - \beta(1 - 2x),$$

$$g = A^{-1}\{\ln(0.5 + y) - \ln(0.5 - y) - 2\beta y\}$$

The integral in eq. 15 is conveniently divided into the ranges $-(0.5 - x) < y < (0.5 - x)$, in which, since $g(y)$ is odd in y, only the term in g^2 contributes to the value of the integral, and the range $(0.5 - x) < y < 0.5$. The series expansion of the integrand diverges as $y \rightarrow 0.5$ but the corresponding series expansion of the integral does not; on integrating we obtain

$$\frac{\bar{v}\Gamma_1^{(v)}}{r_0} = A^{-1/3}\left[1 - (2 - 2^{-1/3})x - \frac{2^{-1/3}x}{6A} + \frac{(2^{-1/3} + 8\beta - 4\beta^2)x - 4x\ln^2 x + \frac{2\beta^2}{3} + 4\sum_{n=1}^{\infty}\frac{(1 - x)^n - \left(\frac{1^n}{2}\right)}{n^2} - 8\beta x\ln x - 4\beta + \ldots}{9A^2}\right] \tag{16}$$

The series $\sum_{n=1}^{\infty}\frac{(1 - x)^n}{n^2}$ converges for $0 \leq x \leq 2$, and in particular has a value $\pi^2/6$ for $x = 0$.[16] The leading term in this expansion, $A^{-1/3}$, is also to excellent approximation equal to $\ln^{-1/3} 1/a$, where a is the activity of the preferentially adsorbed component referred to pure liquid component as standard state.

(c) A binary system for which $\beta > 2$ is one of limited miscibility with limits given by the two roots, other than $x = 1/2$, of

$$\ln\frac{x}{1 - x} + \beta(1 - 2x) = 0 \tag{17}$$

Let x' be the lower of these roots, and $x'' = 1 - x'$ the higher; values of x in the range $x' < x < x''$ do

(16) R. V. Churchill, "Fourier Series and Boundary Value Problems," McGraw-Hill Book Co., Inc., New York, N. Y., 1941, p. 77.

not correspond to stable compositions. For a given $x < x'$ there will be a value u_d of u such that if $u > u_d$, $z < x' - x$, and if $u < u_d$, $z > x'' - x$. For large β $x' \to 0$, $x'' \to 1$, and hence

$$\frac{\bar{v}_1\Gamma_1^{(v)}}{r_0} \longrightarrow u_d = \left\{\ln\left(\frac{x'}{x}\frac{1-x}{1-x'}\right) - 2\beta(x'-x)\right\}^{-1/3} \quad (18)$$

Rigorously

$$\frac{\bar{v}\Gamma_1^{(v)}}{r_0} = u_d(1-2x') + I_1 + I_2 \quad (19)$$

where

$$I_1 = \int_{1-x'}^{1-x} f(z)\,dz,\ I_2 = \int_0^{x'} f(z)\,dz, \text{ and}$$

$$f(z) = \left\{\ln\frac{1-x}{x} + \ln\frac{x+z}{1-x-z} - 2\beta z\right\}^{-1/3}$$

In I_1, let $x + z = 1 - y$, x and y small, use $\ln(1-x) \approx -x$, $\ln(1-y) \approx -y$, and finally $xy \exp[2\beta - (2\beta-1)x] = e^{-t}$ to obtain

$$I_1 = (x'-x)e^B \int_B^\infty e^{-t}\{t + (2\beta-1)(x'-x)e^{B-t}\}^{-1/3}\,dt$$

$$\approx (x'-x)e^B \int_B^\infty t^{-1/3}e^{-t}\left\{1 - \frac{(2\beta-1)(x'-x)}{3t}e^{B-t}\right\}\,dt \quad (20)$$

where $B = -\{2\beta - (2\beta-1)x\} - \ln x(x'-x)$. This can be put in the form

$$I_1 = (x'-x)e^B\Gamma\left(\frac{2}{3}\right)\left\{1 - I\left(B\sqrt{\frac{3}{2}}, -\frac{1}{3}\right)\right\} - (x'-x)^2(2\beta-1)\,e^B B^{-1/3} - e^{2B}\Gamma\left(\frac{2}{3}\right)\left\{1 - I\left(B\sqrt{\frac{3}{2}}, -\frac{1}{3}\right)\right\} \quad (21)$$

in which the function

$$I(u,p) = \frac{\int_0^{u\sqrt{p+1}} e^{-t}t^p\,dt}{\Gamma(p+1)}$$

has been tabulated by Pearson[17] for arguments of interest in the present problem.

An expression for I_1 in terms of asymptotic expansions can be obtained by repeated partial integrations of eq. 20

$$I_1 = \frac{x'-x}{B^{1/3}}\left(1 - \frac{1}{3B} + \frac{4}{9B^2} - \cdots\right) - \frac{(x'-x)^2}{B^{4/3}}\frac{2\beta-1}{6}\left(1 - \frac{2}{3B} + \frac{7}{9B^2} - \cdots\right) \quad (22)$$

The two series in eq. 20 are divergent, but do not differ from the functions they represent by more than the last term included. Hence if the nth term is a small term in one of the series, a representation of the function differing from the function by not more than half the nth term can be obtained by summing the first $n-1$ terms and adding half of the nth term to this sum. This procedure is satisfactory for our purpose. In I_2, let $x + z = y$, x and y be small, use $\ln(1-x) \approx -x$, $\ln(1-y) \approx -y$, and $y/x = e^t$ to obtain

$$I_2 = x'\int_0^p t^{-1/3}e^t + \frac{(2\beta-1)x}{3}t^{-1/3}(e^{2t} - e^t)\,dt \quad (23)$$

(17) K. Pearson, "Tables of the Incomplete Γ-Function," Cambridge University Press, 1934.

in which $p = \ln(1 + x'/x)$. This can be integrated in infinite series form to obtain

$$I_2 = x'p^{-1/3}\left[1 + \frac{1}{3}\frac{x}{x'}\sum_{n=1}^\infty \frac{p^n}{(n-1/3)n!} + \frac{(2\beta-1)x}{3}\sum_{n=1}^\infty \frac{1-2^{-n}}{n-1/3}\frac{(2p)^n}{n!}\right] \quad (24)$$

Both series converge rapidly if p is small, and make small contributions to I_2 if p is large (because x is then small). By combining eq. 18, 19, 21 and 24, we obtain

$$\frac{\bar{v}\Gamma_1^{(v)}}{r_0} = (1-2x')\left\{\ln\left(\frac{x'}{x}\times\frac{1-x}{1-x'}\right) - 2\beta(x'-x)\right\}^{-1/3} + (x'-x)e^B\Gamma\left(\frac{2}{3}\right)\left\{1 - I\left(B\sqrt{\frac{3}{2}}, -\frac{1}{3}\right)\right\} - (x'-x)^2(2\beta-1)\left[e^B B^{-1/3} - e^{2B}\Gamma\left(\frac{2}{3}\right)\left\{1 - I\left(B\sqrt{\frac{3}{2}}, -\frac{1}{3}\right)\right\}\right] + x'p^{-1/3}\left[1 + \frac{1}{3}\frac{x}{x'}\times\sum_{n=1}^\infty \frac{p^n}{(n-1/3)n!} + \frac{(2\beta-1)x}{3}\sum_{n=1}^\infty \frac{1-2^{-n}}{n-1/3}\frac{(2p)^n}{n!}\right] \quad (25)$$

A form of this expression, correct to first order in x' is

$$\frac{\bar{v}\Gamma_1^{(v)}}{r_0} = \ln^{-1/3}\frac{x'}{x}\left[1 + x'\left\{-2 + \frac{(2\beta-1)(1-x/x')}{3\ln x'/x} + \frac{(1-x/x')\left(1 - \frac{1}{3B} + \frac{4}{9B^2}\right)}{\left(\frac{B}{\ln x'/x}\right)^{1/3}} + \frac{1 + \frac{1}{3}\frac{x}{x'}\sum_{n=1}^\infty \frac{p^n}{(n-1/3)n!}}{\left(1 + \frac{\ln(1+x/x')}{\ln x'/x}\right)^{1/3}}\right\}\right] \quad (26)$$

The coefficient of x' is at most 0.9 for $\beta = 3$, at most 1.3 for $\beta = 4$, and at most 2.3 for $\beta = 6$; since for higher β $x' \approx e^{-\beta}$ it is apparent that for large β $\ln^{-1/3} x'/x$ is an excellent approximation to $\bar{v}\Gamma_1^{(v)}/r_0$.

The dependence of the dimensionless group $\bar{v}\Gamma_1^{(v)}/r_0$ on x, the mole fraction of preferentially adsorbed component and on β, the component interaction parameter, is shown graphically for completely miscible components in Fig. 1; the dependence in the case of incompletely miscible components is illustrated in Fig. 2, except that reduced mole fraction (x/x'), mole fraction divided by saturation mole fraction, has been used as abscissa. The trend toward increasing adsorption, at a given mole fraction, with increasing value of β is pronounced in the completely miscible systems; the comparative independence of $\bar{v}\Gamma_1^{(v)}/r_0$ on β, provided reduced mole fraction is used as abscissa, is also evident in the slightly soluble systems.

By establishing the general behavior of the dimensionless group $\bar{v}\Gamma_1^{(v)}/r_0$, we establish the surface excess $\Gamma_1^{(v)}$ except for a constant factor $r_0/\bar{v}$; certain comments can be made as to the character of this factor. An approximate form for estimating van der Waals forces between two molecules is dis-

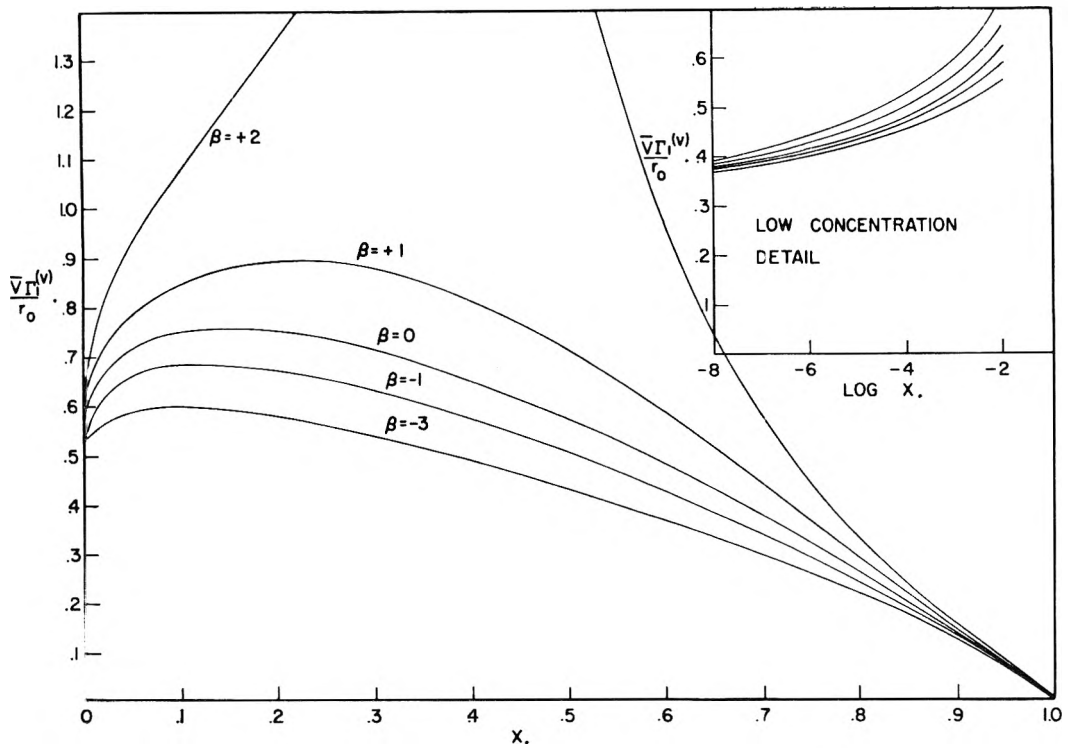

Fig. 1.—Variation in adsorption with mole fraction for completely miscible components.

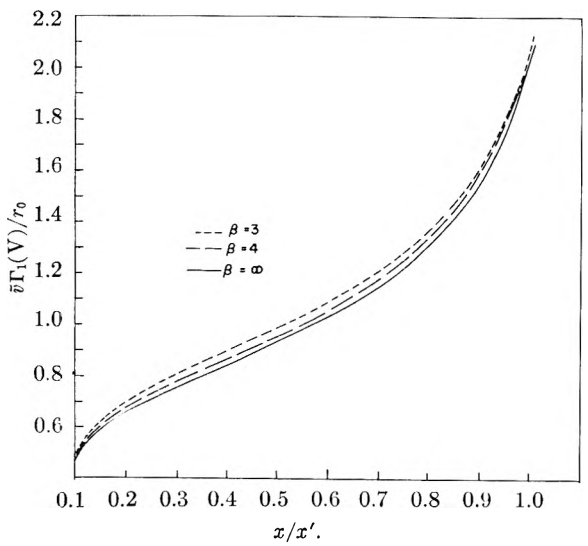

Fig. 2.—Variation in adsorption with reduced concentration for incompletely miscible components.

cussed by Pauling and Wilson.[18] The interaction energy between two molecules A and B, of polarizabilities α_a and α_b, ionization potentials I_a and I_b separated by a distance R is approximately

$$W = \frac{3}{2}\frac{\alpha_a\alpha_b}{R^6}\frac{I_aI_b}{I_a + I_b} \qquad (27)$$

Suppose that the B molecule is located at a distance r from a semi-infinite solid slab of A molecules in which the density of A molecules is ρ molecules per cc.; the total interaction energy between B molecule and the slab is readily found to be

$$W = \frac{\pi\rho}{4r^3}\alpha_a\alpha_b\frac{I_aI_b}{I_a + I_b} \qquad (28)$$

Hence if s denote the adsorbent, 1 and 2 the solution components, by comparison with eq. 5

$$\frac{E_1 - E_2}{RT} = \frac{N_0\pi\rho\alpha_sI_s}{4r^3RT}\left(\frac{\alpha_1}{1 + I_s/I_1} - \frac{\alpha_2}{1 + I_s/I_2}\right) = \left(\frac{r_0}{r}\right)^3 \qquad (29)$$

whence

$$r_0 = \left(\frac{N_0\pi\rho\alpha_sI_s}{4RT}\right)^{1/3}\left(\frac{\alpha_1}{1 + I_s/I_1} - \frac{\alpha_2}{1 + I_s/I_2}\right)^{1/3} \qquad (30)$$

The first factor is a constant for a given adsorbent; the second factor depends on both adsorbent and adsorbate, but dependence on adsorbent could become small if $I_s << I_1, I_2$ and this situation might occur with metal adsorbents. In this case r_0, and hence $\Gamma_1^{(v)}$, will be proportional to the cube root of the difference in polarizabilities between the two components. In any event a polarizability difference is a significant cause for preferential van der Waals adsorption.

Comparison with Experiment

There appear to be available no extensive adsorption data involving regular binary solutions with molecules of approximately equal size; comparison of existing adsorption data with adsorption behavior to be expected from the present model therefore burdens the model *a priori*. It should be noted, however, that adsorption inversion (preferential adsorption of one component over part of the concentration range and of the second component over the remainder of the concentration range) is not consonant with the present model, nor is this lack of consonance likely to be removed by a modification of the theory to account for different molecular sizes, or by a different (but physically reasonable)

(18) L. Pauling and E. B. Wilson, Jr., "Introduction to Quantum Mechanics," McGraw-Hill Book Co., Inc., New York, N. Y., 1935, pp. 387-8.

assumption as to character of activity coefficients. Such adsorption inversion frequently has been reported.[19-23] The inversion may be explained by assuming a heterogeneous surface, part of which preferentially adsorbs one component and part of which preferentially adsorbs the second component. It might also be due to a short range attraction of one component (*e.g.*, hydrogen bonding to an oxidized surface) and a long range attraction of the second component, as has been suggested by Hansen and Fackler.[12]

Several systems have been investigated over the entire concentration range in which no significant inversion occurs. Of these, perhaps the most suitable test of the model is the system water–formic acid–charcoal investigated by Blackburn and Kipling.[24] Judging from the activity behavior of the aqueous-higher fatty acid systems[25] the formic acid-water system should be nearly ideal. Assuming $\beta = 0$, the maximum in the surface excess mole fraction plot should occur at $x = 0.15$, compared to 0.17 observed; the isotherm should approach $x = 1$ almost linearly as is observed, the ratio of maximum adsorption to intercept of tangent at $x = 1$ on the ordinate axis should be 0.56 compared to 0.73 observed. The methanol–benzene–silica gel system investigated by Bartell and Scheffler[21] shows a maximum surface excess at mole fraction 0.20 and a ratio of maximum adsorption to tangent intercept of 0.61 approximately. Assuming $\beta = 1$ (the methanol–benzene system is of course not regular but does show appreciable positive deviation from ideality[10]) the calculated maximum surface excess occurs at $x = 0.22$, and the maximum adsorption to tangent intercept ratio is 0.65. Results published by Hansen and Craig[23] for the systems water–acetic acid–graphon and water–ethanol–graphon do not agree at all well with behavior predicted by the model, in that the adsorption maxima occur at about half the expected mole fraction and the surface excess mole fraction curves approach $x = 1$ with approximately zero slope.

Behavior predicted by the model for slightly soluble systems agrees fairly well with that observed for aqueous solutions of higher alcohols and fatty acids using carbon blacks and graphites as adsorbents by Hansen and Craig.[23] Especially noteworthy are the generally similar behaviors of the isotherms for different solutes when compared as functions of x/x', and the approximate $\ln^{-1/3} x/x'$ behavior as $x \rightarrow x'$.

In so far as the model predicts a surface excess proportional to $\ln^{-1/3} a$ as $a \rightarrow 0$, it predicts a behavior rather similar to the frequently reported Freundlich isotherm behavior and the principle dependence on activity rather than mole fraction also has been emphasized by Hansen and Craig.[23] It must be noted, however, that isotherms investigated at sufficiently low mole fractions are almost invariably linear and not logarithmic, and that at these concentrations the fact that the molecules are not arbitrarily small makes a continuum theory unrealistic.

(19) Wo. Ostwald and R. de Izaguirre, *Kolloid Z.*, **36**, 289 (1925).
(20) F. E. Bartell and C. K. Sloan, *J. Am. Chem. Soc.*, **51**, 1643 (1929).
(21) F. E. Bartell and G. H. Sheffler, *ibid.*, **53**, 2507 (1931).
(22) J. J. Kipling and D. A. Tester, *J. Chem. Soc.*, 4123 (1952).
(23) R. S. Hansen and R. P. Craig, THIS JOURNAL, **58**, 211 (1954).
(24) A. Blackburn and J. J. Kipling, *J. Chem. Soc.*, 1493 (1955).
(25) R. S. Hansen, F. A. Miller and S. D. Christian, THIS JOURNAL, **59**, 391 (1955).

THE MERCURY PHOTOSENSITIZED OXIDATION OF ETHANE

BY J. S. WATSON[1a] AND B. DEB. DARWENT[1b]

Olin Mathieson Chemical Corp., New Haven, Conn.

Received October 15, 1956

The kinetics of the mercury photosensitized oxidation of ethane have been investigated at a variety of pressures, compositions and intensities at temperatures between 40 and 200°. The rate is essentially independent of pressure, composition and temperature within prescribed limits. The quantum yield is approximately unity and independent of the intensity. The reaction is not a chain process and a mechanism has been proposed that is consistent with the kinetics.

I. Introduction

Investigations of the mercury photosensitized reactions of ethane have been reported, in single pass flow systems, by Nalbandyan[2a] and Gray.[2b] Nalbandyan's experiments were conducted at high relative oxygen concentrations ($[O_2]/[C_2H_6] = r = 9.0$), and at temperatures up to 310°. He concluded that peroxides were the initial products and that conditions could be reached such that they were the only products of the reaction. He suggested a mechanism involving the formation of free radicals, by the action of excited mercury on ethane, which reacted with oxygen to give peroxy radicals. The peroxy radicals reacted with ethane to form organic peroxides and regenerated active free radicals—thus resulting in a chain reaction. At long contact times the peroxides decomposed to form aldehydes which then either decomposed or were oxidized to CO and CO_2. The peroxides were not identified but the aldehydes were found to be formaldehyde and acetaldehyde, in the ratio of about 5:1 and approximately independent of contact time.

Gray's experiments,[2b] at lower temperatures and $r \approx 0.1$, confirmed Nalbandyan's conclusion that peroxides were the primary products and also showed that ethyl hydroperoxide was the only

(1) (a) Department of Applied Chemistry; National Research Council, Ottawa, Canada; (b) Department of Chemistry, Catholic University of America, Washington 17, D. C.
(2) (a) A. B. Nalbandyan, *Doklady Akad. Nauk U.S.S.R.*, **66**, 413 (1949); (b) J. A. Gray, *J. Chem. Soc.*, 3150 (1952).

peroxidic substance produced in the initial stages of the reaction. He did not find significant quantities of diethyl peroxide, hydrogen peroxide or water in the products and suggested the mechanism

$$Hg(^1S_0) + h\nu \longrightarrow Hg(^3P_1) \quad (0)$$

$$Hg(^3P_1) + C_2H_6 \longrightarrow C_2H_5 + H + Hg(^1S_0) \quad (a)$$

$$C_2H_5 + O_2 \longrightarrow C_2H_5{\cdot}O{\cdot}O{\cdot} \quad (1)$$

$$C_2H_5{\cdot}O{\cdot}O{\cdot} + C_2H_6 \longrightarrow C_2H_5O{\cdot}OH + C_2H_5 \quad (2)$$

containing the chain reactions 1 and 2.

However, from the known values for the quenching cross-sections of ethane[3] and oxygen,[4] it may be shown[5] that, even with r as small as 0.1, more than 90% of the $Hg(^3P_1)$ atoms should be deactivated by oxygen

$$Hg(^3P_1) + O_2 \longrightarrow O_2^* + Hg(^1S_0) \quad (b)$$

thus requiring fairly long chains if the quantum yield is of the order of unity.

Since neither of the previous investigators[2] attempted to study the kinetics of the reaction there is very little proof of the suggested mechanism, other than the fact that ethyl hydroperoxide is the sole initial product. Such a kinetic study forms the basis of this communication.

II. Experimental

Materials.—High purity, research grade ethane and propane, from the Phillips Petroleum Company, were used to avoid possible complications due to the presence of unsaturated hydrocarbons. Those gases were further purified by trap-to trap distillations *in vacuo* and the middle fractions stored in 2-liter flasks. The oxygen was usually taken from a commercial cylinder and roughly purified by evacuating a sample condensed at −195°. In some experiments high purity oxygen, prepared by heating mercuric oxide, was used to test the effect of possible impurities in the commercial product. The results were found to be independent of the purity of the oxygen.

Apparatus.—A closed system, in which the gases were circulated by a suitable pump, was used to enable the rates of disappearance of O_2 and C_2H_6 to be measured. The apparatus included a quartz spiral reaction vessel of 15-cc. capacity, separated by a cylindrical copper shutter from an axially placed low pressure mercury lamp, enclosed in an electrically heated furnace. The gases were circulated over the surface of mercury warmed to about 80°, through the reaction vessel and traps, maintained at −80° to remove the ethyl hydroperoxide, and through a Beckman Oxygen Analyzer, by which the concentration of oxygen was measured throughout the experiment. The total volume of the reaction system was 720 cc. The pump permitted the contact time (τ) to be varied between 0.5 and 20 sec. with slightly pulsating flow. The measurements of the total pressure and concentration of O_2 were not unduly affected by the pulsation of the pump. Connections were provided to the storage, analytical and vacuum systems.

Procedure.—Before starting an experiment the whole system was thoroughly evacuated. Ethane was added to the requisite pressure and then frozen at −195° in one of the traps which was then isolated from the rest of the system. Oxygen was admitted to the rest of the apparatus to the required pressure and the Beckman analyzer checked against the manometer. The gases were mixed by evaporating the ethane into the rest of the system and operating the pump. The lamp was brought to its steady operating condition with the shutter closed and one of the traps cooled to −80°. The reaction was started by opening the shutter and allowed to proceed for a measured time, during which the total pressure and the O_2 pressure were observed.

Analysis.—The uncondensable products (CO, H_2, CH_4), together with any unreacted O_2 were separated by freezing out the ethane and condensable products at −195°. The pressure of the uncondensable gases was measured and they were then transferred by a Toepler pump to a gas buret. The O_2 was removed by absorption on yellow phosphorus and the residue analyzed by oxidation on copper oxide or mass-spectrometrically.

A second fraction, consisting principally of unreacted C_2H_6 with some CO_2, was separated at −80°, measured and submitted to mass-spectrometric analysis.

The heavier products, contaning C_2H_5OOH, aldehydes, etc., were obtained as a residue at −80° and were analyzed for peroxides iodometrically.[6] The peroxide was not further characterized in view of the very complete identification by Gray.[2]

Light Intensity and Quantum Yield.—The intensity was measured by observing the rate of production of H_2 in the mercury photosensitized decomposition of propane and adopting the values for the quantum yield of that reaction at the requisite temperature as found by Bywater and Steacie.[7] The intensity of the light was varied by altering the current to the primary of the transformer and the relationship between current and intensity determined with propane.

III. Results

Preliminary experiments at room temperature (24–28°) gave rather erratic results. A solid, presumably mercuric oxide, was deposited as a thin film on the walls of the reaction vessel and as a thicker film immediately beyond the illuminated portion of the vessel. A similar complication had been observed previously in the mercury photosensitized oxidation of hydrogen.[8,9] At a slightly higher temperature (40–45°) there was no visible deposit and the results were usually reproducible; this is consistent with a previous observation by Evans.[8] Accordingly, only results obtained at 40° or higher are reported here.

The course of a typical experiment (no. 59) is shown in Fig. 1. The rates of total pressure decrease and of the consumption of oxygen were found to be independent of time, and the rate of consumption of O_2 (0.21 mm./min.) was very close to half of the rate of decrease of the total pressure

TABLE I

EFFECT OF PRESSURE ON RATE AND YIELD

Volume of cell, 15 cm.^{3}; incident intensity, 6.8×10^{-4} einst. hr.$^{-1}$; volume of system, 720 cm.^{3}; temperature, 72° ± 2°; contact time, 0.6 sec.

Expt.	Initial pressures (mm.) C_2H_6	O_2	$10r^a$	Total rate (mm.$^{-1}$ hr.$^{-1}$)	O_2 consumed (mmole)	ROOH produced (mmole)	Yield^b
43	92	10	1.09	19	...	...	...
31	108	12	1.13	24	1.00	1.02	0.98
36	150	17	1.14	21	0.71	0.63	.89
34	210	26	1.24	21	.56	.52	.92
32	271	30	1.10	20	.61	.65	1.06
38	377	42	1.12	16	.44	.51	0.87
45	387	82	2.10	19	1.18	1.30	.91
40	405	45	1.11	20	0.55	0.45	1.22
30	460	48	1.06	22	.28	.28	1.00
44	562	62	1.11	23	1.61	1.32	1.22
37	655	82	1.24	24	1.06	1.16	0.92
42	704	68	0.97	22	2.56	2.47	1.04
41	718	36	0.50	21	1.20	1.10	1.09

^{a} $r = ([O_2]/[C_2H_6])$—at start of experiment.

^{b} yield = moles of peroxide formed per mole of O_2 consumed.

(3) B. deB. Darwent, *J. Chem. Phys.*, **18**, 1532 (1950).

(4) M. W. Zemansky, *Phys. Rev.*, **36**, 919 (1930).

(5) B. deB. Darwent, *J. Chem. Phys.*, **20**, 1979 (1952).

(6) E. J. Harris, *Proc. Roy. Soc. (London)*, **A173**, 126 (1939).

(7) S. Bywater and E. W. R. Steacie, *J. Chem. Phys.*, **19**, 319 (1951).

(8) M. G. Evans, *ibid.*, **2**, 726 (1934).

(9) D. Volman, *ibid.*, **12**, 707 (1946).

TABLE II

EFFECT OF TEMPERATURE ON RATE AND YIELD

(Conditions as in Table I except for temp.)

Expt.	Temp. (°C.)	Initial pressures (mm. Hg) C_2H_6	O_2	Rates- (mm. hr.$^{-1}$) Total	O_2	O_2 consumed (mmole)	ROOH produced (mmole)	Total rate / O_2 rate	Yield
68	42	513	25	19	9	1.06	1.05	2.1	1.00
95	80	208	23	16	8	0.93	0.75	2.0	0.81
47 (B)	100	215	24	20	10	.57	.54	2.0	.95
48	120	180	20	19	9	.60	.50	2.1	.72
89	120	159	20	18	9	.54	.43	2.0	.80
102	150	124	24	21	10	.51	.33	2.1	.64
53	200	221	14	29	..	.41	.18	..	.44
54	200	208	12	23	..	.61	.21	..	.33

(0.41 mm./min.). Hence ethane and oxygen disappeared at equal rates. In that experiment the concentration of ethane changed only by about 10% whereas the pressure of oxygen varied from 18.2 mm. at the start to less than 1 mm. at the end of the experiment. Accordingly, the rate was independent of the pressure of oxygen and of the ratio of O_2/C_2H_6, at least over the range covered in that experiment.

The effect of total pressure of the rate and yield of the reaction are shown in Table I. In those experiments the total pressure was varied between 102 and 754 mm. and the percentage of O_2 in the initial mixture from 5 to 21. The rates of the reactions were essentially constant at 20 ± 4 mm. hr.$^{-1}$ and did not vary with change of the pressure. Similarly, the yield of ethyl hydroperoxide was unity, within 20%, and did not vary with the pressure.

The effect of temperature on the reaction is shown in Table II. The rate appears to be independent of the temperature and, at least up to 150°, the rate of consumption of O_2 is accurately one-half of the rate of decrease of the total pressure. The yield decreased slowly with increasing temperature up to about 120° and more rapidly as the temperature was further increased.

The relationship between the contact time (τ) and the yield of ethyl hydroperoxide is shown in Fig. 2. At all temperatures studied the yield decreased with increasing contact time in a manner which suggests that, at least up to 150°, it approaches 100% as $\tau \rightarrow 0$. If this suggestion is valid, ethyl hydroperoxide is the sole initial product of the mercury photosensitized oxidation of ethane, up to at least 150°, and the decrease in yield at the higher temperatures of Table II was caused by the subsequent decomposition of the hydroperoxide, since the yield decreased with increasing contact time more rapidly at the higher temperatures.

The effect of intensity on the rate of the reaction was investigated and the results are shown as logarithmic plots of the relative rates against the relative intensity (Fig. 3). If the rate varies as I_a^n the slope of the experimental line in Fig. 3 will give the value of n. Three lines are shown corresponding to values of 0.50, 0.66 and 1.00 for n. Although the points are rather badly scattered, they are not inconsistent with a value of unity for the exponent and show quite clearly that n must be greater than 0.66.

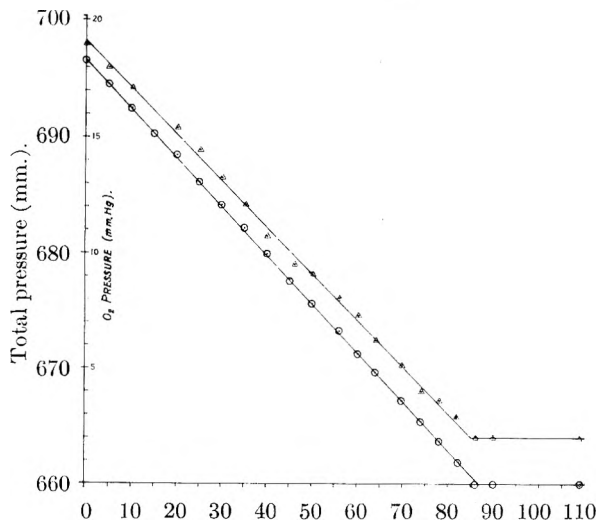

Fig. 1.—The pressure–time relationship (expt. no. 59): △, total pressure; ○, O_2 pressure.

IV. Discussion

At low temperatures, low percentages of oxygen and short contact times, the results were fairly reliable and allow reasonably accurate conclusions to be drawn. Those experiments have shown the rate to be independent of pressure, O_2/C_2H_6 and temperature and the quantum yield to be of the order of unity (0.5–0.75) and independent of the intensity. We shall show that a chain mechanism of the type suggested by Nalbandyan[1] and Gray[2] is inconsistent with those observations and then propose another mechanism that is consistent with the kinetics of the reaction.

For a chain mechanism to be amenable to kinetic test it is, of course, necessary to include the chain terminating steps. Although such reactions have not been proposed for the process under consideration, (3), (4) and (5)

$$R + RO_2 \longrightarrow ROOR \quad (3)$$

$$2R \longrightarrow R\text{-}R \quad (4)$$

$$2RO_2 \longrightarrow \text{Products} \quad (5)$$

where R represents the ethyl radical, are likely termination reactions. These reactions are intrinsically probable and have been suggested[10,11] as termination steps in hydrocarbon oxidation.

(10) J. L. Bolland, *Trans. Faraday Soc.*, **44**, 669 (1949).

(11) L. Bateman, G. Gee, A. L. Morris and W. F. Watson, *Disc. Faraday Soc.*, **10**, 250 (1951).

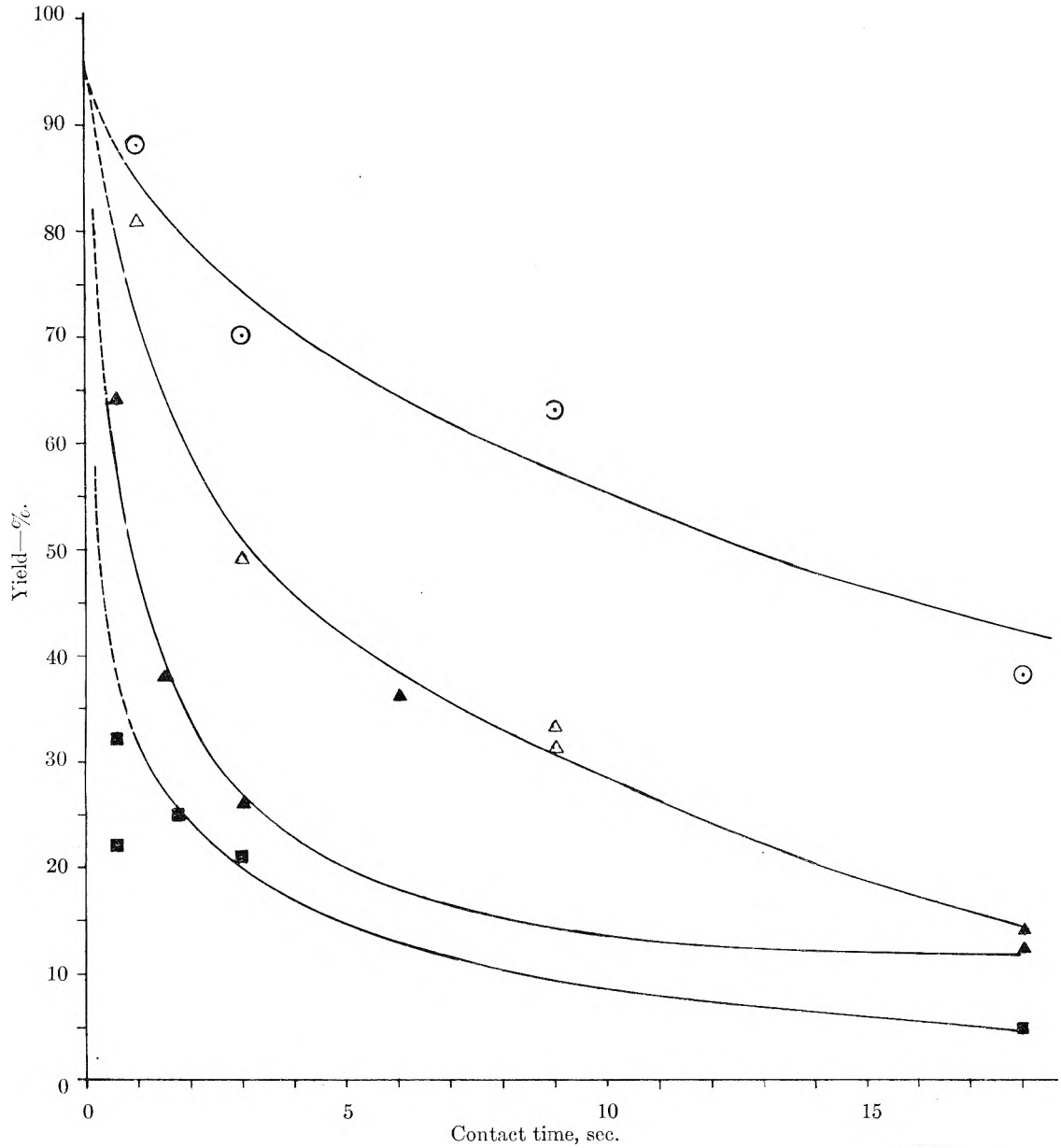

Fig. 2.—The relationship between contact time and yield: ⊙, 30°; △, 80°; ▲, 150°; ■, 200°.

A further possibility of chain termination arises from the likelihood that H atoms, produced in reaction (a), react rapidly with O_2, probably in the presence of a third body, to form HO_2

$$H + O_2 \longrightarrow HO_2 \qquad (6)$$

which causes termination by reacting with RO_2

$$RO_2 + HO_2 \longrightarrow ROOH + O_2 \qquad (7)$$

The various termination reactions lead to the rate equations

$$R = R_i^{1/2}k_1k_2\cdot[O_2\cdot][RH]/(k_2k_4^{1/2})[RH] + k_1k_5^{1/2}[O_2] \qquad (A)$$

for termination by reactions 3, 4 and 5, assuming that $k_3 = (k_4k_5)^{1/2}$ (for this assumption see ref. 10 and 11).

$$R = R_i^{1/2}(k_1k_2[RH][O_2]/2k_3)^{1/2} \qquad (B)$$

for termination by reaction (3) alone

$$R = R_i + R_i^{1/2}k_2[RH]/k_7^{1/2} \qquad (C)$$

for termination by reactions 6 and 7. Equation C is based on the assumption that $[H_2O] \approx [RO_2]$. This assumption probably is correct, since stoichiometry requires $[H] + [HO_2] = [R] + [RO_2]$ and it is very likely that the concentrations of the peroxy radicals are very much greater than those of H and R. The first term represents the non-chain and the second the chain reaction.

The proposed chain mechanism thus requires the rate to be proportional to the square root of the absorbed intensity and to increase with increasing concentration. Both of these requirements are contrary to the experimental results (Figs. 1 and 3), so that it may safely be concluded that the mechanism previously suggested[2] does not represent the reaction under the conditions of our experiments.

The quantum yield of about unity, in the absence of chains and under conditions such that more than 90% of the $Hg(^3P_1)$ atoms are deactivated by oxygen, requires the products of reaction

(b) to be effective in initiating the oxidation. Although the products of reaction (b) are not well established, they are likely to be either O atoms or excited oxygen molecules (O_2^*). The results favor the latter possibility since, if O atoms were formed the products would have contained copious quantities of H_2O, CO and CO_2, which were not found in significant amounts in the experiments at short contact times and temperatures lower than about 120°.

Although very little is known about the reactions of excited oxygen molecules, the reactions

$$O_2^* + C_2H_6 \longrightarrow C_2H_5 + HO_2 \quad (8)$$
$$\longrightarrow C_2H_5O_2 + H \quad (9)$$
$$\longrightarrow C_2H_5OOH \quad (10)$$

are plausible and are not in disagreement with the results obtained. They are kinetically indistinguishable from one another if RO_2 and HO_2 disappear principally by reaction 7, since reactions 1 and 6 are certainly very fast. Mechanisms consisting of reactions b and 10 or of (b), (8), (9), (1) (6) and (7) give identical kinetics which, in agreement with experimental results, require the rate to be equal to the absorbed intensity and independent of the pressure, composition and temperature.

During the course of any one experiment, reaction (a) will assume increasing importance as the reaction proceeds, since r then increases, and reaction (a) will account for about 50% of the quenching when $r = 130$. In experiment 59 that point was reached when the pressure of oxygen had fallen to about 5 mm. but it is evident that there was no observable diminution in the rate (Fig. 1). Hence the oxidation is initiated with equal efficiency by both reactions (a) and (b). This observation is also in accordance with the kinetics, provided that the pressure of oxygen is not so low that the combination of ethyl radicals

$$2C_2H_5 \longrightarrow C_4H_{10} \quad (11)$$

becomes important compared with reaction 1. If the pressure of ethyl radicals is not greater than

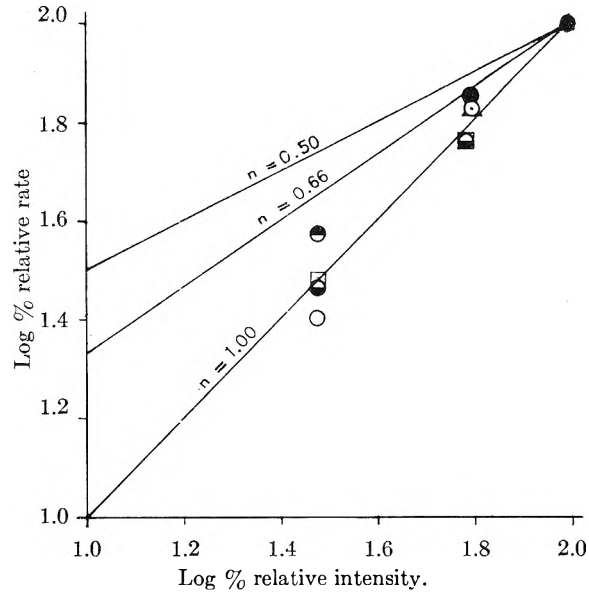

Fig. 3.—The relationship between intensity and rate:

Point	⊙	◓	◒	□	△
Temp. °C.	75	75	75	98	120
Initial press.—(mm.)	102	450	624	239	200

10^{-4} mm. and if k_{11} is not much greater than $10^2 k_1$, the rates of reactions 1 and 11 will not be equal until the pressure of oxygen has fallen to 0.1 mm., at which point it was not possible to follow the reaction.

At long contact times and at high temperatures the products become much more complex. However the manner in which the yield varies with contact time (Fig. 2) indicates strongly that ethyl hydroperoxide is still the primary product. Accordingly, the complications arise from subsequent thermal or photochemical reactions of the ethyl hydroperoxide. This aspect of the reaction has not been fully investigated and is not further considered in this communication.

PHYSICO-CHEMICAL PROPERTIES OF SOLUTIONS OF *PARA* LONG CHAIN ALKYLBENZENESULFONATES

BY JACQUELINE WISE GERSHMAN

Contribution from Colgate-Palmolive Co., Jersey City, New Jersey

Received October 18, 1956

Solubility–temperature curves were determined for the branched alkylbenzenesulfonates with the general formula sodium *p*-(1-methylalkyl)-benzenesulfonate where the alkyl group contained from 10 to 16 carbon atoms. Krafft temperatures and CMC values were derived for each compound. Surface tension measurements were made for aqueous solutions of alkylbenzenesulfonates with the general formula of either sodium *p*-(1-methylalkyl)-benzenesulfonate or sodium *p*-alkylbenzenesulfonate, where the alkyl group varied from 10 to 16 carbon atoms in the former and 8 to 10 in the latter. The surface tension and critical micelle concentration are seen to be lowered by the addition of a methyl group. Electrical conductance measurements were made for aqueous solutions of the above compounds and for sodium *p*-dodecylbenzenesulfonate. The CMC values obtained by solubility, surface tension and conductance are compared and their differences discussed. Contrary to prior experience with commercial sulfonate, it was found possible to form slow draining films with some of the compounds studied.

Introduction

In some recent work, there has been occasion to determine certain physical properties on a series of pure *para*-substituted alkylbenzenesulfonates. Data of this sort, especially for pure isomers, are very limited in the existing literature.

Experimental

Materials.—The compounds studied were sodium alkylbenzenesulfonates, where the alkyl group was *p*-(1-methyldecyl), *p*-(1-methyldodecyl), *p*-(1-methyltetradecyl), *p*-(1-methylhexadecyl), *p*-octyl, *p*-decyl or *p*-dodecyl. The preparation and purity of these compounds are discussed by Gray, *et al.*,[1,2]

Solubility.—The solubilities at various temperatures were determined using the apparatus described by Epstein, *et al.*[3] Sulfonates which are not reported either had a solubility too high for the amount of available material, or too low for convenient operation.

Surface Tension.—Equilibrium surface tensions were determined by the ring method as described by Shedlovsky.[4] In addition, the flask was thermostated in a water-bath so that all except the neck was immersed. Sodium *p*-dodecylbenzenesulfonate was not studied because of its low solubility.

Conductance.—A high precision conductance bridge built on the principles of Edelson and Fuoss[5] was employed (at 1000 cycles) to measure the conductance of sodium *p*-(1-methyldodecyl)- and *p*-(1-methyltetradecyl)-benzenesulfonate, while a Leeds and Northrup 60-cycle conductance bridge was used for the remainder of the measurements. The bath was filled with mineral oil and jacketed with sheets of asbestos covered with aluminum foil. Temperature control of ±0.003° was achieved using an Electron-O-Therm controller.

A cell (2 ml., cell constant 0.9315) whose electrodes consisted of truncated cones of platinum was employed to measure the conductance of sodium *p*-(1-methyldodecyl)-benzenesulfonate while a Shedlovsky flask cell[6] (cell constant, 0.8967) was used in the other conductance measurements. With the former cell, it was necessary to prepare a series of solutions. When the flask cell was used, a weighed amount of deionized water was added to the cell and the desired concentrations obtained by stepwise addition of a stock solution. For the less soluble compounds, where it is necessary to operate at temperatures of 50–60°, it was found necessary to modify the above technique to prevent crystallization of the stock solution. A weighed amount of stock solution was placed in the cell and diluted with successive additions of deionized water from a weight buret. The tendency of the solution to crystallize in the side arms was eliminated by warming the exposed parts of the cell with an infrared lamp.

Film Drainage Transition Temperatures.—Film drainage transition temperatures were measured by the method devised in this Laboratory.[3,7]

Results and Discussion

Because of special methods of preparation and purification, the sulfonates used are thought to be exceptionally free of homologs, unsulfonated materials, *ortho* isomer, or other impurities. The surface tension measurements indicate that the samples are of a high degree of purity.[4]

The solubilities of the alkylbenzenesulfonates (Fig. 1) decrease with increasing chain length as would be expected.[8] The critical micelle concentrations (CMC) and Krafft temperatures as determined by the break in the solubility curves are given in Table I. The CMC decreases and the Krafft temperature increases as the molecular weight increases.

(1) F. W. Gray, J. F. Gerecht and I. J. Krems, *J. Org. Chem.*, **20**, 511 (1955).

(2) F. W. Gray and I. J. Krems, to be published, Research and Development Department, Colgate-Palmolive Company.

(3) M. B. Epstein, A. Wilson, C. W. Jakob, L. E. Conroy and J. Ross, THIS JOURNAL, **58**, 860 (1954).

(4) L. Shedlovsky *Ann. N. Y. Acad. Sci.*, **46**, 430 (1946).

(5) D. Edelson and R. M. Fuoss, *J. Am. Chem. Soc.*, **73**, 269 (1951).

(6) A. Weissberger, "Techniques of Organic Chemistry, Physical Methods of Organic Chemistry," Vol. I, Part II, Interscience Publishers, Inc., New York, N. Y., 1949, p. 1667.

(7) G. D. Miles, J. Ross, and L. Shedlovsky, *J. Am. Oil Chemists' Soc.* **27**, 268 (1950).

(8) H. P. Klevens, *Chem. Revs.*, **47**, 30 (1950).

In the case of sodium *p*-(1-methyldodecyl)-benzenesulfonate (curves B and B′, Fig. 1), the crystals in some solutions appeared to dissolve and then to reform on continued aging of the solutions at the same temperature. This phenomenon, which was not observed with other compounds, is thought to be due to the formation of a metastable phase during the initial precipitation by rapid cooling. Where two solid phases were observed, both solubility temperatures were determined. The values observed for the stable phase were used in determining the Krafft temperature and CMC.

It is apparent from the solubility relationships, that effective separation of homologs could be obtained by crystallization at a temperature which is above the Krafft temperature for the lower and below the Krafft temperature for the higher.

For the branched-chain alkylbenzenesulfonates (Fig. 2), the surface tension values in the micellar regions are in the range of 37 to 39 dynes per cm. for all members of the group. The concentration necessary to attain this lowering of surface tension is, of course, less as the chain length increases. A comparison of the concentrations required to obtain a surface tension of 40 and 41 dynes per cm. gives ratios from 3.2 to 4.0 between successive compounds in the series. This corresponds to a factor of about 1.6 to 2.0 as a measure of the additional energy of adsorption required for each CH_2 group, suggesting a relatively flat orientation on the surface.[9]

For straight-chain sulfonates (Fig. 3), the surface tension in the micellar region is somewhat higher than for branched. Comparison of the decyl and methyldecyl compounds shows the effect of the methyl group in lowering the surface tension for a given concentration and in decreasing the CMC. For all of the above compounds, a value for the CMC was estimated from the surface tension data (Table I). This was taken as the concentration at which the surface tension–concentration curve flattens out. When the curve showed a slight minimum, the concentration at the minimum was taken.

TABLE I

CRITICAL MICELLE CONCENTRATIONS OF *para*-ALKYLBENZENESULFONATES

Alkyl group	From solubility $m \times 10^2$	From solubility T, °C.[a]	From conductance $m \times 10^2$	From conductance T, °C.	From surface tension $m \times 10^2$	From surface tension T, °C.
1-Methyldecyl	0.245	19.0	0.253	35	0.190	40
1-Methyldodecyl	.071	27.7	.072	35	.062	40
1-Methyltetradecyl	.050	32.6	.031	40	.022	40
1-Methylhexadecyl	.014	45.5	.013	50	.014	50
Octyl	...	...	1.47	35	1.11	25
Decyl	...	...	0.381	50	0.314	50
Dodecyl	...	...	0.120	60	...	..

[a] Krafft temperature.

(9) N. K. Adam, "The Physics and Chemistry of Surfaces," Third Edition, Oxford Press, London, 1941, p. 121.

The conductance data are presented in Table II. For brevity, all experimental points are not reported. The data do not permit direct comparisons between compounds because the measurements were not carried out at the same temperature. They may be compared, however, by making corrections for the variation of the viscosity of water with temperature according to Walden's rule.[10,11] Although Walden's rule usually is applied to equivalent conductance at infinite dilution, it can be used for higher concentrations. For experimental data available in the literature,[12] the application of Walden's rule has proven satisfactory at concentrations up to 0.1 *m* (Table III). The product of the equivalent conductance (Λ) and viscosity (η) varies over an 0.8% range at a low concentration (0.005 *N*) and by about 10% in the micellar region (0.1 *N*).

For the compounds studied here, the concentration corresponding to any given $\Lambda\eta$ value in the micellar region is lower as the chain length is increased.

The specific conductance plot is the most accurate and precise method for determining the CMC.

TABLE II

SPECIFIC CONDUCTANCE OF *para*-ALKYLBENZENESULFONATES

Molality × 10⁴	$K \times 10^4$, ohms^{-1} [a]	Molality × 10⁴	$K \times 10^4$, ohms^{-1} [a]
Sodium *p*-(1-methyldecyl)-benzenesulfonate (35°)			
48.1	3.05	25.9	2.09
43.1	2.84	22.3	1.84
38.5	2.66	12.0	1.00
28.1	2.20	7.12	0.595
Sodium *p*-(1-methyldodecyl)-benzenesulfonate (35°)			
27.7	1.592	7.78	0.6669
22.0	1.324	5.52	.5196
16.5	1.083	3.14	.3093
8.77	0.7308	1.21	.1322
Sodium *p*-(1-methyltetradecyl)-benzenesulfonate (40°)			
8.86	0.5675	3.21	0.2801
6.80	.4825	2.28	.2133
4.53	.3522	1.77	.1674
3.23	.2790	0.750	.0680
Sodium *p*-(1-methylhexadecyl)-benzenesulfonate (50°)			
5.16	0.335	1.24	0.131
3.83	.274	1.00	.110
2.61	.211	0.88	.100
1.36	.137	.693	.079
Sodium *p*-octylbenzenesulfonate (35°)			
3.46	1.80	1.44	1.11
2.56	1.51	1.26	0.998
2.27	1.40	1.13	.904
1.55	1.15	0.952	.763
Sodium *p*-decylbenzenesulfonate (50°)			
0.476	0.469	0.344	0.377
.451	.455	.285	.316
.399	.424	.222	.249
Sodium *p*-dodecylbenzenesulfonate (60°)			
0.207	0.211	0.115	0.146
.164	.184	.105	.137
.143	.171	.081	.106
.123	.155	.056	.074

[a] Specific conductance minus that of water at the corresponding temperature.

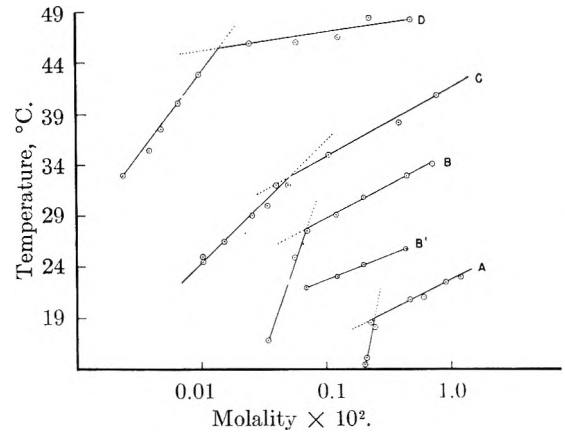

Fig. 1.—Solubilities of the branched sodium alkylbenzenesulfonates: A, methyldecyl; B, methyldodecyl (stable phase); B', methyldodecyl (unstable phase); C, methyltetradecyl; D, methylhexadecyl.

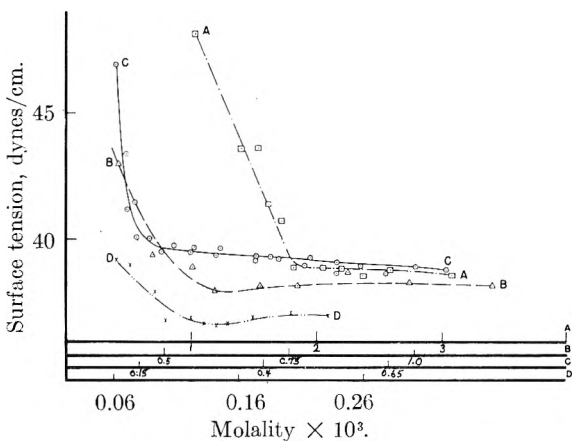

Fig. 2.—Surface tension data of the branched sodium alkylbenzenesulfonates: A, methyldecyl, and B, methyldodecyl, etc.

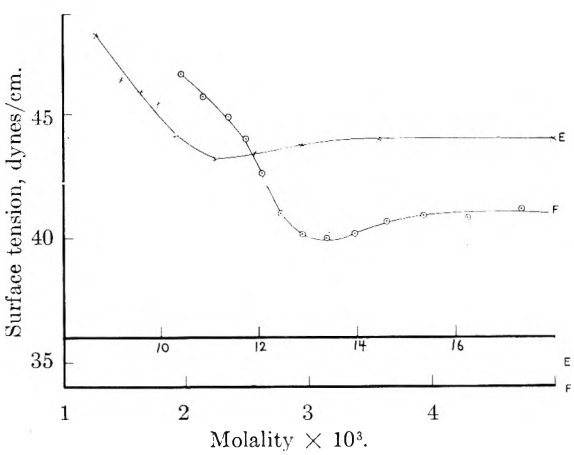

Fig. 3.—Surface tension data of the straight-chain sodium alkylbenzenesulfonates: E refers to octyl and F to decyl.

(10) S. Glasstone, "Textbook of Physical Chemistry," 2nd Edition, D. Van Nostrand Co., New York, N. Y., 1950, p. 897.

(11) H. S. Harned and B. B. Owen, "The Physical Chemistry of Electrolytic Solutions," Reinhold Publ. Corp., New York, N. Y., 1943, p. 184.

(12) R. G. Paquette, E. C. Lingafelter and H. V. Tartar, *J. Am. Chem. Soc.*, **65**, 686 (1943).

TABLE III

APPLICATION OF WALDEN'S RULE TO SODIUM *p*-OCTYLBENZENESULFONATE

Molality	Deg. C.	Λ (ohms^{-1})	η (poises $\times 10^2$)[13]	$\Lambda\eta$
0.1	25	34.9	0.8949	31.2
	40	49.7	.6536	32.5
	60	73.5	.4699	34.5
0.005	25	68.7	0.8949	61.5
	40	93.3	.6536	61.4
	60	129.9	.4699	61.0

The method used is illustrated in Fig. 4 and the results are given in Table I which presents a comparison of CMC values obtained by the various methods. Because of the different temperatures involved, the comparisons are only approximate.

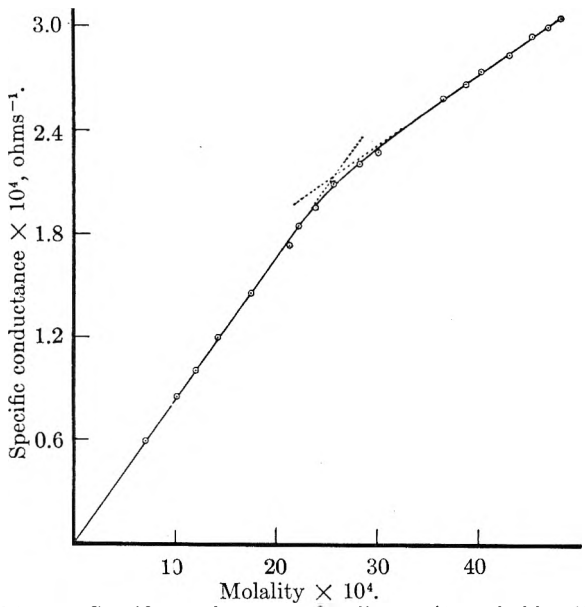

Fig. 4.—Specific conductance of sodium *p*-(1-methyldecyl)-benzenesulfonate at 35°.

(13) "International Critical Tables," Vol. 5, McGraw-Hill Book Co., New York, N. Y., 1927, p. 10.

Roughly, the surface tension method gives values which are 5–30% lower. On the other hand, the solubility method shows good agreement with the CMC's obtained from conductance, with the exception of one compound. The experimental data on this compound, 1-methyltetradecyl)-benzenesulfonate, have been carefully rechecked.

It has been stated previously[4] that alkylarylsulfonates do not give slow draining films in the presence of organic additives. This conclusion was based on a study of commercial sulfonates. In the present study, we have found that slow draining films may be obtained in certain cases. The data in Table IV illustrate this point.

TABLE IV

FILM DRAINAGE TRANSITION TEMPERATURES FOR *para*-ALKYLBENZENESULFONATES WITH MYRISTYL ALCOHOL

Molality × 10²	Sulfonate, g./100 g. soln.	Myristyl alcohol, g./100 g. soln. × 10²	Film drainage transition temp., °C.
	Sodium *p*-(1-methyldecyl)-benzenesulfonate		
0 224	0.0750	1 10	27.0
		0.75	26.4
		.40	24.0
111	0.0370	.55	41.5
		.37	36.5
		.18	[a]
	Sodium *p*-octylbenzenesulfonate		
1 37	0.4000	2.0	32.3
		1.0	30.0
		0.40	23.0
0 685	0.2000	1.0	43.1
		0.50	42.8
		.20	33.6

[a] Only fast draining film observed.

Acknowledgments.—The author wishes to thank Mr. J. V. Schurman and Dr. L. Shedlovsky for their helpful discussion during the preparation of the manuscript and Mr. M. Camara for his assistance with the solubility measurements.

REACTION HEATS OF ORGANIC HALOGEN COMPOUNDS. VIII. THE HEATS OF CHLORINATION OF PERFLUORINATED BUTENE-1, PENTENE-1 AND ISOBUTENE[1]

BY J. R. LACHER, A. KIANPOUR AND J. D. PARK

Contribution from the Department of Chemistry, University of Colorado, Boulder, Colorado

Received October 22, 1956

The heats of chlorination of perfluorobutene-1, perfluoroisobutene and perfluoropentene-1 have been measured in vapor phase reactions and found to be −44.97, −42.22 and −45.61 kcal./mole, respectively. Some physical properties of the reaction products together with their infrared absorption spectra have been determined. The thermochemical data are discussed in connection with the heats of chlorination of some simple perfluoroölefins.

In earlier papers[2,3] we have described a calorimeter which could be used to measure the heat of vapor phase reactions. More recently[4–6] we have modified it to permit the use of condensing vapor baths as a source of constant temperature. The present paper deals with the vapor phase heats of

(1) This research was supported by the Office of Scientific Research, Air Research and Development Command under Contract No. AF 18(600)-1151.

(2) J. R. Lacher, J. D. Park, *et al.*, *J. Am. Chem. Soc.*, **71**, 1330 (1949).

(3) J. R. Lacher, J. D. Park, *et al.*, *ibid.*, **71**, 1334 (1949).

(4) J. R. Lacher, E. Emery, E. Bohmfalk and J. D. Park, THIS JOURNAL, **60**, 492 (1956).

(5) J. R. Lacher, L. Casali and J. D. Park, *ibid.*, **60**, 608 (1956).

(6) J. R. Lacher, A. Kianpour and J. D. Park, *ibid.*, **60**, 1454 (1956).

chlorination of perfluorinated butene-1, isobutene and pentene-1. The experimental procedures used were essentially those previously described.

Experimental Details.—Perfluorobutene-1 and perfluoropentene-1 were prepared by the pyrolysis of the sodium salts of perfluorovaleric and perfluorohexanoic acids, respectively.[7] The olefins were carefully purified by distillation in a Podbielniak column. The infrared spectra of the purified material were identical to those reported in the literature.[8] Perfluoroisobutene was obtained as a gift from the Minnesota Mining and Manufacturing Company. It also was purified by repeated distillation in a 100-plate column. Infrared analysis of the various fractions suggested that the main impurity was perfluorobutene-2. We believe our product was 98 to 99% pure.

The catalyst consisted of ferric chloride on activated carbon. The carbon was sized to pass 6 and be retained on 14 mesh. After treatment with dilute hydrochloric acid, it was washed with water, dried at 120° and finally heated *in vacuo* at 350° for 24 hours. Twenty grams of ferric chloride was sublimed and then dissolved in 50 cc. of anhydrous ether. This solution was mixed with 120 g. of treated carbon. The ether was driven off by a stream of dry nitrogen. The mixture was transferred to the calorimeter catalyst chamber and heated under vacuum at 120° for three hours. After cooling the catalyst chamber was filled with nitrogen and closed to the atmosphere.

In making a run, an excess of olefin was used. The reaction was quantitative and no chlorine could be detected in the exit line by means of the potassium iodide–starch paper test. The rate of formation of product was taken to be equal to the rate of consumption of chlorine. This was determined by diverting the chlorine to a collecting tower filled with glass beads for a known length of time. The gas was absorbed in a 3 *N* potassium iodide solution and the iodine which was liberated was titrated with standard sodium thiosulfate in the usual way.

The products of the reactions were distilled in a micro-Podbielniak column and some physical properties measured which are listed in Table I.

TABLE I

PHYSICAL PROPERTIES OF PERHALOALKANES

Compound	B.p., °C. (760 mm.)	Density at 20°	Refractive Index at 10°
$CF_3CF_2CF_2CFClCF_2Cl$	85	1.7225	1.3095
$CF_3CF_2CFClCF_2Cl$	67	1.6695	1.3082
$(CF_3)_2CClCF_2Cl$	65	1.708	1.3118

Their infrared absorption spectra are shown in Fig. 1. Perfluorobutene-1 and pentene-1 were chlorinated photochemically in the vapor phase. The infrared spectra of the products were identical to those produced by catalytic chlorination.

The results obtained on calorimetric runs which were carried out without experimental difficulty are given in Table II. It would have been desirable to have made more runs on each of the compounds; however, sufficient material was not available.

Discussion of Results.—The data obtained in these experiments together with the chlorinations previously reported[2,3] are summarized in Table III.

For this series of compounds there are strong deviations from the additivity rule. The heat of chlorination of tetrafluoroethylene is strongly exothermic being 57,323 cal./mole as compared to 43,600 cal./mole[9] shown by ethylene. When one fluorine is replaced by a trifluoromethyl group, the heat of reaction drops 10 kcal. Within experimental error, a perfluoroethyl and perfluoropropyl group give the same drop of about 12 kcal. When both trifluoromethyl groups are on the same

(7) J. D. Lazerte, L. J. Hals, T. S. Reid and G. H. Smith, *J. Am. Chem. Soc.*, **75**, 4525 (1953).

(8) "Fluorine Chemistry," Vol. II, J. H. Simons, editor, Academic Press, Inc., New York, N. Y., 1954.

(9) J. D. Conn, G. B. Kistiakowsky and E. Smith, *J. Am. Chem. Soc.*, **60**, 2764 (1938).

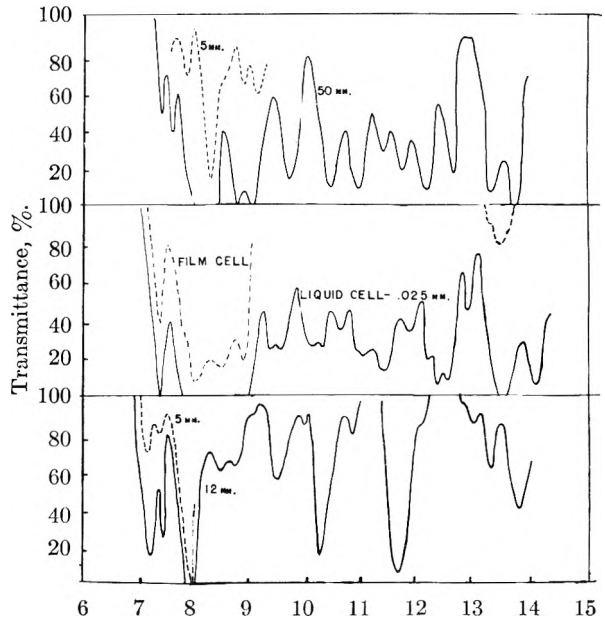

Fig. 1.—Infrared spectra of products of chlorination of perfluorinated butene-1, pentene-1, and isobutene.

TABLE II

CHLORINATION OF PERFLUOROÖLEFINS AT 128°

Chlorine rate, moles/min. × 10^4	Energy rate, cal./min.	$-\Delta H$, cal./mole
	(a) Perfluoropentene-1	
1.195	5.478	45,841
1.298	5.876	45,503
2.041	9.389	46,002
1.955	8.819	45,109
	$-\Delta H_{av}$ = 45.61 ± 0.40 kcal./mole	
	(b) Perfluorobutene-1	
1.465	6.527	44,698
1.694	7.618	44,970
1.408	6.369	45,234
	$-\Delta H_{av}$ = 44.97 ± 0.31 kcal./mole	
	(c) Perfluoroisobutene	
2.298	9.770	42,552
1.899	7.920	41,706
2.070	8.782	42,415
1.390	5.867	42,217
	$-\Delta H_{av}$ = 42.22 ± 0.51 kcal./mole	

TABLE III

VAPOR PHASE HEATS OF CHLORINATION AT 128°

Compound	$-\Delta H$, cal./mole
$CF_2=CF_2$	57,323
$CF_2=CF-CF_3$	47,149
$CF_2=CF-CF_2-CF_3$	44,966
$CF_2=CF-CF_2-CF_2-CF_3$	45,612
$CF_2=C(CF_3)_2$	42,222
$CF=CF$ $\vert \quad \diagdown$ CF_2-CF_2	37,376
$CF_2=CFCl$	48,815
$CF_2=CCl_2$	41,076

carbon, the lowering of the heat of chlorination is 15 kcal.; with a cyclobutene the lowering is 20 kcal. A chlorine atom is less effective if only one is present. One gives a lowering of 8.5 kcal. but two on the same carbon gives a lowering of 16.2 kcal.

THE ELECTROCHEMICAL DOUBLE LAYER ON SILVER SULFIDE[1]

BY W. L. FREYBERGER AND P. L. DE BRUYN

Department of Metallurgy, Massachusetts Institute of Technology, Cambridge, Massachusetts

Received October 29, 1956

Adsorption densities of silver and sulfide ions at the silver sulfide–solution interface were determined as a function of *p*Ag and ionic strength. Silver and sulfide ions were identified as the potential determining ions for this system. The zero-point-of-charge for silver sulfide in solutions containing sodium acetate and sodium metaborate was observed to lie at *p*Ag 10. This zero-point-of-charge was also shown to be independent of the concentration of hydrosulfide ions below 10^{-9} mole/liter and of *p*H in the *p*H range 4.7 to 9.2. From the adsorption data the magnitude of the changes in free energy at the solid–liquid interface was calculated at different *p*Ag values. The differential capacity of the double layer was determined from the adsorption curves. The results indicated that the capacity values were in good agreement with those found for silver iodide and mercury except at high positive polarization of the surface.

Introduction

In the separation of a valuable mineral from the worthless solids by means of the froth flotation process, reactions at the solid–solution and solid–air interfaces are very important.[2] The reagents used in flotation vary widely in their chemical nature and in the effects they produce at the solid interfaces. The mechanisms by which these changes are accomplished are not clearly understood and have been the subject of much investigation in recent years.

One approach to this problem would be to attempt a correlation between the electrical properties of a specific solid–liquid interface under a given set of conditions and the flotation behavior of the same solid under identical conditions. The desirability of such a correlation has been recognized for a long while and a few experiments have been carried out.[3–6] However, the success of this approach until now has been limited by the lack of quantitative knowledge of the electrical properties of the solid–liquid system except for the mercury–solution[7] and silver iodide–solution system.[8] Neither one of these two systems is of much practical interest from a flotation standpoint.

A program of research was initiated to study the electrical and electrochemical properties of a solid–liquid system which is more closely allied to flotation practice. The solid chosen was silver sulfide and this paper reports the results of an electrochemical study of the adsorption of silver and sulfur-bearing ions at the silver sulfide–solution interface in the presence of controlled concentrations of an indifferent electrolyte.

Silver sulfide was chosen as the solid because it is a heavy metal sulfide typical of the ore-forming metal sulfides; because in contact with silver it forms a reversible electrode of the second kind; because it can be prepared as a well flocculated precipitate with high specific surface and because silver has only one important valence state, which simplifies greatly the interpretation of electrochemical results.

Experimental

The experimental technique adopted in this research is similar to that used by Mackor[8] for his studies on silver iodide. This technique consists of adding measured quantities of silver acetate to an aqueous suspension of finely divided silver sulfide and then determining electrochemically the concentration of silver ion in solution after equilibrium has been reached. The amount adsorbed at the solid surface is determined by difference.

Materials.—Finely divided silver sulfide was prepared by precipitation with hydrogen sulfide from an ammoniacal solution of silver hydroxide.[9] After precipitation, the silver sulfide was allowed to stand overnight in contact with the saturated hydrosulfide solution. The precipitate was then washed free of foreign electrolytes by decantation. The precipitation and subsequent washings were carried out as much as possible in a nitrogen atmosphere. Chemical analyses of two of the precipitates gave 86.99 and 86.12% silver and 13.48 and 12.96% sulfur, respectively. Stoichiometrically, silver sulfide should analyze 87.1% silver and 12.9% sulfur. X-Ray diffraction patterns of these two precipitates checked with the data listed by the A.S.T.M. for β-silver sulfide, the low temperature form of silver sulfide. A value of 7.32 g./cm.^{3} was used for the density of silver sulfide. The aging characteristics of several precipitates were checked by measuring electrochemically the change in silver ion concentration in a solution in contact with the precipitate for periods up to six days. This check was necessary because the experimental technique required that the solid should not change its specific surface by recrystallization at a rapid rate. The aging tests showed that during the time of testing, the precipitates decreased in surface area by only a few hundredths of one per cent. A precipitate was used in an experiment for about fourteen days and was not re-used.

Tank prepurified nitrogen which was further purified, provided an inert atmosphere for the electrochemical titrations and was used to remove dissolved oxygen from the solutions. The tank nitrogen was purified by passing it over hot copper punchings, then through a solution of chromous chloride, next over activated charcoal and finally through a suspension of silver sulfide of the same composition as the one being titrated at that time.

Tank hydrogen sulfide, purified according to the recommendation of Dodd and Robinson,[10] was used as a source of

(1) Based on a dissertation submitted by W. L. Freyberger in partial fulfillment of the requirements for the degree of Doctor of Science, MIT.

(2) P. L. de Bruyn, J. Th. G. Overbeek and R. Schuhmann, Jr., *Trans. Am. Inst. Min. & Met. Engrs.*, **199**, 519 (1954).

(3) D. Talmud and N. M. Lubman, *Kolloid-Z.*, **50**, 163 (1930).

(4) P. A. Lintern and N. K. Adam, *Trans. Faraday Soc.*, **31**, 564 (1935).

(5) B. Kamienski, *Z. physik. Chem.*, **A158**, 441 (1932).

(6) O. Jo, *J. Mining Inst. Japan*, **68**, 439 (1952).

(7) D. C. Grahame, *Chem. Revs.*, **41**, 441 (1947).

(8) E. L. Mackor, *Rec. trav. chim.*, **70**, 763 (1951).

(9) W. L. Freyberger, Sc.D. Thesis, Mass. Inst. of Tech., 1955.

(10) R. E. Dodd and P. L. Robinson, "Experimental Inorganic Chemistry," Elsevier Publishing Co., New York, N. Y., 1954.

sulfide for all experiments. The water used in the tests was redistilled in a block-tin still from an alkaline permanganate solution. No water was used which had a specific conductance greater than 0.7×10^{-6} ohm^{-1} cm.$^{-1}$.

Except for silver acetate and sodium hydroxide, all the chemical reagents were of reagent grade and were not purified. Silver acetate of an unspecified purity was recrystallized once from water and was stored in a dark bottle after being pumped dry in a vacuum desiccator. The salt analyzed 64.1% silver as compared to the theoretical value of 64.6%. Sodium hydroxide, free from sodium carbonate, was prepared according to the method of Kolthoff and Sandell[11] and was used immediately after preparation.

Apparatus.—The titrations of the silver sulfide suspensions were conducted in a Pyrex glass vessel having a total volume of about 500 ml. Normally 250 ml. of suspension was used in a test. A rubber stopper sealed the vessel and provided entrance for the silver sulfide electrodes, the reference electrode, a thermometer, two microburets and an inlet and an outlet for nitrogen gas. The suspension was stirred with a magnetic stirrer and the temperature of the suspension was maintained between 20 and 25° by placing a copper plate carrying a water coil between the vessel and the stirrer.

The electromotive force of the cell was measured by means of a Leeds and Northrup Student Potentiometer with a Vibrating Reed Electrometer serving as a null-point indicator. E.m.f. measurements were accurate to ±0.5 mv. The titration vessel was placed inside a grounded copper box and shielded cable was used in the circuit to prevent interference from electrical pick-up.

The electrode system for determining the concentration of silver ion in solution consisted of a reference electrode and a silver–silver sulfide indicating electrode. Two different reference electrodes were used depending on the *p*H of the suspension. At a *p*H of about 5, it was possible to use a glass electrode as reference electrode. When the *p*H was buffered at 9, the glass electrode was sluggish in its response so a saturated calomel electrode connected to the system by means of a salt bridge, was used. The salt bridge was copied from the one described by Mackor.[8] The liquid junction solution in the bridge was 2 *N* NH_4NO_3.

Silver–silver sulfide indicating electrodes were prepared by first plating a platinum wire with silver and then anodizing electrically the silver in the presence of a solution of sodium sulfide.[9] Several sets of these electrodes were prepared. Each set contained two or three electrodes which were used simultaneously during a titration.

From measurements of the standard potential of the silver–silver sulfide:glass electrode couple, the standard potential (E^0) of the half cell reaction

$$2Ag(s) + S^=(aq) \rightleftarrows Ag_2S(s) + 2e^- \qquad (1)$$

was calculated. The average of 23 determinations with eight different silver–silver sulfide electrodes indicated that at 22.5°

$$E^0_{Ag(s)/Ag_2S(s)} = 0.7180 \pm 0.0035 \text{ volt} \qquad (2)$$

The standard potential of the glass electrodes was determined to be

$$E^0_{glass} = -0.7040 \pm 0.0044 \text{ volt} \qquad (3)$$

(A) Ag(s) | Ag_2S(s) | indifferent electrolyte and small concn. of Ag^+, $S^=$, H^+, etc. || HCl (dil. aq.) | AgCl(s) | Ag(s)

or

(B) Ag(s) | Ag_2S(s) | indifferent electrolyte and small concn. of Ag^+, $S^=$, H^+, etc. || NH_4NO_3 aq. (2 *N*) | KCl (sat.) | Hg_2Cl_2(s) | Hg(l)

Determinations were made with the salt bridge–calomel electrode assembly in order to evaluate the effect of the liquid junction potential. The average of 41 such determinations with 13 different Ag/Ag_2S electrodes gave at 22.5°

$$E^0_{Ag(s)/Ag_2S(s)/\text{liq. junction}} = 0.7090 \pm 0.0028 \text{ volt} \qquad (4)$$

The potential of the saturated calomel electrode was taken as[12]

$$E_{\text{sat calomel}} = -0.2415 + 0.00076[t(°C.) - 25] \text{ volt} \qquad (5)$$

A check on the stability of the indicating electrodes was obtained by measuring the standard potential of a pair of electrodes three times over a period of three months. During this time the standard potential varied by about three millivolts.

Procedure.—At the start of an experiment, a suspension of freshly prepared silver sulfide precipitate in an aqueous solution of reagents needed to fix the *p*H and ionic strength, was introduced into the titration vessel. Experiments were run at either *p*H 4.7 or *p*H 9.2 and at several values of ionic strength of solution. At *p*H 4.7 the electrolyte used to fix the ionic strength was sodium acetate and the solution was buffered by maintaining equal molar concentrations of acetic acid and sodium acetate. At *p*H 9.2 boric acid and sodium hydroxide in the molar ratio of 2:1 were used to give equal concentrations of boric acid and sodium metaborate. The latter salt fixed the ionic strength.

Aqueous solutions of silver acetate and sodium hydrosulfide to be used as titrating agents, were prepared essentially free of oxygen and were stored under nitrogen in a modified 5-ml. Koch microburet, from which they were added to the suspension when required. The sodium hydrosulfide solution was prepared by bubbling purified H_2S through a solution of approximately 0.1 *N* sodium hydroxide.

Titrations were run by measuring the equilibrium potential of the silver–silver sulfide electrode against the reference electrode. Then a measured number of moles of silver acetate was added and the new equilibrium e.m.f. value was determined. Equilibrium was usually attained in less than four hours after the addition of silver acetate. The additions of silver acetate were made stepwise until the *p*Ag value was just less than 4. Below *p*Ag 4, the measurements became exceedingly inaccurate because small changes in cell e.m.f. were produced by relatively large additions of silver acetate. At this point sufficient sodium hydrosulfide was added to raise the *p*Ag to about 13. It proved impractical to carry out the addition of sodium hydrosulfide stepwise as was done with the silver acetate addition because in spite of all precautions taken H_2S gas continually escaped from the sodium hydrosulfide solution thereby changing the concentration of the solution. The titration procedure was then repeated, usually three times, until enough points have been obtained to establish the curve of the cell e.m.f. *versus* moles of silver acetate added for a particular value of the ionic strength. The *p*Ag was then again adjusted to about 13 and the ionic strength of the system was increased and the whole sequence was repeated.

Calculation of the Adsorption Density of Silver ions.—To obtain the amount of silver adsorbed at a given *p*Ag value and fixed ionic strength from the experimental e.m.f. values and the known amount of silver added to the system, it is necessary to account for the various forms in which silver might exist in solution. Depending on the reference electrode used, the electrical cell whose e.m.f. is measured corresponds to either

For cell A it is apparent that provided the *p*H is held constant, any change in cell e.m.f. (E) can be related directly to changes in the chemical potential (μ) of the sulfide ion, the hydrosulfide ion and the H_2S molecule, by the relation

$$F\,dE = {}^1/_2 d\mu_{S^=} = {}^1/_2 d\mu_{HS^-} = {}^1/_2 d\mu_{H_2S} \qquad (6)$$

The same interpretation can be given to changes in the e.m.f. of cell B provided the liquid junction potential between the cell solution and the salt bridge does not vary.

(11) I. M. Kolthoff and E. B. Sandell, "Textbook of Quantitative Inorganic Analysis," The Macmillan Co., New York, N. Y., 1936.

(12) S. Glasstone, "An Introduction to Electrochemistry," D. Van Nostrand Co., New York, N. Y., 1942.

By using the relation expressing the solubility product of silver sulfide

$$d\mu_{Ag^+} = -{}^1/_2 d\mu_{S^-} \quad (7)$$

Equation 6 may be written as

$$F\,dE = -d\mu_{Ag^+} = -RT\,d\ln a_{Ag^+} \quad (8)$$

where, R is the gas constant, T, the absolute temperature and a_{Ag^+}, the activity of the silver ion. From equation 8 the activity of the free silver ion in solution is obtained. The other forms that silver could assume in the system include insoluble precipitates, adsorbed ions at the solid–liquid interface, complex ions and undissociated molecules in solution. Care was taken to avoid precipitation of insoluble compounds except, of course, silver sulfide. Possible insoluble compounds that could be formed are silver acetate (AgAc), silver hydroxide and silver metaborate.

The concentrations of sulfide ion, hydrosulfide ion and undissociated hydrogen sulfide were calculated from the measured silver ion activity and the equilibrium constants at 22.5°

$$Ag_2S(s) \rightleftarrows 2Ag^+(aq) + S^=(aq); \quad K = 1.96 \times 10^{-52} \quad (9)$$

$$H_2S(aq) \rightleftarrows H^+(aq) + HS^-(aq); \quad K = 1.00 \times 10^{-7} \quad (10)$$

$$HS^-(aq) \rightleftarrows H^+(aq) + S^=(aq); \quad K = 7.08 \times 10^{-16} \quad (11)$$

The free energy data used for calculating these constants are given in Table I.

TABLE I

STANDARD FREE ENERGY OF FORMATION OF SILVER SULFIDE, SILVER, SULFIDE AND HYDROSULFIDE IONS AND HYDROSULFURIC ACID AT 25°

Substance	$\Delta F°$, cal./mole	Substance	$\Delta F°$, cal./mole
Ag_2S (s)	−9,562[13]	Ag^+ (aq.)	18,448[14]
$S^=$ (aq.)	23,450[14]	H_2S (aq.)	−6,490[14]
HS^- (aq.)	2,980[14]		

Equilibrium data on complexes involving silver and acetate are given by MacDougall and Topol.[15] The equilibrium constants for these complexes are

$$AgAc(aq) \rightleftarrows Ag^+(aq) + Ac^-(aq); \quad K = 0.186 \quad (12)$$

$$AgAc_2^-(aq) \rightleftarrows Ag^+(aq) + 2Ac^-(aq); \quad K = 0.230 \quad (13)$$

The concentrations of these complexes were appreciable under conditions of high silver and acetate concentrations but, in this investigation, the corrections never exceeded 15% of the total amount of silver added to the system.

Concentrations of complex ions of silver and sulfide or hydrosulfide ions were calculated from data given by Treadwell and Hepenstrick.[16]

$$AgHS(aq) \rightleftarrows H^+(aq) + AgS^-(aq); \quad K = 5 \times 10^{-6} \quad (14)$$

$$Ag^+(aq) + H_2S(aq) \rightleftarrows AgHS(aq) + H^+(aq); \quad K = 1.76 \times 10^9 \quad (15)$$

The concentrations of AgS^- and AgHS were never of any significance under the conditions used in this investigation.

To convert the ionic activities calculated from the above equilibrium constants to ionic concentrations the ionic activity coefficients were estimated from the Debye–Hückel relation

$$\log f_i = \frac{-0.513 z_i^2 \sqrt{I}}{1 + \sqrt{I}} \quad (16)$$

where f_i is the activity coefficient of ion i of valence z_i at ionic strength I, was used in these calculations.

The calculated increase in the amount of free silver ion and in the amount of silver ion tied up in solution in the various forms discussed above are subtracted from the total amount of silver added to the system in passing from one pAg value to a lower value. The difference thus obtained is assumed to represent the amount of silver adsorbed. The adsorption densities were thus calculated in moles of silver per gram of solid as a function of the silver ion activity in solution and also of ionic strength.

Results

Zero-point-of-charge.—Experimentally, it is only possible to determine the change in adsorption density of silver ion with pAg. In order to plot an adsorption isotherm, it is necessary to know the absolute value for the adsorption density at at least one pAg value. From the experimental results, therefore, an adsorption isotherm can be constructed only with adsorption density in arbitrary units *versus* pAg. These adsorption curves are shown in Figs. 1 and 2. Figure 1 shows a series of adsorption curves at pH 4.7 and at five different ionic strengths: 2×10^{-3}, 5×10^{-3}, 5×10^{-2}, 0.1 and 0.2 N. Figure 2 shows a series of adsorption curves at pH 9.2 and at ionic strengths 5×10^{-3}, 5×10^{-2} and 0.2 N. The set of curves in each figure was obtained on the same precipitate; the titration was started at the lowest ionic strength. The horizontal dotted lines connecting successive curves indicate the changes in pAg when the ionic strength was increased at constant total silver and sulfide content of the system. These lines are drawn horizontally and are therefore lines of constant adsorption density because the solutions were so dilute with respect to silver and sulfide ion concentration that no measurable change in adsorption density would be expected to take place even though the pAg value changed at times by as much as one-half a unit.

It will be seen from Figs. 1 and 2 that the arbitrary adsorption curves do not cross exactly at one point but that the intersecting points lie very close to a pAg value of 10 for both sets of curves with the exception of the curve at ionic strength 2×10^{-3} N in Fig. 1.

Even though the curve at 2×10^{-3} N ionic strength does not intersect the other curves in the vicinity of pAg 10, its shape, nevertheless, has been determined quite accurately. The anomalous behavior of this curve must be attributed to an experimental error which occurred when changing the

(13) J. R. Goates, A. G. Cole, E. L. Gray and N. D. Faux, *J. Am. Chem. Soc.*, **73**, 707 (1951).

(14) "Handbook of Chemistry and Physics," 34th Ed., Chemical Rubber Publishing Company, Cleveland, 1952.

(15) F. H. MacDougall and L. E. Topol, THIS JOURNAL, **56**, 1090 (1952).

(16) W. D. Treadwell and H. Hepenstrick, *Helv. Chim. Acta*, **32**, 1872 (1949).

ionic strength from 2×10^{-3} N to 2×10^{-2} N. A more recent investigation of this system under the same conditions as to pH and nature of indifferent electrolyte[17] has shown that even at an ionic strength of 10^{-3} N, the adsorption curve intersects at pAg 10.

Since it has been demonstrated that the adsorption density of silver is a function of ionic strength as well as pAg (see Figs. 1 and 2), the point common to all the adsorption curves must represent the point of zero charge on the silver sulfide surface. For silver sulfide there is, therefore, no excess of silver or sulfur-bearing ions at the surface at pAg 10. With the zero-point-of-charge established, the absolute adsorption curves can be plotted.

The reproducibility of the curves shown in Figs. 1 and 2 has been illustrated by redetermining the curves under identical conditions but by using different precipitates.

Adsorption Isotherms.—To express the adsorption density in terms of charge per cm.^{2}, the specific surface of the silver sulfide precipitates must be known. Several attempts to measure the surface area by the B.E.T. nitrogen adsorption method gave unsatisfactory results. The specific surfaces obtained by this method indicate that the average particle size lies between one and three microns whereas observations with the electron microscope showed that the maximum particle size was less than half a μ.

The specific surface of the silver sulfide precipitates was estimated by the same method used by Mackor[8] in determining the surface area of silver iodide. This method involves the assumption that the minimum differential capacity of the double layer for silver sulfide in contact with an aqueous solution of an indifferent electrolyte at low ionic strength has the same value as the minimum differential capacity of mercury in contact with an aqueous solution of sodium fluoride at the same ionic strength. The differential capacity is defined as the differential change in charge with change in potential at constant ionic strength. The change in charge is calculated from the experimental data and the change in potential is measured by the change in pAg.

The validity of this method of arriving at the surface area depends on satisfactory proof that the electrolyte (sodium acetate or sodium metaborate) which fixes the ionic strength of the system is not specifically adsorbed at the interface and that the ionic strength is low enough so that the Gouy model of a diffuse double layer[7] is applicable. If these two conditions are met, then the differential capacity of the double layer should have only a very slight dependence on the chemical nature of the solid surface. From Figs. 1 and 2 it follows that the electrolytes, NaAc and $NaBO_2$, act as indifferent electrolytes since all the curves cross in a narrow pAg region. A specifically adsorbed electrolyte could cause a shift in the zero-point-of-charge of as much as two or three pAg units as the electrolyte concentration is varied. Furthermore, at the lowest ionic strength, 2×10^{-3} N used in these experiments, the diffuse layer model should apply reasonably well. Grahame[18] obtained an experimental value of 7.6 μ farads per cm.^{2} for the minimum differential capacity at this ionic strength. By using this value and knowing the total capacity for a given weight of silver sulfide, specific surfaces varying from 25,000 to 65,000 cm.^{2}/g. were calculated.

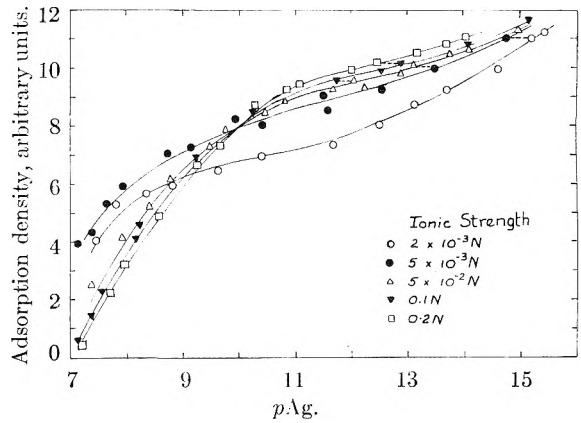

Fig. 1.—Adsorption density of potential determining ions on silver sulfide as a function of the pAg. Adsorption density calculated directly from the titration data. Indifferent electrolyte: sodium acetate; pH 4.64.

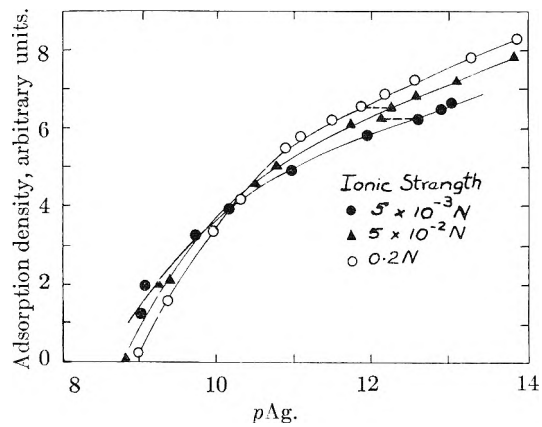

Fig. 2.—Adsorption density of potential determining ions on silver sulfide as a function of the pAg. Adsorption calculated directly from the titration data. Indifferent electrolyte, sodium metaborate; pH 9.19.

In Fig. 3 adsorption density expressed in μ coulombs per cm.^{2} is plotted against pAg at an ionic strength of 0.2 N, to show that pH has no effect on the adsorption density of silver or sulfide ions in the pH range 4.7 to 9.2. Similar results were obtained at ionic strengths 5×10^{-2} N and 5×10^{-3} N.

Figure 4 combines all the experimental results in the form of one series of adsorption isotherms for different ionic strengths. The individual curves have been adjusted to cross at pAg 10, the established zero-point-of-charge. Adjustments were made only in the value of the ordinate since the pAg value was established by the experimentally determined e.m.f. of the cell. The curves at ionic strength 5×10^{-3}, 5×10^{-2} and 0.2 N have been obtained at pH 4.7 and pH 9.2; the curves at the other ionic strengths were determined only at pH 4.7. It is interesting to note the unsymmetrical nature of the adsorption isotherm. A smaller change in pAg below the zero-point-of-charge than above this point gives the same adsorption density.

(17) Unpublished results by I. Iwasaki, Mass. Inst. of Tech.

(18) D. C. Grahame, *J. Am. Chem. Soc.*, **76**, 4819 (1954).

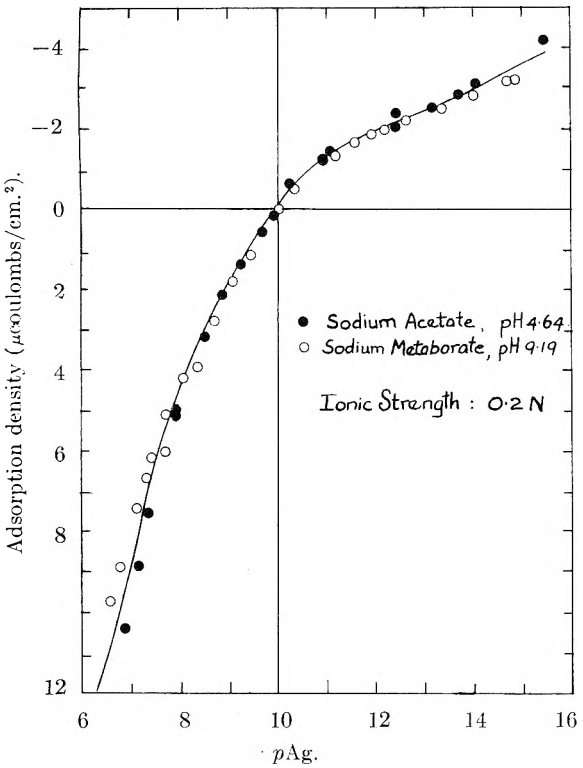

Fig. 3.—Adsorption density of potential determining ions on silver sulfide as a function of the pAg. Curve determined at two pH values with two different electrolytes at the same ionic strength.

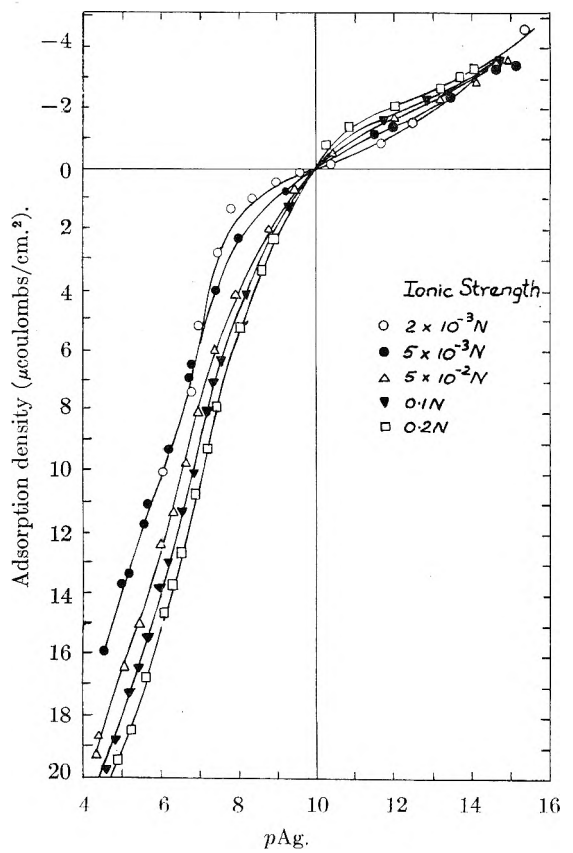

Fig. 4. Adsorption density of potential determining ions on silver sulfide as a function of the pAg.

Discussion

Thermodynamical Considerations.—By applying the well-known Gibbs adsorption equation and by making use of the general theory of the electrochemical double layer Grahame,[7] Mackor[8] Kruyt and Overbeek[19] have succeeded in improving our understanding of interactions at the solid–solution interface.

The general form of the Gibbs equation

$$d\gamma = -\Sigma\Gamma_i d\mu_i \qquad (17)$$

where γ is the interfacial free energy, Γ_i the adsorption density of component i, and μ_i the chemical potential of component i in the bulk solution, may be expanded for silver sulfide in contact with a solution of sodium acetate at constant pH and constant ionic strength to yield

$$d\gamma = -\Gamma_{Ag^+}\,d\mu_{Ag^+} - \Gamma_{S^=}\,d\mu_{S^=} - \Gamma_{HS^-}\,d\mu_{HS^-} - \Gamma_{H_2S}\,d\mu_{H_2S} - \Gamma_{AgAc}\,d\mu_{AgAc} - \Gamma_{AgAc_2^-}\,d\mu_{AgAc_2^-} - \Gamma_{AgS^-}\,d\mu_{AgS^-} - \Gamma_{AgHS}\,d\mu_{AgHS} \qquad (18)$$

Equation 18 may be simplified if the assumption is made that the adsorption density of the silver acetate and silver sulfide complexes is negligible. This assumption is reasonable because the activities of these complexes were always kept very low. Furthermore, by making use of the definition of the solubility product of Ag_2S (equation 7) and by realizing that at constant pH

$$d\mu_{HS^-} = d\mu_{H_2S} = d\mu_{S^=} \qquad (19)$$

Equation 18 simplifies to

$$d\gamma = -(\Gamma_{Ag^+} - 2[\Gamma_{S^=} + \Gamma_{HS^-} + \Gamma_{H_2S}])d\mu_{Ag^+} \qquad (20)$$

When working at constant pH there is no means of distinguishing among the adsorptions of $S^=$, HS^- and H_2S. Experimentally, only the total charge due to an excess of sulfur-bearing species over silver ion at the interface is obtained. However, equation 20 can be simplified further and the specific roles of the $S^=$ and HS^- ions and the H_2S molecule will be clarified by recalling that identical adsorption isotherms for a fixed ionic strength but two different pH values were obtained (see Figs. 3 and 4). At a given pAg, the sulfide ion concentration is fixed regardless of the pH, but the HS^- ion activity in going from pH 4.7 to pH 9.2 changes by a factor of 10^4. The experiments at different pH values therefore indicate that Γ_{HS^-} and Γ_{H_2S} are negligibly small or perhaps zero and that the sulfide ion alone determines the adsorption density at pAg values above the zero-point-of-charge. Equation 20, therefore, reduces to

$$d\gamma = -(\Gamma_{Ag^+} - 2\Gamma_{S^=})d\mu_{Ag^+} \qquad (21)$$

By introducing now the electrochemical relation

$$F\,dE = -d\mu_{Ag^+} \qquad (8)$$

which defines the change in free energy of the reversible cell used in this investigation at constant pH, equation 21 reduces to

$$d\gamma = +F(\Gamma_{Ag^+} - 2\Gamma_{S^=})dE \qquad (22)$$

The silver and sulfide ions are common to both the solid phase and the solution phase; furthermore these ions are involved in the electrode reaction at the Ag/Ag_2S electrode. As a consequence these

(19) H. R. Kruyt, "Colloid Science," Vol. I, Elsevier Publishing Co., New York, N. Y., 1952.

ions are known as potential determining ions because their activity in solution determines the change in the potential difference (Nernst potential) between the solid and liquid. It should be realized that at constant *p*H the electrode reaction at the Ag/Ag_2S electrode can also be written in terms of H_2S or HS^- and under such conditions these species could also be considered as potential determining. However, by changing the *p*H at constant ionic strength, the role of the $S^=$ ion as the only potential determining anion has been established.

Since adsorbed silver and sulfide ions cannot be distinguished from the silver and sulfide ions constituting the silver sulfide crystal lattice, the term $F(\Gamma_{Ag^+} - 2\Gamma_{S^-})$ is referred to as the surface charge. The surface charge will be positive or negative depending on whether an excess of silver or sulfide ions is present. By the establishment of a surface charge, the electrochemical double layer is built up at the interface because an equivalent counter charge must be present in the solution phase adjacent to the solid surface. A surface charge of potential determining ions will have a significance only if the concentration of these ions in solution is small compared to that of the indifferent electrolyte. Only under this condition will the contribution of the potential determining ions toward the counter charge in the solution phase be negligible. This condition was met by working at high ionic strengths.

Equation 22 neglects any contribution to the surface charge by free electrons in the solid. Beta silver sulfide is known to be an electronic as well as an ionic conductor.[20] The role of free electrons in this system may be explained as follows.[21] These electrons will have to come from somewhere since neutral substances are the starting materials (*e.g.*, $AgNO_3$, NaHS, H_2O, etc.). Free electrons may be generated by some disproportionation reaction as, for example

$$S^= \longrightarrow S^- + e^- \qquad (23)$$

The S^- ion is certainly not stable in the solution. It might exist in the solid Ag_2S but in the technique used, the influence of an electron plus a S^- ion is indistinguishable from that of a $S^=$ ion. At the silver sulfide electrode where electrons can be supplied from the silver, the situation might be different, but as long as the electrode behaves according to the Nernst equation, the actual mechanism is not of importance in this study.

By integrating equations 21 or 22 the change of interfacial free energy with silver ion activity in solution may be obtained. From equation 21 it follows that the interfacial free energy will be a maximum at *p*Ag 10, the zero-point-of-charge, and will decrease above and below this point. However, since the absolute value of the interfacial free energy at the zero-point-of-charge is not known only changes in interfacial free energy with respect to the zero-point-of-charge can be determined. In Fig. 5 the difference in interfacial free energy at the silver sulfide–solution interface *versus* *p*Ag for various ionic strengths is plotted. This figure has been obtained by graphical integration of Fig. 4.

(20) M. H. Hebb, *J. Chem. Phys.*, **20**, 185 (1952).

(21) This suggestion was made by Dr. J. Th. G. Overbeek, University of Utrecht, Netherlands, to the authors.

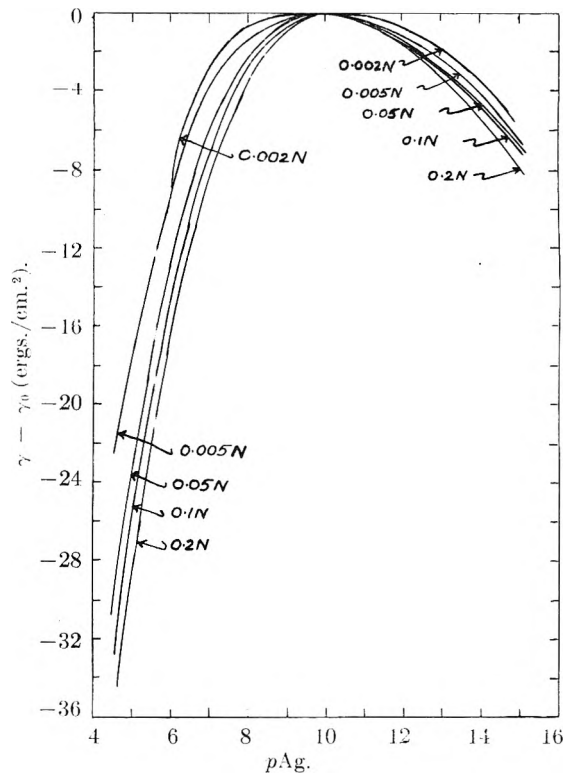

Fig. 5.—Changes in surface tension of the solution–silver sulfide interface due to the adsorption of potential determining ions. Indifferent electrolytes: sodium acetate at *p*H 4.64; sodium metaborate at *p*H 9.19.

Differential Capacity and the Electrical Double Layer.—The electrical double layer at the silver sulfide–solution interface, for the conditions investigated, is visualized to consist of a surface charge due to an excess of silver or sulfide ions at the solid surface and a counter charge contributed by nonspecifically adsorbed ions in the adjacent solution. Sodium acetate and sodium metaborate have been shown to act as indifferent electrolytes and depending on the *p*Ag value of the solution an excess or a deficiency of sodium, metaborate and acetate ions will contribute toward the counter charge. Neither H^+ nor OH^- ions showed any specific affinity for the silver sulfide interface; of course, the concentration of these ions was always kept below 10^{-4} molar. The behavior of these ions is of great interest to the flotation chemist since *p*H regulation has always played an important role in effecting good mineral separations.

The slope of the surface charge (σ^s) *versus* potential (or *p*Ag) curves measures the differential capacity (C_d) of the electrical double layer. Since all the potential jumps except that at the silver sulfide–solution boundary are kept constant, any change in *p*Ag or cell e.m.f. (E) will also measure the change in potential difference across this interface. For the conditions maintained in this investigation, the differential capacity is defined, therefore, by the relation

$$C_d = \left(\frac{\partial \sigma^s}{\partial E}\right)_{\text{all } \mu\text{'s constant except } \mu_{Ag^+},\ (\mu_{S^-})} \qquad (24)$$

The interpretation of σ^s *versus* E or C_d *versus* E

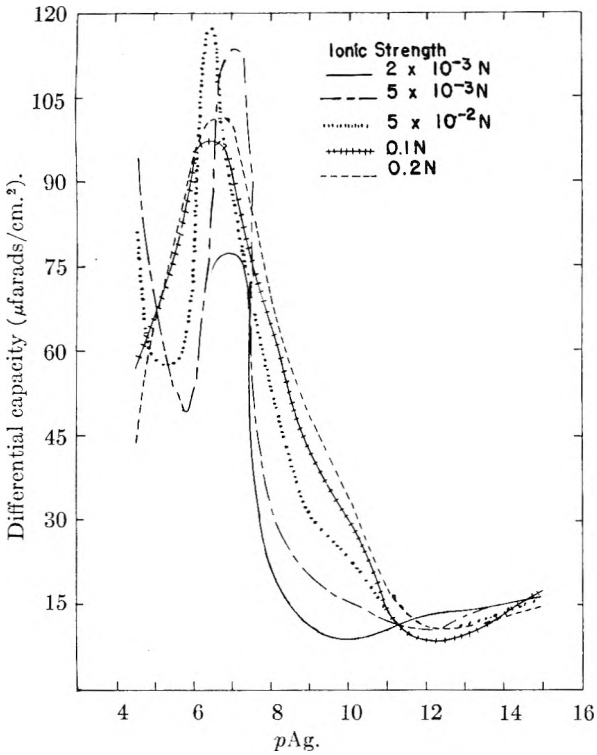

Fig. 6.—Differential capacity of the double layer on silver sulfide as a function of pAg. Indifferent electrolytes: sodium acetate at pH 4.64; sodium metaborate at pH 9.19.

curve lies outside the field of thermodynamics and depends on the choice of the particular physical model to represent the electrochemical double layer.

In Fig. 6 the differential capacity of the double layer on silver sulfide is plotted as a function of pAg for five different ionic strengths. These curves were determined by measuring the slopes of the curves in Fig. 4. Since the adsorption isotherms are quite steep below pAg 8, a small change in the way the adsorption isotherm is drawn will have a profound effect on the slope and the capacity in this region.

The most striking feature of the capacity curves is the steep rise of capacity to the left of the zero-point-of-charge (pAg 10). This is more marked than the measurements made by Mackor[8] on silver iodide and even more so than with mercury in contact with aqueous solutions of sodium fluoride.[7]

The drop in the capacity in the pAg range of 7 to 6 and the minimum indicated between pAg 5 and 6 may or may not be real due to difficulties in establishing the very steep portions of the adsorption isotherms. Grahame[7] has observed a similar behavior for solutions of several electrolytes in contact with mercury.

The minimum in the capacity curve for ionic strength 2×10^{-3} N occurs near pAg 10 and is in accord with the model of a diffuse double layer in the vicinity of the zero-point-of-charge at low ionic strengths. This minimum is, however, not as marked as in the case of mercury.[7] The failure of the curve at 5×10^{-3} N to reach a minimum near pAg 10 is, however, puzzling. It might be that the data are not smooth enough to show this minimum.

The capacity curves approach a plateau at about 15 μ farads per cm.^{2} for negative polarization. This is in good agreement with the qualitative behavior predicted by the theory of Stern and Grahame[7] and with the quantitative results obtained with silver iodide[8] and mercury.[7] The adsorption isotherms plotted in Fig. 4 show that all the curves coincide at high pAg regardless of ionic strength. Thus it would appear that the properties of the double layer on silver sulfide under the conditions investigated, become independent of ionic strength for moderately high negative polarization. This same behavior was observed with silver iodide where it was found by Mackor that the surface charge at negative polarization approaches a limiting value of -4 μ coulombs per cm.^{2}.

Conclusions

This electrochemical investigation of the silver sulfide–solution system established the silver and sulfide ions as potential determining ions in the pH range 5 to 9. Sodium acetate and sodium metaborate were used to determine the ionic strength of the solution and were shown to behave as indifferent electrolytes. Within the pH range 5 to 9 hydroxyl and hydrogen ions showed no specific affinity for the silver sulfide surface.

The zero-point-of-charge for silver sulfide was found to lie at pAg 10; above this pAg, an excess negative charge; and below this pAg an excess positive charge is found at the surface. This surface charge is a function of pAg and ionic strength.

Estimations of the differential capacity from the adsorption isotherms indicate that the structure of the double layer is in qualitative agreement with the models set up by Stern and Grahame. The capacity reaches a plateau in the region of moderately high negative polarization. In general, the capacity curves agree well with those obtained by Grahame for mercury and by Mackor for silver iodide except that a much steeper rise in the capacity curve on positive polarization was observed.

Acknowledgments.—The authors are grateful to the Atomic Energy Commission for financial support in conducting this investigation. To Dr. J. Th. G. Overbeek the authors extend thanks for the valuable advice given and interest shown in this investigation. The authors also wish to express their appreciation to Dr. A. M. Gaudin and Dr. Carl Wagner for helpful discussions.

HEATS OF MICELLE FORMATION OF PARAFFIN CHAIN SALTS IN WATER[1]

BY E. D. GODDARD,[2] C. A. J. HOEVE[3] AND G. C. BENSON

Division of Pure Chemistry, National Research Laboratories, Ottawa, Canada

Received November 2, 1956

Heats of dilution of aqueous solutions of several paraffin chain salts have been measured calorimetrically in the concentration range about the C.M.C. Our experimental data are in agreement with the normally accepted view that the relative amount of paraffin chain salt present in micellar form only becomes significant in the neighbourhood of the C.M.C. and continues to increase smoothly as the total concentration is increased. The heat of micelle formation at 25° is small and positive for the systems studied. It is shown that structural effects exist in water surrounding the single ions and on this basis the small heats of micelle formation can be explained.

I. Introduction

In a recent publication[4] a theoretical treatment was presented for the calculation of heats[5] of micelle formation from experimentally determined thermal data on paraffin chain salts in water, and for "ideal" solutions in which there is aggregation the heat of solution (or dilution) curve was predicted. Measurements were confined to sodium dodecyl sulfate and it was shown that the results were apparently not in accord with the theoretical predictions in view of the sudden jump in the heat data in the range of the critical micelle concentration (C.M.C.). Such a discontinuity is quite inconsistent with the normally accepted model which is based on the law of mass action. Because of the smallness of the measured heats of dilution and the above-mentioned jump, discussion of this phenomenon was withheld until more reliable data became available. It is therefore unfortunate that the title of the above publication, "An Attempt to Measure the Heat of Micelle Formation of Sodium Dodecyl Sulphate" was shortened without the knowledge of the authors to omit the first four words.

Interest in these studies was heightened by the fact that Hutchinson and his co-workers have reported a sudden break in the heat data of paraffin chain salts at the C.M.C. in at least three cases.[6,7] These workers calculate heats of micelle formation by application of "Hess's law" to the data just above and below the C.M.C. An implicit and incorrect assumption involved in this procedure is that there is an abrupt transition from single ions to micelles at the C.M.C. and that only micelles are present above the C.M.C.

In order to pursue these studies and elucidate the nature of the heat change at the C.M.C. we have made measurements on paraffin chain salts of shorter chain length which have a higher C.M.C. and hence enable measurements of the heat to be made with greater accuracy. In addition, for the work on the alkyl sulfates, a calorimeter of somewhat different design, with improved stability and sensitivity, has been used. Measurements on a fatty acid soap were carried out in the original calorimeter.[8]

II. Experimental

The calorimeter used in most of these studies has been described recently[9]; it differs from that used in the previous work in that an electrically heated shield is used for, and permits somewhat greater precision of, adiabatic control. Also the sensitivity of the instrument is increased due to the increase in the number of thermocouple junctions from ten to twelve. Changes of $5 \times 10^{-5°}$ can be detected which corresponds, when the calorimeter contains 170 cc. of water, to *ca.* 0.01 cal. As before, two electrical calibrations were carried out for each run from which heat capacities of the solutions were derived.

The heat of dilution technique was used exclusively. Various quantities of concentrated stock solution were contained in thin wall glass bulbs and broken by a guillotine arrangement within the calorimetric vessel which contained water or other specified aqueous solution. An improvement has been the use of precision bore glass tubing for blowing glass bulbs; in this way a tight fit between Teflon stopper and bulb can be ensured. A further improvement[9] was the introduction of a detachable pin above the guillotine weight; this allowed stirring of the calorimeter vessel before breaking the bulb and was used in the experiments with sodium octyl sulfate and potassium octanoate.

Some of the results at the higher concentrations were obtained by multiple dilution. This involved diluting the stock solution not into water but into the paraffin chain salt solution formed during the preceding run. For alkyl sulfates at the higher concentrations the dilution was at most threefold and usually twofold, but in the case of potassium octanoate up to sevenfold dilutions were performed. The values obtained by this technique were compared with those obtained by single dilutions. Smooth curves could be drawn when all data were plotted on one graph, thus attesting the reliability of the multiple dilution method.

One series of dilutions of sodium octyl sulfate was carried out in the presence of 0.6941 *m* sodium chloride. The addition of potassium hydroxide (final molality 0.0417) to the potassium octanoate solutions served to suppress hydrolysis.

All dilution experiments were carried out at 25°.

A. Materials.—In preparing the solutions conductivity water ($\kappa = 1.1 \times 10^{-6}$ ohm^{-1} cm.$^{-1}$ at 25°) was used.

The sodium alkyl sulfates were all prepared from carefully fractionated normal alcohols. The octyl sulfate was a high purity specimen prepared for us through the courtesy of Lever Brothers Company. The decyl sulfate was prepared by the method of Dreger, *et al.*,[10] recrystallized three times from ethanol and finally extracted four times with light petroleum.

Fractionated octanoic acid having an acid value of 388.0 (calcd. 389.04) and a melting point of 16.48° was used for preparing the potassium octanoate.

Potassium hydroxide was AnalaR grade.

Sodium chloride was AnalaR grade recrystallized three times from water.

The molalities of the stock solutions used in the dilutions were: sodium decyl sulfate 1.0767; sodium octyl sulfate (i)

(1) Issued as N.R.C. No. 4308.

(2) National Research Laboratories Postdoctorate Fellow, 1954-1956.

(3) National Research Laboratories Postdoctorate Fellow 1955-1956.

(4) E. D. Goddard and G. C. Benson, *Trans. Faraday Soc.*, **52**, 409 (1956).

(5) In the present paper the terms heat of solution, dilution and micelle formation are used to denote the increase in heat content, ΔH, of the system during the respective processes.

(6) E. Hutchinson, K. E. Manchester and L. Winslow, THIS JOURNAL, **58**, 1124 (1954).

(7) E. Hutchinson and L. Winslow, *ibid.*, **60**, 122 (1956).

(8) G. C. Benson and G. W. Benson, *Rev. Sci. Instr.*, **26**, 477 (1955).

(9) G. C. Benson, E. D. Goddard and C. A. J. Hoeve, *ibid.*, **27**, 725 (1956).

(10) E. E. Dreger, G. I. Keim, G. D. Miles, L. Shedlovsky and J. Ross, *Ind. Eng. Chem.*, **36**, 610 (1944).

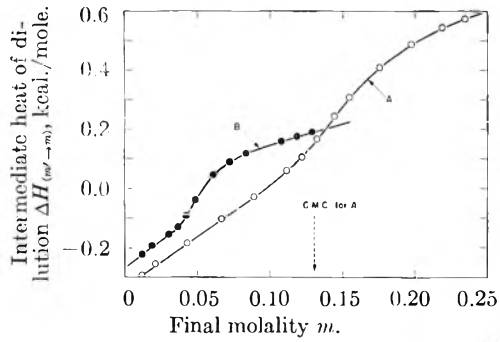

Fig. 1.—Intermediate heats of dilution: $\Delta H_{(m' \to m)}$ plotted as a function of the final molality m: curve A, sodium octyl sulfate in water at 25°; m' = 2.9761; curve B, sodium octyl sulfate in 0.6941 m NaCl solution at 25°; m' = 1.2959.

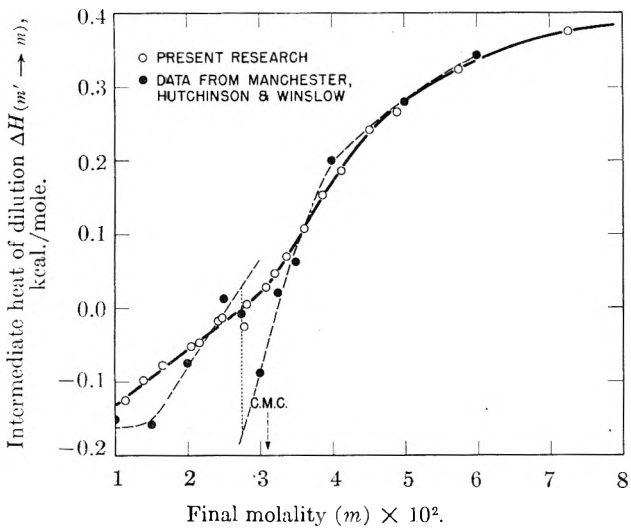

Fig. 2.—Intermediate heats of dilution $\Delta H_{(m' \to m)}$ for sodium decyl sulfate in water at 25° plotted as a function of the final molality m; m' = 1.0767. Solid points are obtained by subtracting 5.85 kcal./mole from the heats of solution tabulated by Hutchinson, Manchester and Winslow.[6]

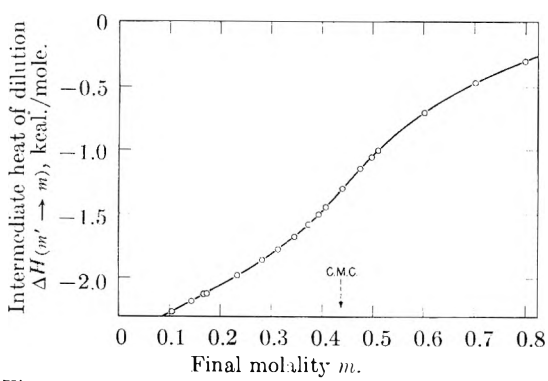

Fig. 3.—Intermediate heats of dilution $\Delta H_{(m' \to m)}$ for potassium octanoate in 0.0417 m KOH solution at 25° plotted as a function of the final molality m; m' = 3.1890.

2.9761, (ii) 1.2959 in 0.6941 m sodium chloride solution as solvent; potassium octanoate 3.1890 in 0.0417 m potassium hydroxide solution as solvent.

III. Results

The data are presented in Figs. 1, 2 and 3, where the increases in heat content per mole on dilution are plotted against the molality of the final solution. Values of the C.M.C. (estimated from tables given by Goette[11] are also indicated on the graphs. In Figs. 4, 5 and 6 a function related to the partial molal heat content, $\bar{H}_2$, of the paraffin chain salt is plotted against the final molality, m. This function is given by

$$\Delta H_{(m' \to m)} + m \frac{\mathrm{d}\ \Delta H_{(m' \to m)}}{\mathrm{d}m} = \bar{H}_2 - \bar{H}_2^\circ - \phi_L'$$

where $\bar{H}_2^\circ$ is the partial molal heat content of the paraffin chain salt at infinite dilution, ϕ_L' is its relative apparent molal heat content at molality m' and $\Delta H_{(m' \to m)}$ is the intermediate heat of dilution per mole of paraffin chain salt.

When the heat capacities of the paraffin chain salt solutions were plotted against their molality, a change of slope was observed in the region of the C.M.C. This change could be measured most accurately for the system having the highest C.M.C.: accordingly the results for potassium octanoate are presented in Fig. 7.

IV. Discussion

A. Comparison with Other Data.—There is a pattern in common to all the curves in Figs. 1, 2 and 3: as the concentration is increased through the C.M.C. a change of slope but no *discontinuity* is observed. This is in accord with earlier predictions. The only data in the literature available for comparison with our heats of dilution are those of Hutchinson, Manchester and Winslow[6] for the heat of solution of sodium decyl sulfate in water. Owing to the difference in the experimental quantity determined the two sets of data should differ by a constant value. However, in contradiction to our results these investigators found a discontinuity in the heat of solution in the range of the C.M.C. By subtracting a constant value of 5.85 kcal./mole from the data of Hutchinson, *et al.*, the two sets can be brought into correspondence at the higher concentrations where experimental accuracy is greatest. In this way experimental data from reference 6 have been included in Fig. 2 and at the lower concentrations they are seen to be scattered about the smooth curve drawn through our points.

In our calorimetric system, one mm. deflection on the scale of the galvanometer indicating the temperature of the calorimeter (total heat capacity about 200 cal. deg.$^{-1}$) corresponds to 5 × 10^{-5}° or 0.01 cal. The estimated experimental error in a single determination is three times this value in unfavorable cases. Each dilution experiment involves two temperature readings and hence there is a possible error of 0.06 cal. in the measured heat effect. The error in determining the heat capacity of the system is negligible in comparison with the error in determining the temperature change in a dilution. The abrupt change observed by Hutchinson, *et al.*, in the integral heat of solution of sodium decyl sulfate in water amounts to 0.2 kcal./mole or about 0.95 cal. for the quantity of material used in our determinations. Such a change would have been detected readily in our calorimeter; a similar change in the heat of solution at the C.M.C. of the shorter chain compounds studied

(11) E. K. Goette, *J. Colloid Sci.*, **4**, 459 (1949).

in the present work would have involved a much larger change in the measured heat and would certainly not have escaped detection.

The apparent discontinuity in the heats of dilution of sodium dodecyl sulfate reported previously[4] corresponded to a difference of 0.1 cal. in the experimentally measured heat and was comparable in magnitude with the estimated error. In view of the failure to find a discontinuity in the heats of dilution for any of the paraffin chain salts in the present work, it is evident that the measurements on sodium dodecyl sulfate should be repeated. A new microcalorimeter more suitable for this purpose is now under construction.

B. Heat of Micelle Formation.—The heat of micelle formation is the increase in heat content when one mole of paraffin chain ions in the single ion form aggregate to the micellar form. In the case of an ideal solution a simple procedure was suggested[4] for obtaining this quantity. It is clear from the variation with concentration of the partial molal heat contents plotted in Figs. 4, 5 and 6 that departures from ideal behavior are considerable. As a result of this and the fact that the C.M.C. as determined by these thermal measurements covers a considerable range, exact assessment of the heat of micelle formation is not possible. Estimated values are given in Table I and all values are seen to be small and *positive*. It is probable that at concentrations above the C.M.C. the values would be different.

TABLE I

HEATS OF MICELLE FORMATION, ΔH_M, OF VARIOUS PARAFFIN CHAIN SALTS IN THE RANGE OF THE C.M.C. AT 25°

Paraffin chain salt	ΔH_M (kcal./mole)
Sodium decyl sulfate	0.5
Sodium octyl sulfate	0.8
Sodium octyl sulfate in 0.6941 *m* NaCl	0.3
Potassium octanoate in 0.0417 *m* KOH	1.7

According to the "sketch of a theory of the micelle" given by Debye[12] and later developments and treatments by Nagagaki[13], Ooshika[14], and Reich[15], micelles are formed because the state in which the hydrocarbon chains are aggregated possesses a lower energy than that in which they are surrounded by water molecules. Although the electrical energy due to the repulsion of the ionic heads increases in the process of micelle formation, the first effect is expected to predominate and hence micelle formation is an energy effect. According to these views no micelles are formed below the C.M.C. since the sacrifice in entropy would be too great. However, experimental results do not confirm this picture. From measurements on the temperature dependence of the C.M.C. several indications exist[16,17] that the increase in heat content on micelle formation may indeed be positive; again our direct thermal measurements (Table I) show that at 25° it is positive for the octyl sulfate, decyl sulfate and potassium octanoate. A smaller change in the heat content would be expected in the presence of added salt as a result of reduced electrical repulsion within the micelles; this is confirmed experimentally in the case of sodium octyl sulfate (Table I).

Stainsby and Alexander[18] were the first to attempt an explanation of the small heat effects involved in aggregation. They assumed that, whereas the hydrocarbon part of the micelle can be regarded as essentially the same as a liquid hydrocarbon, the hydrocarbon part of the single ions sur-

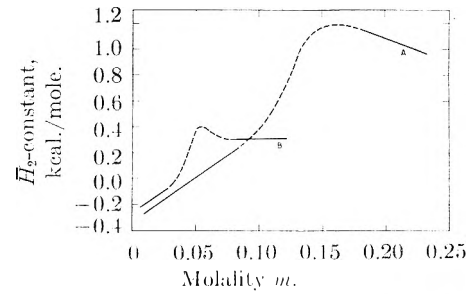

Fig. 4.—Plot of the partial molal heat $\bar{H}_2$ against molality *m*. The constant subtracted in the ordinate is $\bar{H}_2^\circ + \phi_L'$ as defined in the text. Curve A, sodium octyl sulfate in water at 25°; Curve B, sodium octyl sulfate in 0.6941 *m* NaCl solution at 25°.

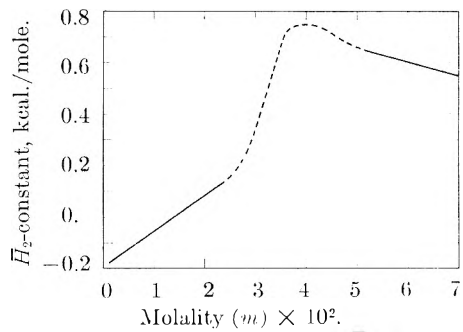

Fig. 5.—Plot of the partial molal heat $\bar{H}_2$ against molality *m*, for the system sodium decyl sulfate–water at 25°. The constant subtracted in the ordinate is $\bar{H}_2^\circ + \phi_L'$ as defined in the text.

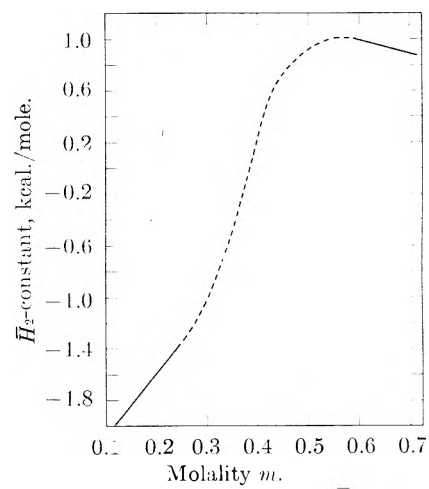

Fig. 6.—Plot of the partial molal heat $\bar{H}_2$ against molality *m* for potassium octanoate in 0.0417 *m* KOH solution at 25°. The constant subtracted in the ordinate is $\bar{H}_2 + \phi_L'$ as defined in the text.

(12) P. Debye, *Ann. N. Y. Acad. Sci.*, **51**, 575 (1949).
(13) M. Nagagaki, *J. Chem. Soc. Japan*, **72**, 113 (1951).
(14) Y. Ooshika, *J. Colloid Sci.*, **9**, 254 (1954).
(15) I. Reich, THIS JOURNAL, **60**, 257 (1956).
(16) A. P. Brady and H. Huff, *J. Colloid Sci.*, **3**, 511 (1948).
(17) B. D. Flockhart and A. R. Ubbelohde, *ibid.*, **8**, 428 (1953).
(18) G. Stainsby and A. E. Alexander, *Trans. Faraday Soc.*, **46**, 587 (1950).

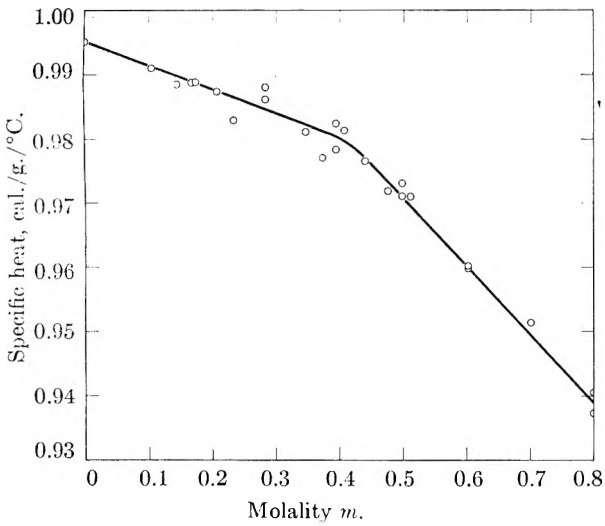

Fig. 7.—The specific heat of potassium octanoate solutions in 0.0417 *m* KOH solution at 25° plotted as a function of molality *m*. One point (specific heat = 0.7681 cal. degree^{-1} gram^{-1} at $m' = 3.1890$) is beyond the range of the graph.

rounded by water is curled up tightly and the internal motions are consequently considerably restricted. According to these views changes in entropy and heat effects due to internal motions in the process of micelle formation should approximately be equal to those in the melting process of a crystalline hydrocarbon and should largely compensate the external effects; the latter consist mainly of the contribution resulting from a reduction of the hydrocarbon–water interface, as electrical effects are shown to be small. It is, however, unlikely that the hydrocarbon part of the single ion surrounded by water is restricted in its internal motions to such an extent as to become comparable with a hydrocarbon in the crystalline state; furthermore one may question the validity of equating the interfacial energy per square centimeter between the hydrocarbon chain of a single ion and water to that between a macroscopic oil drop and water.

1. Structural Effects in Water.—An explanation of the small heat effects is now made in terms of structural effects exhibited in water, as discussed by Frank and Evans.[19] According to these ideas water molecules tend to form a kind of ice structure around the molecules of non-polar solutes. This structure would lower the energy and entropy of the solution and result in an extra specific heat because of the gradual breakdown of the structure on increasing the temperature. It has been shown experimentally[20] that the decrease in heat content on dissolving non-polar gases in water is much larger than in organic solvents and this is paralleled by corresponding entropy effects, and a higher specific heat of the water solutions. If these views also apply to the hydrocarbon part of the single ions, the water solutions of single ions should show this extra specific heat. However, a complicating factor is the ionic head. In the treatment given below for potassium octanoate the contribution of the ionic heads to the specific heats is allowed for by comparing the specific heat at 25° of a potassium octanoate solution with that of a potassium acetate solution of the same molality. On the assumption that no long range order effects exist, below the C.M.C. the heat capacity of a potassium octanoate solution should approximately be equal to that of the potassium acetate solution in which is dissolved an equimolar amount of $(CH_2)_6$ chains. From the specific heat data of potassium acetate[21] and of potassium octanoate plotted in Fig. 7, the partial molal heat capacity of $(CH_2)_6$ chains surrounded by water was found to be 120 cal. degree^{-1} mole^{-1}, which corresponds to 1.4 cal. degree^{-1} gram^{-1}. It is more difficult to draw conclusions above the C.M.C. of potassium octanoate since the CH_3 group of potassium acetate is surrounded by water, whereas the CH_3–$(CH_2)_6$ group of potassium octanoate is mainly surrounded by the same groups of other paraffin chains forming the interior of the micelle. In order to account for this, we can tentatively put

$$\bar{C}_p\{CH_3\} - \bar{C}_p\{CH_3\}_{aq} = \frac{1 \text{ mol. wt. } \{CH_3\}}{6 \text{ mol. wt. } \{CH_2\}} \times (\bar{C}_p\{(CH_2)_6\} - \bar{C}_p\{(CH_2)_6\}_{aq})$$

where $\bar{C}_p$ is the partial molal heat capacity of the groups which follow in brackets; if the environment is water this is indicated by the subscript "aq."; otherwise the environment is hydrocarbon. Knowing $\bar{C}_p\{CH_3 + (CH_2)_6 - (CH_3)_{aq.}\}$ from the value of potassium octanoate above the C.M.C. and the heat capacity of potassium acetate solutions of the same molality,[21] and having obtained above a value for $\bar{C}_p\{(CH_2)_6\}_{aq.}$, we are now able to calculate the value of $\bar{C}_p\{(CH_2)_6\}$, the partial molal heat capacity of $(CH_2)_6$ groups in the micelle. In this calculation the experimental value for the specific heat 0.7681 cal. degree^{-1} gram^{-1}, of the stock solution ($m' = 3.1890$) also was used to determine $\bar{C}_p\{CH_3 + (CH_2)_6 - (CH_3)_{aq.}\}$. It is found that $\bar{C}_p\{(CH_2)_6\} = 47$ cal. deg.$^{-1}$ mole^{-1} which corresponds to 0.55 cal. degree^{-1} gram^{-1}. The above treatment neglects other contributions to the heat capacity which are considered small. These result from the shift with temperature of the equilibrium between micelles and single ions, surface contributions due to the contact between hydrocarbon and water, and electrical effects due to the repulsion of the ionic heads.

It is interesting to make a comparison with data for liquid paraffins at 25° given by Timmermans.[22] These data show that the specific heat varies only 4% in the series liquid *n*-hexane to *n*-dodecane, the average value being 0.53 cal. degree^{-1} gram^{-1}. The agreement between this value and the above calculated value strongly supports the suggestion[23] that the interior of the micelle is liquid in character. On the other hand the partial molal heat capacity of hydrocarbon surrounded by water in the single ion form is nearly three times as large

(19) H. S. Frank and M. W. Evans, *J. Chem. Phys.*, **13**, 507 (1945).

(20) D. D. Eley, *Trans. Faraday Soc.*, **35**, 1421 (1939).

(21) "International Critical Tables," Vol. 5, McGraw-Hill Book Co., New York, N. Y., p. 124.

(22) J. Timmermans, "Physico-chemical Constants of Pure Organic Compounds," Elsevier Press, New York, N. Y., 1950.

(23) G. S. Hartley, "Aqueous Solutions of Paraffin Chain Salts," Hermann et Cie, Paris, 1936.

as in the liquid state, substantiating the view that structural effects exist in the water surrounding the single ions.

It is now possible to provide a qualitative explanation of the change of the heat of micelle formation with temperature in terms of the water structure around the hydrocarbon chains. As a result of the stability of the structure at low temperature aggregation is accompanied by an increase in the energy of the system and is therefore an entropy effect. On elevation of the temperature there is a progressive breakdown of this structure, the energy of the single ion state increases and consequently the increase in heat content on aggregation is smaller and becomes negative.

If the above views are correct, then anomalous volume effects should exist in the single ion state of solutions of paraffin chain salts since the "iceberg" structure around the hydrocarbon chains should decrease the volume of water solutions. It has indeed been observed[24,25] that the partial molal volume of the single ion state is smaller than that of the micellar state, although the difference is small.

2. Estimation of the Heat of Micelle Formation. —An estimate of the heat of micelle formation now can be made. We note first that the environment of the ionic part of the paraffin chain ions is water in both the single ion and micellar state and hence the main contribution is expected from the change of state of the hydrocarbon part. Therefore, it would be expected that energy and entropy changes in the process of micelle formation are approximately equal to the corresponding quantities for the process hydrocarbon in water → hydrocarbon in the bulk liquid with added terms arising from surface effects. No data exist for the hydrocarbons of interest, but it is possible to obtain a rough estimate as follows. From the data given by Egloff[26] we can calculate energy and entropy changes for the process hydrocarbon gas → hydrocarbon liquid at 25°. Morrison[27] determined the solubilities of the hydrocarbon gases from methane to butane in water at different temperatures. From these data the entropy and energy changes can be calculated for the process hydrocarbon gas → hydrocarbon in water at 25°. By extrapolation, a rough estimate can be made of the corresponding changes for the higher hydrocarbons. If the same standard states are taken in the gas phase for both processes, it is possible to estimate energy and entropy changes for the process

hydrocarbon in water → hydrocarbon liquid at 25°

(standard state: mole fraction unity referred to the infinitely dilute solution). We find for decane

$$\Delta H = -1.4 \text{ kcal./mole}$$
$$\Delta S = +29 \text{ cal. degree}^{-1} \text{ mole}^{-1}$$

These values are used to estimate the heat of micelle formation of sodium decyl sulfate.

So far we have neglected surface effects of the micelle. These effects can be regarded as being composed of the surface free energy of an uncharged hydrocarbon drop and the electrical free energy of the charged particle. The latter effect is considered to be rather small since the effective charge on the micelle is known to be small[28] and in view of the already crude procedure this effect is neglected. The former effect can be evaluated approximately for the case of sodium decyl sulfate in the following way. The micelle consists of approximately 50 single ions[29] as determined by light-scattering experiments. Molar volumes of 32.63 cc. for a CH_3 and 16.21 cc. for a CH_2 group as given by Tartar[30] are used to calculate the size of the micelle. Approximate values of 50 ergs cm.$^{-2}$ and 0.035 erg cm.$^{-2}$ degree^{-1} [31] are adopted, respectively, for the surface free energy and entropy of a hydrocarbon–water interface. The surface energy of the micelle is calculated to be 5.1 kcal. mole^{-1} and the surface entropy term 3 cal. mole^{-1} degree^{-1}. Experimentally the C.M.C. is found to be 0.03 *m;* hence we estimate for the process

single ions (0.03 *m*) → micelles at 25°
$\Delta H_M = +3.7$ kcal./mole
$\Delta S_M = 17$ cal. degree^{-1} mole^{-1}
$T\Delta S_M = +5.1$ kcal./mole.

It is observed that the calculated values of $T\Delta S_M$ and ΔH_M are approximately equal, as required for equilibrium. The agreement between these values and the experimental value of $\Delta H_M = 0.2$ kcal./mole given in Table I is rather poor, presumably in view of the roughness of the extrapolation procedures. However, the treatment given shows that the small positive values of micelle formation can be understood on the basis of the fact that structural effects exist in the water surrounding the single ions, although these effects are probably less pronounced than those existing in the water solutions of smaller non-polar molecules.

It is interesting to compare the value calculated here with that based on the assumption that no structural effects exist and that the single ions are curled up to a sphere with the same surface energy per square centimeter as a macroscopic oil drop; electrical effects are neglected, as before. The value obtained in this way is $\Delta H_M = -13$ kcal./mole.

It may seem surprising that the terms due to electrical forces are neglected altogether in the present treatment. Admittedly a complete theory of micelle formation must necessarily take account of the electrical terms, for it is known[32] that extraneous salt lowers the C.M.C. considerably, indicating a reduction of the free energy of the micellar state. Salting out effects on the single ions also exist, but these effects are generally small in comparison with the former. The correctness of these views can be judged from the following example. If sufficient salt be added to a system to

(24) D. G. Davies and C. R. Bury, *J. Chem. Soc.*, 2263 (1930).
(25) K. Hess, W. Philippoff and H. Kiessig, *Kolloid-Z.*, **88**, 40 (1939).
(26) G. Egloff, "Physical Constants of Hydrocarbons," Vol. 5, Reinhold Publ. Corp., New York, N. Y., 1953.
(27) T. J. Morrison, *J. Chem. Soc.*, 3184 (1952).
(28) D. Stigter and K. J. Mysels, THIS JOURNAL, **59**, 45 (1955).
(29) H. V. Tartar and A. L. M. LeLong, *ibid.*, **59**, 1185 (1955).
(30) H. V. Tartar, *ibid.*, **59**, 1195 (1955).
(31) "International Critical Tables," Vol. 4, McGraw-Hill Book Co., New York, N. Y., p. 437.
(32) W. D. Harkins, "The Physical Chemistry of Surface Films," Reinhold Publ. Corp., New York, N. Y., 1952, p. 304.

lower the C.M.C. by a factor of ten and this effect is ascribed wholly to the lowering of the electrical free energy of the micelle, the latter term is decreased by only 1.4 kcal./mole. Therefore it is believed that in view of the crudeness of the present treatment, we are justified in neglecting the electrical terms as a first approximation.

Acknowledgments.—The authors wish to thank Mr. P. D'Arcy for invaluable help in the calorimetric determinations. Also they are most indebted to the Lever Brothers Company for providing the sample of sodium octyl sulfate.

THE SODIUM DIFFUSION FLAME METHOD FOR FAST REACTIONS. II. REACTIONS OF FLUORINATED METHYL CHLORIDES[1,2]

BY JOHN F. REED AND B. S. RABINOVITCH

Contribution from the Department of Chemistry of the University of Washington, Seattle, Washington

Received November 9, 1956

The reaction of sodium atoms with the series CH_3Cl, CFH_2Cl, CF_2HCl and CF_3Cl has been studied. After primary abstraction of chlorine, subsequent reactions of sodium with fluoromethyl radicals are of importance. A new upper boundary condition for the limiting visible sodium pressure has been applied. Various models for the calculation of specific rate constants are discussed and compared. The activation energies of the primary step in the series are found to be 9.8, 10.1, 10.0 and 9.2 kcal./mole, respectively. These are used to obtain $D(CFH_2\text{–}Cl)$ = 81–82, $D(CF_2H\text{–}Cl)$ = 81–82, and $D(CF_3\text{–}Cl)$ = 80–81 based on $D(CH_3\text{–}Cl)$ = 81.2 kcal./mole. These enabled calculations of $\Delta H_f(CF_3)$ = −119.5, $D(CF_3\text{–}F)$ = 117.5 and $D(CF_3\text{–}CF_3)$ = 64 kcal./mole. Some other relevant thermochemical quantities for fluorocarbons and limits of rate constants for sodium atom reaction with radicals are calculated and discussed.

In a previous paper,[3] an analysis of the experimental variables of sodium diffusion flames was presented. In the present work, application is made to the reactions of sodium atoms with the series of compounds CH_3Cl, CFH_2Cl, CF_2HCl and CF_3Cl. The nature and limitations of some of the assumptions made in experimental models used to describe the steady-state phenomena are examined in the light of the experimental findings, in an effort more accurately to define the rate constants. Corrections for radical reactivities are explicitly included. From these reactions, information concerning the effect of fluorine substitution on the magnitude of the carbon–chlorine bond dissociation energy has been obtained, as well as some knowledge of the chemistry of the fluoroalkyl radicals and the magnitude of some bond dissociation energies for fluorocarbons. A brief report of an early value of the heat of formation of CF_3 radical obtained in this work already has appeared.[4]

Experimental

Materials.—Methyl chloride was an Eastman Kodak white label product purified by repeated bulb to bulb distillation.

Monofluoro-, difluoro- and trifluoromethyl chlorides were obtained from the Kinetic Chemicals Division of the E. I. du Pont de Nemours Co. They were distilled in a low temperature fractionating column and the middle fractions were used.

Nitrogen was purified by passage through a metal ketyl solution[5] and then through several cold traps, including one containing silica gel.

Sodium was cut from a large block and was refluxed under vacuum for about 10 hours at 500° to drive off volatile impurities and was handled under dry nitrogen.

Apparatus.—A flow system modeled after those of Polanyi[6] and of Heller[7] was employed. The reaction vessel, a Pyrex tube 6 cm. in diameter with plane windows, was heated by a furnace provided with plane windows for observation of the flame. Nitrogen carrier gas streamed over sodium at 529°K. in the carburetor, and through a nozzle of radius 1.00 mm. into the reaction zone. The flow rate of nitrogen, which was maintained by a three stage mercury vapor pump, was determined from the pressure fall across a capillary, measured by means of a double McLeod gage. Halide was fed to the reaction zone through a calibrated capillary tube. The reaction zone was illuminated with a sodium lamp monitored and controlled at constant irradiation intensity. Volatile products were collected in cold traps, and salts were collected on a plate under the flame. Reaction system pressure was measured by a McLeod gage. Temperatures were measured with calibrated thermocouples. The inside of the reactor was blackened by a soot deposit to provide a uniform dark background for flame observations.

Procedure.—Temperatures, nitrogen pressure in the system and carrier gas flow rate were brought to constant conditions before the halide was introduced. The fluorescence zone was reduced to the steady-state size in a few minutes. The flame radius was measured by sighting at right angles to the flow axis along a thin steel plate mounted on a lucite travelling arm of a steel rule. The lucite allowed observation of the entire flame or, when covered, only the flame edge so that the intense flame center could be obscured. Several readings of flame size together with relevant pressure and temperature readings were made and constituted the measurements of a single run. After these measurements, halide flow was closed off and new conditions were established.

There was no chemiluminescence under dark conditions. Products were isolated in runs of several hours duration.

Sodium Pressure.—The sodium pressure in the carburetor was obtained from the data of Gordon.[8] The limiting visible pressure, p_1, was determined by raising the temperature of the carburetor and reaction zone (the latter always 20° higher than the former), and noting the temperatures when sodium fluorescence was first visible both within and just outside the nozzle tube, while nitrogen was circulated at rates and pressures comparable with a run. The appropriate value to be taken is discussed below.

Halide Pressure.—The halide partial pressure was calculated from the nitrogen and halide flow rates and the total reaction pressure.

Diffusion Coefficient of Sodium.—The ternary diffusion coefficient of sodium into the mixture of halide and nitrogen

(1) Presented before the Physical and Inorganic Division of the American Chemical Society at Los Angeles, March, 1953.

(2) Abstracted in part from a thesis submitted by John F. Reed in partial fulfillment of the requirements for the degree of Doctor of Philosophy at the University of Washington, 1953.

(3) J. F. Reed and B. S. Rabinovitch, THIS JOURNAL, **59**, 261 (1955).

(4) B. S. Rabinovitch and J. F. Reed, *J. Chem. Phys.*, **22**, 2092 (1954).

(5) L. F. Fieser, "Experiments in Organic Chemistry," D. C. Heath and Co., New York 2nd Ed., 1941, p. 396.

(6) H. V. Hartel and M. Polanyi, *Z. physik. Chem.*, **B11**, 97 (1930)

(7) W. Heller, *Trans. Faraday Soc.*, **33**, 1556 (1937).

(8) A. R. Gordon, *J. Chem. Phys.*, **4**, 100 (1936).

was calculated using Wilke's equation,[9] in which the binary diffusion coefficients of sodium into nitrogen and into halide are required along with the mole fractions of the gases. The binary coefficient in nitrogen is in the literature,[10,11] but that of the halide was calculated from kinetic theory[12] using molecular diameters of halides calculated from viscosity data.[13]

Analysis of Products.—Products could be grouped as volatile and non-volatile. The former included products of reactions of the radicals, the latter included halide salts and carbon.

Volatile products were analyzed using a Consolidated Model 21-103 mass spectrometer. The mass spectra of the original reactants, of the total products, and, to assist in identification, of high and low boiling fractions of the products were obtained.

The halide salts were sodium chloride and sodium fluoride. Samples from various portions of the collection plate were analyzed for the chloride to fluoride ratio. The chloride was determined by a semi-micro Mohr method and the fluoride by a spectrophotometric method.[14] Both methods were calibrated against samples of known composition.

Results

Volatile Reaction Products.—Although not all the mass spectral patterns of the products were known, a sufficient number of those of the simpler compounds were available from the API tables to enable deduction of the nature of the products, but not always of their relative amounts. The principal results are listed in Table I. Only trace quantities of higher molecular weight compounds were found.

The product of the reaction of CFH_2Cl was C_2FH_3 and no $C_2F_2H_4$ was detected. The latter would arise from radical recombination of CFH_2 after Cl abstraction by sodium. However, it has been pointed out that this ethane is very unstable toward HF elimination which occurs even at 0°.[15] Likewise in the products of the reaction of CF_2HCl, both $C_2F_4H_2$ and C_2F_3H were detected, the latter presumably also arising by HF split from the somewhat more stable tetrafluoroethane.

TABLE I

VOLATILE REACTION PRODUCTS

	Products
CF_3Cl	C_2F_6 and C_2F_4 (1.00:0.74); C_4F_8 (trace)
CF_2HCl	$C_2F_4H_2$, $C_2F_2H_2$ and C_2F_3H
CFH_2Cl	C_2FH_3, C_2H_4 (small)

The products of the reaction of sodium with methyl chloride were not analyzed.

Non-volatile Reaction Products.—In general the molar ratio of fluoride to chloride salt found decreased slightly with increasing distance from the nozzle. Significant amounts of a dark carbon deposit were evident only with CF_3Cl. Average values over the entire reaction zone of the molar ratios, for the various reactants studied, are given in Table II. The ratio at any point on the collection plate fell within 10% of the average.

TABLE II

AVERAGE NaF/NaCl DEPOSIT RATIOS, c

Reactant	CF_3Cl	CF_2HCl	CFH_2Cl
c	0.75	0.20	0.05

Calculation of Specific Rate Constants.—Four methods of calculating the specific rate constant were used. The first three models have been discussed previously[3] and only their definition and calculation are described here. The fourth model is introduced below.

$k^{(0)}$.—This is the conventional Polanyi diffusion model rate constant, which employs the boundary condition that the pressure of sodium at the nozzle is the carburetor pressure, p^*.

$$k^{(0)} = \frac{(\ln p^* r_0/p_1 R)^2 D}{(R - r_0)^2 p'} \qquad (1)$$

where the observables on the right-hand side have their customary meaning.

$k^{(1)}$.—When the nozzle boundary condition is modified by setting the flow rate of sodium into the system equal to the total amount of reaction per second, $k^{(1)}$ is obtained

$$k^{(1)} = \frac{[\ln v_0 r_0^2 p^*/4Dp_1 R(1 + Cr_0)]^2 D}{(R - r_0)^2 p'} \qquad (2)$$

where v_0 is the linear streaming velocity of the gas in the nozzle and $C^2 = k^{(1)}p'/D$. Since $k^{(1)}$ occurs in C, it was evaluated by successive approximation.

$k^{(2)}$.—This constant utilizes the same boundary condition as $k^{(1)}$ but with a different model. An average streaming velocity is inserted into the equation of continuity and the solution contains a factor exponential in the coördinate along the streaming axis, with a resultant asymmetric flame shape dependent on the streaming velocity.

$$k^{(2)} = \left\{\left[\frac{\ln(\pi_0 r_0/p_1 R) + \alpha Z}{R - r_0}\right]^2 - \alpha^2\right\}\frac{D}{p'} \qquad (3)$$

where Z is the displacement of the flame center along the flow axis, $\alpha = v/2D$, $R^2 = P^2 + Z^2$ and $\pi_0 = r_0 v_0 p^*/[4D(1 + \beta r_0 + \alpha^2 r_0^2/2)]$; P is the flame height; $\beta^2 = \alpha^2 + k^{(2)}p'/D$: v is the average streaming velocity, obtained by averaging an assumed velocity distribution (initially v_0 and decreasing as an inverse square function of the distance from the flow axis), weighted by the sodium pressure over the flame. Typical values of v were of the order of $0.1v_0$, while Z was of the order of 0.2 to 1.0 cm. Since β contains $k^{(2)}$, the latter was obtained by successive approximation.

$k^{(3)}$.—This constant was evaluated with the same lower boundary condition as for $k^{(1)}$, but utilizes a newly applied boundary condition at the flame edge. Observation of the limiting visible fluorescence pressure of sodium at the flame edge actually represents integration of the intensity over the line of sight by the eye. The edge of the flame is characterized by a value of the integral of the sodium concentration over the line of sight, S, normal to the radius at the flame edge. The value of this limiting quantity of sodium was determined by observing the first appearance of sodium fluores-

(9) C. R. Wilke, *Chem. Eng. Prog.*, **46**, 95 (1950).

(10) H. V. Hartel, M. Polanyi and N. Meer, *Z. physik. Chem.*, **B19**, 139 (1932).

(11) R. J. Cvetanovic and D. J. LeRoy, *J. Chem. Phys.*, **20**, 343 (1953).

(12) E. H. Kennard, "Kinetic Theory of Gases," McGraw-Hill Book Co., Inc., New York, N. Y., 1938, p. 194.

(13) John F. Reed, Thesis, University of Washington, 1953, available on microfilm from University Microfilms, Ann Arbor, Michigan.

(14) D. Morrier, R. Vaucher and P. Wagner, *Helv. Chim. Acta*, **31**, 929 (1948).

(15) A. L. Henne and T. Midgley, *J. Am. Chem. Soc.*, **58**, 882 (1936).

TABLE III

SPECIFIC RATE CONSTANTS FOR REACTION WITH SODIUM[a]

Compound	CH_3Cl	CFH_2Cl	CF_2HCl	CF_3Cl	CF_3Cl
No. of runs	14	11	11	11	3
T, °K.	586	586	586	586	525
Over-all rate constants					
$k^{(0)}$	1.49 (0.08)	1.13 (0.17)	1.24 (0.14)	3.82 (0.29)	1.01 (0.17)
$k^{(1)}$	0.55 (.05)	0.44 (.06)	0.52 (.06)	1.85 (.08)	0.17 (.02)
$k^{(2)}$	0.50 (.04)	0.41 (.06)	0.49 (.05)	1.70 (.07)	0.14 (.02)
$k^{(3)}$	1.26 (.05)	0.98 (.11)	1.19 (.08)	3.46 (.15)	0.97 (.08)
Primary step rate constants					
$k_a^{(0)}$	1.49 (0.08)	1.08 (0.16)	1.03 (0.11)	2.18 (0.17)	
$k_a^{(1)}$	0.55 (.05)	0.42 (.06)	0.43 (.05)	1.06 (.04)	
$k_a^{(2)}$	0.50 (.04)	0.39 (.06)	0.41 (.04)	0.97 (.04)	
$k_a^{(3)}$	1.26 (.05)	0.93 (.10)	0.99 (.07)	1.98 (.09)	

[a] Units are 10^{11} cm.^{3}/mole sec.; standard deviation of average in parentheses.

cence, under the same irradiation intensity used in rate studies, both within and outside the nozzle tube. Within the tube, the concentration is constant along the line of sight bounded by the tube walls. Outside the tube, the sodium concentration varies in space and this variation was calculated on the basis of a radial diffusion and streaming model, the latter contribution being negligible. The results for a number of measurements within and outside the tube showed good agreement and the value of 4.7×10^{-14} mole/cm.^{2} was used in rate calculations. The corresponding values of p_1 were 3.2 to 6.5×10^{-6} mm., depending on reaction vessel age, while the integrated intensity showed much less variation. Using this boundary condition, $k^{(3)}$ was determined from the relation

$$4.7 \times 10^{-14} = \frac{v_0 r_0^2 p^* e^{Cr_0}}{4D(1 + Cr_0)} \int_S \frac{e^{-Cr}}{r} ds \qquad (4)$$

where $C^2 = k^{(3)}p'/D$. A family of plots were made of the above integral *versus* C for various values of the parameter, R, the flame radius which, with the reaction vessel size, determines S. From the appropriate value of the integral to fit equation 4, C was obtained.

For all halides the correction to the rate constant for halide depletion in the flame was found to be low, of the order of 2 to 5%, using the diffusion model[16] treatment of Smith.[17] Instead, the Heller[8] correction modified for nozzle size[3] was employed, in as much as this takes into account the effect of streaming on the halide impoverishment in the flame.

The results are summarized in Table III. The data are too numerous to tabulate.[13] The maximum range of experimental variables employed in any run is as follows: halide pressure in the flame from 0.08 to 0.4 mm.; v_0/D from 4.9 to 24 cm.$^{-1}$; total reaction pressure from 2.5 to 5.5 mm.; flame radius from 1.49 to 1.86 cm. Typical data bearing on a discussion of the experimental models is given in Table IV for CF_3Cl.

Correction of Rate Constants for Radical Reactivities.—In the past, corrections have not been made for the further reaction of halogen-containing radical products which also deplete sodium in the flame. Since reaction of sodium with these radicals is bimolecular (Discussion), the over-all rate of depletion of sodium at any point in the flame, in the case of CF_3Cl, is given by

$$k_a pp_{CF_3Cl} + k_b pp_{CF_2} + k_c pp_{CF_2} + k_d pp_{CF}$$

If the ratio of formation of sodium chloride to sodium fluoride in the flame is c, then the rate of disappearance of sodium due to all reactions is $k_a(1 + c)pp_{CF_3Cl}$, and the over-all rate constant is equal to $(1 + c)k_a$. It will be recalled that the average value of c agreed with the value at any point of the flame within 10%. The value of k_a is obtained by dividing the over-all rate constants in Table III by $(1 + c)$ for the particular chloride.

It is to be noted that irrespective of the model employed for calculation, the order of reactivity among the various halides is the same (the minor discrepancy between CFH_2Cl and CF_2HCl for the Polanyi model actually falls within the limit of experimental error). The reactivity of CF_3Cl is greater than that of CH_3Cl, while CFH_2Cl and CF_2HCl react more slowly.

Activation Energies.—From the specific rate constants at 586°K. of the primary step, $k_a^{(3)}$, activation energies were computed assuming a unit steric factor and a value of $\sigma^2 = 3.5 \times 10^{-15}$ cm.^{2}, and are given in Table V. The difference between the activation energies recorded here and those reported earlier[4] is due to the fact that the latter values were based on $k_a^{(1)}$. The approximate activation energy computed from the temperature dependence of the rate of CF_3Cl between 525 and 586°K., assuming the same product distribution at both temperatures, was 12.7 kcal./mole.

Discussion

Evaluation of Experimental Models.—It is seen from Table III that in all cases $k^{(0)} > k^{(3)} > k^{(1)} > k^{(2)}$, as expected.[3] The values of the first two constants are roughly the same as are the last two, the first pair being about twice the value of the second pair.

The specific rate constants, $k^{(0)}$ and $k^{(1)}$, are related as

$$(k^{(0)})^{1/2} = (k^{(1)})^{1/2} + \delta; \quad \delta = -\frac{(D/p')^{1/2} \ln v_0 r_0/4D}{(R - r_0)} \qquad (5)$$

(16) R. J. Cvetanovic and D. J. LeRoy, *Can. J. Chem.*, **29**, 597 (1951).

(17) F. T. Smith, *J. Chem. Phys.*, **22**, 1605 (1954); *cf.* R. J. Cvetanovic, *Can. J. Chem.*, **34**, 54 (1956).

TABLE IV

EXPERIMENTAL DATA FOR CF_3Cl AT 586°K.

v_0/D, cm.$^{-1}$	p', dynes cm.$^{-2}$	D, cm.^{2} sec.$^{-1}$	Pressure, mm.	Flame radius, cm.	$k^{(0)}$	$k^{(1)}$	$k^{(2)}$	$k^{(3)}$
						10^{11} cm.^{3}/mole sec.		
8.06	158	185	3.01	1.51	5.20	1.66	1.60	3.49
8.93	129	178	3.19	1.54	5.75	1.99	1.89	4.16
13.8	156	108	5.31	1.46	3.12	1.44	1.31	3.02
14.5	273	213	2.53	1.49	3.80	1.88	1.75	3.33
14.6	143	138	4.11	1.52	4.46	2.20	2.00	3.97
16.2	128	176	3.23	1.86	3.62	1.91	1.71	3.68
16.3	145	131	4.35	1.68	3.18	1.69	1.60	3.10
16.9	336	199	2.76	1.70	3.02	1.65	1.46	2.99
17.8	264	193	2.82	1.57	3.14	1.77	1.64	3.06
18.4	352	190	2.85	1.41	3.16	1.81	1.57	2.94
24.2	245	167	3.31	1.48	3.60	2.43	2.14	3.91

TABLE V

ACTIVATION ENERGIES OF PRIMARY REACTIONS AND SOME PHYSICAL PARAMETERS FOR FLUOROMETHYL CHLORIDES

Compound	E, kcal./mole	r_e, Å.	eQq (20°K.)Mc.[a]	eQq (gas)
CH_3Cl	9.8	1.78[b]	68.4	75.13[d]
CFH_2Cl	10.1	1.76[c,d]	67.6	70.46[c]
CF_2HCl	10.0	1.73[d]	70.5	
CF_3Cl	9.2[f]	1.75[b]	77.6	78.05[e]

[a] W. Gordy, J. W. Simmons and A. G. Smith, *Phys. Rev.*, **74**, 243 (1948). [b] L. S. Bartell and L. O. Brockway, *J. Chem. Phys.*, **23**, 1860 (1955). [c] N. Muller, *J. Am. Chem. Soc.*, **75**, 860 (1953). [d] L. O. Brockway, THIS JOURNAL, **41**, 747 (1937). [e] D. K. Coles and R. H. Hughes, *Phys. Rev.*, **76**, 858 (1949). [f] J. W. Hodgins and R. L. Haines, *Can. J. Chem.*, **30**, 473 (1952), report 6.2 kcal.

where δ arises only from the difference in lower boundary conditions. The experimental range of δ was greatest (fourfold) for CF_3Cl at 586°K., and a plot of $(k^{(0)})^{1/2}$ *versus* δ is shown for CF_3Cl in Fig. 1. If $k^{(0)}$ is a physically correct quantity, then it should show only random variation with δ, but if $k^{(1)}$ is more precise, the points should cluster about a line of slope one. It can be seen that the data fit the variation expected on the basis of the model associated with $k^{(1)}$. The slope of the least squares line calculated from the data for each of the halides is 0.9 for CF_3Cl, 0.8 for CF_2HCl, 1.4 for CFH_2Cl and 0.3 for CH_3Cl. Although the calculated slopes vary somewhat due to experimental error, the conclusion may be drawn that there is a positive slope in all cases which is of the order of magnitude predicted from the boundary condition of $k^{(1)}$. The smaller standard deviation of the average of $k^{(1)}$ as opposed to that of $k^{(0)}$ further emphasizes the better fit of the data to $k^{(1)}$.

The improvement in the standard deviation of $k^{(2)}$ over that of $k^{(1)}$ is small enough so that it is felt that the introduction of an average streaming velocity into the equation of continuity has not materially altered the results, even though the model more adequately describes the flame contour and does provide some improvement. This is expected since the asymmetry of the flame was not pronounced, the ratio of the flame height to center displacement from the nozzle being of the order of 2 to 5 in all cases. It may be concluded that within this range of flame asymmetry, there is little need for a velocity model. The effect on halide distribution is, of course, an associated problem.

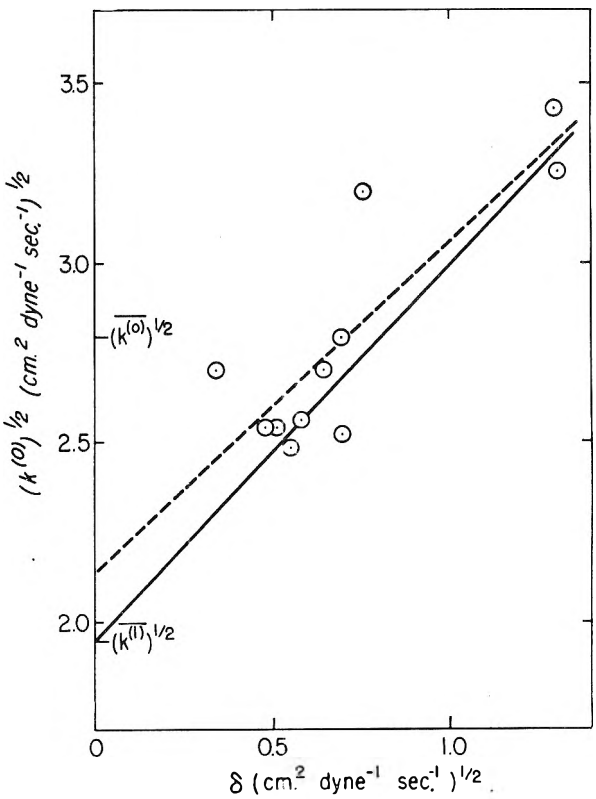

Fig. 1.—Relation between $k^{(0)1/2}$ and δ; solid line is theoretical fit with slope unity, broken line is least squares fit, for reaction of CF_3Cl.

Adoption of the new upper boundary condition yields improved precision in the rate constant, $k^{(3)}$, and also readjusts the magnitude of the rate constant to a greater value. The fortuitous approach toward the value of $k^{(0)}$ stems from the partially compensating errors in both boundary conditions of the model for the latter quantity. The exact extent of the variation of $k^{(0)}$ from $k^{(3)}$ will depend on experimental conditions.

The values of $k^{(3)}$ are not only the most precise, but are here considered to be conceptually the most nearly correct derived from the models examined. The earlier comparison of $k^{(0)}$ and $k^{(1)}$ above is still valid, however, since it may be shown that use of the incorrect upper boundary condition in both models tends to be mutually compensating.

Range of v_0/D.—The range of v_0/D employed extends beyond that recommended by Heller.[7]

Justification for extending the lower limit has been discussed previously and a correction for the sodium depletion, θ, due to back diffusion of halide, derived[3]

$$\theta = \frac{2kp_0'/D'}{(v_0/D')^2[1 + (1 + 4kp^*D'/v_0^2)^{1/2}]} \qquad (6)$$

where p_0' is the pressure of halide at the nozzle and D' is the diffusion coefficient of halide into the gas mixture. Calculations of θ at the lowest v_0/D values employed were made for the various halides and found to be negligible, *e.g.*, for CH_3Cl at v_0/D = 4.9 cm.$^{-1}$, the lowest value used, the sodium depletion was less than 1%. From the data for CF_3Cl at 525°K., it is estimated that a value of v_0/D of less than 2.0 cm.$^{-1}$ would result in sodium depletion of only 2%; the depletion is significantly greater at lower values of v_0/D but, in such cases, a correction may be made readily from the calculated depletion, θ.

Heller's upper limit of v_0/D = 12 cm.$^{-1}$ was exceeded in this work; however, the rate constants of the improved models suffered no pronounced drift to lower values (Table IV). The smaller size of the nozzle employed here, relative to that used by Heller, extends the allowed v_0/D range without onset of turbulence.

Warhurst,[18] working with a nozzle of unspecified size, found no drift in the rate constants for bromobenzene when values of v_0/D up to 19 were used in the modified life period method, the calculations of which are more akin to those of $k^{(3)}$ than of $k^{(0)}$. It is concluded that Heller's upper limit may be exceeded under suitable circumstances.

Mechanism of the Over-all Reaction.—It is clear from previous work[19] that the reaction of sodium atoms with an alkyl halide involves removal of the halide atom leaving a free alkyl radical. In the present study, some radicals produced contained fluorine atoms capable of further reaction with sodium, as evidenced by NaF found in the products. From a consideration of the reaction with CF_3Cl, a general mechanism may be deduced for all the compounds studied.

Primary Reaction.—

$$Na + CF_3Cl \longrightarrow NaCl + CF_3 \qquad (a)$$

This reaction is evidenced by the preponderance of NaCl in the salts collected (Table II), by the similarity in rates and activation energies found for CF_3Cl and CH_3Cl (abstraction of F by Na from a fluorinated methane has an appreciably higher activation energy than 10 kcal.[19]), and is physically reasonable since the C–Cl bond is the weakest. In addition, no chlorofluoroethane dimer products (see below) were detected, but only C_2F_6.

Secondary Reactions.—The secondary reactions involve the subsequent reactions of CF_3 radicals and secondary products and the further reactions of sodium. These reactions are

$$Na + CF_3 \longrightarrow NaF + CF_2 \qquad (b)$$
$$Na + CF_2 \longrightarrow NaF + CF \qquad (c)$$
$$Na + CF \longrightarrow NaF + C \qquad (d)$$
$$2CF_3 \longrightarrow C_2F_6 \qquad (e)$$
$$2CF_2 \longrightarrow C_2F_4 \qquad (f)$$

Reactions (b), (c) and (d) are evidenced by the NaF and carbon found in the products. The formation of CF_2 by reaction (b) leads by recombination (f) to C_2F_4, found in the products in significant amount. Any reactions of CF other than (d) were not detected or recognized.

It is now well known that recombination of CF_3 radicals (e) occurs at these pressures without any concomitant disproportionation.[20]

Abstraction of F by CF_3 is not favored under these conditions.[21] Also, pertinent to reactions of the less fluorinated chloride, hydrogen abstraction by fluorinated radicals is not expected, as known specific rates of hydrogen abstraction by both methyl and trifluoromethyl radicals[22] are much slower than processes occurring in the flames studied here.

This mechanism adequately accounts for all the products of the reaction. Trace amounts of higher compounds, such as C_4F_8 in the reaction of CF_3Cl, could arise from polymerization of unsaturated products. The extent of each of the reactions in the above scheme, x_i, was calculated on the basis of one mole of sodium consumed and is given in Table VI. For the reaction of CF_2HCl with sodium, since the extent of fluorine abstraction compared to chlorine abstraction is low (0.20), and since the ratio of reactions (c) to (b) are low for CF_3Cl, it was arbitrarily assumed that the extent of reaction (c), stripping of the last fluorine of the radical by sodium, may be taken to be zero; sufficient information was not available to determine the ratio of reaction (c) to (b). Thus the entry in Table VI for this reaction implies an assumed value. A dash in the table indicates that no reaction exists.

TABLE VI

EXTENT OF REACTION, MOLES OF PRODUCT/MOLE OF SODIUM CONSUMED

Reaction	x_a	x_b	x_c	x_d	x_e	x_f
CF_3Cl	0.57	0.28	0.072	0.072	0.14	0.11
CF_2HCl	.83	.17	(0)	...	.33	.085
CFH_2Cl	.95	.048	...	...	.45	.024

Specific Rate Constants of Secondary Reactions.—Consider first the case of CF_3Cl. The specific rate constant of the reaction of sodium with CF_3 may be written

$$k_b = x_b b_0 \Big/ \int pp_{CF_3} 4\pi r^2 dr \qquad (7)$$

Since all the quantities in equation 7 are known except p_{CF_3}, the evaluation of k_b rests on the approximation necessary to specify the nature of the variation of p_{CF_3} in the flame, and its magnitude. Two such approximations will now be discussed.

The first approximation is based on the observation that the F^-/Cl^- ratio in the salts was relatively constant throughout the flame. Since NaF is produced mainly by reaction of Na with CF_3, the rates of reactions (a) and (b) are assumed to be in con-

(18) E. Warhurst, *Trans. Faraday Soc.*, **35**, 674 (1939).

(19) E. Warhurst, *Quart. Revs.*, **5**, 44 (1951).

(20) J. R. Dacey, *Disc. Faraday Soc.*, **14**, 84 (1953); P. B. Ayscough and H. J. Emeleus, *J. Chem. Soc.*, 3381 (1954); G. O. Pritchard, H. O. Pritchard and A. F. Trotman-Dickenson, *Chemistry and Industry*, 564 (1955); J. R. Dacey and D. M. Young, *J. Chem. Phys.*, **23**, 1302 (1955).

(21) R. A. Sieger and J. G. Calvert, *J. Am. Chem. Soc.*, **76**, 5197 (1954).

(22) P. B. Ayscough and E. W. R. Steacie, *Can. J. Chem.*, **34**, 103 (1956).

stant ratio. To this approximation, p_{CF_3} may be taken constant throughout the flame at an average value, p_{CF_3}, whose magnitude may be obtained from the extent of the recombination reaction (e)

$$x_e b_o = k_e \int p^2_{CF_3} 4\pi r^2 \, dr \qquad (8)$$

The value of k_e has been reported recently.[23] All other quantities in equation 8 are known. The result obtained at 586°K. is $k_b = 2 \times 10^{14}$ cm.^{3}/mole sec., which should be divided by a factor of 3 for reaction per C–F bond. On assuming a unit steric factor and using a collision number of 5×10^{14} cm.^{3}/mole sec., common to sodium atom reactions, an activation energy, E_b, of 2.4 kcal./mole is obtained.

A second approximation, which embraces the first, leads to a less definite but more rigorous result by use of the Schwarz inequality.[24] Application to the functions involved, p and p_{CF_3}, integrated over the flame yields

$$\int p^2_{CF_3} r^2 \, dr \cdot \int p^2 r^2 \, dr \geq (\int p p_{CF_3} r^2 \, dr)^2 \qquad (9)$$

By inserting the experimental value of the integral given in equation 8, and evaluating the known sodium pressure function, it is found that $k_b \gg 7 \times 10^{13}$ cm.^{3}/mole sec. Treatment of this quantity as before yields an upper limit to the activation energy of 3.5 kcal./mole.

By application of the Schwarz inequality in a similar manner to the other radical reactions with sodium, estimates of the lower limits of the rate constants per C–F bond may be obtained. The results are given in Table VII in terms of the radical recombination rate constant. This latter quantity is known only for CF_3. A good assumption is that all the recombination constants of the fluorine substituted methyl radicals are approximately 2×10^{13} cm.^{3}/mole sec., in line with the values for CF_3 and CH_3.[23,25] It must be concluded that these radical reactions with sodium occur with small activation energy. Furthermore, it appears that CF_3 is more reactive than CF_2H or CFH_2 per C–F bond.

TABLE VII

LOWER LIMITS OF SPECIFIC RATE CONSTANTS PER C–F BOND IN CM.^{3}/MOLE SEC. FOR RADICAL REACTION WITH SODIUM (586°K.)

Radical	CF_3	CF_2H	CFH_2	CF_2
k_b	$(2.5 \times 10^{13} k_e)^{1/2}$	$(7 \times 10^{11} k_e)^{1/2}$	$(1.8 \times 10^{12} k_e)^{1/2}$	$(5 \times 10^{12} k_f)^{1/2}$

Activation Energies and D(C–Cl).—The differences in observed activation energies for the primary reactions of sodium atoms can be related to differences in bond dissociation energies of the C–Cl bond in these molecules. Consideration of the factors affecting an estimate of these differences is made most easily on the basis of the model suggested by previous workers.[26] Ogg and Polanyi[26a] pointed out there should be parallel changes in the activation energy and bond dissociation energy of the bond reacting with sodium, namely, $\Delta E = \alpha' \Delta D$ ($\alpha' < 1$). This relation is valid when the differences in bond dissociation energy arise mainly from differences in radical stabilities and when the ionic repulsion curves of R and X^-Na^+ are of the same shape. If this relation is applied to the compounds studied in this work with α' set at its conventional value[27] of 0.28, the following result is obtained: the C–Cl bond in CF_3Cl is weaker by 2 kcal./mole than that in CH_3Cl ($D(CH_3$–$Cl) = 81.2$[28]), and the bonds in CF_2HCl and CFH_2Cl are stronger by 0.6 and 1.0 kcal./mole, respectively. The relative magnitude of these experimental activation energies and bond dissociation energies correlate very reasonably with the variation of C–Cl bond distances in this series (Table V).

Actually, a number of complicating factors enter in the application of the simple relation between ΔE and ΔD to the compounds studied in this work, and estimation of their magnitude and direction has been made by construction of the appropriate potential energy curves on the basis of the Polanyi–Evans model.[26] First, the polarizability, a, of the various methyl radicals are not the same but increase with increasing fluorine substitution. This effect is greatest for CF_3 relative to CH_3. There is no reliable value of a for CF_3, but it is calculated that this factor would decrease the activation energy for CF_3Cl by an amount of roughly 1.4 kcal./mole from that for CH_3Cl.

A second complicating factor is the fact that the equilibrium internuclear C–Cl bond distances of these compounds differ. This causes a shift of the initial and final state energy curves on a cut along the C–Cl bond distance axis through the transition state of the potential energy surface representing the reaction. A decrease in the C–Cl equilibrium internuclear separation results in an increase in activation energy, for this factor alone. This effect would raise the activation energy for CF_2HCl by 2 kcal./mole over that of CH_3Cl, and by 1.2 kcal./mole for CF_3Cl.

A third and smaller effect is the decrease in the observed activation energy resulting from resonance in the transition state, which increases with the number of fluorine atoms in the molecule. The magnitude of this factor was roughly estimated from the treatment which has been given by Warhurst,[19] in conjunction with some of our preliminary results on the reaction of sodium with CF_3Br and CH_3Br, the bond dissociation energies of which are known[29] to differ by only 3 kcal. The greatest decrease in activation energy to be expected is for CF_3Cl and here this effect was estimated at 0.5 kcal./mole.

(23) P. B. Ayscough, *J. Chem. Phys.*, **24**, 944 (1956).

(24) H. Margenau and G. M. Murphy, "The Mathematics of Physics and Chemistry," D. Van Nostrand Co., Inc., New York, N. Y., 1943, p. 130.

(25) A. Shepp, *J. Chem. Phys.*, **24**, 939 (1956); E. W. R. Steacie, "Atomic and Free Radical Reactions," Vol. II, 2nd Ed., Reinhold Publ. Corp., New York, N. Y., 1954.

(26) (a) R. A. Ogg and M. Polanyi, *Trans. Faraday Soc.*, **31**, 1375 (1935); (b) M. G. Evans and E. Warhurst, *ibid.*, **35**, 593 (1939); (c) however, compare also R. P. Smith and H. Eyring, *J. Am. Chem. Soc.*, **74**, 229 (1952); R. P. Smith, Am. Chem. Soc. Meeting, Buffalo, 1952.

(27) E. T. Butler and M. Polanyi, *Trans. Faraday Soc.*, **39**, 19 (1943); A. G. Evans and H. Walker, *ibid.*, **40**, 384 (1944).

(28) C. F. Mortimer, H. O. Pritchard and A. H. Skinner, *ibid.*, **48**, 220 (1952).

(29) A. H. Sehon and M. Szwarc *Proc. Roy. Soc.* (*London*), **A209** 110 (1951).

These various factors operate as a whole in the direction of cancellation, and together with the small spread in experimental E values leads to the conclusion that there is little variation of D(C–Cl) in the series studied, and that based on $D(CH_3–Cl)$ = 81.2 kcal./mole, a reasonable estimate is $D(CF_3–Cl)$ = 80–81 kcal./mole, while $D(CF_2H–Cl)$ and $D(CFH_2–Cl)$ = 81–82 kcal./mole.

Our data are too sparse to justify any detailed attempt to correlate the bond dissociation energies measured here with the various factors and theories relating to valence binding. It may be remarked that in addition to the qualitative agreement of the observed activation energies, and probable relative order of the dissociation energies, with the variation of the parameter r_{C-Cl} in this series, a similar correspondence may be found with the quadrupole coupling constant for Cl^{35} in these molecules (Table V), of which the relative gas phase values are the more unequivocal. The explanation of this relation may involve the decreasing importance of structures such as $F^-\overset{H}{\underset{H}{C}}=Cl^+$ with increasing fluorine substitution. The variation of eqQ is such, in any case, as to show that inductive factors alone do not determine its magnitude (see reference 26c). However, the nature of this binding, particularly in mixed polyhalogenated methanes, is notoriously complex.

It is possible to give a qualitatively consistent explanation of the relative magnitudes of carbon–halogen bond dissociation energies of mixed polyhalogenated methanes, based on a competition between two competing factors along the lines first pointed out by Scanlan and Warhurst[30]: namely, that the greater is n, in a molecule of the type, $CH_{4-n}X_n$, the greater the ionic resonance energy and stabilization, the effect of which is also to reduce the M–X bond length; on the other hand, increasing substitution of H by X or another atom, Y, increases the non-bonded repulsion between the X atom and the other substituents of the central C atom, the more so, the larger the van der Waals radius of Y.[31] Such an explanation has been applied by Szwarc to the analogous bromides.[29]

Some Derived Thermochemical Quantities for Fluorocarbons.—In an earlier note[4] we gave the following thermochemical quantities, $\Delta H_f(CF_3)$ = −120.5, $D(CF_3–F)$ = 116.5 and $D(CF_3–CF_3)$ = 62, all in kcal./mole at 25°. From $D(CF_3–Cl)$ taken from this study as 80.5 kcal./mole, the above quantities, when recalculated on the same basis as before, become −119.5, 117.5 and 64 kcal./mole, respectively. Although some question has been raised recently[32] regarding the possible inexactitude of $D(F_2)$ = 38 kcal./mole, this value has been retained in the above calculations. Very recently, Lossing, *et al.*,[33] from electron impact studies have reported $\Delta H_f(CF_3)$ = −117 kcal./mole, whil Pritchard, *et al.*,[34] have estimated this quantity a −119 kcal./mole, both quantities being in satis factory agreement with our values. Correspond ence for $D(CF_3–F)$ and $D(CF_3–CF_3)$ follows also.

Some limits may also be set for other related quantities. From the activation energy for the reaction of sodium with CF_3, which has a maximum value of 3.5 kcal./mole, a limit on the heat of formation of CF_2 may be obtained. Using the value of $\Delta H_f(CF_3)$ = −119.5 kcal., ΔH_f(Na) = 26.0 kcal.,[35] and ΔH_f(NaF) = −72 kcal.[35] values of $\Delta H_f(CF_2) \leqslant -18$ kcal./mole and $D(F_2C–F) \leqslant$ 120.5 kcal./mole are obtained. There is an indication that the second bond in CF_4 is weaker than the first, since the data of sodium atom-alkyl halide reactions, in general, show that a reaction characterized by a low activation energy of <3.5 kcal. is not endothermic, *i.e.*, $D(CF_2–F) \leqslant D$(NaF) = 117 kcal./mole, and $\Delta H_f(CF_2) \leqslant -21.5$ kcal./mole. Similar limits may be set for D(CF–F), $D(H_2C–F)$ and D(HFC–F). The above values, when coupled with L(C) = 170 kcal., give D(C–F) ⩾ 112 kcal./ mole. (*cf.* reference 42).

Recently, heats of formation of C_2F_4 have been determined. The values for C_2F_4 are −151, −152 and −162 kcal./mole.[36,37] Using $\Delta H_f(CF_2)$ obtained above, the double bond strength in C_2F_4 is calculated to be <108–119 kcal./mole in agreement with the 112 kcal./mole limit deduced by Atkinson from kinetic studies.[38]

From the value $\Delta H_f(CF_2CH_2)$ = −77.5 kcal./

TABLE VIII

BOND DISSOCIATION ENERGIES (KCAL./MOLE) OF F AND H ANALOGS

	X = H	X = F
$D(CX_3–H)$	102.5[40]	103[33]
		102[40]
$D(CX_3–F)$	107[41]	118[a]
	108[39]	121[33]
		143[42]
$D(CX_3–Cl)$	81[28]	80.5[a]
$D(CX_3–Br)$	67[29]	64[29]
$D(CX_3–I)$	55[43]	49[42]
		57[33]
$D(CX_3–CX_3)$	85[25]	64[a]
		69[33]
		65[34]
		115[42]

[a] This work.

(30) J. Scanlan and E. Warhurst, *Trans. Faraday Soc.*, **45**, 1000 (1949).

(31) D. F. Heath and J. W. Linnett, *J. Chem. Phys.*, **18**, 147 (1950).

(32) K. L. Wray and D. F. Horrig, *ibid.*, **24**, 1271 (1956).

(33) J. B. Farmer, I. H. S. Henderson, F. P. Lossing and D. G. H. Marsden, *ibid.*, **24**, 348 (1956).

(34) G. O. Pritchard, H. O. Pritchard, H. I. Schiff and A. F. Trotman-Dickenson, *Chemistry and Industry*, 896 (1955).

(35) Rossini, *et al.*, "Selected Values of Chemical Thermodynamic Properties," Circular 500 of the N. B. S., Washington, D. C., 1952.

(36) H. V. Wartenberg, *Z. anorg. Chem.*, **278**, 326 (1955); H. C. Duus, *Ind. Eng. Chem.*, **47**, 1445 (1955).

(37) C. A. Neugebauer and J. L. Margrave, THIS JOURNAL, **60**, 1318 (1956).

(38) B. Atkinson, *J. Chem. Soc.*, 2684 (1952).

(39) V. H. Dibeler and R. M. Reese, *J. Research Natl. Bur. Standards*, **54**, 127 (1955).

(40) G. O. Pritchard, H. O. Pritchard, H. I. Schiff and A. F. Trotman-Dickenson, *Trans. Faraday Soc.*, **52**, 849 (1956).

(41) F. P. Lossing, K. U. Ingold and I. H. S. Henderson, *J. Chem. Phys.*, **22**, 1489 (1954).

(42) V. H. Dibeler, R. M. Reese and F. L. Mohler, *J. Research Natl. Bur. Standards*, **59**, 113 (1956).

(43) A. S. Carson, J. Hartley and H. A. Skinner, *Proc. Roy. Soc. (London)*, **A195**, 500 (1959).

mole,[37] and reasonable limits on both $\Delta H_f(CH_2)$ and $\Delta H_f(CF_2)$ as currently known, it appears that the double bond in CF_2CH_2 is stronger than that in C_2F_4.

One further point is worth mentioning. For some time, the presence of three fluorine atoms on a carbon atom has been generally thought to confer extra stability on the fourth bond. There is an appreciable amount of experimental evidence that this notion has no general validity (Table VIII).

Acknowledgment.—We thank Professor G. H. Cady for his generous coöperation in this research, which was supported by the office of Naval Research.

COMBINATION OF PYROPHOSPHATE WITH ACTOMYOSIN STUDIED BY THE CHANGE OF LIGHT SCATTERING[1]

By Yuji Tonomura, Fumi Morita and Koichi Yagi

From the Research Institute for Catalysis, and from the Chemistry Department, Faculty of Science, Hokkaido University, Sapporo, Japan

Received November 16, 1956

The decrease in the scattered intensity of actomyosin solution caused by pyrophosphate was measured quantitatively in the presence of Mg^{++} and Ca^{++}, over a wide range of concentration of pyrophosphate and these cations. From the analyses of the results, it was concluded that there are two kinds of sites for the binding of pyrophosphate with actomyosin, one is for the direct binding of pyrophosphate with protein and the other is for the mediated binding by the cation absorbed on the protein. On the basis of the analyses a mechanism of the overoptimal inhibition of actomyosin-ATPase was proposed.

Since Szent-Györgyi[2] showed that various physical changes can be evoked in actomyosin as a result of the interaction with ATP, this reaction has been studied by many investigators. It has thus been established that this phenomenon is the fundamental mechanism of muscular contraction.[2-4] But the mechanism of this reaction is much complicated, mainly owing to the breakdown of ATP by actomyosin-ATPase.[5,6] PP evokes the same physical change in actomyosin solution as ATP, but it is not decomposed by actomyosin. Therefore, it appears likely that the mechanism of the reaction of PP will be elucidated more readily than that of ATP.

The drop of the viscosity of actomyosin solution by the addition of PP was qualitatively studied by Mommaerts.[7] Recently, Matsumiya, *et al.*,[8] have observed that the reduced viscosity caused by PP recovered to the original value when the added PP was decomposed by the subsequent addition of yeast pyrophosphatase, thus showing that the actomyosin–PP system is a reversible one. A quantitative study on the actomyosin–PP system already has been performed by Tonomura, *et al.*,[9] but it was under limited experimental conditions. In this report, the effect of PP on the turbidity of actomyosin in 0.6 *M* KCl solution was described in various ionic media, and the results were analyzed in greater detail, in the expectation that these analyses might throw some light on the nature of action of polyphosphates on actomyosin.

Experimental

Materials.—Myosin B (natural actomyosin) was prepared from fresh skeletal muscle of rabbit as described in an earlier paper.[9] Pyrophosphate was recrystallized twice from a commercial product. Other materials used were commercial samples.

Procedures.—Relative intensity of the light scattered at 90° by myosin B solution was measured by means of an apparatus described in an earlier paper.[8] The protein solution, containing 0.22–0.28 mg protein/ml., 0.01 mole of tris-(hydroxymethyl)-aminomethane-maleate, 0.6 mole of KCl and a measured amount of a divalent cation, was filtered three times through a filter paper. Ten ml. of this protein solution was carefully pipetted into a cell and the intensity of the scattered light was controlled by an iris stop and a slit so that the reading of the μ-ammeter became 95 μa. Two-tenths ml. of PP was added into myosin B solution, with gentle stirring of the solution. About 10 minutes after the addition of PP the reduced intensity reached a constant value. This reading was used for computation of the grade of the light scattering drop (see below).

Amounts of Mg and Ca contained in myosin B were determined by the following procedure. A measured amount of the stock solution of myosin B preparation, which contained 0.6 mole of KCl besides some amounts of Mg and Ca, was ashed. Quantitative separation of cations contained in the ash was effected by chromatographic analysis on a column (2.3 cm. diameter, 23 cm. high) of colloidal Dowex 50 according to Sutton and Almy.[10] The spectrophotometric determination of Mg^{++} and Ca^{++}, using the dye Eriochrome Black T, in the basic solution, was performed with a Shimazu photospectrometer.[11]

The protein was determined by the Kjeldahl method. *p*H was measured with a Beckman type G *p*H meter.

Results

Contents of Magnesium and Calcium.—The contents of magnesium and calcium contaminated in the preparation of myosin B was about 3.5 *M* and below 1 *M* per 10^5 g. of protein, respectively. As the content of magnesium intrinsically bound on the protein is about 1 *M* per 10^5 g. of protein,[12] the

(1) The abbreviations ATP for adenosine triphosphate and PP for inorganic pyrophosphate will be used.

(2) A. Szent-Györgyi, "Chemistry of Muscular Contraction," 1st ed., Academic Press, New York, N. Y., 1947.

(3) A. Szent-Györgyi, "Chemistry of Muscular Contraction," 2nd ed., Academic Press, New York, N. Y., 1951.

(4) H. H. Weber and H. Portzehl, *Prog. Biophys. Phys. Biochem.*, **4**, 60 (1954).

(5) Y. Tonomura, *J. Research Inst. for Catalysis (Hokkaido Univ.)*, **4**, 87 (1956).

(6) J. J. Blum, *Arch. Biochem. Biophys.*, **55**, 486 (1955).

(7) W. F. H. M. Mommaerts, *J. Gen. Physiol.*, **31**, 361 (1948).

(8) H. Matsumiya, F. Morita, S. Kitagawa, K. Yagi and Y. Tonomura, *J. Biochem. (Japan)*, in press.

(9) Y. Tonomura, S. Watanabe and K. Yagi, *ibid.*, **40**, 27 (1953).

(10) W. J. L. Sutton and E. F. Almy, *Dairy Sci.*, **36**, 1248 (1953).

(11) A. Young, T. S. Sweet and B. B. Backer, *Anal. Chem.*, **27**, 356 (1955).

(12) E. T. Friess, M. F. Morales and W. J. Bowen, *Arch. Biochem. Biophys.*, **53**, 311 (1954).

content of magnesium contaminated in our preparation is about 2.5 M per 10^5 g. of protein. Therefore the reaction solution was contaminated with about 0.005 mM Mg and below 0.002 mM Ca, because the concentration of myosin B in the solution was about 0.2 mg./ml. The intensity of the scattered light of myosin B solution decreased to a certain degree by the addition of PP even when neither Mg^{++} nor Ca^{++} was added. In some cases, this may be partly due to the contamination of these cations, because, as described below, they enhance powerfully the effect of PP.

Effect of Magnesium Ion.—As in the case of the change of viscosity studied by Mommaerts,[7] the decrease of the scattered intensity caused by PP was enhanced by Mg^{++}. Let us denote the grade of the drop (Δ) as[13]

$$\Delta = \frac{I_0 - I_c}{I_0 - I_\infty}$$

where I_0 and I_c represent the scattered intensities before and after the addition of a certain amount of PP, respectively. I_∞ stands for the intensity with a sufficiently large amount of PP.

As shown in Fig. 1, the relation between the grade of the drop and the concentration of PP was dependent remarkably upon the concentration of Mg^{++}. When the concentration of Mg^{++} was low enough, the relation was given as a dissociation curve of the first order

$$\Delta = \frac{1}{1 + K/[PP]} \text{ or } \Delta = \frac{1}{2} + \frac{1}{2}\tanh\left(2.303\,\frac{1}{2}\log\frac{[PP]}{K}\right)$$

where [PP] is the concentration of PP and K is a constant appropriate to [PP] that effects 50% drop. When the concentration of Mg^{++} was considerably high, the relation Δ-[PP] was described as a dissociation curve of the second order

$$\Delta = \frac{1}{1 + K^2/[PP]^2} \text{ or } \Delta = \frac{1}{2} - \frac{1}{2}\tanh\left(2.303\log\frac{[PP]}{K}\right)$$

In this case, the K value decreased with increasing the concentration of Mg^{++}. When the concentration of Mg^{++} was high enough, the relation Δ-[PP] became a mixed curve of the first and the second order, *e.g.*, over a range of high concentrations of PP the relation was the first order but over a range of low concentrations the relation was the second order.

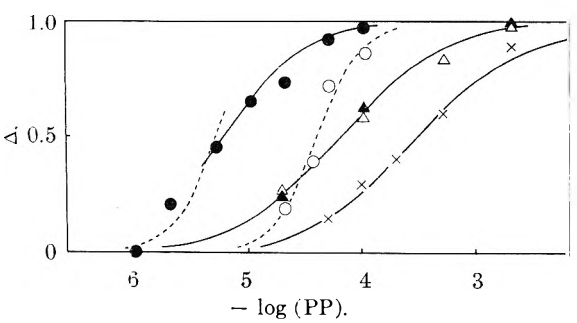

Fig. 1.—Relation between the grade of the drop of light scattering (Δ) and the concentration of PP. 0.6 M of KCl, 5–6°, about 0.2 mg. protein/ml. The solid and the dotted lines correspond, respectively, to $\Delta = 1/2 + 1/2 \tanh (2.303\,(1/2)\log [PP]/K)$ and $\Delta = 1/2 - 1/2 \tanh (2.303 \log [PP]/K)$. ●, protein no. 1, 10 m$M$ of Mg^{++}, pH 7.5. ○, protein no. 2, 10 mM of Mg^{++}, pH 6.7 ×, protein no. 2, 0.1 mM Mg^{++}, pH 6.7. ▲, protein no. 2, 0.1 mM of Ca^{++}, pH 7.5. △, protein no. 2, 0.01 mM of Ca^{++}, pH 7.5.

Values of K observed for three preparations of myosin B are summarized in Table I. It is apparent from the table that the relation Δ-[PP] was somewhat different from one preparation to another. For example, at 5–6° and at pH 7.5, this relation for no. 2 appeared always to be the second order over a full range of concentration of Mg^{++} and the values of K^2 were proportional to the concentration of Mg^{++}, but for no. 1 and 3 the relation of this sort was valid only in a limited range of Mg^{++} concentration.

Influence of pH, Temperature, etc., on the Myosin B–Magnesium Ion–Pyrophosphate System.—The effect of PP was greater at pH 7.5 than at pH 6.7. One of the causes of the pH effect might be the dissociation of PP, $PP^{-3} \rightleftarrows PP^{-4} + H^+$. The effect of PP was somewhat greater at low temperature than at room temperature, *e.g.*, for the preparation no. 2, at pH 7.5 and in the presence of 10 mM of Mg^{++}, the values of K at 5–6° and 16.5° were, respectively, 1.6×10^{-5} and 3.2×10^{-5} M. This result accords with other workers' qualitative finding concerning viscosimetry.[7,14]

The relation between Δ and [PP] was found to depend scarcely on the concentration of the protein. For example, at both concentrations of 0.22 and 2.0 mg. protein/ml., and at 16.5°, pH 7.5 and in 10 mM of Mg^{++}, the relation Δ-[PP] for the sample no. 2 obeyed the dissociation curve of the second order, and its K-value was $2.5–3.2 \times 10^{-5}$ M. The relation was also seemingly independent of the extraction time of myosin B.

Effect of Calcium Ion.—Not only Mg^{++} but also Ca^{++} enhances the effect of PP. However the relation $\Delta - [PP]$ in the presence of Ca^{++} was remarkably different from the one in the presence of Mg^{++}, *i.e.*, it followed the dissociation curve of the first order independently of the concentration of this cation (Fig. 1). At high temperature the value of K was somewhat dependent on the concentration of Ca^{++}, but at low temperature it was independent of its concentration. The enhancing effect of Ca^{++} was largely hindered at higher temperatures, namely, at pH 7.5 and in 0.1 mM of Ca^{++}, K of the preparation no. 2 increased about 10 times when the temperature was raised from 5 to 17° (see Table I). For these reasons at low temperatures and in low concentrations of the divalent ion, Ca^{++} was even more effective than Mg^{++}.

Discussion

According to Szent-Györgyi's view, which has been supported by many experiments, polyphosphate brings about actomyosin to dissociate into myosin and actin.[3,15] But Blum and Morales[16] suggested by means of the light-scattering method, using Zimm's extrapolation method, that ATP causes an elongation of myosin B and leaves the

(13) A small correction due to dilution is necessary.

(14) F. B. Straub, *Studies Inst. Med. Chem., Univ. Szeged*, **3**, 38 (1948).

(15) A. Weber, *Biochim. Biophys. Acta*, **19**, 345 (1956).

(16) J. J. Blum and M. F. Morales, *Arch. Biochem. Biophys.*, **43**, 208 (1953).

TABLE I

APPARENT DISSOCIATION CONSTANTS FOR THE MYOSIN B–PYROPHOSPHATE SYSTEM

Protein no.	Temp., °C.	pH	Divalent cation added, mmoles/l.		Protein concn., mg./ml.	Order[a]	pK[b]
1	5–6	7.5	10	Mg	0.25	2 (?)[c] → 1	5.25 → 5.2
1	5–6	7.5	1	Mg	.25	2 → 1	5.1 → 5.1
1	5–6	7.5	0.1	Mg	.25	2	4.7
1	5–6	7.5	0.02	Mg	.25	2	4.5
1	5–6	7.5	0.015	Mg	.25	2 (?)	4.35
1	5–6	7.5	0.01	Mg	.25	1	3.6
2	5–6	7.5	10	Mg	0.22	2	4.8
2	5–6	7.5	0.1	Mg	.22	2	3.9
2	5–6	7.5	0.01	Mg	.22	2	3.4
2	16.5	7.5	10	Mg	.22	2	4.5
2	16.5	7.5	10	Mg	2.0	2	4.4
2	5–6	6.7	10	Mg	0.22	2	4.45
2	5–6	6.7	0.1	Mg	0.22	1	3.6
3	6	7.5	10	Mg	0.22	2	4.7
3	6	7.5	0.1	Mg	.22	2	4.45
3	6	7.5	0.01	Mg	.22	1	3.9
2	5	7.5	0.1	Ca	0.22	1	4.2
2	5	7.5	0.01	Ca	.22	1	4.2
2	17	7.5	0.1	Ca	.22	1	3.2
2	17	7.5	0.01	Ca	.22		2.7
3	5	7.5	0.1	Ca	0.22	1	3.7
3	5	7.5	0.01	Ca	0.22	1	3.7

[a] The arrow indicates the transition of the order at higher concentrations of PP. [b] Minus logarithm of K (mole/liter). [c] When [PP] is smaller than $10^{-5.5}$ M, $[PP]_f$ may be decreased by its absorption on the protein, because concentration of the absorbing sites is probably about $2 \times 0.25/2 \times 10^{-5} = 2.5 \times 10^{-6}$ M.[9] The apparently second order observed in presence of 10 mM Mg^{++} and low [PP] may be attributable to this situation.

molecular weight unchanged.[17] Therefore it seems to be unsettled whether polyphosphate dissociates myosin B into myosin and actin or leaves the molecular weight unchanged. In either case the value of K obtained from the relation Δ-[PP] may be treated as the "apparent dissociation constant" (see Appendix), because the myosin B–PP system is a reversible one[8] and K, as described above, is almost independent of the protein concentration used. As listed in Table I, the relation Δ-[PP] was extremely affected by divalent cations and, moreover, even in the same ionic medium the value of K changed slightly but clearly from one preparation to another. Similar fluctuation with the "apparent dissociation constant" has also been recognized on the myosin B–nucleotide triphosphate system.[6] The structural basis of this fluctuation is not clear, except that the length of the extraction time of myosin B scarcely influences on the value of K.[18] The variation would not be due to the heterogeneity of actomyosin in each preparation, because, by the ultracentrifugal[16] and the electrophoretical[19] studies, it has been shown that only one major macromolecular component is contained in myosin B prepared according to the method almost identical with ours. Since the qualitative properties of the reaction are common to all the preparations, as described above, it may be assumed, in spite of these difficulties, that the fundamental mechanism of the reaction of PP and divalent cations with myosin B is the same in either preparation but the "true dissociation constant" of each step of the reaction varies from one preparation to the other.

Considering that the change of the light scattering can be evoked even in the presence of sufficiently low concentration of divalent cations and that in the presence of appropriate quantity of Mg^{++} the relation Δ-[PP] is given by a dissociation curve of the second order but in the presence of Ca^{++} the relation is always given by the one of the first order, the mechanism may be proposed[20]

$$M + PP \underset{K_1}{\overset{PP}{\rightleftarrows}} M^* \qquad (1)$$

$$M + Me \underset{K_2}{\rightleftarrows} M.Me \qquad (2)$$

$$M.Me + PP \underset{K_3}{\rightleftarrows} M.Me.PP \qquad (3)$$

(17) Recently, J. Gergely (*J. Biol. Chem.*, **220**, 917 (1956)) showed by means of the Zimm method that the weight-average molecular weights of his actomyosin preparations became smaller by the addition of ATP. However, whether this was due to the complete dissociation of actomyosin into myosin and actin, as he postulated, is not clear. If the dissociation is to take place, the average molecular weight of "actin" in the dissociated state must be calculated from his data and the known molecular weight of myosin. Thus, the present authors have found that the molecular weight of the assumed actin thus calculated is almost equal or sometimes even larger than that of actomyosin. Therefore, it may be concluded that under certain experimental conditions ATP disaggregates actomyosin to a small extent but it does not dissociate actomyosin completely into myosin and actin.

(18) Whether the first-order relation can be observed in the presence of low concentration of added Mg^{++} or not may depend upon the content of contaminated Mg^{++} in each preparation.

(19) M. L. R. Harkness and A. Wassermann, *J. Chem. Soc.*, 1344 (1954).

(20) The simplest mechanism might be as follows: Me + PP ⇄ Me.PP, M + Me ⇄ M.Me, M.Me + PP ⇄ M*.Me.PP. But this could not account for the above facts. Also a mechanism, where the actual reagent was the chelate compound PP–Me–PP, was found to conflict with the data.

$$\mathrm{M.Me} + \mathrm{PP} \underset{K_4}{\overset{\mathrm{PP}}{\rightleftarrows}} \mathrm{M^*.Me} \qquad (4)$$

$$\mathrm{M^*.Me} + \mathrm{PP} \underset{K_5}{\overset{\mathrm{PP}}{\rightleftarrows}} \mathrm{M^*.Me.PP} \qquad (5)$$

$$\mathrm{Me} + \mathrm{PP} \underset{K_6}{\rightleftarrows} \mathrm{Me.PP} \qquad (6)$$

where M and M* are the original and the physically changed myosin B, respectively, and Me is a divalent cation and K_i is the dissociation constant of each step. The exact value of K_6 is not known but in 0.6 M of KCl it might be within the range between 10^{-3} and 10^{-2} M.[21]

The feature of this mechanism is that there are two different sites for the binding of PP to myosin B, one is the site on the protein molecule,[22] and the other the divalent cation absorbed on the protein.[23] If we assume that the physical state of the protein is violently changed by the combination of PP with the former site and that the light scattering due to the species $\mathrm{M^*}^{\mathrm{PP}}$ is practically identical to the one due to the species $\mathrm{M^*.Me}^{\mathrm{PP}}$ and $\mathrm{M^*.Me.PP}^{\mathrm{PP}}$, the relation between Δ and [PP] is given by the formula

$$\Delta = \frac{\left[\mathrm{M^*}^{\mathrm{PP}}\right] + \left[\mathrm{M^*.Me}^{\mathrm{PP}}\right] + \left[\mathrm{M^*.Me.PP}^{\mathrm{PP}}\right]}{[\Sigma \mathrm{M}]} = \frac{1 + \frac{K_5}{[\mathrm{PP}]_f} + \frac{K_2K_4K_6}{K_1[\mathrm{Me}][\mathrm{PP}]_f}}{1 + \frac{K_5}{[\mathrm{PP}]_f} + \frac{K_2K_4K_6}{K_1[\mathrm{Me}][\mathrm{PP}]_f} + \frac{K_4K_5}{K_3[\mathrm{PP}]_f} + \frac{K_4K_6}{[\mathrm{PP}]_f^2}\left(1 + \frac{K_2}{[\mathrm{Me}]}\right)} \qquad (7)$$

and

$$[\mathrm{PP}] = [\mathrm{PP}]_f \left(1 + \frac{[\mathrm{Me}]}{K_6}\right) \qquad (8)$$

where $[\mathrm{PP}]_f$ and [PP] are the concentrations of free and total PP, respectively.[24]

(1) In the case of sufficiently high [Me]

(i) if $K_3 >> K_4$ and $K_5 >> [\mathrm{PP}]_f$

$$\Delta \sim \frac{1}{1 + \frac{K}{[\mathrm{PP}]}}, \quad K = K_4\left(1 + \frac{[\mathrm{Me}]}{K_6}\right)\left(1 + \frac{K_2}{[\mathrm{Me}]}\right) \qquad (9)^{25}$$

and (ii) if $K_5 << [\mathrm{PP}]_f$

$$\Delta \sim \frac{1}{1 + \frac{K^2}{[\mathrm{PP}]^2}}, \quad K^2 = K_4K_6\left(1 + \frac{[\mathrm{Me}]}{K_6}\right)^2\left(1 + \frac{K_2}{[\mathrm{Me}]}\right) \qquad (9^*)^{25}$$

(2) On the other hand, when [Me] is smaller than 10^{-3} M, then

$$[\mathrm{PP}]_f \sim [\mathrm{PP}]$$

(i) When $[\mathrm{Me}] \geq K_2K_4/K_1$, and $[\mathrm{PP}] >> K_5$, $K_2K_3/[\mathrm{Me}]$

$$\Delta \sim \frac{1}{1 + \frac{K}{[\mathrm{PP}]}}, \quad K = \frac{K_4K_5}{K_3} \qquad (10)$$

(ii) when $[\mathrm{Me}] \geq K_2K_4/K_1$ and $K_5\,(1 + K_2/[\mathrm{Me}]) >> [\mathrm{PP}] >> K_5$

$$\Delta \sim \frac{1}{1 + \frac{K^2}{[\mathrm{PP}]^2}}, \quad K^2 = K_4K_5(1 + K_2/[\mathrm{Me}]) \qquad (11)$$

and (iii) when $[\mathrm{Me}] << K_2$, $[\mathrm{PP}] << K_2K_3/[\mathrm{Me}]$, and $1 << K_5/[\mathrm{PP}] + (K_2K_4K_5/K_1\,[\mathrm{Me}][\mathrm{PP}])$

$$\Delta \sim \frac{1}{1 + \frac{K}{[\mathrm{PP}]}}, \quad K = \frac{K_2K_4}{[\mathrm{Me}]}\left(1 + \frac{K_2K_1}{K_1[\mathrm{Me}]}\right) \qquad (12)$$

These deductions fit well with the data observed in the presence of Mg^{++}, that is, when [Me] is sufficiently high, the relation follows a dissociation curve of the first order and when [Me] is relatively high, it obeys the one of the second order, and when [Me] is low, again the first order.

If, in the presence of Ca^{++} smaller than 10^{-3} M, K_3 and K_5 are very large, Δ reduces to

$$\Delta \sim \frac{1}{1 + \frac{K}{[\mathrm{PP}]}}, \quad K = \frac{K_4(1 + K_2/[\mathrm{Me}])}{(1 + K_2K_4/K_1[\mathrm{Me}])} \qquad (13)$$

and when K_2 is sufficiently small

$$\Delta \sim \frac{1}{1 + \frac{K}{[\mathrm{PP}]}}, \quad K = K_4 \qquad (14)$$

that is, K becomes independent of [Me]. These deductions are also consistent with the experimental data.

Because of the rather complicated mechanism the valuation of K_i could not be carried out. But, if the above mechanism is admitted, some interesting conclusions can be deduced. That is, K_2 for Ca^{++} is much less than for Mg^{++} (for example, at 5–6° and at *p*H 7.5 K_2 for Ca^{++} of the preparation no. 2 is less than 10^{-5} M (*cf.* eq. 13 and 14), while K_2 for Mg^{++} must be larger than 10^{-3} M (*cf.* eq. 11)). On the other hand, the binding of PP with Mg^{++} adsorbed to the protein is fairly strong but the binding with Ca^{++} is weak and almost imperceptible (for example, K_5 for Mg^{++} and Ca^{++} of the preparation no. 2 should be sufficiently smaller than $10^{-4.5}$ M (*cf.* eq. 7 and 11) and larger than 10^{-3} M (*cf.* eq. 7 and 13), respectively).

In the case of the actomyosin–ATP system, the relation Δ-[ATP] follows the dissociation curve of the first order, regardless of whether divalent cations are present or not.[5,6] Considering the similarity of the chemical structure of ATP to that of PP, it might be possible to expect that the former

(21) J. R. Van Wazer and D. A. Campanella, *J. Am. Chem. Soc.*, **72**, 655 (1950).

(22) This site may be Mg^{++} fixed intrinsically on the protein,[12] because K. Uchida (personal communication) has recently observed that in certain ionic media PP activates myosin-ATPase just as EDTA does.

(23) These sites should be separated with each other, because if they are situated closely with each other two PP molecules cannot bind due to the strong repulsive electrostatic interaction.

(24) Concentration of free Mg^{++} is practically equal to the one of total Mg^{++}, because in almost all experiments $[\mathrm{PP}] > 10^{-3}\ M \leq K_6$.

(25) Eq. 9 indicates that when $[Mg^{++}]$ becomes to be larger than K_6 and K_2, the K value increases with increasing $[Mg^{++}]$. But this conclusion did not hold good, especially for the preparation no. 2. This might be due to the situation that the step 4 or 5 could be promoted by exceedingly high $[Mg^{++}]$.

could also combine, though weakly, with Mg^{++} absorbed to the protein but not with the bound Ca^{++}. The inhibitory effect of ATP at higher concentrations on the ATPase was reported by Hasselbach[26] and Perry[27] who showed that Mg^{++} activated ATPase is more readily subjected to this inhibition than Ca^{++} activated ATPase, and there is a close relation between the concentration of Mg^{++} and the concentration at which ATP becomes inhibitory. If we presume that the overoptimal inhibition is caused by the chelation of ATP with a divalent cation bound to actomyosin, these phenomena could be interpreted as follows: the reaction $M.Mg + ATP \rightleftarrows M.Mg.ATP$ may proceed to the right only when the concentration of Mg^{++} is appropriate (at rather higher concentrations of Mg^{++} the reaction is inhibited by the chelation of ATP with Mg^{++} and, on the other hand, at lower concentration of Mg^{++} it is accompanied by a diminution in M.Mg), but the reaction $M.Ca + ATP \rightleftarrows M.Ca.ATP$ cannot proceed to the right. It seems also possible that the various kinases[26-30] act as inhibitors of ATPase by increasing the "effective concentration" of ATP near Mg^{++} absorbed on the protein.[31] As is well known ATPase and the physical change of actomyosin caused by ATP are simultaneously affected by many substances such as cations,[5] –SH inhibitors[32,33] and EDTA.[34] So these suggestions may be worthy of consideration.

It has been shown by Portzehl[35] and Bozler[36] that PP has a softening action on glycerol-extracted muscle fibers and that this softening action is closely related with the action of PP on the viscosity of actomyosin solution. Bozler[36] and Bendall[28,37] found that PP induces relaxation of fibers contracted by ATP, but its mechanism is not yet quite clear, although several suggestions have been proposed. In the present paper the binding of PP with actomyosin has been followed by the change in light scattering. Here, we may expect that existence of such bindings by which the scattered intensity, at low concentration of actomyosin, does not change substantially may participate in the softening and relaxing action by decreasing the intermolecular cohesive force between actomyosin molecules. So, it seems to be premature to discuss detailed mechanisms. However, the reaction mechanism could be much more clarified by comparing the result presented here with that of the equilibrium dialysis method, which the present authors are now in a position to perform.

Acknowledgments.—Our thanks are due to Prof. J. Horiuti (Research Inst. for Catalysis), Prof. H. Tamiya (Tokyo Univ.) and Prof. N. Takasugi (Chemistry Dept.) for their support; to Prof. T. Kwan (Research Inst. for Catalysis) for his valuable advice. This study has been aided in part by a grand-in-aid for Fundamental Scientific Research of the Ministry of Education given to the Research Group on the "Chemistry of Muscular Contraction."

Appendix

(1) When PP dissociates actomyosin (AM) into myosin (M) and actin (A)

$$AM + PP \underset{K}{\rightleftarrows} M.PP + A$$

provided that the second virial coefficients can be neglected, then

$$\frac{I_0}{kC_p} = M_{am}P_{am}$$

$$\frac{I_\infty}{kC_p} = M_mP_mX_m + M_aP_aX_a$$

$$\frac{I_c}{kC_p} = \frac{1}{1 + \frac{K}{[PP]}}(M_mP_mX_m + M_aP_aX_a) + \frac{\frac{K}{[PP]}}{1 + \frac{K}{[PP]}} M_{am}P_{am}$$

where P_i is the shape function for the molecule i of molecular weight M_i and weight fraction X_i, C_p is the weight concentration of protein, k is a constant,[38] and the subscripts am, a and m represent actomyosin, actin and myosin, respectively.

(2) On the other hand, if PP changes the shape of actomyosin but leaves the molecular weight unchanged

$$AM + PP \underset{K}{\rightleftarrows} AM^*.PP$$

Then, as described by Blum[5]

$$\frac{I_0}{kC_p} = M_{am}P_{am}$$

$$\frac{I_\infty}{kC_p} = M_{am}P^*_{am}$$

$$\frac{I_c}{kC_p} = M_{am}\left(\frac{1}{1 + \frac{K}{[PP]}} P^*_{am} + \frac{\frac{K}{[PP]}}{1 + \frac{K}{[PP]}} P_{am}\right)$$

Therefore, in either case

$$\frac{I_0 - I_c}{I_0 - I_\infty} = \frac{1}{1 + \frac{K}{[PP]}}$$

(26) W. Hasselbach, *Biochim. Biophys. Acta*, **20**, 355 (1956).
(27) S. V. Perry, 36me Congr. Intern. Biochim., Rapports, Liége, 1955, p. 159.
(28) J. R. Bendall, *Proc. Roy. Soc.* (*London*), **B142**, 409 (1954).
(29) L. Lorand, *Nature*, **172**, 118 (1953).
(30) L. Lorand and C. Moos, *Federation Proc.*, **15**, No. 1, 393 (1956).
(31) W. Hasselbach and H. H. Weber, *Biochim. Biophys. Acta*, **11**, 160 (1953).
(32) K. Bailey and S. V. Perry, *ibid.*, **1**, 506 (1947).
(33) G. Kuschinsky and F. Turba, *ibid.* **6**, 426 (1951).
(34) Y. Tonomura, H. Matsumiya and S. Kitagawa, *ibid.*, in press.
(35) H. Portzehl, *Z. Naturforsch.*, **7b**, 1 (1952).
(36) E. Bozler, *J. Gen. Physiol.*, **38**, 53 (1954).
(37) J. R. Bendall, *Nature*, **172**, 586 (1953).
(38) J. J. Blum and M. F. Morales, *J. Chem. Phys.*, **20**, 1822 (1952).

THE HEATS OF ADSORPTION OF HELIUM AND NEON ON GRAPHITIZED CARBON BLACK[1]

BY J. GREYSON AND J. G. ASTON

Contribution No 88 from the Cryogenic Laboratory of the College of Chemistry and Physics, The Pennsylvania State University, University Park, State College, Pennsylvania

Received November 24, 1956

The partial molal heats of adsorption of helium at 17.3°K. on graphitized carbon have been measured and also calculated from isotherms interpolated to 17.0 and 20.3° from measured data. The partial molal heats of adsorption of neon at 29°K. have likewise been measured and also calculated from isotherms interpolated to 28 and 30°K. The data are in reasonable agreement.

Introduction

Recent investigations of the adsorption of gases on certain samples of highly graphitized carbon black have revealed characteristics of energetic uniformity for adsorption.[2-4] Systematic studies of the heats of adsorption for the systems argon on Spheron-6 (2700°) and krypton on P-33 (2700°) have been published by Beebe and co-workers.[5]

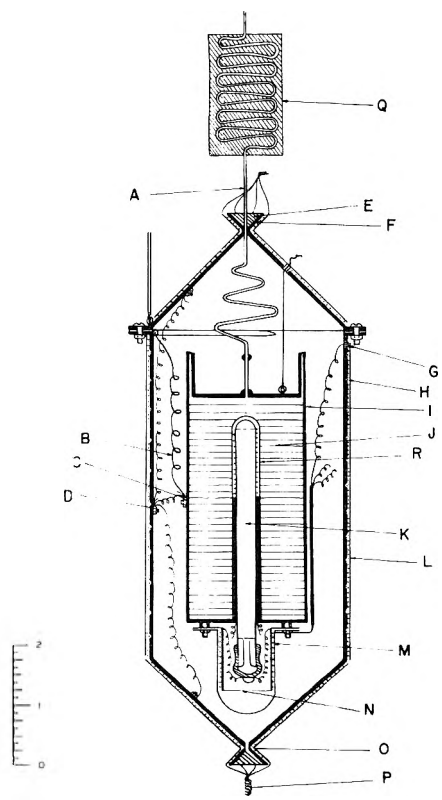

Fig. 1.—Calorimeter, shield and heat exchanger assembly (dimensions approximate): A, calorimeter filling tube; B, difference couple wires; C, calorimeter couple junction; D, shield couple junctions; E, soft solder thermal contact; F, upper cone for wire wrap; G holes for wire outlet; H, adiabatic shield; I calorimeter; J platinum separators; K, resistance thermometer; L, aluminum cover; M, radiation cap; N, copper cylinder around which supply wires are wrapped for thermal contact; O, lower cone for wire wrap; P, wire bundle; Q, heat exchanger.

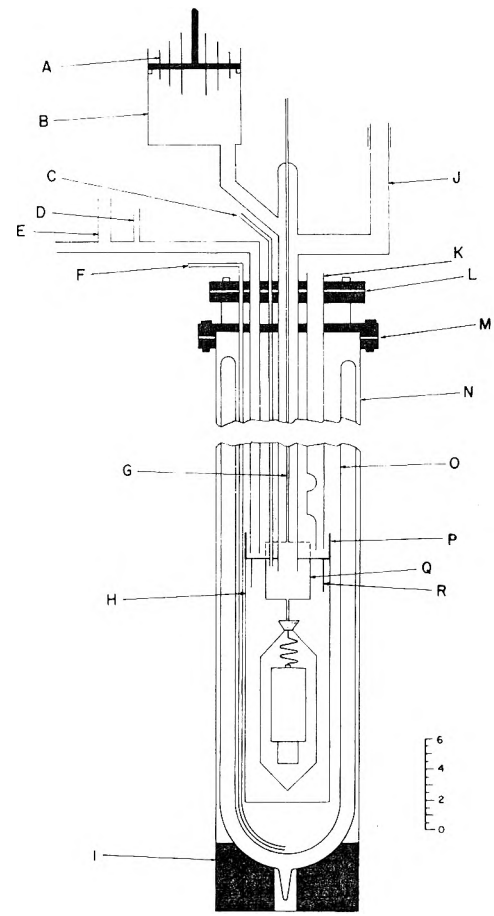

Fig. 2.—Cryostat assembly (dimensions approximate): A, the electrical terminals; B, sealed take-out cup for supply wires; C, thermocouple take-out tube; D, to "U" tube manometer; E, to high speed vacuum pump; F, siphon tube; G, calorimeter filling tube; H, brass can; I, Balsa block; J, to high vacuum system; K, refrigerant filling tube (to accommodate vacuum jacketed transfer tube); L, gasket; M, gasket; N, Dewar case; O, outer Dewar; P, re-entrant cup (can be filled with water while soldering); Q, heat exchanger; R, ring.

For a more detailed interpretation of the characteristics of adsorption on these carbon black surfaces, it is necessary that data be available for the lower boiling members of the rare gas series. This paper, therefore, presents the results of an investigation of the heats of adsorption and isotherms of helium and neon on P-33 (2700°). A paper pre-

(1) This research was carried out under Contract DA-36-061-ORD-509 of the Office of Ordnance Research.

(2) M. H. Polley, W. R. Smith and W. D. Schaeffer, THIS JOURNAL, **57**, 469 (1953).

(3) W. D. Schaeffer, W. R. Smith and M. H. Polley, *Ind. Eng. Chem.*, **45**, 1721 (1953).

(4) J. H. Singleton and G. D. Halsey, THIS JOURNAL, **58**, 1011 (1954).

(5) (a) C. H. Amberg, W. B. Spencer and R. A. Beebe, *Can. J. Chem.*, **33**, 305 (1955); (b) R. A. Beebe and D. M. Young, THIS JOURNAL, **58**, 93 (1954).

senting an interpretation of all the available data for adsorption on these carbon blacks follows.

Experimental

1. **Apparatus and Method.**—For the measurement of the heats of adsorption, an adiabatic calorimeter was constructed based primarily on the designs of this Laboratory.[6] Incorporated into the system was a small heat exchanger whose purpose was to ascertain and control the temperature of the gas entering the calorimeter. Temperatures were measured with a platinum resistance thermometer and pressures with a wide bore mercury manometer in conjunction with a Gaertner cathetometer.

A scale drawing of the adiabatic shield, calorimeter and heat exchanger assembly, with explanatory legend, is shown in Fig. 1. The apparatus was entirely rebuilt using the calorimeter vessel (I) and the platinum resistance thermometer (K) which were previously used by Morrison and Szasz.[7] The details of construction involved improvements which have been described elsewhere.[6] The resistance thermometer was calibrated by Morrison and Szasz, and their temperature scale was used. A determination of its ice point resistance was made previous to installing it into the equipment. The change was insignificant. The method of mounting and general method of operation of the calorimeter and shield is evident from Fig. 2 which is a scale drawing of the entire cryostat assembly with legend. The heat exchanger serves to bring the gas to the temperature of the calorimeter. Such a heat exchanger was not included in the apparatus of Morrison and Szasz. It is made of a copper cylinder in which 12 feet of $^1/_8''$ copper tubing are coiled and held securely by a lead cast which was poured into the cylinder. At the top and bottom of the exchanger are two difference couples which measure the temperature difference between the exchanger and the calorimeter. The efficiency of the exchanger was determined while doing the experimental measurements. No deflection of its lower difference couple was noted with the input of a gas increment. The gas therefore is known to have entered the calorimeter chamber at the temperature of the vessel.

To obtain the heat of adsorption, the temperature rise in the calorimeter was measured after adding gas under adiabatic conditions.

2. **Materials.**—The adsorbent consisted of 58 grams of a Fine Thermal carbon black, P-33, which had been graphitized at 2700°. This was obtained from the Godfrey L. Cabot Company through the courtesy of Dr. W. R. Smith. The calorimeter vessel was vibrated for several days after introduction of the adsorbent to make the packing as uniform as possible. A nitrogen surface area determination using the standard B.E.T. procedure yielded a monolayer capacity of 2.76 cc. S.T.P. per gram. The adsorbent was out-gassed at 350° until the residual pressure in the calorimeter was less than 1×10^{-6} mm. Thereafter, the calorimeter was evacuated before each run at room temperature to the same pressure.

The neon was a reagent grade from a cylinder supplied by the Air Reduction Corporation. A mass spectrometric analysis supplied with the cylinder showed less than 0.01 mole % of helium and no other impurity. The helium was that supplied by the U. S. Naval Lakehurst Air Station and contained less than 0.01 mole per cent. impurity as determined by thermal conductivity. Both gases were passed through a trap packed with activated charcoal and cooled to liquid nitrogen temperatures before their entry into the calorimeter chamber.

3. **Calculations.**—The equations used for calculating the heat of adsorption were those derived by Kington and Aston[8] and are

$$\frac{q_{st}}{22414} = (C_{cal} + C_{Pg} + C_{Ns})\frac{\Delta T}{\Delta V} - V_{cal}\frac{\Delta P}{\Delta V} \quad (1)$$

where

T = temperature
P = pressure
ΔV = volume *adsorbed* in cc. S.T.P.
C_{cal} = heat capacity of the calorimeter plus the adsorbent
C_{Pg} = heat capacity of the gas in the calorimeter free space
C_{Ns} = heat capacity of the adsorbed gas
V_{cal} = volume of the calorimeter free space
q_{st} = partial molar heat of adsorption

and

$$C_{tot} = \frac{\Delta Q}{\Delta T} = (C_{cal} + C_{Pg} + C_{Ns}) - \frac{q_{st}\,\Delta V}{22414\,\Delta T} - V_{cal}\frac{\Delta P}{\Delta T} \quad (2)$$

where Q is the energy input in a heat capacity measurement. Since q_{st} appears in both equations, its final value is established by making both heat capacity and heat of adsorption measurements for a given point and using both equations in a series of successive approximations.

A variety of pressure, temperature and coverage values were available from the heat of adsorption and heat capacity measurements. The initial and final temperatures, respectively, rarely deviated more than several tenths of a

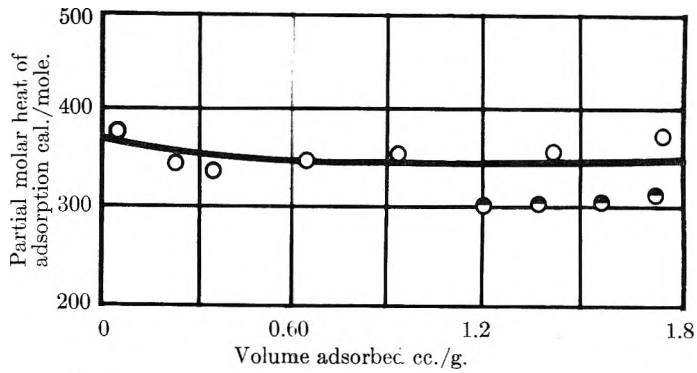

Fig. 3.—Partial molar heats of adsorption of helium on P-33 (2700°) at 17.3°K: ○, calorimetric; ◓, isosteric.

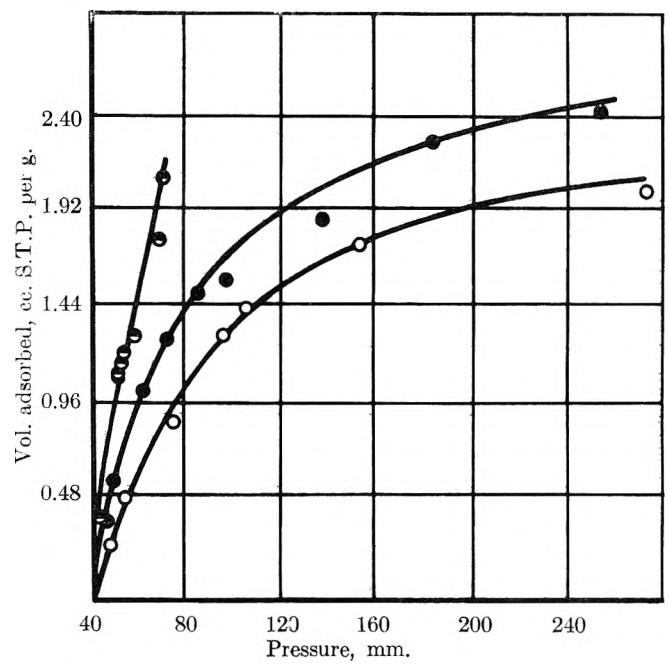

Fig. 4.—Isotherms for helium adsorbed on P-33 (2700°): ○, 20.3°K.; ●, 19.0°K.; ◓, 17.0°K.

(6) J. G. Aston, J. L. Wood and T. P. Zolki, *J. Am. Chem. Soc.*, **75**, 6202 (1953).

(7) J. H. Morrison and G. J. Szasz, *J. Chem. Phys.*, **16**, 280 (1948).

(8) G. L. Kington and J. G. Aston, *J. Am. Chem. Soc.*, **73**, 1929 (1951).

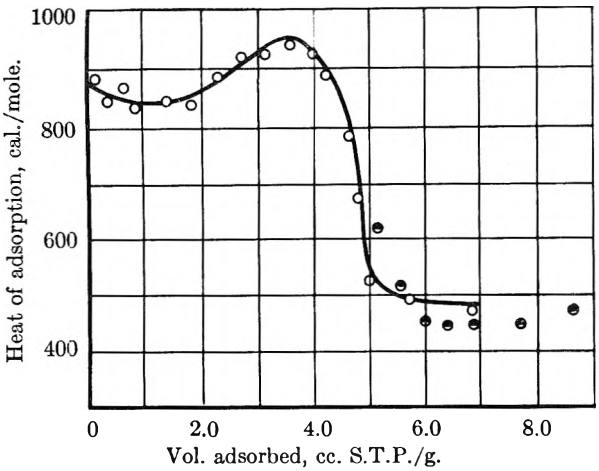

Fig. 5.—Partial molar heats of adsorption of neon on P-33 (2700°) at 29° K.: O, calorimetric; ◓, isosteric.

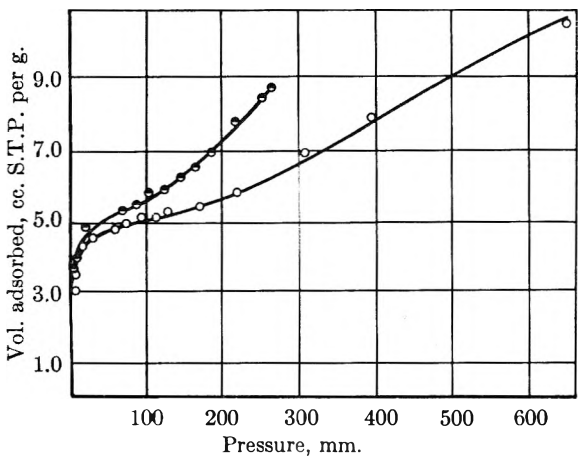

Fig. 6.—Isotherms of neon adsorbed on P-33 (2700°): O, 30°K.; ◓, 28°K.

degree from a mean value. Thus isotherms could be constructed at the mean initial and final temperatures, respectively. The integrated form of the Clapeyron equation

$$\ln P_2 - \ln P_1 = -\frac{q_{st}}{R}\left(\frac{1}{T_2} - \frac{1}{T_1}\right) \qquad (3)$$

was used to correct for deviation of the temperatures from the mean initial or final temperatures. These isotherms were then used to calculate values of the heat of adsorption from the Clapeyron equation for comparison with the measured values.

Results and Discussion

1. The System Helium Plus P-33 (2700°).—Calorimetric heats are recorded in Table I. Figure 3 is a graph showing the partial molar heats of adsorption measured calorimetrically at 17.3° and the calculated isosteric heats from the 19 and 20.3° isotherms. Isotherms constructed from pressure-coverage data are plotted in Fig. 4.

The estimated precision of the measured heats is ±20 cal. where the compression correction is small. The point shown at the highest coverage is probably in error. Its compression correction is about 26% of its value as compared to 10% or less for the other points. It is noteworthy that the heat of adsorption curve is essentially flat. A very slight downward trend is shown at low coverages. Here the values of the heats are most reliable, having low heat of compression corrections so that the effect is certainly real.

TABLE I

PARTIAL MOLAR HEATS OF ADSORPTION OF HELIUM ON P-33 (2700°) AT 17.3°K.

Coverage, cc. S.T.P. per g.	q_{st}, cal./mole	Coverage, cc. S.T.P. per g.	q_{st}, cal./mole
1.740	379	.079	377
1.421	354	1.897[a]	346
0.912	350	1.724[a]	312
.6624	346	1.552[a]	301
.390	336	1.379[a]	304
.252	341	1.207[a]	300

[a] Calculated from 19 and 20.3°K. isotherms.

The calculated isosteric heats deviate from the measured values by about 13%. This deviation and the obvious scatter in the isotherms is attributed to difficulty in making the measurements since, under these conditions, a warm drift of the calorimeter was difficult to avoid. While there was no difficulty in correcting for heat leak, the drift made the pressure uncertain.

The theoretical interpretation of these data together with those which follow for neon is discussed in the following paper.

2. The System Neon Plus P-33 (2700°).—The values of the measured heats of adsorption of neon are listed in Table II and plotted in Fig. 5. Isotherms at 28 and 30° are shown in Fig. 6. The calculated isosteric heats are shown for comparison in Fig. 5.

TABLE II

PARTIAL MOLAR HEATS OF ADSORPTION OF NEON ON P-33 (2700°) at 29°K.

Coverage, cc. S.T.P. per g.	q_{st}, cal./mole	Coverage, cc. S.T.P. per g.	q_{st}, cal./mole
0.136	878	4.591	790
.407	847	4.784	672
.640	862	4.983	574
.990	830	5.786	492
1.457	836	5.021	522
1.895	838	6.891	474
2.352	880	5.172[a]	623
2.779	929	5.603[a]	519
3.207	928	6.034[a]	448
3.660	944	6.465[a]	445
4.012	924	6.896[a]	445
4.276	897	7.758[a]	456
		8.620[a]	473

[a] Calculated from isotherms.

The heat curve, like that of helium, tends downward initially and then rises to a maximum, falling rapidly toward the value of the heat of liquefaction of bulk neon. The estimated error in these measurements is ±10–15 cal. per mole with compression corrections no greater than 20%. It is to be noted that the calculated heats are in fair agreement (about 4–6%) with the calorimetric values.

The isotherms have their knee at 4.65 S.T.P. per gram and are concave upward in shape, the 28° curve being more so than the 30° curve.

Adiabatic conditions were maintained throughout the experimental runs and provided for better

pressure data for isotherm construction than in the case of the helium data. This is plain from the curves and the agreement between the measured heats and those calculated from the isotherms.

Acknowledgments.—The contribution of Mr. L. F. Schultz in making the liquid hydrogen and in the assembly of the apparatus was invaluable. Dr. Donald M. Nace and Dr. Richard N. Selby gave continued assistance in the operation of the adiabatic controls.

THEORY OF HEATS OF ADSORPTION ON A UNIFORM SURFACE. EFFECT OF LATERAL INTERACTION AND GRAIN BOUNDARIES[1]

BY J. G. ASTON AND J. GREYSON

Contribution No. 90 from the Cryogenic Laboratory of the College of Chemistry and Physics, The Pennsylvania State University, University Park, State College, Pennsylvania

Received November 24, 1956

The use of a model whereby the adsorbent surface is composed of edge sites and flat sites, the former being twice the energy of the latter, shows that the effect of edge sites on the surface is too small to be seen with any great precision. The graphitized carbon black surface, therefore, appears to be essentially uniform for adsorption. The observed lateral interaction energies of neon, argon and krypton on graphite indicate patchwise adsorption with each patch under compression.

1. Introduction.—Experimental investigations of adsorption on a uniform surface have been greatly facilitated by the preparation of samples of essentially uniform graphitized carbon black of relatively high surface area.[2,3] Heats of adsorption of argon and krypton on these blacks have been studied by Beebe and co-workers.[4] Heats of adsorption of helium and neon have been obtained in this Laboratory.[5]

This paper presents an interpretation of the heats of adsorption for the series of gases on P-33 (2700°), a partially graphitized carbon black, which is applicable to other uniform surfaces.

2. Heats of Adsorption of Helium and Neon on P-33 (2700°).—The adsorbent was P-33 carbon black which had been partially graphitized by heat treatment at 2700°. Figures 3 and 5 of the previous paper are curves showing the partial molar heats of adsorption of helium and neon on P-33 (2700°) as measured ordinates with the coverage as abscissa. The partial molar heats refer to the change

$$X(\text{gas}) + \text{graphite} \longrightarrow X(\text{on graphite}, \theta = x)$$

This quantity frequently has been loosely called the "differential heat of adsorption."

It is to be noted that the helium curve is essentially parallel to the abscissa except at low coverages. A similar downsweep at low coverages is present in the neon curve also. The rise in heat of adsorption as the monolayer value of the adsorbent is approached in the neon data is in agreement with the data of Beebe and co-workers[4] for argon and krypton and indicates lateral interaction in the adsorbed film.

3. The Low Coverage Heats.—It has been pointed out[3] that one would not expect a partially graphitized carbon black to appear energetically uniform since the characteristics are so strongly dependent upon surface topology. In particular, the effect of high energy edge sites for adsorption should play an important part in the values of the heat of adsorption.

Using the procedure of Aston, Tykodi and Steele[6] it is possible to calculate approximately the heats of adsorption of helium and neon on this surface at low coverages for comparison with the experimental data. The equations derived by these authors are

$$\widetilde{\Delta H} = \frac{1}{\theta}\sum_i \theta_i g_i(\epsilon_i + RT) \qquad (1)$$

$$\theta = \Sigma g_i \left(1 + \frac{f(T)e^{-\epsilon_i/kT}}{P}\right)^{-1} \qquad (2)$$

$$f(T) = \frac{(2\pi mkT)^{3/2}kT}{h^3} \qquad (3)$$

$$q_{st} = \widetilde{\Delta H} + \theta\frac{\partial\widetilde{\Delta H}}{\partial\theta} \qquad (4)$$

where ϵ_i is the energy of the i-th site, $\widetilde{\Delta H}$ is the integral molar heat of adsorption, θ_i is the fraction of the i-th sites covered, and q_{st} is the partial molar heat of adsorption. The value of g_i (a normalized distribution function which is the fraction of the i-th type sites) can be picked if it is assumed that the adsorbent has just two kinds of sites, one kind that of a flat surface, and the other kind on either side of the boundary of the crystallites with double the energy of the flat sites. If every crystallite is considered to have double energy sites around its surface perimeter and single energy sites across its flat surface, then the ratio of edge sites to flat surface sites is simply the ratio of the perimeter of the crystallite to exposed surface area. The average crystallite size as determined by X-ray diffraction[3] is about 200 Å. Thus, the maximum fraction of edge sites is 2% of the total number of adsorption sites in any particle of the carbon.

Choosing the value of ϵ_1 as equal to the energy of adsorption given by the flat part of the heat of adsorption curve and ϵ_2 equal to $2\epsilon_1$, one can then calculate the effect of the edge sites at low cover-

(1) This research was carried out under Contract DA-36-061-ORD-509 of the Office of Ordnance Research.

(2) M. H. Polley, W. R. Smith and W. D. Schaeffer, THIS JOURNAL, **57**, 469 (1953).

(3) W. D. Schaeffer, W. R. Smith and M. H. Polley, *Ind. Eng. Chem.*, **45**, 1721 (1943).

(4) (a) C. H. Amberg, W. B. Spencer and R. A. Beebe, *Can. J. Chem.*, **33**, 305 (1955); (b) R. A. Beebe and D. M. Young, THIS JOURNAL, **58**, 93 (1954).

(5) J. Greyson and J. G. Aston, *ibid.*, **61**, 610 (1957).

(6) J. G. Aston, R. J. Tykodi and W. A. Steele, *ibid.*, **59**, 1053 (1955).

ages. It is easily seen from Fig. 1, which is an expanded plot of the low coverage experimental heats (solid curve) compared to those calculated (dotted curve), that edge effects approximated even as an outside limit are small. It is interesting that the break in the calculated heats occurs just beyond the x value of the first experimental point. If the value of ϵ_2 was chosen as $1.5\epsilon_1$ rather than $2\epsilon_1$, the calculated curve would be essentially the same in shape but would be lower in energy at zero coverage. Thus the integral heat would have a lower value.

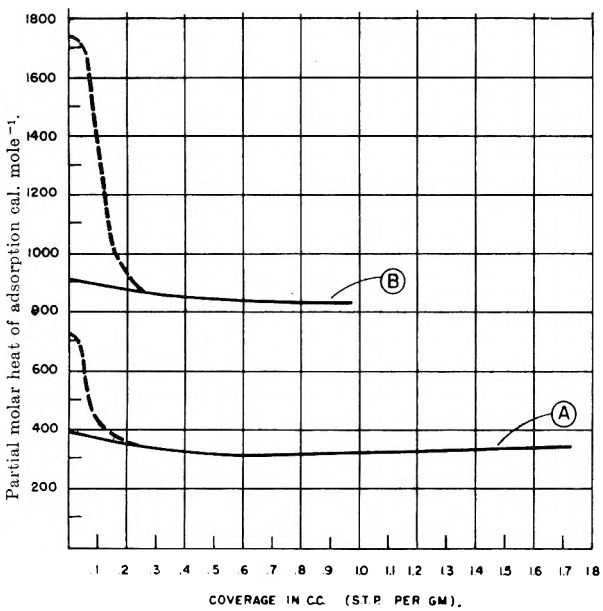

Fig. 1.—Partial molar heats of adsorption of helium (curve A) and neon (curve B) on graphitized carbon at low coverage.

Since the first experimental point[5] is, strictly speaking, an integral heat value, it is interesting to compare it to calculated integral heats. For the curves shown, the calculated integral heat is of the order of 1.5 times the first experimental point. If the value of ϵ_2 is chosen equal to 1.5 ϵ_1, the integral heats agree more closely. It would seem then that the model is very close to the actual case, 1.5 ϵ_1 being an average energy for sites other than single faced. Beebe and co-workers did not observe higher heats at very low coverages but comment on their absence. An examination of Fig. 1 shows that the position of the downsweep of the calculated curve relative to the ordinate would make it very easy to miss surface heterogeneity.

4. Interaction Energy from the Heats of Adsorption of Neon, Argon and Krypton.—A reasonable estimate of the integral lateral interaction energy at any coverage up to the monolayer can be determined from[7,8]

$$E_I = -\frac{a\theta}{2b} \qquad (5)$$

where a and b are the van der Waals constants; θ, the coverage; and E_I, the interaction energy. This formula can be expected to give values within about 50% of the true values if there is a mobile first layer and the layer behaves as a two-dimensional fluid.

Figure 2 shows the heat of adsorption curves for neon,[5] argon,[4b] and krypton[4a] on partially graphitized carbon black. The interaction energies can be approximated by a graphical integration of the area enclosed between the bump in the heat curve and an extrapolation of the flat portion of the heat curve to the monolayer value. Table I shows these experimental values at a monolayer, the values calculated from equation 5, and the heats of liquefaction of each gas. This table also includes values for second and higher layer interaction energies. These will be discussed in the next section.

TABLE I

MEASURED ENERGY OF LATERAL INTERACTION ENERGY (E_I)

	Neon E_I (cal.)	Argon E_I (cal.)	Krypton E_I (cal.)
1st layer meas.	44	169	330
2nd layer meas.	370	1400	2520
3rd layer meas.	..	..	2650
$a\theta/2b$, $\theta = 1$	150	510	710
Liquefaction	405	1600	2500 (sublim.)

It is apparent that the observed energy of lateral interaction is between one-quarter and one-half of the value predicted by equation 5. If the lateral interaction energy is calculated at a portion of a monolayer and compared with the experimental value, the measured value is an even smaller portion of the calculated value. This is evident from the downward concavity of the graphs below a monolayer, whereas, theoretically, the graphs should be straight lines with a slope of $a/2b$. One is therefore led to conclude that the surface film does not behave as a simple two-dimensional fluid.

Since a Lennard-Jones potential adequately describes the behavior of a bulk material in its various states of aggregation, it seems worthwhile to attempt to examine the adsorbed phase in terms of such a potential curve.

In Fig. 3 the Lennard-Jones curves for neon, argon and krypton are reproduced[9] with the values of the observed lateral interaction contribution to the energy of adsorption superimposed upon them (dotted lines). If it is assumed that the nearest neighbor distances between adsorbed molecules on the surface are determined by the intersection of the Lennard-Jones potential curve and the dotted line, then two possible values for the area per cubic centimeter, under standard conditions, for each gas can be calculated. If the computation is based on cubic packing on the surface, the values listed in Table II are obtained for the volume of gas under standard conditions per square meter of surface. The first row of the table is that value calculated by using the distance from the ordinate to the intersection at the *repulsive* side of the potential curve. The second row is that value calculated from the distance between the ordinate and the *attractive* side of the well. The last row contains

(7) R. H. Fowler and F. A. Guggenheim, "Statistical Thermodynamics," Cambridge Univ. Press, Teddington, England, 1939.

(8) T. L. Hill, "Advances in Catalysis," Vol. IV, Ed. P. H. Emmett. Academic Press Inc., New York, N. Y., 1952.

(9) J. O. Hirschfelder, C. F. Curtiss and R. B. Bird, "Molecular Theory of Gases and Vapors," John Wiley and Sons, Inc., New York, N. Y., 1954.

values for the volume under standard conditions of gas per square meter if it is assumed to liquid pack.

TABLE II

VOLUME OF GAS (STANDARD CONDITIONS) ADSORBED PER SQUARE METER OF SURFACE

	Volume, cc. (S.T.P.)/m.²		
	Neon	Argon	Krypton
Repul.	0.50	0.32	0.29
Attract	.12	.08	.08
Liquid	.39	.28	.22

Distances in the monolayer corresponding to the attractive side of the potential curve can be discarded since it is generally agreed that monolayers are liquid packed.

The solid vertical lines on the graphs of Fig 2 indicate the position of the monolayer calculated assuming that the atoms are *liquid packed* (*i.e.*, using the liquid density of the elements in question) and that the correct *area* is obtained from the nitrogen isotherm using B.E.T. theory The dotted vertical lines are drawn at the quantities of rare gas calculated for the monolayer from the nitrogen isotherm using B E.T. theory to compute the number of sites; a rare gas molecule is then assumed to occupy each site. There is no question that the solid vertical line is a better indication of the position of the true monolayer than the value calculated from sitewise adsorption.

There is a serious discrepancy between the liquid packing value and the value of the area per cubic centimeter of gas calculated from the expanded side of the well. At coverages below a monolayer the assumption of sitewise adsorption already excluded would be needed to keep the molecules on the expanded side of the well. Therefore any explanation must deal with the compressed side of the well. Thus, there is at coverages below a monolayer, a need for some sort of compressive constraint for a film without which the adsorbed molecules would pack as a van der Waals liquid. That is, adsorption in compressed patches must be explained. On the other hand, Crowell and Young[10,11] have shown that the energy of interaction between an argon atom and a uniform graphite surface is independent of the position of the argon atom relative to the carbon atoms in the surface. It can be inferred then that there is no force acting tangentially to the surface; therefore, there can be no constraint which could maintain an expanded film if the surface is truly planar. Nevertheless, the assumption of a compressed film implies a constraint and closer approach than liquid packing between adsorbed particles. This can therefore only arise if patches occur in hollow depressions in the surface, thereby giving a tangential component. The result is, of course, the observation of an abnormally low lateral interaction term due to the addition of repulsive terms to the total force between particles. A small reduction in the distance corresponding to liquid packing would significantly affect the interaction energies due to the steep decline of the repulsive side of a Lennard-Jones potential curve.

(10) A. D. Crowell, *J. Chem. Phys.*, **22**, 1397 (1954).

(11) A. D. Crowell and D. M. Young, *Trans. Faraday Soc.*, **49**, 1080 (1953).

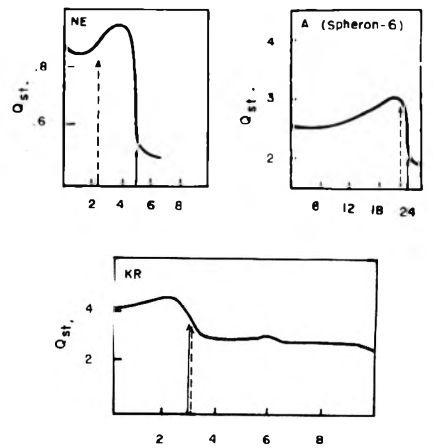

Fig. 2.—Partial molar heats of adsorption of NE, A and KR on graphitized carbon. Abscissas in cubic centimeters per gram; ordinates in kilocalories per mole.

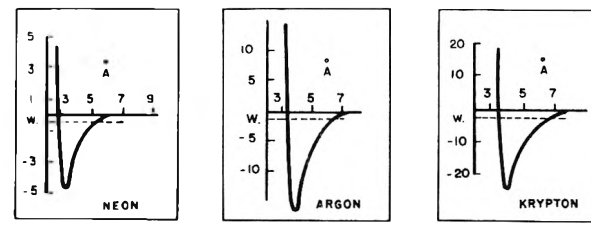

Fig. 3.—Potential energy curves for neon, argon and krypton; ordinates in ergs $\times 10^{15}$.

The argument for compression remains consistent for the second and higher layers as an examination of Table I for the higher layer values will show. The numbers were calculated by assuming that the heat of adsorption curve for the second layer and above is flat enough to equate integral energies to partial molar energies. The cube law for the decay of the energy due to surface interaction was assumed. The higher layer lateral interaction energies were then calculated by subtracting the part due to surface interaction. Figure 4 is a reproduction of typical potential curves calculated for highly compressed liquids and dense gases.[10] These curves show that a compressed liquid (curve C) upon expansion experiences a variation in potential energy which passes through a minimum (curve B) corresponding to a maximum in the lateral interaction energy. It can be seen that an analogous situation occurs in the case of krypton, the second and third layer energies being somewhat higher than the heat of sublimation of the gas. Since the adsorbed film must, at higher coverages, take on the properties of the bulk material, the lateral interaction energy must fall with increasing coverage.

Work to be reported elsewhere[12] has been done on the temperature of the second order transition of solid methane adsorbed on titanium dioxide as a function of coverage. This transition is presumably due to onset of rotation in the solid as the temperature is increased. In the bulk there is a narrowing of a broad line in the nuclear magnetic resonance adsorption due to the onset of rotation. This narrowing is complete at 70°K. For four layers of methane on titanium dioxide the narrow-

(12) N. Fuschillo, C. A. Renton and J. G. Aston, to be published.

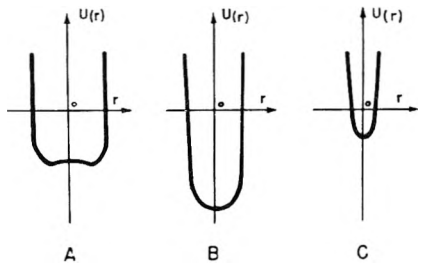

Fig. 4.—Potential curves for condensed gases (curves A, B, and C are for successive stages of compression).

ing is also complete at about 70°K. There is thus little difference in coöperation between the four layers and the bulk solid. As the coverage is lowered, the temperature at which the line narrowing is complete falls until at the monolayer the temperature is about 21°K. As the coverage is further lowered, this temperature starts to increase slightly and continues to increase slightly until about 0.3 monolayer. Experimental difficulties make it hard to get data below this coverage.

This increase of temperature below the monolayer indicates an increase in coöperation which can only be due to an increase in density due to compression. Although the line shape changes with coverage and the range of temperature for broadening of the line to the maximum also varies, the general conclusion from the above result is not changed.

This is a striking confirmation of the theoretical conclusions reached in the foregoing discussion. The fact that titanium dioxide has other sites than those of the flat surface[6] does not affect the argument since more than half of the sites in the monolayer are those of a flat surface. The methane in the high energy sites could only change the line shape slightly and would not affect greatly the degree of coöperation. Previously Mastrangelo and one of us have shown[13] that there is a sharp inflection in the 2.41 °K. isotherm of helium on titanium dioxide at the end of the second layer. This was attributed to a decrease in surface pressure occurring rather suddenly in the formation of the second layer. It was pointed out that such an effect implied that the density of the film was relatively constant throughout a layer. It was thus concluded that "*the film consists largely of regions of the surface completely filled.*"

Acknowledgments.—The coöperation of Dr. William A. Steele in the many discussions of the material presented in this paper is gratefully acknowledged as is also the helpful criticism of Dr. Julian Eisenstein of the Department of Physics.

(13) S. V. R. Mastrangelo and J. G. Aston, *J. Chem. Phys.*, **19**, 1370 (1951).

D-GLUCOSE–WATER PHASE DIAGRAM

BY FRANK E. YOUNG[1]

Contribution from Western Utilization Research Branch, Agricultural Research Service, U. S. Department of Agriculture, Albany 10, California

Received November 25, 1956

The D-glucose–water phase diagram has been investigated between −30 and +62°. Solubility curves have been established for all of the known solid phases: ice, α-D-glucose, β-D-glucose and α-D-glucose monohydrate. The ice–α-D-glucose monohydrate and ice–β-D-glucose eutectics have been observed experimentally. Mutarotatory equilibrium between α- and β-isomers in D-glucose solutions is found to be nearly independent of temperature but may be affected by concentration.

The discovery of new crystalline hydrates in recent studies of phase equilibria in the sucrose–water[2] and D-fructose–water[3] systems, the practical importance of the crystallization of α-D-glucose monohydrate in fruit preservation,[4] and inconsistencies in available data on the D-glucose–water system prompted this new investigation of phase equilibria in aqueous D-glucose solutions.

The temperatures at which ice and D-glucose solutions are in equilibrium have been reported by Abegg[5] and by Pozner and Amerkhanov.[6] The results of these two studies are in good agreement for solutions more dilute than 23% by weight of anhydrous sugar, but at higher concentrations significant differences occur which increase with sugar content. Abegg's ice curve, based on measurements on solutions containing up to 42% glucose, is essentially the same as that found for fructose solutions.[3] On the other hand the Russian investigators found higher ice points at high sugar contents, the result at 71% glucose being about 12° higher than the ice point of a fructose solution of the same concentration and only 1.5° lower than 71% sucrose solution.

Solubility data for α-D-glucose and its monohydrate have been reported by Jackson and Silsbee.[7] Their two measurements at 28° for the anhydrous sugar are in poor agreement with the value obtained by extrapolation of their other data obtained at higher temperatures. No solubility data have been reported for β-D-glucose.

New determinations of the solubility curves of ice, α-D-glucose, β-D-glucose and α-D-glucose monohydrate are reported here for the range from −30 to +62°. These curves have established new values for the eutectics of this system. No crystal-

(1) California State Polytechnic Institute, San Luis Obispo, Calif.

(2) F. E. Young and F. T. Jones, THIS JOURNAL, **53**, 1334 (1949).

(3) F. E. Young, F. T. Jones and H. J. Lewis, *ibid.*, **56**, 1093 (1952).

(4) R. W. Olsen and E. L. Moore, *Food Tech.*, **8**, 175 (1954); G. M. Cole, *ibid.*, **9**, 38 (1955).

(5) R. A. Abegg, *Z. physik. Chem.*, **15**, 209 (1894).

(6) E. Pozner and A. X. Amerkharov, *J. Phys. Chem., U.S.S.R.*, **15**, 1137 (1941).

(7) R. F. Jackson and C. G. Silsbee, *Natl. Bur. Standards Sci. Papers*, **17**, 715 (1922)(No. 437).

line phases were found which had not been observed heretofore. Observations on the ice–α-D-glucose monohydrate eutectic and the ice–β-D-glucose eutectic enable estimates to be made of the isomer composition of D-glucose solutions at mutarotatory equilibrium at these temperatures.

Experimental

Materials.—Measurements were made on solutions which had been allowed to stand overnight at room temperature to reach mutarotatory equilibrium. These solutions were prepared from distilled water and reagent grade α-D-glucose which gave $[\alpha]^{26}D$ 52.79° in water (c 4, *l* 4). At several points, the results were checked on solutions of National Bureau of Standards dextrose Standard Sample No. 41. β-D-Glucose was prepared from the above α-D-glucose by the method of Hudson and Dale,[8] after which it was dried *in vacuo* over anhydrous calcium chloride to remove alcohol and water. Since the solubilities of both α- and β-D-glucose remained unchanged when the ratios of solid phase to solution were increased, the amounts of impurities remaining in these materials were too small to affect the results.

Analysis.—Concentrations were determined by refractometer readings at room temperature. These were converted to D-glucose percentages by the table of Young and Jones.[9] All concentrations in this paper are expressed in grams of anhydrous D-glucose per 100 g. of solution.

Isothermal Measurements.—The solubility curves for α-D-glucose, its monohydrate and ice in the regions in which they are the stable solid phases were determined by equilibrium measurements in constant temperature baths as described previously.[2] Equilibrium was not considered attained until the concentrations of solutions which had approached equilibrium from both above and below saturation differed by less than 0.10% and remained constant for several days. Agreement of measurements for initially under- and oversaturated solutions also ensures attainment of mutarotatory equilibrium when the solid phase is not ice. The final result for each temperature represents the average of at least 4 measurements. Although several successful measurements were made by this method on the metastable portion of the ice curve down to −9°, the frequent spontaneous crystallization of α-D-glucose monohydrate made it necessary to investigate the remainder of the phase diagram by other methods.

Warming Curves.—Points on the ice curve were also determined by the warming curve method[2] over the entire range reported here. Except for the point at −29.55° each result is the average of two or more determinations. That ice points above −9° obtained from warming curves are not in error from lack of time for mutarotation is shown by their agreement with those determined by isothermal measurements. That ice points at lower temperatures are also not affected by mutarotation was indicated by excellent agreement found for the ice points of two 60% D-glucose solutions, one of which had been allowed to reach mutarotatory equilibrium and the other contained practically all the solute in the β form.[10]

Solubility of Anhydrous Phases.—Points on the solubility curves for anhydrous α- and β-D-glucose were determined by stirring powdered D-glucose in excess of the amount needed to produce saturation into a solution containing about 0.1% less D-glucose than the expected equilibrium value. Samples were then withdrawn through fritted glass filter tubes at intervals of several minutes. Usually the concentration rose to the equilibrium value during the first few minutes and then remained constant until α-D-glucose monohydrate began to crystallize. When this occurred, usually after 20 to 30 minutes, the sudden evolution of heat caused a momentary increase in concentration before crystallization rendered the solution too pasty to filter. Each result obtained by this technique was checked by repeating the procedure with a solution whose initial concentration was the equilibrium value indicated by earlier measurements. It was not feasible to check these results with initially oversaturated solutions, because crystallization of the metastable solid phase proceeds so slowly that equilibrium is not attained before crystallization of a stable solid phase begins.

Frequent spontaneous crystallization of glucose monohydrate and extremely slow mutarotation made it impractical to hold these solutions long enough to ensure mutarotatory equilibrium at the temperature of measurement. Separate experiments were performed to determine how much the solubilities of anhydrous D-glucose measured as just described were in error due to lack of attainment of equilibrium between the α- and β-isomers in solution. For this purpose ammonia was used to catalyze mutarotation.

Measurements first were made to demonstrate that ammonia is effective in speeding mutarotation at low temperatures. A D-glucose solution to which 2 drops of concentrated ammonium hydroxide had been added was allowed to equilibrate at −10.65° in the presence of solid α-D-glucose. The solution was then diluted 0.40% and again allowed to equilibrate in the presence of the solid phase. The concentration quickly rose to 50.25%, its value before dilution. Repetition of the dilution and equilibration in the presence of solid α-D-glucose produced the same concentration. Had mutarotation not occurred rapidly in the presence of ammonia, each successive dilution would have reduced the final value by an amount corresponding to the reduction of the β-D-glucose concentration.

Solubilities determined by this procedure were higher for α-D-glucose by 0.35% at −10.65° and by 0.10% at 0°, and lower for β-D-glucose by 0.25% at −16.80°, than those measured without adding ammonia. These figures indicate the equilibrium between α- and β-isomers is not shifted much by rather large changes in temperature, a conclusion in accord with data of Isbell and Pigman[11] at 0 and 20° for a 4% D-glucose solution. The magnitude and direction of the shifts indicated by our solubility data are also in agreement with their rotation data. The small corrections indicated by these figures have been applied to solubility data obtained for α- and β-D-glucose below 20° in the absence of ammonia. At 40° or higher, mutarotatory equilibrium was attained before measurements were completed.

The solubility measurements on anhydrous α- and β-D-glucose at or below 40° were made on about 100 g. solution in a 25 × 200 mm. test-tube in a constant temperature bath. The solutions were agitated with a rotary stirrer and temperatures were read on a calibrated thermometer graduated to 0.1°. Above 40°, solution and excess solid phase were rapidly tumbled end-over-end in partly filled vials in a constant temperature bath.

Results and Discussion

Figure 1 shows the phase diagram established in this investigation and includes the experimental points which determine the solubility curves. It should be emphasized that these curves represent equilibrium between solid phase and solution in which α-D-glucose and β-D-glucose are present in equilibrium proportions at the indicated temperatures. These curves are expressed below as equations fitted to the data by the method of least squares.

Ice

$$(p - 100)t = 11.38p - 9.07 \times 10^{-2}p^2 + 3.455 \times 10^{-3}p^3 - 2.653 \times 10^{-5}p^4 \quad (1)$$

$\sigma = 0.10°$, $n = 19$; $t = 0$ to $-27°$; $p = 0$ to 67%

α-D-Glucose Monohydrate

$$p = 33.78 + 0.6215t + 3.08 \times 10^{-3}t^2 - 2.31 \times 10^{-5}t^3 \quad (2)$$

$\sigma = 0.05\%$, $n = 7$; $t = -4$ to $+52°$; $p = 31$ to 71%

(8) C. S. Hudson and J. K. Dale, *J. Am. Chem. Soc.*, **39**, 320 (1917).

(9) F. E. Young and F. T. Jones, *J. Assoc. Official Agr. Chem.*, **37**, 932 (1954).

(10) The solution of β-D-glucose was prepared by shaking 15 g. of powdered β-D-glucose with 10 g. of water at 0° for several seconds, followed by rapid suction filtration and immediate transfer to a precooled warming curve tube in which it was rapidly cooled to about −20°. Rotation measurements showed that this solution contained initially only 1.4% α-D-glucose. Mutarotation after cooling the solution was assumed to be negligible, since the entire procedure required only 12 minutes and eutectic halts were reproducible on repeated warming curves below −10° on the same solution.

(11) H. S. Isbell and W. W. Pigman, *J. Research Natl. Bur. Standards*, **18**, 141 (1937) (RP 969).

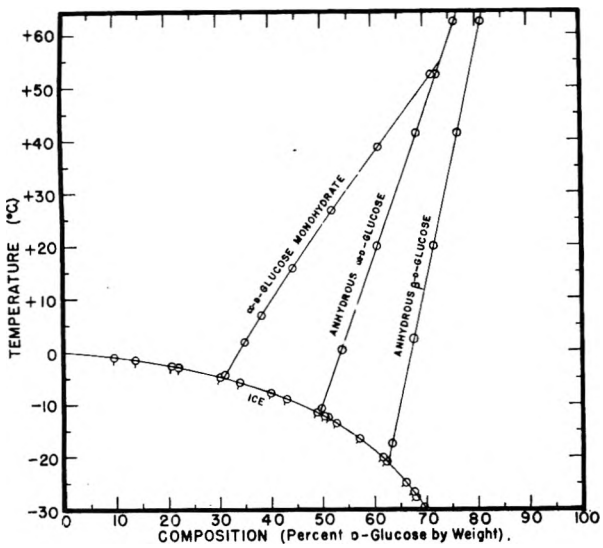

Fig. 1.—D-Glucose–water phase diagram.

Anhydrous α-D-Glucose

$$p = 53.80 + 0.535t + 3.65 \times 10^{-4}t^2 \quad (3)$$

$\sigma = 0.04\%$, $n = 6$; $t = -11$ to $+62°$; $p = 50$ to 76%

Anhydrous β-D-Glucose

$$p = 67.00 + 0.224t \quad (4)$$

$\sigma = 0.07\%$, $n = 8$; $t = -17$ to $+63°$; $p = 63$ to 81%

In these equations p is the anhydrous glucose content of the solution in weight per cent., t is the temperature in °C., σ is the standard deviation of the experimental data from values calculated by the equation, and n is the number of values used in deriving the equation. The range of composition and temperature data on which each equation is based is also shown. Values calculated from these equations at selected values of the composition and temperature are given in Table I.

Ice.—The warming curve method gave readily reproducible data for the ice curve except for the lowest two temperature points shown in Fig. 1 at −27.69 and −29.55°. These two points were not used in obtaining equation 1, since they were of doubtful reliability due to the difficulty in inducing crystallization in these highly viscous solutions. The −29.55° point represents the only successful attempt to induce crystallization of ice from solutions containing over 68% glucose.

The ice curve reported here coincides with that found for D-fructose solutions[3] at sugar contents below about 50%. For solutions containing 60% hexose, the ice point is only about 0.3° lower for a solution containing D-fructose than for one containing D-glucose. Thus structural differences between the two sugars have little net effect on the activity of water in their concentrated solutions.

The ice points of Fig. 1 are markedly lower than those of Pozner and Amerkhanov[6] at high glucose contents. This unexplained discrepancy amounts to 9° at 70% sugar.

α-D-Glucose Monohydrate.—The solubilities of the monohydrate calculated from equation 2 are in good agreement with those of Jackson and Silsbee[7] except at +0.50° and at +50.00°, where their results are about 1% higher.

During the present investigation it was found that anhydrous α-D-glucose dissolves readily in a solution at equilibrium with the solid monohydrate at 50°. Apparently the relatively low rate of crystallization of the monohydrate under these conditions allows the solution to become saturated with respect to anhydrous α-D-glucose. Oversaturation with respect to the hydrate continues as long as anhydrous solid is present. This behavior appears to provide a reasonable explanation for the earlier observation[7] of solid α-D-glucose and its monohydrate apparently at equilibrium with a solution containing 70.91% glucose at 50.00°. If this datum is omitted, the remaining data of Jackson and Silsbee extrapolate to essentially the same transition point between hydrate and anhydrous sugar as found from equations 2 and 3, *viz.*, 54.71° and 73.22% glucose.

The α-D-glucose monohydrate–ice eutectic is determined by the intersection of the ice and the hydrate solubility curves (equations 1 and 2) to be −4.93° and 30.79% glucose. This point corresponds to (mutarotatory) equilibrium between α- and β-isomers in solution. It is difficult to observe by the warming curve technique since melting of monohydrate–ice eutectic initially yields only α-isomer in solution. The eutectic corresponding to no β-isomer in solution can be visualized as the intersection of the ice curve and a solubility curve for solid hydrate in equilibrium with solution containing only α-isomer. This hypothetical solubility curve can be estimated by reduction of the hydrate solubility shown in Fig. 1 by the proportion of β-isomer present at mutarotatory equilibrium at each temperature. Although accurate isomer composition data are not available for thus calculating this curve, it is apparent that this hypothetical eutectic for β-isomer absent must occur at a higher temperature and lower glucose concentration than the values cited above.

TABLE I

SOLUBILITIES IN THE D-GLUCOSE–WATER SYSTEM[a]

Temp., °C.	Concn., wt. %	Temp., °C.	Concn., wt. %
Ice		α-D-Glucose monohydrate	
0.00	0.00	− 4.93[b]	30.79
− 1.20	10.00	0.00	33.78
− 2.70	20.00	10.00	40.28
− 4.74	30.00	20.00	47.26
− 7.72	40.00	30.00	54.57
−12.17	50.00	40.00	62.09
−18.97	60.00	50.00	69.67
−30.01	70.00	54.71[c]	73.22
Anhydrous α-D-glucose		Anhydrous β-D-glucose	
−12.06	49.81[b]	−21.02[b]	62.29
−10.00	50.49	−20.00	62.52
0.00	53.80	−10.00	64.76
10.00	57.19	0.00	67.00
20.00	60.65	10.00	69.24
30.00	64.18	20.00	71.48
40.00	67.78	30.00	73.72
50.00	71.46	40.00	75.96
54.71[c]	73.22	50.00	78.20

[a] The data in this table were calculated from the equations given in the text. [b] Eutectic: ice and solid phase of table. [c] Transition: α-D-glucose monohydrate ⇄ anhydrous α-D-glucose.

Eutectic halts lasting up to 105 minutes in the range −2.29 to −1.83° were observed in warming curves for a number of samples which might be expected to contain monohydrate–ice eutectic. Since mutarotation rates at these temperatures are too slow to produce significant changes in isomer composition during the time required to obtain a warming curve, these variations in observed invariant temperatures presumably correspond to different amounts of β-isomer present, depending upon the seeding and temperature history of the sample prior to the warming curve. If it is assumed that −1.83° is the eutectic temperature for solution containing only α-isomer, it is found from equation 1 that the concentration of α-D-glucose in equilibrium with solid hydrate at this temperature is 14.59%. Since the solubility of hydrate at this temperature is found from equation 2 to be 32.65%, the portion of D-glucose in the α-form at mutarotatory equilibrium at −1.83° is estimated[12] as 35%. This value probably should be regarded as an upper limit since the correct ice-hydrate eutectic temperature in the absence of β-isomer may be higher than −1.83°.

Anhydrous α-D-Glucose.—Since the results of this investigation showed the solubility of α-D-glucose below 50° to vary with temperature somewhat more than reported by Jackson and Silsbee,[7] additional measurements were made at three higher temperatures, *viz.*, 52.22, 62.21 and 75.28°. At the highest temperature, considerable difficulty was encountered in determining the solution concentration refractometrically at room temperature due to crystallization of α-D-glucose on the refractometer prism. This effect usually gave concentrations too low by several tenths per cent., but one well-defined and one poorly defined index were obtained corresponding to 80.64 and 80.80%, respectively. These values are consistent with those at lower temperatures.

No experimental evidence was obtained for the existence of an anhydrous α-D-glucose–ice eutectic. All attempts to obtain this eutectic resulted in crystallization of the hydrate.

Anhydrous β-D-Glucose.—According to equations 3 and 4, the solubility curves for α- and β-D-glucose intersect at 91.4° and 87.5% glucose. Little confidence can be placed in these α-β transition point figures because extrapolation of curves of similar slopes (Fig. 1) is involved. A transition temperature of 108.6° has been reported from solubility measurements of α- and β-D-glucose in methanol.[13]

(12) The assumption is made here that the number of moles of water per mole of D-glucose isomer in solution in equilibrium with solid phase of the same type isomer is independent of the presence of the other type isomer in solution. Results now being prepared for publication show that the presence of D-glucose in solution has little effect on the solubility of D-fructose dihydrate and that D-fructose in solution has little effect on the solubility of D-glucose monohydrate when the solubility is expressed in molality of the saturating sugar. It therefore seems reasonable to assume that the molality of the saturating isomeric form of D-glucose will not be significantly affected by the presence of the other mutarotatory form in solution.

The β-D-glucose–ice eutectic is determined by the intersection of the ice and β-D-glucose solubility curves (equations 1 and 4) to be −21.02° and 62.29% glucose. This point corresponding to mutarotatory equilibrium in solution is not readily observed in warming curves for the reason discussed above in reference to the α-D-glucose monohydrate–ice eutectic. However, eutectic halts at −16.52° were observed in 5 different warming curves on a β-D-glucose solution[10] which was seeded with β-D-glucose. This temperature corresponds to equilibrium between ice, solid β-D-glucose and a solution which contains a total of 56.9% α- and β-D-glucose. When the small amount of α-D-glucose present is taken into account, the solubility of β-D-glucose at −16.52° in the absence of the α-form is calculated to be 56.2%. The corresponding value for β-D-glucose and solution at mutarotatory equilibrium is 63.30%. Thus about 74.4% of the total dissolved glucose at −16.52° is in the β-form.[12] From these results, the β-D-glucose–ice eutectic temperature and concentration are estimated to be approximately −16.1° and 56.4% in the absence of the α form.

Mutarotation of D-Glucose.—Some new information on the effect of temperature and concentration on the mutarotatory equilibrium of D-glucose has been obtained in the course of this study. The temperature effect can be approximated from differences in solubilities of either α- or β-D-glucose in solutions at mutarotatory equilibrium at room temperature and at the temperature of measurement, as already discussed in the Experimental section. These differences indicate a shift in equilibrium isomer composition of at most a few tenths per cent. between 25 and −15° for solutions containing 50 to 65% by weight of D-glucose. The rotation data of Isbell and Pigman[11] likewise indicate a shift of only one-tenth per cent. between 20 and 0° for a 4% solution. The conclusion seems justified that mutarotatory equilibrium in D-glucose solutions has a very low temperature coefficient at all concentrations.

Observations on the ice-α-D-glucose monohydrate eutectic temperature indicated a maximum of 35% of the D-glucose in the α-form in a 33% solution. An isomer composition of 74% β was indicated by ice-β-D-glucose eutectic observations, this value being a maximum for a 63% solution. In 4% D-glucose solution, an α-isomer percentage of 36 has been found.[11] These data suggest either a significant shift in isomer composition with sugar concentration or a dependence of activity coefficient on concentration which could account for this apparent shift.

Acknowledgments.—The author wishes to thank Dr. F. T. Jones for making many of the refractive index measurements and Dr. Fred Stitt for suggestions and considerable assistance in the preparation of the manuscript.

(13) J. Gillis and H. N. Nachtergaele, *Rec. trav. chim.*, **53**, 31 (1934).

THE REACTION OF HYDROGEN ATOMS WITH PHOSPHINE[1]

BY D. M. WILES[2] AND C. A. WINKLER

Contribution from the Physical Chemistry Laboratory, McGill University, Montreal, Canada

Received December 3, 1956

Red phosphorus and molecular hydrogen were the only products of the reaction between hydrogen atoms and phosphine. It is postulated that hydrogen abstraction is followed by combination of PH_2 radicals to give the products. The atomic hydrogen concentration was estimated by measuring the extent of the reactions of HBr and HI with hydrogen atoms under the same experimental conditions.

Introduction

The reactions of atomic hydrogen with a large number of organic compounds have been investigated under a variety of experimental conditions. It is generally accepted that the primary reaction with saturated hydrocarbons is hydrogen abstraction whereas with alkyl halides and alkenes it is thought to involve halogen atom abstraction and hydrogen atom addition, respectively.

Reactions between atomic hydrogen and gaseous inorganic compounds have not been extensively studied in quantitative experiments, although the qualitative effects upon many inorganic substances have been reported in the literature. Phosphine has been subjected to the action of hydrogen atoms produced in an electrodeless discharge[3] in a search for higher hydrides of phosphorus, but no attempt was made to determine the products of the reaction or its mechanism.

In the present work the reaction of hydrogen atoms with phosphine was studied in a Wood–Bonhoeffer fast-flow system. A limited examination of the corresponding reactions with hydrogen iodide and hydrogen bromide was also made with a view to obtaining a measure of the atomic hydrogen concentration in the system.

Experimental

The apparatus and the experimental techniques were similar to those described in an earlier paper from this Laboratory.[4] The pressure in the apparatus before each experiment was always less than 5×10^{-3} mm. Hydrogen from a cylinder was passed through a trap immersed in liquid nitrogen and was admitted through a capillary flow meter to both sides of a V-shaped discharge tube. The total pressure of atomic and molecular hydrogen in the reaction system was 0.87 mm., with a molecular hydrogen flow rate of 1.24×10^{-4} mole/sec. Experiments were made at high temperature with an electrical heater surrounding the reaction vessel and the lower 5 cm. of the tube that connected it to the discharge tube. The temperature was measured with a glass-enclosed, copper–constantan thermocouple located just below the reactant inlet in the center of the reaction vessel. The inner surfaces of the discharge tube and reaction system were poisoned with 2% metaphosphoric acid solution. All experiments lasted 100 seconds.

Phosphine was prepared using three different methods: (i) by decomposing phosphonium iodide with dilute base; (ii) by treating calcium phosphide with dilute acid; (iii) by treating white phosphorus with boiling aqueous potassium hydroxide solution. In each case, hydrogen was passed through the reaction flask, and the mixture of hydrogen and phosphorus hydrides passed through 6 *N* HCl and 25% KOH solutions, through two traps immersed in freezing ethanol, and finally through a liquid nitrogen trap to condense the phosphine. Prior to use, the condensate was distilled twice from a trap cooled to −130°. Phosphine flow rates were controlled by maintaining a constant pressure behind a capillary jet. The flow meter was calibrated by distilling the gas collected during "blank" experiments into a small removable trap that contained dilute silver nitrate solution. The precipitated silver was removed by filtration and excess silver nitrate was determined by the Volhard method.[5] Estimation of unreacted phosphine by the same procedure enabled the amount of reaction in each experiment to be determined.

Hydrogen iodide[6] and hydrogen bromide[7] were prepared by standard methods. The gases were carried in a stream of dry hydrogen through two traps at −100° before they were condensed with liquid nitrogen. They were purified further by bulb-to-bulb distillations and care was taken in subsequent experiments to prevent their contact with mercury. Hydrogen halide flow rates were measured in "blank" experiments by distilling the condensate from the product trap (kept at −100° for HBr, −60° for HI) into a removable trap containing standard NaOH solution and back-titrating the excess alkali with standard acid. The extent of reaction was determined by collecting and measuring unreacted hydrogen halide in the same manner.

Ethyl chloride (b.p. grade) was obtained from Ingram and Bell, Ltd., Montreal, and was vacuum distilled before use. The extent of its reaction with hydrogen atoms was estimated from the amount of hydrogen chloride produced.

Results and Discussion

Figure 1 shows the results obtained in the reactions of HI, HBr and C_2H_5Cl with atomic hydrogen at 65°. The hydrogen halides reacted with 3 times as many hydrogen atoms as did the alkyl halide and the fact that hydrogen iodide and hydrogen bromide reacted to the same extent is a good indication that both consumed all the hydrogen atoms. The following elementary steps must have occurred in the hydrogen halide reactions.

$$H + HX \longrightarrow H_2 + X \quad (1)$$

$$X + X + M \longrightarrow X_2 + M \quad (2)$$

$$H + X_2 \longrightarrow HX + X \quad (3)$$

The activation energy for reaction 1 is approximately 1 kcal./mole.[8] Reaction 3 has a small but significant activation energy, practically the same as for reaction 1. According to Williams and Ogg,[9] the ratio k_3/k_1 is 3.5 for HI and is essentially independent of temperature. For HBr the ratio k_3/k_1 is 8.4.[8] However, since hydrogen atom consumption is apparently complete with excess of either hydrogen halide, the consumption of H atoms by I_2 or by Br_2 under these conditions seems to represent a negligibly small percentage of the total H-atom con-

(1) With financial assistance from the National Research Council of Canada.

(2) Holder of National Research Council Studentships, 1955–1956, 1956–1957.

(3) K. G. Denbigh, *Trans. Faraday Soc.*, **35**, 1432 (1939).

(4) P. A. Gartaganis and C. A. Winkler, *Can. J. Chem.*, **34**, 1457 (1956).

(5) I. M. Kolthoff and E. B. Sandell, "Textbook of Quantitative Inorganic Analysis," 3rd ed., The Macmillan Co., New York, N. Y., 1952.

(6) A. I. Vogel, "A Textbook of Practical Organic Chemistry," Longmans, Green and Co., New York, N. Y., 1951.

(7) J. W. Mellor, "Mellor's Modern Inorganic Chemistry," revised ed., Longmans, Green and Co., New York, N. Y., 1939.

(8) J. C. Morris and R. N. Pease, *J. Chem. Phys.*, **3**, 796 (1935).

(9) R. R. Williams, Jr., and R. A. Ogg, Jr., *ibid.*, **15**, 691 (1947).

centration available. It is assumed, therefore, that the plateau value for the amount of reactant destroyed may be taken as a measure of the hydrogen atom concentration. On this basis the flow rate of atomic hydrogen in the reaction system was 10^{-5} mole/sec. and the ethyl chloride reaction was 32% complete at 65° (*cf.* 10). It is of interest that a previous study of the HBr–H atom reaction[11] indicated 100% consumption of hydrogen atoms.

The only products of the reaction of phosphine with atomic hydrogen were molecular hydrogen and red phosphorus. The latter was deposited in a uniform layer on the inside wall of the reaction vessel and it changed from a light golden to a deep amber color as the thickness increased. When hydrogen atoms reacted with this coating it was consumed completely in such a manner that the clearly defined horizontal boundary between clean and phosphorus-covered glass moved gradually down the reaction vessel and few hydrogen atoms appeared to exist beyond the phosphorus level. This process resulted in conversion of the red phosphorus to phosphine and a small amount of diphosphine. The reactions

$$\left.\begin{aligned} P_{red} + H &\longrightarrow PH^{12} \\ PH + H_2 &\longrightarrow PH_3 \end{aligned}\right\} \Sigma \quad \begin{matrix}(4)\\(5)\end{matrix}$$

would account for the formation of phosphine, and the small amount of disphosphine could have been formed by

$$PH_3 + H \longrightarrow PH_2 + H_2 \qquad (6)$$
$$2PH_2 + M \longrightarrow P_2H_4 + M \qquad (7)$$

Because of the trace of P_2H_4 formed, the conversion of the layer could not be used to determine quantitatively the amount of phosphorus produced in the phosphine–atomic hydrogen reaction. The action of hydrogen atoms on red phosphorus to produce phosphine was observed by Langmuir[13] who found that the process would proceed either in the gas phase or on the vessel wall. The conversion of phosphorus to phosphine observed in the present work occurred at an appreciable rate for temperatures at which the vapor pressure of red phosphorus is quite low. Under these conditions there must have been a considerable proportion of wall reaction.

The results obtained in the reaction of phosphine with H atoms at three temperatures are given in Fig. 2. It is apparent that phosphine reacts with all the available hydrogen atoms at 73°, since the plateau corresponds closely to the maximum amounts of hydrogen iodide and hydrogen bromide destroyed under similar conditions. It is probable that phosphine reacts according to the following mechanism.

$$PH_3 + H \longrightarrow PH_2 + H_2 \qquad (8)$$
$$PH_2 + PH_2 \longrightarrow P_2 + 2H_2 \qquad (9)$$
$$P_2 \longrightarrow P_{red} \qquad (10)$$

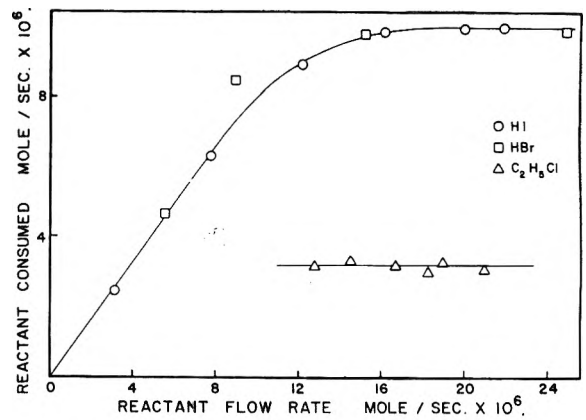

Fig. 1.

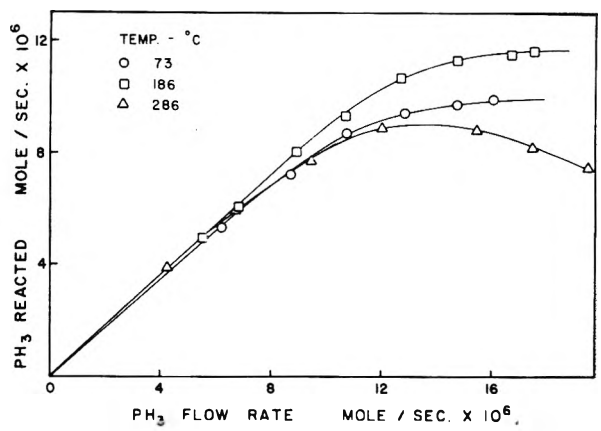

Fig. 2.

The abstraction of hydrogen is typical of the reactions of atomic hydrogen and, because of its exothermicity, reaction 8 is the most reasonable primary step. Reactions 9 and 10 are substantiated by evidence obtained in investigations of the photochemical and mercury photosensitized decomposition of phosphine. Melville, *et al.*,[14] studied the photochemical decomposition of PD_3 and PH_3 and found evidence that PH_2 radicals decompose to give molecular hydrogen. Melville and Gray,[15] in a study of the polymerization of phosphorus, obtained experimental evidence that P_2 molecules condense to red phosphorus so that equations 8 to 10 can account for the products found in the present study.

The following reactions are also possible, although they appear to occur only to a slight extent at room temperature.

$$PH_2 + H \longrightarrow PH + H_2 \qquad (11)$$
$$PH + PH_2 \longrightarrow P_2 + H + H_2 \qquad (12)$$
$$PH + H \longrightarrow P + H_2 \qquad (13)$$
$$PH + PH \longrightarrow P_2 + H_2 \qquad (14)$$

Reactions 11 and 13 should lower the plateau at 73° relative to that representing the available hydrogen atoms, but this was not observed. It is therefore reasonable to assume that, at phosphine flow rates corresponding to complete consumption of hydrogen atoms, the unstable PH_2 species re-

(10) H. M. Chadwell and T. Titani, *J. Am. Chem. Soc.*, **55**, 1363 (1933).

(11) E. Cremer, J. Curry and M. Polanyi, *Z. physik. Chem.*, **B23**, 445 (1933).

(12) The values of heats of formation found in Circular 500, U. S. National Bureau of Standards were used for species occurring in this and subsequent reactions. Values of 30 and 55 kcal./mole were estimated for PH_2 and PH radicals, respectively.

(13) I. Langmuir, *J. Am. Chem. Soc.*, **34**, 1310 (1912).

(14) H. W. Melville, J. L. Bolland and H. L. Roxburgh, *Proc. Roy. Soc.* (*London*), **A160**, 406 (1937).

(15) H. W. Melville and S. C. Gray, *Trans. Faraday Soc.*, **32**, 271 (1936).

acts according to equation 9 rather than equation 11. This rules out steps 12, 13 and 14 since they depend on the formation of PH radicals.

The rates of phosphine decomposition at 73 and 186° are typical of a reaction with a small activation energy, in which the reactant present in smaller amount is completely consumed. The experiments at 286° indicated that a back reaction with a large temperature coefficient appreciably affects the net amount of phosphine decomposed. It is suggested that this back reaction is the attack of hydrogen atoms on phosphorus, represented by 4 and 5. At lower PH_3 flow rates, corresponding to the rising portion of the curve for 286°, red phosphorus produced in (10) should react with hydrogen atoms to make PH radicals. Some of the species would proceed by (5) to regenerate phosphine; others in the presence of excess hydrogen atoms would be decomposed again to give red phosphorus by (13). At higher phosphine flow rates where hydrogen atom consumption is virtually complete, most of the PH radicals would probably regenerate phosphine. Thus, the observed phosphine decomposition may be reduced not only by consumption of atomic hydrogen by red phosphorus, but also by regeneration of phosphine. Consequently in accordance with the observed behavior the curve for 286° might be expected to rise to a maximum and fall off slowly as the phosphine flow rate is increased.

A KINETIC APPROACH TO THE THERMODYNAMICS OF IRREVERSIBLE PROCESSES[1]

BY O. K. RICE

Department of Chemistry, University of North Carolina, Chapel Hill, N. C.

Received December 3, 1956

The study of irreversible processes is considered from the point of view of "transference units," or groups of molecules in a particular energy state capable of causing a certain exchange of molecules. By considering the equilibrium (or steady state) of such a transference unit with the components of the solution, and the relation of this equilibrium in a temperature and concentration gradient with that of an inverse unit (one capable of reversing the exchange of molecules), equations are set up for fluxes of matter and heat. It is shown that the reciprocal relations between the phenomenological coefficients follow from these equations. The usual equations for the Soret effect and for thermocells are derived, and a few remarks on experimental values of heats of transport in electrolyte solutions are included. The extension to heterogeneous systems (systems containing a membrane) is considered and illustrated by application to the Knudsen flow of a gas.

The theory of irreversible processes is commonly based either upon the Thomson principle, which states that the second law of thermodynamics can be applied to all portions of the process which are reversible even though complete equilibrium is not established, or else upon Onsager's reciprocal relations.[2] There have also been some kinetic studies[3] aimed partly at evaluating heats of transport, but also directed toward the understanding of the equations for the Soret phenomenon and related effects. However, no general kinetic study of these relationships seems to have been given. While this is unnecessary in the sense that these relationships are already well established, and the rigor of the treatment is not likely to be improved, such a study should lead to greater physical insight into the nature of these phenomena and of the reciprocal relations.

1. Ideal Solutions

The thermodynamics of irreversible processes is concerned with flows of heat and matter which occur under gradients of temperature and concentration. The flows or fluxes, if not too great, can be expressed as linear functions of certain "forces," related to the gradients, one standard formulation being given in Section 4, below. Of special interest are steady states in which some of the flows have stopped. For example, in the Soret effect, a temperature gradient is maintained and flow of heat always occurs, but a steady state is reached in which the gradients of the different materials present have definite values, and flow of matter stops. The concentration gradients are then dependent on heats of transport, *i.e.*, the heat which must be absorbed from thermostat or surroundings when unit quantity of a particular component is removed from a certain region or, equivalently, the heat rejected when the component is added. Before we go into the general relationships, it may be of interest to consider the special case presented by an ideal solution.

A truly ideal solution is presumably one in which the types of molecule involved have the same size and the same molecular force fields, being distinguished only by some trivial property; otherwise some deviations from ideality would be expected. If we have a solution of this sort, placed in a temperature gradient, it is clear that the distribution of solute and solvent across the gradient will be uniform; that is, the mole fraction will be the same at all temperatures when the system has come to a steady state, because there is no reason for one kind of molecule to be preferred to the other at any temperature. Likewise, the heat of transport will

(1) Work supported by the Office of Naval Research.

(2) For reviews see (a) K. G. Denbigh, "Thermodynamics of the Steady State," John Wiley and Sons, New York, N. Y.; and (b) S. R. de Groot, "Thermodynamics of Irreversible Processes," Interscience Publishers, Inc., New York, N. Y., 1951. See also E. P. Wigner, *J. Chem. Phys.*, **22**, 1912 (1954); N. G. Van Kampen, *Physica*, **20**, 603 (1954).

(3) (a) K. Wirtz and J. W. Hiby, *Physik. Z.*, **44**, 369 (1943); (b) K. Wirtz, *Z. Naturforschung*, **3a**, 672 (1948); (c) I. Prigogine, L. de Brouckère and R. Amand, *Physica*, **16**, 577 (1950); (d) K. G. Denbigh, *Trans. Faraday Soc.*, **48**, 1 (1952); (e) K. F. Alexander, *Z. physik. Chem.* (Leipzig), **203**, 181 (1954); (f) L. Onsager and R. M. Fuoss, THIS JOURNAL, **36**, 2689 (1932); (g) R. B. Parlin, R. J. Marcus and H. Eyring, *Proc. Natl. Acad. Sci. U. S.*, **41**, 900 (1955).

be zero; for obviously, if solute molecules pass from one solution to another at constant temperature (due, say, to a small concentration gradient) no heat will be absorbed or evolved.

The preceding paragraph implies that the number of molecules crossing a given boundary in a concentration gradient at non-uniform temperature depends upon the mole fraction of a given constituent rather than upon the number of molecules per unit volume, since in general the density depends upon the temperature. The reason for this is that transfer actually involves exchange of molecules of both solvent and solute, transfer of solute in one direction being accompanied by transfer of solvent in the other, so that in the whole process of transfer there is no dissymmetry with respect to the density.

The conclusions drawn from an ideal solution can be carried over to other cases under special circumstances. When one has a very dilute solution of some solute in a solvent one has a situation which is essentially ideal with respect to solvent. The solute can be considered as a solvated entity. If the solvated complex is large enough (this requires practically only one or two layers of solvent molecules) the interaction with the solvent molecules outside the solvated complex is just the same as if only solvent molecules were inside the complex. Thus *if these complexes moved as a whole*, and if the solution were dilute enough so that they were never broken up, one should be able to make the same statement as before regarding the heat of transport and the behavior of this system in a temperature gradient. Usually, however, the situation will not be this simple, and we shall proceed at once to a more general formulation. In so doing, we shall also generalize our discussion to include multicomponent systems, but we shall assume that all the gradients of concentration and temperature occur along the same direction, thus avoiding vector interactions.

2. General Description of the Transport Processes

There have been various theories advanced in order to account quantitatively or semi-quantitatively for the magnitudes involved in various kinds of transfer. In one such theory, which may be described as the hole theory of transport[3a,b,c,d] and which is believed to be applicable in many instances, it is supposed that transfer occurs if there happens to be a hole adjacent to some molecule when this molecule simultaneously possesses sufficient energy to jump into the hole. Another example is the theory recently proposed[4] to explain the high conductivity of hydrogen ions in aqueous solutions, in which it is supposed that there is rotation of a water molecule followed by quantum-mechanical tunneling of the hydrogen atom.

In any such theory we see that the transfer of material results because a certain group of molecules in the solution is in a certain energy level. Let us call such a group of molecules in a particular energy level or a definitely defined group of energy levels involving a small energy range a transference or transport unit. We shall assume the energy levels to be sufficiently closely specified so that the probability of a particular exchange of molecules is very closely determined. We purposely leave the exact description of a transference unit vague, since it must depend on the circumstances, but we need to include in a unit a sufficient number of molecules so that its interaction with the rest of the solution is "average" and does not change when the transference process occurs. In other words, the transference process takes place *within* the transference unit. After the transfer process has occurred, it would be possible for the reverse process to take place. A transference unit which is the same as the original unit except that the reverse process can occur will be called the inverse unit. It will now be seen that the flux of any particular component arising from any particular transference unit will be proportional to the difference in concentration of the transference unit and its inverse.

A transference unit may be treated as a chemical species in or tending to equilibrium with its environment. Since it is large enough so that its interaction with the environment is on the average the same as that of that much of the environment itself, and since the concentration of any given transference unit if stringently enough defined is very low, we may assume that the chemical potential of the τth unit is given by

$$\mu_\tau = \mu_\tau^0 + RT' \ln c_\tau \qquad (2.1)$$

where c_τ is the concentration. The chemical potential of the inverse unit will be the same function of concentration as that of the direct unit[5]; there will be a difference between the concentrations of direct and inverse units because of the tendency of a transference unit to come to equilibrium with a specific component of the solution at that particular point (or points) in the gradient where this component actually occurs in the transference unit. Thus we make the assumption that there exists a given concentration and temperature and that the thermodynamic quantities can be defined at any point in the solution, and that the temperature and concentration gradients have a meaning even in the distance across a single transference unit. If a transference unit is not of macroscopic dimensions one might question whether there can be a definite temperature or concentration gradient across it, and of course these would have no meaning for a single transference unit. But temperature and concentration are statistical quantities, and when one considers the average effect over many similar units the idea does have significance. The assumptions regarding the equilibrium are, in my opinion, inherent in the assumption that the thermodynamic functions can be defined at any point in the solution. The procedure suggested here is applied in detail in Section 3. In a general way our hypothesis resembles the Thomson hypothesis, inasmuch as we apply thermodynamic considerations to the equilibrium even though irreversible processes are

(4) B. E. Conway, J. O'M. Bockris and H. Linton, *J. Chem. Phys.*, **24**, 834 (1956).

(5) Since this statement should be correct regardless of whether or not the activity of a transference unit is exactly the same as its concentration, as implied by eq. 2.1, and since a small change in activity will always be proportional to the corresponding change in concentration (so eq. 3.1 would hold with only a slight change in the meaning of λ_τ) all our conclusions would be unaltered if c_τ were interpreted as an activity instead of a concentration.

taking place, but it is applied here to elementary processes.

There may be some overlapping of different kinds of transference units, but this presumably will not matter, since we shall calculate the concentration of each kind of unit, and its effects, separately, then add all the effects together. The effects are in the nature of probabilities, which are thus assumed to be independent; but if they were not independent then those particular transference units would not have an independent existence, but would be part of a single larger unit, so overlapping would be automatically avoided.

3. Calculation of the Fluxes

Suppose that the transference process associated with the rth transference unit results in a transfer of the jth component equivalent to the advance of a molecule of this component through a distance a_{rj}. a_{rj} has the character of a moment; for example advancement of two molecules through a distance $a_{rj}/2$ would be equivalent to the advancement of a single one through a distance a_{rj}; we can refer to a_{rj} as the moment of transfer or transport. We shall denote the excess in the concentration of inverse transference units which have a moment $-a_{rj}$, over that of the direct unit by δc_r. The total flux of component j will then be given by

$$J_j = -\Sigma_r \lambda_r a_{rj} \delta c_r \qquad (3.1)$$

where λ_r is a proportionality constant equal to the probability of occurrence of the transfer process per unit time.

Our next task is to calculate δc_r. The inverse transference unit differs from the direct unit only in that certain molecules have changed position; its external portions are the same and so its interaction with the environment is the same. However, it may in general be expected to lie effectively at a slightly different temperature, depending upon where, on the average, it absorbs or rejects heat in the process of coming into equilibrium with its environment. Also, since some molecules change position in the transfer process, and since there is a concentration gradient, the inverse unit will be in equilibrium with molecules at slightly different concentrations from those in equilibrium with the direct unit. (We shall assume provisionally that the transference units are in equilibrium with the substrate, but will examine this assumption at the end of Section 4.)

Let us consider the entire molal free energy change

$$\Delta G_r = \mu_r - \Sigma_j n_{rj} \bar{\mu}_j \qquad (3.2)$$

when the separate molecules in the solution, with respective average chemical potentials $\bar{\mu}_j$, react to form the transference unit with chemical potential μ_r. The sum Σ_j goes over all components and there are n_{rj} molecules of component j in the unit. The free energy change for formation of the inverse unit will be $\Delta G_r + \delta\Delta G_r$. ΔG_r and $\Delta G_r + \delta\Delta G_r$ will be zero at equilibrium, assuming that the thermodynamic functions can be defined in the temperature and concentration gradients, and that the work-balance principle can be applied to find the state of equilibrium. Noting the thermodynamic relation for constant pressure and concentration, $\partial\Delta G/\partial T = -\Delta S$, we can write

$$\delta\Delta G_r = -\Delta S_r \delta T + (\delta\Delta G_r)_T = 0 \qquad (3.3)$$

The first term between equals signs takes care of the temperature gradient and the second term the concentration gradient, assuming constant pressure. The subscript T means T is held constant in the differentiation. When the direct transference unit is formed, the heat $T\Delta S_r$ is absorbed at average temperature T, and when the inverse unit is destroyed the heat is dissipated at average temperature $T + \delta T$. Every time the transference process occurs, therefore, the heat is transported through a distance equal to $\delta T/\text{grad } T$. Thus we can say that the moment of heat transport, Q_r, is given by

$$Q_r = T\Delta S_r(\delta T/\text{grad } T) \qquad (3.4)$$

For $(\delta\Delta G_r)_T$ we can write

$$(\delta\Delta G_r)_T = (\partial\mu_r/\partial c_r)_T \delta c_r - \Sigma_j n_{rj}(\delta\bar{\mu}_j)_T \qquad (3.5)$$

and from the definition of a_{rj} we see that

$$n_{rj}(\delta\bar{\mu}_j)_T = a_{rj}(\text{grad } \mu_j)_T \qquad (3.6)$$

We can now use (3.4), (3.5) and (3.6) in (3.3), and set $\partial\mu_r/\partial c_r = RT/c_r$ from eq. 21. We thus obtain

$$\delta c_r = (c_r/RT)[(Q_r/T) \text{ grad } T + \Sigma_j a_{rj}(\text{grad } \mu_j)_T] \qquad (3.7)$$

We now use (3.7) in (3.1) to get J_k (k being an alternative designation for the components)

$$J_k = -(RT)^{-1}\Sigma_r \lambda_r c_r a_{rk}(Q_r/T) \text{ grad } T - \Sigma_j L_{kj}(\text{grad } \mu_j)_T \qquad (3.8)$$

where

$$L_{kj} = (RT)^{-1} \Sigma_r \lambda_r c_r a_{rk} a_{rj} \qquad (3.9)$$

The summation Σ_r is to go over all transference units, but if the kth species is not included in any unit the coefficient a_{rk} will be zero. It is of interest to note that if there are no transference units with more than one of the a_{rk} different from zero (as is presumably the case in the hole transport mechanism considered by Wirtz and Hiby[3]), then $L_{kj} = 0$ unless $k = j$.

In analogy to eq. 3.1, but taking into account a heat-conduction term $-\Lambda$ grad T, we can write for the heat flux

$$J_q = -\Lambda \text{ grad } T - \Sigma_r \lambda_r Q_r \delta c_r \qquad (3.10)$$

Again using (3.7) we have

$$J_q = -(\Lambda T + L_{QQ}) T^{-1} \text{ grad } T - \Sigma_k Q_k L_{kk}(\text{grad } \mu_k)_T \qquad (3.11)$$

where

$$L_{QQ} = (RT)^{-1}\Sigma_r \lambda_r c_r Q_r^2 \qquad (3.12)$$

and

$$Q_k = (RT)^{-1}\Sigma_r \lambda_r c_r Q_r a_{rk}/L_{kk} \qquad (3.13)$$

We note that L_{QQ} is the expression which would be obtained from (3.9) for L_{kk}, except that Q_r is substituted for a_{rk}, and $Q_k L_{kk}$ would be obtained from L_{kj} if a_{rj} but not a_{rk} were replaced by Q_r; in other words, heat is much like a component. Q_k, according to its definition (3.13), is the heat of transport of species k at constant temperature, taking into account that part of the flow of k due to the gradient of its own potential. On account of the Gibbs–Duhem relation its own chemical potential could not be the

only one to have a gradient, but if this were possible we would have $Q_k = J_q/J_k$ under these circumstances.[6] If we compare the individual terms in the sum $(RT)^{-1}\Sigma_\tau \lambda_\tau c_\tau Q_\tau c_{\tau k}$ with the individual terms of the sum in (3.9) we see that the ratio is $Q_\tau/a_{\tau k}$, which can be interpreted as the heat of transfer of the transference unit τ referred to transfer of component k in unit τ, and Q_k is an average value.

4. Relation to Irreversible Thermodynamics

The phenomenological equations for the flow of matter and heat can be written[2]

$$\begin{aligned} J_k &= L_{kq}X_q + \Sigma_j L_{kj}X_j \\ J_q &= L_{qq}X_q + \Sigma_j L_{qj}X_j \end{aligned} \qquad (4.1)$$

Here the X's represent the forces, X_q being the force associated with the temperature gradient, while the others are associated with concentration gradients, and the L's are the phenomenological coefficients. The exact choice of the J's and the X's can vary somewhat[6] but they must be related to the rate of production of entropy per unit volume θ by

$$T\theta = \Sigma_k J_k X_k + J_q X_q \qquad (4.2)$$

and if (4.2) is satisfied, the Onsager reciprocal relations hold

$$L_{kj} = L_{jk} \qquad (4.3a)$$

$$L_{qk} = L_{kq} \qquad (4.3b)$$

Let us examine our results in the light of these general ideas. First we shall show that

$$T\theta = -J_q\, T^{-1} \text{ grad } T - \Sigma_k J_k (\text{grad } \mu_k)_T \qquad (4.4)$$

where the J's are defined as in Section 3. It is convenient to consider a volume of unit length and cross-section with uniform gradients of T and μ_k. Heat $-J_q$ per unit time[7] enters the unit volume from the thermostat at temperature T + grad T with loss of entropy of the thermostat equal to $-J_q/(T + \text{grad } T)$ and leaves the unit volume at temperature T with gain of entropy of the thermostat equal to $-J_q/T$; if grad T is small, the net gain is $-(J_q/T^2)$ grad T, which, if multiplied by T, is the first term of (4.4). There is no change in entropy of the unit volume itself due solely to uniform flow of heat (any non-uniformity will be taken care of in the next paragraph).

Let us now consider the entropy change which arises directly from flow of component k. As component k flows from one temperature to a slightly different one there will be additional absorption or rejection of heat, on account of the partial heat capacity of component k, but the gain or loss of entropy of the unit volume will exactly cancel that of the thermostat. However, besides this, there will be a change of entropy of component k, at a rate $J_k(\text{grad } \bar{s}_k)_T$ which would have occurred even if there were no change in temperature, and a change in entropy of the thermostat equal to $-J_k$ $(\text{grad } \bar{h}_k)_T/T$ (where $\bar{h}_k$ is the partial molal enthalpy), because this amount of heat would need to be taken from the thermostat in addition to that needed to take care of the partial heat capacity of component k (it does not matter if the heat is absorbed at T or T + grad T if grad T is small). The total contribution to $T\theta$ from transport of all components is thus

$$\Sigma_k [TJ_k(\text{grad } \bar{s}_k)_T - J_k (\text{grad } \bar{h}_k)_T] = -\Sigma_k J_k (\text{grad } \mu_k)_T$$

This is the last term in (4.4), which is thus verified. Therefore we can write

$$X_k = -(\text{grad } \mu_k)_T$$

and

$$X_q = -T^{-1} \text{ grad } T \qquad (4.5)$$

Comparing these with eq. 3.8 we see that the L_{kj} of Section 3 correspond to the L_{kj} of (4.1). Furthermore $L_{kj} = L_{jk}$, by eq. 3.9. Also, L_{kq}, L_{qk}, and L_{qq} of (4.1) can be expressed in terms of the quantities of (3.11) and (3.8) (compare eqs. 3.8 and 3.13) as

$$L_{qq} = \Lambda T + L_{QQ} \qquad (4.6)$$

and

$$L_{qk} = L_{kq} = Q_k L_{kk} \qquad (4.7)$$

We thus see that the reciprocal relations hold, and our formulation gives the laws of irreversible thermodynamics quite automatically. Equation 4.3a holds because the two a's which enter eq. 3.9 (one coming from the flow equation, eq. 3.1, and the other from eq. 3.7 which, in a sense, gives the force for a single type of transference unit) enter symmetrically. Equation 4.3b follows in just the same way, but Q_τ takes the place of one of the a's.

We have of course made the assumption that the transference units come to equilibrium in the particular way described. In so doing we have assumed either (1) that the transference process must be slow compared to formation and destruction of transference units by other means, or else (2) that the transference process is an integral part of the action by which equilibrium is maintained. The second assumption is not really self-consistent, and we shall now consider the possibility that neither of these assumptions is correct. In any event, the transference units should come to a steady state and we can write $\dot{c}_\tau = 0$ and $\dot{c}_\tau' = 0$, where the dot means time differentiation and the prime refers to the inverse unit. If complete equilibrium were established, the rate of formation and destruction of transference units would be $a_\tau c_{\tau,\text{eq.}}$, where a_τ is a constant.[7a] If equilibrium is slightly disturbed by the transference process the rate of formation from the substrate will still be $a_\tau c_{\tau,\text{eq.}}$ (except possibly for a term proportional to $c_{\tau,\text{eq.}} - c_\tau$, which would not affect the results), but the rate of destruction will be $a_\tau c_\tau$, and the net rate of change of concentration due to transference (*i.e.*, from transformation into and from the inverse unit) will be $\lambda_\tau(c_\tau' - c_\tau)$. Thus

$$\dot{c}_\tau = a_\tau c_{\tau,\text{eq.}} - a_\tau c_\tau + \lambda_\tau(c_\tau' - c_\tau) = 0 \qquad (4.8)$$

(6) Our heats of transport do not include transported enthalpy, but refer strictly to the part of the energy which will be transferred to or from a thermostat when there is any accumulation of material at some point in space. (See *e.g.*, ref. 2a, p. 14; ref. 2b, p. 124). They have sometimes been called "reduced heat flows." Because of their use, our formulas will differ from those of de Groot by some enthalpy terms.

(7) We would call J_q positive if the flow were in the same direction as grad T; actually the flow is in the opposite direction, so the flux $-J_q$ enters the unit volume at the higher temperature T + grad T.

(7a) The constant may of course depend upon the temperature and the concentrations of the components; the probability of "reaction" of a given transference unit is independent of other like units (their concentration being small) but dependent on the general environment.

and

$$\dot{c}_\tau' = a_\tau' c_{\tau,\mathrm{eq}}' - a_\tau' c_\tau' + \lambda_\tau(c_\tau - c_\tau') = 0 \quad (4.9)$$

Solving for $\delta c_\tau' = c_\tau' - c_\tau$ we obtain

$$\delta c_\tau = [a_\tau a_\tau'/(a_\tau a_\tau' + \lambda_\tau a_\tau + \lambda_\tau a_\tau')]\delta c_{\tau,\mathrm{eq}} \quad (4.10)$$

which shows that δc_τ is proportional to $\delta c_{\tau,\mathrm{eq}}$. The proportionality constant can simply be absorbed into the λ_τ in eq. 3.1 and 3.10 and δc_τ treated as though it were $\delta c_{\tau,\mathrm{eq}}$. Everything will then go through as before.

We might, however, imagine a more complicated situation, for a transference unit might be able to take part in several transference processes, having thus several inverses. This would be allowed for by putting one term for each such *process* in (3.1) and (3.10). This means that the sum becomes a sum over what may be designated as coupled pairs of transference units. For each such pair there will be one δc_τ, but there will be some overlapping of the separate c_τ and c_τ'. Thus if the coupled pairs τ and σ have their direct units in common (in which case we shall say they "overlap" on their direct units), $c_\sigma \equiv c_\tau$.

If we have to consider a steady state instead of an equilibrium we must then attempt to express the δc_τ as linear functions of the $\delta c_{\tau,\mathrm{eq}}$. Suppose we have

$$\lambda_\tau \delta c_\tau = \Sigma_\sigma g_{\tau\sigma}\delta c_{\sigma,\mathrm{eq}} \quad (4.11)$$

Then (3.1) will become

$$J_j = -\Sigma_\tau \Sigma_\sigma a_{\tau j} g_{\tau\sigma}\delta c_{\sigma,\mathrm{eq}} \quad (4.12)$$

As we have noted previously, heat acts like another component (aside from the conduction term, $-\Lambda$ grad T, which we can neglect here), and we will not need to consider it explicitly. With this understanding we can use eq. 3.7 for $\delta c_{\sigma,\mathrm{eq}}$ and obtain

$$J_j = -(RT)^{-1} \Sigma_\tau \Sigma_\sigma \Sigma_k c_{\sigma,\mathrm{eq}} a_{\tau j} g_{\tau\sigma} a_{\sigma k} (\mathrm{grad}\ \mu_k)_T \quad (4.13)$$

where one of the $a_{\sigma k}$ stands for Q_σ and one of the $(\mathrm{grad}\ \mu_k)_T$ stands for T^{-1} grad T. We see that

$$L_{jk} = -(RT)^{-1} \Sigma_\tau \Sigma_\sigma c_{\sigma,\mathrm{eq}} a_{\tau j} g_{\tau\sigma} a_{\sigma k} \quad (4.14)$$

and, similarly

$$L_{kj} = -(RT)^{-1} \Sigma_\tau \Sigma_\sigma c_{\sigma,\mathrm{eq}} a_{\tau k} g_{\tau\sigma} a_{\sigma j} = -(RT)^{-1} \Sigma_\tau \Sigma_\sigma c_{\tau,\mathrm{eq}} a_{\sigma k} g_{\sigma\tau} a_{\tau j} \quad (4.15)$$

If $g_{\tau\sigma} \neq 0$, $c_{\tau,\mathrm{eq}}$ and $c_{\sigma,\mathrm{eq}}$ are concentrations of transference units which can, at least indirectly, go over into each other, and hence $c_{\tau,\mathrm{eq}} = c_{\sigma,\mathrm{eq}}$. Thus $L_{jk} = L_{kj}$ provided $g_{\tau\sigma} = g_{\sigma\tau}$. To find out whether this is true or not we set up more general equations like (4.8) and (4.9)

$$\dot{c}_\tau = a_\tau c_{\tau,\mathrm{eq}} - a_\tau c_\tau + \lambda_\tau(c_\tau' - c_\tau) + \Sigma_\sigma' \lambda_\sigma b_{\sigma\tau}(c_\sigma' - c_\tau) = 0 \quad (4.16)$$

$$\dot{c}_\tau' = a_\tau' c_{\tau,\mathrm{eq}}' - a_\tau' c_\tau' + \lambda_\tau(c_\tau - c_\tau') + \Sigma_\rho' \lambda_\rho b_{\rho\tau}'(c_\rho - c_\tau') = 0 \quad (4.17)$$

In these equations the subscript τ refers to a particular coupled pair, the inverse unit being indicated by primes. The summation Σ_σ' or Σ_ρ' is over all other coupled pairs. If a particular coupled pair does not overlap with τ on the direct unit of τ then $b_{\sigma\tau} = 0$; if such overlapping does occur $b_{\sigma\tau} = 1$. Considering the common unit to be the direct one for σ also, $c_\sigma \equiv c_\tau$ and we have written $c_\sigma' - c_\tau$ in the equation; $c_\sigma' - c_\tau = \delta c_\sigma$. Similarly $b_{\rho\tau}' = 0$ or 1. In the latter case the common unit is considered to be the inverse unit in each case; we have $c_\rho' \equiv c_\tau'$ and we have written $c_\rho - c_\tau'$, which is $-\delta c_\rho$, in the equation. Dividing (4.16) by a_τ and (4.17) by a_τ' and subtracting one from the other, we find

$$\delta c_{\tau,\mathrm{eq}} = (\lambda_\tau^{-1} + a_\tau^{-1} + a_\tau'^{-1})\lambda_\tau \delta c_\tau + \Sigma_\sigma'(b_{\sigma\tau}/a_\tau)\lambda_\sigma \delta c_\sigma + \Sigma_\rho'(b_{\rho\tau}'/a_\tau')\lambda_\rho \delta c_\rho \quad (4.18)$$

We note that if we pick out a term in the first sum and one in the second such that $\sigma \equiv \rho$, then the corresponding $b_{\sigma\tau}$ and $b_{\rho\tau}'$ cannot both be equal to 1, so we may write

$$\delta c_{\tau,\mathrm{eq}} = g_{\tau\tau}^{-1}\lambda_\tau \delta c_\tau + \Sigma_\sigma' g_{\tau\sigma}^{-1}\lambda_\sigma \delta c_\sigma + \Sigma_\rho' g_{\tau\rho}^{-1}\lambda_\rho \delta c_\rho \quad (4.19)$$

where the g^{-1} are elements of the inverse of the matrix defined in eq. 4.11 except that if $g_{\tau\sigma}^{-1} \neq 0$, $g_{\tau\rho}^{-1} = 0$ if $\sigma \equiv \rho$, and conversely. We see that $g_{\tau\sigma}^{-1} = a_\tau^{-1}$ or 0 and $g_{\tau\rho}^{-1} = a_\tau'^{-1}$ or 0. Now let us consider another δc_{eq}, say $\delta c_{\xi,\mathrm{eq}}$

$$\delta c_{\xi,\mathrm{eq}} = g_{\xi\xi}^{-1}\lambda_\xi \delta c_\xi + \Sigma_\sigma' g_{\xi\sigma}^{-1}\lambda_\sigma \delta c_\sigma + \Sigma_\rho' g_{\xi\rho}^{-1}\lambda_\rho \delta c_\rho \quad (4.20)$$

where $g_{\xi\sigma}^{-1} = a_\xi^{-1}$ or 0 and $g_{\xi\rho}^{-1} = a_\xi'^{-1}$ or 0. We now consider several possibilities.

1. The pairs τ and ξ do not overlap. Then $g_{\xi\tau}^{-1} = g_{\tau\xi}^{-1} = 0$.

2. The pairs τ and ξ overlap on the direct unit. Then $g_{\tau\xi}^{-1}$ is to be found among the $g_{\tau\sigma}^{-1}$ in (4.19) and $g_{\xi\tau}^{-1}$ is to be found among the $g_{\xi\sigma}^{-1}$ in (4.20). But clearly in this case, since the direct unit τ is identical with the direct unit ξ, $a_\tau = a_\xi$. Hence $g_{\tau\xi}^{-1} = g_{\xi\tau}^{-1}$.

3. The pairs τ and ξ overlap on the inverse unit. Then $g_{\tau\xi}^{-1}$ is found among the $g_{\tau\rho}^{-1}$ in (4.19) and $g_{\xi\tau}^{-1}$ among the $g_{\xi\rho}^{-1}$ in (4.20). Again $a_\tau' = a_\xi'$ and $g_{\tau\xi}^{-1} = g_{\xi\tau}^{-1}$.

The matrix of the inverse transformation of (4.11) being symmetrical, the transformation itself must be, and the reciprocal relations hold. Thus we need to assume only that the equilibrium between transference units and substrate would be established in the way described in Sections 2 and 3 by processes involving no net transfer of matter and of heat. One might question whether such processes actually exist, inasmuch as any transference unit has special properties both with respect to the positions of the molecules and the amount of energy it contains; however, by net transfer we refer only to the result of motions along the gradients, and motions normal thereto will also occur. Along with processes involving no net transfer we will also have to include in the first terms of (4.16) and (4.17) any random transference processes involving transference units which are distinct in composition and energy from those which are coupled, but which happen to overlap with them in a trivial or random way, as explained at the end of Section 2. We include here as overlapping pairs only such as are essentially connected with respect to the transference processes. Otherwise we could not set $c_{\tau,\mathrm{eq}} = c_{\sigma,\mathrm{eq}}$ in eq. 4.14 and 4.15. Nevertheless, the consideration of the steady state offers a worthwhile generalization.

The original derivation of the reciprocal relations[2] was based on the law of microscopic reversibility, and it is of interest to note that this law is in-

volved in our deduction. For it is essential to our argument that the rate of a transfer process should, at true equilibrium, exactly balance the rate of the inverse process. The linear character of the phenomenological relations follows from the linear dependence of the elementary processes on the δc_r. Another familiar element in the usual discussion of irreversible thermodynamics is also present here, namely, the consideration of fluctuations, for a transference unit is actually a fluctuation of a special type. One of the advantages of our procedure is that it brings out clearly the relation of the fluctuations to the macroscopic process.

The law of microscopic reversibility applies directly only to the equilibrium situation. If a steady state in which the J_k's are zero is set up under a system of gradients, it clearly does not mean that the contribution to the flux arising from each kind of transference unit (*i.e.*, from each term in the sum of eq. 3.1) vanishes separately.[8] It simply means that there is as much flux in one direction as in the other, and the result of net zero flux arises from a certain kind of cyclic process in which the flux in one direction, arising from certain energy levels, cancels the flux in the other direction, arising from other levels. Since each type of transference unit has its own characteristic moment of heat transport Q_r, not necessarily directly related to the moment of transport a_{rk}, there can be a net flow of heat due to flow of component k even when $J_k = 0$. An expression for this heat flow will be given in Section 5.

5. The Soret Effect

Strictly, since we have shown that the kinetic formulation yields the reciprocal relations, this is all that is necessary, as we now know that the equations for the special effects can be obtained. However, it will be of some interest to see their relation to the quantities which are defined in terms of the kinetic picture.

If we maintain a temperature gradient and allow the concentration gradients to adjust themselves as the flows proceed we arrive at a steady state in which, finally, all the J_k will be zero. Remarking that

$$(\text{grad } \mu_j)_T = \Sigma_l'(\partial\mu_j/\partial x_l) \text{ grad } x_l \qquad (5.1)$$

where the summation Σ_l' goes over all x_l but one, since they are not all independent, we can set $J_k = 0$ in eq. 3.8, use eq. 3.13, and obtain

$$(Q_k/T) + \Sigma_l'(\partial\mu_k/\partial x_l)\, dx_l/dT + \Sigma_{j(j\neq k)}\Sigma_l'(L_{kj}/L_{kk})(\partial\mu_j/\partial x_l)\, dx_l/dT = 0 \qquad (5.2)$$

Equation 5.2 is the equation for the Soret effect, but is not quite in its usual form. This is because the Q_k overlap to some extent, and any transference unit which involves the transfer of more than one component will contribute to the Q_k of all of them, as is readily seen from eq. 3.13.

We can define another set of heats of transfer, Q_j^*, which avoid the overlapping but are not as readily interpreted in terms of a sum over transference units, by the equation[9]

$$J_q = \Sigma_j Q_j^* J_j, \text{ for grad } T = 0 \qquad (5.3)$$

(8) See J. Meixner, *Ann. Physik*, **43**, 244 (esp. p. 258) (1943).

(9) See ref. 2b, pp. 112, ff.

Using (3.8) with grad $T = 0$, this gives

$$J_q = -\Sigma_j\Sigma_k Q_j^* L_{jk}(\text{grad } \mu_k)_T \qquad (5.4)$$

Comparing coefficients of $(\text{grad } \mu_k)_T$ in (3.11) and (5.4)

$$Q_k L_{kk} = \Sigma_j Q_j^* L_{jk} \qquad (5.5)$$

Using eq. 5.5 with eq. 3.13 in eq. 3.8

$$J_k = -\Sigma_j Q_j^* L_{jk} T^{-1} \text{ grad } T - \Sigma_j L_{kj}(\text{grad } \mu_j)_T \qquad (5.6)$$

Since we have shown that $L_{jk} = L_{kj}$, it can be seen that $J_k = 0$ if

$$(Q_j^*/T) \text{ grad } T + (\text{grad } \mu_j)_T = 0 \qquad (5.7)$$

or

$$Q_j^*/T + \Sigma_k(\partial\mu_j/\partial x_k)\, dx_k/dT = 0 \qquad (5.8)$$

which is the expression generally given for the Soret effect. It can also be shown that this is the only solution. If we set $-(Q_j^*/T)$ grad $T - (\text{grad } \mu_j)_T = y_j$, eq. 5.6 can be written $J_k = \Sigma_j L_{jk} y_j$. The general condition that such a set of equations have a solution is that the determinant of the L_{jk} not vanish; then the only solution for all $J_k = 0$ is $y_j = 0$.

As we have noted, when J_k is equal to zero this may be only because the amount of component k transported in one direction is equal to that transported in the other. Since that transported in one direction may carry a different amount of heat than that transported in the opposite direction, the contribution to J_q from the Q_k or Q_k^* may not vanish. An interesting formula for the value of J_q at the Soret steady state is obtained by substituting eq. 5.7 into eq. 3.11. This gives

$$J_q = -(\Lambda T + L_{QQ} - \Sigma_k Q_k Q_k^* L_{kk})T^{-1} \text{ grad } T \qquad (5.9)$$

It has been noted previously that the expression for J_q under the condition that all $J_k = 0$ involves coefficients other than L_{qq}, and the quantity multiplying grad T in (5.9) has been identified with the thermal conductivity[10]; however the interpretation in terms of the cyclic flow of matter and, in particular, the interpretation of the various quantities involved through eq. 3.9, 3.12, 3.13 (or 4.14) and 5.5 have apparently not been given.

6. Equations for Charged Particles

Systems with charged particles differ from those that we have already considered in that there is a condition on the concentrations, in order to maintain all parts of the system neutral. Actually there is a slight separation of positive and negative charges where gradients exist, which results in the production of a potential. However, the differences in concentration are so small that they do not need to be considered explicitly. We will take care of the resultant electrical potential ϕ by writing for the chemical potential μ_j of ion species j

$$\mu_j = \zeta_j + z_j e\phi F \qquad (6.1)$$

ζ_j is the value the chemical potential would have if the particle were uncharged, z_j is the valence (which may be positive or negative), $z_j e$ being the charge on the particle, and F is a conversion factor. Some objections have been expressed to this method of dividing the chemical potential explicitly into

(10) See ref. 2a, p. 76.

electrical and non-electrical parts,[11] but for a kinetic theory it seems entirely adequate.

The condition of electrical neutrality is

$$\Sigma_j \nu_j z_j = 0 \qquad (6.2)$$

where ν_j is the number of moles of the jth ion per mole of electrolyte.

At the Soret steady state for a strong electrolyte we again have $J_j = 0$ for all species of particle. We apply eq. 5.7 to the jth ion, using eq. 6.1, multiply by ν_j, and add over all species of ion. The term grad ϕ will have as a factor $\Sigma_j \nu_j z_j$, which vanishes, so finally we obtain

$$(\Sigma_j \nu_j Q_j^*/T) \text{ grad } T + (\text{grad } \Sigma_j \nu_j \zeta_j)_T = 0 \qquad (6.3)$$

Now $\Sigma_j \nu_j Q_j^*/T$ is the heat of transfer of the salt and $\Sigma_j \nu_j \zeta_j$ is the chemical potential of the salt. Thus eq. 6.3 actually says that (5.7), or (5.8), holds for a dissociated salt just as for any other type of component.

To get ϕ we go through the same process, except that we subtract the terms for the negative ions from the terms for the positive ones. Noting that $\Sigma_j{}^+ \nu_j z_j = -\Sigma_j{}^- \nu_j z_j$ we obtain

$$\begin{aligned} 2\Sigma_i{}^+ \nu_i z_i eF \text{ grad } \phi \\ = (\Sigma_i{}^- \nu_i Q_i^* - \Sigma_i{}^+ \nu_i Q_i^*) T^{-1} \text{ grad } T \\ + [\Sigma_i{}^- \nu_i \text{ grad } \zeta_i - \Sigma_i{}^+ \nu_i \text{ grad } \zeta_i]_T \end{aligned} \qquad (6.4)$$

which gives grad ϕ in terms of the heats of transfer and chemical potentials of the individual ions.

In the case of a thermocell we have a junction at which there is a temperature gradient but no concentration gradient. Thus in this case grad $\zeta = 0$ for each ion and for the solvent grad $\mu = 0$. We cannot set $J_k = 0$, but the condition of neutrality when no current is taken from the system demands that $\Sigma_k z_k J_k = 0$, where the sum extends over all ions. We thus find from (5.6)

$$\begin{aligned} 0 = \Sigma_k \Sigma_j z_k Q_j^* L_{jk} T^{-1} \text{ grad } T \\ + \Sigma_k \Sigma_j z_k L_{kj} z_j eF \text{ grad } \phi \end{aligned} \qquad (6.5)$$

where the sum Σ_k extends over all ions but the sum Σ_j includes the solvent in the first term. If grad T and all concentration gradients were zero, but the system were in an applied electric field, we would have

$$J_k = \Sigma_j L_{kj} z_j eF \text{ grad } \phi \qquad (6.6)$$

where in this case Σ_j goes only over the ions since $z_j = 0$ for the solvent. We see that $z_k \Sigma_j L_{kj} z_j$ is proportional to t_k the transference number of the kth ion, and eq. 6.5 becomes, exchanging j and k in the first term and noting that $\Sigma_k t_k = 1$ in the last

$$0 = [\Sigma_k (t_k/z_k) Q_k^* + t_0 Q_0^*] T^{-1} \text{ grad } T + eF \text{ grad } \phi \qquad (6.7)$$

We have used the subscript zero to indicate the solvent; t_0 is defined by the relation $t_0 = (t_j/z_j) J_0/J_j$ for grad T and all grad ζ_j equal to zero, and may be called the transference number of the solvent.[12] The quantities t_k/z_k and t_0 are proportional to the molal flows J_k and J_0. The velocities of flow are proportional to J_k/x_k and J_0/x_0, where the x's are the mole fractions. Thus the velocity of ion k with respect to the solvent will be proportional to $J_k/x_k - J_0/x_0$ and the rate of flow relative to the solvent will be

$$J_k(J_k/x_k - J_0/x_0)/(J_k/x_k) = J_k - J_0 x_k/x_0 \qquad (6.8)$$

Now we note from the Gibbs-Duhem relation, since eq. 5.7 can hold for all j, that

$$\Sigma_j x_j Q_j^* = 0 \qquad (6.9)$$

where Σ_j includes the solvent. This relation has been discussed by Denbigh.[3d] Therefore

$$Q_0^* = -\Sigma_k (x_k/x_0) Q_k^* \qquad (6.10)$$

and so eq. 6.7 becomes

$$0 = \Sigma_k (t_k^*/z_k) Q_k^* T^{-1} \text{ grad } T + eF \text{ grad } \phi \qquad (6.11)$$

where

$$t_k^*/z_k = t_k/z_k - t_0 x_k/x_0 \qquad (6.12)$$

By eq. 6.8 and the discussion preceding it, t_k^* is the transference number with respect to solvent. Equation 6.11 is the equation originally derived by Eastman.[13] It was also derived by de Groot[14] on the basis of the Onsager reciprocal relations, a derivation which is not fundamentally different from that given here; but since the reduction to motion relative to the solvent was made at an earlier stage de Groot did not go through (6.7).

There have been various efforts to estimate heats of transport, but the results are not entirely in accord.[13,15] If reliable results for them can be obtained, it is clear that they will be quite useful in making inferences concerning the mechanism of the transference process, especially when taken in conjunction with the temperature coefficient of the equivalent conductance. In view of the uncertainties, however, we will confine our comments to some remarks on the heats of transfer of OH^- and H^+.

The OH^- ion, according to Goodrich, *et al.* (and in this case, the Soret coefficient of KOH agrees reasonably well), has a heat of transport of roughly 4500 cal. per mole (the entropy of transport actually given by them seems to be in error by a factor of ten). If, as seems likely, this is correct at least as far as the sign is concerned, it indicates that heat must move in the same direction as the ion, and in fact farther than the ion, since the activation energy for conductance is only about 3100 cal. per mole.[16] This would seem to be evidence against a mechanism[4] in which a water molecule near the OH^- undergoes a rotation, a proton then jumping from the water molecule to the OH^-. The OH^- ion would then appear to move into the rotating water molecule, and this would presumably be followed by adjustment to the environment through rotation of the newly formed water molecule behind the new OH^-. Since its rotation requires an activation energy heat would move in the wrong direction. On the other hand, the OH^- itself might be the rotating element.

If Eastman's[13] original positive value for the heat of transfer of H^+ is correct, this is similarly evidence against a mechanism in which an H_2O molecule rotates ahead of the H_3O^+ ion which is to transfer the proton.

(11) E. A. Guggenheim, THIS JOURNAL, **33**, 842 (1929).

(12) See H. A. Hartung, Thesis, University of North Carolina, Chapel Hill, p. 157.

(13) E. D. Eastman, *J. Am. Chem. Soc.*, **50**, 292 (1928).

(14) Ref. 2b, pp. 133, ff.

(15) J. G. Goodrich, F. M. Goyan, E. E. Morse, R. G. Preston and M. B. Young, *J. Am. Chem. Soc.*, **72**, 4411 (1950); H. J. V. Tyrrell and G. L. Hollis, *ibid.*, **73**, 2402 (1951); ref. 12, pp. 79 ff, 113, 147.

(16) G. Milazzo, "Elektrochemie," Springer-Verlag, Vienna, 1952, p. 43.

7. Relation of the Fluxes to the Surroundings

Although, as noted, the deduction of eq. 6.11 from eq. 5.7 is not in principle different from de Groot's derivation of (6.11), it is of some interest since it shows how the fluxes which originally came out of the use of the transference units are related to the fluxes of solute with respect to solvent. Actually our original fluxes are fluxes with respect to the transference units. Since the transference units are large enough to have an average interaction with the substrate, they must all have the same average motion and must effectively move with the molecular structure of the substrate. This is a somewhat hazy concept, to be sure, but one which has been discussed previously by Alexander.[3e] It is certainly precise enough to handle steady states, where all the fluxes vanish, and it is always possible by a linear transformation to reduce the fluxes to fluxes with respect to a particular component. In such a transformation the Onsager reciprocal relations are preserved.[17]

8. Heterogeneous Systems

There has been much interest in the steady state for systems in which there are two reservoirs at different temperatures, these being separated by a membrane of some kind. In such a case the temperature gradient occurs in the membrane, and eq. 5.7 holds for the material within the membrane. Let the temperature on one side of the membrane be T and on the other side be $T + dT$. From $(\partial\mu_j/\partial T)_{x_k} = -\bar{s}_j$ and (5.7) we can write

$$d\mu_j = -\bar{s}_j dT - (Q_j^*/T)\, dT \qquad (8.1)$$

In the solutions outside the membrane we may write

$$d\mu_{j,0} = -\bar{s}_{j,0} dT + \Sigma_k'(\partial\mu_{j,0}/\partial x_{k,0})_T dx_{k,0} + \bar{v}_{j,0} dp \qquad (8.2)$$

where Σ_k' goes over all components but one, where the subscript zero indicates a quantity in the solution, and where we have also allowed for the possibility that the membrane can sustain a difference in pressure, dp. Equating $d\mu_j$ and $d\mu_{j,0}$, since in a steady state the component will be in equilibrium inside and outside the membrane[18,19]

$$(\bar{s}_j - \bar{s}_{j,0} + Q_j^*/T)\, dT + \Sigma_k'(\partial\mu_{j,0}/\partial x_{k,0})_T\, dx_{k,0} + \bar{v}_{j,0}\, dp = 0 \qquad (8.3)$$

Now $(\bar{s}_j - \bar{s}_{j,0})T$ is the heat absorbed when one mole of component j is removed from the solution and enters the membrane at equilibrium. It can therefore be considered to be a contribution to the heat of transport. If we write $Q_{j,0}$ for the total heat of transport (8.3) can be written

$$(Q_{j,0}/T)dT + \Sigma_k'(\partial\mu_{j,0}/\partial x_{k,0})_T\, dx_{k,0} + \bar{v}_{j,0}dp = 0 \qquad (8.4)$$

If there is only one component the summation does not occur and we have the well-known equation

$$(Q_0/T)\, dT + v_0\, dp = 0 \qquad (8.5)$$

The application of (8.5) to the Knudsen flow of an ideal gas through a porous plug is especially interesting. The chemical potential of the gas outside the porous plug is $e_0 + p_0v_0 - Ts_0$ where e_0 is the molal energy. Inside the porous plug the gas is effectively "dissolved" since a gas molecule makes many collisions with the wall compared to the collisions with other molecules, and the chemical potential is $\bar{e} + p\bar{v} - T\bar{s}$. If the porous plug does not interact with the gas, $\bar{e} = e_0$, but we will have $\bar{v} = 0$, since addition of gas does not affect the total volume. Hence at equilibrium $p_0v_0 - Ts_0 = -T\bar{s}$, or for an ideal gas, $T(\bar{s} - s_0) = -RT$. On the other hand, the heat of transport within the plug is equal to $+{}^1/_2\,RT$, because the molecules which cross any point in a pore in the porous plug have an average energy ${}^1/_2\,RT$ larger than that of all the molecules.[20] Thus $Q_0 = -{}^1/_2\,RT$, which gives the usual result for the Knudsen flow.

(17) Ref. 2b, Chapter XI.

(18) See S. Weller, *Nature*, **165**, 199 (1950); K. G. Denbigh and G. Raumann, *ibid.*, **165**, 200 (1950); *Proc. Roy. Soc.* (*London*), **A210**, 377 (1951). Our treatment is a generalization of Denbigh and Raumann.

(19) The effect of pressure is generally negligible except for gases. Any effect of the pressure gradient *within* the membrane could be taken into account, but will be neglected.

(20) O. K. Rice, *Phys. Rev.*, **89**, 793 (1953).

THERMOLUMINESCENCE STUDIES OF ALUMINUM OXIDE[1]

BY JAMES K. RIEKE AND FARRINGTON DANIELS

Contribution from the Department of Chemistry, University of Wisconsin, Madison, Wisconsin

Received December 3, 1956

Gamma-ray induced thermoluminescence of aluminum oxides depends on the extent of hydration and the crystal form produced by different calcining treatments. A peak at 236° depends on sodium impurity. Surface thermoluminescence can be induced by visible light in partially hydrated alumina.

The influence of structure and impurities on the thermoluminescence glow curves of aluminum oxides was the object of this investigation. It is part of a broader program in this Laboratory in which an attempt has been made to understand better the factors which determine the thermoluminescence of crystals and to find chemical applications for this phenomenon. These glow curves may have a bearing on the catalytic behavior of aluminum oxides.

(1) Adapted from a portion of a Ph.D. thesis by James K. Rieke, filed in the University of Wisconsin Library, 1954.

Experimental

Thirty samples of aluminum oxide, representing various crystal phases, degrees of hydration and chemical purity have been studied. They were prepared and characterized by Dr. Allen S. Russell of the Aluminum Company of America and kindly given to us for this investigation. In general, the samples were crystalline powders ranging in size from 5 to 100 mesh. The samples were ground uniformly to pass a 100 mesh screen and be retained on a 200 mesh screen.

TABLE I

DESCRIPTIONS OF Al_2O_3 SAMPLES

Sample No.	Name[1,4]	Description	Purity
1	α-Alumina trihydrate	Monoclinic, from Na_3AlO_3 (Bayer)	0.38% Na_2O
2	β-Alumina trihydrate	Monoclinic, rapid ppt. with CO_2 at 40° from Na_3AlO_3	0.28% Na_2O
3	α-Alumina monohydrate	Digested no. 1 with H_2O at 200°	
5	High purity, α-monohydrate	Orthorhombic, hydrolyzing pure Al isopropoxide	<0.10% impurity
6	Alcoa, Alumina A-1	Calcined no. 1 at 1100°	0.5% Na_2O
7	Alcoa alumina A-14 (porous alpha)	Calcined hydrate	0.04% Na_2O
8	Alcoa alumina F-10	Catalyst support, 120 m.²/g.	0.1% Na_2O
9	Alcoa alumina T-61	Highly calcined hydrate	0.02% Na_2O
10	χ-Al_2O_3	Cubic (not spinel), calcined 600°	
11	γ-Al_2O_3	No. 1 calcined at 700°	
12	ϵ-Al_2O_3	Cubic (spinel), no. 2 calcined at 800°[c]	
13	δ-Al_2O_3	Orthorhombic, no. 1 calcined at 900° in steam, almost anhydrous	
14	θ-Al_2O_3	Hexagonal, no. 2 calcined at 1000° in steam	
15	κ-Al_2O_3	Orthorhombic, no. 8 calcined at 850° in steam	
16	α-Al_2O_3	Hexagonal, no. 8 calcined at 1000° in steam, anhydrous	
31	Sapphire	Powder fused in electric arc	

γ-Irradiation of about 145,000 roentgens was accomplished by exposure of 1-gram samples in gelatine capsules to a cobalt-60 source.[2] The samples were placed in glass containers and stored on Dry Ice until their thermoluminescence glow curves were determined. The thermoluminescence apparatus of improved design is described elsewhere.[3] The samples were heated at the rate of 25° per minute to 450° and the intensity of emitted light recorded.

Effect of Light.—In this investigation it was first found that thermoluminescence in crystals sometimes occurs without previous exposure to γ-rays or other high energy radiation. For studying this phenomenon samples of aluminum oxide powder were placed in the thermoluminescence apparatus (without previous exposure to γ-radiation) and heated to between 350 and 400° until the emission of light practically ceased. These "drained" samples were then cooled in the dark in a desiccator evacuated to 0.1 mm. of mercury. Repeated heating and cooling failed to activate the aluminum oxide to give thermoluminescence, but exposure to the light of the room or to a AH-4 mercury lamp did activate the samples so that they exhibited glow curves when heated in the thermoluminescence apparatus. A beam of light from the mercury lamp was focussed through the thick Pyrex desiccator and onto the sample. After such an exposure the sample exhibited thermoluminescence glow curves with broad maxima around 350°. Visual observation showed that the thermoluminescence light is pale blue or blue-green. In some cases, the light was emitted for as long as ten minutes when kept at 370°. In other experiments, before exposing to the light, the drained samples were exposed to water vapor in the desiccator at 1 mm. and at 15 mm.

Description of Aluminum Oxides.—The thirty samples are described in Tables I and II.

Samples 17 to 30 were prepared from monoclinic alumina trihydrate, $Al_2O_3 \cdot 3H_2O$, by calcining under conditions recorded in the tables which follow.

Results

Typical examples of glow curves are shown in Figs. 1–3 from the thirty curves which are available. These curves have been corrected for dark current with shutters at periodic intervals and for black body radiation using an empty dish. In these figures the light intensity of the actual experiments measured with the photomultiplier cell, has been reduced by a suitable factor so as to get all the curves on a comparable scale. The reduction factor is labeled on each curve. Thus, in sample 22 of Fig. 3, the relative intensity of the low temperature peak is 4 × 10 or 40, whereas the high temperature peak is 31 × 40 or 1240. The areas under the various peaks of the original glow curves were measured with a planimeter. Different determinations of area for a given material agreed within about 10%.

γ-Ray Induced Thermoluminescence.—Thermoluminescence glow curves are produced after irradiation with γ-rays for nearly all samples of aluminum oxide, but the intensity of light and the peak temperatures at which maxima occur, vary greatly. The quantity of light emitted generally increases as the degree of calcination increases from the lower hydrates through α-alumina and is greatest for synthetic sapphire, made in an electric arc, which is highly crystalline α-alumina.

All the thermoluminescence peaks are found to lie in one of four temperature ranges; 103 ± 5°, 123 ± 5°, 164 ± 5° and 236 ± 5°. The 103 and 123° peaks do not usually occur together in the same sample. The thermoluminescence behavior is recorded in Table II.

Light-induced Thermoluminescence.—Thermoluminescence sometimes occurred without previous exposure to γ-radiation as already described. This phenomenon was observed in the hydrated or partially hydrated aluminas and did not occur in the highly calcined samples or the sapphire. Several experiments were carried out with sample 22 which had been heated to 220° for two hours and originally consisted of a mixture of α-trihydrate and α-monohydrate. The material was heated to 370° for varying periods of time to convert more of the trihydrate to monohydrate and then exposed to the light for varying periods of time before obtaining the thermoluminescence glow curves. The results are recorded in Table III.

Similar experiments were carried out with sample 20 which also showed light induced thermoluminescence except that after calcining at 370° the aluminum oxide was exposed to water vapor for 160 minutes and then exposed to the light for 130 minutes. The blank run without water vapor gave a light induced thermoluminescence area of 15.0 (square inches on the chart) whereas the one with

(2) D. F. Saunders, F. F. Morehead and F. Daniels, *J. Am. Chem. Soc.*, **75**, 3096 (1953).

(3) J. K. Rieke, THIS JOURNAL, **61**, 633 (1957).

(4) A. C. Stumpf, A. S. Russell, J. W. Newsome and C. M. Tucker, *Ind. Eng. Chem.*, **42**, 1398 (1950).

TABLE II

CORRELATIONS OF AREA UNDER DIFFERENT PEAKS

Sample no.	Temp. of calcination, °C.[a]	Area under peak	% crystal forms		Surface area m.²/g.
			123° Peak		
1	140	0.4		100 monoclinic	
28	200	1.4	25 orthorhombic	75 monoclinic	
22	220	1.9	35 orthorhombic	65 monoclinic	7
21	230	1.9	40 orthorhombic	60 monoclinic	45
24	245	2.2	50 orthorhombic	50 monoclinic	169
27	250	2.0	50 orthorhombic	50 monoclinic	110
25	400	3.3	50 orthorhombic	50 cubic	400
26	300	3.0	90 orthorhombic	10 cubic	300
23	282	3.7	95 orthorhombic	5 cubic	282
3	200(s)	8.2	100 orthorhombic	.....	
10	600	0.2	99 cubic	1 gamma	
17	500	1.0	95 cubic	5 gamma	310
18	740	...	60 cubic	40 gamma	172
19	830	0.9	.....	100 gamma	134
11	700	3.0	100 cubic	.....	
12	800	5.7	.....	75 gamma	
13	900(s)	8.7	25 orthorhombic	.....	
15	850(s)	13.0	100 orthorhombic		
6	1100	22.5			
14	1000(s)	64.0			
			103° peak		
18	740	0.4	60 cubic	40 gamma	
20	1000	3.9	100 gamma		
15	850(s)	11.6	100 orthorhombic		
30	1100	7.2	100 theta		
29	1200	46.0	100 hexagonal		
9	...	25.0	100 hexagonal		
			164° peak		
28	200	0.9			
10	600	0.2			
20	1000	3.2			
13	900(s)	7.5			
15	950(s)	13.0			
6	1100	9.0			
30	1000(s)	7.2			
14	1000	82.0			
29	1200	65.6			
16	1000(s)	152			
7	...	200			
9	...	240			
			236° peak		
					% Na_2O
9	...	13.0	100 alpha		0.02
7	...	25.0	100 alpha		.04
16	1000(s)	62.0	100 alpha		.1
29	1200	141.2	100 alpha		.3

[a] (s) indicates that the calcination was carried out in steam.

TABLE III

RELATIVE AREAS UNDER GLOW CURVES OF THERMOLUMINESCENCE INDUCED BY LIGHT FOR SAMPLE 22

Time of heating at 370°, min.	Time of subsequent exposure to light, hr.	Relative thermoluminescence, glow curve area	Time of heating at 370°, min.	Time of subsequent exposure to light, hr.	Relative thermoluminescence, glow curve area
20–30	5	23.6	50–30	2	9.2
20–30	10	19.8	60–70	1	6.5
20–30	1	18.4	90–100	3	9.3
30–40	2	11.7	Over 100	10	7.3
30–40	0.5	5.3	Over 100	10	5.7
40–50	4	9.3	Over 100	1	5.0
50–60	10	11.1			

1 mm. of water vapor gave 1.3 and the one with 15 mm. of water vapor gave 1.2.

Discussion

The glow curves indicate that thermoluminescence is induced by high γ-irradiation, but that the locations of the maxima and the areas under the maxima vary markedly. The quantity of thermoluminescent light increases as the removal of water increases. It is largest with synthetic sapphire which is highly crystalline α-Al_2O_3 without water.

The thermoluminescence glow curves can be re-

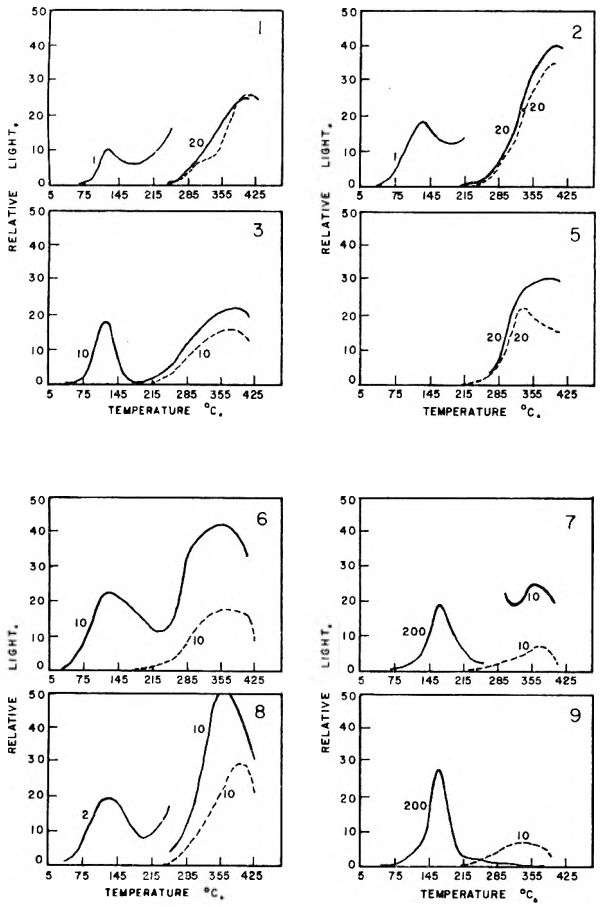

Fig. 1.—Thermoluminescence of Al_2O_3 (samples 1,2,3,5–9).

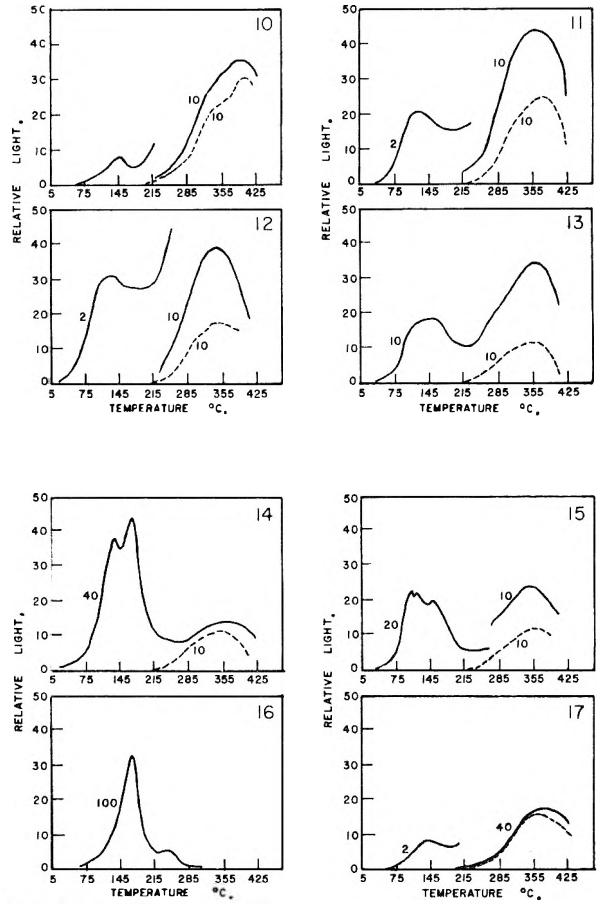

Fig. 2.—Thermoluminescence of Al_2O_3 (samples 10–17).

solved into four peaks occurring at approximately 103, 123, 164 and 236°. The 123° peak is the most characteristic peak for aluminum oxide, hydrates and partial hydrates. It is found in almost all samples until a very high degree of calcination has been reached and then with further removal of water it disappears abruptly. To a limited extent, the area under the curve can be correlated with the crystal phases of the material. The area increases as the orthorhombic phase replaces the monoclinic alpha trihydrate and it reaches a maximum for orthorhombic α-monohydrate. As the temperature is increased and the orthorhombic phase disappears, the peak continues, but to a lesser extent than in the case of the α-monohydrate. The peak area again increases as the orthorhombic α-phase forms at still higher temperatures and continues to increase as the theta phase appears. It then disappears rapidly with further calcination.

The 103° peak occurs in most samples which do not show the 123° peak, except in no. 7 and no. 16. Only in no. 15 do both peaks appear. Both the 103° peak and the 164° peak appear at intermediate stages in the calcination which removes water from the crystal.

The 164° peak appears first when the alumina has been calcined to 600° and then increases progressively as the calcination increases. It is greatest for samples 7 and 8 and the synthetic sapphire. No correlation with impurities was found.

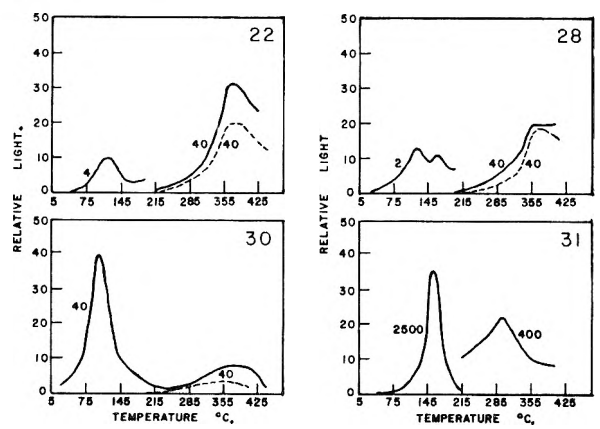

Fig. 3.—Thermoluminescence of Al_2O_3 (samples 22,28,30,31).

The 236° peak occurs only in samples which have been calcined above 1000°. The thermoluminescence area increases in an approximately linear manner with concentration of sodium ion present as an impurity. The synthetic sapphire no. 31 shows an additional peak at 300°.

The 103, 123 and 164° peaks appear to be characteristic of lattice imperfections rather than impurity imperfections. The fact that the thermoluminescence shifts to higher temperatures as the degree of calcination increases indicates that the 103 and 123° trapping centers are in regions of partial hydration. The loss of water during calcination would tend to make these regions more posi-

tive and these centers may be of the $Al(OH)_2^+$ type. The 164° peak may be related to $Al_2(O)_x^{+(6-2x)}$ where x is between 2 and 3. The 236° peak which occurs only in the presence of sodium and complete dehydration is probably connected with a sodium ion trapping center.

The light-induced thermoluminescence is found in the partially hydrated samples. The fact that it is quickly quenched by adsorbed water suggests that the trapping centers are predominantly surface sites and that H_2O must be chemically bound. Anderson[5] observed that luminescence occurs at aluminum anodes after an oxide film has been built up. Phosphorescent after-glow decayed rapidly after the current was stopped. Anderson concluded that the oxide layer acts as an excess conductor under these conditions. Work by Charlesby[6] supports this view and indicates that the traps are at or near the crystal surface. Ewles[7,8] studied the excitation and emission spectra of several oxides. He found that the wave length of the exciting light most effective in producing luminescence lies in the spectral region where the hydroxyl ion is absorbing. Ewles found further that by chemical analysis there was marked oxygen deficiency at the surface. The emission maxima observed by Anderson and by Ewles were 4590 and 4500 Å., respectively. The visible light produced by light-induced thermoluminescence also lies in this spectral region. The electron transition which produces light emission appears to be the same in all three cases, and it is likely that the emission centers occur in surface regions where OH radical or ions exist.

The authors are grateful to Dr. Allen Russell of the Aluminum Company of America for furnishing the samples of aluminum oxide and characterizing them. They are also appreciative of the financial support for this research program by the Atomic Energy Commission under Contract AT(11-1)-178.

(5) S. Anderson, *J. Appl. Phys.*, **14**, 611 (1943).
(6) A. Charlesby, *Proc. Phys. Soc. (London)*, **66B**, 317 (1953).
(7) J. Ewles and G. C. Farnell, *ibid.*, **62A**, 216 (1949).
(8) J. Ewles and C. N. Heap, *Trans. Faraday Soc.*, **48**, 331 (1952).

THERMOLUMINESCENCE OF SOME INORGANIC CRYSTALS AND GLASSES

By James K. Rieke[1]

Contribution from the Department of Chemistry, University of Wisconsin, Madison, Wisconsin

Received December 3, 1956

Over fifty inorganic compounds and glasses have been examined for γ-ray induced thermoluminescence. Impurities are important and only limited generalizations can be made now.

When some crystals are exposed to ionizing radiation, and then heated in the dark, light is emitted at definite temperatures below red heat. The emission of light is due to the release of electrons trapped in imperfections in the crystal, and released when the kinetic energy becomes equal to the trapping energy. The light intensity is plotted against temperature (or against time when the crystal is heated at a uniform rate) and a "glow curve" showing a series of peaks is obtained which is characteristic of the chemical and physical nature of the crystal, its imperfections and its impurities. These "glow curves" have been studied intensively in this Laboratory, with lithium fluoride,[2] alkali halides,[3a] aluminum oxides,[3b] sulfates, carbonates and oxides,[4] and many limestones and minerals.

This communication records the results of a survey of the thermoluminescence of over fifty inorganic compounds and glasses in an attempt to find how wide-spread the phenomenon of radiation-induced thermoluminescence is and to try to obtain data from which wider generalizations can be made.

Experimental

The inorganic crystals taken from fresh bottles were mostly of analytical reagent quality. Usually the purity as given on the bottle was over 99.5% and frequently it was better than 99.9%. Thermoluminescence frequently is affected by traces of impurities less than 0.01%.

All samples except a few which were in the form of powders, were ground in a porcelain mortar to between 100 and 200 mesh, dried at 60° and bottled. They were then exposed to a cobalt-60 γ-source,[5] giving about 5000 roentgens per hour. Each sample received 5000, 25,000 or 100,000 roentgens at room temperature and was then stored on Dry Ice until used.

The specimens were transferred to small iron dishes 0.75 inch in diameter and 0.15 inch deep and leveled off to give an "infinitely thick" layer. The dish was then placed in the thermoluminescence apparatus[6] and heated at the rate of 25° per minute, to about 350°.

The apparatus was the result of considerable development of earlier types used in this Laboratory. It consists of a light-tight box divided in the middle by a horizontal shelf with a hole in its center. The furnace in the bottom of the box consists of a pancake arrangement with a coil of No. 20 nichrome wire in spiral grooves of ceramic, covered with a silver block which can be heated up to 1° per second. Holes in the ceramic housing permit air cooling after the completion of an experiment. The temperature of the silver block is recorded with the help of a thermocouple. Vertical internal reflecting rods of clear fused silica 1.1 inch in diameter carry the thermoluminescent light directly from the heated sample to the photomultiplier at the top of the box. This photomultiplier tube (RCA 1P28) is enclosed in a housing through which cooled air can be circulated if necessary to reduce the dark current.

An automatic switch is attached to the door in such a way that the photomultiplier tube is always disconnected when it is exposed to the day-light of the room, thus preserving the high sensitivity of the tube. Corrections are made for

(1) Dow Chemical Company, Midland, Michigan.
(2) C. A. Boyd, *J. Chem. Phys.*, **17** 1221 (1949).
(3) (a) L. F. Heckelsberg and F. Daniels, This Journal, **61**, 414 (1957); (b) J. K. Rieke and F. Daniels, *ibid.*, **61**, 629 (1957).
(4) L. E. Moore, *ibid.*, **61**, 636 (1957).
(5) D. F. Saunders, F. F. Morehead and F. Daniels, *J. Am. Chem. Soc.*, **75**, 3096 (1953).
(6) J. K. Rieke, Ph.D. thesis, Chapt. II, University of Wisconsin, 1954.

TABLE I

THERMOLUMINESCENCE OF γ-IRRADIATED INORGANIC CRYSTALS

Materia	5000 roentgens Peak temp., °C.	Area	25,000 roentgens Peak temp., °C.	Area	100,000 roentgens Peak temp., °C.	Area
Li_2O	111	9	109	8	114	11
	180	49	183	57	183	99
	283	136	296	56	282	23
Li_2SO_4	80	9	93	12	106	29
	134	4	146	14	146	41
	302	56	318	25	320	29
Na_2CO_3	100	3050	100	22,000	91	67,000
	133	1450	137	9,400	126	18,800
					158	20,800
$K_2Cr_2O_7$			100	<1	111	2
			196	<1	212	2
			244	<1		
K_2HPO_4	220	5	219	34	225	90
	305	6	320	29	336	51
$MgCO_3$ 60% MgO 40%	334	118	350	216	350	424
MgO	115	..	115	..	115	..
	200	..	225	..	215	..
	325	..	335	..		
MgF_2	91	81	100	200	93	200
	153	200	150	570	144	1820
			268	140	264	620
			338	450	350	1480
$Ca_3(PO_4)_2$	108	825	110	4780	114	10,400
BaO	106	1300	105	2440	103	2710
	184	1240	192	1580	196	1790
$BaCO_3$	84	29	79	80	95	145
	158	43	112	68	147	445
			153	270	183	165
$Ba(NO_3)_2$					85	1
	192	1	234	1	211	7
$BaCl_2$	90	10	89	20	91	
	330	164	345	240	347	524
$BaBr_2$	87	168	89	266	86	370
$AlPO_4$	265	4	171	2		
	305	<1	250	14		
			325	18		
MnO_2[a]	97	1	102	2	159	13
	173	<1	175	4	210	26
MnO_2[a]			138	4	135	4
			202	3	192	4
$Pb(NO_3)_2$			114	2	114	4
					194	4
					247	3
$PbCl_2$	66	2	60	1	..	..
	102	1	96	2	..	..
			156	4		

[a] Chemical, from different sources.

dark current by closing a shutter for brief intervals during the determination of the thermoluminescence glow curve, and for black body radiation by making the same determination in an empty dish.

The current from the photomultiplier tube is amplified by a Leeds and Northrup model 9836-A D-C amplifier with a wide range of sensitivities. The amplification is raised to give maximum deflections without going off the scale and the amplification is checked periodically with a standard tritiated phosphor button imbedded in clear plastic. The intensity of the thermoluminescence light and the temperature of the sample are recorded on a continuous two pen recorder Model 153, manufactured by the Brown Instrument Co.

The temperature increase is controlled by hand with a Variac or with an automatic device consisting of a Brown Model 152 circular chart proportionating control with an integral mounted Electro-line relay, connected to a slide wire and valve control of a Brown model MS.801 industrial reversing motor geared to a 10 ampere Variac.

The recorder chart was operated at the rate of 1 inch per minute The temperature of the maximum and the area under each peak was determined. The areas in arbitrary units are proportional to the light emitted within the tem-

perature range and are probably correct to within 20% and the peak temperatures to within 10°.

Results

The results are summarized in Table I.

The following materials exhibited no thermoluminescence detectable with this apparatus even after exposure to 100,000 roentgens: $K_2S_2O_8$, $K_3Fe(CN)_6$, $K_2S_2O_5$, $KHSO_4$, K_2CrO_4, $KMnO_4$, KNO_3, NH_4NO_3, $(NH_4)_2Cr_2O_7$, MnO_2 (electrolytic), $MnCO_3$, $MnCl_2$, $FeCl_2{\cdot}4H_2O$, Fe_2O_3, NiF_2, $CuCl_2$, $Cu_3(PO_4)_2{\cdot}3H_2O$, CuI, Ag_2O, Ag_2SO_4, $HgCl_2$, $HgBr_2$, $PbBr_2$, PbI_2.

In addition to exploring thermoluminescence of several inorganic salts, a few glasses containing varying amounts of iron were studied. It is known that exposure of some glasses to X-rays or γ-rays gives coloration, which disappears on heating. Such glasses exhibit thermoluminescence and provide information concerning the types of imperfections which can act as electron traps. Six plates of glass were exposed to 240,000 roentgens and run in the thermoluminescence apparatus with a 1P21 photomultiplier tube. The glass plates and the chemical analyses were supplied by Mr. J. V. Fitzgerald of the Pittsburgh Plate Glass Company. All the glasses had the following approximate composition: Na_2O, 20%; CaO, 20%; SiO_2, 60% with varying traces of iron oxide.

The results are summarized in Table II.

TABLE II

THERMOLUMINESCENCE OF GLASS

% iron oxide	Peak temp., °C.	Peak area, arbitrary units
0.01	170, 210	82
.05	190	45
.10	215	20
.10[a]	208	43
.10[b]	185	50
.50	..	3

[a] All oxidized. [b] All reduced.

In general, the thermoluminescence decreases as the iron content increases, at least after a minimum amount is present. The presence of 0.5% iron oxide practically destroys the thermoluminescence. There is little difference in the thermoluminescence whether the iron is in the form of the oxidized ferric or reduced ferrous compound. There is a difference, however, in the absorption color of the glass. After irradiation, the 0.01, 0.05 and 0.10% iron oxide glasses are brown-black, brown and light brown, respectively. All become colorless after heating. The glass with 0.50% iron oxide is very light brown after irradiation, and after heating it retains the same light color. The reduced iron at 0.10% gives a very light brown with no apparent change on heating; whereas the oxidized iron gives a dark brown after irradiation, which disappears completely on heating.

A dozen other glasses of varying compositions were studied also. With exposures of 5000 roentgens most of them did not exhibit thermoluminescence; but with 300,000 roentgens most of them did.

Discussion

In view of the large number of alkali halides, oxides, carbonates and sulfates, and the thousands of mineral samples that have shown radiation-induced thermoluminescence in this Laboratory, it was somewhat surprising to find so many inorganic compounds which exhibit no thermoluminescence. Probably many of these would show thermoluminescence at temperatures below room temperature if exposed to radiation at still lower temperatures.

The presence of chemical impurities greatly affects thermoluminescence, sometimes increasing it and sometimes decreasing it. The relation between impurity content and thermoluminescence has been studied in calcium carbonate. Impurities so low in concentration as to be undetectable by many standard methods of analysis can still affect thermoluminescence. But impurities are not the only factors. The type of crystal, the physical treatment of the crystal and the extent of the exposure to γ-radiation are variables which affect thermoluminescence.

Only tentative generalizations can be offered now. Radiation-induced thermoluminescence is more apt to occur in hard, colorless crystals with simple lattices and small cations and anions as indicated in Table III.

TABLE III

ROUGH CLASSIFICATION OF THERMOLUMINESCENCE INTENSITIES

Anions	Cations
High intensity	
F^-, Cl^-, $CO_3^=$, $SiO_3^=$, $O^=$	Li^+, Na^+, K^+, Mg^{++}, Ca^{++}, Sr^{++}, Al^{+++}
Intermediate intensity	
$HPO_4^=$, Br^-, I^-, $PO_4^{\equiv}$	Pb^{++}, Cd^{++}, Ba^{++}
Low intensity	
$CrO_4^=$, $Cr_2O_7^=$, $S_2O_8^=$, $Fe(CN_6)^=$, HSO_4^-, MnO_4^-, NO_3^-	Fe^{+++}, Fe^{++}, Mn^{+++}, Mn^{++} Co^{++}, Ni^{++}, Cu_2^{++}, Cu^{++}, Ag^+, Hg^{++}, NH_4^+

These generalizations are only tentative and much more needs to be done, particularly with crystals of extraordinary purity before firm conclusions can be drawn. Although the thermoluminescence glow curves are reproducible for a given sample of material, there may be great differences in the glow curves for a given chemical compound prepared under different conditions and with different impurity contents.

The author is glad to acknowledge the advice of Professor Farrington Daniels and the support of the Atomic Energy Commission, Contract AT-(11–1)-178 in this work.

THERMOLUMINESCENCE OF SODIUM SULFATE AND LEAD SULFATE, AND MISCELLANEOUS SULFATES, CARBONATES, AND OXIDES[1]

BY LOUISE E. MOORE[2]

Department of Chemistry, University of Wisconsin, Madison, Wisconsin

Received December 8, 1956

Radiation-induced thermoluminescence has been studied for several sulfates, carbonates and oxides. The thermoluminescence of sodium sulfate is affected by the method of dehydration and by the impurities taken up on crystallization. Lead sulfate is not thermoluminescent, but is rendered so by the addition of certain impurity ions.

The thermoluminescence of crystals has been studied in this Laboratory,[3a] particularly the alkali halides[3b] and calcium carbonate. After exposing the crystals to γ-radiation they are heated in the dark and the temperatures at which light is emitted are recorded, giving a "glow curve."

The glow curve of calcium carbonate is markedly affected by the impurities in the solution from which the material is precipitated. Maxima in the light intensity–temperature curves can be induced, increased or decreased by the addition of various impurities. In some cases, impurity content can be predicted from the glow curve and *vice versa*. This fact suggested that thermoluminescence might be useful as an analytical tool in studies of nearly pure crystalline compounds. It is sensitive to very small quantities of impurities—reagent grade purity is far from thermoluminescence purity.

Thermoluminescence may or may not be an inherent property of the host crystal. The pure crystal may give a basic thermoluminescence pattern which is modified by imperfections, or the thermoluminescence may arise from the presence of impurity ions or from effects of radiation on the crystal.

The purpose of this investigation was to determine the thermoluminescence of the sulfates, and to study particularly sodium sulfate which can be easily purified, and lead sulfate which is free from the complication of hydrate formation. Other salts such as carbonates and oxides were measured also in an exploratory study.

Experimental

Reagent grade sulfates were used with the exception of calcium sulfate and manganese sulfate, both of which were described as "purified." "Specpure" samples obtained from the Jarrell-Ash Company, designated as "spectroscopically pure," were used for the carbonates and oxides.

Any samples which were not powders were ground and sieved to 100 to 200 mesh. The "Specpure" samples were neither dried nor ground.

Sodium sulfate was recrystallized from distilled water and from conductance water. The recrystallizations from conductance water were made in polyethylene containers (except for the filtration steps) by cooling from room temperature to 0°. The lead sulfate precipitations and the preparations of sodium sulfate with added impurities were carried out in Pyrex containers.

Sodium sulfate samples were ground to 100 to 200 mesh. Lead sulfate samples precipitated as powder. All lead sulfate samples and most of the sulfates, except sodium sulfate, were dried at 150°.

Sulfates were tested for thermoluminescence before and after irradiation in a cobalt-60 source.[4] The radiation level within this source is approximately 3000 roentgens per hour. Most of the sulfates were irradiated for periods of 24, 48 and 72 hours. The sodium sulfate samples were irradiated for 24 hours and the lead sulfate samples for 72 hours. The samples were irradiated in gelatine capsules and stored on Dry Ice until used.

Samples were then packed in a thin silver dish, 1.2 cm. in diameter and 1 mm. deep, and were heated in a light-tight box from 0 to 400°. A linear temperature rise of about 1° per second was provided by manual operation of a Variac which controlled the furnace current. The furnace consisted of heating coils of Nichrome wire, electrically insulated from the silver plate on which the sample dish was placed.

Light was detected with an RCA 5819 phototube with a maximum response in the blue. The current from the phototube was passed through a Leeds and Northrup amplifier to a Speedomax recorder. This responded alternately to the light impulse and to the output of a copper–constantan thermocouple. The sensitivity to thermoluminescent light could be varied 300-fold.

Results

Sulfates.—The peak temperatures at which maxima occurred in the glow curves of the sulfates are recorded in Table I.

TABLE I

RADIATION-INDUCED THERMOLUMINESCENCE OF SULFATES

Compound	Peak temp., °C.	Compound	Peak temp., °C.
$Li_2SO_4 \cdot H_2O$	85–120	$3CdSO_4 \cdot 8H_2O$	110–130
	230–260[a]	$PbSO_4$	110–130
$Na_2SO_4 \cdot 10H_2O$	80–130	Tl_2SO_4	60– 80
K_2SO_4	80–100	Ag_2SO_4	None
$MgSO_4 \cdot 7H_2O$	120–145[b]	$MnSO_4$	80–110
	90–120	$NiSO_4 \cdot 6H_2O$	None
$SrSO_4$	120–135	$CuSO_4 \cdot 5H_2O$	None
$CaSO_4$	120–140	$Fe_2(SO_4)_3 \cdot 6H_2O$	None
$BaSO_4$	100–120		
	180–190		

[a] High temperature peak only after grinding. [b] Low temperature peak only after heating to 260°.

Drying sometimes increased and sometimes decreased the area of the thermoluminescence peaks. The peak temperature and the peak area could not be correlated either with the position of the element in the periodic table nor with the impurity content given by the manufacturer.

Dried $LiSO_4 \cdot H_2O$ always exhibited a very small peak between 85 and 120°. This was a very low, broad peak; and it was impossible to determine precisely the temperature of the maximum. When the material was ground, either before or after drying, a second, large peak appeared at 230 to 260°. This peak could be found only in samples which

(1) Supported by the U. S. Atomic Energy Commission, Contract AT(11-1)-178.

(2) Armour Research Foundation, Chicago, Illinois.

(3) (a) J. K. Rieke, THIS JOURNAL, **61**, 633 (1957); (b) L. F. Heckelsberg and F. Daniels, *ibid.*, **61**, 414 (1957).

(4) D. F. Saunders, F. F. Morehead and F. Daniels, *J. Am. Chem. Soc.*, **75**, 3096 (1953).

were dried and ground. Since 12 hours or more of heating at 150° did not destroy the effects of grinding, a relatively permanent type of trap must have been produced. The production of a new peak in radiation-induced thermoluminescence by grinding has been observed before and will be discussed in another communication.

In the case of calcium and manganese sulfates (which were less pure), thermoluminescence peaks were observed *before* irradiation. This crystallization-induced thermoluminescence has been noted before.[5] These peaks appeared against a background rising to red heat. The peak for manganese sulfate, previously dried at 260°, came in at 290°. The undried material did not give this peak. The curve for calcium sulfate had a peak at 310° before drying. After the material was dried at 150°, two peaks appeared at 345 and 355°. These pre-irradiation peaks were usually not observed in the irradiated samples, probably because of a high background from the larger peaks induced by radiation.

Carbonates and Oxides.—Table II shows the effect of different radiation periods on a group of "Specpure" carbonates.

TABLE II

INFLUENCE OF γ-RADIATION EXPOSURE ON THERMOLUMINESCENCE

Compound	Approx. peak temp., °C.	Peak height after exposure to 145,000 r.	Peak height after exposure to 215,000 r.
Li_2CO_3	140	0.025	0.103
Na_2CO_3	110	1.3	2.8
	230	4.4	4.6
Tl_2CO_3	100	0.0077	0.0153
$CaCO_3$	155	4.8	4.9
	235	1.3	1.3
	340	1.5	1.2
$BaCO_3$	125	0.25	0.29
	165	0.14	0.14

For about half of these materials there was little change in peak height produced by additional radiation beyond 145,000 roentgens. The electron-traps were largely filled by this exposure. The greatest increase produced by additional radiation was observed for lithium carbonate which had a very low peak. With sodium carbonate a 50% increase in radiation did not affect a high temperature peak, but it doubled the intensity of light emitted at a low temperature peak.

Figure 1 shows the relative thermoluminescence peaks induced in a number of "Specpure" compounds obtained from the Jarrell-Ash Company by exposure to 145,000 roentgens. Each bar indicates the temperature of the maximum light intensity of a peak, and the length of the bar represents the relative height of the peak. It is to be emphasized that the scales of the ordinates are not the same for the different materials.

The following samples of "Specpure" materials gave no thermoluminescence detectable with the present apparatus after exposure to 145,000 roentgens: $BeCO_3$, Cs_2CO_3, K_2CO_3, Ag_2O, Bi_2O_3, CdO,

(5) E. J. Zeller, J. L. Wray and F. Daniels, *J. Chem. Phys.*, **23**, No. 11, 2187 (1955).

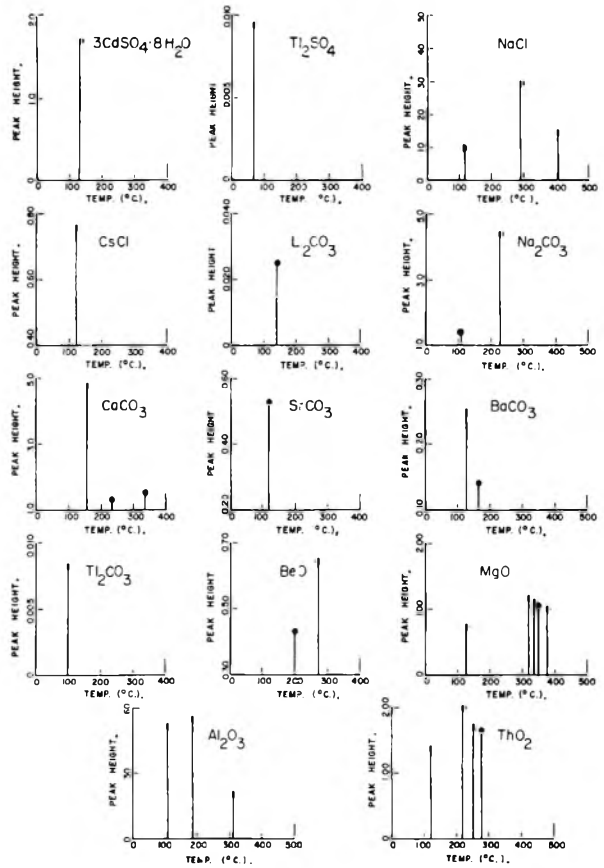

Fig. 1.—Relative thermoluminescence peak heights of thermoluminescent "Specpure" carbonates and oxides.

Cr_2O_3, CuO, Fe_2O_3, Mn_3O_4, MoO_3, Sb_2O_4, SiO_2, SnO_2, Ta_2O_5, TiC_2, Tl_2O_3, U_3O_8, V_2O_5, WO_3 and Si.

Sodium Sulfate.—Sodium sulfate was studied in more detail because it is easy to recrystallize. The study is divided into two parts—drying and recrystallization. Since the material crystallizes as the decahydrate, it is necessary to consider the effect of drying on the thermoluminescence pattern. Removal of the water of crystallization from the solid creates crystal defects which contribute electron traps. This complicates any basic thermoluminescence pattern and its interpretation.

Samples of anhydrous sodium sulfate were used to test reproducibility and to determine the limits of the apparatus and of the method of determining area and peak temperature. Variations of 5 to 20° are possible for the maximum of a peak. The area under the peak, determined by planimetry, varied by about 10%.

Anhydrous sodium sulfate also was used to test the irradiation time necessary for saturation and to show that storage on Dry Ice for periods up to a week does not reduce the thermoluminescence. The peak area after 72, 48 and 24 hours of irradiation was essentially the same. Twenty-four hours, about 70,000 roentgens, was sufficient for saturation.

Samples of the decahydrate from a single bottle were dried at 70, 120, 320°, and at room temperature over concentrated sulfuric acid for periods ranging from one hour to 52 days. Peak temperatures and areas varied with drying time and tem-

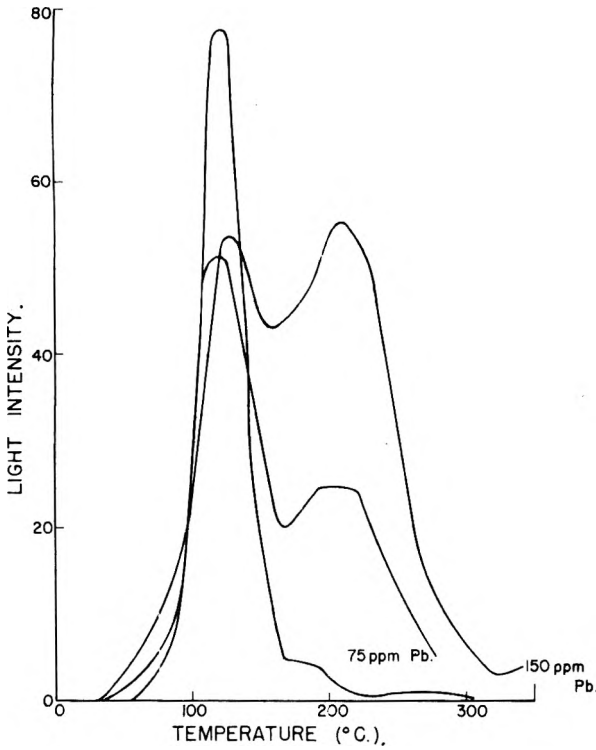

Fig. 2.—Glow curve of sodium sulfate recrystallized three times and glow curves with additions of lead (p.p.m. referred to Na_2SO_4). Intensity is in arbitrary units.

perature, but for any given method the reproducibility was fair. Areas generally increased with heating time. For samples heated first at low temperatures, the area increased with drying at 320°. Usually the area for a sample heated for 24 hours at 320° was approximately twice that of a sample heated for 1 hour at 320°.

Usually drying at temperatures below 320° produced one peak at 110–140°. Increasing the time of heating tended to lower the temperature of this peak and to cause a second peak to appear between 150 and 280°. The contribution of such an unresolved peak would raise the apparent maximum of the low temperature peak. In addition a very low temperature peak appeared between 40 and 60° in all samples heated at 320° except those previously dried for 52 days over concentrated sulfuric acid. This room temperature drying was associated with a pink coloration of the sample after irradiation.

Apparently the defects produced by drying play an important role in the production of thermoluminescence in this hydrate. Two or three types of traps can be produced during drying. When water was removed slowly at room temperature by standing over concentrated sulfuric acid, the decahydrate did not go into solution and recrystallize. After prolonged treatment over sulfuric acid, no high temperature peak developed even after later heating at 320°. Apparently when much of the water was carefully removed at room temperature, fewer defects were produced. It may be that the 110° peak is characteristic of the material and that the peaks at 150–280° and at 40–60° are produced by rapid removal of part of the water.

In general, recrystallization of sodium sulfate from distilled water or conductance water decreased the thermoluminescence, but in each series of recrystallizations the area increased at least once. This occasional increase may have been due to variations in crystallization or drying, or possibly to accidental traces of impurities. The addition of traces of K_2SO_4, $CaSO_4$ and $PbSO_4$ to solutions of the products of several such series gave erratic results although checks on each individual sample agreed well. The difficulty probably was due in part to differences in the amount of impurity taken up in the crystal.

The product of the third recrystallization of a sample of $Na_2SO_4 \cdot 10H_2O$ was used to determine the effect of impurities on the glow curve. All samples were dried at 120° and later at 320°. The samples without added impurities showed a single, sharp peak. All samples have a background of many impurities, as shown by spectrographic analysis.

Addition of lead sulfate in small amounts produced a second peak, the area of which increased roughly with the concentration of the lead sulfate, as shown in the thermoluminescence glow curves given in Fig. 2. Addition of potassium sulfate produced a second peak which was smaller than that produced by lead sulfate. Calcium sulfate apparently did not affect the thermoluminescence pattern.

Lead Sulfate.—Lead sulfate was chosen for further study because it is not complicated by water of crystallization. Reagent grade lead sulfate showed very little thermoluminescence. Precipitation of lead sulfate by mixing 0.1 *M* $Pb(NO_3)_2$ with 0.1 *M* H_2SO_4 gave a material with no measurable thermoluminescence. A thermoluminescence peak at 110–140° could be induced in this material by deliberate addition of certain impurities. In all experiments the lead sulfate was subjected to γ-radiation of 215,000 roentgens.

A series of lead sulfate precipitates was prepared in which silver nitrate, cupric sulfate pentahydrate, ammonium sulfate, potassium sulfate, lithium sulfate monohydrate, nickel sulfate hexahydrate or hydrated ferric sulfate was added to the solution. Equal volumes of 0.1 *M* lead nitrate and a solution 0.1 *M* in sulfuric acid and 0.1 *M* in the impurity salt were mixed. The precipitates from solutions containing ammonium sulfate, potassium sulfate or lithium sulfate gave a thermoluminescence peak at about 120°.

The thermoluminescence is not due to that of the added impurity alone. Pure lithium sulfate showed less thermoluminescence than lead sulfate precipitated in the presence of lithium sulfate. Silver sulfate, calcium sulfate, strontium sulfate, magnesium sulfate and manganese sulfate were also used as impurities and none of the lead sulfates prepared with these impurities gave thermoluminescence peaks although most of these sulfates alone, as reagent grade chemicals, are thermoluminescent.

Concentration effects were studied with added sodium sulfate. Equal volumes of 0.1 *M* lead nitrate and 0.1 *M* sulfuric acid containing various amounts of sodium sulfate were mixed. The precipitated lead sulfate was not thermoluminescent

if the sodium sulfate concentration in the sulfuric acid was 6×10^{-5} to 3×10^{-2} M. It was thermoluminescent if the concentration of sodium sulfate in the sulfuric acid was raised to 0.2 to 0.8 M. If the precipitating solution contained only sodium sulfate, a thermoluminescent lead sulfate could be prepared by mixing equal volumes of 0.1 M lead nitrate and 0.1 M sodium sulfate. As the sodium sulfate solution was increased to 0.8 M, the area of the thermoluminescence peak increased. In each case the thermoluminescence of lead sulfate precipitated from a solution containing a given concentration of sodium sulfate was greater if no acid was added.

Two concentration series were run with potassium sulfate. When potassium was the added impurity, an increase in acid concentration increased the area of the thermoluminescence peak. The area also increased with increasing concentration of potassium in the solution. If a small amount of silver sulfate was added to the solution of potassium sulfate, the thermoluminescence area was changed. For high potassium concentrations it usually increased, while for low concentrations it generally decreased. If sulfuric acid was present, the decrease in area seemed to be greatest for high potassium concentrations. Both acid and silver sulfate alone gave lead sulfates with no thermoluminescence.

The results may be due to complex combinations of the effects of several impurities in the lattice or to changes in the amount of impurity taken into the lattice when other impurities are present in the solution.

Lead sulfate was precipitated from solutions containing one of several sodium or potassium salts. The salt was added to the sulfuric acid solution in each case. Lead sulfate precipitated in the presence of chlorides, bromides and acetates was not thermoluminescent, but lead sulfates precipitated in the presence of iodides and hydroxides were thermoluminescent. Potassium carbonate, potassium nitrate and potassium phosphate gave thermoluminescent precipitates while the corresponding sodium salts did not.

These results indicate that anion impurities also affect the thermoluminescence pattern. All samples gave the lead sulfate X-ray pattern with some modifications. Samples from the solutions containing iodides showed the X-ray pattern of lead iodide in addition to that of lead sulfate. There were minor changes in line intensities, perhaps due to the substitution of sodium or potassium for lead.

Conclusions

Radiation-induced thermoluminescence glow curves provide a means for studying factors in crystallization and the purity of the crystals. Many of the sulfates exhibit thermoluminescence even when highly purified. Others definitely require the presence of impurities.

The quantity of impurity which affects the thermoluminescence may be so low as to be difficult to measure by analytical methods.

The effects on thermoluminescence of various impurities at different concentrations are very complicated. In order to affect thermoluminescence, the impurities must be taken up into the crystal structure to give special types of imperfections.

In one reagent bottle of $Na_2SO_4 \cdot 10H_2O$ of high quality, different crystals in the bottle gave widely varying thermoluminescence glow curves. The variations probably were due to slight differences in impurities taken up by the crystals at different stages in the crystallization process or to differences in the physical conditions of crystallization. Thermoluminescence measurements might be used as a control for uniformity in certain types of crystallization operations.

The thermoluminescence of sodium sulfate is changed by the method of heating the decahydrate. Apparently the rate of heating affects the defects in the crystal and their ability to trap electrons. The nature and concentration of foreign ions taken up into the sodium sulfate crystal also affects the glow curve. Lead and potassium produce an additional high temperature peak.

Pure lead sulfate is uncomplicated by dehydration. It does not exhibit radiation-induced thermoluminescence. Large amounts of impurities of sodium, ammonium, potassium, lithium and iodide and hydroxide added to the solutions from which lead sulfate is precipitated, produce a thermoluminescence peak while many other impurities are without effect. The peak temperature in lead sulfate is always the same with the different impurities, and the area depends on the concentration of sulfuric acid at the time of precipitation and on an interaction of both cation and anion impurities.

It is hoped that studies of thermoluminscence will lead eventually to a better understanding of the up-take of impurities and the nature of imperfections in crystals.

Acknowledgments.—The author wishes to express her gratitude to Dr. Farrington Daniels who directed this work and to the U. S. Atomic Energy Commission which supported it.

STREAMING POTENTIAL STUDIES ON CORUNDUM IN AQUEOUS SOLUTIONS OF INORGANIC ELECTROLYTES[1]

BY H. J. MODI AND D. W. FUERSTENAU[2]

Department of Metallurgy, Massachusetts Institute of Technology, Cambridge, Massachusetts

Received December 5, 1956

Streaming potential measurements show that corundum is positively charged in water and indicate that H^+ and OH^- are potential-determining ions for corundum. The zero point of charge occurs at *p*H 9.45. Under no conditions do monovalent ions, such as Na^+, Cl^- and NO_3^-, change the sign of the zeta potential, ζ, and hence they must act as surface-inactive counterions. Provided the surface is oppositely charged, multivalent ions, such as Ba^{++}, $SO_4^=$ and $S_2O_3^=$, change the sign of ζ and must function as surface-active counter ions. Under conditions of like charge, however, these same ions function as surface-inactive ions at the corundum–solution interface.

Introduction

Information concerning conditions which exist at solid–solution interfaces has so far been principally derived from adsorption measurements, employing electrochemical or radiotracer techniques. The electrokinetic method affords another sensitive approach to elucidating the structure of the electrical double layer, especially for oxide systems. By using streaming potential techniques to evaluate the electrokinetic or zeta potential, ζ, the structure of the negatively charged quartz–solution interface recently has been studied extensively.[3-5] However, quartz is negatively charged except at low *p*H, and consequently an electrokinetic study of a positively charged quartz surface is experimentally difficult. Corundum, on the other hand, has been reported to be positively charged in water, but published data on its surface electrical properties are exceedingly scant.[6,7] Accordingly, the object of this paper is to present a study of the effect of various inorganic electrolytes on the zeta potential of corundum, and to postulate the function of different types of ions at the corundum–solution interface.

Experimental Materials and Method

Materials.—Since natural corundum gives results that range from a high negative charge to a high positive charge in water,[8,9] synthetic sapphire boules manufactured by Linde Air Products Company were used in this investigation. This material is extremely pure and has a specific gravity of 3.98. A spectrographic analysis indicated the presence of several oxides totalling less than 0.02%; Na_2O and SiO_2 were present to the extent of 0.001%. The material was crushed and sized into the two fractions used for the streaming potential studies, namely, a 48/65-mesh fraction for the plug and a 28/35-mesh fraction to cover the holes in the platinum electrodes. A considerable portion of the iron impurity introduced during crushing was removed with a hand magnet and the last traces were removed by treatment with hydrochloric acid. The material was next washed with distilled water till free from chloride ion. Finally, it was washed several times with conductivity water and stored under the same till used.

To avoid contamination of corundum with surface-active impurities, all solutions were prepared with conductivity water, which had been double-distilled from a block-tin still. Only water with a specific conductance of less than 5×10^{-7} ohm^{-1} $cm.^{-1}$ was used. The water was stored and dispersed in an atmosphere free of carbon dioxide.

Except for sodium hydroxide and hydrochloric acid, all inorganic chemicals used in the experiments were of reagent grade and were used without further purification. Sodium hydroxide, free from sodium carbonate, was prepared by the standard methods and stored in a carbon dioxide-free atmosphere. Hydrochloric acid solutions of various normalities were prepared by dilution from a stock solution of constant boiling acid.

Apparatus and Procedure.—The apparatus used in this study consists essentially of the cell assembly, a flow system and the electrical measuring equipment which have been described in detail previously.[10] The apparatus has been suitably modified to overcome polarization difficulties encountered with platinum electrodes for potential measurements in concentrated solutions. Silver–silver chloride electrodes, prepared according to the method of Brown,[11] were substituted for platinum electrodes and proved to be unpolarizable with respect to all electrolytes investigated. The design and construction of these electrodes, as well as the manner of their introduction in the experimental setup has been described in a thesis by Modi.[12]

In dilute solutions, surface conductance plays an important role in the evaluation of the zeta potential from streaming potential experiments.[10,13] Because of surface conductance, the calculated zeta potential in dilute solutions is depressed and it appears to rise initially as the concentration of 1–1 valent electrolytes is increased although it may actually be decreasing. In this work, the experimental values are strictly correct only if the ionic strength is greater than 4×10^{-6}. If the effect of surface conductance is kept in mind, the data can still be interpreted satisfactorily.

Experimental Results

Zeta potentials of corundum were determined in solutions of 1–1 valent, 1–2 valent, and 2–1 valent inorganic electrolytes. The data are presented graphically in the accompanying figures in plots of ζ against logarithm of the electrolyte concentration. Some of the points have been omitted for the sake of clarity. For corundum in conductivity water, ζ averaged +66.7 mv. The standard deviation based on 32 values was less than 1.6 mv.

Monovalent Electrolytes.—Figure 1 presents the zeta potentials of corundum in solutions of sodium chloride, sodium nitrate, sodium hydroxide and hydrochloric acid. ζ in conductivity water is

(1) Condensed from a thesis submitted by H. J. Modi in partial fulfillment of the requirements for the degree of Doctor of Science at the Massachusetts Institute of Technology.

(2) Metals Research Laboratories, Electro Metallurgical Company, Niagara Falls, New York.

(3) A. M. Gaudin and D. W. Fuerstenau, *Trans. A.I.M.E.*, **202**, 66 (1955).

(4) A. M. Gaudin and D. W. Fuerstenau, *Trans. A.I.M.E.*, **202**, 958 (1955).

(5) D. W. Fuerstenau, THIS JOURNAL, **60**, 981 (1956).

(6) F. Hazel, *ibid.*, **42**, 409 (1938).

(7) H. R. Kruyt, "Colloid Science," Vol. I, Elsevier Publishing Co., New York, N. Y., 1952, Chapters IV, V, and VIII.

(8) D. J. O'Connor, N. Street and A. S. Buchanan, *Australian J. Chem.*, **7**, 245 (1954).

(9) D. J. O'Connor, P. G. Johansen and A. S. Buchanan, *Trans. Faraday Soc.*, **52**, 229 (1956).

(10) D. W. Fuerstenau, *Min. Eng.*, **8**, 834 (1956).

(11) A. S. Brown, *J. Am. Chem. Soc.*, **56**, 646 (1934).

(12) H. J. Modi, "Electrokinetic Properties and Flotation Behavior of Corundum," Sc.D. Thesis, Massachusetts Institute of Technology, 1956.

(13) J. Th. G. Overbeck and P. W. O. Wijga, *Rec. trav. chim.*, **65**, 556 (1946).

taken as the initial point for the various ζ–log C curves. With sodium chloride and sodium nitrate, ζ increases in absolute value with electrolyte concentration up to about 4×10^{-6} M; thereafter, it undergoes a logarithmic decrease with concentration until 10^{-2} M solutions are reached, the slope, $d\zeta/d(\log C)$, being -17 mv. At still higher concentrations, ζ approaches zero as a limiting value, but does not change sign. Both the curves are very similar, with the sodium nitrate curve being about 5 mv. higher than the sodium chloride curve.

In solutions of hydrochloric acid, ζ markedly increases with concentration to reach a maximum of about +125 mv. at 3×10^{-5} M. Further additions cause a substantial reduction in its value till it finally drops to 45 mv. at 10^{-1} M. Since surface conductance can scarcely be expected to play a more significant role in hydrochloric acid solutions than in sodium chloride solutions, this observation suggests that the role of H^+ is distinctly different from that of Na^+.

Aqueous solutions of sodium hydroxide change ζ from positive to negative values at relatively low concentrations. The isoelectric point occurs at a hydroxyl ion concentration of 2.8×10^{-5} N. In other words, the value of ζ is zero at pH 9.45. The magnitude of the negative ζ decreases somewhat beyond 10^{-3} equivalent per liter. The striking difference between the curves for sodium hydroxide and sodium chloride once again points to a special function of OH^- in the system as compared with Cl^-.

Sodium Chloride at Different pH Values.—To ascertain the effect of ionic strength on the zeta potential of corundum when the solid is positively or negatively charged, ζ was measured as a function of the concentration of NaCl at pH 4, 6.5, 10 and 11. As can be seen from Fig. 2, sodium chloride has no effect on ζ until the ionic strength is changed. For a given pH, ζ decreases in absolute value as a linear function of the ionic strength until the ionic strength exceeds approximately 10^{-2}. The rate of decrease appears to increase with increasing surface charge.

Sodium Hydroxide and Hydrochloric Acid in 10^{-4} M Sodium Chloride Solutions.—The effect of H^+ and OH^- on ζ indicates that these ions play a special role at the corundum surface as compared with Na^+ and Cl^-. To confirm this belief, the effect of adding sodium hydroxide and hydrochloric acid to solutions containing 10^{-4} M sodium chloride was investigated. Such experiments would indicate the effect of H^+ and OH^- in the absence of surface conductance and initial change of ionic strength. Figure 3 shows that relatively small additions of sodium hydroxide and hydrochloric acid have a marked effect on ζ long before the ionic strength is changed (compare with Fig. 2). This indicates that the marked effect of H^+ and OH^- is real.

Effect of Ionic Strength and pH on ζ.—Since the zeta potential of corundum depends on both pH and the ionic strength of the solution, the value of ζ is plotted as a function of pH for different ionic strengths in Fig. 4. The different ionic strengths and pH values were obtained by making solutions with sodium chloride, and hydrochloric acid or sodium hydroxide. Observation of Fig. 4 shows that the only point which is common to all the curves is the point where ζ is zero, namely, pH 9.45. These data indicate that ζ is determined by pH even though the ionic strength of the solution remains constant, whereas Fig. 2 shows that if pH remains constant, the addition of an inert electro-

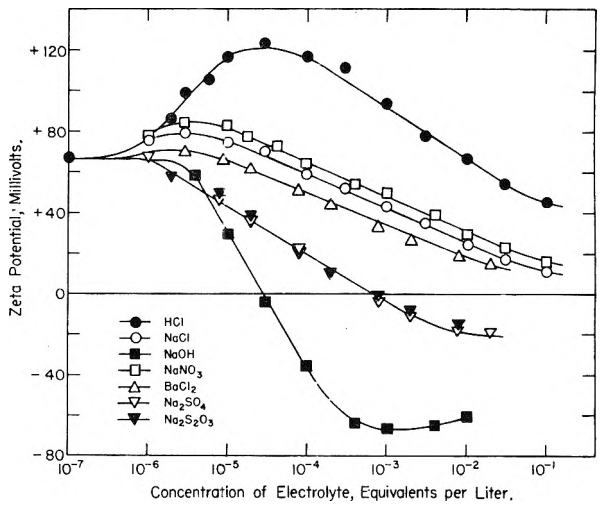

Fig. 1.—Zeta potential of corundum in solutions of various electrolytes.

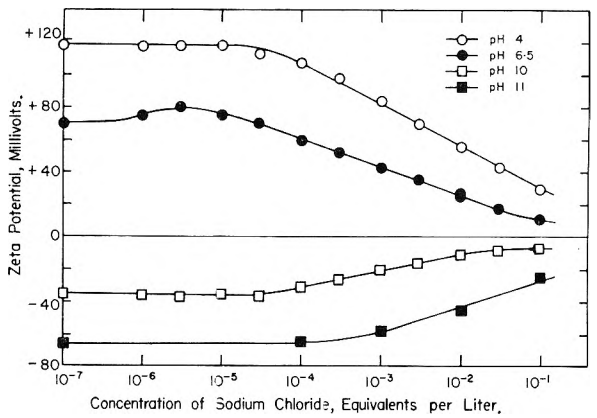

Fig. 2.—Zeta potential as a function of the sodium chloride concentration at different pH values.

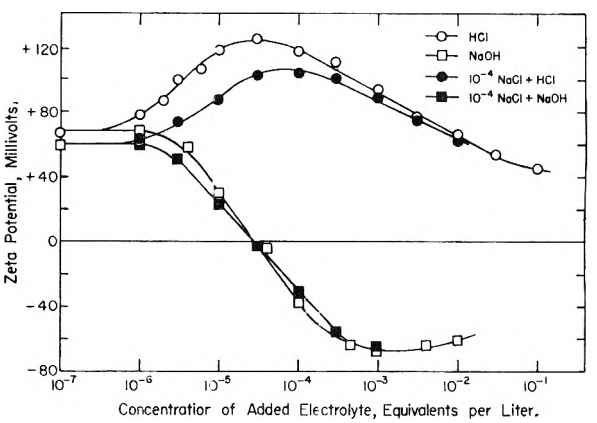

Fig. 3.—Zeta potential of corundum as a function of the addition of sodium hydroxide and hydrochloric acid in conductivity water and 10^{-4} N sodium chloride solutions.

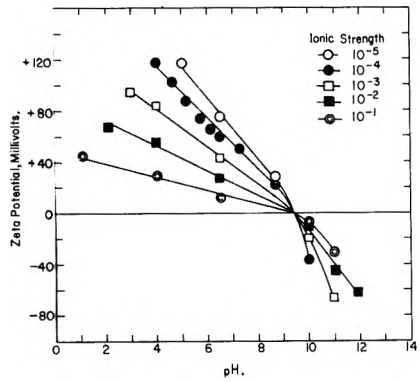

Fig. 4.—Zeta potential of corundum as a function of *p*H for different total ionic strengths.

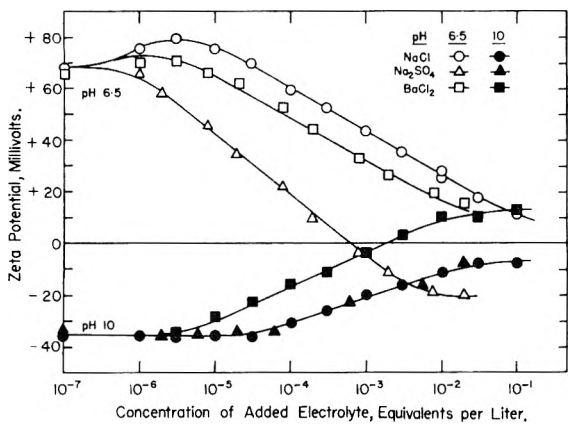

Fig. 5.—Zeta potential of corundum in solutions of barium chloride, sodium chloride and sodium sulfate at different *p*H values.

lyte like sodium chloride does not affect ζ until the ionic strength is changed. The facts presented in Fig. 4 firmly establish that H^+ and OH^- have a special function at the corundum surface, distinctly different from that of either Na^+ or Cl^-.

Divalent Electrolytes.—Zeta potential-concentration curves for corundum in solutions of barium chloride, sodium sulfate and sodium thiosulfate are presented in Fig. 1. These electrolytes scarcely show the effect of surface conductance, as evidenced by the absence of the hump. The reduction in ζ brought about by additions of barium chloride is analogous to that by sodium chloride, except that it is achieved at lower concentrations; likewise, the slope of the ζ–log C curve is -17 mv. The value of ζ approaches zero at high concentrations but does not change sign. The observed similarity in the behavior of sodium and barium chlorides indicates that Cl^- has no special effect at the interface.

The experiments also show that sodium sulfate and sodium thiosulfate exert an identical influence on ζ of corundum over the entire concentration range investigated. ζ is positive in dilute solutions but negative in concentrated solutions. The reversal of sign occurs with about 3×10^{-4} molar solutions. Thus, $SO_4^=$ and $S_2O_3^=$ behave differently from Cl^- and NO_3^- in that they are capable of changing the sign of ζ, whereas the latter do not. Even though these divalent ions reverse the sign of ζ, monovalent OH^- reduces the zeta potential to zero at a concentration nearly twenty times more dilute. This further indicates a special role of OH^- at the corundum surface.

Barium Chloride and Sodium Sulfate at *p*H 10.—The behavior of divalent ions at the solid–solution interface under conditions of negative surface charge was further studied by determining ζ in aqueous solutions of barium chloride and sodium sulfate at *p*H 10. The experimental data are shown in Fig. 5, together with measurements for sodium chloride added for comparative purposes.

When the corundum surface is negatively charged, ζ is affected in an identical fashion by additions of sodium chloride and sodium sulfate. This similarity of behavior suggests that neither Na^+, Cl^- nor $SO_4^=$ have any special effect at the surface. Ba^{++}, on the other hand, seem to have a special affinity for the negative surface. The zeta potential decreases in absolute value with increasing concentration of barium ions, and finally becomes positive at about 10^{-3} M. This fact indicates that the behavior of Ba^{++} is remarkably different from that of Na^+; barium chloride solutions can change the sign of ζ at high concentrations, whereas sodium chloride solutions do not. In addition, it is possible to conclude that Ba^{++} act just the same at a negative surface as $SO_4^=$ or $S_2O_3^=$ at a positive surface.

In brief, all these results seem to indicate that the counter ions charged oppositely to the surface play the determining role in the electrokinetic behavior of corundum. It also appears that specific adsorption of counter ions depends mainly on valency. Thus, divalent counter ions reverse the sign of ζ, but monovalent counter ions do not.

Discussion of Results

In this paper the model of the double layer proposed by Stern[14] will be used to interpret the experimental results. An excellent discussion of Stern's treatment of the double layer is presented by Overbeek.[7]

The total potential across the double layer, commonly referred to as the surface potential, ψ_0, is determined only by the concentration of potential-determining ions in solution. Indifferent electrolytes do not affect its value unless they have secondary effects.

The zeta potential is more complex and affected by all electrolytes, the effect depending not only on concentration but also on the valence and sign of charge of the ions. Increasing the concentration of indifferent electrolytes in solution reduces the value of ζ by compression of the double layer because more ions are forced into the Stern layer.

In this work, two main types of ions are considered: (1) potential-determining ions, and (2) indifferent ions, which are subdivided into surface-active and surface-inactive indifferent ions. Each of these types of ions can be characterized by its effect on the zeta potential.

Potential-determining Ions.—Results of streaming potential measurements indicate *p*H plays an exceptional role at the corundum surface as shown by the following observations.

(14) O. Stern, *Z. Elektrochem.*, **30**, 508 (1924).

(1) H^+ cause ζ to become more positive than any other cation tested (Fig. 1).

(2) OH^- change the sign of ζ at *p*H 9.45, where Cl^- and NO_3^- merely reduce it to zero at infinitely high concentrations (Fig. 1).

(3) In solutions of surface-inactive indifferent electrolytes at a given total ionic strength (same thickness of the double layer), the value of ζ is determined by *p*H (Figs. 2 and 4).

(4) Na^+ and Cl^- do not affect ζ until the ionic strength of the solution is changed, but H^+ and OH^- change ζ under conditions where the ionic strength remains constant (Figs. 2 and 3).

(5) ζ is zero only at *p*H 9.45 regardless of the ionic strength of the solution (Fig. 4).

Because of the manner in which ζ is affected by the *p*H of the solution, it must be concluded that H^+ and OH^- function as potential-determining ions for corundum, in agreement with the findings of Verwey.[15] If H^+ and OH^- are potential-determining ions, they must enter into an electrolytic reaction at the surface which leaves the surface with a net positive charge in water. Since corundum is uncharged at *p*H 9.45, the double layer ceases to exist at this *p*H and there is an equal number of anions and cations in the solution next to the surface.

The total double layer potential ψ_0 may be calculated from the relation

$$\psi_0 = \frac{kT}{ve} \ln \frac{C_{H^+}}{C_{H_0^+}} = -\frac{kT}{ve} \ln \frac{C_{OH^-}}{C_{OH_0^-}}$$

where k is the Boltzmann constant, T is the absolute temperature, v is the valence of the ion in question, e is the electronic charge, C_{H^+} and C_{OH^-} are the concentrations of the potential-determining ions in solution, and $C_{H_0^+}$ and $C_{OH_0^-}$ are their concentrations at the zero point of charge. Since the zero point of charge for corundum occurs at *p*H 9.45, in pure water the double layer potential is, therefore, positive ($\psi_0 = +145$ mv.). As mentioned before, in dilute solutions, surface conductance lowers the experimental values of ζ. In the absence of surface conductance a near identity of ζ and ψ_0 should, therefore, be expected. Consequently, the true zeta potential of corundum in conductivity water should be about +125 mv.

Surface-inactive Indifferent Ions.—Since surface-inactive electrolytes reduce the value of ζ by compression of the double layer without changing its sign, ζ approaches zero as a limiting value at higher concentrations. Sodium chloride and sodium nitrate are electrolytes of this type as seen from Fig. 1, Cl^- and NO_3^- functioning as counterions. The difference between the curves, although small, is believed to be due to the difference in anions, and points out that valency alone does not determine the behavior of counterions at the interface. Experimentally, the results agree with the relative positions of Cl^- and NO_3^- in the lyotropic series. As seen from Fig. 2, the reduction in potential by the addition of NaCl is more rapid at *p*H 4 than at *p*H 6.5. Similar is the case for *p*H 11 as compared with *p*H 10. Qualitatively, the increased adsorption of counter ions with increasing H^+ and OH^- concentration can be explained by the increasing potential drop across the double layer.

Surface-active Indifferent Ions.—If the counterions are attracted to the surface not only by simple electrostatic forces, but also by strong chemical or covalent forces, they may reverse the sign of ζ as in the case of Ba^{++}, $SO_4^=$ and $S_2O_3^=$ (Figs. 1 and 5). When potential-determining ions, such as OH^-, change the sign of ζ, the charge at the surface as well as ψ_0 must change sign; whereas when a surface-active counter ion changes the sign of ζ, there must be a higher charge in the Stern plane than at the surface. This results in the formation of a triple layer.[7]

At *p*H 10, Ba^{++} must be surface active since ζ is reversed in 10^{-3} molar solutions. However, this affinity of Ba^{++} for the surface is not apparent in neutral solutions, where ζ merely approaches zero as a limiting value at high concentrations. If Ba^{++} were specifically adsorbed, ζ would have become more positive on increasing the concentration of barium chloride, but this has not been observed. Similarly $SO_4^=$ are also specifically adsorbed but only when the surface is positively charged.

The specifically adsorbed ions, Ba^{++}, $SO_4^=$ and $S_3O_3^=$, are all divalent; in contrast no monovalent ion was found to be specifically adsorbed. It has been shown by Gaudin and Fuerstenau[3] that Ba^{++} and Al^{+++} are specifically adsorbed by quartz with a negative surface charge, but significantly no monovalent inorganic ion was found to be specifically adsorbed. On the basis of these results, it seems that multivalent but not monovalent counter ions can function as surface-active indifferent ions and reverse the sign of zeta potential. The specific adsorption probably results from a multivalent ion sitting on a single site at the surface.

Summary and Conclusions

By means of streaming potential techniques, it has been shown that corundum is positively charged in water. Hydrogen and hydroxyl ions are potential-determining ions for corundum, and the zero point of charge occurs at *p*H 9.45. Sodium, chloride and nitrate ions function as surface-inactive indifferent ions under all conditions and, therefore, cannot change the sign of ζ. Barium, sulfate and thiosulfate ions function as surface-active counter ions, provided the surface is oppositely charged, and are able to change the sign of ζ. Under conditions of like charge, however, these same ions function as surface-inactive indifferent ions. Thus the reversal of zeta potential seems to be a characteristic property of multivalent inorganic counter ions.

Since *p*H determines the nature of the surface charge and also the magnitude of the surface potential, ψ_0, it will be expected to affect markedly the adsorption of all other ions by corundum.

Acknowledgments.—This research was made possible through the financial support provided by the Aluminum Company of America. The authors wish to give thanks to Professors A. M. Gaudin and P. L. deBruyn for their interest in this work.

(15) E. J. W. Verwey, in "Colloid Chemistry, Theoretical and Applied," ed. J. Alexander, Vol. III, Reinhold Publ. Corp., New York, N. Y., 1950, p. 50.

A LOW TEMPERATURE SCALE FROM 4 TO 300°K. IN TERMS OF A GOLD–COBALT *VERSUS* COPPER THERMOCOUPLE[1]

BY N. FUSCHILLO

Department of Physics, The Pennsylvania State University, University Park, Pa.

Received December 7, 1956

A low temperature scale has been obtained by comparing the e.m.f. from the Au + 2.1 atomic % Co *vs.* Cu thermocouple with the temperature values obtained from a constant-volume helium gas thermometer. By paying appropriate attention to considerations concerning temperature gradients and the homogeneity of the alloy, the absolute thermodynamic scale can be realized to between 0.1 and 0.2° from 4 to 10°K. and to better than 0.1° above this temperature. The e.m.f.'s are shown to be reproducible to within these limits on successive reductions to helium temperatures. The thermoelectric scale has also been transferred to wire from a different batch to a precision of 0.2° from 4 to 300°K., using helium and nitrogen bath temperatures as fixed points. The use of a composite three limb Au–Co *vs.* Cu *vs.* constantan thermocouple is described. This thermoelement enables the use of the nitrogen temperature fixed point to be avoided, and the Au–Co *vs.* Cu and Cu *vs.* constantan thermoelectric scales to be checked with respect to each other. The methods described are applicable to a wide variety of experimental measurements where moderate precision is required.

Introduction

A large variety of experiments in physical chemistry, physics and engineering physics requires the measurement of absolute temperatures in the range 4.0 to 300°K with a precision between 0.1 and 1.0°. The thermoelectric thermometer is in principle an ideal instrument[2–4] for such purposes. Copper *vs.* constantan thermocouples have long been used in temperature measurements down to 77°K.[4,5] This thermoelement has also been used at temperatures as low as 14°K.[4–6] The sensitivity at this temperature is, however, only 4.0 μv./°K.[5] Thus temperature measurement to 0.2° below 20°K. is somewhat unsatisfactory. This is especially the case in view of e.m.f. changes equivalent to 0.5° at 14°K. on successive reductions to hydrogen temperatures,[6,7] and the rapid loss of sensitivity with temperature.

In a study of the thermoelectric power of the alloy system cobalt-in-gold by the differential method, Keesom, *et al.*,[8,9] found that the alloy Au + 2.1 atomic % Co *vs.* Ag + 0.37 atomic % Au had a thermoelectric power 9.3 μv./°K. at 10.3°K. and 16 μv./°K. at 20°K. It was thus suggested that this combination would provide a superior low temperature thermoelectric thermometer. It has, however, been stated[10] that, presumably due to instability, such a thermocouple is only of use as an indicator of the approximate equality of two temperatures. In this investigation it is shown that thermocouples of Au — 2.1 atomic % Co *vs.* Cu instead of Ag + 0.37 atomic % Au and utilizing silver soldered junctions, instead of the rose metal junctions of Keesom, *et al.*,[8] can be used in various experimental arrangements, in the temperature range 4 to 300°K., with a precision between 0.1 and 0.2°. It is the purpose of this article to describe the use, performance and construction of this thermometer and to present a thermoelectric reference table for use in the manner described by Aston[5] and Adams[11] for the copper *vs.* constantan thermoelement.

Experimental

1. **Construction of Thermoelement.**—A 500 cm. length of 0.03 inch diameter enameled Au + 2.1 atomic % Co wire was doubled by bending at its mid-point. The two wires thus formed were silver soldered to single 34 B and S Constantan and 36 B and S copper wires to form the cold junction. Borax flux, a thin strip of silver solder and a gas microburner were used in this operation. The Au–Co wire was doubled in the manner described to average out partially any systematic variations in chemical composition. Silver solder was used because this material does not become superconducting in the temperature range under consideration.[8] Two separate ice junctions were formed with copper wire leads in the same fashion. Thus the thermoelement could be used either as a Au + 2.1 atomic % Co *vs.* Cu or as a constantan *vs.* copper thermocouple. The constantan wire also served as a structural member supporting the fine Au–Co limbs of the thermocouple. Previous to the formation of these junctions, the wires were wrapped with silk thread and lightly covered with GE type varnish. Insulation resistance was tested at every stage of construction. The ice junctions were embedded in tight-fitting, thin-walled polyethylene tubing which was sealed off at both ends as a precaution against the condensation of moisture.

2. **Cryostat.**—The thermocouple was brought down through a vacuum enclosure to the massive copper bulb of a helium gas thermometer. This was enclosed in a re-entrant well in a brass can of capacity 2 liters, initially containing liquid helium or nitrogen, depending on the temperature range to be covered. The re-entrant well was designed to form an experimental chamber into which an apparatus for measuring the mechanical properties of materials could be lowered after the establishment of the temperature scale and upon removal of the gas thermometer bulb. The helium can was contained in an evacuated enclosure which could be nitrogen cooled to secure better temperature control below 70°K. The thermoelement was in metallic contact with the thermometer bulb and 80 cm. of the thermocouple wire was wrapped around the bulb as a precaution against heat leak. Isothermal temperature control was effected by the appropriate use of helium exchange gas and non-inductively wound electrical heating coils. For temperatures above 10°K. the helium can was evacuated to 10^{-4} mm. Thermoelectric measurements were taken to 0.5 microvolt with a Wenner Potentiometer, using the precautions described by White[2a] and Giauque.[4] The reference junctions were maintained at the ice point using the pro-

(1) Supported by the United States Atomic Energy Commission.

(2) (a) W. P. White, *Phys. Rev.*, **31**, 159 (1910); **31**, 470 (1906); (b) R. B. Scott, "Temperature," Vol. 2, Reinhold Publ. Corp., New York, N. Y., 1955 p. 179.

(3) N. Fuschillo, *Proc. Phys. Soc.*, **64**, 649 (1953); **55**, 896 (1952).

(4) W. F. Giauque, R. M. Buffington and W. A. Schulze, *J. Am. Chem Soc.*, **49**, 2343 (1927).

(5) J. G. Aston, E. Willihnganz, and G. H. Messerly, *ibid.*, **57**, 1642 (1935).

(6) J. G. Aston, "Temperature," Vol. 1, Reinhold Publ. Corp., New York, N. Y., 1941, p. 219.

(7) C. C. Stephenson and W. F. Giauque, *J. Chem. Phys.*, **5**, 149 (1937).

(8) W. H. Keesom and C. J. Matthijs, *Physica*, **2**, 623 (1935).

(9) G. Borelius, W. H. Keesom, C. H. Johannesson and J. O. Linde, Leiden Comm. No. 217d (1932).

(10) C. T. Linder, Westinghouse Research Report R-94433-2-A (1950).

(11) L. H. Adams, "International Critical Tables," Vol. I, McGraw-Hill Book Co., New York, N. Y., 1926.

cedure recommended in the international temperature scale.[12]

3. Gas Thermometry.—The copper bulb of the constant-volume gas thermometer had a total mass 1 kg., and volume 80.1 cc. A steel capillary led to the short limb of a mercury manometer in the manner described by Beattie, *et al.*[13] The i.d. of the Pyrex walls of the manometer was 0.89 cm. Corrections for the meniscus volume, surface tension, dead space correction and thermal expansion of the mercury and bulb, were made as described in the literature.[13,14] Four copper *vs.* constantan thermocouples and two mercury thermometers were placed along the dead space for the calculation of the gas thermometric dead space correction. The gas thermometer was filled with helium after purification in the manner described by Aston.[5] Temperatures in the range from 4.2 to 295°K. were obtained with an initial filling with helium at 824.0 mm. at 273.16°K. To increase the precision of the gas thermometric measurements at temperatures below liquid nitrogen temperatures, the thermometer was refilled with helium at 77.7°K. to a pressure of 766.0 mm. This procedure has been described elsewhere.[14] The temperature of the filling was determined under identical conditions by using the thermoelectric results of the previous run. Manometric precision of the order 0.01 cm. enabled temperatures to be determined on the normal helium scale to 0.03°K. The normal helium scale was corrected where necessary to the absolute thermodynamic scale from the data given by Keesom.[15] Other details were similar to those described in the literature.[5,13-16]

Results

A shortened form of the thermoelectric reference table is shown in Table I. Comparison of the thermoelectric scale with the oxygen vapor pressure scale[17-19] gave a temperature lower by 0.03°K. at 77.77°K. than the precise work of Henning. The e.m.f.–temperature relationship is approximately linear in the range 90 to 300°K. A cubic equation $E = 8952.7 - 4.180T - 0.3226T^2 + 0.001226T^3$ represents the data between 4 and 90°K. with an average deviation of 0.17° and a maximum deviation of 0.3° at 90°K. The change in sensitivity of the thermocouple as a function of temperature is shown in Fig. 1. The thermoelectric power dE/dT was obtained by first differences from the initial e.m.f. *versus* temperature table. A single equation of the form $dE/dT = 38\ [1 - \exp(-41/T)]$ represents this curve with an average deviation irrespective of sign of 0.5% between 30 and 300°K. These equations, however, are principally of academic interest since the reference table itself provides a more convenient interpolation device. The reproducibility of the Au + 2.1 atomic % Co *vs.* Cu thermometer was such that on five successive reductions to helium temperatures in a three-month period, the variation in e.m.f. at the helium bath temperature was no greater than one microvolt, corresponding to a temperature variation of no greater than 0.17°. Greater thermoelectric precision may have been obtained; however, the accuracy in temperature measurement required for the envisaged applications was 0.2°.

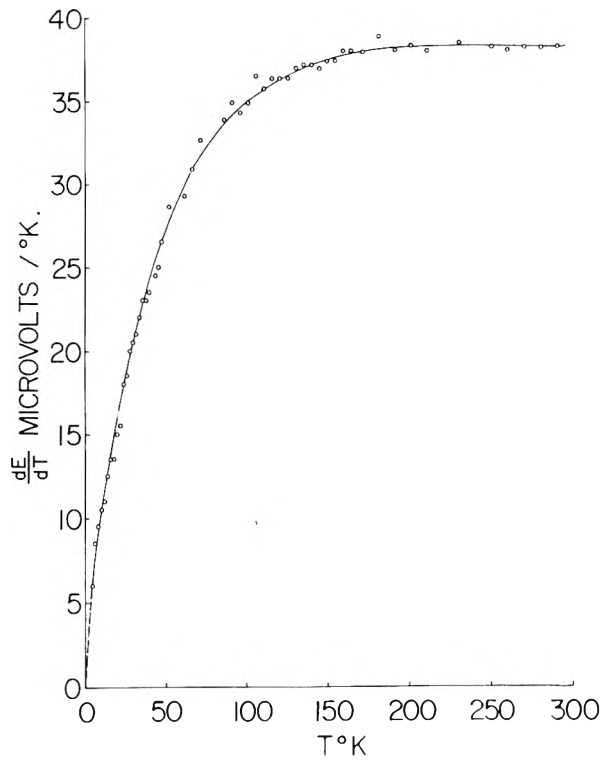

Fig. 1.—Change in sensitivity of the Au + 2.1 atomic % Co *vs.* Cu thermocouple as a function of temperature.

Table I

Thermoelectric Reference Table[a]

T, °K.	μv.	T, °K.	μv.	T, °K.	μv.	T, °K.	μv.
4.0	8930	22.0	8721	65.0	7662	145.0	4871
5.0	8924	24.0	8686	70.0	7508	150.0	4686
6.0	8916	26.0	8649	75.0	7345	160.0	4316
7.0	8907	28.0	8610	77.0	7279	170.0	3938
8.0	8898	30.0	8571	80.0	7182	180.0	3561
9.0	8888	32.0	8529	85.0	7015	190.0	3175
10.0	8877	34.0	8486	90.0	6846	200.0	2797
11.0	8866	36.0	8441	95.0	6672	210.0	2417
12.0	8855	38.0	8397	100.0	6501	220.0	2041
13.0	8844	40.0	8348	105.0	6327	230.0	1651
14.0	8831	42.0	8302	110.0	6145	240.0	1262
15.0	8819	44.0	8255	115.0	5967	250.0	873
16.0	8806	46.0	8205	120.0	5786	260.0	494
17.0	8792	48.0	8154	125.0	5605	270.0	117
18.0	8779	50.0	8099	130.0	5424	280.0	− 261
19.0	8765	55.0	7956	135.0	5240	290.0	− 639
20.0	8750	60.0	7808	140.0	5055	300.0	−1017

[a] Thermoelectric reference table for the Au + 2.1 at. % Co *vs.* Cu thermocouple. The reference junction is at 273.16°K. and the variable junction is at T°K. Seebeck e.m.f.'s are expressed in microvolts (μv.).

Discussion

An inhomogeneity test through liquid nitrogen of a typical Au–Co wire, using the reference gradient[20] method indicates an average inhomogeneity e.m.f. of 4.2 μv. and a maximum of 10.0 μv. The temperature gradient was of the order 200° in five centimeters. The contribution to the Seebeck e.m.f. arising from the inhomogeneity e.m.f. is indistinguishable in its effects from the e.m.f. due

(12) *Trav. Bur. Int. Poids. Mes.*, 19 (1934).

(13) J. A. Beattie, *Proc. Am. Acad. Arts Sci.*, **74**, 327 (1941).

(14) H. J. Hoge and F. G. Brickwedde, *J. Research Natl. Bur. Standards*, **22**, 351 (1939).

(15) W. H. Keesom, "Helium," Elsevier Press, Houston, Texas, 1942, p. 71.

(16) F. Henning, "Temperaturmessung," Johann Ambrosius Barth, Leipzig, 1951.

(17) F. Henning and J. Otto, *Physik. Z.*, **37**, 633 (1936).

(18) J. G. Aston and G. W. Moessen, *J. Chem. Phys.*, **21**, 948 (1953).

(19) G. W. Moessen, J. G. Aston and R. G. Ascah, *ibid.*, **22**, 2096 (1956).

(20) N. Fuschillo, *J. Sci. Instr.*, **31**, 133 (1954).

to the Thomson thermoelectric potential.[21] Thus e.m.f.'s of this kind and their variations with temperature are included in the thermoelectric reference table. It is therefore important to keep the variation in temperature gradients with temperature as reproducible as possible from one experiment to another. This, however, cannot be accomplished if the Au–Co wire is in direct contact with the refrigerant liquid because of the steep localized temperature gradient at the liquid surface and the changing of the liquid level by evaporation as a function of time. Under these circumstances fluctuations in inhomogeneity e.m.f. of 5.0 μv. can easily occur. While this would not prevent a precision of 0.2° down to 70°K., its effect would be to give an inaccuracy of one degree near 4°K. However, most of the cryostat designs operating the range 4 to 300°K. are either based on the isothermal calorimeter or involve the use of cold helium gas. In these designs, the thermocouple limbs are easily prevented from coming into contact with the refrigerant and in addition, the temperature difference is spread out over a considerable length of the cryostat. The consequent reduction in the magnitude of the temperature gradient is usually between 10 and 15. This results in a considerable reduction[3] in the inhomogeneity e.m.f. In the type of cryostat under discussion the position of the temperature distribution is far more constant and unsystematic changes in the residual inhomogeneity e.m.f. are substantially reduced. The apparatus used in this work is an example of this class of temperature control.

The temperature scale summarized in Table I has been applied to Au–Co wire from a different batch. The thermocouple was a composite Au + 2.1 atomic % Co *vs.* Cu *vs.* constantan instrument, and was used for temperature measurement in the gas controlled apparatus described by Kline.[22] The constantan wire carried the Penn State copper–constantan temperature scale.[5] The thermometer gave a higher e.m.f. (9167 μv. at 4.2°K.) than the previous thermocouple. This difference was most likely due to departures from the stated composition of the Au–Co alloy wire. On obtaining a fixed point calibration from the helium bath temperature and one at nitrogen temperatures, a deviation plot[6] using Table I was obtained. The temperatures thus derived agreed with those given by the Penn State scale with a maximum deviation of 0.2° at 17 temperatures in the range 19 to 70°K. Similar results have been obtained in a nuclear magnetic resonance isothermal cryostat[23] in operation between 20 and 295°K. Here, however, comparisons were made at only two temperatures.

(21) A. Sommerfeld and N. H. Frank, *Revs. Mod. Phys.*, **3**, 1 (1931).

(22) D. E. Kline *J. Polymer Sci.*, in press (1956).

Conclusion

On taking precautions to ensure the absence of steep and fluctuating temperature gradients, the Au + 2.1 atomic % Co *vs.* Cu thermocouple can be used in the measurement of absolute temperature to at least 0.2° from 4 to 20°K. and to 0.1° from 20 to 300°K. by utilizing single fixed points at helium and nitrogen temperatures and a reference table. The use of a composite Au–Co Cu *vs.* constantan thermometer enables the two thermoelectric scales to be checked with respect to each other. The constantan limb also provides a convenient supporting member to prevent the straining of the fine Au–Co wire. A small diameter is often desirable because of the high thermal conductivity of the alloy. Care should be used in the handling of the thermocouple wire as the inhomogeneity e.m.f.'s are increased by cold work. If Leeds and Northrup constantan wire is used, the upper fixed point may be obtained from the Leeds and Northrup tables to a precision between 0.1 and 0.2°.

The thermocouple has been shown to be stable to at least 1.0 μv. at 4.2°K. The limiting factor here is the reproducibility and stability of the temperature gradients and associated inhomogeneity e.m.f.'s, rather than any intrinsic instability in the thermometer. The improvement in the performance of this thermocouple is principally the metallurgical problem of producing more homogeneous alloy wires. However, until these become available it is better to select, or at least check, the wire by test methods.[20] The replacement by copper wire of the Ag + 0.37 atomic % Au limb of the combination originally suggested enables a reference table to be employed with more certainty, and results in no significant loss in sensitivity. In addition, the relatively high cost of the thermocouple is reduced by half. Improvements might also be effected by using many loops of Au–Co wire in parallel or alternatively in series in the construction of the thermoelement.[3,20]

Acknowledgments.—The author is indebted to Professor H. S. Sack for permitting part of this work to be done at Cornell University and to Professor J. G. Aston for the use of the Penn State copper *vs.* constantan temperature scale for purposes of comparison. Thanks are also due to G. H. Dishong and Virginia Wolfe for computational aid.

(23) N. Fuschillo, *Rev. Sci. Instr.*, **27**, 394 (1956).

ADSORPTION OF HYDROGEN ON GERMANIUM

BY KENZI TAMARU

Frick Chemical Laboratory, Princeton University, Princeton, N. J.

Received December 10, 1956

The adsorption of hydrogen on a germanium surface has been studied using a clean germanium film prepared by germane decomposition on glass wool. The adsorption was an activated chemisorption and the activation energy of adsorption on a bare germanium surface was 14.6 kcal./mole, and the heat of adsorption was 23.5 kcal./mole at 0.05 coverage. Statistical mechanical considerations suggest that the initial adsorption is an immobile dissociative adsorption, which is supported by a hydrogen deuterium exchange reaction on a germanium surface. The saturation point of the adsorption corresponds to one adsorbed hydrogen atom per one surface germanium atom.

Introduction

As has been shown in previous papers,[1,2] the decomposition of germane on germanium is a zero-order reaction and its activation energy is 41.2 kcal./mole. It was suggested in the papers that during the decomposition of germane the germanium surface is covered by adsorbed molecules, radicals and atoms decomposing at the measured rate. This implies that the rate of breaking the bond between hydrogen and germanium atoms on the surface to form a hydrogen molecule is a comparatively slow reaction with high activation energy, which suggests that the heat of adsorption of hydrogen on germanium might be large enough to enable an adsorption measurement to be made.

Nitrogen gas is not chemisorbed on germanium at temperature of 20° or higher according to Law and Francois,[3] but germanium forms its nitride when it is heated with ammonia at 700°.[4] Even at a temperature as low as 278° ammonia is chemisorbed on a germanium surface, dissociating to NH_2(a) and H(a).[5] This fact shows that nitrogen from ammonia is comparatively easily chemisorbed on germanium with hydrogen, though no nitrogen is chemisorbed at the same temperature from nitrogen gas.

Recently Law[6] studied the adsorption of various gases on germanium and found that hydrogen appeared to be chemisorbed on a germanium surface at room temperature or higher, though it was impossible to calculate the heat of chemisorption from the data.

As it was found that fresh pure germanium with a large surface area could be prepared by the decomposition of germane on a clean Pyrex glass wool, hydrogen adsorption on this surface has been studied.

Experimental

The apparatus used for the measurements consists essentially of three parts: a glass vessel for germanium film, a McLeod pressure gage and a pumping system. A cylindrical Pyrex vessel filled with clean Pyrex glass wool was used for the deposition of germanium film. The inside diameter of the vessel was 2.7 cm. and its volume was 69 cc. Pure germane gas prepared from $GeCl_4$ and $LiAlH_4$, as has been shown in the previous paper,[1,7] was decomposed in the vessel at 302°. The temperature of this vessel was controlled satisfactorily using vapor baths of mercury, diphenylamine, acenaphthene and naphthalene under various constant pressures. The vessel was attached to the apparatus *via* a liquid nitrogen trap[8] and the pressure of hydrogen was followed by a McLeod gage.

A pumping system consists of two mercury diffusion pumps backed up by a Cenco Hy-Vac oil pump, which could easily give a pressure of less than 10^{-6} mm. Hydrogen was obtained from a cylinder and was purified by passing through a palladium–kieselguhr tube at 300°, a liquid nitrogen trap, and finally through a palladium thimble at 300°.

After the deposition of germanium film, the vessel was evacuated to a pressure of less than 10^{-6} mm. for at least several hours at 302°,[9] and then a known amount of hydrogen was introduced, and the adsorbed amount was determined from the dead space measurement using helium. The adsorption rate near equilibrium at 218° was so slow that the equilibrium points were obtained by extrapolating adsorption and desorption curves.

Experimental Results and Discussion

Adsorption Isotherms at Various Temperatures.—The adsorption was reversible and the amounts of adsorbed hydrogen on germanium film at various temperatures are shown in Fig. 1. If the logarithms of the adsorbed amounts are plotted against those of the corresponding pressures, it can be shown that the Freundlich isotherm, $v = cp^{1/n}$, is applicable except at lower pressures as shown in Fig. 2. The value of $1/n$ in the isotherm ranges from 0.20 at 218° to 0.54 at 348°. All the straight lines in Fig. 2 appear to converge and meet at one point which is assumed to mean a saturation point of the adsorption. This "saturation point" corresponds to 0.40 cc. (S.T.P.) hydrogen adsorption.

Surface Area of the Germanium Film and the Adsorption at Full Coverage.—The surface area of the germanium film was measured by the B.E.T. method using nitrogen adsorption at −196° and *n*-butane adsorption at −78°. The former gave 2.5×10^4 cm.^{2} and the latter, 2.8×10^4 cm.^{2}.[11]

(1) K. Tamaru, M. Boudart and H. S. Taylor, THIS JOURNAL, **59**, 801 (1955).

(2) P. J. Fensham, K. Tamaru, M. Boudart and H. S. Taylor, *ibid.*, **59**, 806 (1955).

(3) J. T. Law and E. E. Francois, *Ann. N. Y. Acad. Sci.*, **58**, Art. 6, 925 (1954).

(4) W. C. Johnson, *J. Am. Chem. Soc.*, **52**, 5160 (1930).

(5) K. Tamaru, THIS JOURNAL, **60**, 612 (1956).

(6) J. T. Law, *ibid.*, **59**, 543 (1955).

(7) This preparation was carried out without trouble as described in the previous paper.[1] Dr. M. D. Banus of Metal Hydrides Inc., Beverly, Mass., kindly called our attention to the fact that solutions of lithium aluminum hydride or any chloride in a glycol ether should not be heated or extensively evaporated, as otherwise explosion sometimes takes place.

(8) During the germane decomposition experiment a solid carbon dioxide trap was used.

(9) This evacuation is thought to be enough to remove practically all the hydrogen in the vessel on the basis of the desorption rate of chemisorbed hydrogen on germanium, which will be shown later,[10] and also from the fact that the adsorption results were not changed by raising the evacuating temperature to 444°.

(10) K. Tamaru and M. Boudart, submitted to the International Congress on Catalysis in Philadelphia, Pa., September, 1956.

(11) The surface area can be roughly estimated from the decomposition rate of germane on the film. The decomposition rate of germane on the film was 1.4×10^{-2} cc. (S.T.P.) per minute at 218°. It was shown in the previous paper that the decomposition rate on 108 cm.^{2} geometrical surface area was 7.6×10^{-3} cc. (S.T.P.) per minute at 278° and the activation energy was 41.2 kcal./mole. The comparison of the two decomposition rates gives the surface area of the film on the

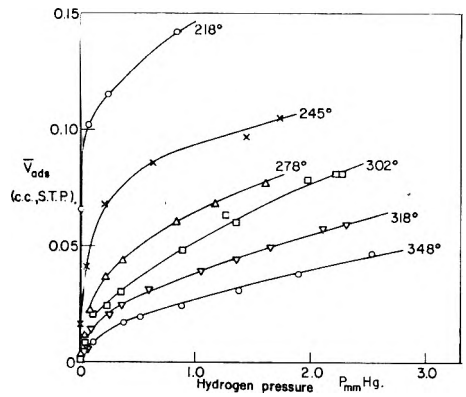

Fig. 1.—Adsorption of hydrogen on germanium (temperatures shown are in °C.).

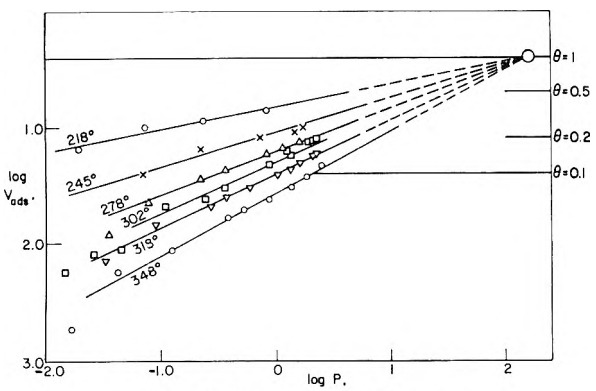

Fig. 2.—Freundlich isotherms.

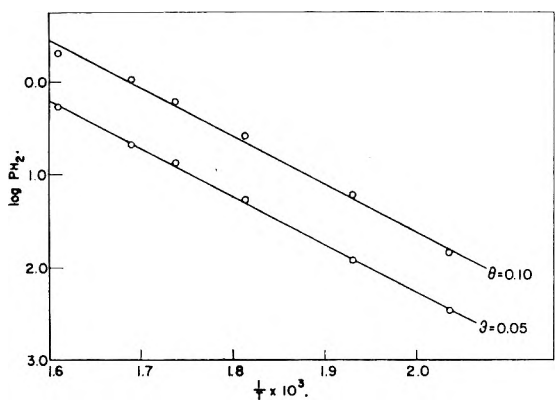

Fig. 3.—Heat of adsorption at lower coverages.

From the crystal structure of germanium,[12] it is calculated that 0.90×10^{15} and 0.73×10^{15} germanium atoms are exposed on unit surface area of (110) and (111) crystal faces, respectively. Consequently the total number of germanium atoms on the germanium surface is $\sim 2.15 \times 10^{19}$. The saturation point of adsorption, on the other hand, corresponds to 1.1×10^{19} hydrogen molecules, which means that the saturation corresponds to one hydrogen atom per one surface germanium atom. From the saturation point thus obtained the fraction of the surface covered by adsorbed hydrogen (θ) can be calculated as shown in Fig. 2. It is interesting to note, as will be shown later,[10] that this "saturation point" agrees well with the amount of hydrogen adsorbed on the germanium film while germane is being decomposed.

Heat of Adsorption.—The heat of adsorption can be obtained by plotting the logarithms of the equilibrium pressure at each coverage against the corresponding temperatures as shown in Fig. 3. The heat is 23.5 kcal./mole at $\theta = 0.05$ and 23.3 at $\theta = 0.10$. At higher coverages it tends to decrease with increasing coverages, getting to zero at full coverage as shown in Fig. 2.

The Langmuir Isotherm and Theoretical Considerations.—The adsorption isotherms at low pressures are shown in Fig. 4, where the coverages

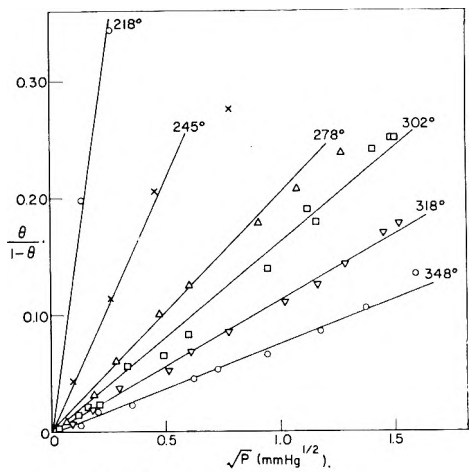

Fig. 4.—Langmuir isotherms.

of the surface by hydrogen calculated from the saturation point are plotted against square roots of the corresponding equilibrium pressures. It is found in the figure that the Langmuir isotherm of dissociative adsorption is applicable at lower pressures, that is

$$\frac{\theta}{1-\theta} = \sqrt{ap}$$

This fact suggests that the heat of adsorption of hydrogen stays nearly constant at low coverages, as is found in Fig. 3.

Statistical mechanics give an approximate value of $\sqrt{a}$ in the Langmuir isotherm from partition functions of the hydrogen gas molecule, assuming that the adsorption is an immobile dissociative adsorption on an uniform surface.[13] The observed slope at 318° in Fig. 4, for example, is 0.11 ($mm.^{-1/2}$), while the calculated slope is 0.12 ($mm.^{-1/2}$) using the heat of adsorption of 23.5 kcal./mole. The agreement of the two values is satisfactory, which suggests that the adsorption is an immobile dissociative adsorption as has been assumed in the calculation.[13] The fact that the saturation of the adsorption corresponds to one adsorbed hydrogen atom per one germanium atom on the surface shows that all the germanium atoms on the surface take part in the chemisorption. As the behavior of the initial adsorption obeys what can be expected from the immobile dissociative adsorption on an uniform surface, all the germanium atoms on the surface may be considered to be homogeneous

glass wool as, at least, 2.0×10^4 cm.^{2} assuming that the roughness of the surface is unity.

(12) *Cf.*, "Crystal Structure," by R. W. G. Wyckoff, Vol. 1, Interscience Publishers Inc., New York, N. Y.

(13) T. Kwan, *Advances in Catalysis*, **6**, 67 (1954).

in their behavior for the initial hydrogen adsorption. It was shown in the previous paper[5] that the surface of this germanium film behaves as though it is homogeneous in its properties for ammonia decomposition, and it is also the case, as will be shown in a later paper, for germane decomposition.

Exchange Reaction between Hydrogen and Deuterium on the Germanium Film.—2.1 cm. of hydrogen and 2.9 cm. deuterium were admitted to a germanium film, with a surface area comparable with those in the preceding adsorption measurements, at 302° for 130 minutes. The mass spectrometric analysis showed a large amount of hydrogen deuteride produced in it, which supports the dissociative adsorption of hydrogen on the germanium film. The increased surface area and the longer reaction times account for the deviations from the previous observations.[1,2]

Activation Energy of Adsorption.—The activation energy of the adsorption was obtained from the dependence of the initial rate of adsorption at 0.065 mm. hydrogen pressure on a bare germanium surface upon temperature. The results are shown in Fig. 5 and the activation energy was 14.6 kcal./mole. The initial adsorption rate calculated from this activation energy and absolute rate theory,[13] is 4.2×10^9 molecules/sec. cm.^{2}, while the observed rate is 3.0×10^{11} molecules/sec. cm.^{2}, when the hydrogen pressure is 0.065 mm. The heat of adsorption on a bare surface is approximately 23.5 kcal./mole and, consequently, the activation energy for desorption becomes 38 kcal./mole under this condition.

Acknowledgment.—The assistance of Mr. B. W. Steiner in the mass spectrometric analyses is gratefully acknowledged. The author is also indebted to Dean Hugh Taylor and Professor M. Boudart for their valuable suggestions and assistance, and to Yokohama National University, Japan, for a leave of absence.

This work was carried out on a post-doctoral fellowship kindly provided Princeton University by the Shell Fellowship Committee of the Shell Companies Foundation, Inc., New York City. We wish to express our appreciation of this support. The work in question is also a part of a program of research supported by the Office of Naval Research N6onr-27018 on Solid State Properties and Catalytic Activity. Acknowledgment is made also to this research project for facilities used and for consultation with workers in the project.

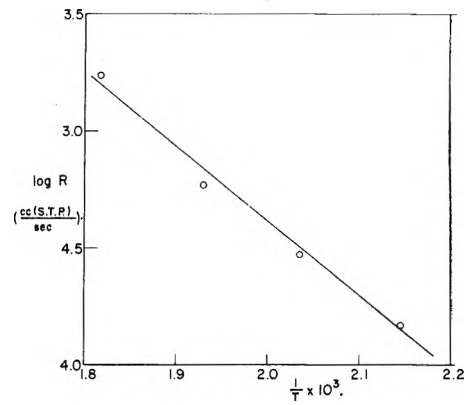

Fig. 5.—Adsorption rates on bare surface at different temperatures.

THE SEDIMENTATION OF DEOXYRIBONUCLEATE IN $MgCl_2$ SOLUTIONS

By H. Kahler and J. Shack

National Cancer Institute, National Institutes of Health, U. S. Public Health Service, Bethesda 14, Maryland

Received December 12, 1956

The sedimentation of DNA in $MgCl_2$ solutions was compared with its sedimentation in KCl solutions. At infinite dilution both sediment with similar velocity. At finite concentrations the S coefficient in $MgCl_2$ is higher than in KCl, and the boundaries are less sharp. The viscosity in $MgCl_2$ is also less than in KCl. Addition of 0.16 N KCl to 0.05 $MgCl_2$ diminishes the sedimentation coefficient at finite concentrations of DNA. The effects are not the result of charge effects as outlined by Tiselius.[4] Mg^{++} and K^+ compete for sites on the DNA structure, the resultant effect depending on the concentrations of the two ions.

The velocity of sedimentation of DNA (deoxyribonucleate) decreases rapidly as the concentration increases. This decrease in sedimentation velocity with concentration results in self sharpening during sedimentation, the sharpness of the boundary gradient being greater for greater changes in sedimentation velocity across the boundary.

The attempts at a theoretical interpretation of the concentration effect in the sedimentation of DNA presumably would be more successful if this effect were studied under as wide a range of conditions as possible. Numerous studies have been reported on the sedimentation of DNA in NaCl and KCl solutions, but only a single observation has been published[1] on its sedimentation in a bivalent salt, $CaCl_2$. The present work is concerned with a comparison of the sedimentation of DNA in KCl or NaCl and $MgCl_2$ solutions.

Materials and Methods

One sample of DNA was prepared from calf thymus by the Simmons method.[2] Other samples prepared from calf thymus and mouse lymphoma by a modified Mirsky–Pollister method previously described[3] were used. After preparation the fibers were cut into small pieces and thoroughly mixed so that small portions taken for separate experiments would be truly representative of the whole preparation.

The concentration of DNA in saline solutions was estimated by measuring the optical density at 260 mμ and using the ε (P) value determined for each preparation under the same conditions.

All sedimentation experiments were performed in a

(1) H. Kahler, This Journal, **52**, 676 (1948).

(2) N. S. Simmons, S. A. Chavos and H. K. Orbach, U.C.L.A. Report 184 (1952).

(3) J. Shack and J. M. Thompsett, *J. Biol. Chem.*, **197**, 17 (1952).

Spinco E ultracentrifuge with schlieren optics and a bar or wire at the diaphragm position at speeds of 50,740, 37,020 and 23,150 r.p.m. It is advantageous to run DNA at a relatively low speed since diffusion is negligible; leakage, cell distortion and temperature changes are all less at low speeds, thus giving higher precision. The photographic image of the DNA boundaries generally consisted of a diffraction pattern, and these were directly measured with a Mann micron-comparator. The position of a band was taken as the central line of symmetry of the pattern. All sedimentation coefficients were corrected to 20° and standard conditions.

A few viscosity measurements were made using Ostwald viscometers.

Results

Stability Tests.—The stock solutions of DNA were made in 0.1 *M* sodium cacodylate buffer, *p*H 6.8, either (a) cold (3°) or (b) at room temperature. Solutions for centrifugal analysis were made by mixing these stock solutions with solutions of KCl or $MgCl_2$ in the same buffer. Since DNase is activated by magnesium ions, it was necessary to ensure that no active enzyme was present in the solutions. This was tested by following the viscosity of the DNA solutions in KCl and in $MgCl_2$ (0.05 *M*) for periods up to several days. All solutions in KCl (no added Mg) were stable. All solutions made from DNA dissolved at room temperature were also stable. The same was true of all solutions of mouse lymphoma DNA whether dissolved in the cold or at room temperature. However, certain of the preparations of calf thymus DNA, when dissolved at 3°, exhibited a gradual decrease of viscosity when tested in 0.05 *M* $MgCl_2$ soon after solution was complete. However, these were also stable with constant viscosity if, before the addition of $MgCl_2$, the solutions were either (a) stored at 3° for about one week or (b) stored at room temperature for one day. The viscosities did not measurably change during this storage and also the viscosities in $MgCl_2$ of such stored solutions were the same as the initial viscosity in $MgCl_2$ of the freshly dissolved (at 3°) DNA.

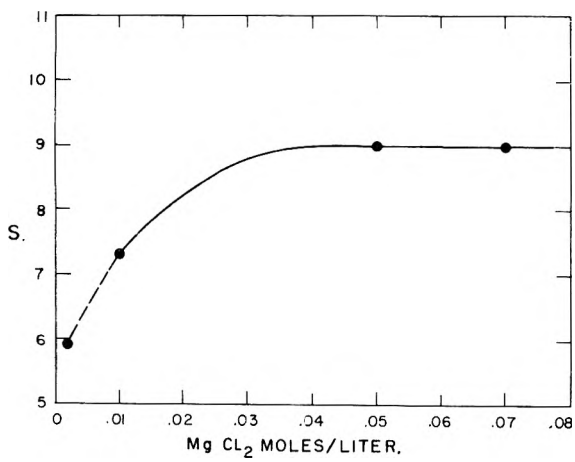

Fig. 1.—Sedimentation coefficients for 0.1 g./100 ml. DNA (calf thymus) in magnesium chloride.

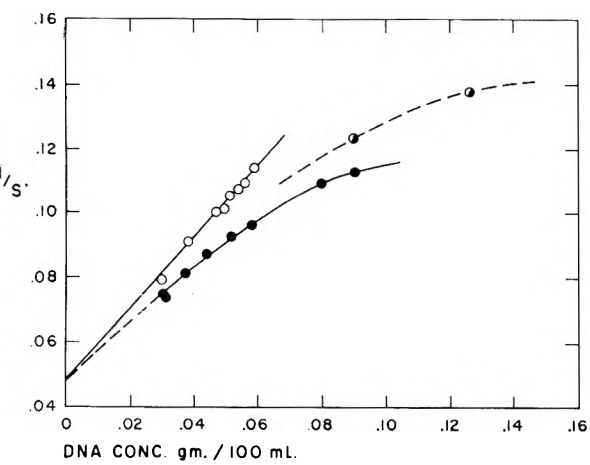

Fig. 2.—$1/S$ plotted against DNA concentrations in different solvents: ○, DNA in solutions of 0.3 *N* KCl + 0.01 *M* cacodylate buffer; ●, in 0.05 *M* $MgCl_2$ + 0.01 *M* cac.; ◑, in 0.05 *M* $MgCl_2$ + 0.15 *N* NaCl + 0.01 *M* cac.

These results suggest that some DNA preparations may contain trace amounts of enzyme which is destroyed when the DNA is dissolved in potassium chloride solutions at room temperature but not at low temperature. All of the experiments in $MgCl_2$ solutions were therefore carried out with calf thymus DNA dissolved at room temperature or with the mouse lymphoma DNA. The method of dissolving the DNA was without influence on results in NaCl or KCl.

The specific viscosity of 0.05% DNA in NaCl solutions from 0.1 to 0.3 *N* was approximately 10% greater than in 0.05 *M* $MgCl_2$.

The sedimentation coefficient for 0.1% DNA (calf thymus) in $MgCl_2$ solutions is shown in Fig. 1. It appears from this curve that the maximum is reached at 0.04 to 0.05 *M* $MgCl_2$. Since several of the studies reported in the literature have been carried out at 0.3 *N* KCl or NaCl the comparison between the sedimentation of DNA in Mg and K salts was made at 0.05 *M* and 0.3 *N*, respectively. Such a comparison is shown in Fig. 2. It is evident from this figure that DNA has a higher sedimentation coefficient in magnesium chloride (lower values of $1/S$ where S is in Svedberg units) than in KCl at finite concentrations of DNA and that at infinite dilutions the two curves extrapolate to values which are similar but which, because of unavoidable errors at higher dilutions, have not been proven to be identical. In addition, there is shown an intermediate curve corresponding to the case where DNA was sedimented in 0.05 *M* $MgCl_2$ + 0.15 *N* NaCl + 0.01 *M* buffer. This indicated that addition of NaCl at similar ionic strength to a solution of $MgCl_2$, in which the charge effect was suppressed, diminished the sedimentation coefficient. The addition of 0.002 *M* $MgCl_2$ to 0.1 *N* NaCl caused no detectable increase in sedimentation velocity of 0.1% DNA indicating that the change in S depends on the proportions of the two salts used.

It was observed that the sedimentation boundary of the DNA in $MgCl_2$ solutions was always broader than in KCl solutions.

No difference was found between the S values for speeds of 50,740, 37,020 and 23,150 r.p.m.

These effects were further studied with solutions of the mouse lymphoma DNA. Aliquots of a concentrated stock solution of DNA in 0.01 *M* cacodylate buffer diluted with different salt + buffer solutions to a DNA concentration of 0.1% were

used in these tests. The first solution in 0.3 N KCl + buffer gave S = 7.92 with a typical sharp boundary. Another aliquot in 0.05 M $MgCl_2$ + buffer was characterized by S = 9.48 with a broader and lower boundary. A third solution made up in 0.05 M $MgCl_2$ + buffer, which stood for the same length of time required to make the previous run, was then adjusted to 0.05 M $MgCl_2$ + 0.16 N KCl + 0.01 M buffer and found to have S = 8.51 with an intermediate sharpness. Finally the solution in 0.05 M $MgCl_2$ + buffer was dialyzed against 0.3 N KCl + buffer overnight and the following day gave an S value of 7.98 which is similar to the original value in 0.3 N KCl (S = 7.92) and the boundary was of similar sharp appearance. The results on the mouse lymphoma preparation thus show the same qualitative effects as the calf thymus preparation.

Discussion

According to the Tolman–Tiselius theory[4] of the charge effects, the primary charge effect is eliminated on using salts of sufficient conductivity such as 0.3 N KCl or 0.05 M $MgCl_2$. The secondary charge effect is caused by differences in sedimentation velocity of the salt cation and anion. For salts, with lighter cations than anions such as $MgCl_2$, the sedimentation rate of a colloid ion would be slightly diminished. Since there is actually an increase in the nucleate velocity in $MgCl_2$, this must be attributable to causes other than these charge effects.

The decrease in sharpness of the DNA boundaries in $MgCl_2$ solutions as compared to KCl is a result of a smaller change in the dependence of sedimentation on concentration (see Introduction).

The similarity in sedimentation values at infinite dilution for DNA in $MgCl_2$ and KCl indicates that the free particles of DNA have the same diameter in both solvents but no conclusions can be drawn concerning small differences in length or bending of the flexible rods. If the ultimate explanation of differences in salt effect is on a morphologic rather than on an electrical basis, these results would be consistent with a shortening of the DNA particle in $MgCl_2$ solutions.

Limited observations[5] on light scattering at higher salt strengths than those used here indicated that the length of infinitely dilute DNA is the same in magnesium and KCl solutions. On the other hand, Katz[6] found a shortening of the length in $HgCl_2$ solutions.

The reversal of the magnesium effect by the addition of KCl to DNA solutions at finite concentrations indicates that Mg^{++} ion and K^+ ion are in competition for sites on the DNA, probably at the P–O positions.

The evidence[7-9] from experiments on the relative binding of Mg^{++} and Na^+ indicates that at low salt concentrations Mg^{++} binds to DNA more strongly than does Na^+, but there is no direct evidence as yet indicating that the DNA particle has a smaller charge in the presence of large amounts of Mg^{++} than in Na^+ or K^+.

(4) T. Svedberg and K. O. Peterson, in "The Ultracentrifuge," Oxford University Press, 1940.

(5) J. W. Rowen, *Biochim. Biophys. Acta*, **10**, 391 (1952).

(6) S. Katz, *J. Am. Chem. Soc.*, **74**, 2238 (1952).

(7) J. Shack, R. J. Jenkins and J. M. Thompsett, *J. Biol. Chem.*, **203**, 373 (1952); **198**, 85 (1952).

(8) J. M. Creeth and D. O. Jordan, *J. Chem. Soc.*, 1409 (1949).

(9) L. F. Cavalieri, *J. Am. Chem. Soc.*, **74**, 1242 (1952).

THE WATER-CATALYZED OXIDATION OF CARBON MONOXIDE BY OXYGEN AT HIGH TEMPERATURE

BY C. P. FENIMORE AND G. W. JONES

Research Laboratory, General Electric Co., Schenectady, N. Y.

Received December 13, 1956

By sampling burnt gases from lean flat hydrocarbon flames at one atmosphere pressure, the oxidation rate in the presence of ample water at 1700–2000°K. is determined to be $-1/(O_2)(d\ln(CO)/dt) = 1.2 \times 10^9\, e^{-24{,}000/RT(\text{moles/l.})^{-1}}$ sec.$^{-1}$. In the burnt gas from carbon monoxide flames, containing very little water, $-d\ln(CO)/dt$ is independent of oxygen and roughly proportional to water. The slower rate of comparatively dry carbon monoxide flames is raised toward the value appropriate to hydrocarbon flames by adding hydrogen to the carbon monoxide. A partial mechanism is suggested which is consistent with these results.

Introduction

In principle, water-cooled porous burners[1] offer a simple method of studying certain fast reactions at high temperatures. The burners produce steady flames which are flat unless the normal burning velocity is exceeded. The temperature of the burnt gas can be varied several hundred degrees by varying the supply of reactants to the burner. If the burnt gas, downstream of the flat luminous zone, maintains a reasonably constant temperature for a distance of 1 cm. or more, and if some reaction is still occurring in this region, one might follow it by probe sampling.

This report will discuss measurements of the clean up of carbon monoxide in burnt gases from lean flames. The reaction studied is the water-catalyzed oxidation of carbon monoxide by oxygen. A succeeding paper reports the application of the same method to the decomposition of nitric oxide.

(1) J. P. Botha and D. B. Spalding, *Proc. Roy. Soc. (London)*, **A225**, 71 (1954).

Experimental

Two different burners were used in this work. One possessed a porous burner surface, made of $^3/_{32}$-inch thick sintered bronze, of 11.09 cm.^{2} area. The surface was cooled by a water coil pushed against the upstream side.

A central tube, also pushed against the upstream side, covered 1.9% of the entire area of the burner surface. This central tube was fed separately from the remainder of the burner with 1.9% of the total reactant flow. Sodium chloride dust could be supplied to the central tube when desired, and burnt gas temperatures determined by the sodium line reversal method.

For acetylene flames, cooling was insufficient in the burner just described, and we used a burner obtained from W. E. Kaskan, of this Laboratory. The burner had a surface area of 22.3 cm.^{2}. It was made of a half-inch thick layer of sintered copper shot with a cooling coil immersed in the layer. Burnt gas temperatures for this burner for acetylene flames were supplied by Kaskan's measurements made with quartz coated thermocouples.[2]

The burnt gas was sampled through small uncooled quartz probes. The distance between probe tip and burner surface was varied by racking the burner, mounted on a micro-manipulator, up or down. The question must be considered, does the presence of the probe invalidate our measurements of the reaction rate? At the higher temperatures, the probe slowly closed up and it was sometimes necessary to renew the tip. But this did not change the slopes of our curves within experimental error, though it might slightly displace the entire curve of logarithm of carbon monoxide *vs.* distance. The displacement of the curves was presumably due to some cooling of the gas upstream of the probe tip, different for different size probes. Since different probes gave the same slope of ln(CO) *vs.* distance, we concluded that the reaction within this cooler region was a negligible contribution to the total reaction measured. That is, when the probe was moved out a distance, ΔX, the burnt gas flowing to it enjoyed a greater time, $V\Delta X$, to react at the temperature measured in the absence of the probe (V = streaming velocity of the burnt gas).

A second question arises—is the hot burnt gas unaffected by its mode of preparation? Or, for example, might an inordinate concentration of radicals from the flame reaction zone carry over into the burnt gas? Since our results are independent of the kind of fuel burnt, we believe the answer to this question is no.

Finally, different sampling positions were converted to different reaction times by assuming that the gas flow did not diverge and that the velocity of the burnt gas was given by multiplying the approach velocity of the reactants by the product of volume change due to reaction and the temperature ratio. Some support for this is offered by the fact that two different size burners were used and gave consistent results.

The gas samples drawn through the quartz probes were collected at a pressure low enough (<0.2 atm.) to ensure critical flow through the probe. In this way the sample spent the minimum time possible in the probe tip. Water in the sample was absorbed on magnesium perchlorate, carbon dioxide on Ascarite. The residue was passed through a liquid nitrogen trap, compressed to one atmosphere in a Toepler pump, passed over hot copper oxide, and the water and carbon dioxide so formed subsequently absorbed. Sampling times were up to one hour for burnt gases containing very little carbon monoxide. The absence of hydrocarbons in the sample was proven mass spectroscopically. Mass spectroscopic measurements also checked the relative flow measurements by determining oxygen.

Air and gas flows were measured with calibrated critical flow orifice meters. The gases were Matheson C.P. methane, ethane, ethylene and Prest-o-lite acetylene. Acetone was removed from acetylene with charcoal traps.

Results

The carbon monoxide in burnt gases from lean flames (containing 1.1 times the stoichiometric amount of air or more) may amount to several per cent. of the total carbon fed in the fuel, far more than the equilibrium quantity. As one samples further downstream, the logarithm of the carbon monoxide content is found to decrease linearly with distance. This first-order decrease agrees with Friedman and Cyphers'[3] result on a 2.15% uncooled propane flame burning at 46 mm. pressure.

The amount of hydrogen is generally considerably less than carbon monoxide and does not change much with distance. For all flames examined, the hydrogen found in the burnt gas corresponded to $P_{H_2} = 4$ to 6×10^{-4} atm.

Figure 1 shows the residual carbon monoxide for a number of acetylene flames. If the probe is placed too close to the luminous zone of the flame, carbon monoxide increases to a value greater than an extrapolation of the curves. This may result from disturbing the zone of vigorous oxidation. Curves similar to those of Fig. 1 were obtained for other fuels.

From the experimental data, we derive $-$ d ln(CO)/dx. Since the disappearance of carbon monoxide by reaction is opposed by its accumulation through diffusion down the concentration gradient thus formed, the measured slopes must be converted to $-$ d ln(CO)/dt by use of the expression given by Friedman and Cyphers.

$$-\frac{\mathrm{d}\ln(\mathrm{CO})}{\mathrm{d}t} = \frac{V^2}{4D}\left[\left(-\frac{2D}{V}\frac{\mathrm{d}\ln(\mathrm{CO})}{\mathrm{d}x} + 1\right)^2 - 1\right]$$

where V = linear velocity of the burnt gas, D = diffusion coefficient of carbon monoxide in the burnt gas. We took D = 3.5, 4.3, 5.1, 6.0 cm.^{2}/sec. at 1600, 1800, 2000 and 2200°K., respectively.

When the resulting values of $-$ d ln(CO)/dt are examined, it is obvious that they vary with oxygen concentration in the burnt gas unless the concentration of water is very small. Since the consumption of oxygen is small over the region sampled, we consider it constant and equal to the oxygen in excess over that required to burn the fuel to carbon dioxide and water. In Fig. 2 we plot both $-$d ln(CO)/dt and $-$ [1/(O$_2$)] (d ln(CO)/dt) against

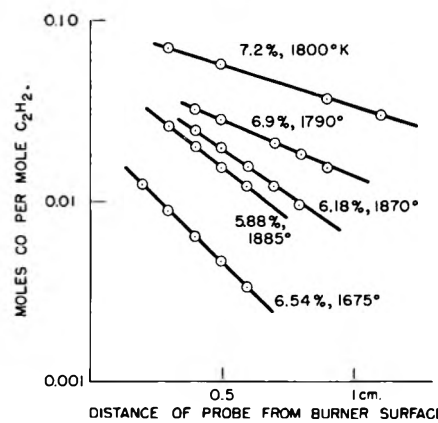

Fig. 1.—Clean up of CO in burnt gases from various C_2H_2, air flames. % C_2H_2 in reactants and burnt gas temperature noted on each curve.

the reciprocal of absolute temperature. We conclude that unless the concentration of water is very small

$$-\frac{1}{(\mathrm{O_2})}\frac{\mathrm{d}\ln(\mathrm{CO})}{\mathrm{d}t} = 1.2 \times 10^9 e^{-24{,}000/RT(\mathrm{moles/l.})^{-1}}\ \mathrm{sec.}^{-1}$$

(2) W. E. Kaskan, Sixth Symposium on Combustion, New Haven, August, 1956.

(3) B. Friedman and J. A. Cyphers, *J. Chem. Phys.*, **23**, 1875 (1955).

If the concentration of water is very small, the rate does not depend on oxygen, but rather appears to depend on the water concentration in the burnt gas. Roughly, at least

$$-\frac{1}{(H_2O)}\frac{d\ln(CO)}{dt} = f(T)$$

when the water concentration is very small in the burnt gas. The data are collected in Table I.

TABLE I

DATA ON CO CLEAN UP IN BURNT FLAME GASES

Fuel	% Fuel	T burnt gas, °K.	$-\frac{d\ln(CO)}{dz}$	$-\frac{d\ln(CO)}{dt}$	$-\frac{1}{O_2}\frac{d\ln(CO)}{dt}$
C_2H_2	5.88	1885	2.70	700	2.1×10^6
	6.18	1870	2.48	500	1.8
	6.54	1675	3.00	270	1.1
	6.90	1790	1.45	186	1.2
	7.20	1800	1.16	140	1.4
	7.30	1728	0.91	79	1.0
CH_4	8.01	1905	3.75	540	2.6
	8.67	1943	1.82	249	2.3
C_2H_4	5.41	1963	2.31	600	2.7
	5.80	2006	0.99	229	2.9
C_3H_8	3.00	1800	3.86	533	1.5
	3.24	1780	3.96	386	1.2
	3.24	1848	4.20	640	2.1
	3.63	1830	2.00	188	1.4
	3.63	2020	1.40	314	2.5
CO	26.6	2061	0.26	24	0.17
(0.74% H_2)	27.0	1993	0.24	20	0.16
CO	28.6	1909	0.43	30	0.65
(1.67% H_2)	25.2	2093	0.40	50	0.24
	26.3	2170	0.38	53	0.36
CO[a] (46% H_2)	25.5	1763	1.80	240	1.4

[a] To the mixture of 25.5% fuel in air, N_2 was added = 1.9 × CO so as to give a burnt gas similar to that obtained from hydrocarbon fuels.

Discussion

Figure 2 shows that $-d\ln(CO)/dt$ varies directly with oxygen concentration when ample water is present. But when very little water is present, as in the CO mixtures, $-d\ln(CO)/dt$ varies roughly with the concentration of water and does not depend on oxygen. These observations strongly suggest that the oxidation is catalyzed by water. A possible mechanism will now be offered.

The reaction

$$OH + CO \longrightarrow CO_2 + H \qquad (1)$$

is generally accepted as an important step for the oxidation of carbon monoxide in systems containing hydrogen or water. According to Avromenko and Lorentso,[4] its activation energy is $E_1 = 7$ kcal.

The hydrogen atoms from eq. 1 would certainly react, in part at least, with oxygen

$$H + O_2 \longrightarrow OH + O \qquad (2)$$

and Lewis and Von Elbe[5] have proposed the value, $E_2 = 17$ kcal.

(4) L. Avromenko and Lorentso, *Zhur. Fiz. Khim.*, **24**, 207 (1950); *C. A.*, **44**, 6245 (1950).

(5) B. Lewis and G. von Elbe, "Combustion, Flames and Explosions in Gases," Academic Press, New York, N. Y., 1951.

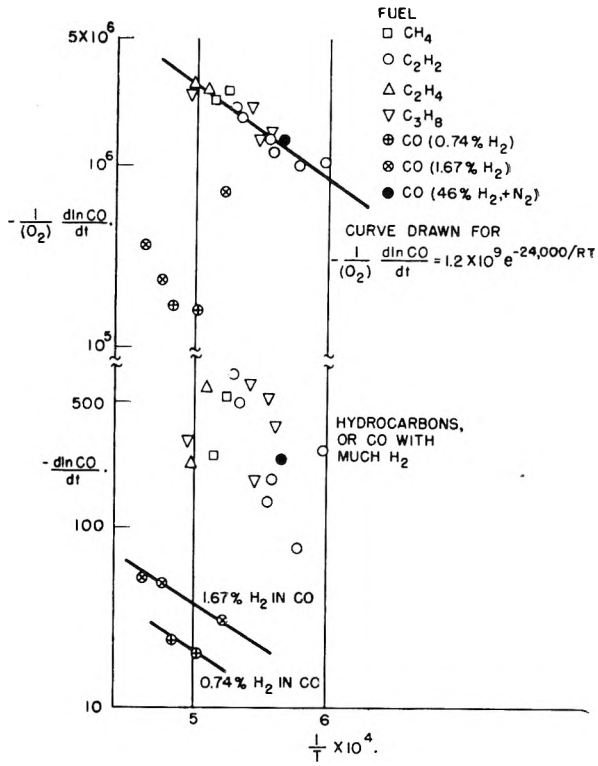

Fig. 2.—Temperature dependence of CO oxidation. Same data plotted in two ways.

If eq. 2 is a branching reaction in our system, that is, if the O atom continues the reaction chain, and if the radicals reach a steady concentration, then eq. 2 must be opposed by some chain terminating reaction. We postulate as the terminating step

$$H + OH + M \longrightarrow H_2O + M \qquad (3)$$

whence the steady hydroxyl concentration can be obtained by equating the rate of branching to terminating reactions, and

$$-\frac{1}{(O_2)}\frac{d\ln(CO)}{dt} = \frac{k_1k_2}{k_3(M)} = k$$

In this expression, M is any inert molecule which absorbs part of the energy released in reaction 3.

The expected activation energy is 24 kcal. $= E_3$. Since E_3 should be very small, our experimental value (24 ± 5) is consistent with the suggested mechanism.

The mechanism requires that k vary inversely with pressure. The ratio of Friedman and Cyphers' single determination at 46 mm. P, 1605°K., to our extrapolated result at 1 atmosphere is about 8, while the inverse ratio of the pressures is 17. Thus, the variation of k with pressure is qualitatively correct, and one can imagine factors which would surely decrease the expected ratio of rates in a more complete reaction mechanism; for example, the loss of radicals by diffusion would be expected to be more serious at low pressures.

In mixtures poor in hydrogen or water, reactions 1–3 should still occur, but the assumption that reaction 2 is always a branching reaction may be false, the O atom may not always regenerate OH in the absence of ample water. In that case, the steady hydroxyl concentration might very well

become independent of oxygen and proportional to water, as is suggested by our results for carbon monoxide flames containing 0.74 or 1.67% hydrogen. On adding 20 or 46% hydrogen to carbon monoxide, the rate of clean up of carbon monoxide in the burnt gas is raised toward the value appropriate to hydrocarbon flames. The rate is still low, however, (by about 40%) unless enough nitrogen is added to give a burnt gas with the same nitrogen concentration as was obtained from hydrocarbon flames. Then the rate for the carbon monoxide flame becomes the same as the rate obtained from hydrocarbon flames. The requirement that nitrogen be added may mean that carbon dioxide and/or water are more efficient third bodies than is nitrogen.

NITRIC OXIDE DECOMPOSITION AT 2200–2400°K.

BY C. P. FENIMORE AND G. W. JONES

Research Laboratory, General Electric Co., Schenectady, N. Y.

Received December 13, 1956

Flat premixed flames of nitrous oxide and fuel are burnt at controlled temperatures on a water-cooled porous burner. The nitrous oxide decomposes entirely in the flame, partly to nitric oxide, and the subsequent decay of nitric oxide in the burnt gas downstream of the flame is observed by probe sampling The decay is second order in nitric oxide, impeded by oxygen, and adequately described by $[(O_2)^{1/2}d(1/NO)/dt] = 2 \times 10^{12} e^{-98,000/RT}$(mole/l.)$^{-1/2}$ sec.$^{-1}$. The range of variables covered is $O_2 = 10^{-3} - 10^{-7}$ moles/l., $(NO)/(O_2) = 0.5 - 2.000$. We agree fairly well with Zeldovich's experimental results obtained by a different technique. However, his proposed mechanism must be modified in part at least.

Introduction

Zeldovich[1] carried out an ingenious, non-isothermal study of the nitrogen oxygen reaction at 2000–2900°K. Assuming that the high temperature reactions were

$$O + NO \underset{-1}{\overset{1}{\rightleftharpoons}} N + O_2$$

$$N + NO \underset{-2}{\overset{2}{\rightleftharpoons}} N_2 + O^{1a}$$

and supposing that oxygen atoms were in equilibrium with oxygen molecules, he derived an expression equivalent to I.

$$\frac{(O_2)^{1/2}\, d\left(\frac{1}{NO}\right)}{dt} = \frac{2Kk_2\left\{1 - \frac{(NO_{equ})^2}{(NO)^2}\right\}}{1 + \frac{k_2(NO)}{k_{-1}(O_2)}} \qquad (I)$$

where (NO_{equ}) is the equilibrium concentration of nitric oxide and $K = k_1(O)/k_{-1}(O_2)^{1/2}$ = the equilibrium constant for the reaction

$$NO = N + 1/2O_2, \Delta H = 91 \text{ kcal.}$$

Zeldovich set the denominator of I equal to one, since $(NO)/(O_2)$ was generally small, and obtained

$$2Kk_2 = 5 \times 10^{11} e^{-86,000 + 10,000/RT} \text{ (mole)/l.)}^{-1/2} \text{ sec.}^{-1}$$

Two comments can be made about this work. First, the higher dissociation energy of nitrogen, 225 kcal./mole, accepted since Zeldovich published, requires that K contribute 91 kcal. to the activation energy of Kk_2. This is not a major matter perhaps, for he recognized that his technique would give too low an activation energy. He allowed 4 kcal. correction, but there is room for a larger correction within the assigned error, and one can read his result as indicating an activation energy of 91–96 kcal. if the mechanism is retained.

Second, $(O_2)^{1/2}$ d $(1/NO)/dt$ should decrease with increasing values of the ratio, $(NO)/(O_2)$. Zeldovich never found this to happen up to $(NO)/(O_2)$ ratios of about one. Consequently, his data give no real indication that the nitrogen atom concentration is maintained by reaction 1 and its reverse. It is obvious that, granting his mechanism, he measured only reaction 2, and that the concentration of nitrogen atoms was determined by the equilibrium with nitric oxide and oxygen.

At far lower temperatures, 1400–1600°K., Kaufman and Kelso[2] showed that the decomposition of nitric oxide is strictly second order and independent of oxygen with an activation energy of 63.8 kcal. They gave reasons for believing this low temperature reaction to be the direct decomposition $2NO \rightarrow N_2 + O_2$, involving no intermediates, and showed that many previously published data agree with their determination, so the low temperature gas phase mechanism seems well established.

Because of its smaller temperature dependence, the low temperature decomposition could not contribute appreciably to the reaction in Zeldovich's temperature range. But Vetter[3] found a composite reaction at 1500–1900°K.

$$-\frac{d(NO)}{dt} = k_\infty (NO)^2 + k\beta(NO)(O_2)^{1/2} \text{ approximately}$$

and Kaufman and Kelson recomputed his data, assuming that the term in k_β was due to I. Then $k_2 (NO)/k_{-1}(O_2) >> 1$ necessarily, and they obtained

$$2Kk_{-1} = 4.5 \times 10^{12} e^{-101,000/RT} \text{ (mole/l.)}^{-1/2} \text{ sec.}^{-1}$$

A comparison of Vetter s recomputed result with Zeldovich shows that k_2/k_{-1} must assume a value of order unity at 1800°K., but this is inconsistent with the magnitude assigned to k_2/k_{-1} in recomputing Vetter's work. Without further measurements it is uncertain in a given situation how the high temperature decomposition will be affected by oxygen.

(1) J. Zeldovich, *Acta Physicochim. URSS*, **21**, 577 (1946).

(1a) Zeldovich called his scheme a chain reaction, and so it is as written. But his subsequent assumption that oxygen is in equilibrium with respect to dissociation destroys the chain character. Reaction 2 no longer creates an active center to carry on the decomposition, since the number of oxygen atoms is unchanged whether 2 occurs or not.

(2) F. Kaufman and J. Kelso, *J. Chem. Phys.*, **23**, 1709 (1954).

(3) K. Vetter, *Z. Elektrochem.*, **53**, 369 (1949).

We have studied the high temperature decomposition again, using a more direct method than did Zeldovich, and working at higher temperatures than Vetter could obtain. We confirm Zeldovich's experimental results but partly doubt his mechanism, because over a wide range of $(NO)/(O_2)$ ratios, 0.5–10^3, $(O_2)^{1/2}$ d $(1/NO)/dt$ remains constant at constant temperature, and this would require incredibly large values of k_{-1} if the data were fairly represented by I. The results always agree with I, of course, if the denominator of this expression is set equal to unity. This suggests that nitrogen atoms are always in equilibrium with nitric oxide and oxygen, and the measured reaction is reaction 2.

Vetter's results are puzzling. It seems impossible that the high temperature term of his composite rate could be a contribution of the high temperature homogeneous decomposition observed by Zeldovich and now confirmed by us.

Experimental Details

The hot gases in which we observed the reaction were obtained by combustion of flat premixed flames of nitrous oxide with hydrogen or carbon monoxide. The carbon monoxide always contained hydrogen. Sometimes, nitric oxide or oxygen was also added to the reactants. The flat burner had a surface of 22.3 cm.² area made of a layer of sintered copper shot 1.3 cm. thick with a water cooling coil embedded in it. The excess nitrous oxide decomposed to nitrogen, oxygen and nitric oxide in the combustion zone very close to the burner surface. Less than 0.1% of the nitrous oxide fed was ever recovered in the burnt gas. Under varying conditions, 5–30% of the nitrous oxide fed appeared in the burnt gas as nitric oxide.

The decomposition of nitric oxide in the burnt gas was followed by sampling through stout quartz probes of 1–2.5 mm. o.d.: very small i.d. at the tip. The probe never attained a temperature near the gas temperature and its cooling effect on the gas extended upstream an undetermined distance. We assume that when the probe was moved out a distance ΔX, the burnt gas flowing to it enjoyed a greater time, $V\Delta X$, to react at the burnt gas temperature measured in the absence of the probe (V = streaming velocity of the hot gas). The assumption is supported by the fact that large changes in the probe diameter did not change the measured rate of decay of nitric oxide.

A further assumption is that the flow of the burnt gas is one-dimensional, so that its streaming velocity can be calculated from the flow of reactants, the burnt gas analysis, and the temperature increase on combustion. We think that this assumption introduces an error of less than 10% in our rate constants, because attempts to approach one-dimensional flow more nearly with a screen did not change the rate of decay of nitric oxide. The screen was placed downstream of the sampling region so as to force the conical sheath of hot gas extending far downstream from the burner surface to become strictly cylindrical over the region sampled. The hot gas was visible because of the nitrogen dioxide emission continuum. It should be added that even in the absence of a screen, the hot gases were very nearly cylindrical over the region sampled.

Temperature of the burnt gas was controlled by varying the reactant flow, and measured by the sodium line reversal method. The image of the tungsten strip in the comparison lamp extended over the region of the burnt gas subsequently sampled. Thus the measured temperature was an average over the region studied. The flame was colored by inserting a small salt packed quartz tube into it at the burner surface. This occasionally dirtied the burner, but dilute hydrochloric acid and water cleaned the surface nicely. In a series of runs at ostensibly constant temperature, we think our temperature may have varied about 10° and we consider this our greatest source of error.

The pressure in a collecting bottle attached to the probe was maintained below 2 mm., and the sample system flushed carefully. Samples were analyzed by the mass spectrometer. The advantage of low pressure samples, of course, is

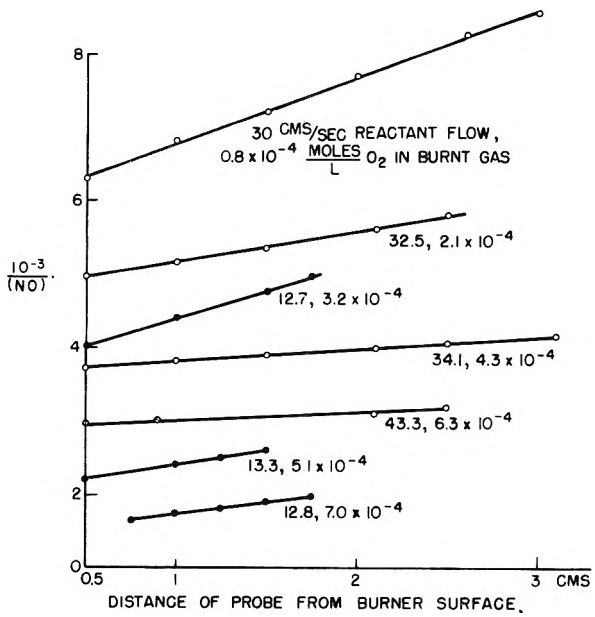

Fig. 1.—Decomposition of nitric oxide in burnt gases at 2337°K.: open symbols, H_2 fuel; solid symbols, CO (11.6% H_2) fuel.

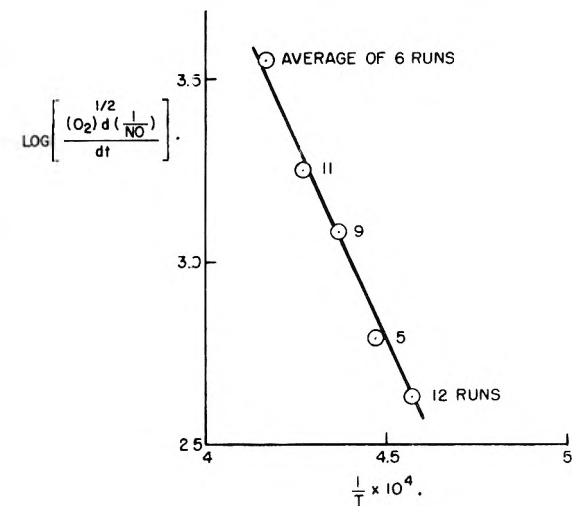

Fig. 2.—Temperature dependence of nitric oxide decomposition.

that mixtures containing both nitric oxide and oxygen could be analyzed easily. No nitrogen dioxide peak was ever observed. Water was generally absorbed from the sample before analysis by passing the gas over magnesium perchlorate, and sometimes carbon dioxide by ascarite.

All reactants were analyzed. C.P. Matheson gases were used and corrections for impurities were negligible except that the nitric oxide contained 1–3% nitrogen. We metered reactants through critical flow orifices to an accuracy of about 1%. Nitrous oxide cooled the meter considerably as it expanded through it; but the flow calculated from the known fuel flow and the burnt gas analysis agreed closely with that metered, perhaps because the cooling in the runs was nearly equal to the cooling during calibration.

Results

We sampled at about five positions for each of some forty runs, and found that the best linear graphs of our data were obtained by plotting the reciprocal of nitric oxide concentration against the distance of the probe from the burner surface. A sample of the results is shown in Fig. 1, and the runs are listed in Table I.

TABLE I

DATA ON NO DECOMPOSITION

Reactants N_2O +	Reactants at 298°K., cms/sec	T, °K.	$(NO)^a/(O_2)$	Burnt gas $(O_2)^{1/2} \times 10^{2a}$, (moles/l.)$^{1/2}$	$\frac{d(1/NO)}{dt} \times 10^{-4}$, (moles/l.)$^{-1}$ sec.$^{-1}$
0.46 CO (11.3% H_2)	10.2	2188	0.9	2.4	1.8
0.69 CO	11.0		1.0	1.7	2.7
.93 H_2	23.9		4.8	0.5	10.2
.58 H_2	24.4		0.6	2.2	1.8
.80 H_2	20.2		0.9	1.4	3.3
.42 H_2	21.4		0.5	2.7	1.4
.79 H_2 + 0.28 NO	23.4		2.6	1.6	2.5
.79 H_2 + 0.38 NO	25.6		3.0	1.7	2.6
.88 H_2 + 0.43 NO	24.1		4.3	1.4	3.1
1.17 H_2	34.6		550	0.038[b]	100
1.31 H_2	42.6		1200	0.023[b]	180
1.52 H_2	48.7		2400	0.014[b]	250
0.59 CO (15.6% H_2)	13.4	2288	0.9	2.1	5.0
.77 H_2	23.4		0.9	1.5	8.1
.88 H_2	22.4		1.8	1.0	13.4
.77 H_2 + 0.23 NO	38.1		1.9	1.7	6.7
.76 H_2 + 0.10 NO	38.0		1.4	1.6	7.5
.75 H_2 + 0.51 NO	40.0		2.9	1.8	6.1
1.15 H_2	38.9		110	0.080[b]	180
1.36 H_2	51.2		410	0.037[b]	310
1.29 H_2 + 0.19 NO	37.2		230	0.088[b]	160
0.50 CO (11.6% H_2)	13.3	2337	1.0	2.3	6.6
.36 CO	12.8		0.9	2.6	5.4
.60 CO	13.2		0.8	2.2	7.3
.71 CO	13.2		1.1	1.7	10.9
.79 CO	12.7		0.8	1.8	10.4
.59 H_2	34.1		0.6	2.1	7.7
.77 H_2	32.5		1.0	1.5	13.3
.45 H_2	43.3		0.5	2.5	6.7
.88 H_2	30.0		2.1	0.9	25.2
.76 H_2 + 0.22 NO	40.7		1.7	1.7	10.0
0.84 H_2 + 0.23 NO	40.9		2.0	1.5	15.1
.46 CO (0.9% H_2)	11.0	2400	1.0	2.3	14
1.10 CO	16.0		1.4	1.2	25
0.78 H_2	46.0		0.5	1.9	22
.68 H_2	47.8		0.7	1.8	22
.58 H_2	57.6		0.5	2.2	16
.86 H_2	40.9		1.1	1.1	33
.50 CO (10.5 H_2) + 0.25 O_2	10.4	2238	0.8	3.0	1.8
.50 CO + 0.37	10.9		0.7	3.3	1.6
.60 H_2	25.2		0.6	2.2	2.9
.57 H_2	27.7		0.6	2.1	3.1
.69 H_2	24.6		0.7	1.9	3.8

[a] Average values of $(NO)/(O_2)$ and of $(O_2)^{1/2}$ over the region sampled. [b] For these runs, O_2 determined from $P_{O_2}^{1/2} = K_P P_{H_2O}/P_{H_2}$ with $K_p = 1.05 \times 10^{-3}$ at 2188°, 2×10^{-3} at 2288°.

The slopes $d(1/NO)/dx$, such as are shown in Fig. 1, were multiplied by the velocity of the burnt gas to get $d(1/NO)/dt$. The disappearance of nitric oxide by decomposition is opposed by its accumulation through diffusion and this effect tends to make $d(1/NO)/dt$ smaller than the decomposition rate. But the difference is not significant for our conditions.

The decomposition is always measured in the presence of other gases. The rate constant is unchanged whether the fuel is hydrogen or carbon monoxide, containing some hydrogen. Furthermore, the presence of unburnt fuel in a few rich runs did not affect the rate constant. Oxygen markedly hinders the decay of nitric oxide in such a way that $(O_2)^{1/2}d(1/NO)/dt$ is approximately constant at constant temperature.

The second-order constants obtained are always at least ten times greater than the values predicted by extrapolating Kaufman's and Kelso's low temperature rate constant. Therefore we ignore any correction for a contribution from the low temperature mechanism.

Since $(NO_{equ})^2/(NO)^2 << 1$, the high temperature mechanism of Zeldovich requires that $(O_2)^{1/2} \cdot d(1/NO)/dt$ be constant for small $(NO)/(O_2)$, but depend on the $(NO)/(O_2)$ ratio when this is sufficiently large. Our data must be interpreted, however, with allowance for the probable error of actually obtaining a constant burnt gas temperature

in flames of different mixtures and flow rates. Since a single run might miss by about 10° in a series at ostensibly constant temperature, we must anticipate errors of 10–20% in the determination of the rate constant from a single run. Within this error, we find $(O_2)^{1/2}d(1/NO)/dt$ independent of the $(NO)/(O_2)$ ratio over a wide range. For example, at 2188°K., nine runs with $(NO)/(O_2) = 0.5 - 5.0$ give $(O_2)^{1/2}d(1/NO)/dt = 430 \pm 30$; while we find $(O_2)^{1/2}d(1/NO)/dt = 380, 410, 350$ when $(NO)/(O_2) = 550, 1200$ and 2400, respectively. If Zeldovich's mechanism is accepted, $k_2/k_{-1} < 3 \times 10^{-4}$ conservatively at 2188°K. Similarly, $k_2/k_1 < 10^{-3}$ at 2288°K.

Averaging our values of $(O_2)^{1/2}d(1/NO)/dt$ at each of five temperatures, we plot the results in Fig. 2 and obtain

$$(O_2)^{1/2}d(1/NO)/dt = 2 \times 10^{12}e^{-98000/RT} \text{ (mole/l.)}^{-1/2} \text{ sec.}^{-1}$$

We consider this in good agreement with Zeldovich. The two studies agree well within the error assigned to his determination by Zeldovich.

According to the Zeldovich mechanism, the rate constant above should be $2Kk_2$ as stated in the introduction. From the equilibrium constants tabulated by Lewis and von Elbe[4], one can derive K after correcting for the fact that their tables are based on $D_{N_2} = 170.2$ kcal./mole rather than 225 kcal. This leads to $K = 31\ e^{-91,000/RT}$, and substituting in our experimental result

$$k_2 = 3 \times 10^{10}\ e^{-7,000/RT} \text{ (mole/l.)}^{-1} \text{ sec.}^{-1}$$

(4) B. Lewis and G. von Elbe, "Combustion, Flames, and Explosions in Gases," Academic Press, New York, N. Y., 1951.

The value of k_2 is possible. However, the insignificance of $k_2(NO)/k_{-1}(O_2)$ relative to unity at 2188°K., requires $k_{-1} > 2 \times 10^{13}$ (mole/l.) sec.$^{-1}$ which appears impossibly large. We conclude that the Zeldovich mechanism contains a flaw of some nature, though we cannot state certainly what it is. Probably nitrogen atoms are maintained in equilibrium with nitric oxide and oxygen by some additional means than reactions 1 and −1. In this case, $(O_2)^{1/2}d(1/NO)/dt = 2Kk_2$ still but the reactions which maintain the equilibrium concentration of nitrogen atoms would be unknown, and might even change for changing reaction mixtures. Or nitrogen atoms may not be involved in the high temperature decomposition at all, though this seems extreme because other likely modes of decomposition of nitric oxide are ruled out by the existence of a low temperature decomposition reaction of known mechanism.[2]

The oxidation of nitrogen to nitric oxide, the reverse reaction, was attempted briefly at 2400°K. with flames of nitrogen, oxygen and hydrogen. About 1–3% of the equilibrium amount of nitric oxide was formed in 5×10^{-3} sec. when nitrogen and oxygen concentrations in the burnt gas were 10^{-3} moles/l. This amount was too little to measure accurately, but is about the yield expected according to the equation

$$\frac{(O_2)^{1/2}\,d(1/NO)}{dt} = 2Kk_2\left\{1 - \frac{(NO_{equ})^2}{(NO)^2}\right\}$$

with (NO_{equ}) expressed in terms of nitrogen and oxygen.

THE ELECTROMOTIVE FORCE CENTRIFUGE, FACTORS AFFECTING PRECISION

BY ROBERT L. KAY* AND D. A. MACINNES

Contribution from The Rockefeller Institute for Medical Research, New York, N. Y.

Received December 15, 1956

In order to improve the precision of measurements with the electromotive force centrifuge studies have been made of (a) the circuit for measuring cell potentials; (b) the commutator for making electrical connection between the galvanic cell in the rotor with the potentiometer; (c) the design of the cell and its mounting; (d) thermal effects due to centrifugal compression; and (e) the effect of thermal insulation of the cell and its mounting on the measured potentials. A means for correcting these potentials for thermal effects is described.

The electromotive force generated by a simple galvanic cell situated in a centrifugal field was first studied by des Coudres[1] and later by Tolman[2] who used a cell of the type

$$(Pt)\ ;\ \underset{r_1}{I_2, KI, I_2}\ ;\ \underset{r_2}{(Pt)} \qquad (A)$$

In this cell two, otherwise identical, iodide–iodine electrodes are situated at radii r_1 and r_2 from the center of rotation. For the potential E developed by this cell Tolman derived the expression in

$$-EF = 2\pi^2n^2(r_2^2 - r_1^2)\,[t_k(M_{KI} - \bar{V}_{KI}\rho) - {}^1/_2(M_{I_2} - \bar{V}_{I_2}\rho)] \quad (1)$$

which F is the Faraday, n is the number of revolutions per second, t_k is the cation transference number of the iodide KI, M_{KI} and M_{I_2} are molecular weights, $\bar{V}_{KI}$ and $\bar{V}_{I_2}$ partial molal volumes, and ρ is the density of the solution. A series of papers from this Laboratory[3] describe further work on this subject. As a method for determining the transference number, t_k, the method has the advantage, over the procedures now in use, that the electrodes do not have to carry appreciable current. This is of special utility in dealing with non-aqueous solutions. However, in the development of the method it has been necessary to eliminate a

* Merck Postdoctoral Fellow from Canada, 1952.

(1) Th. des Coudres, ANN. PHYSIK CHEM., **49**, 294 (1893); **57**, 232 (1896).

(2) R. C. Tolman, *Proc. Am. Acad. Arts Sci.*, **46**, 109 (1910); *J. Am. Chem. Soc.*, **33**, 121 (1911).

(3) (a) D. A. MacInnes, *Ann. N. Y. Acad. Sci.*, **43**, 243 (1942); (b) B. R. Ray and D. A. MacInnes, *Rev. Sci. Inst.*, **20**, 52 (1949); (c) D. A. MacInnes and B. R. Ray, *J. Am. Chem. Soc.*, **71**, 2987 (1949); (d) D. A. MacInnes and M. O. Dayhoff, *J. Chem. Phys.*, **20**, 1034 (1952); (e) D. A. MacInnes, *Proc. Am. Phil. Soc.*, **97**, 51 (1950).

number of disturbing effects which result in errors in the potential measurements. Some of these efforts to obtain greater accuracy have been discussed in earlier papers, including the precision measurement of the speed of rotation, n,[4] and the elimination of the effects of suspended particles in the solution.[3b,3d] An investigation of the effect on the measured potentials of the ratio of iodine to iodide concentrations in the cell solution has been made.[3b,3d] Other researches in this Laboratory have been concerned with the determination of the density, ρ, and of the partial molal volumes, $\bar{V}$.[5]

The present paper is concerned with further efforts to obtain accuracy in the measurements.

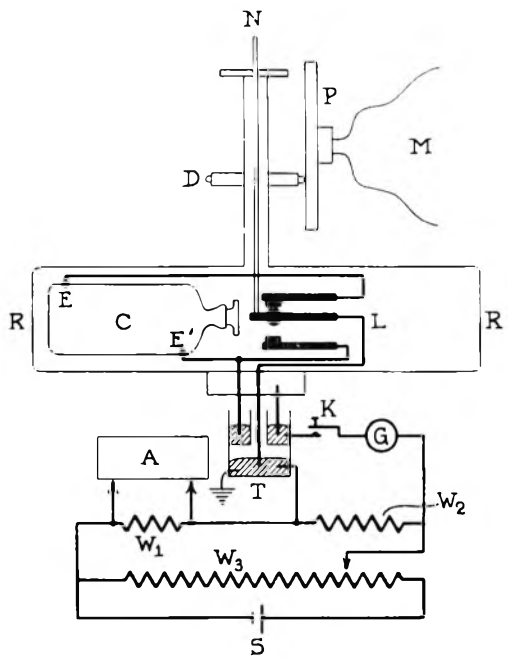

Fig. 1.—The apparatus and the potential measuring system.

The Apparatus and the Potential Measuring System.—An assumption underlying the derivation of equation 1 is that the solution contained between the electrodes in the cell A is uniform as to composition. This can be true only for relatively low values of the speed of rotation, n, of equation 1. At high speeds, *i.e.*, of the order of 60,000 r.p.m., both the salt and iodine will increase in concentration at the end of the cell near the periphery of the rotor and decrease at the other end. This will continue until the chemical potentials of both components are constant throughout the cell, and the resulting electromotive force will be zero. The tendency toward this sedimentation exists at all speeds, and is, as a matter of fact, responsible for the measured potentials of the cell. With rotations up to 7,200 r.p.m., the maximum used in our work, decreases of potential with time that could, with certainty, be ascribed to sedimentation have not been observed in our study of aqueous solutions. As will be shown in a later paper the results are affected by sedimentation when using methanol as solvent. It is clear from these considerations that there are definite advantages in working with low speeds of rotation, involving small values of the electromotive force, which must be measured with accuracy. Disturbances such as thermoelectromotive forces must be carefully eliminated. This has required some alterations of the apparatus and of the measuring circuit which will be outlined below.

The centrifuge and the potentiometer circuit are shown diagrammatically in Fig. 1. The rotor R-R, a disk of magnesium 23 cm. in diameter and 5 cm. thick, is turned in a horizontal plane by the pressure of the disk D on the plate P, which is rotated by the synchronous motor M, the rotor speed being varied by changing the position of the disk with relation to the plate. The cell C has electrodes E and E′ which are connected through the switch L with the commutator T which leads to the potentiometer system. The Rubicon potentiometer used has a precision of 1 microvolt. This has been increased tenfold by means of an arrangement, similar to that used by Grinnell and Koenig[6] in which the cell potential is balanced by the drop across the 10 ohm standard resistance W_2. The adjustment is indicated by the galvanometer G when the key K is depressed. A variable potential drop through W_2 is obtained by adjusting the resistance W_3 (adapted from a L. and N. type K potentiometer), with the primary cell S as the source of electrical energy. In series with W_2 and W_3 is the 100 ohm standard resistance W_1, the potential across which is determined with the Rubicon potentiometer A mentioned above. Thus a measured variation of 1 μv. corresponds to 0.1 μv. in the potential of the cell C. In order to obtain accuracy in accord with this precision it is necessary to eliminate, or correct for, potentials arising at the commutator and from thermoelectric effects. The latter have been avoided as much as possible by dispensing with soldered joints, by enclosing the whole potentiometer system in a metal box provided with means for making adjustments from the outside, and by using a constant temperature room. Any extraneous potentials not eliminated by these precautions, and those arising from the commutator, can be measured and corrected for by the use of the switch L. Normally it is in the position shown in the figure in which the cell is connected with the potentiometer circuit. If, however, the rod N is depressed the cell is disconnected, and the residual potential, if any, may be directly measured. As described in previous papers[3b,3c] the rotor R-R and the commutator T are contained in a vessel in which a vacuum of about 10μ is maintained. It was therefore necessary to arrange for a vacuum seal for the rod N by which the switch L is operated. A change from our previous practice is to provide for the exhausting of the channel containing the cell C. This aids in insulating the cell thermally from the rotor.

The Commutator.—A very important part of the e.m.f. centrifuge is the commutator, T of Fig. 1, by which electrical contact of the electrodes of the cell C in the rotor is made with the potentiometer.

(4) D. A. MacInnes, *Rev. Sci. Inst.*, **14**, 14 (1943).

(5) D. A. MacInnes, M. O. Dayhoff and B. R. Ray, *ibid.*, **22**, 643 (1951); D. A. MacInnes and M. O. Dayhoff, *J. Am. Chem. Soc.*, **74**, 1017 (1952).

(6) S. W. Grinnell and F. O. Koenig, *ibid.*, **64**, 682 (1942).

The commutator now in use is shown in Fig. 2 and is the result of much research. In this figure the relative horizontal dimensions have been expanded. The contact C is fitted with a copper needle which dips into the pool of mercury M. Projecting from the contact C′ is a hollow copper cylinder about 2 mm. inner diameter projecting into the annular mercury ring M′. It has been found quite essential to keep the peripheral speed of the contacts low to reduce heat effects, which result in thermoelectric potentials, and also to reduce the loss of mercury due to spattering. The leads K, K′ and L, L′ connect, respectively, with the cell in the rotor and with the potentiometer. Supporting and insulating the two contacts is the plastic cylinder P which fits into the rotating element E, which is kept in strict alignment with the aid of the ball bearings B and B′, which are, in turn, mounted on the cylinder D. This is held in place by the heavy aluminum frame F which is firmly connected with the support of the centrifuge. The main break with our earlier designs is the use of the rubber tube T to furnish a flexible connection of the rotor R with the commutator. This allows for precession of the rotor, and also insulates the rotor thermally from the commutator. Some slack must be allowed in the leads K, K′ to avoid breakage during the precession of the rotor. The potential developed in this commutator, at full speed, is of the order of 0.5 μv., and can be measured with the aid of the switch L shown in Fig. 1. The precision alignment prevents pressure of the needle and cylinder of the contacts C and C′ with the thin plastic wall S which holds mercury in the annular ring. Due to frictional heat such pressure results in relatively large and erratic potentials in the cell circuit.

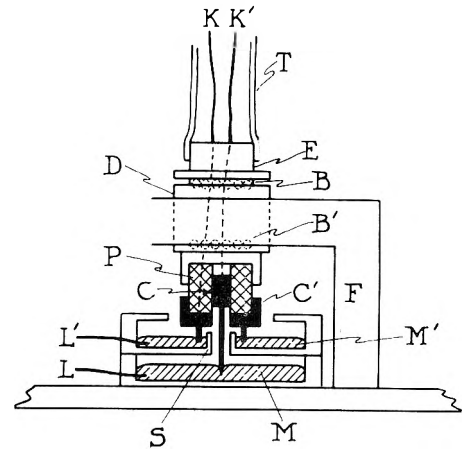

Fig. 2.—Details of the commutator.

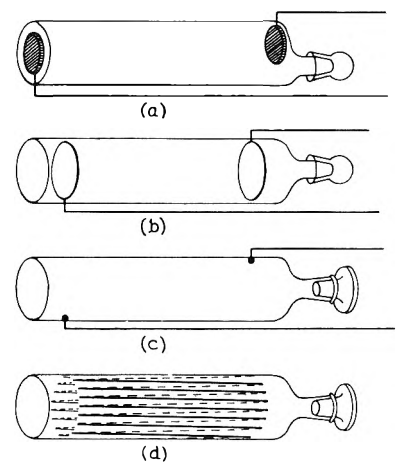

Fig. 3.—The galvanic cells.

The Design of the Galvanic Cells.—As already mentioned, the galvanic cells used in these experiments consist of vessels containing iodide–iodine electrodes at two different radii in the rotor. The vessel of the first cell was made of plastic. All later ones were formed from Jena glass and are shown in Fig. 3. In the form represented by (a) the circular disk electrodes are sealed in place at the ends of the cell and platinum leads pass through the glass wall. The disadvantage of this type of cell is that suspended particles of dust and oil are centrifuged to the electrodes, and these particles have definite effects on the potentials. However, by ultrafiltration of the solutions contained in the cell the effect was largely, if not entirely, eliminated. The necessity for such ultrafiltration was overcome by the design of cell shown by (b). Here the electrodes are rings of platinum wire sealed in the wall of the cell some distance from the ends. Centrifugation in this case forces the particles past the electrodes. However it has not been found possible to make these cells accurately enough to give single values to the radii, r, of the electrodes. On account of this fact, in our most recently reported work[3d] it was found necessary to replace the term $(r_2^2 - r_1^2)$ in equation 1 by an empirically determined cell constant K.

It has however become increasingly evident that for maximum precision all points on an electrode should have the appropriate value of r, and should thus lie on a cylindrical surface, otherwise when the centrifuge is in rotation different positions on the electrode will be at various potentials with the result that "local action" will occur. This action amounts to short-circuited galvanic cells, the operation of which may tend to change the composition and potentials at the electrodes. Such effects of local action have been discussed in a recent paper by Uhlig.[7] The construction of cells in which the electrodes have appreciable areas which are cylindrical surfaces around the axis of rotation with definite values of the radii represents serious mechanical difficulties. One solution is to reduce the electrode area as near as possible to a point. This has been done in the design of cell shown in Fig. 3c. Here the electrodes consist of platinum spheres about 1 mm. in diameter sealed into the cell wall.

Any of these glass cells may burst if placed in a strong centrifugal field. The means for overcoming this difficulty is illustrated in Fig. 4. Here a cell of the type (c) of Fig. 3 is shown enclosed by a shield S made of brass or plastic. In the space between the cell and shield is placed a silicone lubricant which has a low vapor pressure. The effect of this semi-fluid material is to balance, to a suffi-

(7) H. H. Uhlig, *Proc. Nat. Acad. Sci.*, **40**, 276 (1954); *J. Electrochem. Soc.*, **100**, 173 (1953).

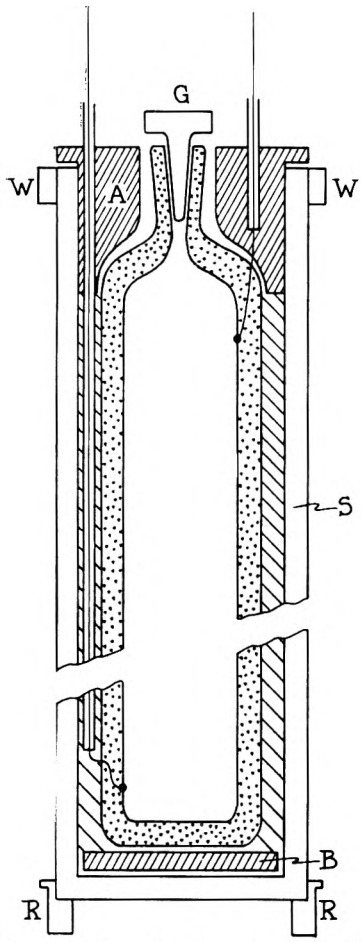

Fig. 4.—The galvanic cell and shield.

cient extent, the pressures on the glass wall of the liquid in the cell. The spacers A and B hold the cell and leads in place in the shield. The cell is closed by the Teflon plug G, which furnishes a vacuum seal. Other details shown will be discussed later in this paper.

Temperature and Heat Effects.—If the two electrodes in the cell are at different temperatures large errors can arise in the measurements. The magnitude of the potential difference is approximately 660 μv. per degree[8] which means that differences must be eliminated to 0.001° if errors of more than one microvolt are to be avoided. To study and attempt to control this effect, a cylindrical rack holding 25 copper–constantan thermojunctions was placed, in some of our earlier work,[3c] outside the brass shield S of Fig. 4. Well-founded suspicion that the potential measurement on the thermojunctions, thus arranged, did not reflect the thermogradients in the cell itself, led to the use of the expedient shown in (d) of Fig. 3, where the 25 junctions were attached directly to the cell with silicone varnish and were inserted into the semi-fluid material, between the brass shield and the glass wall of the cell.

Some of the results of the experiments with this arrangement are shown in Fig. 5. During the times represented by the abscissa the rotor speed was increased, at the intervals indicated, from zero by three stages to 6000 r.p.m., and then reduced to 3600 and to rest. It will be observed that at each change of speed there is a sudden development of a potential of the set of 25 thermojunctions indicating a thermal gradient in the system. The potential decreases rapidly, then tends slowly toward zero after a new constant speed is established. On lowering the rotational rates these effects occur in the reverse direction.

Beams[9] has pointed out that the maximum radial temperature difference due to adiabatic compression may be calculated from the equation[10] which

$$\frac{\Delta T}{\Delta P} = \frac{T}{C_p}\left(\frac{\partial V}{\partial T}\right)_p$$

for a centrifugal field takes the form

$$\Delta T = \frac{2\pi^2 T}{C_p}\left(\frac{\partial V}{\partial T}\right)_p (r_2^2 - r_1^2)(n_2^2 - n_1^2)\rho$$

in which n_1, n_2 are the number of revolutions per second before and after the change of speed. Computations with this equation yield at least the right order of magnitude for the effects. However, the junctions are in direct contact with the plastic material between the shell S and the glass wall of the cell, as is shown in Fig. 4, so that the temperature differences observed are affected by the adiabatic compression of this material as well as that of the solution in the cell. This is shown by the fact that temperature gradients of the same order as those shown above are observed if the solution is left out of the cell. Conversely, if the viscous material is omitted and the solution retained much the same effects as those shown in Fig. 5 are observed. However, if both the solution and the viscous material are omitted very slight temperature effects are observed on changing speeds.

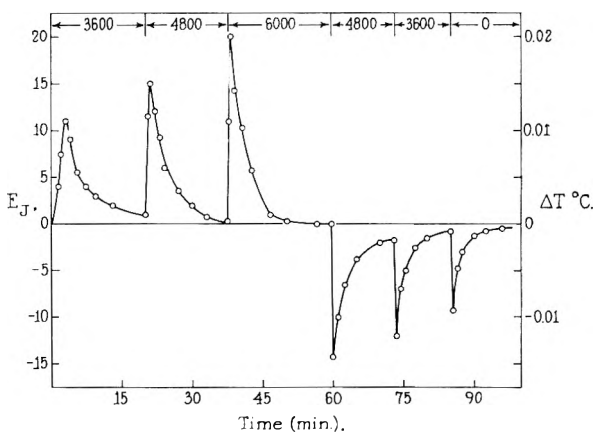

Fig. 5.—Measurement of the adiabatic compression effect.

Thermal Insulation of the Galvanic Cell.—In spite of the fact that the rotor turns in a vacuum of 10 μ, thus greatly reducing air friction, our experiments indicate that a radial temperature gradient may exist and this will necessarily affect the potential of the galvanic cell. This effect is however much modified by the way the cell and accessories are thermally connected with the rotor. The results of measurements of the potentials, at

(8) J. N. Agar and W. G. Breck, private communication.

(9) J. W. Beams, *J. App. Phys.*, **8**, 795 (1927).

(10) Lewis and Randall, "Thermodynamics," McGraw-Hill Book Co., New York, N. Y., equation 25, p. 137.

6000 r.p.m., of a cell mounted as shown in Fig. 4, containing 1.0 *M* KI and 0.08 *M* I_2, are shown in Fig. 6. In this plot values of the potential in microvolts are given as functions of the time. It will be observed from curves A, B and C that after an initial period of about 30 minutes the values become essentially constant for as long as the measurements are made. In this initial period the effect on the potential of the adiabatic compression is dissipated. The observed steady-state potentials are however greatly dependent upon the thermal connection of the cell sheath with the rotor. For curve A the best available thermal insulation was used. Contact of the shield S with the rotor was made only through the Lucite rings R-R and W-W of Fig. 4. In the case of the data shown in curve B the brass sheath was replaced by one made of Lucite. In obtaining the data for curve C the bottom of the brass sheath S was in direct metallic contact with the magnesium rotor by replacing the Lucite ring R-R with an aluminum cylinder. The steady potentials of the cell under these varying conditions are evidently quite different. To arrive at an estimate of the potentials in the cell due to thermal gradients the following procedure was adopted. After the measurements had reached a steady state as shown in curves A, B and C, the rotor was stopped as quickly as possible and e.m.f. readings were again taken as functions of the time. The results are plotted in curves A′, B′ and C′ in the lower portion of Fig. 6. It is interesting to note that these curves converge toward a value of zero for the cell potential at the moment the rotation was stopped. This is undoubtedly due to the fact that an air bubble, held in the inner side of the cell by centrifugal force, is released when the rotor stops, producing stirring which, along with precession of the rotor, temporarily equalizes the temperatures at the two electrodes.[11] However the temperature gradient existing in the cell wall, the semifluid material, and the sheath, soon begins to produce a difference of temperature at the electrodes. After about 30 minutes the potentials become constant for the conditions A′ and B′ in which the cell had the most thermal insulation. For the case shown by curve C′ there was thermal contact with the rotor so that the potentials were influenced by temperature changes in the rotor. If the linear portions of the curves A′, B′, and C′ are extrapolated to zero time and resulting values are added to the corresponding steady state voltages at 6000 r.p.m., a constant 647 ± 1 μv. is obtained, which is presumably the

(11) A test of this explanation was made by inserting ground glass into the cell, thus immobilizing the solution in the spaces between the glass particles. A large positive potential due to the adiabatic decompression during deceleration was observed immediately on stopping the rotor.

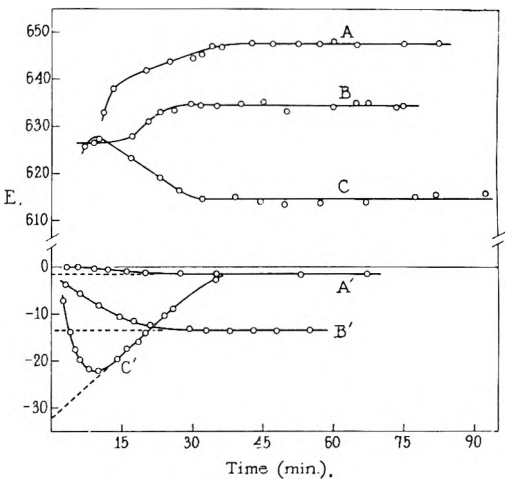

Fig. 6.—The effect of thermal insulation on potentials.

potential of the cell as corrected for the effect of the thermal gradients. In Table I these figures are combined with data obtained in the same manner at other speeds. From equation 1 it is evident that the quotient E/n^2 should be independent of the rotational speed n. In the Table E_m is the measured potential after steady-state conditions have been obtained as shown in Fig. 6, and E_c is the corresponding correction obtained as described above. The final column gives values of $E/n^2 = (E_m - E_c)/n^2$, which, as can be seen, are nearly constant. Due to the relative complexity of the heat flow the greater variation of the figures for the thermal contact condition C, is perhaps to be expected. It is to be noted that the corrections are quite small for condition A, *i.e.*, the best thermal insulation. It is perhaps significant that these results were obtained with cells of type (c) of Fig. 4 in which the effects of local action, due to uncertain values of the radii r_1 and r_2, are reduced to a minimum.

TABLE I

Thermal Contact	Speed, r.p.m.	E_m	E_c	$\frac{E_m - E_c}{n^2} \times 10^4$
A	3600	232.4	− 0.5	646.9
	4800	413.0	− 2.0	648.4
	6000	646.1	− 1.5	647.6
	7200	932.2	− 2.4	649.0
B	6000	634.5	−13.6	648.1
C	3600	215.0	−19.4	651.1
	4800	389.4	−24.9	647.3
	6000	614.7	−32.2	646.9

A study of solutions of iodides in methanol, with the aid of the e.m.f. centrifuge, including the improvements in technique outlined above, will appear in a forthcoming paper.

A REDETERMINATION OF THE VALUE OF THE FARADAY WITH THE IODINE COULOMETER

I. A PRECISION CONSTANT CURRENT APPARATUS

By D. A. MacInnes, Chia-chih Yang and Alfred R. Pray*

Contribution from the Laboratories of the Rockefeller Institute for Medical Research, New York, N. Y.

Received December 17, 1956

A device for obtaining currents constant to about 1 part per million is described. The value of the current is determined by standard cells and resistances. Adjustments are made by the motion of a line of light impinging on differential photocells, which, through a relay system, operate a reversing motor which changes the length of a column of electrolytic resistance. The apparatus is in use in the determination of the value of the Faraday with the aid of the iodine coulometer.

Introduction

The Faraday, *i.e.*, the number of coulombs necessary to produce one gram equivalent of electrochemical reaction by the passage of current across a metal-electrolyte boundary, has received relatively little study in recent years. Since the work of Washburn and Bates[1] and of Bates and Vinal[2] on the iodine coulometer, the only electrochemical research on the subject is that of Craig and Hoffman[3] who employed the electrolytic decomposition of sodium oxalate as the coulometer reaction. The investigations of Birge, DuMond, Bearden and their associates have amply demonstrated that the Faraday is of prime importance in evaluating other physical constants, such as the charge and mass of the electron, and the Planck quantum constant. A re-study of the iodine coulometer using modern techniques and standards has therefore been instigated. In addition to the coulometer itself the research involves methods of purification and analysis of iodine, accurate time measurement, and

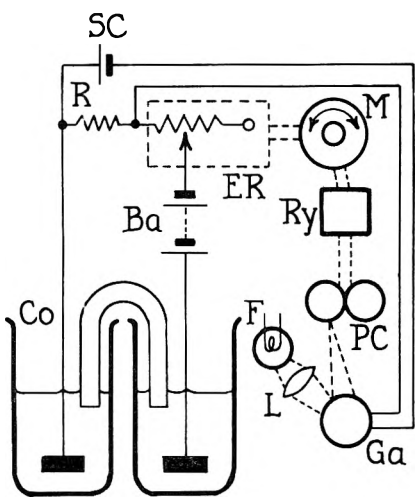

Fig. 1.—Principle of the apparatus.

a constant current apparatus, the last of which is described in this paper. The instrument is a development of the constant current devices which have been used extensively in this Laboratory in connection with the determination of transference numbers by the moving boundary method.[4]

In its simplest elements the device now in use is shown in Fig. 1. The coulometer, Co, is connected in series with storage cells, Ba, a standard resistance, R, and an adjustable resistance, ER. In parallel with R are a standard cell, SC, and a galvanometer, Ga. Light from a lamp, F, passes through a lens, L, to the galvanometer mirror, and an image of the filament is focussed on two differential photo-cells, PC. Movement of the light spot on these cells causes a relay, Ry, to vary the direction of rotation of a reversible motor, M, producing small alterations of an electrolytic resistance, ER. Thus the current through the coulometer is continually in process of adjustment to a value determined by the potential of the standard cell SC and the standard resistance R.[5]

The actual apparatus is complicated by the fact that it must be operating with the desired current flowing through an auxiliary resistance up to the instant of commencing the electrochemical reactions in the coulometer. Provision must also be made for automatic opening of the circuit containing the galvanometer and standard cell in case of any failure of the apparatus. Description of these details is given below.

The Coulometer.—On passage of electric current through a system which may be represented by

$$+ \text{Pt; KI, } I_2 : \text{KCl} : \text{KI, } I_2 \text{ ; Pt} -$$

the reaction $3I^- = I_3^- + 2e^-$ occurs at the anode and the reverse reaction at the cathode. The interposition of a solution of potassium chloride is to keep the anode and cathode portions of the system entirely separate. After passing a determined number of coulombs these portions are titrated with a solution of sodium thiosulfate. Fuller descriptions of the coulometer and of the method of analysis will be given in later articles.

The Adjustable Resistance.—The changes of resistance and electromotive force which occur during the passage of current through the coulometer must be compensated if the current is to remain constant. Since comparatively slight deviations of the filament image from a point between photo-cells PC of Fig. 1 can result in failure of the operation of

* Aided by a fellowship from the Dazian Foundation for Medical Research.

(1) E. W. Washburn and S. J. Bates, *J. Am. Chem. Soc.*, **34**, 1341 (1912).

(2) S. J. Bates and G. W. Vinal, *ibid.*, **36**, 916 (1914).

(3) D. N. Craig and J. I. Hoffman, "Electrochemical Constants," Nat. Bur. Stand. Circular 524, p. 13; *Phys. Rev.*, **80**, 487 (1950).

(4) D. A. MacInnes, I. A. Cowperthwaite and K. C. Blanchard, *J. Am. Chem. Soc.*, **48**, 1909 (1926); L. G. Longsworth and D. A. MacInnes, *J. Optical Soc. Am.*, **19**, 50 (1929); L. G. Longsworth and D. A. MacInnes, *J. Am. Chem. Soc.*, **60**, 3070 (1938).

(5) This is an adaptation of a principle originally suggested by M. Gouy, *J. Physique*, **6**, 479 (1897), for securing continuous control of an on-off temperature regulator.

the constant current apparatus, it is essential that the adjustable resistance ER of that figure be free from the small but erratic changes of resistance such as can frequently occur when one metal conductor scrapes or rolls on another. The variable electrolytic resistance shown in Fig. 2 has been found to be useful in this connection. The copper anode A and the copper cathode C are contained in a glass cylinder V which holds a solution of copper sulfate and sulfuric acid. The anode must be on the upper side in order that the copper sulfate formed by the electrolysis will descend through the solution, maintaining an approximately constant concentration. (If the current is reversed a concentrated solution is formed in the lower layers and hydrogen gas may be evolved at the upper electrode with an attendant large rise in resistance.) The anode disk A is secured to a stainless steel rod, S, which in turn is supported by a silver chain, D. The current is led to the anode by a helix of platinum wire, P, which is strung with small glass beads to prevent possible shorting across adjoining turns. The distance between the anode and cathode, and thus the resistance, changes when the silver chain winds on or unwinds from the spool R, which is on a shaft with the grooved conical pulley T. This is driven by the pulley T′ which is joined to a reversing motor M (Haydon Mfg. Co. Type 2200A-KEB-1RPM). Different rates of rise and fall of the anode disk A can be arranged by shifting the elastic belt B along the pulleys T and T′. The anode disk A is prevented from going too far up or down by a chain E which is attached to the shaft of pulley T. If the chain winds too far in either direction, it opens a contact K which is in the circuit operating the motor M. A chuck, F, makes it possible to adjust the silver chains D and E independently. Backlash, which causes unnecessary motion of the light from the galvanometer, is avoided by having a sufficiently heavy anode disk A.

The Electrical Connections.—A diagram of the electrical connections of the complete apparatus is shown in Fig. 3. The coulometer circuit, indicated by heavy lines, contains the standard resistance, R1, a variable electrolytic rheostat, ER1, a milliameter, MA, the storage cells, Ba1, and the adjustable electrolytic resistance, ER2, described above and shown in Fig. 2. Included in this circuit are the terminals of a four-pole, double-throw, switch, S1, which is shown in the position for sending current through the coulometer. The standard resistance, R1, is connected in series with a Weston saturated standard cell, SC, a galvanometer, Ga1, (Rubicon No. 3202) and the third blade of switch S1. The fixed contacts of the first and second blades of switch S1 are raised so that current passes before the galvanometer circuit is completed. This prevents wide swings of the galvanometer, arising from any surge in the coulometer circuit at the moment it is completed. It is also useful to have a second galvanometer, Ga2, (Leeds and Northrup lamp and scale type 884N) used in place of Ga1 during manipulations other than the operation of the coulometer. Also in series with the galvanometer are the contacts of a protective relay, Ry3,

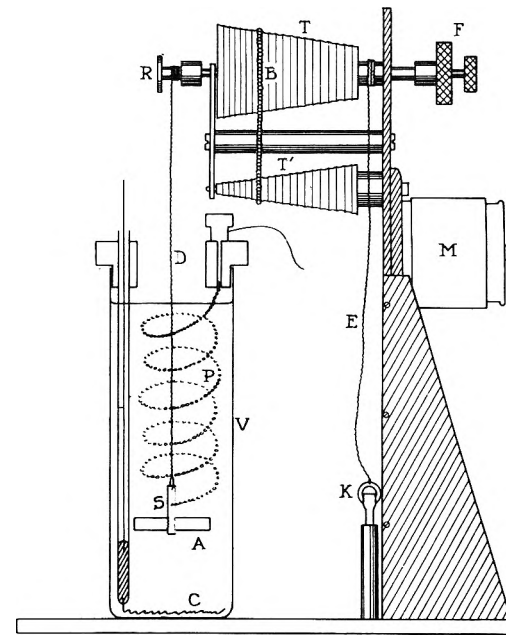

Fig. 2.—The adjustable electrolytic resistance.

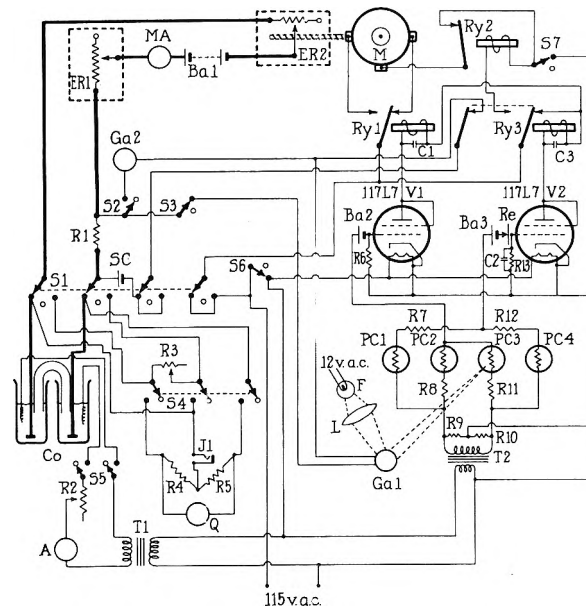

Fig. 3.—The electrical connections.

further discussed below. A fourth blade of switch S1 breaks the circuit containing the reversing motor M, if current is not flowing through the coulometer or through resistance R3.

Automatic adjustment of the variable electrolytic resistance, ER2, to maintain constant current through the coulometer, is accomplished as follows. Light from the lamp F, (Sound Reproducer type G. E. 4A/T8/25) is focussed by the lens, L, and the mirror of the galvanometer Ga1, normal to a line between two cadmium sulfide photo-conductive cells, PC2 and PC3 (Sensiton type SS-2). These cells are in a bridge system including as the other arms two 10K resistances, R9 and R10. Any deviation of the current through the coulometer circuit from that determined by the standard resistance, R1, and the standard cell, SC, will cause the galvanometer, Ga1, to deflect the line of

light on one of the photo-cells, PC2 or PC3. If the light falls on PC2, a potential will be impressed on the grid of the tube V1 (RCA type 117L7/M7-GT), in phase with the plate voltage so that current passes which operates the relay Ry1 (Allied model BK-6A), with the result that the reversing motor turns to produce an increase in the resistance of the electrolytic rheostat, ER2. This diminishes slightly the current in the coulometer circuit and causes the galvanometer mirror to shift the reflected line of light back again from photo-cell PC2 to cell PC3. In this condition the potentials impressed on the grid will be out of phase with the plate voltage of the tube, V1. This in turn releases the relay, Ry1, so that the motor, M, operates in the opposite direction. In this way the electrolytic rheostat, ER2, is continually receiving slight adjustments to maintain the current constant. A difference of potential at the galvanometer terminals of less than one-tenth microvolt will cause the motor, M, to reverse its direction. Since the standard cell, SC, has a potential of about one volt, the regulation, as now used, is thus of the order of one part in ten million, under the best conditions. Momentum of the anode of the electrolytic rheostat, its motor and the coil of the galvanometer, causes the image of the filament to move somewhat more than the minimum needed for reversal: one microvolt at the galvanometer terminals deflects the image by two centimeters. A conservative estimate of the regulation attainable with this apparatus is thus one part per million. As shown, the photo-cells PC2 and PC3 are each in series with 15K protective resistances R8 and R11, and form a bridge with two 10K resistances, R9 and R10. The operation of the apparatus is thus uninfluenced by the illumination of the room since changes in the background lighting produce substantially equal variations in the resistances of the two photo-cells.

To protect the galvanometer and the standard cell in case of any failure in the apparatus, provision is made to release the contacts of the relay, Ry3, in case the light reflected from the galvanometer mirror reaches the photo-cells, PC1 or PC4. Normally, current passes through the tube, V2, holding the contacts of the relay, Ry3, in closed position. However, illumination of PC1 or PC4 will change the grid bias of the tube V2, thus effecting the release of these contacts with the result that the galvanometer circuit is opened and the relay Ry2 breaks the circuit of the motor M. To make this system also independent of the background lighting the photo-cells PC1 and PC4 with their series resistances form a bridge with the 10K resistances R9 and R10. Normally the mid-point between R7 and R12 will be at zero potential with respect to the center of the bridge arms R9 and R10. If, however, the light from the galvanometer mirror reaches PC1 or PC4, this point will be subject to a fluctuating potential. This potential is converted into a pulsating negative bias on tube V2 with the germanium diode rectifier Re (1N68), the 10M resistance R13, and a 0.05 microfarad condenser C2. This bias causes V2 to stop conducting, thus releasing the relay, Ry3, and opening the galvanometer and motor circuits. The microfarad condensers C1 and C3 eliminate the chatter of the relays Ry1 and Ry3. The batteries Ba2 and Ba3 furnish adjustable biases on the grids of tubes VI and V2.

As already stated, it is necessary for the purpose of this research that current be passing through the principal circuit, with the value determined by the quotient of the values of the potential of the standard cell and the standard resistance, R1, at the moment at which the current is started through the coulometer. To meet this requirement the switch S1 is turned to the position opposite to that shown in Fig. 3, so that the current is passing through a variable resistance, R3, which must have a resistance equal to that of the coulometer, Co. In order to make the appropriate adjustment, a bridge system is provided by opening switch S1 and closing switch S4. Audiofrequency current from the generator Q is impressed on the bridge as shown. Since the resistance arms R4 and R5 are both 100 ohms, equality of the resistances of Co and of R3 is secured by adjusting R3 and is indicated by a minimum of sound in a telephone connected at jack J1. Switch S4 is then opened, and S1 is put in the position opposite to that shown in the figure until it is desired to pass current through the coulometer, when it is reversed.

EXCHANGE AND ISOMERIZATION OF *trans*-ETHYLENE-d_2 ON NICKEL IN THE PRESENCE OF DEUTERIUM[1]

BY TED B. FLANAGAN AND B. S. RABINOVITCH

Contribution from the Department of Chemistry of the University of Washington, Seattle, Washington

Received December 17, 1956

The products of the exchange and isomerization reactions of *trans*-ethylene-d_2 and deuterium on nickel wire can be satisfactorily explained by assuming that the reactions proceed through an half-hydrogenated state. The activation energies for isomerization and exchange from 0–56° were found to be 6.9 and 7.3 kcal., respectively. In this range of temperature and extent of reaction investigated, hydrogenation and excess exchange (ethylene-d_3 minus ethylene-d_1) were unimportant.

(1) Abstracted in part from a thesis submitted by Ted B. Flanagan to the Graduate School in partial fulfillment of the requirements for the degree of Doctor of Philosophy at the University of Washington.

Introduction

The exchange reaction, $C_2H_4 + D_2 \rightarrow C_2H_3D$

+ HD, was discovered by Farkas, Farkas and Rideal[2] in their study of the nickel-catalyzed hydrogenation of ethylene with deuterium. The mechanism of this exchange has been controversial since its discovery. Much support has been given a reaction proceeding from associatively absorbed ethylene through a half-hydrogenated intermediate,[3] *e.g.*

$$H_2C(*)—CH_2(*) + D(*) \longrightarrow CH_2D—CH_2(*) \longrightarrow H_2C(*)—CDH(*) + H(*) \quad (1)$$

although there have been a number of different proposals regarding the mechanism of the over-all process. Jenkins and Rideal[4] have recently presented evidence in support of an alternative mechanism suggested by their adsorption studies of ethylene on nickel.

$$C_2H_4(g) + D(*) \longrightarrow DCH_2—CH_2(*) \longrightarrow C_2H_3D + H(*) \quad (2)$$

In recent studies of nickel-catalyzed isomerization and exchange of *trans*-ethylene-d_2 in the absence of hydrogen, Flanagan and Rabinovitch[5,6] found strong experimental evidence favoring the half-hydrogenated state as an intermediate.[7] Pliskin and Eischens[8] have presented spectral evidence for the existence of the half-hydrogenated state when ethylene was added to a hydrogen covered nickel catalyst. Thus, there is strong but not unequivocal evidence regarding the half-hydrogenated state as an intermediate in the exchange reactions of ethylene in the presence of hydrogen. To obtain further information, a study of isomerization and exchange of *trans*-ethylene-d_2 in the presence of deuterium was undertaken; circumstances have prevented as detailed a study as would have been desirable.

Experimental

Materials and Apparatus.—The ethylenes were the same as used in earlier work.[5,6] Deuterium (99.5%), obtained from the Stuart Oxygen Co., was passed over hot platinized asbestos and through liquid nitrogen traps before use; mass-spectral analysis showed it to be free from contaminants. The vacuum apparatus and catalyst (nickel wire) were the same as employed earlier. The catalyst was activated in the same manner and was protected at all times from stopcock grease and mercury with a cold trap.

Procedure.—*trans*-Ethylene-d_2 was frozen into the catalyst chamber, the required deuterium was added and the *trans*-ethylene-d_2 was allowed to evaporate. To stop the reaction, the gases were removed by evacuation through a liquid nitrogen trap. The deuterium lost in this way was replaced with fresh material after each determination; since the reaction was only carried to a small percentage reaction where excess exchange (defined below) was negligible, replacement of deuterium made no significant difference in the isotopic content of the deuterium.

The catalyst was found to maintain its activity in the presence of deuterium, as contrasted to the situation in the absence of deuterium, so that no difficulty was encountered in working with a catalyst of constant activity.

Analysis.—The isomerization and exchange reactions were followed as before by infrared and mass-spectral analysis. Greater weight is attached to the experimental percentage of ethylene-d_3 than those of ethylene-d_1, since the mass spectral analysis for ethylene-d_3 was more accurate.

Results and Discussion

Time Reaction Order.—Table I shows a typical run in which percentages of isomerization and exchange of *trans*-ethylene-d_2 in the presence of added deuterium are shown at various times (0°, 5.8 cm. of each reactant); hydrogenation was negligible. The rate constants were calculated from the equations

$$\frac{dC_c}{dt} = k_i(C_2^0 - 2C_c - 2C_3) \quad (3)$$

$$\frac{d(C_3 + C_1)}{dt} = k_e(C_2^0 - 2C_3) \quad (4)$$

where C_n refers to an ethylene with n deuterium atoms, C_c refers to *cis*-ethylene-d_2 and C_2^0 refers to the initial *trans*-ethylene-d_2. These expressions are for first-order reactions (reversible for isomerization). Equation 3 is solved by approximate methods and (4) may be integrated directly. The rate constants for exchange refer to rates of inter-exchange; excess exchange, defined below, was unimportant where quantitative significance was attached to the rate constants, *e.g.*, activation energy determination. The justification and adequacy of these approximate equations was discussed earlier.[5]

Relative Rates of Isomerization and Exchange.—From Table I it may be seen that isomerization proceeded faster than exchange (ethylene-d_1 plus ethylene-d_3); this was also true in all other runs. The rates of isomerization and exchange of *trans*-ethylene-d_2 were many times faster in the presence of added deuterium than in its absence, and isomerization and exchange were accelerated in a quantitatively similar manner by the addition of deuterium. Both reactions were also affected equally by variation of catalyst activity.

TABLE I

Sample run (0°, 5.8 cm. of deuterium and ethylene-d_2)

Time, min.	C_1, %	C_3, %	C_c, %	$k_i \times 10^2$, min.$^{-1}$	$k_e \times 10^2$, min.$^{-1}$
4	..	0.54	1.8	4.8	2.7
10	1.2	1.23	4.6	4.5	2.3
12	(2.6)	1.49	5.1	4.6	2.5
14	1.7	1.53	5.9	4.4	2.2
16	2.0	2.03	6.5	4.5	2.6
18	2.3	2.20	7.4	4.5	2.5

Inter-exchange and Excess Exchange.[9]—In spite of the presence of added deuterium, excess exchange was negligible under the conditions of the run in Table I; in runs with higher pressures of deuterium or at higher temperatures (>60°), excess exchange became appreciable (Table II). The sample data of Table II refer to runs made with a catalyst of es-

(2) A. Farkas, L. Farkas and E. K. Rideal, *Proc. Roy. Soc.* (*London*), **A164**, 630 (1934).

(3) J. Horiuti and M. Polanyi, *Trans. Faraday Soc.*, **30**, 1164 (1934).

(4) G. I. Jenkins and E. Rideal, *J. Chem. Soc.*, 2490, 2496 (1955).

(5) T. B. Flanagan and B. S. Rabinovitch, THIS JOURNAL, **60**, 724 (1956).

(6) T. B. Flanagan and B. S. Rabinovitch, *ibid.*, **60**, 730 (1956).

(7) Various mechanisms were eliminated as possibilities in the earlier work by virtue of their inability to explain the observed ratios of isomerization to exchange; upon further examination, however, it is found that a mechanism involving an associatively adsorbed vinyl radical, *i.e.*, $C_2H_4(g) \rightarrow CH_2—CH\cdot + H$ (*, *, *), cannot be eliminated for these reasons but is unlikely on other grounds (see ref. 11).

(8) W. A. Pliskin and R. P. Eischens, *J. Chem. Phys.*, **24**, 482 (1956).

(9) The difference, ethylene-d_3–ethylene-d_1, will be called excess exchange and twice ethylene-d_1 will be called inter-exchange; "hydrogen" and "ethylene" will be used as general terms without regard to isotopic content.

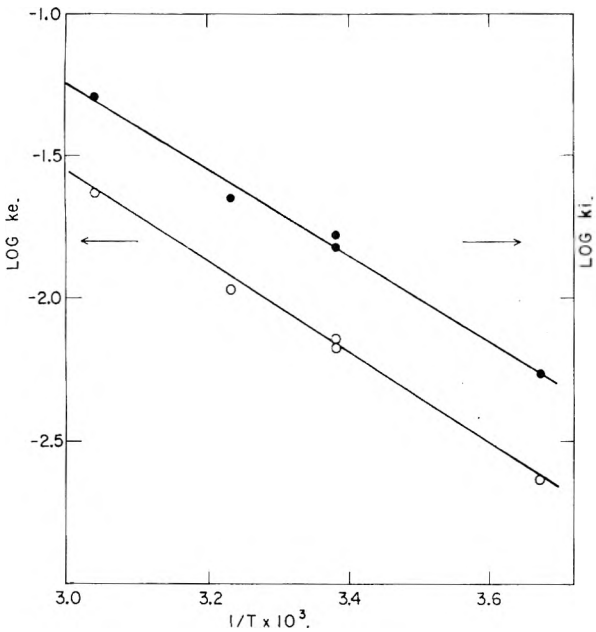

Fig. 1.—Temperature dependence of isomerization and inter-exchange of *trans*-ethylene-d_2 with deuterium at equal concentrations (2.1×10^{18} molec. cm.$^{-3}$).

sentially constant activity; the catalyst activity was determined experimentally by the activity toward the reactions being studied at particular standard concentrations and temperature. Under given conditions, the relative proportions of excess and inter-exchange depend somewhat upon catalyst activity, although this effect was not examined in detail.

It has been shown by previous workers that below 60° excess exchange is slower than hydrogenation and faster above 60°,[2] which is a consequence of the high heat of desorption of hydrogen. Inter-exchange, however, still takes place much faster than hydrogenation at the lower temperatures.

TABLE II

EFFECT OF TEMPERATURE AND PRESSURE OF DEUTERIUM ON EXCESS EXCHANGE AT CONSTANT CONCENTRATION OF ETHYLENE-d_2 (2.1×10^{18} MOLEC./CM.^{3})

Temp., °C.	Concn. deuterium/ concn. ethylene-d_2	C_1, %	C_2, %	$C_2 - C_1$, %
0	1	1.21	1.23	0.02
0	1	2.00	2.03	0.03
22	1	0.76	1.09	0.27
22	1	1.89	2.00	0.11
36	1	1.63	1.17	(−0.46)
36	1	0.63	0.81	0.18
56	1	1.30	1.50	0.20
56	1	2.22	2.06	(−0.16)
90	1	0.76	1.77	1.01
90	1	3.50	4.74	1.24
157	0.05	2.90	2.94	0.04
157	0.28	2.40	4.00	1.60
157	3.50	2.0	12.5	10.5

Activation Energies.—Rate constants have been determined from 0 to 56° for the isomerization and inter-exchange reactions at equal and constant concentrations (2.1×10^{18} molec. cc.$^{-1}$) of *trans*-ethylene-d_2 and deuterium. Most runs were carried to about 8% isomerization; at this (constant) catalyst activity and extent of reaction, both hydrogenation and excess exchange were unimportant. The data are given in Fig. 1. The activation energies are 6.9 and 7.3 kcal./mole for isomerization and exchange respectively.

Mechanism.—From the results given above it is seen that for both isomerization and exchange the time reaction orders are the same, the absolute magnitudes of the rates are closely similar, the variation of the catalyst activity affects each reaction similarly, both reactions are enhanced equally by the addition of deuterium and the activation energies for isomerization and exchange are of the same magnitude (the small difference may be readily explained by the isotope effect for C–H, C–D bond rupture). It is concluded that in the presence, as in the absence of added hydrogen, isomerization and inter-exchange take place by the same mechanism.

The observed ratios of isomerization to exchange may be explained by a mechanism in which the double bond is broken to permit isomerization. As before, a number of mechanisms cited in our earlier work, and which need not be listed again, may be immediately eliminated as not accounting properly for the product ratios. Some variations which have recently been proposed[10] may also be eliminated because they predict either no isomerization or an incorrect product ratio.

A mechanism involving a half-hydrogenated intermediate is successful in interpreting the present results for exchange and isomerization in the presence of deuterium. Such a mechanism was applied to these reactions in the absence of hydrogen and the values of α, the C–H/C–D bond rupture ratios in the half-hydrogenated intermediate, were determined over a wide range of temperatures.[5] Using these values of α, the percentage of isomerization may be calculated from the observed amounts of exchange and are compared with some experimental values in Table III.[11]

(10) B. M. W. Trapnell, "Chemisorption," Butterworths Pub. Co., London, 1955, pp. 247, 249.

(11) An associatively adsorbed vinyl radical intermediate is nominally

$$C_2H_4 \rightleftharpoons \underset{*}{H_2C}\text{—}\underset{*}{CH}\cdot + \underset{*}{H}$$

compatible with the ratios of isomerization and exchange observed here and in our earlier work; however, this mechanism does not appear to be correct. The value of α', the (C–H)/(C–D) rupture probability necessary to explain the observed ratios if CHD=CHD is adsorbed as an associatively adsorbed vinyl radical, is related to α in the following manner

$$\alpha' = (\alpha + 1/\alpha) + \sqrt{\alpha^2 + 1};$$

α' is approximately 2α at low temperatures. The values of α' required to predict the proper ratios of product at high temperatures[5] are much higher than the classical limit of 1.4 (*viz.*, $\alpha' = 4.1$ and $\alpha = 1.4$ at 430°); α' does not approach the classical limit if extrapolated to infinitely high temperature. Values of (C–H)/(C–D) rupture probability determined for the gas phase decomposition of 1,2-dideuteroethyl radicals at low temperature (B. S. Rabinovitch and D. H. Dills, unpublished results) agree quite well with α values from the half-hydrogenated state intermediate. The fact that α values appear to be independent of catalyst type, *e.g.*, Pd on charcoal gives the same α values as nickel, suggests the comparison is valid. The usual arguments against dissociative-type mechanisms apply, *e.g.*, inability to explain double bond migration and the close relation of hydrogenation to exchange.

The experimental evidence is vastly in favor of a half-hydrogenated state as an intermediate, but an unequivocal differentiation between

TABLE III

COMPARISON OF SOME EXPERIMENTAL AND CALCULATED PERCENTAGES OF ISOMERIZATION[a]

Temp., °C.	α	C_1, %	C_3, %	C_c (calc.), %	C_c (exp.), %
0	4.9	0.69	0.75	3.6	3.2
22	3.9	1.7	2.1	7.2	6.2
22	3.9	0.76	1.09	3.1	3.3
36	3.3	0.63	0.81	2.4	2.6
56	2.8	1.3	1.5	4.2	4.8
56	2.8	2.1	2.6	6.8	7.2

[a] To illustrate the validity of the mechanism for excess exchange, some runs were especially chosen where excess exchange was highest. The catalyst activity was in some cases quite different from the runs of Table II.

The tremendous increase in rate (100–1000 fold) when deuterium is used is readily explained in terms of a half-hydrogenated intermediate since deuterium species, chemisorbed from the gas phase on the surface, furnished many more sites for half-hydrogenated state formation than is the case in the absence of gaseous deuterium. If no equilibration of the surface and gaseous hydrogen takes place, excess exchange is negligible (the amount of excess deuterium adsorbed on the surface being negligible). It follows from our previous work,[5] that the product ratio of isomerization, C_c, to inter-exchange, $2C_1$, should *not* depend on whether light hydrogen or deuterium is the addend, if excess exchange is negligible. At high pressures of deuterium and/or high temperatures, excess exchange (and hydrogenation) increases. Under these conditions, the product ratio, $C_c/(C_1 + C_3)$, should depend on the addend.

Stepwise Exchange.—As in the case of exchange in the absence of deuterium, equilibration of the surface ethylenes with gaseous ethylene takes place after one exchange reaction, since only ethylene-d_1 and ethylene-d_3 were found initially from *trans*-ethylene-d_2 plus deuterium, and only ethylene-d_1 from ethylene-d_0 and deuterium. This is similar to the results of Turkevich, *et al.*[12]

For the observed single step exchange to occur, either exchange by an associative mechanism takes place on low energy ethylene sites so that the rate of ethylene desorption is faster than the experimental reaction rate,[13] or a Rideal[4] type mechanism is operative which results in automatic ethylenic equilibration with the gas phase.

Adsorption studies of ethylene on nickel films led Jenkins and Rideal[4] to the conclusion that ethylene is not associatively adsorbed, but adsorbed irreversibly as acetylenic complexes. However, our earlier work, *i.e.*, exchange in the absence of added hydrogen on supported nickel, nickel films and nickel wire, shows that some reversible adsorption of ethylene on a small area must take place on a fully-covered ethylene surface. This reversible adsorption of ethylene could still be of the form C_2H_4 (g) + H $\rightleftarrows$ C_2H_5, although Kemball[14] has pointed out that associative adsorption may be a factor in the adsorption of ethylene in the presence of hydrogen, and that the Rideal mechanism in any case cannot explain the initial multiple exchange found under his low temperature ($-100°$) conditions; spectral evidence has been found[8] for associative adsorption when ethylene is exposed to a supported nickel catalyst.

Concluding Remarks.—It is of interest to point out that the isotope effect is of importance in determining the proportions of exchange in the reactions of ethylene and deuterium. The three investigations where initial product analyses on nickel have been made are those of Turkevich, *et al.*,[12] at 90°, Kemball[14] at $-100°$ and the present investigation. α has been measured from -78 to 400° and was found to vary considerably with temperature.[5] For the reaction of ethylene-d_0 and deuterium at 90° (α = 2.4), each time a half-hydrogenated state is formed, $DH_2C\text{-}CH_2$, 17% of the decomposition events lead to reformation of ethylene-d_0, at 20° (α = 4.0), this percentage drops to 11%, and at $-100°$ (α = 24 extrapolated), ethylene-d_0 is reformed only 2%. This is a factor in giving rise to higher proportions of more highly deuterated ethylenes at early times in low temperature work. Exchange activation energies measured or compared over a large temperature range have an isotope effect superimposed on them; this is true even if the detailed mechanism for which α is defined is supplanted by another mechanism.

It will be recalled that the observed activation energies for isomerization and inter-exchange are 6.9 and 7.3 kcal; the small difference is presumably due to the isotope effect. Kemball[14] found 7 kcal. for both hydrogenation and exchange of ethylene and deuterium on nickel film at $-100°$. The observed activation energy for inter-exchange in the presence of hydrogen, 7.3 kcal., thus declines from the value of 15 kcal. observed in the absence of hydrogen in the same temperature region. It is possible to construct explanations for this decline on both a Rideal and associative basis. However, since the precise meaning of the observed activation energy in the absence of hydrogen is not established,[5] such explanations are of an *ad hoc* nature and need not be presented.

Acknowledgments.—We thank the Office of Naval Research for their support under Contract N8-52009, Project No. 051217.

the two mechanisms could be made by careful determinations of *cis*-ethylene-d_2 and exchange percentages at temperatures above 400° in the absence of deuterium, and high temperature (200°) experiments with added deuterium, where the two mechanisms predict different products if excess exchange is significant.

(12) J. Turkevich, D. O. Schissler and P. Irsa, THIS JOURNAL, **55**, 1078 (1951).

(13) Calculations have been made of rates of desorption of ethylene for various heats of adsorption by absolute rate theory (K. Laidler, "Catalysis" Ed. P. Emmett, Vol. III, Reinhold Publ. Corp., N. Y., 1954, p. 203). 13 kcal. was used as the heat of adsorption on a fully covered surface; this is an average of values in the literature and it is also a value which is of the correct magnitude for such an interpretation of our results in the absence of hydrogen. The rate of desorption is appreciably faster than the rate of reaction at 0° or above, but is slower at $-100°$ (*cf.* Kemball's data, ref. 14).

(14) C. Kemball, *J. Chem. Soc.*, 735 (1956).

CONDUCTANCE OF UNASSOCIATED ELECTROLYTES

BY RAYMOND M. FUOSS AND LARS ONSAGER

Contribution No. 1400 from Sterling Chemistry Laboratory, Yale University, New Haven, Conn.

Received December 28, 1956

The relaxation field for unassociated electrolytes is obtained as a function of concentration by solving the Onsager–Fuoss equation of continuity, subject to boundary conditions for charged spheres (rather than point charges) to represent the ions, and with retention of higher order terms. Combined with the previous value of the electrophoretic term, a conductance equation is obtained which has the limiting form $\Lambda = \Lambda_0 - (\alpha\Lambda_0 + \beta)c^{1/2} + Dc \ln c + (J_1c - J_2c^{3/2})(1 - \alpha c^{1/2})$ in which the constants J_1 and J_2 are explicit functions of ion size, Λ_0 and properties of the solvent; D is independent of ion size. Up to concentrations of the order of hundredth normal, the equation has the form $\Lambda = \Lambda_0 - (\alpha\Lambda_0 + \beta)c^{1/2} + cB(\kappa a)$. Numerical tables are given which permit calculation of $B(\kappa a)$. A method of obtaining the two parameters Λ_0 and a from Λ,c-data is described. The equation reproduces experimental data for the alkali halides in water up to about 0.01 N. Limitations of the theory are discussed.

Experimental results for a wide variety of electrolytic systems show that their phoreograms approach the Onsager[1] tangent

$$\Lambda = \Lambda_0 - (\alpha\Lambda_0 + \beta)c^{1/2} \qquad (1)$$

in the limit of vanishingly small concentrations. In most non-aqueous systems, the phoreograms lie below the limiting tangent (catabatic phoreograms[2]); ion association[3] or else incomplete dissociation usually provides a satisfactory explanation. But an important class of electrolytes, exemplified by the alkali halides in water, diverge upwards from the limiting tangent (anabatic phoreograms) as concentration increases from zero. The question of the theoretical origin of the positive deviations from the limiting tangent naturally arises: is a new hypothesis necessary or is the shape of the curves predictable by further development of present theory?

Underlying eq. 1 is a model in which the ions are represented as point charges. An earlier calculation of the electrophoresis term,[4] using as the model for the ion charged spheres of average diameter a, showed that the $\beta c^{1/2}$ term should be replaced by $\beta c^{1/2}/(1 + \kappa a)$ for symmetrical electrolytes; the transcendental term Ei $(2\kappa a)$ vanishes. The divisor, of course, diminishes the magnitude of the term as concentration increases, and produces a curve which is concave-up. This result obviously suggests that the relaxation term $\alpha\Lambda_0c^{1/2}$ should also be reinvestigated, using the spherical model. Integration of the appropriate differential equation with electrostatic boundary conditions corresponding to charged spheres does indeed modify this term in the expected direction; Falkenhagen[5] has shown that terms of first order (and higher) in concentration appear in the limiting equation. But his differential equation was already an approximation in which terms had been neglected which also would have led to terms of order c, and still more important to transcendental terms of limiting order $c \ln c$ in the relaxation field. We therefore have re-examined the integration with consistency of order of retained terms as the guiding principle. In a preliminary paper,[6] it was stated that integration of the fundamental equation of continuity, with retention of higher terms than those linear in the charge of the reference ion and subject to boundary conditions for spherical ions, would lead to a conductance equation which accurately reproduced experimental data for the alkali halides in water up to moderate concentrations (*i.e.*, less than 0.1 normal). The purpose of this paper is to present the details of the derivation, and to describe a practical method of solving the final conductance equation for the two empirical parameters, Λ_0 and a, which appear in the theoretical development.

1. Equation of Continuity

Limitations of space prohibit a detailed repetition of essential but previously published introductory material.[7] The derivation which follows will therefore be presented in the form of the solution of a mathematical problem, after definition of the variables and a brief recapitulation of their significance.

The average concentration of ions of species i is $n_i = N_i/V$ where N_i is the number of such ions present in the total volume V. Local concentrations differ from this value due to mutual attraction and repulsion between the charged ions; the concentration of i-ions in an element of volume located by a vector $\mathbf{r}_{21}$ with respect to a j-ion at the origin will be denoted by $n_{ji}(\mathbf{r}_{21})$. The symmetrical distribution functions

$$f_{ji}(\mathbf{r}_{21}) = n_jn_{ji}(\mathbf{r}_{21}) = n_in_{ij}(\mathbf{r}_{12}) = f_{ij}(\mathbf{r}_{12}) \qquad (1.1)$$

satisfy the general conservation condition

$$\mathrm{div}_1(f_{ij}\mathbf{v}_{ij}) + \mathrm{div}_2(f_{ji}\mathbf{v}_{ji}) = 0 \qquad (1.2)$$

where $\mathbf{v}_{ij}$ is the velocity of a j-ion in the vicinity of an i-ion. The distribution functions and the potentials ψ_j are assumed to satisfy the Poisson equation

$$\Delta\psi_j = -(4\pi/D)\Sigma_i f_{ji}e_i/n_j \qquad (1.3)$$

The velocity depends on the various forces, which are in turn derivable from the potentials; combination of (1.2) and (1.3) thus in principle should lead to the relaxation field as a function of concentration. We assume that the external field strength X is so small that no appreciable Wien effect occurs; we may then set

(1) L. Onsager, *Physik. Z.*, **27**, 388 (1926); **28**, 277 (1927).

(2) R. M. Fuoss, *J. Chem. Education*, **32**, 527 (1955).

(3) R. M. Fuoss, *Chem. Revs.*, **17**, 27 (1935).

(4) L. Onsager and R. M. Fuoss, THIS JOURNAL, **36**, 2689 (1932); eq. (4.2.10).

(5) H. Falkenhagen, M. Leist and G. Kelbg, *Ann. Physik*, [6] **11**, 51 (1952).

(6) R. M. Fuoss and L. Onsager, *Proc. Nat. Acad. Sci.*, **41**, 274, 1010 (1955).

(7) Especially pp. 2689–2704 and 2735–2744 of ref. 4 and pp. 274–280 of ref. 6. See also H. S. Harned and B. B. Owen, "Physical Chemistry of Electrolytic Solutions," Reinhold Publ. Corp., New York, N. Y., 1950, pp. 75–85; and L. Onsager and S. K. Kim, THIS JOURNAL, **61**, 215 (1957).

$$\psi_j(\mathbf{r}_{21}) = \psi^\circ{}_j(r) + \psi'_j(\mathbf{r}) \quad (1.4)$$

$$\psi_i(\mathbf{r}_{12}) = \psi^\circ{}_i(r) - \psi'_i(\mathbf{r}) \quad (1.5)$$

and

$$f_{ji}(\mathbf{r}_{21}) = f^\circ{}_{ji}(r) + f'_{ji}(\mathbf{r}) = f^\circ{}_{ij}(r) - f'_{ij}(\mathbf{r}) = f_{ij}(\mathbf{r}_{12}) \quad (1.6)$$

where the primed terms, denoting the asymmetric terms in potentials and distributions, are proportional to X. For $\psi^0{}_j(r)$, the spherically symmetric part of the potential of a j-ion (*i.e.*, the potential in the absence of an external field), we shall use the Debye–Hückel result

$$\psi^\circ{}_j(r) = e_j e^{-\kappa r} e^{\kappa a}/Dr(1 + \kappa a) = e_j e^{-\kappa r}/\mu Dr \quad (1.7)$$

where μ is an abbreviation for $e^{-\kappa a}(1 + \kappa a)$. For the special case of simple electrolytes ($i = 1, j = 2$), the equation of continuity[8] reduces to a single differential equation for $f'_{21}(\mathbf{r})$

$$kT(\omega_1 + \omega_2)\Delta f'_{21} - [(4\pi f^\circ{}_{21}/D)(e_1{}^2\omega_1/n_2 + e_2{}^2\omega_2/n_1)]f'_{21} = X(e_1\omega_1 - e_2\omega_2)(\partial f^\circ{}_{21}/\partial x) + T(g_1) + T(g_2) + T(g_3) + T(a) + T(v) \quad (1.8)$$

Equation 1.8 differs from the 1932 equation[9] by the presence of the new inhomogeneous terms designated by the T's. The latter will be discussed after an outline of the derivation of (1.8) from (1.2) is given. In (1.2), let $\mathbf{I}_{ji}$ represent the current $f_{ji}\mathbf{v}_{ji}$, where

$$\mathbf{v}_{ji}(\mathbf{r}_{21}) = \mathbf{v}_i(\mathbf{r}_{21}) + \omega_i[\mathbf{K}_{ji} - kT\nabla_2 \ln f_{ji}(\mathbf{r}_{21})] \quad (1.9)$$

$\mathbf{v}_i(\mathbf{r}_{21})$ is the vector velocity of an i-ion due to the presence of a j-ion in its vicinity, $\mathbf{K}_{ji}$ is the electrical force on the i-ion and the ∇_2-term is the diffusion term due to Brownian motion. In turn, the force $\mathbf{K}_{ji}$ is made up of three terms

$$\mathbf{K}_{ji} = Xe_i\mathbf{i} - e_i\nabla_2\psi_i(a) - e_i\nabla_2\psi_j(r_{21}) \quad (1.10)$$

where $\mathbf{i}$ is a unit vector in the direction of the applied field. The first term is due to the applied field, the second to the asymmetry of the atmosphere of the i-ion and the third to the presence of a j-ion and its atmosphere (of which the i-ion is, of course, a member). The term $\nabla_2\psi_i(a)$ reduces to $\nabla_2\psi'_i(a)$ because a central force can produce no motion.

The following sequence of operations converts (1.2) into (1.8). Substitute (1.10) into (1.9) and the result into (1.2). Expand, except in the six gradient terms, using the theorem for divergence of the product of a scalar φ and a vector $\mathbf{A}$: div $(\varphi A) = \mathbf{A}\cdot\text{grad}\ \varphi + \varphi\ \text{div}\ \mathbf{A}$. Note that $\nabla\cdot(\text{const}) = 0$ and that $\nabla\cdot\mathbf{v}_i = 0$ (incompressibility condition). Use the identity $f_{12} = f_{21}$ and the operator relations $\nabla_2 = -\nabla_1 = \nabla$, $\nabla_1\cdot\nabla_1 = \nabla_2\cdot\nabla_2 = \Delta \equiv$ laplacian in variables (r, θ). Substitute (1.4) and (1.5) to reduce the potentials to functions of r and $\mathbf{r}$. This sequence best keeps track of the sign changes involved in reducing the equation to one variable $\mathbf{r} = \mathbf{r}_{21} = -\mathbf{r}_{12}$. Then open the remaining terms, substitute $f_{ji}(\mathbf{r}) = f^\circ{}_{ji}(r) + f'_{ji}(\mathbf{r})$ and drop the $f'\psi'$ terms of order X^2. Cancel out the spherically symmetric $f^\circ\psi^\circ$ terms because $\mathbf{v}_{ji} = \mathbf{v}_{ij} = 0$ when $X = 0$. Reduce the (grad·grad) terms to products of scalar derivatives by use of the relations given immediately after eq. 14 of ref. 6, which are based on the fact that $\psi'(\mathbf{r}) = \varphi(r)\cos\theta$. Use the Poisson equation 1.3 to eliminate the potentials ψ', specialize to $i = 1$, $j = 2$ and use $\Delta\psi^0{}_j \approx \kappa^2\psi^0{}_j$ to simplify $T(g_2)$. The result is (1.8).

(8) Ref. (6), Eq. 19.

(9) Ref. 4, eq. (4.3.6), after specialization to $s = 2$ and substitution of (4.4.1) to eliminate the potentials.

2. Order of Terms in Concentration

The last five terms on the right of (1.8) are explicitly

$$T(g_1) = -\left\{e_1\omega_1\frac{\partial}{\partial x}\left(\frac{\psi'_2}{\cos\theta}\right) - e_2\omega_2\frac{\partial}{\partial x}\left(\frac{\psi'_1}{\cos\theta}\right)\right\}\frac{\mathrm{d}f^\circ{}_{21}}{\mathrm{d}r} \quad (2.1)$$

$$T(g_2) = -(e_1\omega_1\psi^\circ{}_2 + e_2\omega_2\psi^\circ{}_1)\kappa^2 f'_{21} \quad (2.2)$$

$$T(g_3) = -\left(e_1\omega_1\frac{\mathrm{d}\psi^\circ{}_2}{\mathrm{d}r} + e_2\omega_2\frac{\mathrm{d}\psi^\circ{}_1}{\mathrm{d}r}\right)\frac{\partial}{\partial x}\left(\frac{f'_{21}}{\cos\theta}\right) \quad (2.3)$$

$$T(a) = \left\{e_1\omega_1\frac{\partial}{\partial x}\left(\frac{\psi'_1}{\cos\theta}\right)_a - e_2\omega_2\frac{\partial}{\partial x}\left(\frac{\psi'_2}{\cos\theta}\right)_a\right\}\frac{\mathrm{d}f^\circ{}_{21}}{\mathrm{d}r} \quad (2.4)$$

$$T(v) = (v_{1r} - v_{2r})(\mathrm{d}f^\circ{}_{21}/\mathrm{d}r) \quad (2.5)$$

The origin of the last two is obvious by inspection of the expressions for force and velocity. The origin of the first three is made clear by considering the expansion

$$\begin{aligned}\text{div}\,(f\,\text{grad}\,\psi) &= \text{grad}\,\psi\cdot\text{grad}\,f + f\,\text{div grad}\,\psi \\ &= (\nabla\psi^\circ + \nabla\psi')\cdot(\nabla f^\circ + \nabla f') + (f^\circ + f')(\Delta\psi^\circ + \Delta\psi') \\ &= (\nabla\psi^\circ\cdot\nabla f^\circ) + \nabla\psi'\cdot\nabla f^\circ + \nabla\psi^\circ\cdot\nabla f' + [\nabla\psi'\cdot\nabla f'] + (f^\circ\Delta\psi^\circ) + f'\Delta\psi^\circ + f^\circ\Delta\psi' + [f'\Delta\psi']\end{aligned}$$

The final terms in square brackets are quadratic in the field and by hypothesis negligible. The terms in parentheses are the radial functions for the system in the absence of an external field and the sum of these terms in the expansion of (1.2) must vanish. Hence

$$\text{div}\,(f\,\text{grad}\,\psi) \longrightarrow \{f^\circ\Delta\psi' + \nabla\psi'\cdot\nabla f^\circ + f'\Delta\psi^\circ + \nabla\psi^\circ\cdot\nabla f'\}$$

in (1.8). The first of these terms, $f^0\Delta\psi'$, is proportional to f^0f'/n (*cf.* Poisson equation) and is moved to the left side of (1.8), because it is of the same order in concentration as $\Delta f'$ and of course contains the unknown function f'. (The coefficient of f' is $f^0/n \sim n \sim \kappa^2$, and application of the laplacian to f' brings down a multiplier of order κ^2, assuming that f' contains $\exp(-\kappa r)$. Hence $\Delta f' - f^0\Delta\psi' \sim \kappa^2 f'$.) The next three contribute, respectively, to the gradient terms $T(g_1)$, $T(g_2)$ and $T(g_3)$.

We now proceed to examine the order of the various terms of (1.8), considered as functions of concentration. The equation has the form

$$\Delta f' - \gamma^2 f' = \Sigma_k l_k \cos\theta \quad (2.6)$$

where

$$\gamma^2 = q^2\kappa^2 = \frac{4\pi}{DkT}\frac{n_1e_1^2\omega_1 + n_2e_2^2\omega_2}{\omega_1 + \omega_2} \qquad (2.7)$$

and the t_k's are of the functional form $e^{-\kappa r}/r^k$. (Some terms have $e^{-\lambda\kappa r}$ instead of $e^{-\kappa r}$, where λ is a pure number. Since λ is dimensionless, its presence will not affect the argument which follows.) The solution of (1.8) is, of course, the general solution of the homogeneous equation plus a particular solution of the inhomogeneous equation; the latter is the sum of particular solutions of equations of the form

$$\Delta_{r,\theta}\, u_k(r,\theta) - q^2\kappa^2 u_k = e^{-\kappa r}\cos\theta/r^k \qquad (2.8)$$

Dividing by κ^2, this reduces to a function of the dimensionless independent variable $\xi = \kappa r$

$$\Delta_{\xi,\theta}\, u_k - q^2 u_k = \kappa^{k-2}\, e^{-\xi}\cos\theta/\xi^k$$

Hence if $U_k(\xi,\theta)$ is the solution of

$$\Delta U_k - q^2 U_k = e^{-\xi}\cos\theta/\xi^k$$

the solution of (2.8) is $u_k = \kappa^{k-2}U_k$ where U_k is dimensionless. Consequently a term $e^{-\kappa r}/r^k$ on the right of (1.8) will give a term of order κ^{k-2} in the solution, multiplied by whatever powers of κ which may appear in the coefficient of that term.

Several examples will be given to illustrate the use of the above theorem, and then the final result will be stated. Consider the first term on the right of (1.8), disregarding irrelevant multipliers. We require the order in κ of the solution of

$$\Delta u - \gamma^2 u = \partial f^0_{21}/\partial x$$

It will be recalled that $\kappa^2 \sim n_1 \sim n_2 \sim c$; to first approximation

$$f^0_{21} = n_2n_1(1 - e_1e_2e^{-\kappa r}/rDkT)$$

The operator $(\partial/\partial x)$ brings in a multiplier $e^{-\kappa r}(1 + \kappa r)\cos\theta/r^2$ when applied to $e^{-\kappa r}/r$, so we consider

$$\Delta v - \gamma^2 v = \kappa^4 e^{-\kappa r}\cos\theta/r^2$$

Integration of $e^{-\kappa r}/r^2$ gives a multiplier κ^{2-2}, so $v = 0(\kappa^4)$.

Now, consider $T(g_1)$, the second term on the right of (1.8); the corresponding symbolic equation is

$$\Delta u - \gamma^2 u = (\partial\psi'/\partial x)(\mathrm{d}f^0/\mathrm{d}r)$$

Earlier calculations[10] show that $\psi' \sim \kappa^{-2}r^{-2}$, so $\partial\psi'/\partial x \sim \kappa^{-2}r^{-3}$ and we have $\mathrm{d}f^0/\mathrm{d}r \sim \kappa^4 r^{-2}$; the order of the term in f'_{21} arising from $T(g_1)$ is thus obtained by considering

$$\Delta v - \gamma^2 v = \kappa^2 e^{-\kappa r}\cos\theta/r^5$$

whence $v = 0(\kappa^5)$, which is therefore of higher order than the integral of the first term of (1.8). In fact, since we know that the latter gives rise to a $c^{1/2}$ term in the final conductance equation, we already see that $T(g_1)$ will lead to a term of order $\kappa c^{1/2}$, *i.e.*, a linear term in conductance. (It also produces a transcendental term of *limiting* order c ln c, as will be shown later. Here, we are considering algebraic terms only.) In a similar fashion, we can show that the other T's of (1.8) are of higher order in κ than the first term.

(10) Ref. 4, eqs. 4.5.2, 4.5.9 and 4.5.10. See also eq. 4.7 of this paper.

This investigation suggests the method of solving the problem. Let

$$f'_{21} = F_{21} + g_{21} \qquad (2.9)$$

and

$$\psi'_j = \Psi_j + p_j \qquad (2.10)$$

and define F_{21} as the solution of the equation which we obtain by dropping the higher order terms of (1.8), *i.e.*, the T's. This requires the solution of

$$kT(\omega_1 + \omega_2)\Delta F_{21} - [(4\pi f^0_{21}/D)(e_1^2\omega_1/n_2 + e_2^2\omega_2/n_1)]F_{21} = X(e_1\omega_1 - e_2\omega_2)(\partial f^0_{21}/\partial x) \qquad (2.11)$$

Once the solution of (2.11) is obtained, we can then substitute (2.9) in (1.8) and use F_{21} as an approximation for f'_{21} in the inhomogeneous terms. The κ^4 terms will cancel by virtue of (2.11) and there will remain a differential equation which will determine g_{21}. (In each of these steps, the number of terms retained in the expansion of the Boltzmann factor in f^0_{21} is chosen to be consistent with our approximation principle.)

3. Boundary Conditions

The above statement of the problem was deliberately oversimplified, in order to permit postponing discussion of the boundary conditions. To compute the conductance, the potentials, rather than the distribution functions, are needed. They are obtained from the latter by integration of the Poisson equation; in other words, we must integrate the fourth order differential equation

$$\Delta\Delta\psi_j - \gamma^2\Delta\psi_j = \Sigma\ (\text{inhomogen.})$$

in order to obtain the relaxation field. Consequently four boundary conditions are necessary for evaluation of the four constants of integration which will appear in the formal treatment. Three of these are the familiar electrostatic conditions: the field must vanish for $r = \infty$ and potential and field strength must be continuous at $r = a$; that is

$$(\partial\psi'/\partial r)_{r=\infty} = 0 \qquad (3.1)$$

$$\psi'(a - 0) = \psi'(a + 0);\quad (\partial\psi'/\partial r)_{a-0} = (\partial\psi'/\partial r)_{a+0} \qquad (3.2)$$

For $r \leqslant a$, the potential satisfies the Laplace equation

$$\Delta\psi'_j = 0$$

and is given by

$$\psi'_j(r \leqslant a) = -\beta x = -\beta r\cos\theta$$

where β is a constant. Then $(\partial\psi'_j/\partial r)_{a-0} = -\beta\cos\theta$ and $(r\,\partial\psi'/\partial r)_{a-0} = \psi'_j(a - 0) = \psi'_j(a + 0)$. Hence condition (3.2) may be expressed as

$$(r\,\partial\psi'_j/\partial r - \psi'_j)_a = 0 \qquad (3.3)$$

The fourth boundary condition requires a little more care. Our model for the ions consists of rigid spheres of diameter a, which cannot interpenetrate; this fact must be used explicitly in the calculation. This is the most directly achieved by requiring that the radial components of relative velocity of any two ions vanish at contact. This leads to the result

$$[(f_{ij}\mathbf{v}_{ij} - f_{ji}\mathbf{v}_{ji})\cdot\mathbf{r}]_{r=a} = 0 \qquad (3.4)$$

By substitution and expansion similar to that which led to (1.8), we obtain for the flow vector in the above brackets

$$\mathbf{Y} = (e_1\omega_1 - e_2\omega_2)f^\circ_{21}\mathbf{Xi} - kT(\omega_1 - \omega_2)\nabla f'_{21} - f^\circ_{21}(e_1\omega_1\nabla\psi'_2 - e_2\omega_2\nabla\psi'_1) - f'_{21}(e_1\omega_1\nabla\psi^\circ_2 + e_2\omega_2\nabla\psi^\circ_1) + f^\circ_{21}[e_1\omega_1\nabla\psi'_1(a) - e_2\omega_2\nabla\psi'_2(a)] + (\mathbf{v}_1 - \mathbf{v}_2)f^\circ_{21}$$

For later use, it is convenient to define a scalar function

$$Z(r) = (\mathbf{Y}\cdot\mathbf{r})/x$$

the boundary condition (3.4) then may be stated

$$Z(a) = 0 \tag{3.5}$$

Expanding as before, we find

$$(e_1\omega_1 - e_2\omega_2)Xf^\circ_{21} - kT(\omega_1 + \omega_2)\frac{\mathrm{d}}{\mathrm{d}r}\left(\frac{f'_{21}}{\cos\theta}\right) - f^\circ_{21}\left\{e_1\omega_1\frac{\mathrm{d}}{\mathrm{d}r}\left(\frac{\psi'_2}{\cos\theta}\right) - e_2\omega_2\frac{\mathrm{d}}{\mathrm{d}r}\left(\frac{\psi'_1}{\cos\theta}\right)\right\} - \frac{f'_{21}}{\cos\theta}\left(e_1\omega_1\frac{\mathrm{d}\psi^\circ_2}{\mathrm{d}r} + e_2\omega_2\frac{\mathrm{d}\psi^\circ_1}{\mathrm{d}r}\right) + f^\circ_{21}\left\{e_1\omega_1\frac{\mathrm{d}}{\mathrm{d}r}\left(\frac{\psi'_1}{\cos\theta}\right)_a - e_2\omega_2\frac{\mathrm{d}}{\mathrm{d}r}\left(\frac{\psi'_2}{\cos\theta}\right)_a\right\} + (v_{1r} - v_{2r})f^\circ_{21}/\cos\theta = Z(r) \tag{3.6}$$

where v_{jr} is the radial component of velocity of an ion of species j due to the presence of other ions.

Examination as before of the terms of (3.6) shows that the last three are of higher order in κ than the first three. The appropriate boundary condition for the solution of (2.11) for F_{21} is accordingly

$$\left[(e_1\omega_1 - e_2\omega_2)Xf^\circ_{21} - kT(\omega_1 + \omega_2)(\mathrm{d}h_{21}/\mathrm{d}r) - f^\circ_{21}\left\{e_1\omega_1\left(\frac{\mathrm{d}\Phi_2}{\mathrm{d}r}\right) - e_2\omega_2\left(\frac{\mathrm{d}\Phi_1}{\mathrm{d}r}\right)\right\}\right]_a = 0 \tag{3.7}$$

where the radial parts of F_{21} and Ψ_j have been separated by the definitions

$$F_{21}(\mathbf{r}) = h_{21}(r)\cos\theta \tag{3.8}$$

$$\Psi_j(\mathbf{r}) = \Phi_j(r)\cos\theta \tag{3.9}$$

in accordance with the known[11] angular dependence of F_{21} and Ψ_j.

4. First Approximation: Finite Ion Size

In preparing (2.11) for explicit integration, the equation is divided by $kT(\omega_1 + \omega_2)$ and f^0_{21} is replaced by the approximation

$$f^\circ_{21} = n_1n_2(1 - e_1e_2e^{-\kappa r}/\mu DkTr) \tag{4.1}$$

where

$$\mu = e^{-\kappa a}(1 + \kappa a) \tag{4.2}$$

(The next term in the expansion of the Boltzmann factor in f^0_{21} will be included in the calculation of the perturbation term g_{21}.) The neutrality condition

$$n_1e_1 + n_2e_2 = 0 \tag{4.3}$$

and the abbreviation q^2 defined by (2.7) aid in simplifying (2.11) to

$$\Delta F_{21} - \gamma^2F_{21} = \frac{n_1e_1\gamma^2X}{4\pi\mu kT}\frac{\partial}{\partial x}\left(\frac{e^{-\kappa r}}{r}\right) \tag{4.4}$$

The boundary condition $Z(a) = 0$ can be simplified to

$$X - (4\pi e_1/Dn_2\gamma^2)(\mathrm{d}h_{21}/\mathrm{d}r)_a - (\mathrm{d}\Phi/\mathrm{d}r)_a = 0 \tag{4.5}$$

if we anticipate the result that $\Phi_1 = \Phi_2$ and write Φ for both potentials. We must now integrate (4.4), substitute the result into the Poisson equation and integrate the latter, subject to (4.5) and the three electrostatic boundary conditions. Among these, the natural conditions for $r \to \infty$ serve to eliminate solutions of the homogeneous equations in $e^{\gamma r}$ and $e^{\kappa r}$. Routine methods give

$$F_{21} = \frac{n_1e_1q^2X}{4\pi\mu kT(1 - q^2)}\frac{\partial}{\partial x}\left(\frac{e^{-\kappa r}}{r} - \frac{Ae^{-\gamma r}}{r}\right) \tag{4.6}$$

and

$$\Psi = \frac{\epsilon_1e_2q^2X}{\mu DkT(1 - q^2)}\frac{\partial}{\partial x}\left\{\frac{e^{-\kappa r}}{\kappa^2r} - \frac{Ae^{-\gamma r}}{\gamma^2r} + \left(\frac{1}{\gamma^2} - \frac{1}{\kappa^2}\right)\frac{B}{r}\right\} \tag{4.7}$$

Substitution of Ψ in (3.3) gives an equation relating A and B

$$q^2e^{-\kappa a}(1 + \kappa a + \kappa^2a^2/3) - Ae^{-\gamma a}(1 + \gamma a + \gamma^2a^2/3) + (1 - q^2)B = 0$$

Substitution of Φ and h_{21} in (4.5) evaluates B

$$B = e^{-\kappa a}(1 + \kappa a + \kappa^2a^2/2) - \mu\kappa^2a^2/2b$$

where b is the Bjerrum parameter

$$b = -e_1e_2/aDkT > 0 \tag{4.8}$$

this is a positive number because e_1 and e_2 necessarily have opposite signs.

We are now ready to evaluate the relaxation field

$$-\Delta X = \mathrm{grad}_x\,\Psi(a) = (\partial\Psi/\partial x)_{r=a} \tag{4.9}$$

The potential is of the form

$$\Psi = KxH(r)$$

where K is a constant and H depends solely on r. Use of the boundary condition (3.3) shows that $(\mathrm{d}H/\mathrm{d}r)$ vanishes at $r = a$; hence it follows that

$$(\partial\Psi/\partial x)_a = KH(a)$$

Making the appropriate substitutions, we finally obtain

$$\Delta X = \Delta X_0\left\{\frac{1 + {}^1/_2\kappa a(1 + q)[1 - (1 + \kappa a)/b]}{(1 + \kappa a)(1 + q\kappa a + q^2\kappa^2a^2/3)}\right\} \tag{4.10}$$

where ΔX_0 is the previous solution obtained for the point charge model

$$\Delta X_0 = e_1e_2q^2\kappa X/3DkT(1 + q) = \alpha c^{1/2}X \tag{4.11}$$

Examination of the above result shows that it can be expanded in powers of κa

$$\Delta X = \Delta X_0(1 + \alpha_1\kappa a + \alpha_2\kappa^2a^2 + \ldots)$$

where α_1 is negative. Consequently the relaxation field for spherical ions increases *less* rapidly with increasing concentration than that for point charges; the initial deviation of the conductance curve from the limiting tangent can obviously be represented by a positive linear term in concentration in the conductance equation. The above explicit form is, however, not very convenient for numerical calculations. Since, as we shall see later, the range of applicability of our theory is limited to moderate concentrations, expansion in the form

$$\Delta X = \Delta X_0(1 - \Delta_1)$$

(11) Ref. 4, eq. 4.3.3 and 4.3.4, and accompanying discussion.

followed by approximation of Δ_1 is justified. We shall also specialize the result to symmetrical salts, for which $q^2 = {}^1/_2$. The final result is

$$\Delta_1 = (1 + q)(b + 1)\kappa a/2bp_3; \quad \kappa a < 0.3 \quad (4.12)$$

where

$$p_3 = 1 + q\kappa a + \kappa^2 a^2/6 \quad (4.13)$$

The next step in the derivation consists in returning F_{21} and Ψ as approximations for f'_{21} and ψ' in the inhomogeneous terms of (1.8) and then solving for the perturbation functions g_{21} and p_j. Before proceeding to this operation, however, it is necessary to obtain an explicit expression for the velocity terms in (2.5) and (3.6).

5. The Velocity Field

The external electrical field $X\mathbf{i}$ exerts a force $\mathbf{F}$ per unit volume of the solution; if we assume a continuous charge density ρ, then

$$\mathbf{F} = X\rho\mathbf{i} \quad (5.1)$$

This force on the ions is transmitted to the solvent; it is therefore clear that the moving ions will set up a velocity field $\mathbf{v}$ in the solution which will depend on local ion concentrations n_{ji} rather than on average concentrations n_i. The charge density is related to the potential through the Poisson equation

$$\Delta\psi = -4\pi\rho/D \quad (5.2)$$

and the force is related to velocity and pressure through the fundamental hydrodynamic equation

$$\eta\nabla \times \nabla \times \mathbf{v} = \mathbf{F} - \nabla p \quad (5.3)$$

Equations 5.1, 5.2 and 5.3, together with the hydrodynamic statement of incompressibility

$$\nabla\cdot\mathbf{v} = 0 \quad (5.4)$$

thus constitute a system of equations whose solution gives $\mathbf{v}$ in terms of r and $\cos\theta$. This problem was first solved by Debye and Hückel[12]; we shall develop an alternative derivation of the velocity field below, in which the boundary conditions for all but one small term are stated in terms of a, the distance of nearest approach.

Let $\mathbf{u}$ be a vector defined in terms of $\mathbf{v}$ by the differential equation

$$\eta\mathbf{v} = \nabla(\nabla\cdot\mathbf{u}) - \Delta\mathbf{u} = \text{grad (div } \mathbf{u}) - \text{lap } \mathbf{u} \quad (5.5)$$

Constructing curl (curl $\mathbf{v}$), we obtain

$$\eta\nabla \times \nabla \times \mathbf{v} = \Delta\Delta\mathbf{u} - \nabla(\nabla\cdot\Delta\mathbf{u}) \quad (5.6)$$

Equating corresponding terms in (5.3) and (5.6), gives

$$\mathbf{F} = \Delta\Delta\mathbf{u} \quad (5.7)$$

and[13]

$$\nabla p = \nabla(\nabla\cdot\Delta\mathbf{u}) \quad (5.8)$$

Combining (5.1), (5.2) and (5.7) gives

$$\Delta\Delta\mathbf{u} = -(DX\mathbf{i}/4\pi)\,\Delta\psi$$

Integrating once

$$\Delta\mathbf{u} = -(DX\mathbf{i}/4\pi)\psi + \Delta\mathbf{w}$$

where $\Delta\mathbf{w}$ is the solution of the homogeneous equation. Since $\Delta\Delta\mathbf{w} = 0$

$$\Delta\mathbf{w} = \mathbf{i}(\alpha + \beta/r)$$

To keep the velocity finite at $r = \infty$, α must vanish while β can be absorbed in later constants; we may therefore disregard $\mathbf{w}$ at this point. In order to solve the equation

$$\Delta\mathbf{u} = -(DX\mathbf{i}/4\pi)\psi \quad (5.9)$$

for $\mathbf{u}$, it is convenient to consider separately the potential ψ_A due to the atmosphere of the reference ion and the potential ψ_s due to the charge on that ion itself. Using the Debye–Hückel potential, we have

$$\psi_A = (e/D)(e^{-\kappa r}/\mu r - 1/r) \quad (5.10)$$

while

$$\psi_s = e/Dr \quad (5.11)$$

It can be verified readily that

$$(\partial\psi_A/\partial r)_{r=a} = 0 \quad (5.12)$$

Substituting (5.10) into (5.9)

$$\Delta\mathbf{u}_A = -(Xe\mathbf{i}/4\pi)(e^{-\kappa r}/\mu r - 1/r) \quad (5.13)$$

for $r > a$; at $r = a$

$$\Delta\mathbf{u}_A = (Xe\mathbf{i}/4\pi)[\kappa/(1 + \kappa a)] \quad (5.14)$$

Equation 5.14 must also determine $\mathbf{u}_A$ for $r < a$, because there obviously are no charges inside a except that of the reference ion, whose effect will be computed later as $\mathbf{u}_s$.

Integration of (5.13) gives

$$\mathbf{u}_A = \frac{Xe\mathbf{i}}{4\pi}\left(\frac{r}{2} - \frac{e^{\kappa a}}{1 + \kappa a}\frac{e^{-\kappa r}}{\kappa^2 r} + \frac{B}{r}\right), \; r > a \quad (5.15)$$

disregarding a constant which differentiates out by application of (5.5), while integration of (5.14) gives

$$\mathbf{u}_A = \frac{Xe\mathbf{i}}{4\pi}\left(\frac{\kappa}{1 + \kappa a}\frac{r^2}{6} + C\right), \; r < a \quad (5.16)$$

We require that $\mathbf{u}_A$ and its derivative be continuous at $r = a$; using these conditions to evaluate B and C, we find

$$\mathbf{u}_A = \frac{Xe\mathbf{i}}{4\pi}\left(\frac{r}{2} + \frac{1 + \kappa a + \kappa^2 a^2/2 + \kappa^3 a^3/6 - e^{\kappa(a-r)}}{\kappa^2 r(1 + \kappa a)}\right), \; r > a \quad (5.17)$$

and

$$\mathbf{u}_A = \frac{Xe\mathbf{i}}{4\pi}\left(\frac{1 + \kappa a + \kappa^2 a^2/2 + \kappa^2 r^2/6}{\kappa(1 + \kappa a)}\right), \; r < a \quad (5.18)$$

Carrying out the differentiation (5.5), we obtain for the velocity field due to the atmosphere of the reference ion

$$\eta\mathbf{v}_A = \frac{Xe}{4\pi}\left\{\mathbf{r}_1\cos\theta\left(\frac{3B}{r^3} - \frac{1}{2r} - \frac{3e^{\kappa(a-r)}(1 + \kappa r + \kappa^2 r^2/3)}{\kappa^2 r^3(1 + \kappa a)}\right) + \mathbf{i}\left(-\frac{B}{r^3} - \frac{1}{2r} + \frac{e^{\kappa(a-r)}(1 + \kappa r + \kappa^2 r^2)}{\kappa^2 r^3(1 + \kappa a)}\right)\right\} \quad (5.19)$$

For later computation of the relaxation field, we shall need the radial component of $\mathbf{v}_A$; recalling that $\mathbf{i}\cdot\mathbf{r}_1 = \cos\theta$, we have

$$\eta v_{rA} = \frac{Xe\cos\theta}{4\pi}\left\{-\frac{1}{r} + \frac{2(1 + \kappa a + \kappa^2 a^2/2 + \kappa^3 a^3/6) - 2e^{\kappa(a-r)}(1 + \kappa r)}{\kappa^2 r^3(1 + \kappa a)}\right\} \quad (5.20)$$

(12) P. Debye and E. Hückel, *Physik. Z.*, **24**, 305 (1923); Sections VII and VIII.

(13) The pressure is determined by (5.8): integration gives p = (div. $\Delta\mathbf{u}$ + const.) and once $\mathbf{u}$ is found, the pressure is obtained by simple differentiation. Alternatively, application of $(\nabla\cdot)$ to (5.3) and use of (5.4) gives $\Delta p = \nabla\cdot\mathbf{F}$. However, we shall not need the pressure so the derivation is omitted.

We next consider the contribution to v from the charge of the central ion. The corresponding differential equation for $\mathbf{u}_s$ is

$$\Delta \mathbf{u}_s = -Xei/4\pi r$$

with the solution

$$\mathbf{u}_s = \frac{Xei}{4\pi}\left(-\frac{r}{2} + \frac{E}{r}\right) \tag{5.21}$$

Differentiation gives

$$\nabla(\nabla\cdot\mathbf{u}_s) = \frac{Xe}{4\pi}\left\{\mathbf{i}\left(-\frac{1}{2r} - \frac{E}{r^3}\right) + (\mathbf{i}\cdot\mathbf{r})\mathbf{r}_1\left(\frac{1}{2r^2} + \frac{3E}{r^4}\right)\right.$$

The second component above is the radial component of the velocity (5.5) and must vanish at the hydrodynamic surface of the reference ion; *i.e.*, at $r = R$, where R is the Stokes radius. Accordingly

$$E = -R^2/6$$

Substituting in (5.5), we obtain for the radial component

$$\eta v_{sr} = \frac{Xe\cos\theta}{4\pi}\left(\frac{1}{r} - \frac{R^2}{3r^3}\right), r > R \tag{5.22}$$

Finally, combining (5.20) and (5.22), the radial component of the velocity field is found to be

$$v_r = \frac{Xe\cos\theta}{2\pi\eta}\left(\frac{1 + \kappa a + 11\kappa^2a^2/24 + \kappa^3a^3/8 - e^{\kappa(a-r)}(1+\kappa r)}{\kappa^2r^3(1+\kappa a)}\right)$$

The algebraic function of κa in the numerator above is closely approximated by

$$p_1 = 1 + \kappa a + \kappa^2a^2/2$$

over the practical working range of the variable $0 \leqslant \kappa a < 0.3$. We therefore shall use the following expression for v_r in subsequent derivations

$$v_r = \frac{Xe\cos\theta}{2\pi\eta}\frac{p_1 - e^{\kappa(a-r)}(1+\kappa r)}{\kappa^2r^3(1+\kappa a)} \tag{5.26}$$

The velocity term $T(v)$ in the inhomogeneous differential equation 1.8 thus leads to the equation

$$\Delta g_v - \gamma^2 g_v = \frac{n}{\mu Dk^2T^2}\frac{n_2e_1e_2(v_{1r} - v_{2r})}{(\omega_1 + \omega_2)}\frac{\mathrm{d}}{\mathrm{d}r}\left(\frac{e^{-\kappa r}}{r}\right) \tag{5.27}$$

for evaluating the contribution of the velocity field to the relaxation effect. Substituting (5.26) in (5.27) and using the identity

$$n_1n_2(e_2 - e_1) = DkT\kappa^2n_1/4\pi e_2$$

leads to the equation

$$\Delta g_v - \gamma^2 g_v = \frac{n_1e_1X}{8\pi^2\mu kT\eta(\omega_1+\omega_2)(1+\kappa a)}\left\{p_1\left(\frac{xe^{-\kappa r}}{r^6} + \frac{\kappa xe^{-\kappa r}}{r^5}\right) - e^{\kappa a}\left(\frac{xe^{-2\kappa r}}{r^6} + \frac{2\kappa xe^{-2\kappa r}}{r^5} + \frac{\kappa^2xe^{-2\kappa r}}{r^4}\right)\right\} \tag{5.28}$$

6. Higher Field Terms

In Section 4, it was shown that the approximate equation 4.4, when applied to charged spheres, leads to terms of order c and higher in the conductance equation. The analysis in Section 2 showed that the terms of (1.8), the general equation of continuity, which were dropped in order to obtain (4.4), would also lead to terms of order c and higher. We therefore proceed to the evaluation of these terms by the perturbation method described in Section 2; specifically, the problem is to evaluate the functions g_{21} and p_j defined by equations 2.9 and 2.10. Substitution of F_{21} and Ψ in the inhomogeneous terms of (1.8) and (3.6), followed by cancellation of the leading terms by virtue of (4.4) and (3.7), and neglect of higher order terms (κ^3, etc.), leads after rearrangement to the equations

$$\Delta g_{21} - \gamma^2 g_{21} = \frac{n_2e_1e_2^2\gamma^2X}{8\pi D(\mu kT)^2}\frac{\partial}{\partial x}\left(\frac{e^{-2\kappa r}}{r^2}\right) - \frac{e_1e_2\gamma^2e^{-\kappa r}F_{21}}{\mu DkTr} + \frac{n_2e_2\gamma^2}{4\pi\mu kT}\frac{\mathrm{d}}{\mathrm{d}r}\left(\frac{e^{-\kappa r}}{r}\right)\frac{\partial\Phi}{\partial x} - \frac{e_1e_2\kappa^2e^{-\kappa r}F_{21}}{\mu DkTr} -$$
$$\frac{e_1e_2}{\mu DkT}\frac{\mathrm{d}}{\mathrm{d}r}\left(\frac{e^{-\kappa r}}{r}\right)\frac{\partial h_{21}}{\partial x} - \frac{r_2e_2\gamma^2}{4\pi\mu kT}\frac{\mathrm{d}}{\mathrm{d}r}\left(\frac{e^{-\kappa r}}{r}\right)\left(\frac{\partial\Phi}{\partial x}\right)_a + \frac{n_1n_2e_1e_2(v_{1r} - v_{2r})}{\mu Dk^2T^2(\omega_1+\omega_2)}\frac{\mathrm{d}}{\mathrm{d}r}\left(\frac{e^{-\kappa r}}{r}\right) \tag{6.1}$$

and

$$Z'(r) = \frac{n_1e_1\gamma^2Xe^{-\kappa r}}{4\pi\mu kTr} - \frac{\mathrm{d}}{\mathrm{d}r}\left(\frac{g_{21}}{\cos\theta}\right) + \frac{n_2e_2\gamma^2e^{-\kappa r}}{4\pi\mu kTr}\frac{\mathrm{d}\Phi}{\mathrm{d}r} - \frac{e_1e_2h_{21}}{\mu DkT}\frac{\mathrm{d}}{\mathrm{d}r}\left(\frac{e^{-\kappa r}}{r}\right) + \frac{n_2\gamma^2D}{4\pi e_1}\left(\frac{\mathrm{d}\Phi}{\mathrm{d}r}\right)_a - \frac{v_{1r} - v_{2r}}{\omega_1+\omega_2}\frac{n_1n_2}{kT\cos\theta} \tag{6.2}$$

where $Z'(r)$ includes the terms of $Z(r)$ which survive after subtracting those used in Section 4 for the first-order solution. The first terms on the right sides of (6.1) and (6.2) result from retaining one more term than in (4.4) and (3.7) of the expansion of the Boltzmann exponential in f^0_{21}. The boundary conditions for the potentials are of course exactly similar to (3.1) and (3.3), with p_j replacing ψ_j.

The formal attack of (6.1) would now proceed as follows: to a particular solution of the inhomogeneous equation, we would add the general solution of the homogeneous equation. The result would be substituted in the corresponding (part of the) Poisson equation which would then be integrated in a similar fashion. Finally, the boundary conditions would be used to evaluate the two non-trivial constants of integration. Even casual inspection of (6.1) shows that this approach rapidly leads to algebraic chaos. A less direct but far more manageable method was devised. First, g_{21} was broken up into the sum of four terms

$$v_r = \frac{Xe\cos\theta}{4\pi\eta}\left\{\frac{2(1+\kappa a+\kappa^2a^2/2+\kappa^3a^3/6) - 2e^{\kappa(a-r)}(1+\kappa r)}{\kappa^2r^3(1+\kappa a)} - \frac{R^2}{3r^3}\right\} \tag{5.23}$$

Investigation of the two terms in v_r shows that the major contribution comes from the first term: for κa small, it approaches $e^{\kappa a}/r(1+\kappa a) \approx 1/r$. To a fair approximation, the Stokes radius should be about equal to half the center-to-center distance a; if we set $R = a/2$, we find

$$v_r = \frac{Xe\cos\theta}{4\pi\eta r}\left(1 - \frac{a^2}{12r^2}\right) \tag{5.24}$$

At $r = a$, the Stokes term is thus only a twelfth of the total, and its contribution decreases rapidly as r increases. Consequently, we shall make the approximation

$$R = a/2 \tag{5.25}$$

and use it to simplify (5.23) to

$$g_{21} = g_B + g_{2,3} + g_a + g_v \quad (6.3)$$

to parallel the T's of (1.8), and $Z'(r)$ was separated in a similar fashion. The subscript B terms come from the higher terms of the expansion of the Boltzmann function, the subscript 2,3 terms from the cross-gradient terms in the original expansion, the subscript a terms from the $\nabla\psi'(a)$ terms of (1.10) and the subscript v terms from the local velocity field. The potential is also expanded as a sum of corresponding terms. The problem is thus reduced to finding the sum of the solutions of four equations, each a component of (6.3).

Even with this simplification, the algebraic manipulations required to evaluate the integration constants from the boundary conditions are still formidable. A method was accordingly devised which leads directly from the differential equation and boundary conditions to the corresponding contribution to the relaxation field which is

$$\Delta X' = \Delta X_B + \Delta X_{2,3} + \Delta X_a + \Delta X_v \quad (6.4)$$

In order not to break the continuity of the argument, a description of this method is presented in Appendix I, where it is shown that

$$-\Delta X_v = (4\pi e_2 K/3Dn_1)\{\int^a y(r)\,dr + {}^1/_2 a^2 U(a)\} \quad (6.5)$$

Here ΔX_v is the contribution to $\Delta X'$ arising from that part of g_{21} defined by

$$\Delta g - \gamma^2 g = Kf(r)\cos\theta \quad (6.6)$$

with

$$g(r,\theta) = K\left\{y(r)\cos\theta + A\frac{\partial}{\partial x}\left(\frac{e^{-\gamma r}}{r}\right)\right\} \quad (6.7)$$

as the pertinent part of the complete solution of (6.1).

The method will be illustrated by application to the Boltzmann term of (6.1). The differential equation is

$$\Delta g_B - \gamma^2 g_B = -\frac{n_1 e_2^2 e_2 \gamma^2 X}{8\pi D(\mu kT)^2}\frac{\partial}{\partial x}\left(\frac{e^{-2\kappa r}}{r^2}\right) = -K\left(\frac{\kappa x e^{-2\kappa r}}{r^3} + \frac{x e^{-2\kappa r}}{r^4}\right) \quad (6.8)$$

From the boundary condition

$$U(a) = \left(\frac{dh_B}{dr}\right)_a = \frac{n_1 e_1 \gamma^2 X}{4\pi\mu kT}\frac{e^{-\kappa a}}{a}$$

The integral tables (Appendix II) are used to evaluate the functions $\int^a y(r)\,dr$ and $(dy/dr)_a$ arising from the two terms on the right of (6.8). Substitution in (6.5) gives

$$\Delta X_B = \frac{b(1+q)\kappa a \Delta X_0}{p_2(1+\kappa a)^2}\left(\frac{1+\kappa a}{2b} - \frac{1}{4} - \frac{T_2}{2}\right) \quad (6.9)$$

where

$$T_2 = \mathrm{Tr}[(2+q)\kappa a] \quad (6.10)$$

and

$$\mathrm{Tr}(x) \equiv e^x \int_x^\infty e^{-t}\,dt/t \quad (6.11)$$

Similar calculations were made for the other terms of $\Delta X'$; the results are tabulated below. In order to keep the formulas reasonably compact for type setting, it is necessary to introduce a number of auxiliary formulas, which are also listed. Even with these abbreviations, the equations are unwieldy; a number of simplifications were therefore made beforehand. The pattern of these approximations is based on the following arguments. The general form of the explicit terms of $\Delta X'$ is given by

$$\Delta X' = \kappa a\,\Delta X_0[A + Bx + cx^2 + \ldots + (\alpha + \beta x + \gamma x^2 + \ldots)\,\mathrm{Tr}\,(kx)]/P(x) \quad (6.12)$$

where $x = \kappa a$, $P(x)$ is a polynomial of the form $(1 + ax + bx^2 + \ldots)$ and the other symbols represent constants. For large values of x, $\mathrm{Tr}(x)$ behaves asymptotically as $(1/x)$ while for small values it behaves like (const. + ln x). Since ΔX_0 contains a factor κ, the coefficient $\kappa a \Delta X_0$ of the bracketed quantity above is linear in concentration, and a first approximation to [. . .] would be simply $[A + \alpha' + \alpha \ln x]$. A numerical test showed that a wider range of concentration could be covered by retaining the βx term. Accordingly, the explicit integrals were approximated by

$$\Delta X' = \kappa a \Delta X_0[A + (\alpha + \beta x)\,\mathrm{Tr}\,(kx)]/P(x) \quad (6.13)$$

In the final calculations, exact rather than approximate values of the transcendental functions are used, because the useful working range of values comes precisely in the range where neither the series expansion nor the asymptotic expansion of Tr (x) are good approximations unless a cumbersomely large number of terms are retained.[14] Furthermore, a number of other approximations were made which involved inserting terms of order $\kappa^2 a^2$ inside the brackets to construct polynomials which would cancel against some of the terms in $P(x)$. Alternatively, terms of order κa were retained when they would cancel against terms in $P(x)$. Due to the hazard of making the same blunder on the repetition of a calculation, the results presented were checked by repeating the whole calculation from the beginning with the special value $q^2 = {}^1/_2$ (symmetrical electrolytes). This result agreed with that obtained by setting $q^2 = {}^1/_2$ in the final formulas obtained for the general case.

The part of $\Delta X'$ arising from the Boltzmann term is given by (6.9). The other three are

$$\Delta X_a = -\frac{\Delta X_0 q^2 b\kappa a \zeta_1^2(\kappa a)}{3p_2p_3(1+q)(1+\kappa a)^2} \quad (6.14)$$

where

$$\zeta_1 = 1 + \frac{(1+q)\kappa a}{2}\left(1 - \frac{1+\kappa a}{b}\right) \quad (6.15)$$

$$\Delta X_{2,3} = -\frac{\Delta X_0(1+q)b\kappa a\zeta_2(\kappa a)}{p_2p_3(1-q^2)(1+\kappa a)^2} \quad (6.16)$$

where

$$\zeta_2 = (2 - q + 4q^2 - 7q^3 + 2q^4)/8q - (1-q^2)[1 + (1+2q)\kappa a]T_0/4q^2 + (1-q^2)^3[1 + (1+q)\kappa a]T_1/4q^2 + q^2(1+q^2)(1+q\kappa a)T_2/4 + (1-2q^2)(1+\kappa a)T_3/2 \quad (6.17)$$

with $T_0 = \mathrm{Tr}(\kappa a)$, $T_1 = \mathrm{Tr}\,[(1+q)\,\kappa a]$, $T_2 = \mathrm{Tr}\,[(2+q)\,\kappa a]$ and $T_3 = \mathrm{Tr}\,[(1+2q)\,\kappa a]$.

$$\Delta X_v = \frac{X\kappa}{6\pi\eta(\omega_1+\omega_2)}\left(\frac{-b\kappa a\zeta_3(\kappa a)}{p_2(1+\kappa a)^2} + \frac{11\kappa a\zeta_4(\kappa a)}{48p_2}\right) \quad (6.18)$$

where

$$\zeta_3 = (2 + 5q - 2q^2)/16q - p_1p_2T_0/8q^2 - p_1T_1(2q^2 - q^4 - 1)/8q^2 + T_3(4 - q^2)/8 \quad (6.19)$$

and

(14) R. M. Fuoss, This Journal, **58**, 682 (1954).

$$\zeta_4 = (1 + 3\kappa a/11)/(1 + \kappa a) \qquad (6.20)$$

For the case of symmetrical electrolytes, $e_1 = -e_2$ and q^2 reduces to one-half; consequently the polynomials in q simplify considerably. For this case

$$\Delta X_B = -\frac{e_1 e_2 \kappa}{3DkT}\frac{b\kappa a}{p_2(1+\kappa a)^2}\left(\frac{1}{8} - \frac{1+\kappa a}{4b} + \frac{T_2}{4}\right) \qquad (6.21)$$

$$\Delta X_a = -\frac{e_1 e_2 \kappa}{3DkT}\frac{b\kappa a}{p_2 p_3(1+\kappa a)^2}\left(\frac{1}{2} - \frac{\sqrt{2}}{3}\right) \qquad (6.22)$$

$$\Delta X_{2,3} = -\frac{e_1 e_2 \kappa}{3DkT}\frac{b\kappa a \zeta_5(\kappa a)}{p_2 p_3(1+\kappa a)^2} \qquad (6.23)$$

where

$$\zeta_5 = (9\sqrt{2} - 9)/16 + 3p_3T_2/16 + p_1p_3T_1/16 - p_1p_2p_3T_0/4 \qquad (6.24)$$

and

$$\Delta X_v = \frac{X\kappa}{6\pi\eta(\omega_1+\omega_2)}\left(\frac{11\kappa a\zeta_4(\kappa a)}{48p_2} - \frac{b\kappa a\zeta_6(\kappa a)}{p_2(1+\kappa a)^2}\right) \qquad (6.25)$$

where

$$\zeta_6 = (\sqrt{2} + 5)/16 - p_1p_2T_0/4 + p_1T_1/16 + 7T_2/16 \qquad (6.26)$$

The coefficient of the term arising from the velocity field ΔX_v has several factors in common with the leading electrophoresis term; for that reason, it will be convenient to combine the two terms in the final formula for the conductance.

7. Conductance Equation for Symmetrical Electrolytes

For symmetrical electrolytes, the electrophoresis term $\beta c^{1/2}$ in the conductance equation is simply replaced[15] by $\beta c^{1/2}/(1+\kappa a)$ because the coefficient of the transcendental term contains the sum $n_\sigma e_\sigma^2 \mathbf{k}_\sigma \sim n_\sigma e_\sigma^3$ which vanishes. The conductance equation is

$$\Lambda = [\Lambda_0 - \beta c^{1/2}/(1+\kappa a)](1 + \Delta X/X) \qquad (7.1)$$

where

$$-\Delta X/X = \alpha c^{1/2}(1 - \Delta_1 + \Delta_2) + \beta c^{1/2}\Delta'_3/\Lambda_0 \qquad (7.2)$$

and the Δ's are abbreviations for the higher terms which were derived in the preceding sections: Δ_1 is the modification due to finite ion size, Δ_2 summarizes the contributions arising from ΔX_B, $\Delta X_{2,3}$ and ΔX_a, and Δ_3' is the term from the velocity field. For $q^2 = 1/2$, these quantities are explicitly given below. (In several places, q is not replaced by $2^{1/2}/2$, in order to keep the formulas compact)

$$\Delta_1 = (1+b)(1+q)\kappa a/2bp_2 \qquad (7.3)$$

$$\Delta_2 = \frac{b(1+q)\kappa a}{(1+\kappa a)^2}\left(\frac{11\sqrt{2}-3}{24p_2p_3} + \frac{1}{4p_2} + F(\kappa a)\right) - \frac{(1+q)\kappa a}{2p_2(1+\kappa a)} \qquad (7.4)$$

and

$$\Delta'_3 = -\frac{b\kappa a}{(1+\kappa a)^2}\left(\frac{\sqrt{2}+5}{32p_2} + \frac{F(\kappa a)}{4}\right) + \frac{11\kappa a}{96p_2(1+\kappa a)} \qquad (7.5)$$

where

$$F(\kappa a) = (7T_2 + p_1T_1 - 4p_2p_3T_0)/8p_2 \qquad (7.6)$$

The general form of the conductance equation is a product which can be written symbolically as

$$\Lambda/\Lambda_0 = (1 - f_1)(1 - f_2)$$

where

$$f = c^{1/2}(1 - k_1\kappa a + k_2\kappa a \ln \kappa a + k_3\kappa^2 a^2 + \ldots)$$

Since the derivation started by dropping terms in the differential equation which would lead to terms of order $c^{3/2}$ and higher in conductance, the product can, consistent with the initial approximation, be expanded as a sum

$$\Lambda/\Lambda_0 = 1 - f_1 - f_2 + f_1f_2$$

where $f_1 f_2$ is simply approximated as $\alpha\beta c$ and the higher terms in the product are dropped. The identity

$$\beta c^{1/2}/(1+\kappa a) = \beta c^{1/2} - \beta c^{1/2}\kappa a/(1+\kappa a)$$

provides a convenient separation of the electrophoresis term into a sum. Substitution of (7.2) into (7.1), followed by expansion as just described gives

$$\Lambda = \Lambda_0 - (\alpha\Lambda_0 + \beta)c^{1/2} + \alpha\Lambda_0 c^{1/2}(\Delta_1 - \Delta_2) - \beta\Delta_3' c^{1/2} + \alpha\beta c + \beta c^{1/2}\kappa a/(1+\kappa a) + O(\kappa^3 a^3)$$

Substitution of the values of the Δ's then gives the final conductance equation in a form convenient for numerical calculations

$$\Lambda = \Lambda_0 - (\alpha\Lambda_0 + \beta)c^{1/2} + cB(\kappa a) \qquad (7.7)$$

where

$$B(\kappa a) = (\kappa^3 a^2 b^2/c)[(1+2b)\phi_1/b^2 - \phi_2]\Lambda_0 + (\beta\kappa a b/c^{1/2})(\phi_3 + \phi_4/b) + \alpha\beta = B_1\Lambda_0 + B_2 \qquad (7.7')$$

The symbol $B(\kappa a)$ is introduced above as a reminder of the B in Shedlovsky's extrapolation function[16]

$$\Lambda_0 = (\Lambda + \beta c^{1/2})/(1 - \alpha c^{1/2}) - Bc = \Lambda' - Bc \qquad (7.8)$$

It turns out that $B(\kappa a)/(1 - \alpha c^{1/2})$ is remarkably insensitive to κa over a fairly wide range of concentration; this result therefore is theoretical justification for the form of Shedlovsky's function.

The auxiliary functions[17] in (7.7) are

$$\phi_1(\kappa a) = 1/12p_3 = 1/12(1 + q\kappa a + \kappa^2 a^2/6) \qquad (7.9)$$

$$\phi_2(\kappa a) = \frac{1}{6(1+\kappa a)^2}\left(\frac{11\sqrt{2}-3}{24p_2p_3} + \frac{1}{4p_2} + F(\kappa a)\right) \qquad (7.10)$$

$$\phi_3(\kappa a) = \frac{1}{(1-\kappa a)^2}\left(\frac{\sqrt{2}+5}{32p_2} + \frac{F(\kappa a)}{4}\right) \qquad (7.11)$$

$$\phi_4(\kappa a) = 8/9(1 + \kappa a) \qquad (7.12)$$

These functions[18] are given in Table I; they represent the simplest form into which $B(\kappa a)$ can be separated. Attention is called to the fact that each of the variable terms of B contains two terms, one of which depends on a (through the Bjerrum parameter b) and one of which is independent of a. The coefficients are independent of a and of concentration, of course, because

$$ab = e^2/DkT$$

(15) Ref. 1, eq. 12.10.

(16) T. Shedlovsky, *J. Am. Chem. Soc.*, **54**, 1405 (1932).

(17) Several minor approximations were made in defining the ϕ's: for example, ϕ_4 is explicitly $[1/(1+\kappa a) - 11/96p_2(1+\kappa a)]$ and in ϕ_1, p_3 approximates $p_2(1+\kappa a)$.

(18) Grateful acknowledgment is made to the Office of Naval Research for funds which made this compilation and relevant computations possible. We wish to express our thanks to the following for their patient work: John H. Baldrige, Miss Lue-yung Chow, Jerrold Post and Miss Elizabeth van Straelen.

and

$$\kappa^2/c = N\pi e^2/125DkT$$

TABLE I

FUNCTIONS FOR EQUATION 7.7

κa	ϕ_1	ϕ_2	ϕ_3	ϕ_4
0.01	0.08275	0.30761	0.4691	0.8801
.02	.08217	.24944	.3826	.8715
.03	.08159	.21534	.3320	.8630
.04	.08102	.19114	.2963	.8547
.05	.08045	.17238	.2686	.8466
.06	.07990	.15720	.2465	.8386
.07	.07934	.14436	.2276	.8308
.08	.07879	.13333	.2116	.8230
.09	.07825	.12370	.1976	.8155
.10	.07771	.11512	.1849	.8081
.11	.07717	.10745	.1737	.8008
.12	.07664	.10050	.1637	.7937
.13	.07612	.09425	.1545	.7867
.14	.07560	.08848	.1461	.7797
.15	.07508	.08313	.1383	.7730
.16	.07458	.07824	.1313	.7663
.17	.07407	.07375	.1246	.7597
.18	.07357	.06951	.1184	.7533
.19	.07308	.06560	.1128	.7470
.20	.07258	.06191	.1073	.7407
.21	.07209	.05850	.1023	.7346
.22	.07161	.05525	.0976	.7286
.23	.07114	.05224	.0930	.7227
.24	.07066	.04937	.0888	.7169
.25	.07019	.04668	.0849	.7111

8. Approximate Form of Conductance Equation

In order to test eq. 7.7, it is obviously necessary to have numerical values for the arbitrary constants Λ_0 and a. As a consequence of the complicated form of $B(\kappa a)$, one cannot simply substitute observed values of Λ and c into (7.7) for two concentrations and then solve for the constants. A graphical solution of the problem was therefore devised: it depends on approximating the transcendental functions in B by the familiar expression

$$\mathrm{Ei}(x) = -\Gamma - \ln x + x + O(x^2) \qquad (8.1)$$

where $\Gamma = 0.5772$ is Euler's constant. By approximating the polynomials in $F(\kappa a)$ by exponentials ($p_1 = 1 + \kappa a + \kappa^2 a^2/2 \approx e^{\kappa a}$, etc.), we first obtain

$$F(\kappa a) = (7T_2 + e^{\kappa a}T_1 - 4e^{(1+q)\kappa a}T_0)/8e^{q\kappa a} + O(\kappa^3 a^3) \approx e^{2\kappa a}\{7\mathrm{Ei}[(2+q)\kappa a] + \mathrm{Ei}[(1+q)\kappa a] - 4\mathrm{Ei}(\kappa a)\}/8$$

Then the $(1 + \kappa a)^2$ in the denominators of Δ_2 and Δ'_3 approximately cancels the exponential coefficient $e^{2\kappa a}$ in F. Substitution of (8.1) in the expression above for F gives

$$F(\kappa a)/(1+\kappa a)^2 \approx -1.2269 - (1/2)\ln \kappa a + O(\kappa a)$$

where the numerical constant is

$$[-4\Gamma - 7\ln(2+q) + \ln(1+q)]/8 \qquad (8.2)$$

with $q = 2^{1/2}/2$.

This result is substituted in (7.7); conventional algebraic expansion and neglect of higher terms finally leads to an approximation Λ''' for Λ_0 which is the limiting form of (7.7) at low (but non-zero) concentrations

$$\Lambda''' = \Lambda'' - J_1 c + J_2 c^{3/2} \qquad (8.3)$$

The terms of (8.3) are defined by the equations

$$\Lambda''(1 - \alpha c^{1/2}) = \Lambda + \beta c^{1/2} - (\alpha'\Lambda_0 - \beta')c\ln c \qquad (8.4)$$

$$\alpha' = \kappa^2 a^2 b^2/24c \qquad (8.5)$$

$$\beta' = \kappa a b\beta/16c^{1/2} \qquad (8.6)$$

$$J_1 = \theta_1\Lambda_0 + \theta_2 \qquad (8.7)$$

$$J_2 = \theta_3\Lambda_0 + 8\beta\kappa^2 a^2/9c \qquad (8.8)$$

$$\theta_1(a) = 2\alpha'[b^{-2}(1+2b) + 0.9074 + \ln(\kappa a/c^{1/2})] \qquad (8.9)$$

$$\theta_2(a) = \alpha\beta + 8\beta\kappa a/9c^{1/2} - 2\beta'[0.8504 + \ln(\kappa a/c^{1/2})] \qquad (8.10)$$

$$\theta_3(a) = (\alpha'\kappa a 2^{1/2}/c^{1/2})[b^{-2}(1+2b) - 1.0774] \qquad (8.11)$$

Equation 8.3 contains a term in $c^{3/2}$. It should be mentioned that this is not inconsistent with our approximation principles. Equation 7.7, which is the one we shall finally use, indeed neglects terms of order $\kappa^3 a^3$ as it should. But it contains transcendental functions for which no safe approximation can be made except at extremely low concentrations. Equation 8.3 is thus a numerical approximation to the explicit function of eq. 7.7. Retention of the $c^{3/2}$ term (which has its source in the linear term in κa retained in the expansion of the exponential integral) simply extends the range of usefulness of (8.3) and reduces curvature in the functions which will be plotted in order to evaluate Λ_0 and a. Also, while (8.4) contains an explicit expression for the coefficient of the *limiting* $c \ln c$ term, it cannot be expected to agree with values of the empirical constant D in the extended Shedlovsky equation

$$\Lambda_0 = \Lambda' + B'c + Dc\ln c \qquad (8.12)$$

because the latter has been applied at concentrations at which the logarithmic expansion of the exponential integral is invalid. No theoretical significance can therefore be attributed to the B' and D of (8.12), although the B of (7.8) does have an (approximate) theoretical value: it is the average of $B(\kappa a)/(1 - \alpha c^{1/2})$ over a concentration range.

9. Evaluation of Λ_0 and a

In the preceding section, it was shown that the conductance equation approached the limiting form

$$\Lambda''' = \Lambda'' - J_1 c + J_2 c^{3/2} \qquad (9.1)$$

at very low concentrations ($c < 0.01\ N$ for 1–1 salts in water). In this equation, the quantity

$$\Lambda^r = [\Lambda + \beta c^{1/2} - (\alpha'\Lambda_0 - \beta')c\ln c]/(1 - \alpha c^{1/2}) \qquad (9.2)$$

may be calculated directly from experimental data (Λ, c) and an approximate value of Λ_0, because the logarithmic term in the numerator is much smaller than $\beta c^{1/2}$. Extrapolation by Shedlovsky's Λ'-method is adequate to evaluate Λ_0 for the $c \ln c$ term of (9.2). The $J_1 c$ term is considerably larger than the $J_2 c^{3/2}$ term. Hence (9.1) is effectively

$$\Lambda''' = \Lambda^{iv} - cJ_1(a) \qquad (9.3)$$

When the correct value of a is inserted in $J_1(a)$, Λ''' will equal Λ_0 for any (small) value of c. The form of (9.3) suggests the method of finding the desired value of a: several trial values of a are chosen, and Λ''' is computed by (9.1) for a series of concentrations for each value. Then $\Lambda'''(a)$ is plotted against c; a set of curves should result, all inter-

secting at $c = 0$ on the ordinate axis at the final value of Λ_0. These curves become linear in concentration at low concentrations. If one of these lines is horizontal, the corresponding a-value is the value sought. In general practice, this coincidence seldom occurs, but investigation of $J_1(a)$ shows that J is nearly linear in a in the range $3 < a \times 10^8 < 5$. Hence a plot of the slopes of the Λ'''-c plots against the a-values used will be nearly linear, and it is then easy to interpolate to find the value of a which would give zero slope.

The method will be illustrated by application to a specific example: potassium bromide[19] in water at 25°. Using the literature value for Λ_0 to evaluate the coefficient of the logarithmic term, and inserting the other constants, we have

$$\Lambda'' = (\Lambda + 60.20\, c^{1/2} - 59.71 c \log c)/(1 - 0.2289\, c^{1/2})$$

As shown in Table II, the logarithmic term is small compared to $\beta c^{1/2}$ but by no means negligible. (In the example, an extra place was carried in Λ and rounded off at the end of the calculation.) It will be noted that Λ'' is a slowly increasing function of c. Then J_1 and J_2 were computed for $a = 3.6$, 4.0 and 4.4 ($J_1 = 221.72$, 246.16, 270.52; $J_2 = 85.74$, 115.62, 150.01). The table gives the higher terms for $a = 3.6$. A plot of Λ''' (3.6) (Fig. 1) is nearly

TABLE II

CONDUCTANCE[19] OF POTASSIUM BROMIDE IN WATER AT 25°

$10^4 c$	Λ	$\beta c^{1/2}$	$Dc \ln c$	Λ''	$J_1(3.6)c$
13.949	148.27	2.248	0.238	152.056	0.309
27.881	146.91	3.179	.425	152.356	.618
42.183	145.88	3.909	.598	152.657	.935
59.269	144.90	4.634	.788	153.018	1.314
71.696	144.30	5.097	.918	153.286	1.590

$J_2(3.6)c^{3/2}$	$\Lambda'''(3.6)$	$B_1\Lambda_0$	B_2	B
0.004	151.751	−67.34	114.31	46.97
.013	151.751	−45.65	107.20	61.55
.023	151.745	−32.21	102.89	70.68
.039	151.743	−21.28	99.20	77.92
.052	151.748	−15.27	97.13	81.86

$(\alpha\Lambda_0 + \beta)c^{1/2}$	$\Delta\Lambda$	Λ (calcd.)	δ
3.545	0.066	148.27	0.00
5.013	.172	146.91	.00
6.165	.298	145.89	.01
7.308	.462	144.91	.01
8.038	.587	144.30	.00

horizontal. Plots of Λ''' for $\mathring{a} = 4.0$ and 4.4 are also shown. It is obvious that the correct value of $\mathring{a}$ is near 3.6; a plot of the slopes of the lines of Fig. 1 against a is linear and interpolates to $\mathring{a} = 3.58$ for zero slope. The three lines intersect at $\Lambda_0 = 151.75$ for $c = 0$. Next, with $\mathring{a} = 3.58$, we have $\kappa a = 1.174\, c^{1/2}$; hence κa values at each concentration are determined. Using Table I, values of the ϕ's of eq. 7.7 are interpolated, and B is computed. Over this range of concentration $B_1\Lambda_0$ is negative and increasing, becoming positive around $c = 0.01$, while B_2 is positive and decreasing. Both terms change more and more slowly as concentration increases, so that B approximates constancy; for example, $B = 92$ at $c = 0.015$ and $B = 111$ at $c = 0.10$. If we denote by $\Delta\Lambda$ the distance

(19) B. B. Owen and H. Zeldes, *J. Chem. Phys.*, **18**, 1083 (1950).

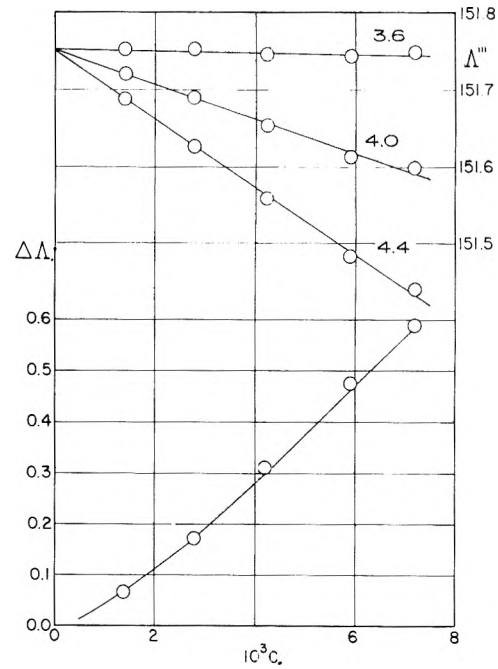

Fig. 1.—Extrapolation functions (top) and test of eq. 7.7 for KBr in water at 25°.

from the Onsager tangent to the conductance curve

$$\Delta\Lambda = \Lambda + (\alpha\Lambda_0 + \beta)c^{1/2} - \Lambda_0 \qquad (9.4)$$

we may compare observed values obtained by substituting Λ(obsd.) in (9.4) with the calculated value $\Delta\Lambda$(calcd.) $= cB(\kappa a)$. The comparison is shown in the lower half of Fig. 1. (The region near the origin will be discussed later. We mention in passing, however, that the $\Delta\Lambda$-c curve of Fig. 1 can be approximated well within the experimental error by a straight line *with a negative intercept* at $c = 0$.)

In making such calculations, it is convenient to prepare mimeographed work-sheets with spaces blank for filling in the quantities: D, T, DT $(DT)^{1/2}$, $(DT)^{3/2}$, η, $\eta(DT)^{1/2}$, $\alpha = 8.204 \times 10^5/(DT)^{3/2}$, $\beta = 82.43/\eta\,(DT)^{1/2}$, $8\beta/9$, $\alpha\beta$, $\kappa^2/c = 2529.5 \times 10^{16}/DT$, $8\beta\kappa^2/9c$, $\kappa/c^{1/2} = 50.29 \times 10^8/(DT)^{1/2}$, $8\beta\kappa/9c^{1/2}$, log $(10^{-8}\ \kappa/c^{1/2})$, ln $(10^{-8}\ \kappa/c^{1/2})$, $ab = 16.708 \times 10^{-4}/DT$, a^2b^2, $\kappa^2\ a^2b^2/c$, $\kappa ab/c^{1/2}$, $(\kappa ab/c^{1/2})^3$, $\kappa^2a^2b^2/12c$, $D_1 = 0.09594\ \kappa^2\ a^2b^2/c$, $\kappa ab\beta/c^{1/2}$, $\kappa ab\beta/8c^{1/2}$, $D_2 = 0.14391\ \kappa ab\beta/c^{1/2}$, $0.05893\ (\kappa ab/c^{1/2})^3$, Λ_0(initial), $D_1\ \Lambda_0$ and $(D_1\ \Lambda_0 - D_2)$. While the above expressions contain both a and c, these quantities only occur in such combinations as (ab) or (κ^2/c) which are, of course, constants for a given DT product, *i.e.*, for calculating data for a given solvent at fixed temperature.

10. Comparison with Experiment

Extrapolation plots for potassium chloride, bromide and iodide[19] at temperatures from 5 to 55° were made. All were approximately linear. The results of the calculation are given in Table III, and the Λ'''-c curves for potassium iodide are shown in Fig. 2. Since Λ_0 changes by nearly a factor of three in going from 5 to 55°, several ordinate scales are used as indicated in the figure. The plots based on the Owen and Zeldes data were all linear up to $c \approx 0.01$ within experimental error, except

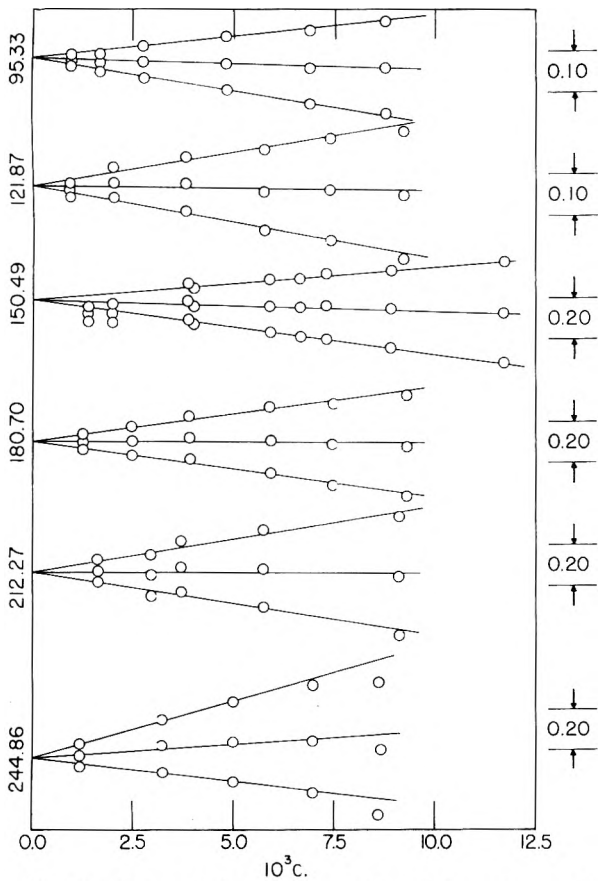

Fig. 2.—Extrapolation functions for KI in water at 5° (top), 15, 25, 35, 45 and 55° (bottom). Λ_0 values shown at left; Λ-scale shown between arrows at right.

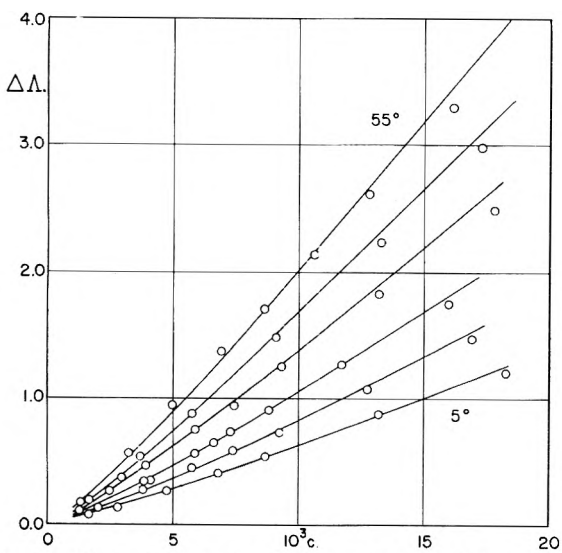

Fig. 3.—Test of eq. 7.7 for KI in water at 5–55°: circles, observed; solid lines, calculated.

the 55°-KI curves, which are concave down. Back-calculation gave close agreement between calculated and observed values, as shown in Fig. 3. The Gunning and Gordon KCl curves were slightly concave up at 15°, and increasingly concave-down for 25, 35 and 45°, so that it was difficult to obtain an a-value; using $\mathring{a} = 3.60$, the maximum deviation between calculated and observed was 0.07, with an average deviation of 0.03.

TABLE III

CONSTANTS FOR POTASSIUM HALIDES

t, °C.	Λ_0	Λ_0 (lit.)	$\mathring{a}$	t, °C.	Λ_0	Λ_0 (lit.)	$\mathring{a}$
Potassium chloride[19]				Potassium iodide[19]			
5	94.27	94.26	3.29	5	95.33	95.32	3.94
25	149.89	149.88	3.50	15	121.87	121.83	3.95
55	245.97	245.69	3.39	25	150.49	150.34	3.90
Potassium bromide[19]				35	180.70	180.60	4.01
				45	212.27	212.13	3.98
5	96.01	96.00	3.58	55	244.86	244.73	4.15
25	151.75	151.68	3.57				
55	247.32	247.15	3.61	Potassium chloride[21]			
				15	121.04	121.09	3.55
				25	149.90	149.88	3.60
				35	180.54	180.50	3.60
				45	212.53	212.49	3.60

Figure 4 shows $\Delta\Lambda$ at 25° for potassium chloride, using $\Lambda_0 = 149.90$ and $\mathring{a} = 3.50$. The agreement among the three independent sets of data (Shedlovsky[20] 1932, Gunning and Gordon[21] 1942 and Owen and Zeldes[19] 1950) is excellent. It will be noted that our value of Λ_0 is somewhat higher than the literature value. The difference is due to the presence of the transcendental function which causes $\Delta\Lambda$ to behave peculiarly near the origin. For *very* small values of concentration

$$\Delta\Lambda \approx Dc \ln c + J_1 c \qquad (10.1)$$

Consequently $\Delta\Lambda$ equals zero at $c_0 = \exp(-J_1/D)$, goes through a minimum at $c_m = \exp[-(J_1 + D)/D]$ and approaches zero from the negative side with a vertical tangent. In other words, the conductance curve for an unassociated salt *crosses* the limiting tangent from above at a low concentration and then approaches the tangent from *below* as zero concentration is approached. When seen on a scale which is realistic from the point of view of experimental error, the curve will therefore appear to lie directly on the tangent at very low concentrations. For potassium chloride at 25°, for example, $c_0 = 1.82 \times 10^{-4}$ and $c_m = 0.668 \times 10^{-4}$ where $\Delta\Lambda_m = -0.0017$. The details are shown as the lower curve of Fig. 5; the structure probably would be just barely detectable by the highly precise methods which Kraus[22] has recently applied to aqueous systems. (Unfortunately the equation cannot be tested against any of Kraus' published data, because all the salts which he studied are slightly associated.)

The effect of the transcendental terms on the extrapolation for Λ_0 is shown by the upper curves of Fig. 5. The solid curve is the theoretical curve; as shown in Fig. 4, it quantitatively reproduces the experimental data up to $c \approx 0.01$; to avoid confusion, the corresponding points are omitted in Fig. 5. The circles represent Shedlovsky's values for higher concentrations; within the experimental error, the actual data may be closely approximated by the linear function

(20) T. Shedlovsky, *J. Am. Chem. Soc.*, **54**, 1411 (1932).

(21) H. E. Gunning and A. R. Gordon, *J. Chem. Phys.*, **10**, 126 (1942).

(22) R. W. Martel and C. A. Kraus, *Proc. Nat. Acad. Sci.*, **41**, 9 (1955).

$$\Delta\Lambda = kc \qquad (10.2)$$

through the origin (dotted in Fig. 4). The theoretical function, on the other hand, can be imitated within the precision of available data by the function

$$cB(\kappa a) = k'c - \delta\Lambda_0 \qquad (10.3)$$

for concentrations above c = 0.001. Most of the limiting conductances in the literature depend on extrapolations based on data up to 0.1 N (or even higher!); the data at low concentrations were usually given less weight on account of their lower precision. Consequently $\delta\Lambda_0$ was completely missed. Testing Fig. 4 with a straight-edge shows that a line *could* be laid through the origin and the experimental points, but a Λ_0 based on this line would be low because the theoretical function approaches from below. The algebraic types of extrapolations all imply that $d\Lambda/dc^{1/2}$ is less than $(\alpha\Lambda_0 + \beta)$ for $c > 0$, and hence they must undershoot a limit which is approached by a curve which actually has a steeper slope over the last part of its course. The empirical extrapolation functions containing a c log c likewise miss the mark somewhat, because they are three-constant equations, applied over a fairly high range of concentrations, and inspection shows that the theoretical equation can be approximated as $[\Lambda_0 - (\alpha\Lambda_0 + \beta)c^{1/2} + Bc + Dc \log c]$ only at extreme dilutions.

11. Discussion

In the preceding sections, it has been shown that the Debye-Hückel theory of long range forces suffices to account for the shape of conductance curves of unassociated electrolytes at non-zero concentrations. It is now necessary to point out some of the limitations of our result.

In the first place, the formulas were specialized to symmetrical electrolytes ($q^2 = {}^1/_2$) in order to simplify the algebraic form of the equations both for convenience in printing and to save labor in the numerical calculations necessary for comparison with experiment. (For example, the ϕ-tables apply to *all* symmetrical electrolytes while their equivalent would have to be computed for *each* individual unsymmetrical electrolyte because single-ion conductances enter explicitly into q^2.) This restriction was also based on practical grounds; some ion association must occur for 2–1 and higher type salts, and also the errors due to the incompatibility of the Boltzmann distribution and the Poisson equation are more serious for unsymmetrical electrolytes than for symmetrical. Since we are unable to evaluate these effects at present, we prefer to limit the explicit statement of our result to the case where these corrections may be presumed to be small. Furthermore, while the algebraic forms are correct for 2–2 and (hypothetical) higher salt types, their applicability is for practical purposes restricted to 1–1 salts in water and other solvents of high dielectric constant. Since a 2–2 salt like copper sulfate in water is electrostatically the equivalent of a 1–1 salt in ammonia ($4e^2/78 \approx e^2/22$), and since association of 1–1 salts in ammonia is well established, our equations cannot be directly applied to data for 2–2 salts in water. They may, however, serve as a basis for computing ideal behavior of 2–2 salts in water and thus give a reference system with which data for real systems may be compared in order to estimate the extent of association of the latter.

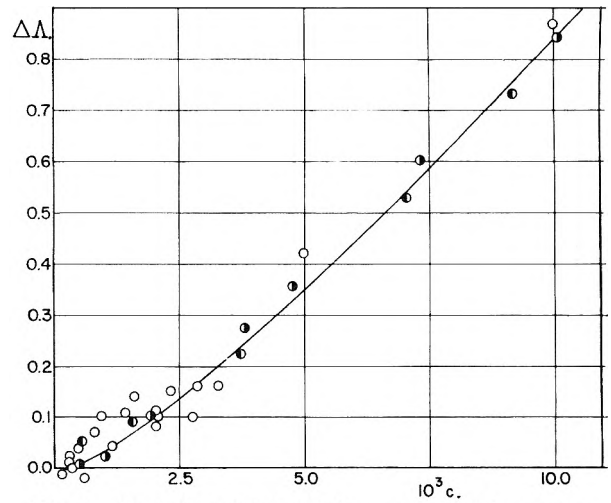

Fig. 4.—Test of eq. 7.7 for KCl in water at 25°: ◐, Owen and Zeldes; ◑, Gurning and Gordon; ○, Shedlovsky; solid curve calculated for $\mathring{a} = 3.50$.

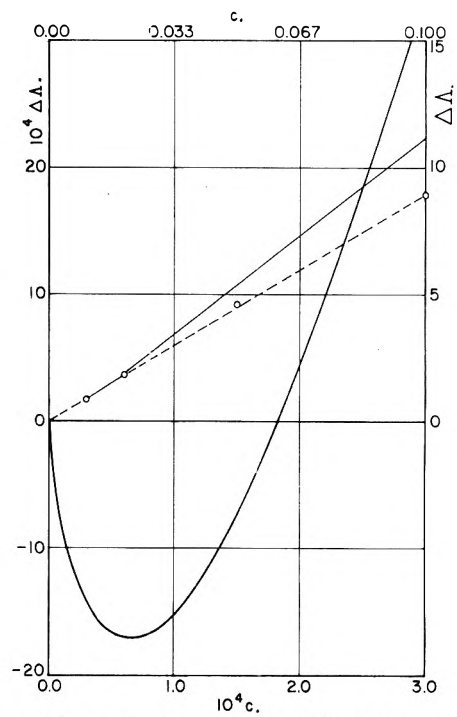

Fig. 5.—Theoretical behavior for KCl at 25°; scales for lower curve ($0 < c < 3 \times 10^{-4}$) left and below; scales for upper curve ($0 < c < 0.10$) right and above; points, Shedlovsky data.

Ion association also limits the extent to which our formulas may be applied to data for 1–1 salts in water. The results of Kraus[21] for sodium bromate in water can be fitted by eq. 7.7, but the a-value found is 3.00, which seems too small. If a Bjerrum association function is assumed, such that the same a-value is used in $K(a)$ and in $B(\kappa a)$, the more reasonable value of 3.38 results. But then this value does not fit the data for sodium bromate in 90:10 water–dioxane. This discrepancy will be discussed in more detail elsewhere. Also, Kraus's

data for a variety of quaternary salts in water clearly show association, because the conductance curves are catabatic. We may not use the mere shape of the conductance curve as a criterion for the absence of association: if the curve is concave-down at low concentrations, association is necessarily present, but if it is concave-up, association to a small extent may still be present, as in the case of sodium bromate. As a matter of fact, just as soon as we introduce ions of non-zero size, we imply by use of boundary conditions for $r = a$ that some ions do approach to contact, and for the duration of the contact those ions must in principle be counted as associated ions which do not contribute to conductance. Consequently our results must for the present be limited to unassociated 1–1 salts, and the only criterion we can offer for the absence of association is the magnitude of a which results from the application of the equations.

It does not appear practical at present to calculate association when K approaches unity. To first approximation

$$\Lambda = \Lambda_0 - (\alpha\Lambda_0 + \beta)c^{1/2} + cB(\kappa a) - c\Lambda_0 f^2/K \quad (11.1)$$

which is essentially of the form

$$\Lambda = \Lambda_0 - (\alpha\Lambda_0 + \beta)c^{1/2} + (B - \Lambda_0/K)c + O(c^{3/2}) \quad (11.2)$$

Analysis of the data would give the coefficient of the linear term, but the coefficient could not be separated into its components. Only if data of high precision at low concentrations were available could K be estimated from the $O(c^{3/2})$ term above which arises from the presence of the activity coefficient f^2. But (8.3) is only an approximation; we have already seen (Fig. 5) that it is at higher rather than at lower concentrations that $B(\kappa a)$ may be approximated by a constant. Within the error of approximating the curve of Fig. 4 by a straight line, an empirical analysis based on (7.8), with B equal to the slope of the line, could give useful estimates of K, but then the B has no physical significance. Furthermore, the neglected $c^{3/2}$ terms from the equation of continuity would be absorbed in the calculated value of K.

If association could be ascribed solely to electrostatic forces, then the same a-value should appear both in $K(a)$ and in $B(\kappa a)$. If the functional form of $K(a)$ were known, then (11.1) might be used as the basis of analysis: as a decreases, $B(\kappa a)$ decreases and $1/K$ increases, so the difference which appears as the coefficient of c in (11.2) goes from positive to negative as the product aD decreases, *i.e.*, as b increases. The Bjerrum function appears to be an excellent approximation to $K(a)$ when K is small, but when K gets larger than about 0.01, it becomes entirely too sensitive to the cut-off value at $R = e^2/2DkT$. This cut-off is a convenient but completely artificial device; $(1/K)$ should approach zero as b approaches zero, rather than as b approaches some arbitrary positive value such as 2.00.

Mention must be made of a number of other effects which were disregarded in our derivation. They all may be expected to give rise to linear (and higher) terms in the conductance equation. The fact that our equation duplicates data for the alkali halides in water suggests either that these neglected terms are individually small, or else they compensate by being both positive and negative.

We have neglected the change of viscosity and dielectric constant with concentration. Linear superposition of fields was assumed. No allowance was made for the volume occupied by the ions. A kinetic effect due to non-zero velocity of colliding ions was not included. The discontinuous nature of the solvent has been completely ignored, both in electrostatics and in hydrodynamics. There may, of course, be still other sources of higher terms which are at present unknown to us.

Finally, the limitations as to concentration range must be considered. First, purely mathematical approximations limit the validity of the formulas to values of κa less than about 0.3. Second, physical approximations limit the range to this or probably to even smaller values. For aqueous solutions, κa is numerically almost equal to $c^{1/2}$ for ordinary 1–1 salts. Hence $c = 0.1\ N$ corresponds to $(1/\kappa) \approx 3a$. Our whole theory is based on the Poisson–Boltzmann equation, which implies that all of the ions except the reference ion may be replaced by a continuous charge distribution. Now $(1/\kappa)$ is the distance at which the charge density in the ionic atmosphere reaches its maximum. The continuum approximation appears hazardous when $(1/\kappa)$ reaches the order of a few ionic diameters: the total charge in the whole atmosphere equals one unit charge, and hence the approach of any one ion to the reference ion will produce a large fluctuation in potential. We have therefore limited the application of our equation to concentrations less than 0.02 N, *i.e.*, to $(1/\kappa) \geqslant 7a$. Up to this concentration, the deviations between calculated and observed values are randomly positive and negative; at higher concentrations (*cf.* Fig. 5), the calculated $\Delta\Lambda$'s based on the a-value obtained from data in the range $c \leqslant 0.02$ are too large. We can, of course, force a fit by choosing an a-value that will send the calculated curve through *any* point at higher concentrations (say the one at 0.1 N). Then a fairly close fit will obtain at all lower concentrations, but the deviations, although practically invisible on a large scale plot, are seen to be systematic on a scale where 0.02 Λ-units is visible. We prefer a fit with random deviations over a smaller range of concentration to an approximate fit with systematic deviations over a wider range. There are a number of semi-empirical formulas in the literature which are of the latter type; their success depends on the presence of $(1 + \kappa a)$ or its equivalent in the denominator. As we have seen, this type of denominator is indeed present, but the rigorous derivation leads to a sum of terms, each with a somewhat different damping denominator.

The problem of concentrated solutions cannot, in our opinion, be solved by any extension of the present theory, which is based on a smoothed ionic distribution. The approach must start by an adequate theory for fused salts, which must then be followed by the theoretical treatment of the effect on the radial distribution function of adding uncharged (solvent) molecules. At high concentrations, the distribution function must be a damped periodic function of interionic distances; as concen-

tration decreases, this function will approach the $e^{-\kappa r}$ type of functions as the asymptotic limit. Unfortunately, knowledge of this limit does not permit prediction of the function of which it is the limit.

Appendix I.

Evaluation of Constants from Boundary Conditions.—Consider the differential equation

$$\Delta g_{21}(r, \theta) - \gamma^2 g_{21} = Kf(r) \cos \theta \qquad (I.1)$$

where $g_{21} = h_{21}(r) \cos \theta$ in turn defines a function p_1 by the equation

$$\Delta p_1 = (4\pi e_2/Dn_1) g_{21} \qquad (I.2)$$

Let the boundary conditions be

$$\{r(\partial p_1/\partial r)\theta - p_1\}_{r=a} = 0 \qquad (I.3)$$

and

$$(dh_{21}/dr)_{r=a} = V(a) \qquad (I.4)$$

plus the condition that (dp_1/dr) must vanish for $r = \infty$. Assume that $f(r)$ is of the form $\exp(-\lambda\kappa r)/r^{n-1}$ and that solutions of the equation

$$\Delta(y \cos \theta) - \gamma^2 y \cos \theta = f(r) \cos \theta \qquad (I.5)$$

are known for relevant values of n (Appendix II). Then

$$g_{21} = K\left\{y(r) \cos \theta + A \frac{\partial}{\partial x}\left(\frac{e^{-\gamma r}}{r}\right)\right\} \qquad (I.6)$$

is the solution of (I.1); the $\exp(+\gamma r)/r$ term from the solution of the homogenous equation drops out by virtue of the condition at $r = \infty$. Then

$$h_{21} = K\left\{y(r) + A \frac{\partial}{\partial r}\left(\frac{e^{-\gamma r}}{r}\right)\right\} \qquad (I.7)$$

Integrating again

$$p_1 = \frac{4\pi e_2 K}{Dn_1}\left\{z(r) \cos \theta + \frac{A}{\gamma^2}\frac{\partial}{\partial x}\left(\frac{e^{-\gamma r}}{r}\right) + \frac{B}{\kappa^2}\frac{\partial}{\partial x}\left(\frac{1}{r}\right)\right\} \qquad (I.8)$$

where z satisfies $\Delta(z \cos \theta) = y \cos \theta$. This immediately reduces to

$$p_1 = \frac{4\pi e_2 K \cos \theta}{Dn_1}\left\{z(r) + \frac{A}{\gamma^2}\frac{d}{dr}\left(\frac{e^{-\gamma r}}{r}\right) - \frac{B}{\kappa^2 r^2}\right\} \qquad (I.9)$$

The first constant of integration is seen to be

$$A = \left\{\frac{V(a)}{K} - \left(\frac{dy}{dr}\right)_a\right\} \Big/ \left(\frac{d^2(e^{-\gamma r}/r)}{dr^2}\right)_a \qquad (I.10)$$

From the first boundary condition and the above values of p_1 and A, B is then determined, and

$$p_1 = (4\pi e_2 K/Dn_1) x F(r) = Qx F(r) \qquad (I.11)$$

where $F(r)$ is a known function (too long for convenient printing). The relaxation field is given by $(\partial p_1/\partial x)$ at $r = a$

$$(\partial p_1/\partial x)_{y,z} = QF(r) + (Qx^2/r)(dF/dr) \qquad (I.12)$$

but by the first boundary condition, it can be shown that

$$(dF/dr)_a = 0 \qquad (I.13)$$

Consequently

$$(\partial p_1/\partial x)_a = QF(a) \qquad (I.14)$$

On substitution of the known functions, this becomes

$$\left(\frac{\partial p_1}{\partial x}\right)_a = \frac{4\pi e_2 K}{3Dn_1}\left\{\frac{2z(a)}{a} + \left(\frac{dz}{dr}\right)_a + \frac{a^2}{2}U(a)\right\} \qquad (I.15)$$

where

$$U(a) = \frac{V(a)/K - (dy/dr)_a}{1 + \gamma a + \gamma^2 a^2/2} \qquad (I.16)$$

The result can be further simplified by use of the relation between the functions y and z: expanding the laplacian operator in spherical coördinates and dividing out $\cos \theta$ gives

$$\frac{d^2 z}{dr^2} + \frac{2}{r}\frac{dz}{dr} - \frac{2}{r^2}z(r) = y(r) \qquad (I.17)$$

Integrating once, and then performing an obvious partial integration, shows that

$$\left(\frac{dz}{dr}\right)_a + \frac{2}{a}z(a) = \int^a y(r)\, dr \qquad (I.18)$$

where the expression on the right means the indefinite integral of $y(r)$ taken for the value at $r = a$. The relaxation field is therefore given by the compact expression

$$\left(\frac{\partial p_1}{\partial x}\right)_a = \frac{4\pi e_2 K}{3Dn_1}\left\{\int^a y(r)\, dr + a^2 U(a)/2\right\} \qquad (I.19)$$

For its evaluation, we need only values of the integrals and derivatives of the y_n's; explicit values of the z_n's need not be computed. The method of evaluating the functions $y(r)$ for the various values of n in $f(r) = \exp(-\lambda\kappa r)/r^{n-1}$ is described in Appendix II.

Appendix II.

Integral Tables.—Determination of the potentials depends on solving the equation

$$\Delta\Delta u - \gamma^2 \Delta u = \Sigma_{n,m} a_{nm} x e^{-\lambda\kappa r}/r^n$$

whose solution is the sum of constants times solutions of equations of the form

$$\Delta\Delta v - \gamma^2 \Delta v = x e^{-\lambda\kappa r}/r^n \qquad (II.1)$$

where $v(r, \theta)$ is separable as $w(r) \cos \theta$. In the following, we shall disregard the solution of the homogeneous equation and establish a general method of obtaining particular integrals of (II.1).

Consider

$$\Delta(y_1 \cos \theta) - \gamma^2 y_1 \cos \theta = x e^{-\lambda\kappa r}/r \qquad (II.2)$$

This equation cannot be integrated by inspection. The right side is a function of x, r and κ; λ is a numerical constant. Since $(\partial r/\partial x)_{y,z} = x/r$, and since the partial operators $\partial/\partial x$ and $\partial/\partial\kappa$ commute, (II.2) is easily shown to be the same as

$$\Delta(y_1 \cos \theta) - \gamma^2 y_1 \cos \theta = \frac{\partial}{\partial x}\left\{\frac{1}{\lambda^2\kappa}\frac{\partial}{\partial \kappa}\left(\frac{e^{-\lambda\kappa r}}{r}\right)\right\} \qquad (II.3)$$

which now integrates by inspection to

$$y_1 \cos \theta = \frac{\partial}{\partial x}\left\{\frac{1}{\lambda^2\kappa}\frac{\partial}{\partial \kappa}\left(\frac{e^{-\lambda\kappa r}}{r(\lambda^2\kappa^2 - \gamma^2)}\right)\right\} \qquad (II.4)$$

on recalling the familiar Debye–Hückel result

$$\Delta\psi = \kappa^2\psi \longrightarrow \psi = e^{-\kappa r}/r$$

and using the fact that the laplacian operator commutes with the other partial operators above. (Caution: while $\gamma^2 = q^2\kappa^2$, it is to be considered as a constant parameter for these manipulations. Proof is simple.) Since $\partial/\partial x$ commutes with $\partial/\lambda^2\kappa\,\partial\kappa$, the differentiation with respect to x may now be carried out; on dividing out $x/r = \cos \theta$, we then obtain

$$y_1(r) = -\frac{1}{\lambda^2\kappa}\frac{\partial}{\partial\kappa}\left\{\frac{e^{-\lambda\kappa r}(1+\lambda\kappa r)}{r^2(\lambda^2\kappa^2-\gamma^2)}\right\}$$

and one more differentiation gives the explicit result

$$y_1(r) = \frac{e^{-\lambda\kappa r}}{\lambda^2\kappa^2-\gamma^2}\left\{\frac{1}{r} + \frac{2(1+\lambda\kappa r)}{r^2(\lambda^2\kappa^2-\gamma^2)}\right\} \quad \text{(II.5)}$$

Now consider

$$\Delta(y_2\cos\theta) - \gamma^2 y_2\cos\theta = xe^{-\lambda\kappa r}/r^2 \quad \text{(II.6)}$$

Differentiation with respect to κ gives

$$\Delta\left(\frac{\partial(y_2\cos\theta)}{\partial\kappa}\right) - \gamma^2\frac{\partial(y_2\cos\theta)}{\partial\kappa} = -\frac{\lambda x e^{-\lambda\kappa r}}{r} \quad \text{(II.7)}$$

Similarity of the right side with that of (II.2) suggests integration of (II.2) between limits κ and ∞

$$\Delta\int_\kappa^\infty y_1\cos\theta\,dt - \gamma^2\int_\kappa^\infty y_1(t)\cos\theta\,dt = \int_\kappa^\infty \frac{xe^{-\lambda rt}}{r}\,dt = \frac{xe^{-\lambda\kappa r}}{\lambda r^2} \quad \text{(II.8)}$$

and comparison then shows that

$$y_2(r,\kappa) = \lambda\int_\kappa^\infty y_1(r,t)\,dt \quad \text{(II.9)}$$

By iteration of this process, it is thus possible to construct solutions of (II.1) for any value of n, starting with the explicit value of y_1 given by (II.5). In the present problem, values $1 \leqslant n \leqslant 6$ are involved. A table of these integrals has been prepared, together with values of dy_n/dr and $\int^r y_n(s)\,ds$ which are also needed in the calculation of the conductance.

One term of y_2 will be considered in some detail here because it is typical of all the integrals involving $n \geqslant 2$ in the inhomogeneous function. The first term of y_2 is

$$f(r) = \lambda\int_\kappa^\infty \frac{e^{-\lambda rt}dt}{\lambda^2t^2-\gamma^2} \quad \text{(II.10)}$$

The integration proceeds by the steps

$$f(r) = \frac{\lambda}{2\gamma}\int_\kappa^\infty\left(\frac{e^{-\lambda rt}}{\lambda t-\gamma} - \frac{e^{-\lambda rt}}{\lambda t+\gamma}\right)dt \quad \text{(II.11)}$$

$$= \frac{e^{-\gamma r}}{2\gamma}\int_{r(\lambda\kappa-\gamma)}^\infty (e^{-u}/u)\,du - \frac{e^{\gamma r}}{2\gamma}\int_{r(\lambda\kappa+\gamma)}^\infty (e^{-u}/u)\,du$$

$$= (1/2\gamma)\{e^{-\gamma r}\mathrm{Ei}[(\lambda\kappa-\gamma)r] - e^{\gamma r}\mathrm{Ei}[(\lambda\kappa+\gamma)r]\}$$

The appearance of the exponential integral[23] is thus a consequence of the terms in the inhomogeneous equation which contains inverse quadratic and higher powers of the distance. These transcendental functions are responsible for the appearance of the terms of limiting order $c \ln c$ in the final conductance equation.

TABLE IV

INTEGRALS OF II.12

$$\int y_1(r)\,dr = -\frac{e^{-\lambda\kappa r}}{\lambda^2\kappa^2-\gamma^2}\left(\frac{1}{\lambda\kappa} + \frac{2}{r}\frac{1}{\lambda^2\kappa^2-\gamma^2}\right)$$

$$\int y_2(r)\,dr = -\frac{\lambda\kappa e^{-\lambda\kappa r}}{\gamma^2 r(\lambda^2\kappa^2-\gamma^2)} + \gamma^{-2}\,\mathrm{Ei}(\lambda\kappa r) - U/2\gamma^3 r$$

$$\int y_3(r)\,dr = e^{-\lambda\kappa r}/\gamma^2 r - \lambda\kappa\gamma^{-2}\,\mathrm{Ei}(\lambda\kappa r) + \lambda\kappa U/2\gamma^3 r$$

$$\int y_4(r)\,dr = -\lambda\kappa e^{-\lambda\kappa r}/2\gamma^2 r + (\lambda^2\kappa^2/2\gamma^2)\,\mathrm{Ei}(\lambda\kappa r) - (\lambda^2\kappa^2-\gamma^2)U/4\gamma^3 r$$

$$\int y_5(r)\,dr = \lambda^2\kappa^2 e^{-\lambda\kappa r}/6\gamma^2 r - (\lambda^3\kappa^3/6\gamma^2)\,\mathrm{Ei}(\lambda\kappa r) + \lambda\kappa(\lambda^2\kappa^2-3\gamma^2)U/12\gamma^3 r - G/6r$$

$$\int y_6(r)\,dr = -e^{-\lambda\kappa r}\left(\frac{1}{8r^2} + \frac{\lambda^3\kappa^2}{24\gamma^2 r}\right) + \frac{\lambda^4\kappa^4}{24\gamma^2}\,\mathrm{Ei}(\lambda\kappa r) + \frac{\lambda\kappa}{6r}G - \left(\frac{\lambda^4\kappa^4}{48\gamma^3 r} - \frac{\gamma}{16r} - \frac{\lambda^2\kappa^2}{8\gamma r}\right)U$$

In Table IV, we give the values of $\int y_n(r)\,dr$ for $n = 1, 2, \ldots, 6$, where $y_n(r)$ is the solution of the differential equation

$$\Delta(y_n\cos\theta) - \gamma^2 y_n\cos\theta = xe^{-\lambda\kappa r}/r^n \quad \text{(II.12)}$$

The functions $y_n(r)$ and dy_n/dr which are needed for the relaxation potential are readily obtained by direct differentiation with respect to r. For the present problem, λ takes the values 1, 2 and $(1+q)$. For possible later use, the solutions are given before specialization to $q^2 = 1/2$ (symmetrical electrolytes) in terms of γ where $\gamma^2 = q^2\kappa^2$. The following auxiliary functions are introduced in order to make the table more compact

$$G(\kappa r) = e^{\gamma r}\,\mathrm{Ei}[(\lambda+q)\kappa r] + e^{-\gamma r}\mathrm{Ei}[(\lambda-q)\kappa r] \quad \text{(II.13)}$$

$$U(\kappa r) = e^{\gamma r}\,\mathrm{Ei}[(\lambda+q)\kappa r] - e^{-\gamma r}\mathrm{Ei}[(\lambda-q)\kappa r] \quad \text{(II.14)}$$

(23) E. Jahncke and F. Emde, "Funktionentafeln," Teubner, Leipzig, 1933, pp. 83-86. Our Ei (x) is the $[-\mathrm{Ei}(-x)]$ of these tables

KINETICS OF GRAPHITE OXIDATION

BY GEORGE BLYHOLDER AND HENRY EYRING

Department of Chemistry, University of Utah, Salt Lake City, Utah

Received January 8, 1957

A description of an apparatus for studying heterogeneous gas–solid reactions in the one to one hundred μ pressure and 600 to 1300° temperature range is presented. The data for the graphite–oxygen reaction from 600 to 800° are presented. The surface reaction is zero order with an 80 kcal. per mole activation energy. On samples thicker than 0.1 mm., the diffusion of oxygen into the pores in the graphite results in an observed one-half order reaction with a 42 kcal. per mole activation energy. Carbon monoxide is shown to be the primary reaction product.

Introduction

A great deal of material has appeared in the literature on the reaction of oxygen with carbon. Most of this deals with coal, coke, charcoal and similar materials. The interpretation of the reactions of these complex materials is complex and difficult, especially in view of the general lack of understanding of the reactions of pure graphite. In the literature one can find activation energies from 15 to 90 kcal. per mole and pressure dependences from zero to greater than first order. It was found in this study that not only the impurities, which undoubtedly account for a great deal of the differences in the literature, but also the particle size and poros-

ity affect the kinetics observed for graphite oxidation. There is considerable confusion in the literature as to whether carbon monoxide or carbon dioxide or both are primary products. A number of authors have discussed the significance of a variety of carbon monoxide to carbon dioxide ratios which have been observed. With the furnaces used below 900°, it appears inevitable that whatever the primary products really are, homogeneous and heterogeneous oxidation of carbon monoxide to carbon dioxide will result in large amounts of carbon dioxide being observed. The presence of free radical inhibitors for the homogeneous oxidation of carbon monoxide to carbon dioxide has been tried.[1-7] This results in the products of the graphite-oxygen reaction being about 90% carbon monoxide. However, recently E. Wicke[8] has demonstrated that these inhibitors have a considerable effect on the reaction. Their use is therefore not an acceptable way of investigating primary products.

In the work reported here, a constant activation energy was found from 600 to 800°. Above 800° both the activation energy and order of the reaction change with the temperature. Since the theoretical equations to interpret the reaction above 800° are not in the literature, the data and theoretical treatment necessary will be given in a subsequent publication.

Experimental System

A general diagram of the apparatus is shown in Fig. 1. The system is designed to oxidize graphite samples in the 600 to 1300° temperature range at pressures of 1 to 150 μ of Hg. The furnace, which has been described elsewhere,[9] was designed to preheat the oxygen to the reaction temperature before passing over the sample. It is a flow system in which the primary products are swept out of the hot zone before secondary reactions occur. The pressure range was selected to eliminate bulk diffusion effects. Oxygen is maintained at 30 to 100 mm. of Hg pressure in the oxygen reservoir. Before entering the oxygen reservoir the oxygen is dried over $Mg(ClO_4)_2$. From the reservoir the oxygen enters the furnace section through a 10-inch piece of 0.5 mm. bore capillary tube. The pressure in the reaction tube is maintained by the mercury diffusion pump. The oxygen pressure in the reaction tube is controlled by the oxygen reservoir pressure. This system of pressure control results in the flow rate of oxygen through the furnace tube increasing with increasing pressure in the reaction tube, if, as was usually done, the power input to the mercury diffusion pump is maintained constant. The reaction rate was found to be independent of the flow rate. The pressure in the reaction tube is obtained from the readings of the two thermocouple gages located just above the furnace. Due to the high linear flow rate of over 1000 cm. per second through the reaction tube, there is a noticeable pressure drop due to flow resistance between these two gages. The actual pressure at the sample is found by a linear extrapolation of the two thermocouple gage readings. These gages were calibrated by comparison with the McLeod gage readings. The thermocouple gages are on static side arms so that their readings are independent of the flow rate.

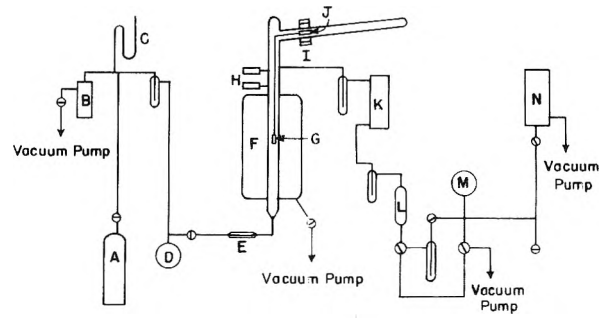

Fig. 1.—Reaction system: A, oxygen tank; B, cartesian manostat; C, mercury manometer; D, 3 liter reservoir; E, capillary tube; F, furnace; G, graphite sample; H, thermocouple gages; I, movable magnet; J, steel rod; K, mercury diffusion pump; L, catalyst; M, 3 liter reservoir; N, McLeod gage.

After the furnace, the product gas which is over 90% unreacted oxygen is passed over hot copper oxide in the catalyst chamber. Here all carbon monoxide is converted to carbon dioxide. The carbon dioxide is removed from the oxygen stream by a liquid nitrogen trap. The oxygen is then pumped out of the system. In actually making a run, the oxygen and carbon monoxide mixture from the furnace is run through the by-pass around the liquid nitrogen trap while steady-state flow conditions are being reached. After steady-state conditions are reached, the flow is diverted through the liquid nitrogen trap for a given length of time. The amount of carbon dioxide collected during a run is measured by allowing it to expand into the previously evacuated 3.35 liter measuring system, whose pressure is measured by the McLeod gage. For some runs, the 3-liter flask on the measuring system was replaced by a cap. This reduced the volume of the measuring system by a factor of 8.3. The initial volume of the measuring system was determined by measuring the pressure of carbon monoxide produced when a known weight of sodium formate was treated with an excess of sulfuric acid.

The efficiency of the catalyst and the liquid nitrogen trap was demonstrated by weighing a sample before and after burning it. The weight of carbon burned calculated from the pressure of carbon dioxide collected agreed within a few per cent. with the weight loss of the sample.

The sample is suspended on a 10 inch length of platinum wire (0.030 inch diameter) which passes through a small hole drilled in one end. This heavy wire is in turn supported by a length of fine platinum wire (0.005 inch diameter) which is flexible enough to let the sample hang freely. This wire is attached to a small steel rod which may be moved by a magnet to raise the sample out of or lower it into the reaction tube. This whole assembly is contained within the vacuum system. Upon being placed in the system samples were outgassed at 800° and one micron pressure overnight. Following this at least the top few layers of carbon atoms were burned off before runs were recorded. Between runs on the same sample, it was kept in the system at 25° and one micron pressure.

The samples were cut from one-quarter inch diameter rods manufactured by the National Carbon Company for use as spectroscopic electrodes. These rods were made by graphitizing a mixture of petroleum coke and pitch at 3000°. The spectroscopic analysis furnished by the manufacturer shows only traces of impurities in these samples.

Samples are prepared from the quarter-inch diameter graphite rod in several ways. For samples numbered 1 through 4, a hole is drilled down the center of the rod leaving walls 1 mm. thick. The resulting cylinder is then sawed in half lengthwise. Lengths of these semi-cylinders from 0.5 to 2.5 cm. long are used. For samples 5 and 6 a thin disk is cut from the end of the solid graphite rod. These disks are then sanded and polished to thicknesses from 0.0018 to 0.0032 inch. Samples 7 and 8 are prepared by rubbing the graphite rod against ceramic rods which are 2" long with $^1/_4$ inch diameter. This leaves a very thin coating of graphite which looks much like a pencil mark on the ceramic rods. The areas and thickness of the samples are given in Table I.

(1) C. Duffraise, *Compt. rend. acad. sci. (Paris)*, **192**, 564 (1931).
(2) J. R. Arthur, *Nature*, **157**, 732 (1946).
(3) J. R. Arthur and J. R. Bowring, *Ind. Eng. Chem.*, **43**, 528 (1951).
(4) J. R. Arthur and D. H. Bangham, *J. chim. phys.*, **47**, 559 (1950).
(5) J. R. Arthur, *Trans. Faraday Soc.*, **47**, 164 (1951).
(6) G. W. Bridger and H. Appleton, *J. Soc. Chem. Ind.*, **67**, 445 (1948).
(7) E. Mertens and L. Hellinclex, "Third Symposium on Combustion and Flame and Explosion Phenomena," The Williams and Wilkins Company, Baltimore, Maryland, 1949, p. 466.
(8) E. Wicke, "Fifth Symposium on Combustion," Reinhold Publ. Corp., New York, N. Y., 1955, p. 245.
(9) J. S. Binford, Jr., and H. Eyring, THIS JOURNAL, **60**, 486 (1956).

TABLE I

Sample	Area (cm.²)	Thickness (cm.)
1	6.94	0.1
2	1.77	0.1
3	7.78	0.1
4	1.40	0.1
5	0.59	1.26×10^{-3}
6	0.59	0.71×10^{-3}
7	9.88	2×10^{-4}
8	9.88	2×10^{-4}

Experimental Results

One of the major problems in this study is obtaining reproducible rates. There are two major causes of the variation in reaction rate from run to run. First, the total surface area of a sample changes as the sample is consumed. As the inner pore structure of the sample is developed and enlarged, the surface area increases. This process continues until enough of the sample has been consumed that continued consumption removes walls between pores resulting in a decreasing surface area. This has been shown very nicely by Wicke.[8] An attempt was made to burn the sample until it was close to its maximum surface area. Unfortunately, at all but the lowest temperatures where this effect is small anyway, the reaction rate is so fast that the reaction does not penetrate very deeply into the pores of the sample. This results in the surface of the sample becoming powder-like long before a maximum rate is reached. Once graphite particles start powdering off the surface of a sample incorrect results are obtained. For this reason, the reaction rates usually show a 5 to 7% increase from one similar run to the next. In order to obtain meaningful results, a set of conditions for a run were selected as standard. A standard run is then made between each run in which the conditions are varied. The results are then normalized so that all the standard runs are the same. After this adjustment the true relationship among runs at varying conditions is seen. Where the sample area changes slowly, it is not deemed necessary to make a standard run between every other run.

The second major factor causing variation in similar runs is the adsorption of vapors other than oxygen. Whenever the sample sits overnight in the system the reactivity is found to be roughly one-half of what it was the previous night. This effect is observed even though the sample whether at 25 or 800° sits in a vacuum of about 0.1 μ of Hg pressure. The reactivity of the sample is restored by oxidizing off the top layer of carbon. The two most likely poisoning vapors are water and mercury. The effect may be produced in a few minutes by passing water vapor over the sample. In spite of attempts to keep all water vapor out of the system including leaving liquid nitrogen on the trap nearest the sample, the effect is still observed upon leaving the sample sitting overnight. This effect has not been observed at 1000° or over, but no special attempt has been made to observe it at these elevated temperatures where the reaction rate is quite fast. After being noted and understood, this effect presented no particular difficulty. The variations in the reaction rate after different runs at the same condition are thus seen as understandable trends rather than as random irreproducibilities.

The pressure dependence of the reaction at 611° is given in Fig. 2. In Fig. 3 is given the pressure dependence of the reaction at 708°. The data for Figs. 2 and 3 were obtained using sample number 1. The pressure dependence of the reaction at 807°, shown in Fig. 4, was obtained using sample number 2. The temperature dependence of the reaction from 600 to 800° at 26 μ of Hg pressure was obtained using sample number 1. This is shown in Fig. 5. Runs from thin samples 5 and 6 are shown in Table II.

TABLE II

PRESSURE DEPENDENCE OF SAMPLES 5, 6 AND 7

Rate μ/3 min. into a 0.404 l. system at 300°K.	Pressure, μ of Hg	Temp. °C.
	Sample no. 5	
18.9	21	726
23.7	68	724
15.0	21	724
	Sample no. 6	
0.8	18	729
1.4	67	729
1.1	24	729
1.8	44	729
	Sample no. 7	
49	27	801
79	66	801
61	27	803

The results show a small, if not actually negligible, pressure dependence for the reaction of these samples. The data on the temperature dependence of the reaction using the very thin coatings on the ceramic rods, samples 7 and 8, are shown in Fig. 6. The data extend from 800 to 900° since below 800° the reaction was too slow to measure. The pressure dependence of sample number 7 is given in Table II. The rate of the reaction was too slow to obtain an accurate determination of the pressure dependence of the reaction on sample 7 at 800° but it is within experimental error of being zero order.

The results obtained by making runs with the copper oxide catalyst cold are recorded in Table III. By comparing the results of these runs with previous runs under the same conditions the amount of carbon dioxide in the product gases can be determined. The percentage of carbon dioxide in the product gases is given in the last column of this table.

TABLE III

RESULTS WITH CATALYST COLD

Rate, μ of Hg/3 min. into a 0.404 l. system at 300°K.	Pressure, μ of Hg	Temp., °C.	% CO_2
	Sample no. 3		
16.2	27	702	6
1.5	26.5	606	4
	Sample no. 4		
17	27	804	3
63	27	900	6
57	28	800	10

Interpretation of Results

The mechanism which best fits the data is one of a zero-order surface reaction of 80 kcal. per mole ac-

tivation energy with diffusion into pores of the sample controlling the rate of the reaction. According to Wheeler[10], the expression for the rate of reaction in a single pore where the surface reaction is zero order and is fast enough to consume all of the reactant gas in the pore before it can diffuse to the end of the pore is given by

$$R = 2\pi r\sqrt{rDk_1C_0} \qquad (1)$$

where

R = reaction rate molecules per pore-sec.
r = pore radius in cm.
D = diffusion constant cm.²/sec.
k_{-1} = intrinsic reactivity of the surface in molecules O_2/cm.²-sec.
C_0 = concn. of gas outside sample, molecules/cm.³

The total rate of reaction is given by the rate per pore multiplied by the number of pores. Equation 1 states that the reaction rate should be proportional to the gas pressure to the one-half power. Figures 2, 3 and 4 show that at 600, 700 and 800° the reaction rate is proportional to the pressure to the one-half power.

If thin enough samples are used, the pore length will be short enough so that at low temperatures the reaction rate will be slow enough for the reactant gas to diffuse to the end of the pore. In this case the observed reaction will be zero order. Samples 5 and 6 were prepared in order to observe this. From the data given in Table II, it is seen that the reaction is close to zero order with these samples. Unfortunately, the reaction with these small samples is so slow as to be difficult to measure accurately. These samples are thick enough for the kinetics to revert to those described by equation 1 when the temperature is raised enough for the reaction rate to become appreciable.

Since the rate constant k_{-1} in equation 1 appears under the square root sign, the observed activation energy for this equation is one-half the activation energy for the surface reaction. An activation energy twice that observed for diffusion conditions described by equation 1 should be found for conditions where the surface reaction is unaffected by diffusion. From Fig. 6 it is seen that with the very thin coatings of graphite rubbed on ceramic rods an activation energy of 80 kcal./mole is observed at 800°. This is close to twice the activation energy of 42 kcal./mole observed in Fig. 5 for samples 1 mm. thick where the rate is described by equation 1. From Table II the pressure dependence of the reaction at 800° on the very thin graphite coatings is seen to be small.

In addition to the work in this Laboratory, work from other laboratories reported in the literature supports the proposed mechanism. Gulbransen and Andrews[11] working with samples of spectrographic graphite between 425 and 575° with oxygen pressures of 0.15 to 9.8 cm. reported for the pressure dependence of the reaction an equation of the form

$$R = A + BP \qquad (2)$$

where

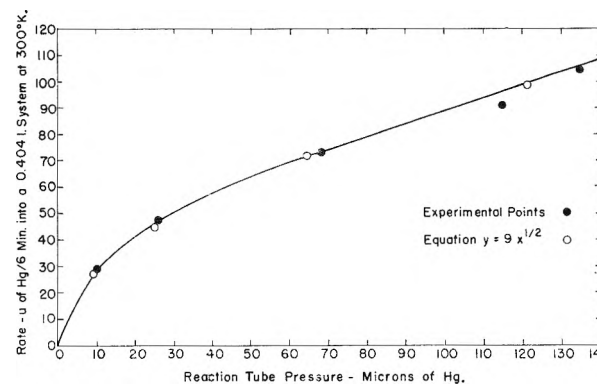

Fig. 2.—Pressure dependence of reaction at 611°.

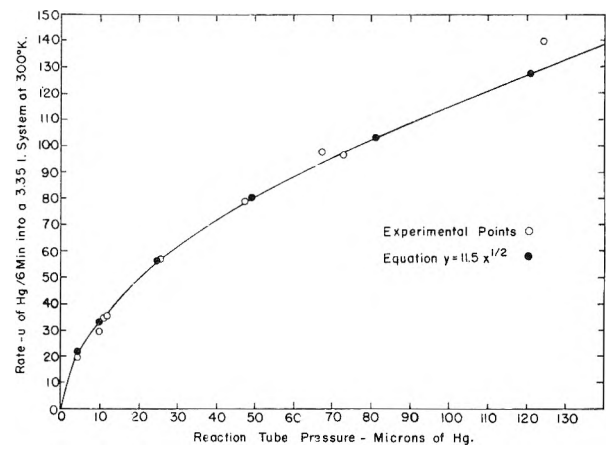

Fig. 3.—Pressure dependence of reaction at 708°.

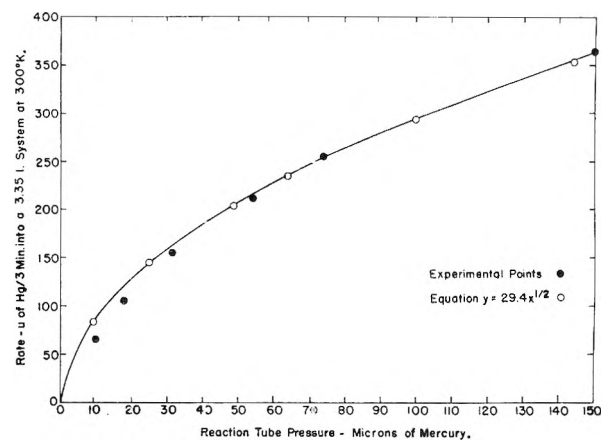

Fig. 4.—Pressure dependence of reaction at 807°.

R = rate of reaction
A and B = constants
P = oxygen pressure

Gulbransen called the reaction first order but offered no explanation for the appearance of the constant A. His data also fits quite well an equation of the form $R = CP^{1/2}$ where C is a constant. This form of fit is identical to equation 1. He found an activation energy of 37 kcal./mole which is not too far from our value of 42 kcal.

P. L. Walker[12] and associates have demonstrated by gasification of graphite with carbon dioxide that spectrographic graphite similar to the samples used

(10) A. Wheeler, "Advances in Catalysis," Vol. II, Academic Press Inc., New York, N. Y., 1951, p. 250.

(11) E. A. Gulbransen and K. F. Andrew, *Ind. Eng. Chem.*, **44**, 1034 (1952).

(12) P. L. Walker, Jr., F. Rusinko Jr., and E. Raats, THIS JOURNAL, **59**, 245 (1955).

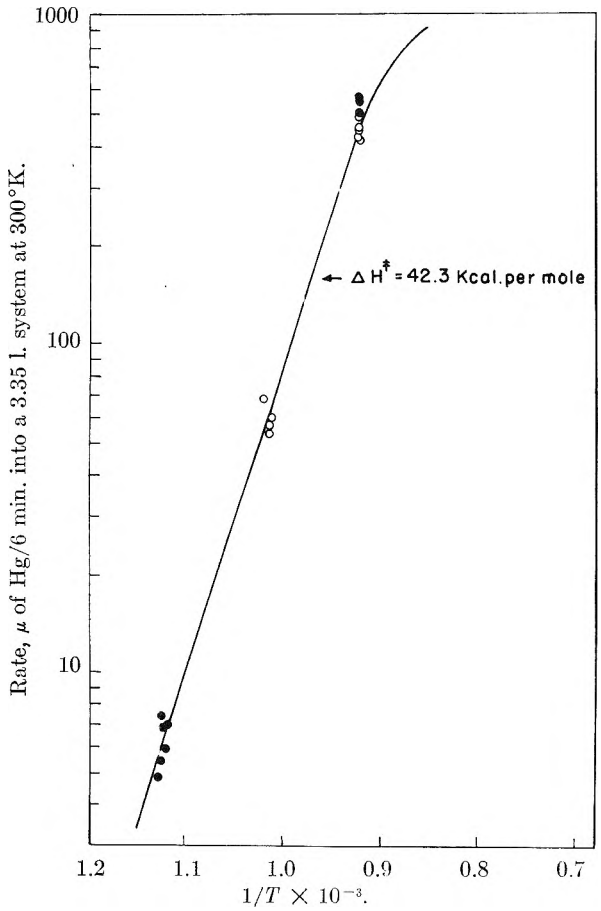

Fig. 5.—Log of rate *vs.* $1/T$.

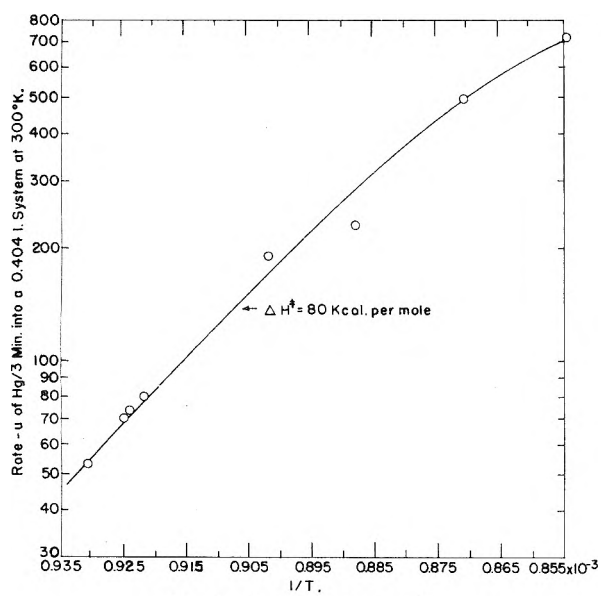

Fig. 6.—Log of rate *vs.* $1/T$.

here is consumed throughout the entire sample and not just on the surface.

Regarding now the role of pore diffusion in graphite oxidation in the 400 to 800° temperature range to have been placed on a firm experimental foundation, a detailed mechanism of the surface reaction is presented. As an oxygen molecule is adsorbed on the graphite surface it dissociates so that oxygen appears on the surface only as oxygen atoms attached to carbon atoms by covalent bonds. A carbon atom to which an oxygen atom is bonded then breaks its bonds with the surface giving a carbon monoxide molecule in the gas phase. Since the adsorption of an oxygen molecule would be expected to be a process which is first order in oxygen pressure, the breaking of the carbon–carbon bonds in liberating the carbon monoxide molecule is the rate controlling step. With a fast adsorption process, which completely covers the surface reaction sites with oxygen, followed by a slower breaking of carbon–carbon bonds, the observed reaction would be zero order with respect to oxygen. This mechanism has carbon monoxide as the primary reaction product. From the data in Table III carbon monoxide is the observed primary product for the reaction in the temperature range below 800°.

The energy variation along the reaction coördinate for this mechanism is shown in Fig. 7. The value of ϵ_1, the activation energy for chemisorption of oxygen on the graphite surface, is unknown. The value of ϵ_2, the heat of adsorption of oxygen, may be estimated in several ways. The value may be calculated from the bond energies of the (C=O) bond and the (O=O) bond. This calculation gives 183 kcal./mole of oxygen. In 1931 Bull, Hall and Garner[13] measured a value of 97 kcal./mole for oxygen adsorption. Trapnell[14] points out that this value would be expected to be rather low since it is doubtful that the carbon surface was really clean. The value of ϵ_3, the activation energy for carbon monoxide breaking loose from the surface, is found to be 80 kcal./mole in this work. The value of ϵ_4, the heat of reaction of carbon and oxygen to give carbon monoxide, is 26.8 kcal./mole. If a value for ϵ_2 near the theoretical value of 91.5 kcal./mole of carbon monoxide is taken, Fig. 7 readily shows why oxygen is removed only as oxides of carbon and never as molecular oxygen whenever it is adsorbed on a graphite surface. Considering a chemisorbed oxygen atom as the initial state, since the activated complex in going either to molecular oxygen or to carbon monoxide could be expected to be a surface complex, the entropy of activation for either process would be very small. This would leave the free energy of activation in both processes essentially equal to the activation energy. Since ϵ_3 is considerably less than $\epsilon_2 + \epsilon_1$, all chemisorbed oxygen would leave the surface as an oxide of carbon rather than as molecular oxygen.

The rate at which carbon monoxide breaks loose from the surface can be calculated from the absolute rate theory.[15] The velocity of the reaction is given by

$$v = C_s k' \qquad (3)$$

where

v = reaction rate in molecules of CO per cm.^{2}-sec.
C_s = surface sites per cm.^{2} taken as 3.5×10^{15} (the number of carbon atoms per cm.^{2} of graphite lattice)
k' = rate constant in sec.$^{-1}$

(13) H. L. Bull, M. H. Hall and W. E. Garner, *J. Chem. Soc.*, 837 (1931).

(14) B. M. W. Trapnell, "Chemisorption," Butterworths Scientific Publications, London, England, 1955, p. 146.

(15) S. Glasstone, K. J. Laidler and H. Eyring, "The Theory of Rate Processes," McGraw-Hill Book Co., New York, N. Y., 1941.

The value of k' is given by absolute rate theory as

$$k' = \kappa \frac{k_B T}{h} \frac{f^{\pm}}{f_s} e^{-\Delta H^{\pm}/R_G T} \quad (4)$$

where

κ = transmission coefficient
k_B = Boltzmann constant
h = Planck constant
T = temperature °K.
$f^{\pm}$ = partition function of activated complex
f_s = partition function of surface with oxygen on it
$\Delta H^{\pm}$ = activation energy, cal./mole
R_G = gas constant, cal./mole-degree

κ is assumed to be one. Since both partition functions involve only vibrational degrees of freedom, $f^{\pm}/f_s$ is taken to be one. Using the experimental value of 80 kcal/mole for $\Delta H^{\pm}$, the results are

$$k' = 1.4 \times 10^{-3} \text{ sec.}^{-1}$$

and

$$v_{\text{calcd}} = 5.2 \times 10^{12} \text{ molecules of CO per cm.}^2 \text{ sec.}$$

The experimental velocity of the surface reaction of spectrographic graphite is taken from Fig. 6. The value at 800° from the graph is 53 μ per three minutes into a 0.404 liter system at 300°K. In more conventional units this is 3.83×10^{15} molecules per second. Since the surface area of the sample is about 10 sq. cm. and the surface roughness may reasonably be taken[11] as 100, the final result is $v_{\text{exptl}} = 3.8 \times 10^{12}$ molecules of CO per cm.^{2}-sec. The experimental and calculated values are seen to agree very well.

Having a value for the intrinsic reactivity of the surface, the validity of equation 1 may now be tested. The total reaction rate per sq. cm. is given by

$$R_T = n_p R \quad (5)$$

where

R_T = rate per sq. cm.-sec.
n_p = no. of pore mouths per unit area
R = rate per pore from eq. 1

Substituting in equation 1 gives

$$R_T = n_p 2\pi \bar{r} \sqrt{\bar{r} D k_1 C_0} \quad (6)$$

where $\bar{r}$ is the average pore radius. According to Wheeler[10]

$$\bar{r} = \frac{2V_g}{S_g} \quad (7)$$

where

S_g = surface area/g. = 15×10^3 sq. cm./g.[16]
V_g = pore vol./g. = 0.3 cm.^{3}/g.[16]

This gives

$$\bar{r} = 3.7 \times 10^{-5} \text{ cm.}$$

The number of pores per sq. cm. is given by

$$n_p = \frac{\theta'}{\pi \bar{r}^2} \frac{1}{\sqrt{2}} \quad (8)$$

where θ' = porosity (fraction of sample which is space).

$$\theta' = \rho_s V_g \quad (9)$$

where ρ_s = density of sample = 1.3 g./cubic cm. Putting in values for ρ_s and V_g, θ' is evaluated as

(16) P. L. Walker, Jr., and E. Raats, THIS JOURNAL, **60**, 364 (1956).

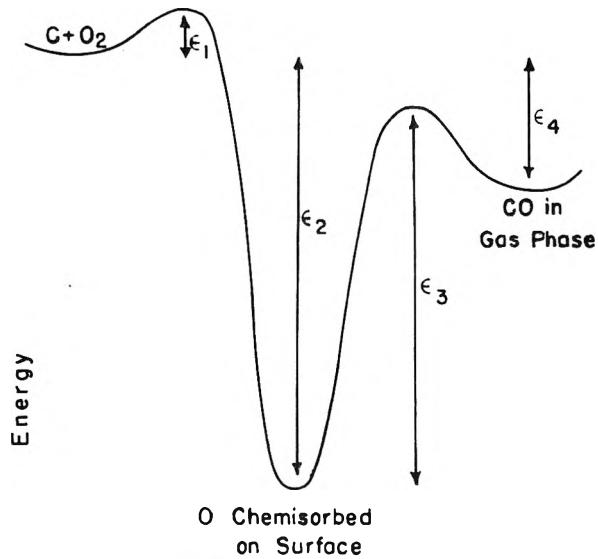

Fig. 7.—Reaction coördinate oxygen reaction with surface.

$$\theta' = (1.3)(0.3) = 0.4$$

From the value of θ' and $\bar{r}$, it is found that

$$n_p = 6.5 \times 10^7 \text{ pores/sq. cm.}$$

Since the mean free path of the gas is much greater than the pore diameters, the diffusion coefficient is for molecular flow. This if given by

$$D = \frac{2\bar{r}}{3} \bar{V} \quad (10)$$

where $\bar{V}$ is the average molecular speed given by

$$\bar{V} = \sqrt{\frac{8k_B T}{\pi m}} \quad (11)$$

in which m is the molecular mass of the gas. For oxygen

$$\bar{V} = 2.19 \times 10^3 \sqrt{T}$$

The intrinsic reactivity of the surface, k_{-1}, is $v/2$, which is 2.5×10^{12} molecules of O_2/sq. cm.-sec. The gas concentration is given by

$$C_0 = \frac{NP}{R_G T} \quad (12)$$

where

N = Avogadro's number
P = pressure in mm.
k_G = gas constant

Putting in numbers gives

$$C_0 = 9.65 \times 10^{18} P/T$$

Substituting values of constants but not measured variables into equation 6 yields

$$R_T = 1.68 \times 10^{11} \theta' \sqrt{\frac{k_{-1} P}{T^{1/2}}} \quad (13)$$

At a pressure of 26 μ of Hg and 800° this gives

$R_T = 3 \times 10^{15}$ molecules of O_2/sq. cm.-sec.
$R_T = 6 \times 10^{15}$ molecules of CO/sq. cm.-sec.

It should be noted that this rate is per sq. cm. of geometric surface. As shown by Fig. 5, at 26 μ of Hg pressure and 800°, the experimental rate is 380 μ per six minutes into a 3.35 liter system at 300°K. In more conventional units the rate is

1.14×10^{17} molecules per second. Dividing by the geometric surface area of 6.94 sq. cm. gives

$$R_{T\ exptl} = 16 \times 10^{15} \text{ molecules of CO/sq. cm.-sec.}$$

Thus the calculated rate is in good agreement with the experimental rate.

We are now in a position to understand the wide differences in data on graphite oxidation in the literature. Impurities in graphitic materials result in a wide variety of low activation energies being observed. The appearance of pore diffusion effects, which are influenced by particle size and porosity, results in the possibility of observing an activation energy anywhere between the value for the plane surface reaction and one-half of that value. Since impurities may change the rate controlling step in the reaction they may also change the observed order of the reaction. A surface reaction of order n will result in an observed order of $n + 1/2$ if the surface reaction is controlled by pore diffusion. In this study the true surface reaction of graphite with oxygen has been found to be zero order with an 80 kcal./mole activation energy. On samples thicker than 0.1 mm., the diffusion of oxygen into the pores in the graphite results in an observed one-half order reaction with a 42 kcal. per mole activation energy. In the previous studies no successful precautions were taken to prevent the secondary reaction of carbon monoxide being oxidized to carbon dioxide. This resulted in the confusion over whether carbon monoxide or carbon dioxide or both are primary products. By the use of a very fast flow rate of oxygen past the sample this study has unequivocally shown carbon monoxide to be the primary product from 600 to 800°.

Acknowledgment.—The authors gratefully acknowledge the California Research Corporation for a fellowship which supported G. B. during much of this work and the U. S. Air Force for support under contract no. AF 33(038)20839.

THE THERMODYNAMICS OF HYDROGEN CHLORIDE IN ETHYL ALCOHOL FROM ELECTROMOTIVE FORCE MEASUREMENTS[1]

BY HARRY TANIGUCHI AND GEORGE J. JANZ

Department of Chemistry, Rensselaer Polytechnic Institute

Received January 24, 1957

Electromotive force measurements of the cell without liquid junction: Pt, H_2 (1 atm.) |HCl in Ethanol (m) | AgCl-Ag have been carried out at 25° over a concentration range from 0.0048 to 0.12 molal. New experimental techniques were devised and the best theoretical treatment was employed. The standard molal electrode potential of the silver, silver chloride electrode in anhydrous ethanol is −0.08138 volt. This value and the activity coefficients of hydrogen chloride computed from the data are recommended for the practical standardization of the silver–silver chloride electrode in anhydrous ethanol at 25°.

Introduction

In contrast to the number of measurements of the activity coefficients of hydrogen chloride in water–ethyl alcohol mixtures, relatively few have been attempted in pure anhydrous ethyl alcohol.

Harned and Fleysher[2] first carried out an extended series of measurements on the cell without liquid junction

$$\text{Pt, } H_2 \text{ (g., 1 atm.) } |\text{HCl}(m)|\ \text{AgCl-Ag} \qquad \text{I}$$

over the concentration range from 0.001 to 3.6 m at 25°. It was estimated by Scatchard[3] and shown experimentally by Woolcock and Hartley[4] that the ethanol was of 99.9% purity, containing 0.1% water. This led to a discrepancy of about 12 mv. in the e.m.f. values. Although Danner[5] used cell I with mercury–mercurous chloride electrodes instead of silver–silver chloride electrodes, his results may be used to evaluate the preceding e.m.f. data since the difference in potential between these two electrodes should be independent of the solvent. This difference was found to be 0.0467 v. in methanol by Nonhebel and Hartley,[6] in agreement with that in water. Noting that the results of Harned and Fleysher and of Danner indicated a difference of only 0.0350 v., the possibility of an error in one or both series of measurements is apparent.

New measurements of cell I in ethyl alcohol were presented by Woolcock and Hartley[4] at 25° from 0.0003 to 1.2 m. Values of the activity coefficient were based on a standard cell potential obtained by direct extrapolation. The value of the limiting slope was found to be greater than that predicted by the Debye theory. Butler and Robertson[7] used cell I with pure ethanol for the concentration range of 0.01 to 1.0 m at 15, 25 and 35°. This represents the only available estimate of the temperature coefficient of e.m.f. for hydrogen chloride in ethanol. While agreement was found with Harned and Fleysher at 1.0 m, the results of the latter were high by 8 mv. at 0.1 m and 17 mv. at 0.01 m. On the other hand, their results agreed with those of Woolcock and Hartley at 0.1 m and at 1.0 m, but were about 3 mv. high between these limits. It was concluded that the difference with

(1) Abstracted in part from a thesis submitted by Harry Taniguchi in partial fulfillment of the requirements for the degree Doctor of Philosophy, Rensselaer Polytechnic Institute. Presented at the Symposium on Electrolytes, Electrochemical Society Meeting, Washington, D. C., May, 1957.

(2) H. S. Harned and M. H. Fleysher, *J. Am. Chem. Soc.*, **47**, 82 (1925).

(3) G. Scatchard, *ibid.*, **48**, 2026 (1926).

(4) J. W. Woolcock and H. Hartley, *Phil. Mag.*, [7] **5**, 1133 (1928).

(5) P. S. Danner, *J. Am. Chem. Soc.*, **44**, 2832 (1922).

(6) G. Nonhebel and H. Hartley, *Phil. Mag.*, [6] **50**, 729 (1925).

(7) J. A. V. Butler and C. M. Robertson, *Proc. Roy. Soc.* (*London*), **125A**, 694 (1929).

the first series probably was due to insufficiently dry alcohol.

The experimental data of Woolcock and Hartley were re-examined by MacInnes[8] in 1939, using the Hitchcock[9] method of extrapolation as extended by Brown and MacInnes.[10] The standard electrode potentials, −0.0740 and −0.0864 v., on the molal and molar scales, respectively, and the activity coefficients from this re-analysis had been accepted as the most reliable values for hydrogen chloride in ethanol until new values were proposed by Mukherjee[11] in 1954. Mukherjee, re-investigating the system, reported a new value, *i.e.*, +0.00977 v., which differed not only in magnitude but also in sign from the accepted value.

It is apparent that a serious discrepancy exists as to the correct values to be assigned at 25°. A redetermination using the best experimental and theoretical techniques was, therefore, undertaken as one of the prime objectives. In addition, a resolution of the uncertainties pertaining to the thermodynamics of hydrogen chloride in anhydrous ethanol could be expected. The determination of the activity coefficient of hydrogen chloride in ethanol at an experimentally convenient concentration, say, 0.01 *m*, serves to standardize the practical potential of the silver–silver chloride electrode by the method of Bates, *et al.*,[12] as in water.

Experimental

Cell Design.—The all-glass cell was basically an H-type cell, designed to permit the use of three silver–silver halide electrodes and two types of hydrogen electrodes—the normal platinized foil electrode and the platinum powder catalyst electrode, first used in aqueous solutions by Hills and Ives.[13] The silver–silver halide chamber was an 80 mm. length of 30 mm. tubing, terminating in three mercury-sealed 10/30 standard taper outer ground glass joints. Tubing of 20 mm. was chosen for the hydrogen electrode chamber, the lower 12 mm. length being constricted to 10 mm. where the bright platinum foil was sweat-sealed into the conical bottom. The platinum cone was shaped from a 10 mm. diameter circle of 0.0004 inch thick foil by cutting out a segment subtending a 4 mm. arc at the circumference. A 2 mm. wide strip for electrical contact was cut along one of the edges left by the removal of the segment. The 1 mm. stopcock permitted the hydrogen to be by-passed when desired, the gas being vented through a bubbler made from a 65 mm. length of 25 mm. glass tubing. The two pre-saturation bubblers for the incoming hydrogen were each made from a 150 mm. length of 20 mm. tubing, with a spiral of 7 to 9 turns of 2 mm. glass rod on a 10 mm. tube to lengthen the pass through the solution.

The approximate solution requirements of each part were as follows: each bubbler, 35 ml.; hydrogen half-cell and exit bubbler, 35 ml.; silver–silver chloride half-cell, 65 ml.

Electrodes.—From a comparison[14] of the three main types of the silver–silver chloride electrodes, the thermal-electrolytic electrodes were selected as most suitable for multiple preparation. The preparation, reproducibility and stability of these have been described elsewhere in detail.[15] Stable electrodes of low bias potential (0.01 mv.) prepared by the above method were transferred to alcoholic hydrochloric acid for storage. In the present work, a set of electrodes was used repeatedly instead of limiting the use of electrodes to one measurement. This had the advantage of using completely equilibrated, anhydrous electrodes. The hydrogen foil electrodes, 7 mm. × 9 mm. × 0.15 mm. platinum, were platinized in 1% platinic chloride solution at 3 ma. for 5 minutes to give a very light platinized surface. These were thoroughly washed with de-ionized water and pre-soaked in alcoholic hydrochloric acid. The platinum black catalyst powder was prepared as described by Hills and Ives,[15] and stored over anhydrous magnesium perchlorate. The present work represents the first use of the catalyst hydrogen electrode in a solvent other than water. It was found that in 0.05 *m* HCl, agreement to 0.01 mv. was obtained within 20 minutes for both foil and catalyst electrodes. The most notable difference for the catalyst electrode in ethanol as compared with water was a somewhat longer period of hydrogen gas flow (about 2 hours) before equilibrium was attained. The test for equilibrium was a constant e.m.f. with the gas by-passing.

Chemicals.—The starting alcohol was "Absolute Ethyl Alcohol, U.S.P." grade (U. S. Industrial Chemicals, Inc.). It was subjected to purification using magnesium ethylate after the procedure of Lund and Bjerrum,[16] and fractional distillation in an all-glass system with a solenoid controlled take-off, a magnetic distributing adaptor,[17] with no stopcocks or greased ground joints in the system. The presence of less than 0.005% water, and a conductivity of less than 1×10^{-8} ohm^{-1} cm.$^{-1}$ in the distillate were taken as the criteria for ethyl alcohol of sufficient quality for this work. Anhydrous hydrogen chloride was prepared by the action of concentrated sulfuric acid on sodium chloride in an all-glass apparatus described elsewhere.[18] All solution flasks were of special design with guard tubes of magnesium perchlorate to ensure anhydrous conditions. Solutions below 0.01 *m* were prepared by weight dilution, while the stronger solutions were prepared by bubbling HCl directly into the ethanol which was maintained at 0–5° until required for use. The ethanol was de-oxygenated by a slow stream of dry hydrogen gas before the solutions were prepared. The concentrations of hydrogen chloride were determined by precision analyses using the differential potentiometric titration of MacInnes and Dole.[19] All weights were corrected to vacuum. The hydrogen gas, an electrolytic grade of 99.8% purity (Matheson Co.), was passed over a palladium catalyst to remove last traces of oxygen, and through a series of magnesium perchlorate, P_2O_5, and ascarite towers, and admitted to the e.m.f. cell through all-metal packless needle valves (Fisher Scientific Co.) for flow control.

Apparatus and Procedure.—All measurements were made in a water-bath thermostated to 25 ± 0.005°. Temperatures were measured with a Type G-2 Mueller bridge (Leeds and Northrup Co.) and certified N.B.S. platinum resistance thermometers. A type 2782 Bonn five-dial potentiometer (Rubicon Co.) was used for the e.m.f. measurements. The system was shielded for potential leaks after White.[20] The e.m.f. measurements were corrected to 1 atmosphere partial pressure of hydrogen gas.[21] The solutions were, in each case, freshly prepared and analyzed just before use in an experiment. The electrodes were conditioned to the solutions in a pre-soaking cell with at least four changes of solutions over a five-hour period. The cleaned e.m.f. cell and pre-saturation bubblers were oven dried at 125°, assembled while hot, purged with dry nitrogen to displace all the air. With the electrodes in place at room temperature and the catalyst powder in, the assembled cell was swept with dry hydrogen for a period of 15 minutes before being filled with the solution. After a period of one hour, this solution was replaced by fresh solution, and hydrogen gas was bubbled rapidly through the assembly to displace some of the solution from the pre-saturators. This ensured smooth operation of the bubblers at a slower rate during the actual measurements. After transfer of the assembly to the ther-

(8) D. A. MacInnes, "The Principles of Electrochemistry," Reinhold Publishing Corp., New York, N. Y., 1939, p. 213.

(9) D. I. Hitchcock, *J. Am. Chem. Soc.*, **50**, 2076 (1928).

(10) A. S. Brown and D. A. MacInnes, *ibid.*, **57**, 1356 (1935).

(11) L. M. Mukherjee, THIS JOURNAL, **58**, 1042 (1954).

(12) R. G. Bates, E. A. Guggenheim, H. S. Harned, D. J. G. Ives, G. J. Janz, C. B. Monk, J. E. Prue, R. A. Robinson, R. H. Stokes, and W. F. K. Wynne-Jones, *J. Chem. Phys.*, **25**, 361 (1956).

(13) G. J. Hills and D. J. G. Ives, *J. Chem. Soc.*, 305 (1951).

(14) G. J. Janz and H. Taniguchi, *Chem. Revs.*, **53**, 397 (1953).

(15) H. Taniguchi and G. J. Janz, *J. Electrochem. Soc.* **104**, 123 (1957).

(16) H. Lund and J. Bjerrum, *Ber.*, **64B**, 210 (1931).

(17) G. J. Janz and E. J. Rock, *Anal. Chem.*, **22**, 626 (1950).

(18) H. Taniguchi and G. J. Janz, *ibid.*, **28**, 287 (1956).

(19) D. A. MacInnes and M. Dole, *J. Am. Chem. Soc.*, **51**, 1119 (1929).

(20) W. P. White, *ibid.*, **36**, 2001 (1914).

(21) F. A. Berry, Jr., E. Bollay and N. R. Beers, Editors, "Handbook of Meteorology," McGraw-Hill Book Co., Inc., N. Y., 1945, p. 84.

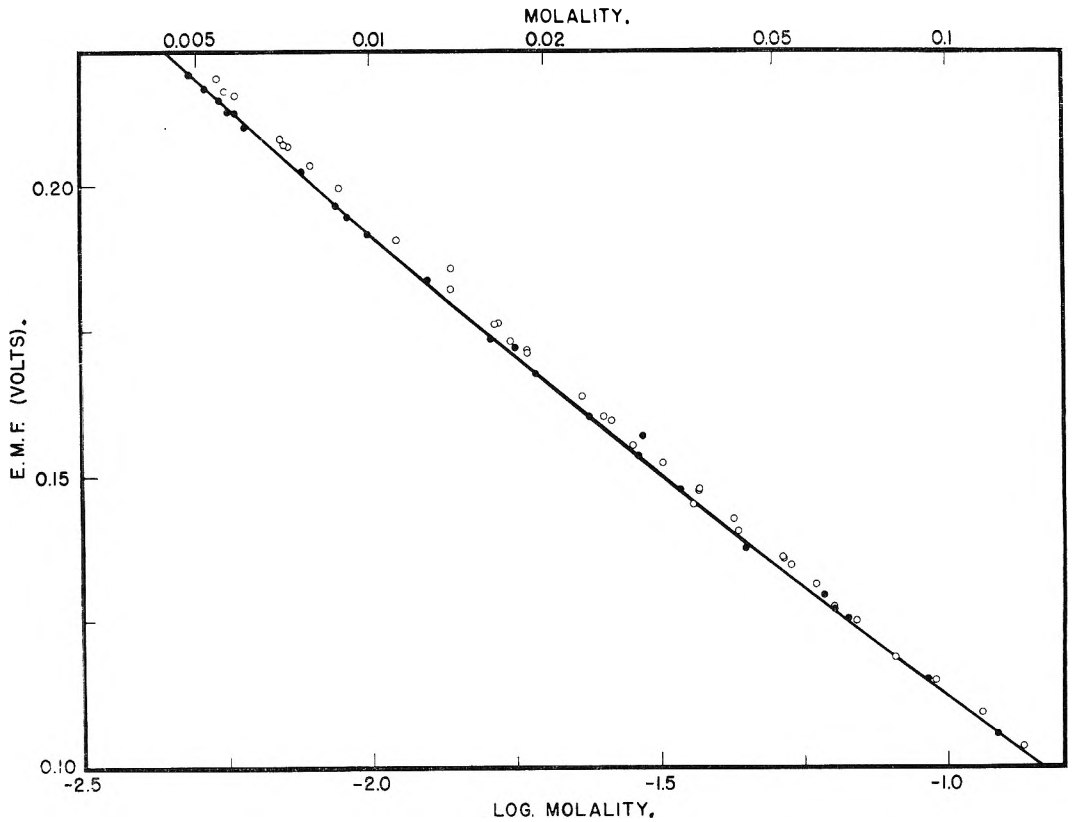

Fig. 1.—E.m.f. of the H_2, Ag–AgCl cell at 25°: O, Woolcock and Hartley; ●, this investigation.

mostat the potentials between pairs of similar electrodes and the nine possible combinations of the three hydrogen electrodes against the three silver, silver chloride electrodes were taken. Equilibrium was considered to be established when the potential remained constant to ±0.01 mv. for an hour.

Results and Calculations

The results are summarized in Table I in order of increasing concentration. The measurements were made in a random order of concentration so that systematic errors, if present, would be detected. The average deviation, δ, is presented as a measure of the reproducibility of the electrodes. The composition of the cell solutions is accurate within 0.02%. The weights of the solutions taken for dilution were sufficiently great to introduce no error from the dilution technique. The corresponding molarities were calculated assuming that the density of the solution did not differ appreciably from that of the pure solvent (d_0, 0.78056/25°). The equations, and the concentration ranges for each, found by the method of least squares and the Gauss criterion to express the experimental results were

$$E = 0.012551 - 0.089381 \log m, \quad 0.0048 < m < 0.0064 \quad (1)$$

$$E = 0.037821 - 0.068385 \log m + 0.0043201 (\log m)^2, \quad 0.0064 < m < 0.044 \quad (2)$$

In Fig. 1 this composite function is shown as the smooth curve together with the e.m.f. data of Woolcock and Hartley and the present results.

For evaluation of the standard electrode potential, when the electrolyte in the cell solution exhibits ion association, this must be accounted for by an extrapolation of the following form[22]

$$(E^{0\prime} - E_\alpha) = E + 2k \log \alpha c y_\alpha = E_c^0 \quad (3)$$

where degree of dissociation α, and the activity coefficient y_α, at an ionic concentration of αc are determined from the simultaneous solution of the thermodynamic dissociation constant equation and the Gronwall, La Mer and Sandved extended equation for the activity coefficient

$$\alpha = \frac{1}{2}\left(-\frac{K}{y_\alpha^2 c} + \left(\frac{K^2}{y_\alpha^4 c^2} \frac{4K}{y_\alpha^2 c}\right)^{1/2}\right] \quad (4)$$

In the present calculations, a dissociation constant of 0.0113 mole liter^{-1}, as found by Bezman and Verhoek[23] was used as the most reliable value. This is in close agreement with an earlier value of 0.0112 mole liter^{-1} reported by Ogston.[24] For each value of the distance of closest approach, a, the molar activity coefficient was calculated from the Gronwall, La Mer and Sandved extension of the Debye–Hückel theory at round values of the square root of the concentration. The degree of dissociation and the activity coefficients were thus found by a series of approximations, and used to compute E_c^0. These calculations are summarized in Table II for a = 3.99 Å. The results for a series of values are shown graphically in Fig. 2, where it is seen that the extrapolation based on a = 3.99 Å. is in complete accord with the theoretical predictions of a straight line with zero slope up to a concentration of 0.008 m. This led to an unam-

(22) H. S. Harned and B. B. Owen, "The Physical Chemistry of Electrolytic Solutions" 2nd Ed., Reinhold Publ. Corp., New York, N. Y., 1950, pp. 122, 334.

(23) I. I. Bezman and F. H. Verhoek, *J. Am. Chem. Soc.*, **67**, 1330 (1945).

(24) A. G. Ogston, *Trans. Faraday Soc.*, **32**, 679 (1936).

biguous extrapolation to $E_c^0 = -0.09383$ v. at 25°. In a similar manner, on the standard molal scale, the extrapolation gave $E_m^0 = -0.08138$ volt.

The variation of the logarithm of the rational activity coefficient with the square root of the molality is shown graphically in Fig. 3, together with the slope predicted by the Debye limiting law. For comparison, the corresponding activity coefficients for hydrogen chloride in water, obtained from the recent results of Bates and Bower[25] are included with the limiting Debye slope.

TABLE I

ELECTROMOTIVE FORCES AT 25° OF THE CELL: Pt, H_2 (g., 1 atm.) |HCl in ethanol(m)| AgCl-Ag

m, equiv. kg.$^{-1}$ solvent	c, equiv. l.$^{-1}$ solution	E, volt	δ, mv.
0.004872	0.0038243	0.21914	0.007
.005190	.0040740	.21686	.005
.005488	.0043067	.21477	.02
.005690	.0044661	.21269	.02
.005855	.0045957	.21258	.001
.006091	.0047809	.21016	.04
.007636	.005993	.20237	.01
.008744	.006862	.19649	.005
.009154	.007184	.19452	.02
.009915	.007781	.19158	.01
.012642	.009920	.18360	.007
.016152	.012672	.17347	.005
.017828	.013987	.17196	.007
.019336	.015169	.16742	.003
.023946	.018783	.16008	.006
.029110	.022829	.15334	.004
.029640	.023244	.15671	.005
.034364	.026944	.14760	.01
.044594	.034952	.13745	.02
.06102	.047798	.12929	.03
.06360	.049813	.12679	.006
.06707	.05263	.12519	.01
.09227	.07219	.11479	.005
.12172	.09514	.10535	.06

TABLE II

EVALUATION OF $(E^{0\prime} - E\alpha)$ FOR $a = 3.99$ Å. ON MOLARITY SCALE

No.	c, equiv. l.$^{-1}$ soln.	$E_{calcd.}$ v.	α	y_α	$-2k \log \alpha c y_\alpha$, v.	$-(E^{0\prime} - E\alpha)$,[a] v.
1	0.0038243	0.21922	0.8820	0.6696	0.31307	0.09385
2	.0040740	.21677	.8779	.6627	.31060	.09383
3	.0043067	.21461	.8744	.6564	.30844	.09383
4	.0044661	.21320	.8722	.6522	.30703	.09383
5	.0045957	.21209	.8702	.6491	.30592	.09383
6	.0047809	.21056	.8676	.6448	.30439	.09383
7	.0059930	.20196	.8523	.6192	.29577	.09381
8	.0068624	.19688	.8428	.6037	.29069	.09381
9	.0071840	.19517	.8396	.5984	.28898	.09381
10	.0077808	.19219	.8338	.5893	.28603	.09384
11	.0099201	.18319	.8159	.5613	.27716	.09397
12	.012672	.17422	.7973	.5332	.26841	.09419
13	.013987	.17063	.7898	.5218	.26493	.09430
14	.015169	.16769	.7836	.5125	.26209	.09440
15	.018783	.16000	.7668	.4885	.25469	.09469

[a] $(E^{0\prime} - E\alpha) = E + 2k \log \alpha c y_\alpha$.

The mean molal activity coefficients, $\gamma_\pm$, were calculated from the thermodynamic equation

$$\log \gamma_\pm = \frac{E_m^0 - E}{2k} - \log m \qquad (5)$$

(25) R. G. Bates and V. E. Bower, *J. Research Natl. Bur. Standards*, **53**, 283 (1954).

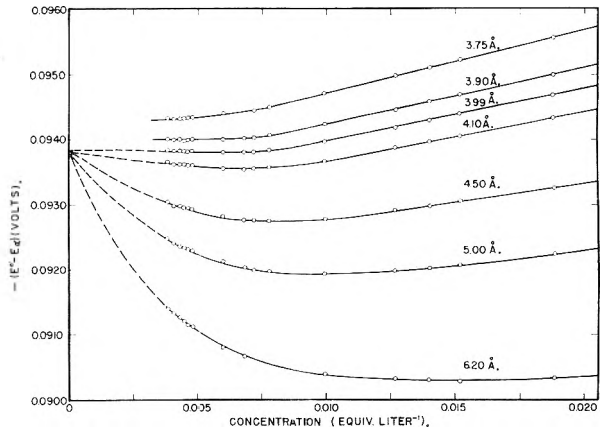

Fig. 2.—Extrapolation of $(E^{0\prime} - E_\alpha)$ for E_c^0.

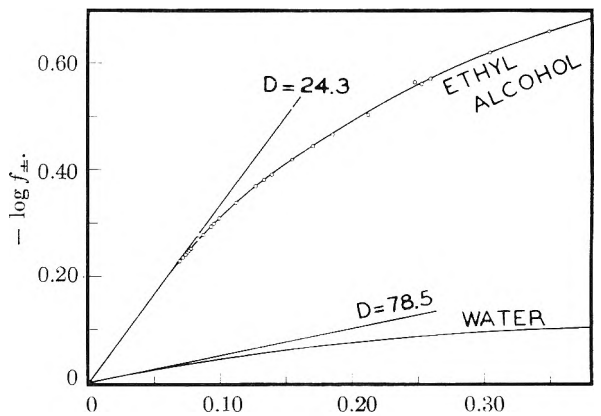

Fig. 3.—Log $f_\pm$ for HCl solutions at 25°.

using the value of −0.08138 v. for the molal standard electrode potential. The activity coefficients at round concentrations are given in Table III, where the last figure has been retained only for computational purposes. Values of the degree of dissociation, calculated in this work, are given in Table IV, the entries at the two lowest concentrations, enclosed in brackets, being extrapolated from the experimental region.

Discussion

As seen in Fig. 1, the present e.m.f.'s are consistently lower than those of Woolcock and Hartley.[4] The difference is 1.2 mv. at 0.1 m, but continuously increases with dilution, being 2.8 mv. at 0.01 m and 3.3 mv. at 0.005 m. This deviation is in the direction to be expected from small amounts of water in the earlier work showing that it becomes increasingly difficult to obtain reliable measurements at low concentrations. Solutions below 0.005 m were not used in the present investigation; instead of relying on critical measurements at extreme dilutions, theoretical aids to extrapolations requiring only moderate dilutions were applied. Thus, a value of −0.08138 v. was realized for E_m^0 when the extrapolation was based on the presence of ion association. The nature of the extrapolations was, however, influenced considerably by the choice of the a parameter, the distance of closest approach. For values greater than that leading to a linear extrapolation, pronounced curvature was

observed, decreasing as this value was approached. For the latter extrapolation, a variation in the distance of closest approach of only 0.1 Å. (3.9 and 4.1 Å., respectively) showed a small, but noticeable slope. The value of 6.2 Å. found to be most satisfactory by Mukherjee[11] to account for the properties of hydrogen chloride in ethanol, is not applicable here. The smallest distance used in the calculations, 3.75 Å. and intermediate values of 4.50 and 5.00 Å. confirm the choice of a = 3.99 Å. as the most satisfactory. The courses of all plots are expected to converge to that for a = 3.99 Å., since in the limiting case the extrapolation is independent of the distance of closest approach.

A distance of closest approach of 3.99 Å. in alcohol is not incompatible with that of 4.3 Å. in water,[25] in spite of the larger alcohol molecule. With the more polar water molecule, it is assumed that the solvation sheath of water molecules is thicker than the sheath of alcohol molecules. In water-organic solvents, the ions become preferentially solvated with water so that the ion-water to ion-center distance remains essentially constant. It is of interest to note that the present value (3.99 Å.) is lower than that used by Scatchard[3] (4.46 Å.) and MacInnes[8] (5.9 Å.) and corresponds to the value used by Bezman and Verhoek[23] in accounting for the conductance of hydrogen chloride in ethanol.

TABLE III

MEAN MOLAL ACTIVITY COEFFICIENTS OF HCl IN ETHANOL AT 25°

m, equiv. kg.$^{-1}$ ethanol	$\gamma_\pm$	m, equiv. kg.$^{-1}$ ethanol	$\gamma_\pm$
0.005	0.5871	0.03	0.3552
.007	.5397	.05	.3000
.01	.4903	.07	.2632
.02	.4018	.1	.2316

Extrapolation of the e.m.f. data by the method based on the Gronwall, La Mer, Sandved extended term theory[12] assuming hydrogen chloride is a strong electrolyte was found possible using an a value of 2.95 Å. but led to an erroneously low value, −0.08022 v., for E_m^0. The Bjerrum critical distance for ion-pair formation in ethanol is 11.53 Å. at 25° so that the extrapolation method based on ion association is theoretically more sound. Although the extrapolations were unambiguous to within 0.02 mv., the experimental variations of the observed e.m.f.'s indicate an accuracy of 0.1 mv. in the values −0.08138 and −0.09383 v. on the molal and molar concentration scales, respectively, for the standard electrode potential of the silver–silver chloride electrode in anhydrous ethyl alcohol at 25°. The values of −0.0740 and −0.0864 v. on the molal and molar scales, respectively, by MacInnes,[8] and −0.0883 v. on the molar scale by Woolcock and Hartley[4] have represented the accepted values to date. The value reported by Mukherjee[11] of +0.00977 v. on the molar scale, on critical examination, is unacceptable since the e.m.f.'s were at 35° rather than 25°. The present values, based on precise data treated by the most theoretically sound extrapolation, may be accepted as reference standards for the silver–silver chloride electrode in absolute ethanol.

It should be noted that the present value of the standard potential of the silver–silver chloride electrode suggests the necessity of revising the value of E_c^0 = −0.0216 v. assigned to the calomel electrode by Danner.[7] If the values of Bates and Bower[25] and of Hills and Ives[13] for the silver–silver chloride electrode and the calomel electrode in water, 0.22234 and 0.26796 v., respectively, are accepted, the difference between the standard potentials is 0.04562 v. Assuming that the difference is the same irrespective of solvents, the standard potential of the calomel electrode in ethyl alcohol would be −0.0358 v. on the molal scale, or −0.0482 v. on the molar scale.

The activity coefficients of hydrogen chloride in ethanol calculated from the results of Woolcock and Hartley[4] deviate from those of the present investigation (Table III) in the direction to be expected by the presence of small amounts of water. At the highest concentrations considered (0.1 m), the difference is about 0.035 unit. This divergence may also be attributed, in part, to the different methods used in extrapolating for the standard electrode potential of the silver–silver chloride electrode. Since the two series of activity coefficients differ by this relatively large amount, a tabular comparison was not attempted.

The relatively great departure from ideality of the activity of hydrogen chloride in ethyl alcohol noted above may be partially attributed to the presence of association of the ions into ion-pairs. In this case, the experimentally observed activity coefficients are not a true measure of the activity coefficients of the *ions* in the solution. The latter coefficients, $\gamma\alpha$ may be termed the quasi-activity coefficients, after Marshall and Grunwald.[26] (The prefix *quasi* has been used here since ion association is not a typical chemical equilibrium in that the two ionized species are parts of a single electrolyte.)

TABLE IV

DEGREE OF DISSOCIATION OF HCl IN ETHANOL AT 25°

m, equiv. kg.$^{-1}$ ethanol	α	m, equiv. kg.$^{-1}$ ethanol	α
0.001	(0.9595)	0.01	0.8332
.002	(.9315)	.015	.8030
.005	.8800	.02	.7812
.007	.8582	.025	.7634

Where there is only partial dissociation, α, the quasi-activity coefficient, γ_α, is given by the simple relation

$$\gamma_\pm = \alpha\gamma_\alpha \qquad (6)$$

where $\gamma_\pm$ is the experimentally observed value. Application of this relation to the present results gave complete agreement between observed and the calculated activity coefficients up to 0.012 m. The concept of ion-pair formation, therefore, is completely adequate at this moderate dilution. At this concentration, hydrogen chloride in ethyl alcohol is 82% present as free ions (Table IV). In contrast to the foregoing, when hydrogen chloride

(26) H. P. Marshall and E. Grunwald, *J. Chem. Phys.*, **21**, 2143 (1953).

in ethyl alcohol is considered as a strong electrolyte and the activity coefficients calculated from the extended term theory (with $a = 3.99$ Å.), there is no agreement even at the lowest experimental concentration.

The considerations presented favor the presence of ion-pairs in solutions of hydrogen chloride in ethyl alcohol at 25°. Since calculations based on this conclusion hold up to at least 0.01 *m*, the results at this concentration cannot be in serious error. Therefore, in the practical standardization of the silver–silver chloride electrode in anhydrous ethyl alcohol at 25° by the method of Bates, *et al.*,[12] the mean molal activity coefficient of hydrogen chloride in ethyl alcohol may be taken as 0.490 (Table III). This contrasts with the value 0.904 proposed[12] for aqueous solutions at 25°.

Acknowledgments.—The authors wish to acknowledge with thanks stimulating discussions with Dr. Roger E. Bates, National Bureau of Standards, in the course of this research. This work was supported by the United States Air Force, Office of Scientific Research, Air Research and Development Command.

NOTES

THE CATALYTIC REDUCTION OF COBALT WITH HYDROGEN FROM AMMONIACAL COBALT SULFATE SOLUTIONS

By Welby G. Courtney[1]

Contribution from Chemical Construction Corporation, New York, N. Y.

Received June 4, 1956

Kaneko and Wadsworth[2] reported observations on the rate of disappearance of Co^{++} from ammoniacal aqueous solution by the graphite-catalyzed reduction of Co^{++} with H_2 to form cobalt metal plus NH_4^+ and/or H^+ at elevated temperatures and pressures.[3] They reported linear reduction rates and proposed that the rate-controlling step in reduction was a reaction between H_2 and $Co(NH_3)_2(H_2O)_2SO_4$ on the surface of the colloidal graphite ("Aquadag," Acheson Colloid Company) added. This note presents several conflicts between the K-W results and interpretations and this writer's observations.

Experimental

The experimental technique generally followed that outlined by K-W. Briefly, a three liter stirred autoclave was used. Teflon packing without lubrication was used in the stuffing box because other work suggested that reduction could be initiated with oil particles. Temperature was controlled to within 0.5° by an electric immersion heater located directly in the charge solution inside the autoclave together with an electrically heated Dowtherm jacket around the body of the autoclave. All metal parts in contact with the charge solution were titanium. Bomb samples were cooled, the sample filtered on the bench, and the filtrate analyzed for cobalt by electrodeposition. Other work indicated negligible dissolution of any basic salt or metal in the sample with this technique. Reagent grade chemicals were used. The H_2 was obtained from the Air Reduction Company and used from the cylinder without purification.

Results indicated that solutions containing 0.1–0.5 *M* $CoSO_4$ and a NH_3/Co^{++} mole ratio of 1.5–5 (typical K-W conditions) precipitated a blue basic cobalt salt at both ambient and elevated temperatures. The presence of $(NH_4)_2SO_4$ increased the solubility of this basic cobalt salt, presumably by buffering the NH_3–NH_4^+ equilibrium. Chemical analysis of the basic salt gave variable results, and a variety of basic cobalt salts have been reported in the literature.[4] Attempts to measure equilibrium solubilities of the basic cobalt salt were unsatisfactory. For example, Co^{++} concentrations which remained constant for 30 minutes at 204° ranged from 0.10 to 0.26 *M* in three runs with solutions initially containing 0.5 *M* $CoSO_4$ and 2 NH_3/CO^{++} and ranged from 0.25 to 0.73 *M* in seven runs initially containing 0.75 *M* $CoSO_4$, 3 NH_3/Co^{++}, and 0.33 *M* $(NH_4)_2SO_4$.

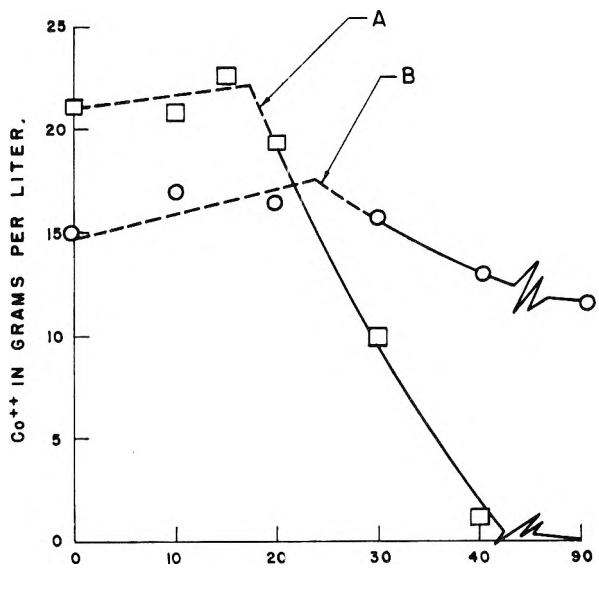

Fig. 1.—Rate of reduction of Co^{++} with H_2 (500 p.s.i.g. partial pressure) at 204°. Zero time was taken at addition of H_2 to the hot autoclave. Dotted lines indicate basic cobalt salt was observed in microscopic examination of a sample; solid lines indicate no basic salt observed. Charges: curve A, 44 g./l. Co^{++} (as the sulfate), 2.1 NH_3/Co^{++}, 100 g./l. cobalt metal seed powder; curve B, 29 g./l. Co^{++} (as the sulfate), 1.9 NH_3/Co^{++}, 44 g./l. $(NH_4)_2SO_4$, 100 g./l. cobalt metal seed.

Typical results of an exploratory study of reduction kinetics in the Co^{++}–H_2 reaction are given in Fig. 1. Both runs were made at 204° and a constant 500 p.s.i.g. H_2 partial pressure. Curve A was obtained with a charge initially containing 0.75 *M* $CoSO_4$, 2.1 NH_3/Co^{++}, and 100 g./l. cobalt metal seed powder (−100 mesh), or typical K-W conditions except for the metal seed added. Curve B was

(1) Experiment Incorporated, Richmond, Virginia.

(2) T. M. Kaneko and M. E. Wadsworth, This Journal, **60**, 457 (1956).

(3) F. A. Schaufelberger and T. K. Roy, *Bull. Inst. Mining Met.*, **581**, 375 (1955); U. S. Patent 2,694,005.

(4) C. W. Stillwell, This Journal, **33**, 1217 (1929); W. Feitknecht and W. Bedert, *Helv. Chim. Acta*, **24**, 676 (1941).

obtained with a charge initially containing 0.5 *M* $CoSO_4$, 1.9 NH_3/Co^{++}, 0.33 *M* $(NH_4)_2SO_4$, and 100 g./l. cobalt metal seed, or conditions where the Co^{++}–H_2–H^+ equilibrium[3] prevents quantitative reduction of Co^{++} to metal. No colloidal graphite was added to either run.

Discussion

The principal K-W arguments for their mechanism appear to be: (1) linear reduction rates "would not be expected if the rate-controlling step takes place at the surface of the growing cobalt metal particle"; (2) the reduction rate was "virtually independent of the nature of the cobalt metal deposit produced"; (3) the reduction rate was proportional to the concentration of colloidal graphite added and was extremely small in the absence of the graphite; and (4) the excellent agreement between the data and their mechanism.

Regarding (1), this writer has observed linear reduction rates during 80% of the reaction in the reduction of Ni^{++} by H_2 from aqueous solutions containing nickel metal seed powder but having no salt precipitate or colloidal graphite.[5] However, these linear rates were proportional to the surface area of the metal particles present. No reduction could be observed in identical runs without seed, indicating negligible homogeneous nucleation of metal particles under the conditions tested. Therefore, the rate-controlling step in the seeded runs was at the surface of the growing nickel metal particles although linear reduction rates were observed, contrary to K-W's assumption. This writer does not have strictly similar data for the Co^{++}–H_2 reaction, but the assumption in (1) is in question.

It may also be noted that K-W analyzed for cobalt in a sample after any cobalt metal had been removed with a magnet. They therefore apparently analyzed the *total* Co^{++} in a sample (solution plus salt) rather than the Co^{++} concentration in the solution alone. Although K-W did not mention the formation of a basic cobalt salt in their work, this writer's results (curve A in Fig. 1) suggest that with typical K-W conditions the Co^{++} concentration *in solution* remains roughly constant during a large portion of the reduction because the basic salt dissolves, tending to maintain the Co^{++} concentration in solution at its equilibrium value. (The early increase in Co^{++} concentration in each curve in Fig. 1 is attributed to the increased equilibrium solubility of the basic salt due to the formation of $(NH_4)_2SO_4$ during the reduction.) Therefore, a constant rate of disappearance of total Co^{++} during the early part of a run would at first glance be not unexpected since growth kinetics are probably concerned with solution composition if anything. However, this writer has observed that with conditions similar to those used by K-W the growing cobalt metal particles were intimately mixed with, and sometimes imbedded in, the salt precipitate during the early part of reduction. Growth kinetics in such a case is difficult to interpret.

Further, linear reduction rates *per se* when the initial mole ratio of NH_3/Co^{++} is less than about 2 (K-W's Fig. 1) is not supported by the present work. In curve B in Fig. 1 of this note, the reduction rate decreased markedly because of approach to equilibrium.

(5) W. G. Courtney, in preparation.

Regarding (2), the "nature" of the metal deposit which K-W produced could perhaps be described more fully. The effect of the surface area of the metal deposit on the gross reduction rate in metal reductions was noted earlier and was also briefly discussed by Schaufelberger.[6]

Regarding (3), this writer had no success in catalyzing the Co^{++}–H_2 reaction with up to eight times the concentration of Aquadag used by K-W. Whether unknown impurities inhibited catalysis in this writer's work or unknown impurities catalyzed K-W's work is of course uncertain.

Regarding (4), an evaluation of K-W's mechanism is difficult in view of the above uncertainties, particularly regarding the importance of linearity of reduction rates. However, the reduction rate of about 60 mg. Co^{++} cc.$^{-1}$ hr.$^{-1}$ obtained in this work with cobalt metal seed alone (the latter part of curve A) is comparable to or even somewhat greater than the reduction rates obtained by K-W with their Aquadag catalyst (K-W's Fig. 1), suggesting that in K-W's work the roles of Aquadag and the metal powder which is formed once reduction has begun must be carefully delineated.

The writer is pleased to acknowledge the advice of Dr. F. A. Schaufelberger, Dr. H. M. Hulburt and Mr. H. Boeckino. Particular thanks are due to Mr. J. Shaw, who conducted the experimental work.

(6) F. A. Schaufelberger, *J. Metals*, **8**, 695 (1956).

THE STABILITY OF METAL CHELATES OF N,N′-ETHYLENEDIANTHRANILIC ACID

BY THOMAS R. SWEET AND WILLIAM F. HARRIS[1]

Department of Chemistry, The Ohio State University, Columbus 10, Ohio

Received August 29, 1956

The stability constants of several transition metals with N,N′-ethylenedianthranilic acid were determined during an investigation of the analytical properties of substituted anthranilic acids. The Bjerrum[2] titration method as modified by Calvin and Wilson[3] was adapted to the present work.

Experimental

Materials.—The N,N′-ethylenedianthranilic acid was prepared by modifying the method of Frankel and Spero.[4] Fifty grams of methyl anthranilate and 15 g. of ethylene bromide were mixed and heated on an oil-bath for 6 hours at 156°. The mixture was cooled and extracted three times with 25-ml. portions of 2 *N* hydrochloric acid. The dianthranilate is insoluble in dilute acid while the unreacted anthranilate is soluble. The insoluble residue was refluxed overnight with 250 ml. of alcoholic potassium hydroxide. The potassium salt of the dianthranilic acid remained as a residue and was filtered and dissolved in water. The dianthranilic acid was precipitated from the water solution with acetic acid. The acid was redissolved in base and reprecipitated with acetic acid from a solution containing 20% alcohol. This gave a slower precipitation and a more crystalline precipitate.

(1) Taken in part from the doctoral dissertation of W. F. Harris presented to the Graduate School of The Ohio State University, August, 1955.

(2) J. Bjerrum, "Metal Amine Formation in Aqueous Solution," P. Haase and Son, Copenhagen, 1941.

(3) M. Calvin and K. W. Wilson, *J. Am. Chem. Soc.*, **67**, 2003 (1945).

(4) J. Frankel and K. Spero, *Ber.*, **28**, 1686 (1895).

The metal solutions were prepared and standardized as indicated in an earlier publication.[5]

The dioxane was purified by the method suggested by Calvin and Wilson.[3]

Procedure.—The weighed reagent was added as a solid to 50 ml. of purified dioxane. Sufficient water, nitric acid and metal nitrate, in the order mentioned were added to bring the final volume to 100 ml. The titrating procedure was the same as that described previously.[5]

Calculations.—The calculations were made by adapting the method of Calvin–Bjerrum to the present situation.

H_2R represents the reagent, N,N′-ethylenedianthranilic acid
K_{a_1} and K_{a_2} represent the acid ionization constants of the reagent
T_M represents the total added metal concentration
T_{H_2R} represents the total added reagent concentration
A represents the total added concentration of HNO_3

From the equations for the conservation of species, charge balance, and ionization constants the following expressions for $R^=$ and $\bar{n}$ were obtained

$$(R^=) = \frac{2T_{H_2R} + A + (OH^-) - (Na^+) - (H^+)}{\frac{2(H^+)^2}{K_{a_1}K_{a_2}} + \frac{(H^+)}{K_{a_2}}}$$

$$\bar{n} = \frac{T_{H_2R} - \frac{(H^+)^2}{K_{a_1}K_{a_2}}(R^=) - \frac{(H^+)}{K_{a_2}}(R^=) - (R^=)}{T_M}$$

Since a titration of the reagent with NaOH showed that the pK value of the protonated nitrogen is less than 2, a consideration of this ionization constant was omitted from the calculations.

Determination of the Ionization Constants of the Reagent.—A titration of the reagent showed only one break even though two carboxyl groups are present. Therefore the ionization constants were determined by Schwarzenbach's graphical method.[6] The experimental procedure was the same as that used for the determination of the formation constants except for the fact that metal salt was not added to the acidified 50% dioxane solution of the reagent.

From the equations for charge balance, conservation of the reagent, and ionization constants the following equation was obtained

$$\frac{1}{K_{a_1}} = \frac{(2T_{H_2R} - b)}{b(H^+)^2}K_{a_2} + \frac{(T_{H_2R} - b)(H^+)}{b(H^+)^2}$$

where

$$b = (H^+) + (Na^+) - (OH^-) - (NO_3^-)$$

A graph $1/K_{a1}$ *versus* K_{a2} was plotted. Each experimental point of the titration curve was represented by one line with a y-intercept given by $[(T_{H_2R} - b)(H^+)]/b(H^+)^2$ and an x-intercept given by $[(b - T_{H_2R})(H^+)]/(2T_{H_2R} - b)$. The lines were found to intersect at the point where $1/K_{a1} = 2.8 \times 10^6 \pm 0.4 \times 10^6$ and $K_{a2} = 6.7 \times 10^{-8} \pm 0.6 \times 10^{-8}$. Therefore $pK_{a1} = 6.45 \pm 0.07$ and $pK_{a2} = 7.17 \pm 0.04$.

Results and Discussion

Using metal concentrations between 0.9×10^{-3} and 1.3×10^{-3} molar and reagent concentrations from 3.5×10^{-3} to 5.2×10^{-3} molar, the following K values for the copper, nickel, cobalt, zinc and cadmium complexes were obtained at 35°: 1.8×10^{10}, 3.6×10^8, 2.8×10^6, 1.2×10^6 and 1.1×10^6.

The order of stability of the metals with N,N′-ethylenedianthranilic acid was found to be copper, nickel, cobalt, zinc and cadmium.

In general there is a significant increase in stability of metal complexes of the N,N′-derivative of anthranilic acid over previously studied stabilities of complexes of anthranilic acid and substituted anthranilic acids in 50% dioxane.[7]

(5) W. F. Harris and T. R. Sweet, *J. Am. Chem. Soc.*, **77**, 2893 (1955).

(6) G. Schwarzenbach, A. Willi and R. D. Bach, *Helv. Chim. Acta*, **30**, 1303 (1947).

(7) W. F. Harris and T. R. Sweet, THIS JOURNAL, **60**, 509 (1956).

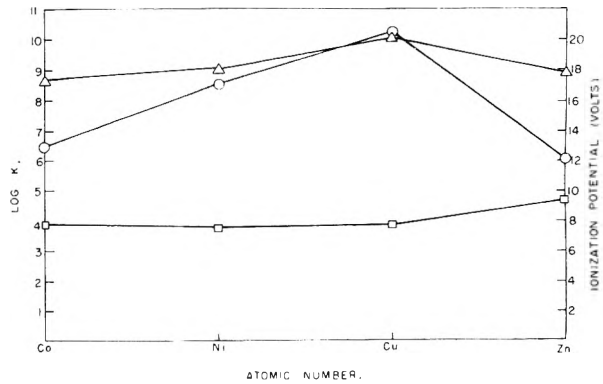

Fig. 1.—○, log K N N′-ethylenedianthranilic acid; □, first ionization potential; △, second ionization potential.

A correlation between the stability of the metal complexes of N,N′-ethylenedianthranilic acid in 50% dioxane and the second ionization potential of the metal is shown in Fig. 1. The figure also shows that there is very little relationship between the stability and the first ionization potential. This is similar to the relationship found by Calvin and Melchior[8] between metal chelates of 5-salicylaldehyde sulfonate and the ionization potentials of the metals.

(8) M. Calvin and N. C. Melchior, *J. Am. Chem. Soc.*, **70**, 3270 (1948).

ON THE MENISCUS IMAGE IN THE ULTRACENTRIFUGE

BY PING-YAO CHENG[1]

Contribution from the Church Laboratories of Chemical Biology, California Institute of Technology, Pasadena, California

Received November 15, 1956

The recent modification of the Archibald method[2] for the determination of molecular weight, developed by Klainer and Kegeles,[3] is reported to give results in agreement with those obtained by other methods.[3,4] In the modified method the concentration gradient, dc/dr, at the meniscus is determined by extrapolation carried out to the center position of the image produced by the meniscus on a photographic plate.[4] The present communication summarizes an investigation of the effect of surface tension at the meniscus on the reliability of the molecular weight value so obtained.

A cell filled with a solution of 0.1% desoxyribonucleic acid (DNA) in 0.2 N NaCl was balanced against a reference cell to within 10 mg. It was then ultracentrifuged at 59,780 r.p.m. in a Spinco (Model E) to form a sharp DNA boundary; after that the speed was varied. Photographs were taken at the different speeds, and the widths of the meniscus and the DNA boundary images were measured at the same level well above the base line with the aid of a high-precision microphotometer (in the Department of Astrophysics of this Institute). The widths of both decreased, but by different amounts, as the speed increased. The width of the meniscus

(1) The Rockefeller Foundation Virus Laboratories, New York.

(2) W. J. Archibald, THIS JOURNAL, **51**, 1204 (1947).

(3) S. M. Klainer and G. Kegeles, *ibid.*, **59**, 952 (1955).

(4) S. M. Klainer and G. Kegeles, *Arch. Biochem. Biophys.*, **63**, 247 (1956).

image changed from 0.016 cm. at 10,000 r.p.m. to 0.010 cm. at 55,000 r.p.m., while that of the DNA boundary decreased only 0.003 cm. under the same conditions. Part of the decreased width of the DNA boundary must be attributed to the strong concentration dependence of sedimentation coefficient of DNA.

If the centrifugal force at low speed were sufficient to overcome the surface tension of the meniscus, the decrease in the width of the meniscus image would have been somewhat smaller than the decrease in the width of the DNA boundary. That the contrary was found to be the case indicates that at low speed the effect of residual surface tension is manifested at the meniscus, and that the radius of curvature of the meniscus may be measurably less than the radius of rotation. Thus the effective meniscus position at which the Archibald method applies may differ, in general, from the center position of the image of the meniscus. As shown by the typical example in Table I, the extrapolated concentration gradient at the meniscus, hence the molecular weight, is inaccurate by 1%, when an error of 0.001 cm. is allowed in the calculation of the meniscus position. Therefore, because of the surface tension effect alone, the reliability of the molecular weight values obtained by the modified Archibald method is greater for experiments performed at high rotor speeds.

TABLE I

REFRACTIVE INDEX-GRADIENT CURVE OF BOVINE SERUM ALBUMIN SOLUTION[a]

r, cm.	Δr, cm.	Ordinate, cm. $\omega dc/dr$	Δ(dc/dr)/(dc/dr)
5.987		0.126	
	−0.026		0.6
5.961		0.247	
	−0.025		0.5
5.936		0.428	
	−0.025		0.4
5.911		0.648	
	−0.025		0.3
5.886		0.867	

[a] A 1% protein solution in 0.15 *M* NaCl and 0.05 *M* sodium acetate buffer, *p*H 4.4, was centrifuged at 8,500 r.p.m. for 32 min. The curve was obtained by the schlieren optical system equipped with a phase plate.[5]

Acknowledgment.—The author is indebted to Dr. L. G. Longsworth for his critical examination of the manuscript and to Professors G. Munch and J. E. Snoke for making their instruments available.

(5) R. Trautman and V. W. Burns, *Biochim. Biophys. Acta*, **14**, 26 (1954).

SULFATE COMPLEXES OF TIN(IV)

BY CARL H. BRUBAKER, JR.

Kedzie Chemical Laboratory, Michigan State University, East Lansing, Mich.

Received December 4, 1956

In an earlier paper[1] we described the changes which occur in the ultraviolet absorption spectrum of tin(IV) solutions as the sulfuric acid concentration is varied and an interpretation of these changes was offered. However, later work[2] indicated that the predominant species of tin(IV) present in dilute acid is not a partially hydrolyzed one, such as the SnO^{++} we originally proposed,[1] but rather is $SnSO_4^{++}$. In addition, our earlier work was based on data on the dissociation of sulfuric acid which appear to be incorrect in the light of recent studies by Smith.[3]

Carter[4] has suggested that the first spectral change corresponds to the formation of $SnSO_4^{++}$ and has based his arguments on the sulfate ion concentrations found by Smith.[3] However, since our later work showed that, even in very dilute sulfuric acid, $SnSO_4^{++}$ is the principal species, still another interpretation had to be sought.

We now believe that the two spectral changes, which we observe as the sulfuric acid concentration is changed from 1 to 17 *M*, correspond to the complex formation steps

$$SnSO_4^{++} + SO_4^{=} = Sn(SO_4)_2(aq.) \quad K_1 \quad (1)$$

$$Sn(SO_4)_2(aq.) + H_2SO_4 = H_2Sn(SO_4)_3(aq.) \quad K_2 \quad (2)$$

Indeed, if we can accept our findings concerning $SnSO_4^{++}$ and the evidence[5] on the probable existence of the tris-(sulfato) complex in concentrated sulfuric acid, we could scarcely escape such conclusions.

Consider, first, reaction 1. We write the equilibrium constant expression

$$K_1 = \frac{a_{Sn(SO_4)_2}}{a_{SnSO_4^{++}}\, a_{SO_4^{=}}} = \frac{[Sn(SO_4)_2]}{(SnSO_4^{++})(SO_4^{=})y^2_{\pm}} \quad (3)$$

where $y\pm$ is the mean activity coefficient for the 2–2 electrolyte $(SnSO_4^{++})(SO_4^{=})$.

We noted[1] that the extinction coefficient, ϵ_2, of the second species must be much less than, ϵ_1, of the initial species. Then in less than 4 *M* sulfuric acid (*i.e.*, when there is negligible $H_2Sn(SO_4)_3$) we see that since

$$D_{obsd}/0.1(Sn^{IV}) = \epsilon_{obsd}$$

$$D_{obsd} \cong 0.1\epsilon_1(SnSO_4^{++})$$

and

$$(Sn^{IV}) \cong (SnSO_4^{++}) + (Sn(SO_4)_2)$$

then, 4.

$$\frac{1}{\epsilon_{obsd}} = \frac{1}{\epsilon_1} + \frac{1}{\epsilon_1} K_1(SO_4^{=})y^2_{\pm} \quad (4)$$

$D_{obsd.}$ is the observed optical density, 0.1 is the length of cell path and (Sn^{IV}) is the total tin(IV) concentration.

Following the reasoning we have previously employed,[2] we estimate the empirical correction constants, α_{12}, and obtain γ_1, the corrected activity coefficients for $(SnSO_4^{++})(SO_4^{=})$ from γ_{10}, the activity coefficients of a typical "pure" 2–2 electrolyte. Then γ_1 are converted to $y_{\pm}$, the activity coefficients on the molar scale (Table I).

Our values of ϵ_{obsd} at 240 mμ are taken from the earlier work[1] and are given in Table I, column 9.

Now according to equation 4, we plot $1/\epsilon_{obsd}$ against $(SO_4^{=})\ y^2_{\pm}$ (Fig. 1) and find a reasonably good straight line. We obtain $\epsilon_1 = 2.5 \times 10^3$ and $K_1 = 1.9 \times 10^2$.

Previously we had estimated $\epsilon_1 = 1.6 \times 10^3$ on the basis of spectrophotometric examinations

(1) C. H. Brubaker, Jr., *J. Am. Chem. Soc.*, **76**, 4269 (1954).
(2) C. H. Brubaker, Jr., *ibid.*, **77**, 5255 (1955).
(3) H. M. Smith, Ph.D. thesis, University of Chicago, 1949.
(4) P. R. Carter, private communication.
(5) R. F. Weinland and H. Kuhl, *Z. anorg. Chem.*, **54**, 244 (1907).

TABLE I

OBSERVED MOLAR EXTINCTION COEFFICIENTS, SULFURIC ACID CONCENTRATIONS, ACTIVITY COEFFICIENTS AND VARIOUS DERIVED QUANTITIES FOR 1.65×10^{-3} M Sn(IV) IN SULFURIC ACID

1 (H_2SO_4), M	2 (SO_4^-), M	3 μ (molal)	4 γ_{10} ($ZnSO_4$)	5 γ_{20} (H_2SO_4)	6 $-\alpha_{12}$	7 γ_1	8 $y^{\pm}$	9 $\epsilon_{obsd.} \times 10^{-3}$
3.48	1.13	6.70	0.0364	0.174	0.067	0.102	0.119	0.648
3.19	1.03	6.02	.0368	.157	.069	.096	.110	0.743
2.24	0.703	3.98	.0434	.130	.078	.089	.097	1.02
1.80	.554	3.12	.0488	.124	.085	.090	.097	1.33
1.50	.450	2.56	.0543	.124	.091	.093	.099	1.41
1 35	.400	2.26	.0590	.123	.093	.096	.101	1.51
0 910	.248	1.45	.0759	.130	.105	.107	.110	1.56

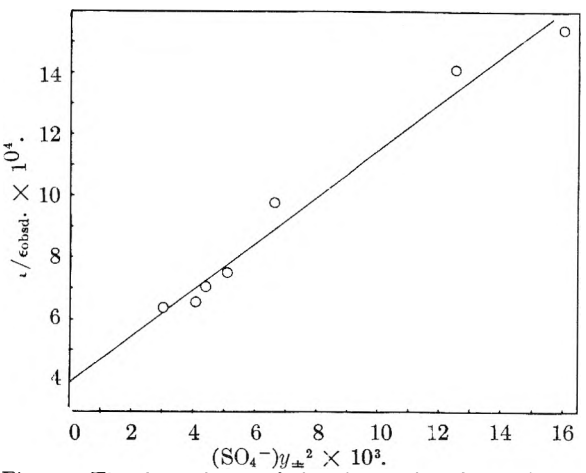

Fig. 1.—The dependence of the observed molar extinction coefficient on sulfate ion activity.

of tin(IV) in perchloric acid, but in view of our later findings that $SnSO_4^{++}$ is the predominant species in dilute sulfuric acid, we can hardly expect the limiting molar extinction coefficient, ϵ_1, in sulfuric acid to be the same as is observed in perchloric acid.

In view of the values of the activity coefficients for 2–2 electrolytes and the fact that there is necessarily some uncertainty in the correction of them, we should probably accept ϵ_1 and K_1 as representing orders of magnitude only. However, we have found that the treatment is not particularly sensitive to the magnitude of $y_{\pm}$ and thus the scatter (Fig. 1) is probably experimental.

Thus it seems safe to conclude that the first spectral change does correspond to the formation of $Sn(SO_4)_2$ from $SnSO_4^{++}$ and that the equilibrium constant is about 10^2.

The second spectral change should correspond to equation 2 and the interpretation which was offered in the previous work will still apply.

This work was supported by the U. S. Atomic Energy Commission.

LATTICE CONSTANTS OF POTASSIUM BROMIDE–POTASSIUM IODIDE SOLID SOLUTIONS[1]

BY EUGENE T. TEATUM AND NORMAN O. SMITH

Department of Chemistry, Fordham University, New York, N. Y.

Received December 20, 1956

(1) Presented before the Division of Physical and Inorganic Chemistry of the American Chemical Society at Atlantic City, September, 1956.

In the course of studies of the mutual solubility of partially miscible solids it became necessary to measure the variation of lattice constant with composition for solid solutions of potassium bromide in potassium iodide. The only previous values of lattice constants in this system are those of Havighurst, Mack and Blake,[2] but the range of compositions studied was very limited and the data inconsistent and meager. These two salts form an incomplete series of solid solutions at room temperature[3] but their mutual solubility increases to complete miscibility at temperatures well below the melting point.[4] By quenching molten mixtures of the two salts it is easy to obtain solid solutions over the entire range of composition at room temperature even though the solids in the large central portion of this range are then metastable.

Reagent grade potassium bromide and potassium iodide were recrystallized from water and dried. Various mixtures, weighing about one gram, were placed in Pyrex tubes (7 mm. o.d.) sealed at one end, and melted together under vacuum. (This was necessary to prevent decomposition and discoloration.) They were then sealed off while evacuated, and quenched in mercury. Compositions which fell within the miscibility gap maintained their metastability for a period more than long enough to permit taking X-ray powder photographs. This was done using a G.E. XRD-3 unit with Cu $K\alpha$ radiation, the wedge technique being adopted in all cases. The films were measured with a G. E. Fluorline Illuminator and the various lattice constants calculated. Simultaneously each sample was analyzed by potenticmetric titration with standard silver nitrate, using silver and saturated calomel electrodes with an ammonium nitrate salt bridge. Both the bromine and iodide end-points were observed. Such analysis was necessary because the composition of the original mixture could not be relied upon after the heating under vacuum.

TABLE I

LATTICE CONSTANTS OF KBr–KI SOLID SOLUTIONS

Composition, mole fraction of KI	Lattice constant, Å.	Dev. from additivity Å. $\times 10^3$	Composition, mole fraction of KI	Lattice constant, Å.	Dev. from additivity Å $\times 10^3$
0.0000	6.599	...	0.568	6.881	+21
.0707	6.624	− 8	.658	6.925	+23
.0977	6.64_	− 8	.740	6.947	+12
.2128	6.705	+ 8	.766	6.949	− 2
.2685	6.734	+11	.878	7.001	− 2
.3352	6.760	+ 7	.902	7.030	+16
.448	6.820	+15	.918	7.060	+39
.495	6.848	+21	1.000	7.059	...

(2) R. J. Havighurst, E. Maek, Jr., and F. C. Blake, *J. Am. Chem. Soc.*, **47**, 29 (1925).

(3) M. Amadori and G. Pampanini, *Atti. accad. Lincei*, **20**, [II] 473 (1911).

(4) J. B. Wresnewsky, *Z. anorg. Chem.*, **74**, 95 (1912).

Table I gives the resulting data. Each lattice constant is an average of the values calculated for the three or four lines with greatest glancing angle, and the average deviation for any one film was about 0.005 Å. The inherent lack of accuracy of the wedge technique, however, is good reason for believing that the uncertainty in the lattice constants is about 0.008 Å. The compositions are believed accurate to a mole fraction of 0.0002. The lattice constants for the pure components, *viz.*, 6.599 and 7.059 Å. for the bromide and iodide, respectively, may be compared with the most recent figures of the National Bureau of Standards,[5] 6.6000 and 7.0655 Å., at 25°. Lack of temperature control in the present work would not account for differences greater than 0.002 Å. Except for some irregularity for the highest potassium iodide contents, the cause of which is not certain, the values lie on a smooth curve within experimental error. Shown also in Table I are the deviations of the experimental values from those predicted by Vegard's rule of additivity. The positive deviations in the central composition range are believed to be real.

(5) H. E. Swanson and E. Tatge, "Standard X-Ray Diffraction Powder Patterns," Vol. 1, National Bureau of Standards, 1953, pp. 66, 68.

THE INTENSITY OF INFRARED O–H ABSORPTION FOR SOME TERTIARY ALIPHATIC ALCOHOLS; THE INDUCTIVE PROPERTIES OF THE CYCLOPROPYL GROUP

BY THEODORE L. BROWN, J. M. SANDRI AND H. HART

A Joint Contribution from Noyes Chemical Laboratory, University of Illinois, Urbana, Ill., and Kedzie Chemical Laboratory, Michigan State University, East Lansing, Michigan

Received December 21, 1956

Measurement of the integrated intensity of infrared absorption for compounds in solution is capable of providing information about the electronic properties of molecules, particularly when the variation in intensity throughout a series of related compounds is investigated. Recently it has been shown that the intensity of absorption of the O–H group in aliphatic alcohols is determined almost completely by the inductive properties of the groups attached to the hydroxyl.[1] In the present paper these results are used in interpreting the measurements of the O–H intensity for a series of tertiary alcohols.

Experimental

Method.—The procedure used in determining the intensities has been described previously.[1] In the present work a Perkin–Elmer Model 112 spectrometer with lithium fluoride optics was employed. Use of a mechanical slit width of 0.1 mm. resulted in a spectral slit width of about 4.5 cm.$^{-1}$. A cell thickness of 1.00 mm. was employed; solution concentrations were in the range 0.03–0.01 *M*.

Materials.—Fresh bottles of reagent grade carbon tetrachloride were used in making up the solutions. *t*-Butyl alcohol and 3-ethyl-3-pentanol were Eastman White Label materials, carefully fractionated prior to use. The preparation and properties of tricyclopropylcarbinol have been described.[2] The other alcohols have been described elsewhere.[3]

(1) T. L. Brown and M. T. Rogers, *J. Am. Chem. Soc.*, **79**, 577 (1957).

Results

The results of measurements on six tertiary alcohols are shown in Table I. The first column after the compound name lists the integrated intensity A', in units of 1×10^4 mole^{-1} liter cm.$^{-2}$. The second column lists the half-intensity width, $\Delta\nu_{1/2}$, in units of cm.$^{-1}$, and the third lists the frequencies of band maxima, ν_m. From the values of $\Delta\nu_{1/2}$ listed it is possible to apply wing corrections as described by Ramsey.[4] These corrections would be of the same order of magnitude for all the compounds listed, and would not change the relative values of intensity appreciably. The relative intensity values are probably correct to 0.02 intensity unit, while the values of ν_m are within 2 cm.$^{-1}$.

TABLE I

RESULTS OF THE MEASUREMENT OF THE O–H BAND INTENSITY FOR SIX TERTIARY ALIPHATIC ALCOHOLS

Compound	A'[a]	$\Delta\nu_{1/2}$ (cm.$^{-1}$)	ν_m (cm.$^{-1}$)
t-Butyl alcohol	0.33	22	3613
Triethylcarbinol	.25	19	3617
Triisopropylcarbinol	.22	25	3625
Diisopropylcyclopropylcarbinol	.28	24	3622
Isopropyldicyclopropylcarbinol	.33	25	3617
Tricyclopropylcarbinol	.37	20	3620

[a] In units of 1×10^4 mole^{-1} liter cm.$^{-2}$.

Discussion

It is noteworthy that although different optics were used, the result obtained here for *t*-butyl alcohol is in excellent agreement with that obtained previously.[1]

The decrease in intensity which accompanies increased branching of the alkyl groups attached to the carbinol is to be expected, since the intensity is known to decrease with increasing electron-donating power of the attached groups.[1] The intensity for the tricyclopropyl compound, however, is much larger than that for the triisopropyl compound, and is in fact larger than that for the trimethyl. Since the value of intensity for the tricyclopropyl compound lies between that for *t*-butyl alcohol and methyl alcohol ($A' = 0.45$),[1] it is to be concluded that the cyclopropyl group exhibits a +I effect relative to hydrogen, but is less electron-donating than the methyl group. This behavior may be compared with that shown by the vinyl group; the intensity result for allyl alcohol ($A' = 0.48$)[1] shows that the vinyl group exhibits a −I effect relative to hydrogen. The intensity for trivinylcarbinol would probably be much larger than 0.48, and considerably greater than that for the tricyclopropyl compound.

In the picture of the cyclopropyl group given by Walsh the bonds to cyclopropyl are made with carbon sp^2 hybrid orbitals.[5] Since this is the same hybridization as that possessed by the carbons in the vinyl group it might be expected that the inductive properties of the two groups would be similar, and Walsh has cited some evidence that this is the case.

(2) H. Hart and J. M. Sandri, *Chemistry and Industry*, 1014 (1956).
(3) J. M. Sandri, Ph.D. Thesis, Michigan State University, 1956.
(4) D. A. Ramsey, *J. Am. Chem. Soc.*, **74**, 72 (1952).
(5) A. D. Walsh, *Trans. Faraday Soc.*, **45**, 179 (1949).

The present results indicate that the vinyl group is more electron-withdrawing than the cyclopropyl, but are not seriously at variance with this picture. The correlation of the intensity results with pK_a values for the various groups attached to carboxyl is reasonably good.[6]

There does not appear to be any systematic frequency effect present, especially in those compounds containing the cyclopropyl group.

Acknowledgment.—Thanks are due Dr. H. G. Drickamer for his coöperation in the use of the infrared instrument.

(6) E. A. Braude and F. C. Nachod, "Determination of Organic Structures by Physical Methods," Academic Press, Inc., New York, N. Y., 1955, p. 573.

STUDY OF THE ISOTOPIC EXCHANGE BETWEEN Te(IV) AND Te(VI) IN ACID SOLUTION[1]

BY M. W. HANSON AND T. C. HOERING

Department of Chemistry, University of Arkansas, Fayetteville, Arkansas

Received January 10, 1957

It has been observed[2] that there is no appreciable exchange at the end of six hours, either at ordinary temperature or at 90 to 95°, between tellurium in H_2TeO_6 and H_6TeO_6. An exchange has been detected and the rate constant determined[3] at different temperatures for the system $Te/TeCl_4$ in $0.1M$ hydrochloric acid.

An investigation was undertaken to determine if there was an exchange between Te(IV) and Te(VI) of the system TeO_2/H_6TeO_6 in acid solution. It was found that both concentrated and $6M$ hydrochloric acid reduced Te(VI) to Te(IV) so rapidly the reaction could not be studied in this medium. Perchloric acid was then chosen as a reaction medium because of its non-complexing nature.

Subsequent studies showed there was no detectable exchange over a period of four days between $0.05M$ solutions of the two ions in $6M$ perchloric acid at a temperature of 30°. Heating an identical mixture at a temperature of 95 to 100° for a period of 24 hours did not induce an exchange between the ions.

A solution was prepared which was $6M$ in hydrogen ion and $3M$ in chloride ion and $0.05M$ in Te(IV) and Te(VI) ions. There was no evidence, after a period of 4 days, of an exchange between Te(IV) and Te(VI) in the solution which was maintained at a temperature of 30°. Heating an identical mixture for 24 hours at 95° to 100° did not cause an exchange between the two ions.

The radio-tellurium, ^{132}Te, was separated from the fission products of irradiated U_3O_8. The experimentally determined 77 hour half-life corresponds to the accepted value for ^{132}Te. The TeO_2 was prepared by the method of Marshall[4] and the H_6TeO_6 by the method of Horner and Leonard.[5]

(1) This work made possible through an A.E.C. contract.

(2) M. Haissinsky and M. Cottin, *Anal. Chim. Acta*, **3**, 226 (1949).

(3) M. Haissinsky, M. Cottin and B. J. Varjabedian, *J. chim. phy.*, **45**, 212 (1948).

(4) H. Marshall, "Inorganic Preparations," Vol. III, McGraw-Hill Book Co., Inc., New York, N. Y., p. 1-3.

(5) H. J. Horner and G. W. Leonard, Jr., *J. Am. Chem. Soc.*, **74**, 3694 (1954).

THE KINETICS OF THE DECOMPOSITION OF OXALIC ACID IN NON-AQUEOUS SOLVENTS

BY LOUIS WATTS CLARK

Contribution from the Department of Chemistry, Saint Joseph College, Emmitsburg, Maryland

Received January 21, 1957

The decarboxylation of malonic acid has been studied in several non-aqueous solvents including quinoline, aniline, dimethylaniline, pyridine and picolines.[1-4] Ogata and Oda[2] observed that the undissociated form of the acid decomposed in aniline and dimethylaniline, and Corey[5] has shown that malonic acid is not appreciably dissociated in pyridine or quinoline. Fraenkel and co-workers[1] have postulated that an intermediate unstable compound is formed between acid and quinoline, in which a carboxyl carbon atom solvates with the unpaired electrons on nitrogen. The monoion has been found to be more stable than the diacid, and the malonate ion appears to be unreactive.[6] In view of the close similarity in structure between malonic acid and oxalic acid, it would be expected that oxalic acid would undergo decarboxylation in the same media as malonic acid and that the mechanism would be similar in both cases. The decomposition of oxalic acid has been studied previously in dioxane[7] and in glycerol[8] wherein decarboxylation took place smoothly in accordance with first-order kinetics.

The present paper describes the results of kinetic studies made in this Laboratory on the decomposition of oxalic acid in the solvents dimethyl sulfoxide, triethyl phosphate, quinoline, aniline, N-methylaniline and N,N-dimethylaniline.

Experimental

Reagents.—(1) Oxalic acid, anhydrous, Analytical Reagent Grade, Assay 100.0%; (2) dimethyl sulfoxide (99.9%); (3) triethyl phosphate, sp. gr. 20°/4°, 1.065–1.070, chlorides, less than 5 p.p.m., sulfates none, acidity not more than 0.03% calculated as H_3PO_4, ester content 97% minimum, b.p. 216°, refractive index $n^{25}D$ 1.404; (4) quinoline, Reagent Grade, boiling range 235–237°; (5) aniline, Reagent Grade, boiling range 183.9–184.3°; (6) N-methylaniline, Reagent Grade, sp. gr. 0.989 boiling range 81–82° (14 mm.); (7) N,N-dimethylaniline, Reagent Grade, boiling range 194.0–194.3°.

Apparatus and Technique.—The kinetic experiments were conducted in a constant temperature oil-bath by measuring the volume of CO_2 evolved at constant pressure, as described in a previous paper.[9] In each experiment a 0.1605-g. sample of oxalic acid (the amount required to produce 400 ml. of CO_2 at STP on complete reaction) was introduced in the usual manner into the reaction flask containing 100 ml. of the solvent which had been previously saturated with dry CO_2 gas.

Results and Discussion

The final corrected volume of CO_2 obtained was

(1) G. Fraenkel, R. L. Belford and P. E. Yankwich, *J. Am. Chem. Soc.*, **76**, 15 (1954).

(2) Y. Ogata and R. Oda, *Bull. Inst. Phys. Chem. Research (Tokyo), Chem. Ed.*, **23**, 217 (1944); *C. A.*, **43**, 7904d (1949).

(3) L. W. Clark, THIS JOURNAL, **60**, 1340 (1956).

(4) L. W. Clark, *ibid.*, **60**, 1583 (1956).

(5) E. J. Corey, *J. Am. Chem. Soc.*, **75**, 1172 (1953).

(6) G. A. Hall, *ibid.*, **71**, 2691 (1949).

(7) A. Dinglinger and E. Schéber, *Z. physik. Chem.*, **A179**, 401 (1937).

(8) L. W. Clark, *J. Am. Chem. Soc.*, **77**, 6191 (1955).

(9) L. W. Clark, THIS JOURNAL, **60**, 1150 (1956).

98–100% of the theoretical yield for all experiments except those in dimethyl sulfoxide at higher temperatures. In this solvent a very slow secondary decomposition of formic acid appeared to take place above 170°. When log $(a - x)$ was plotted against t, where a is the maximum theoretical yield of CO_2 and x is the volume of gas produced at the time t, straight lines resulted in each case, hence the reactions were first order. From the slopes of the lines thus obtained the rate constants were calculated. Typical plots of the original data and their logarithm-plot equivalent are shown in Fig. 1, and the rate constants in each solvent at each temperature studied are collected in Table I.

TABLE I

FIRST-ORDER RATE CONSTANTS FOR THE DECARBOXYLATION OF OXALIC ACID IN SEVERAL NON-AQUEOUS SOLVENTS AT VARIOUS TEMPERATURES

Solvent	Temp., °C.	$k \times 10^5$ (sec.$^{-1}$)
Triethyl phosphate	160.9	128
	170.8	273
	180.8	583
Dimethyl sulfoxide	155.9	47.4
	166.1	148
	170.9	246
Quinoline	165.9	89.7
	175.9	251
	186.1	676
Aniline	149.4	44
	157.9	118.5
	167.9	350
N-Methylaniline	162.4	76.8
	164.1	92
	166.4	115
	177.6	318
N,N-Dimethylaniline	159.4	60
	164.1	92
	169.8	150
	174.3	200

tion in quinoline and in aniline (lines 3 and 4), we see that the activation energy and enthalpy of activation are lower in quinoline than in aniline. This suggests that the unshared electrons on nitrogen are slightly more available in quinoline than in aniline. The enthalpy of activation, which is related to the probability of the formation of the activated complex, is lower in quinoline than in aniline. The data for malonic acid in these two solvents[1,3] parallel those for oxalic acid. These results are in line with the expectation that an increase in molecular complexity should cause a decrease in the entropy of activation.[10]

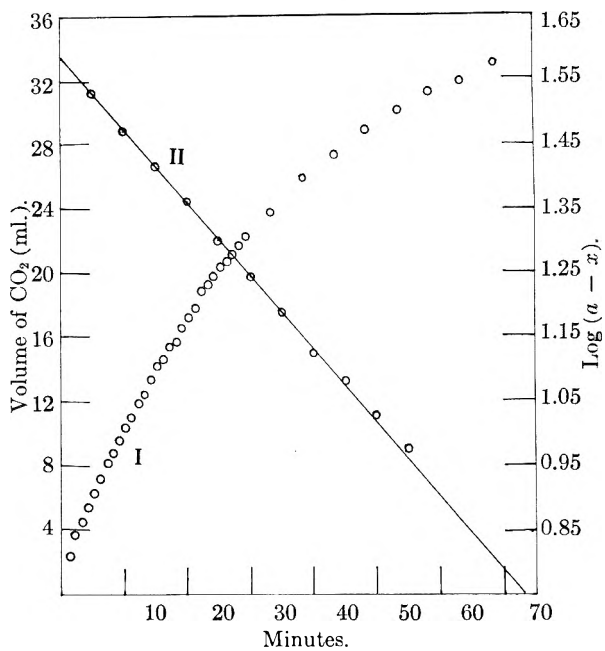

Fig. 1.—Decomposition of 0.1605 g. of oxalic acid in 100 ml. of aniline at 149.4°: I, volume of CO_2 (ml.); II, log $(a - x)$.

The effect on the reaction of varying the structure of aniline by introducing first one, and then two, methyl groups on nitrogen is brought out by

TABLE II

KINETIC DATA FOR THE DECOMPOSITION OF OXALIC ACID IN SEVERAL NON-AQUEOUS SOLVENTS

	Solvent	E^* (cal.)	A (sec.$^{-1}$)	ΔH^* (cal.)	ΔS^* (e.u.)	ΔF^* (cal.)	$k \times 10^5$ (sec.$^{-1}$) (at 140°)
(1)	Dimethyl sulfoxide	40,650	3.0×10^{17}	40,600	+20.7	31,050	9.5
(2)	Triethyl phosphate	29,950	1.74×10^{12}	28,850	− 5.8	31,250	22.0
(3)	Quinoline	40,130	1.0×10^{17}	38,900	−15.75	45,400	5.0
(4)	Aniline	41,450	1.45×10^{18}	40,280	+16.2	33,580	14.5
(5)	N-Methylaniline	35,850	5.76×10^{14}	35,500	+ 8.25	32,100	5.8
(6)	N,N-Dimethylaniline	33,100	3.39×10^{13}	32,400	+ 1.25	31,900	9.5

Straight lines were obtained in each case on plotting log k *vs.* $1/T$ according to the Arrhenius equation. Activation energies and frequency factors for the reaction in each solvent were thus obtained. From the Eyring equation enthalpies of activation, entropies of activation and free energies of activation at 140° were calculated. The results are summarized in Table II.

If we consider the data in Table II for the reaction the data in lines 4, 5 and 6 of Table II. If the mechanism for the decomposition of oxalic acid is similar to that for malonic acid, it would be anticipated that a methyl group on nitrogen, would, due to the positive inductive effect, increase the availability of electrons on nitrogen and thus bring about a decrease in the enthalpy of activation.

(10) L. P. Hammett, "Physical Organic Chemistry," McGraw-Hill Book Co., New York, N. Y., 1940, p. 126.

At the same time the steric factor would be expected to decrease the entropy of activation, in other words render less probable the formation of the activated complex. Both these expectations are verified by the data.

By introducing two methyl groups, doubling the positive inductive effect, it would be predicted that the activation energy or heat of activation would be lowered still further, and, at the same time, the increased steric hindrance would decrease the probability of the formation of the activated complex still more manifesting itself by a further decrease in the entropy of activation. Again the results completely confirm these expectations. Two methyl groups have almost double the effect, in each case, of a single methyl group.

It appears highly probable, in the light of these results, that the mechanism for the decomposition of oxalic acid in aromatic amines and other nonaqueous solvents is quite similar to that for malonic acid. Evidently the unshared pair of electrons on the basic atom links with the undissociated acid to form the activated complex, facilitating cleavage.

Acknowledgment.—This research was supported by the Raskob Foundation, Wilmington, Delaware.

ON THE DETERMINATION OF THE DIFFERENTIAL CAPACITY AT A DROPPING MERCURY ELECTRODE

BY DAVID C. GRAHAME

Contribution from the Moore Laboratory of Chemistry, Amherst College, Amherst, Mass.

Received January 11, 1957

In the determination of the differential capacity at a dropping mercury electrode there is a minor experimental difficulty which seems to give trouble to most investigators, including ourselves. It is necessary to measure with precision the time which elapses from the moment at which the mercury droplet starts to form to the moment at which a bridge balance appears on the screen of an oscilloscope.[1] An electric clock (2 r.p.s.) is used for this purpose in our laboratory, but considerable electronic and mechanical skill is needed to keep the whole mechanism functioning correctly. A much simpler method has now been devised, and its accuracy is such that it can be used to calibrate and to check the older method.

In the new method an electric clock is used as before to produce pulses at the rate of 2 per second. It does this by having its fast-moving (electrically charged) hand touch "cat's whiskers" suitably placed at the periphery of the dial. These pulses trigger the linear sweep of a conventional oscilloscope provided with a long-persistence screen (a Du Mont type 304-A is used in our laboratory) and the sweep speed is set to cover exactly ten centimeters before the next sweep is initiated half a second later. The screen is marked off with ink at half-centimeter intervals.

The bridge is set to provide a balance point preferably within half a second of the moment of fall of the mercury droplet. Under these conditions the moment of fall is clearly marked on the screen because of the abrupt change of impedance at that moment. The persistence of the image on the screen gives one time to read its position relative to the inked-on scale. Then when the next balance point is achieved, its position can also be read off, and the difference gives the fraction of a sweep to be added to an integral number of accurately timed half-second sweeps. The integer is determined simply by counting the sweeps.

The non-linearity of the sweep is not serious in our instrument, but its effects can be eliminated entirely by adjusting the bridge so that the balance point is achieved after an exactly integral number of half seconds.

The advantages of this method are that it is relatively foolproof and easy to build, and that it eliminates uncertainties concerning the time lost in closing mechanical relays. This last is of major importance because the time loss cannot be kept strictly constant and may easily become significantly large as a result of a very slight malfunctioning of the apparatus.

Another experimental matter has to do with the fact that the rate of flow of the mercury through a capillary is not strictly constant owing to the back pressure exerted by the surface tension of the growing droplet.[2] The back pressure is $2\sigma/r$, where σ is the interfacial tension and r is the radius of the drop. Assuming that m, the rate of flow, is *nearly* constant, the radius of the droplet at any time t is $(3mt/4\pi\rho)^{1/3}$. ρ is the density of mercury. If h is the head of mercury, the effective pressure is $h\rho g - 2\sigma(4\pi\rho/3mt)^{1/3}$.

The rate of flow at any instant is proportional to the effective pressure P, so that the volume of the mercury V in the droplet is proportional to $\int P\mathrm{d}t$ or

$$V = k_1 h\rho g t - 3\sigma k_1(4\pi\rho/3m)^{1/3}t^{2/3} \quad (1)$$

$$= k_1 t[h\rho g - 3\sigma(4\pi\rho/3)^{1/3}s^{-1/2}] \quad (2)$$

where k_1 is the constant of proportionality and $s = (mt)^{2/3}$. The area is proportional to the $^2/_3$ power of V, so that

$$\text{Area} = k_2 t^{2/3}[h - (3\sigma/g\rho)(4\pi\rho/3)^{1/3}s^{-1/2}]^{2/3} \quad (3)$$

If the area is considered to be proportional to $t^{2/3}$ when the computation of the differential capacity is made, the result will be too low in the ratio

$$[h - (3\sigma/g\rho)(4\pi\rho/3)^{1/3}s^{*-1/2}]^{2/3} \div [h - (3\sigma/g\rho)(4\pi\rho/3)^{1/3}s^{-1/2}]^{2/3} \quad (4)$$

where s^* is $(mt^*)^{2/3}$ and t^* is the drop time.

Putting $\rho = 13.53$ g./cm.^{3} and expressing h in centimeters gives for small values of the error

$$\text{error} = (0.58\sigma/h)(s^{-1/2} - s^{*-1/2})\ \% \quad (5)$$

Experimentally, the deviation of the apparent value of the capacity with time conforms to this equation rather well. Thus in a wholly typical case, where an error of 1.32% was predicted, an error of 1.45% was observed. In an extreme case an error of 3.98% was predicted and an error of 3.75% observed. In dilute solutions (<0.01 N) there are other sources of error of comparable magnitude which tend to mask the agreement, however.

(1) D. C. Grahame, *J. Am. Chem. Soc.*, **71**, 2975 (1949).

(2) I. M. Kolthoff and J. J. Lingane, "Polarography," 2nd ed., Interscience Pub. Co., Inc., New York, N. Y., 1952, p. 79.

This work has been supported by the Office of Naval Research.

THE CALCULATION OF THE LIMITING RETENTION VOLUME IN GAS–LIQUID PARTITION CHROMATOGRAPHY

By S. A. Greene

Aerojet-General Corporation, Azusa, California

Received November 2, 1956

James and Martin[1] have shown that the apparent retention volume must be corrected to a limiting retention volume in order to take into account compressibility of the vapor phase and resultant gas velocity gradient down the column. The correcting equation is

$$V^0_m = \frac{V_m}{2/3}\left(\frac{P_1/P_0^3 - 1}{P_1/P_0^2 - 1}\right) = \frac{al}{R_F} = \frac{V_g}{R_F} \qquad (1)$$

where

V^0_m = limiting retention volume
a = cross-sectional area of gas phase
l = column length
R_F = usual chromatographic meaning
P_1 = column inlet pressure
P_0 = column outlet pressure
V_g = volume of gas phase when column is uniformly packed
V_m = apparent retention volume

Partition coefficients are calculated from the data of gas–liquid partition chromatography by the expression[2]

$$V^0_m = kV_l + V_g \qquad (2)$$

where

k = partition coefficient
V_l = liquid phase volume

and the rather tedious correction as in 1 must be made. We define the quantity ${}^cV^0_m$ as the limiting retention volume of the carrier gas

$${}^cV^0_m = F'{}^ct_m E = \frac{V_g}{R_F} = V_g \qquad (3)$$

where

F' = carrier gas flow rate
${}^ct_m$ = apparent retention time of carrier gas which is measured by a gas such as hydrogen which is negligibly soluble in the liquid

$$E = 3/2\left(\frac{P_1/P_0)^2 - 1}{P_1/P_0)^3 - 1}\right)$$

R_F = unity for this condition

Then

$$V^0_m = F't_m E = \frac{V_g}{R_F} \qquad (4)$$

where

t_m = apparent retention time of zone

Dividing 3 by 4 we have

$$\frac{{}^ct_m}{t_m} = R_F \qquad (5)$$

and

$$V^0_m = V_g \frac{t_m}{{}^ct_m} \qquad (6)$$

R_F is seen to be the ratio of apparent retention time of carrier and zone. Although the method outlined here obviates the correction, ${}^ct_m$ is usually a small number as compared to t_m and the accuracy of the ratio might not ordinarily be good. It should also be noted that equation 3 permits the calculation of V_g from flow pressure parameters.

(1) A. T. James and A. J. P. Martin, *Biochem. J.*, **50**, 679 (1952).
(2) P. E. Porter, C. H. Deal and F. H. Stross, *J. Am. Chem. Soc.*, **78**, 2999 (1956).

THE PERIODATE OXIDATION OF *cis*- AND *trans*-CYCLOPENTANEDIOL-1,2

By Vernon C. Bulgrin

Contribution from the Department of Chemistry, University of Wyoming, Laramie, Wyoming

Received December 1, 1956

The periodic acid oxidative cleavage of vicinal glycols may proceed by at least two mechanisms, usually, however, involving the formation of an intermediate coördination compound between the oxidant and the reductant, the rate-determining step being the disproportionation of the intermediate. Duke and Bulgrin[1,2] assigned this type of mechanism to the oxidation of ethylene glycol and a series of methylated ethylene glycols, including propylene, *meso*- and *levo*-butylene and trimethylethylene glycols. The reaction scheme was suggested

$$IO_4^- + G \underset{\text{rapid}}{\overset{K}{\rightleftharpoons}} C \xrightarrow[\text{slow}]{k} \text{products}$$

This scheme leads to the kinetic expression

$$-\frac{d[P]_T}{dt} = k[C] = k'[P]_T \qquad (1)$$

where

$$\frac{1}{k'} = \frac{1}{k} + \frac{1}{kK[G]}\left(1 + \frac{1}{K_D} + \frac{A_{H^+}\gamma_{IO_4^-}}{K_1K_D\gamma_{H_5IO_6}}\right)$$

A_{H^+} = activity of hydrogen ion
$\gamma_{IO_4^-}$ and $\gamma_{H_5IO_6}$ are the respective activity coefficients
K_1 and K_D are defined by the equilibria

$$H_5IO_6 \overset{K_1}{\rightleftharpoons} H^+ + H_4IO_6^-$$

$$H_3IO_6^- \overset{K_D}{\rightleftharpoons} 2H_2O + IO_4^-$$

[C] = concentration of intermediate
[G] = concentration of uncoordinated glycol
$[P]_T$ = concentration of total periodate

In a study of the effect of pH on the rate of the reaction it was found that for all of the aforementioned glycols, equation 1 was followed down to pH values of less than one, thus substantiating the postulate that a monovalent periodate ion is the reactive species in the acid range.

Pinacol, on the other hand, was found to oxidize at a much slower rate than any of the others, and to exhibit a first-order hydrogen ion catalysis. No evidence for any intermediate could be demonstrated from the kinetic data, the reaction being second order over the range of concentrations studied. It was suggested that the same type intermediate does not exist in the case of pinacol, and that the formation of the intermediate has become

(1) F. R. Duke, *J. Am. Chem. Soc.* **69**, 3054 (1947).
(2) F. R. Duke and V. C. Bulgrin, *ibid.*, **76**, 3803 (1954).

rate determining. An alternative mechanism, one which would account for the observed hydrogen ion catalysis, would be the formation of an intermediate monoperiodate ester, the disproportionation of which is rate determining.

A kinetic study of oxidation of *cis*- and *trans*-cyclopentanediol-1,2 was undertaken in an effort to shed some light on apparently important steric factors.

Experimental

Cyclopentene was prepared by dehydration of cyclopentanol over activated alumina at 150–200°.

cis-Cyclopentanediol-1,2 was prepared from cyclopentene by the method of Bartlett.[3] The crude glycol was distilled at a pressure of 10 mm.; the fraction boiling from 101–112° (uncorrected) was redistilled at 7 mm. pressure, the portion boiling at 91.5–94° (uncorrected) being collected. Analysis by periodate oxidation showed a purity of 97.3%.

trans-Cyclopentanediol-1,2 was prepared from cyclopentene by means of formic acid and hydrogen peroxide.[4] The crude glycol was vacuum distilled at 10 mm. pressure; a 60-ml. fraction was redistilled at 12 mm. pressure, a 30-ml. fraction boiling at 110–110.3° (uncorrected) being collected. Analysis by periodate oxidation showed a purity of 97.0%.

Rate determinations were made by the procedure outlined in a previous paper,[2] using 10% KI in saturated sodium bicarbonate solution, containing a measured excess of standard sodium arsenite, as a quenching solution, and titrating the excess arsenite with standard iodine solution.

Discussion and Results

***cis*-Cyclopentanediol-1,2.**—The rate of oxidation of the *cis*-isomer proved to be so rapid at 0° that only limited information could be obtained. Only the pseudo second-order rate constants expected at very low concentrations of both reactants could be determined. The *p*H behavior was found to be similar to that predicted by equation 1, the rate being independent of *p*H in the range 2–6, falling off rapidly below *p*H 2. It is presumed that the usual type intermediate is involved in the oxidation.

***trans*-Cyclopentanediol-1,2.**—The rate of cleavage of this compound proved to be quite rapid at 0° but much slower than that of the *cis*-compound. By using a threefold excess of glycol, pseudo first-order rate constants, k', were determined as a function of *p*H. The plot is shown in Fig. 1; such behavior is predicted by equation 1.

Variation of pseudo first-order rate constants as a function of glycol concentration, using a three- to sixfold excess of glycol, was determined in the *p*H range 4–5. Figure 2 shows a plot of the reciprocal first-order rate constants *vs.* the reciprocal glycol concentrations. For the purpose of the plots, the average glycol concentration during the course of the reaction was used. The extrapolation of the resulting straight line to an intercept of zero indicates second-order kinetics over the entire concentration range.

Second-order rate constants were determined using glycol–periodate ratios varying from one to five. The constants k_2 were calculated by multiplying the pseudo second-order rate constants k_2', obtained from the slopes of the second-order plots, by the factor $(1 + 1/K_D)$, the term K_D having its previous significance. The results for five temperatures are given in Table I.

(3) P. D. Bartlett and A. Bavley, THIS JOURNAL, **60**, 2416 (1938).
(4) A. Roebuck and H. Adkins, *Org. Syntheses*, **28**, 35 (1948).

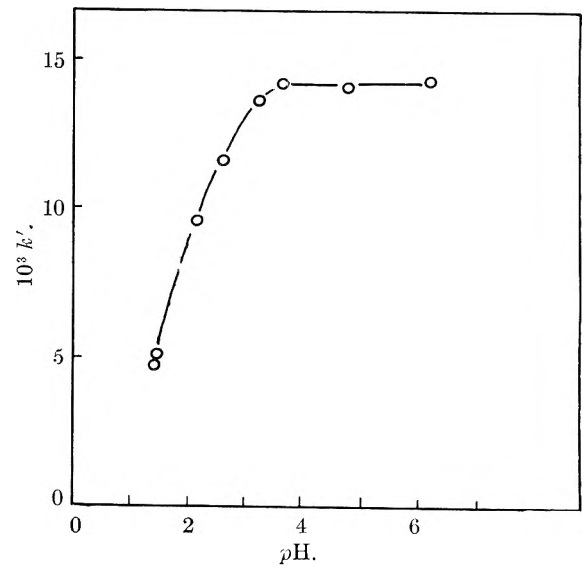

Fig. 1.—*trans*-Cyclopentanediol-1,2: pseudo first-order rate constants *vs.* *p*H at 0°.

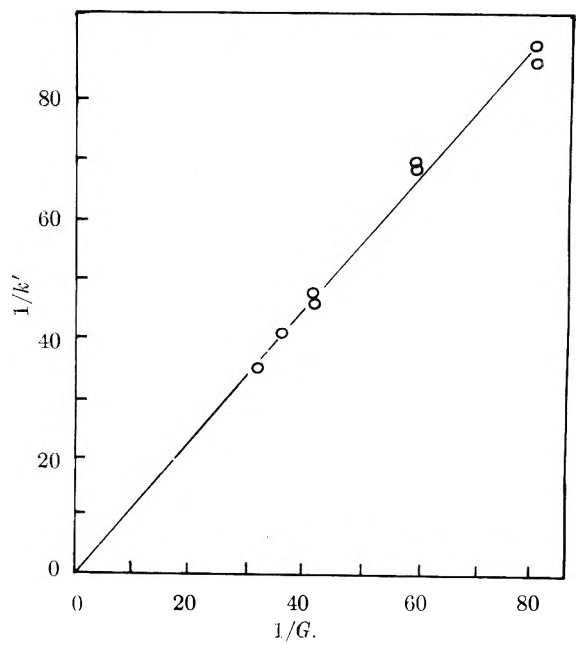

Fig. 2.—*trans*-Cyclopentanediol-1,2: plot of reciprocal pseudo first-order rate constants *vs.* reciprocal glycol concentration at 0° in the *p*H range 4–5.

TABLE I

SECOND-ORDER RATE CONSTANTS FOR *trans*-CYCLOPENTANEDIOL-1,2

Temp., °C.	k_2'	K_D	k_2 (l. moles^{-1} sec.$^{-1}$)
0.00	0.86 ± 0.01[5]	7.4	0.96
5.30	0.93[5]	11.0	1.02
11.03	1.03	16.2	1.09[5]
17.88	1.18	25.4	1.23
25.24	1.34	40.	1.37

The calculated activation energy, E_a, determined from the straight line plot of log k_2 *vs.* the reciprocal temperature, was 2.41 kcal.; the entropy of activation, −52 e.u.

The observed second-order kinetics might be explained on the basis of a small equilibrium constant for the formation of an intermediate (of the order of magnitude of unity or less) or, more likely, that the complex-forming step has become rate determining. Both explanations seem plausible in view of the larger than "normal" oxygen–oxygen distance for this glycol.

COMMUNICATION TO THE EDITOR

ON THE REALITY OF THE LOW *p*H EXPANSION OF BOVINE PLASMA ALBUMIN

Sir:

In a recent paper Loeb and Scheraga[1] have presented a theory which attempts to explain the now well-known anomaly in the titration behavior of bovine plasma albumin. Their calculations are based on the premise that the low *p*H expansion of this protein is minor and, further, independent of ionic strength. The purpose of this communication is to point out that this premise is in all probability false and to attempt to prevent confusion which may result from publication of their paper.

They reject the published evidence for expansion on the grounds that previous workers have not taken cognizance of the heterogeneity resulting from aggregation of plasma albumin at low *p*H. On the contrary all workers involved have considered aggregation and have presented reasonable proof that such aggregation is either negligible or at least not present to a sufficient extent to invalidate the conclusion that expansion[2] does occur.[3,4,5,6] Further, all of these workers found the expansion to be strongly dependent on ionic strength. There is thus no justification for applying hydrodynamic results obtained at ionic strength 0.5 and *p*H 4 to interpretation of the titration curve at ionic strength 0.15 and down to *p*H 3.0.

The importance attached to aggregation by Loeb and Scheraga appears to be based to a large extent on ultracentrifugal studies conducted at relatively high ionic strength (0.3–0.5).[7] At low ionic strength the results showed clear evidence for aggregation only when solutions were aged several months, which observation has little pertinence in the present case. Related studies,[8,9] quoted also by Loeb and Scheraga as supporting aggregation, actually led to the conclusion that such aggregation does not invalidate evidence for expansion. We have found Dural ultracentrifuge cells to promote gross aggregation of plasma albumin at low *p*H.[10] A related observation has been reported by Phelps and Cann.[11] Using Kel-F centerpieces we have found no evidence for aggregation in some 50 ultracentrifuge runs conducted over the *p*H range 2.0–4.5 at ionic strength 0.02. It is presumed, in absence of any statement to the contrary, that the published ultracentrifugal[7,8,9] results were obtained in the conventional Dural cells; if so, repetition in Kel-F cells is most desirable.

Reichmann and Charlwood[4] claimed slow aggregation and eventual precipitation of plasma albumin to take place below *p*H 2.9 in absence of salt. This observation merits further study but is in conflict with the observations reported by ourselves[3] and by Tanford, *et al.*[5] In these latter cases some apparent aggregation was observed which was traced to impurities, possibly fatty acids, in the protein.

We are indebted to the National Cancer Institute, National Institutes of Health, and to the National Science Foundation for support of this work.

DEPARTMENT OF CHEMISTRY
PURDUE UNIVERSITY JOSEPH F. FOSTER
LAFAYETTE, INDIANA

RECEIVED FEBRUARY 11, 1957

(1) G. I. Loeb and H. A. Scheraga, THIS JOURNAL, **60**, 1633 (1956).

(2) It is not intended to imply by the use of this term that no elongation of the molecule occurs. We used[3] the phrase "essentially isotropic" by no means intending to imply that there is no change in axial ratio. Whether some slight increase in asymmetry does occur is in my opinion still unknown and of relatively little importance for purposes of this discussion.

(3) J. T. Yang and J. F. Foster, *J. Am. Chem. Soc.*, **76**, 1588 (1954).

(4) M. E. Reichmann and P. A. Charlwood, *Canadian J. Chem.*, **32**, 1092 (1954).

(5) C. Tanford, J. G. Buzzell, D. G. Rands and S. A. Swanson, *J. Am. Chem. Soc.*, **77**, 6421 (1955).

(6) W. F. Harrington, P. Johnson and R. H. Ottewill, *Biochem. J.*, **62**, 569 (1956).

(7) H. A. Saroff, G. I. Loeb and H. A. Scheraga, *J. Am. Chem. Soc.*, **77**, 2908 (1955).

(8) P. Bro, S. J. Singer and J. M. Sturtevant, *ibid.*, **77**, 4924 (1955).

(9) M. J. Kronman, M. D. Stern and S. N. Timasheff, THIS JOURNAL, **60**, 829 (1956).

(10) M. J. Kronman and J. F. Foster, *Arch. Biochem. Biophys.*,

(11) R. A. Phelps and J. R. Cann, *ibid.*, in press, **61**, 51 (1956).

CHEMICAL NOMENCLATURE

Number eight of the
Advances in Chemistry Series
Edited by the staff of *Industrial and Engineering Chemistry*

A collection of papers comprising the Symposium on Chemical Nomenclature, presented before the Division of Chemical Literature at the 120th meeting—Diamond Jubilee—of the American Chemical Society, New York, N. Y., September 1951

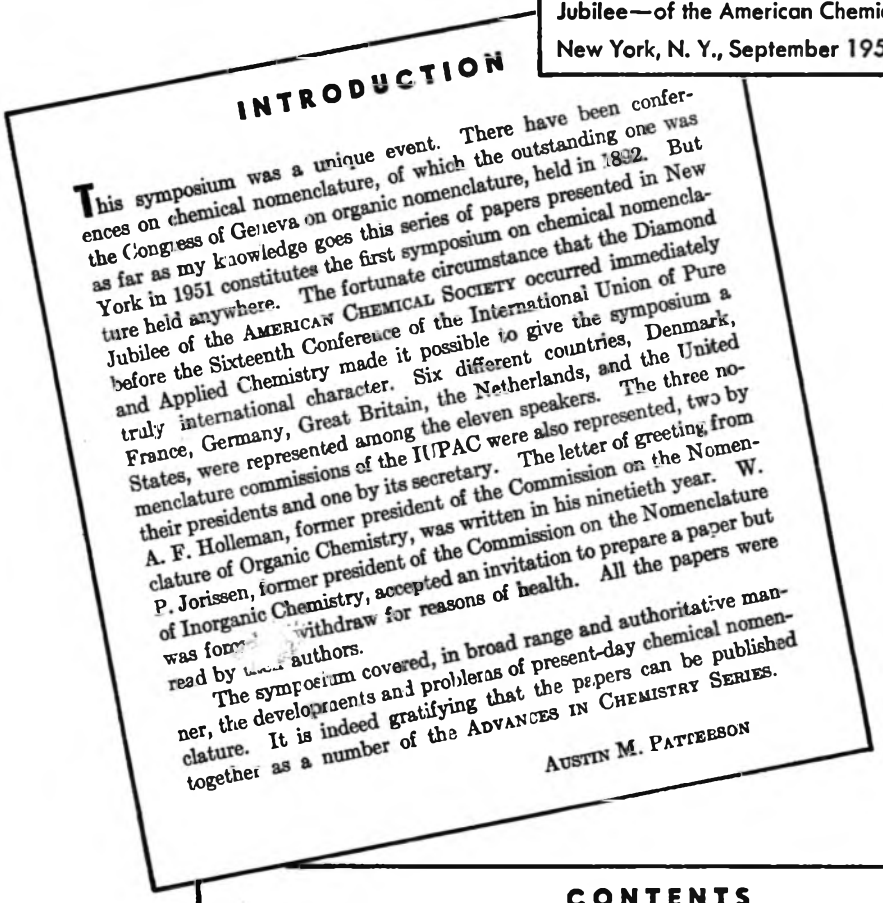

INTRODUCTION

This symposium was a unique event. There have been conferences on chemical nomenclature, of which the outstanding one was the Congress of Geneva on organic nomenclature, held in 1892. But as far as my knowledge goes this series of papers presented in New York in 1951 constitutes the first symposium on chemical nomenclature held anywhere. The fortunate circumstance that the Diamond Jubilee of the AMERICAN CHEMICAL SOCIETY occurred immediately before the Sixteenth Conference of the International Union of Pure and Applied Chemistry made it possible to give the symposium a truly international character. Six different countries, Denmark, France, Germany, Great Britain, the Netherlands, and the United States, were represented among the eleven speakers. The three nomenclature commissions of the IUPAC were also represented, two by their presidents and one by its secretary. The letter of greeting from A. F. Holleman, former president of the Commission on the Nomenclature of Organic Chemistry, was written in his ninetieth year. W. P. Jorissen, former president of the Commission on the Nomenclature of Inorganic Chemistry, accepted an invitation to prepare a paper but was forced to withdraw for reasons of health. All the papers were read by their authors.

The symposium covered, in broad range and authoritative manner, the developments and problems of present-day chemical nomenclature. It is indeed gratifying that the papers can be published together as a number of the ADVANCES IN CHEMISTRY SERIES.

AUSTIN M. PATTERSON

112 pages

paper cover

$2.50

CONTENTS

Published August 15, 1953, by
AMERICAN CHEMICAL SOCIETY
1155 Sixteenth Street, N.W.
Washington, D. C.

AZEOTROPIC DATA

-- Advances in Chemistry Series Volume No. 6

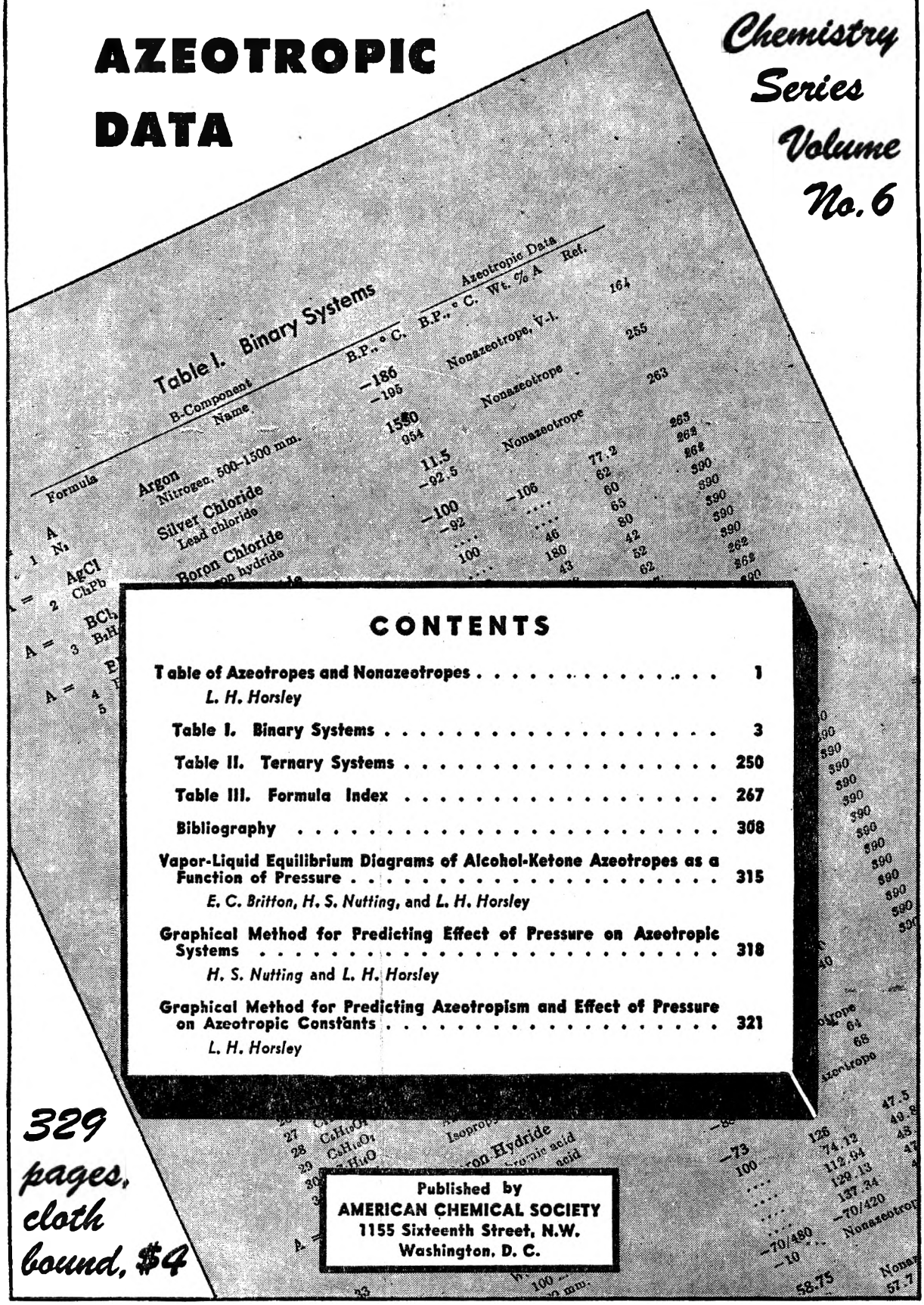

CONTENTS

329 pages, cloth bound, $4

Published by
AMERICAN CHEMICAL SOCIETY
1155 Sixteenth Street, N.W.
Washington, D. C.